

---

**A multi-method approach to study the  
geodynamic evolution of eastern Dronning  
Maud Land in East Antarctica by integrating  
geophysical data with surface geology**

---

DISSERTATION

Zur Erlangung des Grades Dr. rer. nat.  
vorgelegt dem Fachbereich Geowissenschaften  
der Universität Bremen

von

ANTONIA STEFANIE RUPPEL

März 2019

**First reviewer:** PD Dr. Frank Lisker  
University of Bremen, Department of Geosciences

**Second reviewer:** Prof. Dr. Laura Crispini  
University of Genova, Department of Earth, Environmental and Life  
Sciences

**Date of defence:** 09.07.2019

**Versicherung an Eides Statt / *Affirmation in lieu of an oath***  
**gem. § 5 Abs. 5 der Promotionsordnung vom 18.06.2018 /**  
***according to § 5 (5) of the Doctoral Degree Rules and Regulations of 18 June, 2018***

Ich / I, Antonia Stefanie Ruppel wohnhaft in der Podbielskistraße 135, 30177 Hannover, versichere an Eides Statt durch meine Unterschrift, dass ich die vorliegende Dissertation selbständig und ohne fremde Hilfe angefertigt und alle Stellen, die ich wörtlich dem Sinne nach aus Veröffentlichungen entnommen habe, als solche kenntlich gemacht habe, mich auch keiner anderen als der angegebenen Literatur oder sonstiger Hilfsmittel bedient habe und die zu Prüfungszwecken beigelegte elektronische Version (PDF) der Dissertation mit der abgegebenen gedruckten Version identisch ist. / *With my signature I affirm in lieu of an oath that I prepared the submitted dissertation independently and without illicit assistance from third parties, that I appropriately referenced any text or content from other sources, that I used only literature and resources listed in the dissertation, and that the electronic (PDF) and printed versions of the dissertation are identical.*

Ich versichere an Eides Statt, dass ich die vorgenannten Angaben nach bestem Wissen und Gewissen gemacht habe und dass die Angaben der Wahrheit entsprechen und ich nichts verschwiegen habe. / *I affirm in lieu of an oath that the information provided herein to the best of my knowledge is true and complete.*

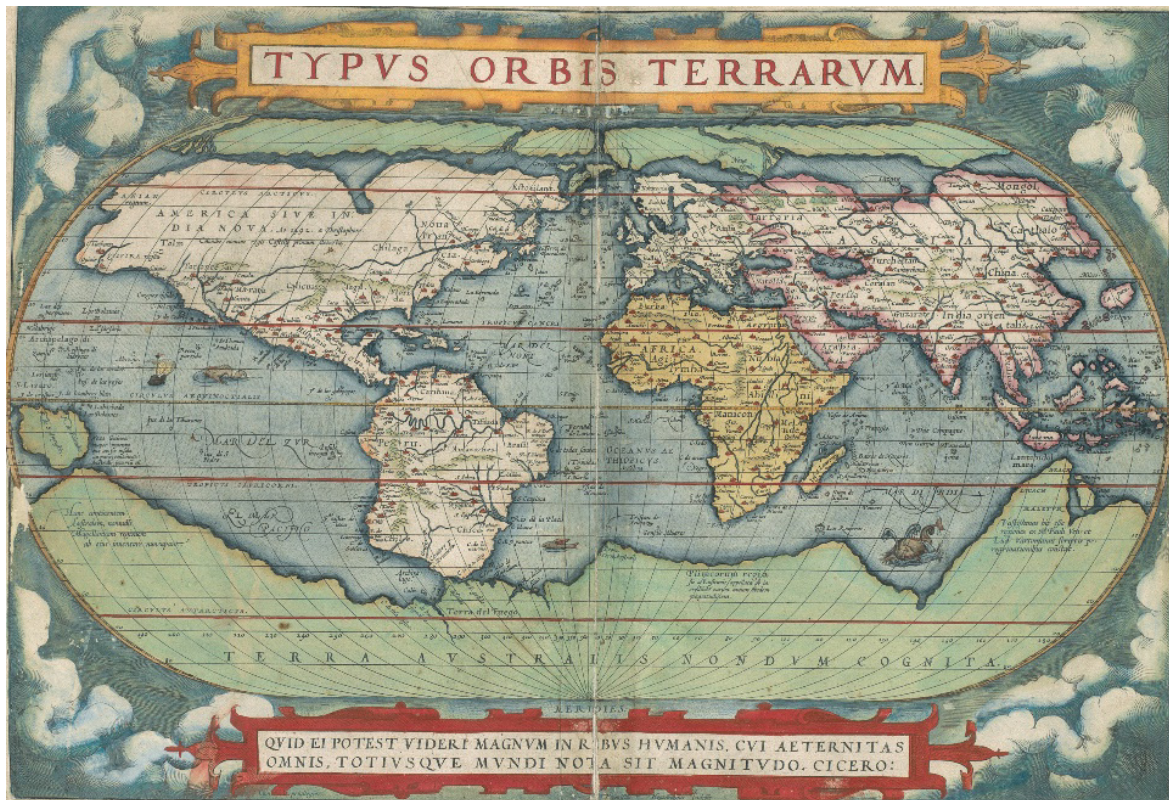
Die Strafbarkeit einer falschen eidesstattlichen Versicherung ist mir bekannt, namentlich die Strafandrohung gemäß § 156 StGB bis zu drei Jahren Freiheitsstrafe oder Geldstrafe bei vorsätzlicher Begehung der Tat bzw. gemäß § 161 Abs. 1 StGB bis zu einem Jahr Freiheitsstrafe oder Geldstrafe bei fahrlässiger Begehung. / *I am aware that a false affidavit is a criminal offence which is punishable by law in accordance with § 156 of the German Criminal Code (StGB) with up to three years imprisonment or a fine in case of intention, or in accordance with § 161 (1) of the German Criminal Code with up to one year imprisonment or a fine in case of negligence.*

Hannover, 11. März 2019

Ort / Place, Datum / Date

Unterschrift / Signature

**"Terra Australis Incognita"- the unknown land of the south.**



*Historical map from the Atlas Theatrum Orbis Terrarum (Theatre of the World) by Abraham Ortelius (Original edition from 1571 with additions from 1573, 1579 and 1584).*

# Preface

This thesis is part of the GEA project and partly funded by the DFG project LI 745/15-1 & LA 1080/9-1 ‘Long term structural development and landscape evolution of eastern Dronning Maud Land, and implications for the geological evolution of the Weddell Sea region’.

GEA, an acronym for ‘Geodynamic Evolution of East Antarctica’, represents an ongoing collaboration between the Federal Institute for Geosciences and Natural Resources (BGR) and the Alfred Wegener Institute, Helmholtz Centre for Polar and Marine Research (AWI) as well as several cooperations with national and international universities. Since GEA was launched in 2010, it has comprised five stages (GEA I-V) each implementing geological, geophysical or combined expeditions to Dronning Maud Land.

This project pursues a multi-methodological approach in order to improve common understanding of geological processes that resulted in the final amalgamation and the break-up of Gondwana by enlightening it from different scientific perspectives. This study is closely interconnected with other PhD theses as well as research projects by participants of the expedition(s) joining from associated universities and cooperating research facilities like the AWI.

# Structure of the Thesis

The present work is written as a cumulative dissertation and comprises a compilation of ‘first-authored’ and ‘co-authored’ contributions to scientific journals. The introductory remarks below aim to provide a comprehensive overview and guideline through the following chapters.

## Chapter 1 - Introduction and Motivation

Chapter 1 provides a brief overview of Antarctica being the last discovered and least explored continent on our planet. It deals with the continent itself, how we know it from today being extensively covered by ice as well as being part of several supercontinent cycles within Earth’s history. Furthermore, the chapter introduces the study area of Sør Rondane situated in eastern Dronning Maud Land on the East Antarctic continent. At the end, it outlines overarching questions and defines the scope of this thesis.

## Chapter 2 - Methods

Chapter 2 gives a methodological introduction, which forms the basis for the structure of this thesis. The presented scientific contributions focus on different methods that have been applied within the framework of the project. The study area of Sør Rondane and its surroundings were investigated by using a multi-methodological approach with the main part of this thesis focusing on structural geology, aeromagnetism, geochronology as well as subordinately geochemistry and petrography.

## Chapter 3 - Contributions to Scientific Journals

Chapter 3 documents the ‘first-author’ and ‘co-author’ contributions. It provides an overview of the submission histories as well as a content-related outline and the author contributions to each part. However, contributions are not presented in an overall chronological order, instead they are separated into a chronological submission history of ‘first-author’ contributions and followed by a chronological list of ‘co-authored’ publications. Therefore, the aim of this chapter is to clarify the two different timelines and provide an overview of all contributions linked to the multi-methodological approach applied.

## Chapter 4 to 6 - ‘First-author’ Contributions

‘First-author’ contributions include two accepted and published contributions and one manuscript that is currently being finalized for submission. Contributions include studies of a regional structural feature referred to as Main Shear Zone. This geological structure was supposed to represent one of the candidates for the location of the E-W-Gondwana suture zone within the Late Neoproterozoic/Early Palaeozoic East African-Antarctic Orogen, which stretched from NE Africa through Madagascar and Mozambique into the coastal mountains of Dronning Maud Land, East Antarctica (Chapter 4). Aeromagnetic surveys were conducted in order to investigate the subglacial nature of a key region in East Antarctica and trace boundaries/ shear zones by integrating geological field investigations. Another survey was realized south and east of the main mountain range of Sør Rondane (Chapter 5).

Geochronological studies were carried out to constrain the timing of deformation and cooling of Sør Rondane after the amalgamation of Gondwana by using Ar/Ar dating on biotite and amphibole as well as U-Pb age dating on zircon (Chapter 6).

#### Chapter 7 to 12 - 'Co-author' Contributions

These chapters include 'co-author' contributions published in close collaboration within the GEA project. Mieth et al. (2014) used aeromagnetic and geological data to refine the tectonic and structural framework of Sør Rondane itself (Chapter 7). Geological, geochronological and geochemical studies of a previously poorly known region between western Sør Rondane and central Dronning Maud Land were carried out by Jacobs et al. (2015) (Chapter 8). Geochronological methods e.g. U-Pb, Lu-Hf and trace element dating on zircon were applied by Elburg et al. (2015) in order to gain detailed information about the early Neoproterozoic history of the southern part of Sør Rondane (Chapter 9). Late- to post-tectonic granitoids were systematically sampled and dated (U-Pb, Lu-Hf dating on zircon) by Elburg et al. (2016) aiming to unravel the magmatic and metamorphic history of Sør Rondane in more detail (Chapter 10). The subglacial landscape and its gravimetric signature of Sør Rondane and adjacent regions were studied by Eagles et al. (2018) and provide evidence for erosional processes at an extended passive continental margin (Chapter 11). Krohne et al. (in prep.) examined the thermal history of Sør Rondane and investigated the break-up of Gondwana and the subsequent long-term landscape evolution (Chapter 12).

#### Chapter 13 - Synopsis

The synopsis highlights, integrates and critically examines the findings of this thesis in the context of the previous state of research.

#### Chapter 14 - Conclusions

This chapter addresses the main research questions raised at the beginning and provides a comprehensive summary of the new findings drawn from the cumulative and multi-methodological approach of this thesis.

#### Chapter 15 - Continuing Work & Outlook

Last but not least, this work has raised several new scientific questions. Some have already become an issue of ongoing research or are designated projects-to-come. Many research questions might benefit from a multi-methodological approach. For example, integrated geophysical and geological studies were attested to be a powerful tool to unveil the subglacial geology of Antarctica. Therefore, this chapter highlights possible future fields for research in and adjacent to Sør Rondane.

# Abstract

Planet Earth has not always been as it appears today. Since billions of years, continents have been drifting continually caused by lateral variations of mantle density resulting in convection. Analyzing the movement of lithospheric plates back in earth's history is essential for the determination of the shape of ancient supercontinents. It further provides paleogeographic information and is vital for biogeographic and climate studies.

Whereas the break-up of the former extensive landmass of Gondwana can be reconstructed fairly well by analyzing seafloor-spreading anomalies of the oceanic crust, the amalgamation of Gondwana still needs to be understood in more detail. This is because oceanic crust, that rarely exceeds 180 million years in age, does not provide any direct evidence for the amalgamation of Gondwana in Late Neoproterozoic/Early Palaeozoic times as well as for older supercontinent cycles.

East Antarctica, once centerpiece of Gondwana, can be considered a rather stable region as it has not been affected by orogenic processes since the Early Paleozoic except for its Palaeo-Pacific margin. Furthermore, the Antarctic plate is mainly surrounded by mid-ocean ridges and features continental rift systems widely related to the break-up of Gondwana. Therefore, exposed regions that can be found in Sør Rondane, East Antarctica, are well suited for studying the formation and break-up of Gondwana as well as preceding collision and break-up processes. Sør Rondane is situated in eastern Dronning Maud Land and exposes the contact zone of crustal blocks of different origin and architecture. Therefore, it is considered to be a site of at least one suture between East and West Gondwana.

This study examines the final amalgamation and break-up history of Gondwana by investigating Sør Rondane and adjacent regions. To answer those questions, a detailed understanding of the crustal architecture is essential. This encompasses the number of involved crustal fragments, the location of their boundaries and their geological evolution. Moreover, this comprises the structural and metamorphic evolution as well as the shallow crustal dynamics of Sør Rondane.

Due to the extensive ice-coverage of this region, the study of exposed rocks by various geological methods was combined with regional aerogeophysical investigations. In the austral summers 2010/11 and 2011/12, structural field work and geological sampling were executed by the Federal Institute for Geosciences and Natural Resources (BGR). Additional airborne geophysical surveys were flown in collaboration with the Alfred Wegener Institute, Helmholtz Centre for Polar and Marine Research (AWI), between 2010 and 2015. The data set includes ice-penetrating radar, aeromagnetic and aerogravity measurements. These combined geological and geophysical data sets are used to analyse the structure and composition of rock units and enable to map units beneath the ice not accessible to geological methods. For instance, fault systems may correlate with magnetic lineaments gained from aeromagnetic anomaly data. These can be tracked over large distances underneath the ice and thus facilitate interpretations at a larger scale.

Substantial findings of this study regarding the crustal architecture of East Antarctica are based on the geological characterization and the estimation of the minimum extent of a distinct aeromagnetic province in southeastern Dronning Maud Land. The basement of this region consists mainly of juvenile Early Neoproterozoic rocks and is defined as the Tonian Oceanic

Arc Super Terrane (TOAST), which includes Sør Rondane. The juvenile oceanic arc complex corresponds to at least 5 % of East Antarctica's size and represents a major remnant of the Mozambique Ocean that developed outside Rodinia. During the amalgamation process of Gondwana the TOAST may have first accreted to the cryptic Valkyrie Craton before this newly formed fragment collided with southern Africa (Kalahari) in the west and Indo-Antarctica in the east.

Newly acquired aeromagnetic data over Sør Rondane lead to the identification of several smaller terranes, fault zones, and tectonic boundaries. One of these fault zones is the Main Shear Zone, formerly assumed to represent one candidate for the location of a possible suture. Based on this study it is now interpreted as a lithotectonic boundary and linked to bipolar lateral escape of the East African-Antarctic Orogen in late Ediacaran-Cambrian times. Further, comprehensive Ar/Ar dating yield new age constraints for the individual terranes and sheds new light on the Late Neoproterozoic/Early Paleozoic tectono-thermal history of Sør Rondane. A correlation of magmatic pulses persisting over 150 Myrs with cooling ages is very likely. Additionally, the long-lasting magmatic activity suggests an accretionary history that resulted in the final amalgamation of Gondwana. Thermochronological and geophysical investigations provided new evidence for the geological history of Sør Rondane regarding the time after Gondwana was established and started its subsequent disintegration during Jurassic times. Modelling of apatite fission track (AFT) and apatite (U-Th-Sm)/He ages shed new light on the geological and long-term landscape evolution since the Late Paleozoic and indicate various exhumation and burial stages of Sør Rondane. New ice-penetrating radar and gravity data reveal first time insights into the East Antarctic Ice Sheet and the bed topography of Sør Rondane with adjacent regions.

Thus, investigating Sør Rondane and adjacent regions by aerogeophysical methods and their integration with surface geology significantly contributed to a more comprehensive conception of the final amalgamation and break-up history of Gondwana. The outcome emphasises the importance of applying a multi-method approach in order to reliably analyse the tectonic structure and geodynamic evolution of mainly ice-covered East Antarctica for present and future studies.

# Kurzfassung

Seit Milliarden von Jahren verändert sich die Gestalt der Erde kontinuierlich. Die Erklärung dafür sind Konvektionsprozesse im Erdmantel, die aufgrund lateraler Dichteunterschiede Bewegungen der Kontinentalplatten auf der Erdoberfläche verursachen. Verfolgt man die Verschiebung dieser Platten in der Erdgeschichte zurück, ist es möglich, elementare Aussagen zum Erscheinungsbild früher Superkontinente zu treffen. Diese Informationen fließen in paleogeographische Studien und darüber hinaus in die Bearbeitung von Fragestellungen aus der Biogeologie und der Klimatologie ein.

Obwohl der Zerfall der einst beträchtlichen Landmasse Gondwana durch die Analyse von Ozeanbodenspreizungsanomalien der ozeanischen Kruste relativ gut rekonstruiert werden kann, wirft die Entstehung Gondwanas weiterhin grundlegende Fragen auf. Der Grund dafür ist, dass das Alter der ozeanischen Kruste selten 180 Millionen Jahre überschreitet und dementsprechend keinen unmittelbaren Hinweis auf den Zusammenschluss von Gondwana während des späten Neoproterozoikums/frühen Paläozoikums oder die Entwicklung früherer Superkontinente liefern kann.

Die Ostantarktis, einst zentraler Teil von Gondwana, kann als relativ stabile Region betrachtet werden, da sie seit dem frühen Paläozoikum mit Ausnahme des paläopazifischen Kontinentalrandes nicht mehr von gebirgsbildenden Prozessen betroffen war. Heutzutage ist die Antarktische Platte von mittelozeanischen Rücken umgeben und durch kontinentale Grabenbrüche gekennzeichnet, die sich im Zuge des Aufbruchs von Gondwana gebildet haben. Demzufolge eignen sich Aufschlüsse in Sør Rondane, einer Region in der Ostantarktis, dazu, sowohl Entstehung und Aufbruch Gondwanas, als auch vorherige Kollisions- und Aufbruchprozesse zu untersuchen. Sør Rondane befindet sich im östlichen Dronning Maud Land und zeigt in dort vorkommenden Aufschlüssen das Aufeinandertreffen zweier Krustenblöcke unterschiedlicher Herkunft und Struktur. Das lässt vermuten, dass es sich hierbei um eine Region handelt, die eine oder mehrere Kollisionszonen zwischen Ost- und Westgondwana dokumentiert.

Die vorliegende Studie untersucht die Fragestellung, welche Erkenntnisse aus der Analyse der Aufschlüsse in Sør Rondane und den angrenzenden Gebieten für die Entstehung und die Aufbruchgeschichte von Gondwana gewonnen werden können. Diese Analyse setzt ein tiefgreifendes Verständnis des Krustenaufbaus voraus und umfasst weiterhin die Anzahl der Krustenfragmente, deren Grenzen sowie deren geologische Entstehung. Weiterhin wird die strukturelle, metamorphe sowie die dynamische Entwicklung der Erdkruste in die Betrachtungen miteinbezogen.

Aufgrund der ausgedehnten Eisbedeckung dieser Region, wurde die Untersuchung von Aufschlüssen mithilfe unterschiedlicher geologischer Herangehensweisen durch regionale aerogeophysikalische Untersuchungen unterstützt. Im Südsommer 2010/11 und 2011/12 wurden strukturelle Geländearbeiten und geologische Beprobungen durchgeführt, die von der Bundesanstalt für Geowissenschaften und Rohstoffe (BGR) geleitet wurden. Zusätzliche aerogeophysikalische Befliegungen konnten in Zusammenarbeit mit dem Alfred-Wegener-Institut, Helmholtz Zentrum für Polar und Meeresforschung (AWI), von 2010 bis 2015 realisiert werden. Die gewonnenen Datensätze geben Auskunft über Eisdicken sowie die magnetischen und gravimetrischen Eigenschaften der Gesteine. Die Zusammenführung

geologischer und geophysikalischer Daten soll ein verbessertes Verständnis der Struktur und Zusammensetzung einzelner Gesteinseinheiten liefern und weiterhin eine Kartierung dieser Einheiten, die zum Teil unter dem Eis verborgen liegen und somit nicht für geologische Untersuchungen zugänglich sind, ermöglichen. Beispielsweise können größere Störungssysteme mit magnetischen Lineamenten aus aeromagnetischen Untersuchungen im Zusammenhang stehen. Diese können dann über große Distanzen unterhalb des Eises weiterverfolgt werden und so Interpretationen in einem größeren Rahmen ermöglichen.

Eine wesentliche Erkenntnis dieser Studie zum Krustenaufbau der Ostantarktis resultiert aus den Ergebnissen der geologischen Charakterisierung und Abschätzung der minimalen Ausdehnung einer sich geophysikalisch deutlich abgrenzenden Provinz im südöstlichen Dronning Maud Land. Demnach besteht das Grundgebirge hauptsächlich aus juvenilen früh-neoproterozoischen Gesteinen, welche als 'Tonian Oceanic Arc Super Terrane (TOAST)' bezeichnet wird und die Region Sør Rondane mit einschließt. Dieser juvenile ozeanische Inselbogenkomplex entspricht in etwa 5 % der ostantarktischen Landmasse und stellt ein bedeutendes Relikt des Mozambique-Ozeans dar, welches sich außerhalb von Rodina entwickelt hat. Weiterhin wird davon ausgegangen, dass das TOAST während des Entstehungsprozesses von Gondwana zuerst entlang des Valkyrie Craton akkretionierte, bevor dieses neu gebildete Fragment im Westen mit dem südlichen Teil von Afrika (Kalahari) und im Osten mit Indo-Antarktika kollidierte.

Die neugewonnenen aeromagnetischen Daten in der Region Sør Rondane führten zur Identifikation mehrerer kleinräumiger Terranes, Störungszonen sowie tektonischer Grenzen. Bei einer dieser Störungszonen handelt es sich um die Main Shear Zone, welche ursprünglich als mögliche Suturzone gehandelt wurde. Auf Basis dieser Studie wird diese Scherzone nun als lithotektonische Grenze und Teil eines bipolaren Extrusionssystems interpretiert, welches während des späten Ediacariums bis zum Kambrium aktiv war. Zusätzlich liefern umfassende Ar/Ar-Altersdatierungen Hinweise auf die spät-neoproterozoisch bis früh-paläozoische tektonische und thermale Entwicklung der einzelnen Krustenfragmente Sør Rondanes. Hierbei ist anzunehmen, dass ein Zusammenhang zwischen magmatischen Schüben, die über einen Zeitraum von 150 Millionen Jahren andauerten, und den Abkühlaltern besteht. Diese lang andauernde magmatische Aktivität deutet auf eine akkretionäre Entwicklungsgeschichte hin, die zum finalen Zusammenschluss von Gondwana führte. Thermochronologische und geophysikalische Untersuchungen lieferten neue Hinweise auf die geologische Entwicklung von Sør Rondane, nachdem Gondwana entstanden war und anschließend im Jura zu zerfallen begann. Die Modellierung von Apatit-Spaltspuren (AFT) und Apatit (U-Th-Sm)/He-Altern erlaubt Rückschlüsse auf die Geologie und Landschaftsentwicklung und liefert Hinweise auf mehrere Hebungs- und Beckenbildungsprozesse seit dem späten Paläozoikum. Eisdicken und gravimetrische Daten zeigen erstmals sehr detailgetreu die Ausdehnung des ostantarktischen Eisschildes und die subglaziale Topographie von Sør Rondane und benachbarter Gebiete.

Folglich hat die Untersuchung von Sør Rondane und benachbarter Gebiete mit kombinierten aerogeophysikalischen und geologischen Methoden dazu beigetragen, wesentliche neue Erkenntnisse über die finale Kollision und den Aufbruch von Gondwana zu erlangen. Das Ergebnis betont die Relevanz eines multimethodischen Ansatzes für diese und zukünftige Studien mit dem Ziel, ein besseres Verständnis der tektonischen Struktur und geodynamischen Entwicklung der größtenteils eisbedeckten Ostantarktis zu erlangen.

## Acknowledgements

*In my experience no one can accomplish demanding challenges without any help. This already applies to everyday work and life routines but especially to my expeditions to Antarctica that made me realize how insignificant and dependent a single person can be. I am grateful for everyone's support – my supervisors, colleagues, friends and family – who provided invaluable feedback and helped me to improve myself.*

First of all, I would like to thank Frank Lisker and Andreas Läufer who offered me the great opportunity to study the least known continent on earth. I am grateful for their supervision, discussions and constructive criticism over the course of the last few years.

A special thanks goes to Frank Lisker and Laura Crispini for reviewing my doctoral thesis. I am profoundly indebted to Joachim Jacobs for his support, the constructive meetings and inspiring scientific discussions enhancing my work significantly.

I had the great opportunity to join international research teams during my first and most memorable land-based expedition to Sør Rondane, and I would like to thank all members of the science crew including Andreas Läufer, Joachim Jacobs, Marlina Elburg, Detlef Damaske and Nicole Krohne for the excellent cooperation.

My work would not have been possible without the support of the science and flight crews of AWI-Polar aircraft. Here, a special thanks goes to the chief scientists of the airborne campaigns Matthias Mieth and Graeme Eagles who put a lot of effort into the successful realization.

I would like to thank Cornelia Spiegel and the working group 'Geodynamics of the Polar Regions' in the Department of Geosciences at the University of Bremen for the warm reception in their group, as well as Lothar Ratschbacher and his group at TU Bergakademie Freiberg.

I would like to express my gratitude to Christoph Gaedicke who supported and motivated me to complete my PhD thesis besides ongoing project work. I would also like to thank the entire polar research group at BGR, Solveig Estrada, Karsten Piepjohn, Nikola Koglin, Felix Goldmann and Christoph Kasch, for keeping an open door, fruitful discussions and profound technical support.

Many thanks go to my colleagues at BGR Roland Stumpf, Frithjof Bense and Heidrun Stück for proofreading and editing of this thesis. Furthermore, thanks to my lunch crew for all the on- and off-topic discussions.

Special thanks goes to my family. I am grateful for their support and excitement during the expeditions and their interest in my work.

Michael - I am more than thankful for your patience, support and steady motivation.

# Contents

<b>Preface</b> .....	<b>I</b>
<b>Structure of the Thesis</b> .....	<b>II</b>
<b>Abstract</b> .....	<b>IV</b>
<b>Kurzfassung</b> .....	<b>VI</b>
<b>Acknowledgements</b> .....	<b>VIII</b>
<b>Chapter 1</b> .....	<b>1</b>
<b>1. Introduction and Motivation</b> .....	<b>1</b>
1.1 Palaeogeographic Overview and Location of the Study Area	1
1.2 Objectives of the Thesis	4
<b>Chapter 2</b> .....	<b>7</b>
<b>2. Methods</b> .....	<b>7</b>
2.1 Structural Geology	7
2.2 Aeromagnetics	8
2.2.1 Platform and Measurement Systems	8
2.2.2 Temporal Variations of the Earth Magnetic Field	8
2.2.3 Processing	9
2.2.4 Ground-Based Geophysics	10
2.3 Geochronology	12
2.3.1 <sup>40</sup> Ar/ <sup>39</sup> Ar Geochronology	12
2.3.2 U-Pb Zircon Data	15
2.4 Geochemistry and Petrography	15
2.4.1 XRF Analyses	15
2.4.2 Petrographical Studies	16
<b>Chapter 3</b> .....	<b>17</b>
<b>3. Contributions to Scientific Journals</b> .....	<b>17</b>
<b>Chapter 4</b> .....	<b>28</b>
<b>4. The Main Shear Zone in Sør Rondane, East Antarctica: Implications for the Late Pan-African tectonic evolution of Dronning Maud Land</b> .....	<b>28</b>
4.1 Abstract	28
4.2 Introduction	28
4.3 Geological Overview of Sør Rondane	31
4.4 Structural Geology	33
4.5 Discussion	39
4.5.1 The Main Shear Zone of Sør Rondane	39
4.5.2 Geodynamic Significance of the MSZ in the EAAO	41
4.6 Conclusions	44
4.7 Acknowledgements	45

<b>Chapter 5.....</b>	<b>46</b>
<b>5. New Geophysical Data from a Key Region in East Antarctica: Estimates for the Spatial Extent of the Tonian Oceanic Arc Super Terrane (TOAST) .....</b>	<b>46</b>
5.1 Abstract	46
5.2 Introduction	47
5.3 Geological-Geophysical Background of the Study Area and Adjacent Regions	48
5.3.1 Sør Rondane	49
5.3.2 Belgica Mts. and Yamato Mts.	51
5.3.3 Lützow-Holm Bay	51
5.3.4 Tonian Oceanic Arc Super Terrane (TOAST)	51
5.4 Data Acquisition and Processing	52
5.5 Results	53
5.5.1 Bed Topography	53
5.5.2 Airborne Magnetism	53
5.6 Interpretation and Discussion	57
5.6.1 Spatial Extent of the SE DML Province	57
5.6.2 Southern Extent of the TOAST	59
5.6.3 Minimum Eastern Extent of the TOAST	59
5.6.4 Coastal Magnetic Low	61
5.6.5 Spatial Extent of the TOAST	61
5.7 Summary and Conclusion	62
5.8 Acknowledgements	62
<b>Chapter 6.....</b>	<b>63</b>
<b>6. New Constraints on Deformation and Cooling History of Sør Rondane, East Antarctica, with Implications on the Final Assembly of Gondwana from <math>^{40}\text{Ar}/^{39}\text{Ar}</math> and U-Pb Geochronology .....</b>	<b>63</b>
6.1 Abstract	63
6.2 Introduction	64
6.3 Regional Geology of Sør Rondane	66
6.4 Samples and Methods	67
6.4.1 Samples	67
6.4.2 $^{40}\text{Ar}/^{39}\text{Ar}$ Analyses	68
6.4.3 U-Pb Zircon Analyses	68
6.5 Results	69
6.5.1 $^{40}\text{Ar}/^{39}\text{Ar}$ Dating on Biotite and Amphibole	69
6.5.2 U-Pb Age Data of Zircons	86
6.6 Interpretation and Discussion	89
6.7 Summary and Conclusions	96
6.8 Acknowledgements	97

<b>Chapter 7.....</b>	<b>98</b>
<b>7. New Detailed Aeromagnetic and Geological Data of Eastern Dronning Maud Land: Implications for Refining the Tectonic and Structural Framework of Sør Rondane, East Antarctica.....</b>	<b>98</b>
7.1 Abstract	98
7.2 Introduction	99
7.3 Geological Overview of Sør Rondane	99
7.4 Data Acquisition and Processing	103
7.5 Results	104
7.5.1 Airborne Magnetism	104
7.5.2 Magnetic Susceptibility Measurements	105
7.5.3 Magnetic High Near Dufekfjellet Intrusion	106
7.6 Interpretations and Discussion	108
7.6.1 Magnetic Domains and Tectonic Terranes	108
7.6.2 Granitic Intrusions	111
7.6.3 Open Questions	113
7.7 Conclusion	113
7.8 Acknowledgements	114
<b>Chapter 8.....</b>	<b>115</b>
<b>8. Two Distinct Late Mesoproterozoic/Early Neoproterozoic Basement Provinces in Central/Eastern Dronning Maud Land, East Antarctica: The Missing Link .....</b>	<b>115</b>
8.1 Abstract	115
8.2 Introduction	116
8.3 Geological Background	118
8.3.1 Sør Rondane (22–28°E)	118
8.3.2 Eastern Central Dronning Maud Land (11–14°E)	120
8.3.3 Geology Between Taggen and Payerfjellet (15–21°E)	120
8.4 Samples and Methods	122
8.4.1 Samples	122
8.4.2 U-Pb Zircon Geochronology and Whole Rock Sm–Nd Isotope Analyses	123
8.5 Results	123
8.5.1 U-Pb Zircon Geochronology	123
8.6 Summary of Geochronological Data	136
8.6.1 Geochemistry and Nd Isotope Composition	136
8.6.2 Interpretation and Discussion	140
8.7 Regional Implication	145
8.8 Summary and Conclusions	148
8.9 Acknowledgements	149

<b>Chapter 9.....</b>	<b>151</b>
<b>9. Early Neoproterozoic Metagabbro-Tonalite-Trondhjemite of Sør Rondane (East Antarctica): Implications for Supercontinent Assembly .....</b>	<b>151</b>
9.1 Abstract	151
9.2 Introduction	151
9.3 Geological Background	152
9.4 Sample Description	154
9.4.1 Field Appearance	154
9.4.2 Petrography	154
9.5 Analytical Techniques	157
9.6 Zircon U-Pb and Lu-Hf Data	157
9.7 Geochemistry	163
9.7.1 Major and Trace Elements	163
9.7.2 Sr and Nd Isotopic Systems	167
9.7.3 Zircon Trace Element Data	167
9.8 Discussion	170
9.8.1 U-Pb Zircon Age Groups	170
9.8.2 Comparative Geochemistry	171
9.8.3 Timeline of Events and Possible Tectonic Scenarios	176
9.9 Conclusion	177
9.10 Acknowledgements	178
<b>Chapter 10.....</b>	<b>179</b>
<b>10. One Hundred Fifty Million Years of Intrusive Activity in the Sør Rondane Mountains (East Antarctica): Implications for Gondwana Assembly .....</b>	<b>179</b>
10.1 Abstract	179
10.2 Introduction	179
10.3 Regional Geology	181
10.4 Samples and Methods	182
10.5 Results	183
10.6 Discussion	198
10.6.1 Comparison with Published Pan-African Zircon U-Pb Ages	198
10.6.2 Age of Deformation	201
10.6.3 Lu-Hf Data	202
10.7 Recapitulation and Conclusions	204
10.8 Acknowledgements	207
<b>Chapter 11.....</b>	<b>209</b>
<b>11. Erosion at Extended Continental Margins: Insights from New Aerogeophysical Data in Eastern Dronning Maud Land .....</b>	<b>209</b>
11.1 Abstract	209
11.2 Introduction	210

11.2.1	Background and Rationale	210
11.2.2	Geological History of Dronning Maud Land and the Riiser-Larsen Sea	211
11.3	Aerogeophysical Data	214
11.3.1	Radar	214
11.3.2	Gravity	214
11.4	Interpretation	216
11.4.1	Bed Topography	216
11.4.2	Free-Air Gravity	218
11.4.3	Bouguer Anomaly	219
11.5	Erosion and Sedimentation Across the Continental Margin	220
11.5.1	Background	220
11.5.2	Sedimentation and Basins of the Riiser-Larsen Sea	221
11.5.3	Sediment Volume Balance Test of Great Escarpment Erosion History	223
11.6	Discussion	224
11.6.1	Great Escarpment Erosion: Mechanism and History	224
11.6.2	Sediments Transported by the ‘Ragnhild River’	225
11.7	Conclusion	225
11.8	Acknowledgements	226
<b>Chapter 12</b>	<b>.....</b>	<b>227</b>
<b>12.</b>	<b>Exhumation and Uplift of Sør Rondane (East Antarctica) – Inversion of an East Gondwana Triple Junction .....</b>	<b>227</b>
12.1	Abstract	227
12.2	Introduction	227
12.3	Geologic Overview	229
12.3.1	Sør Rondane Basement	229
12.3.2	Regional Phanerozoic Geological Evolution	231
12.4	Geomorphology of Eastern DML and Sør Rondane	232
12.5	Brittle Fault-Slip Data	233
12.6	Thermochronology	234
12.6.1	Sampling	234
12.6.2	Apatite Fission Track Results	237
12.6.3	(U–Th–Sm)/He Results	238
12.6.4	Thermal History Modeling	240
12.7	Exhumation of Western Sør Rondane	242
12.7.1	Permo-Triassic Sag Basin	242
12.7.2	Early Jurassic Basin Inversion	243
12.7.3	Jurassic-Early Cretaceous Continental Basin	244
12.7.4	Basin Inversion, Uplift and Major Geomorphological Modification	245

12.8	Conclusions	247
12.9	Acknowledgements	247
<b>Chapter 13</b>		<b>248</b>
<b>13.</b>	<b>Synopsis</b>	<b>248</b>
13.1	Geophysical and Geo(chrono)logical Evidence Obtained from Sør Rondane	250
13.2	Crustal Provinces of East Antarctica	253
13.3	From Rodinia to Gondwana	254
13.4	Break-up of Gondwana	258
<b>Chapter 14</b>		<b>260</b>
<b>14.</b>	<b>Conclusion</b>	<b>260</b>
<b>Chapter 15</b>		<b>264</b>
<b>15.</b>	<b>Continuing Work &amp; Outlook</b>	<b>264</b>
15.1	The Forster Magnetic Anomaly	264
15.2	The Eastern and Southern Extent of the TOAST	265
15.3	Unveiling the Cooling History of the SW Terrane S	266
<b>16.</b>	<b>References</b>	<b>267</b>
<b>Electronic Appendix</b>		<b>A</b>
<b>A.</b>	<b>Supplementary Material Chapter 4</b>	<b>A</b>
A.1.	Structural Measurements	A
<b>B.</b>	<b>Supplementary Material Chapter 6</b>	<b>B</b>
B.1.	Age-spectrum and Isochron Plots	B
B.2.	$^{40}\text{Ar}/^{39}\text{Ar}$ Analytical Data	B
B.3.	U-Pb Zircon Data	B
B.4.	Results of X-Ray Fluorescence (XRF) Spectrometry	B
<b>C.</b>	<b>Supplementary Material Chapter 8</b>	<b>C</b>
C.1.	U-Pb Analytical Details	C
C.2.	U-Pb Zircon Data	C
C.3.	Sm-Nd Data	C
<b>D.</b>	<b>Supplementary Material Chapter 9</b>	<b>D</b>
D.1.	Analytical Details	D
D.2.	U-Pb and Lu-Hf Zircon Data	D
<b>E.</b>	<b>Supplementary Material Chapter 10</b>	<b>E</b>
E.1.	Analytical Data	E
<b>F.</b>	<b>Supplementary Material Chapter 12</b>	<b>F</b>
F.1.	AFT and AHe Results	F
F.2.	Analytical Procedures	F

# Chapter 1

## 1. Introduction and Motivation

Exploring is ingrained into human nature, and in the very beginning of Earth exploration ‘Terra Australis’ was the name for a hypothetical and unknown continent in the south first mentioned in ancient times. In those days, there was an idea about a comparative landmass that balanced the known continental land in the northern hemisphere.

Even today, Antarctica remains to be one of the least known continents on earth because of its hostile environment and isolated position. Nowadays, national Antarctic research programs maintain about 75 permanent and non-permanent Antarctic research stations. These facilitate Antarctic interdisciplinary research covering e.g. life sciences, physical sciences, social sciences as well as geosciences with the latter being the focus of this thesis.

In general, the Transantarctic Mountains/West Antarctic Rift System form a morphological and geological boundary subdividing the southernmost continent into East and West Antarctica.

Large parts of West Antarctica lie near or below sea level, whereas East Antarctica is covered by a thick inland ice sheet. Furthermore, East and West Antarctica are quite distinct from each other in terms of geology. Whereas East Antarctica comprises basement rocks of Archean to Early Paleozoic age with the oldest known rocks, some exceed the age of three billion years, found in Enderby Land. Apart from that, West Antarctica is represented by a collage of distinct crustal blocks with independent geotectonic histories (e.g. Dalziel and Elliot, 1982).

During Earth’s history, Antarctica was part of at least two supercontinents and its study helped and continues to improve our knowledge of how Earth’s continents assembled and dispersed through time, and thus impacting on the change of global environmental conditions, e.g. from warmer to colder climate periods. Therefore, it is necessary to gain detailed knowledge of the few scattered ice-free exposures (~2 %) which can provide at least a glimpse of the geology and deeper crustal structure of the mainly ice-covered continent.

### 1.1 Palaeogeographic Overview and Location of the Study Area

Today, tectonic movement of plates can be monitored by satellite data. The Pacific Plate reaches e.g. ~ 7-11 cm per year moving to the northwest, whereas the Antarctic plate’s movement is estimated to be at least one cm per year towards the Atlantic Ocean (e.g. Argus et al., 2010). Until today, our knowledge of plate tectonic configurations is limited by the availability of data through time. Relative plate movements can be reconstructed in detail based on the fabric and geophysical signatures preserved in oceanic basins (e.g. magnetic anomalies along a spreading center). The Mesozoic break-up history of Gondwana and the subsequent Mesozoic and Cenozoic amalgamation / separation of Pangea is relatively well known (Figure 1.1). However, the Paleozoic to Neoproterozoic tectonic history of Gondwana’s amalgamation as well as the Precambrian histories of the earlier supercontinents Rodinia and Columbia are less well understood because of the lack of preserved oceanic basins and paleomagnetic data. Due to its unique position in the central part of Gondwana (and Rodinia), the region of Dronning Maud



Land in East Antarctic represents a key region for studying and exploring this part of Earth's history. Dronning Maud Land lies between Coats Land (ca. 20°W) and Enderby Land (ca. 45°E) and is covered by a several kilometers thick ice-sheet. The sparse exposures of Dronning Maud Land continue for approximately 150-250 km subparallel to the coastline and can be subdivided into a western, central, and eastern part (Figure 1.2).

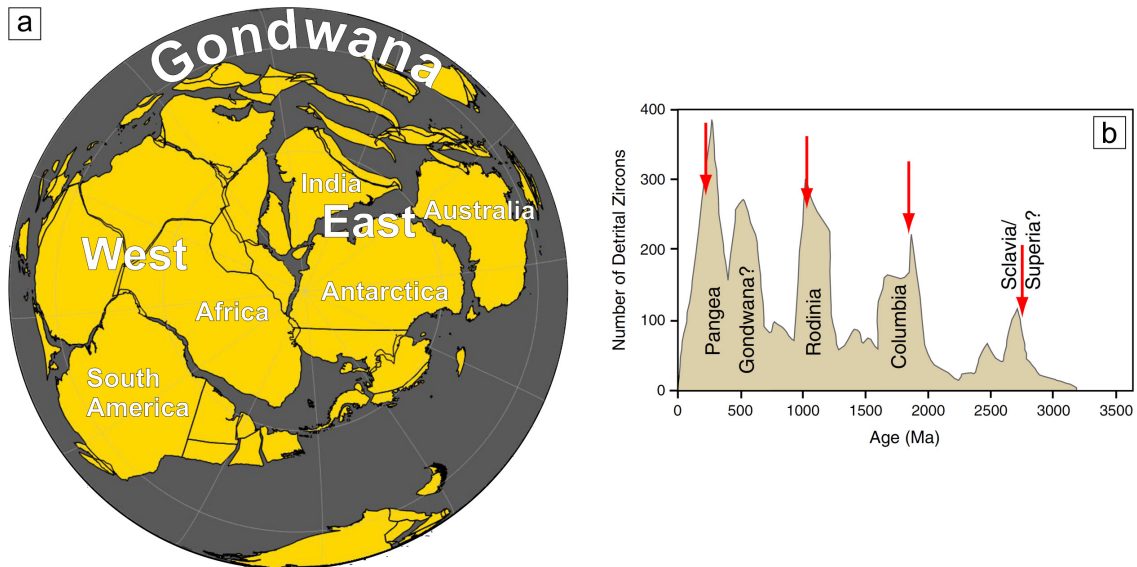


*Figure 1.1: Extensive landmasses and supercontinents. a) GPlates reconstruction of Gondwana at ca. 400 Ma (Matthews et al., 2016). b) Detrital zircon spectra (Hawkesworth et al., 2010) compared to orogenic peaks marked with arrows (Runcorn, 1962). Supercontinents include Columbia, Rodinia and Pangea. Per definition, supercontinents should include ~75 % of the preserved continental crust at the time of maximal packing. Pangea, Rodinia and Columbia meet these criteria. However, Gondwana was represented by a smaller yet still extensive landmass but does not qualify as a supercontinent (modified after Meert, 2012).*

The few exposures of the Dronning Maud Land region provide evidence for two major continent collision phases during late Mesoproterozoic times (1200-1000 Ma) and late Neoproterozoic/early Paleozoic times (650-500 Ma). The older phase is related to the Grenvillian orogeny and the assembly of Rodinia whereas the younger phase is related to the Pan-African orogeny that led to the assembly of Gondwana (e.g. Jacobs et al., 1996b; 1998). After the final collision of various parts of proto-East and proto-West Gondwana, Dronning Maud Land was situated in direct prolongation of the pan-African-aged Mozambique Belt of East Africa also known as East African-Antarctic Orogen (Jacobs and Thomas, 2004). East Gondwana comprised parts of today's landmasses of India, Madagascar, Antarctica, and Australia, whereas West Gondwana was made up of Africa and South America. The exact dimensions of this ancient orogeny, which is comparable to the extent of today's Himalayan Mountains, the geometries of the colliding crustal fragments, as well as the position of suture zones are still poorly known due to the subglacial nature of Antarctica.

The main emphasis of this study was on Sør Rondane and adjacent regions with the geological investigations mainly focused on its western part. Figure 1.3 shows western Sør Rondane and its subdivision by the Main Shear Zone and Sør Rondane Suture as it was captured in 2011. In general, Sør Rondane is situated in eastern Dronning Maud Land and located between 22°E and 28°E and 71.5°S and 72.5°S. The mountain chain rises from sea level up to an altitude of about 3400 m.



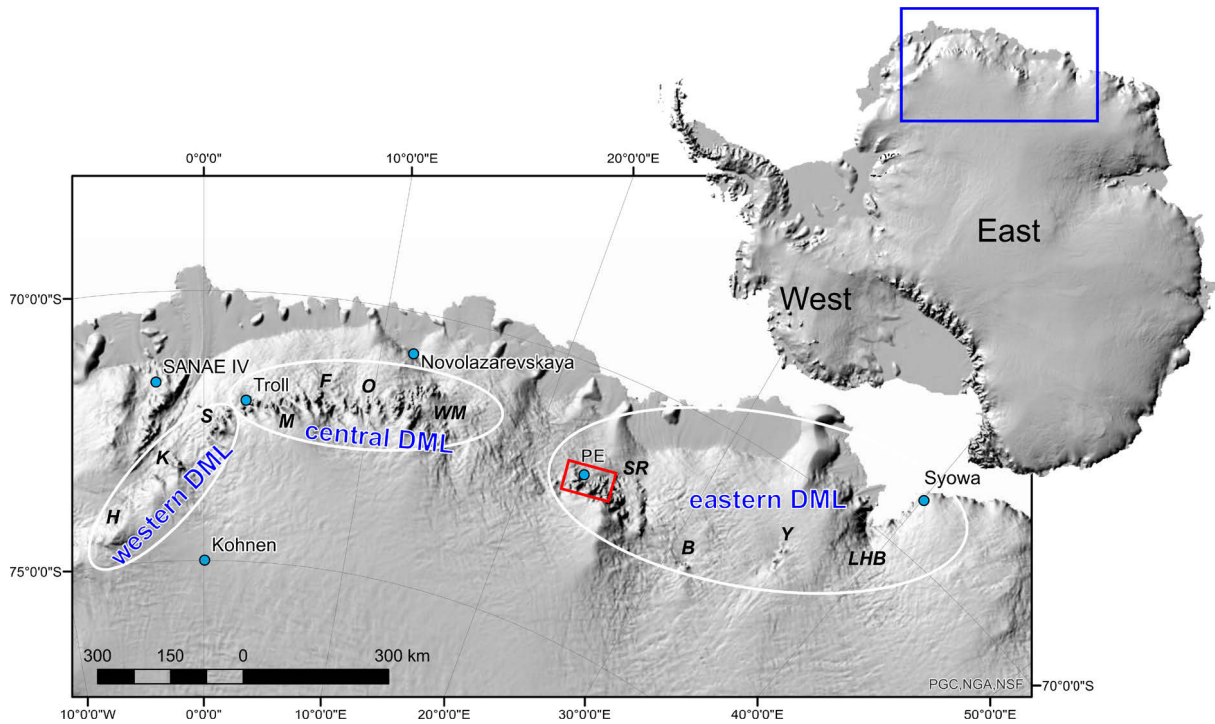


Figure 1.2: Overview of Dronning Maud Land (DML) indicating the main mountain ranges and locations of research stations (light blue points). A high-resolution digital surface model 'Reference Elevation Model of Antarctica' ('REMA2018' used as backdrop (<https://www.pgc.umn.edu/data/rema/>)). Main mountain ranges are: (i) Western DML: Heimefrontfjella (H), Kriwanveggen (K), and Sverdrupfjella (S); (ii) Central DML: Mühlig-Hofmann Gebirge (M), Filchnerfjella (F), Orvinfjella (O), Wohlthatmassiv (WM); (iii) Eastern DML: Sør Rondane (red box cf. Figure 1.3) F, Belgica and Yamato Mtns., Lützow Holm Bay. Inset shows the subdivision of Antarctica into East and West Antarctica as well as the location of Dronning Maud Land (blue box).

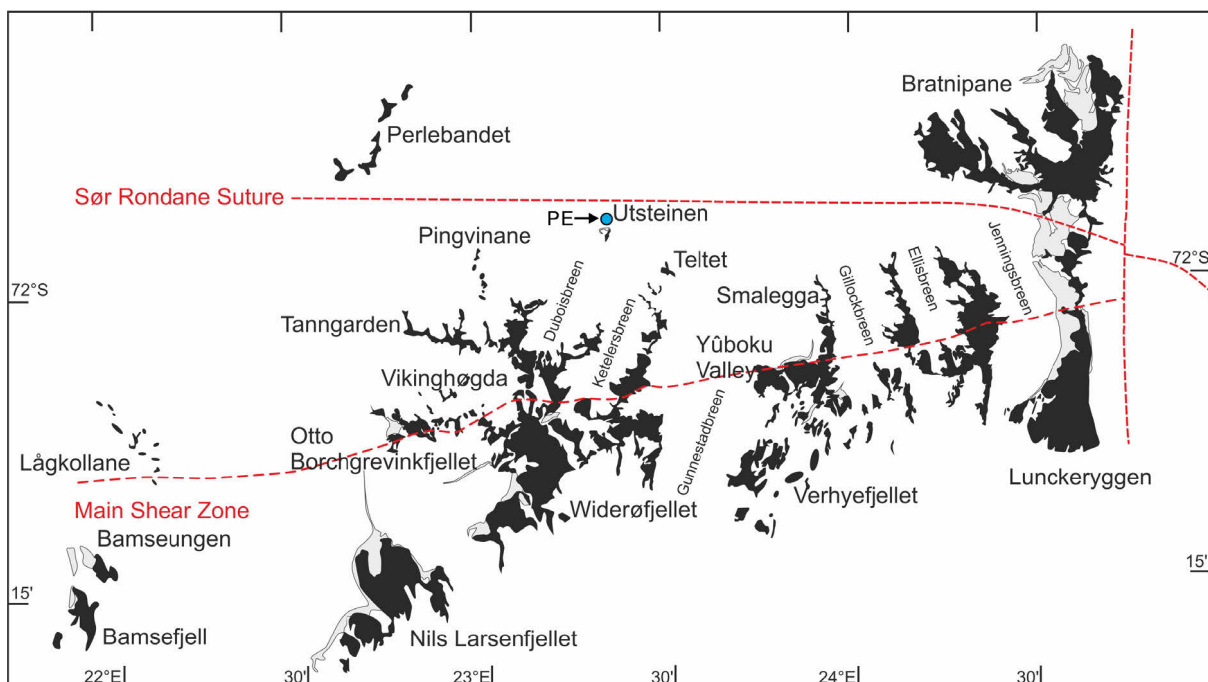


Figure 1.3: Overview of western Sør Rondane within eastern Dronning Maud Land (cf. red box in Figure 1.2) showing the distribution of rock exposures (black), moraines (grey), ice and snow (white), structural features like the Main Shear Zone, as well as names of major geographic location (modified after Osanai et al., 1996c).



## 1.2 Objectives of the Thesis

Due to the fact that East Antarctica was the centerpiece of Gondwana and also part of Rodinia the region of Dronning Maud Land represents one of the key areas for studying the processes of their geodynamic evolution. During the last decades our image of East Antarctica, once considered a single large stable craton of ancient times, changed by intense geoscientific studies across the continent (e.g. Fitzsimons, 2000a; Boger et al., 2001; Fitzsimons, 2003; Meert, 2003; Boger and Miller, 2004; Boger, 2011) raising further questions of origin, composition, number of crustal fragments as well as their extent and possible suture zones.

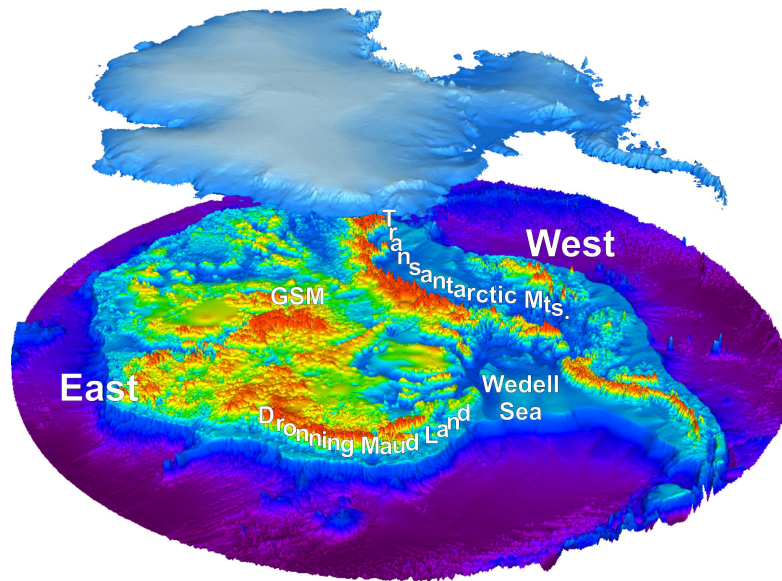


Figure 1.4: Digital map of bedrock under the Antarctic ice sheet, *Bedmap 2* (modified after Fretwell et al., 2013). GSM: Gamburtsev Subglacial Mountains.

The challenge to gain a better understanding of the configuration of plate tectonics in Antarctica through time is simply a matter of sparse exposures. Therefore, geophysical methods like airborne magnetics, gravity and radar are applicable for unveiling the subglacial structure of Antarctica's crust (Figure 1.4). Geophysical data combined with surface geology provide a huge potential for gaining an improved comprehension of the tectonic evolution of a specific region.

In this study, a multi-methodological approach is applied to Sør Rondane and adjacent regions in eastern Dronning Maud Land encompassing structural geology, geophysics, geochronology, geochemistry, and thermochronology in order to investigate the following objectives:

### 1) *Determination of the structural and metamorphic evolution of Sør Rondane with focus on Pan-African times*

Main and overarching objective is the reconstruction of the structural and metamorphic development of the basement of Sør Rondane as one of the possible candidates for the location of the E-W-Gondwana suture zone. Therefore, main emphasis lies on the Pan-African events in order to verify kinematics and crustal development of the E-W-Gondwana border zone. Thermochronological methods and structural analyses of brittle fault zones are implemented in order to investigate the Phanerozoic shallow crustal dynamics of Sør Rondane.



**a) *Study of the Late Pan-African tectonic and structural evolution of Sør Rondane***

The reconstruction of the geodynamic evolution of the basement units of Dronning Maud Land requires detailed structural analysis in the field and investigation of the deformation and metamorphic histories. A particular task is the structural analysis of the Main Shear Zone representing a prominent structural element in Sør Rondane.

So far, only little is known about its kinematics, extent, timing, and role during the Pan-African orogenic cycle. Structural measurements and samples have been taken along and across the shear zone in order to perform microtectonic/textural analyses and to reconstruct the kinematic and structural development of this zone in combination with geochemical and petrological investigations.

**b) *Study of the cooling history of Sør Rondane by using geochronological methods***

Systematic Ar/Ar analyses of syntectonic minerals of the Main Shear Zone, Ar/Ar analyses on biotite and U-Pb dating on zircon across all terranes of Sør Rondane will be performed to unveil the geodynamic evolution and metamorphic history.

i) Ar/Ar analyses:

The Main Shear Zone will be dated by using the Ar/Ar technique on syngenetic minerals, such as mica. The combination of structural investigations and age determinations will provide a detailed picture of the evolution of the Main Shear Zone. Further, systematic sampling across all terranes of Sør Rondane for Ar/Ar age dating will help to gain a better understanding of the cooling history of the entire region after Gondwana amalgamation.

ii) U-Pb dating on zircon:

In addition to the study of syntectonic minerals of the Main Shear Zone, crosscutting relationships may provide further evidence for the timing of deformation. Therefore, syn-kinematically deformed rocks like granitoids as reported for the Vengen granite (Shiraishi et al., 2008) can provide an upper age constraint for the shearing event by using U-Pb dating on zircon.

**c) *Study of different rock suites by using mainly U-Pb datings on zircons***

Rarely visited and uncharted nunataks are located west of Sør Rondane and are situated within the magnetically characterized SE DML province which exhibits a distinct magnetic anomaly pattern (Mieth and Jokat, 2014). Geochronological and geochemical analyses are used to identify the nature of this proposed geological unit.

Further, protolith and metamorphic ages are determined for meta-igneous rocks of the southwestern part of Sør Rondane. Additional isotopic and geochemical analyses are accomplished (Lu-Hf data and trace element data) to reveal indications for the tectonic setting during magma formation.

In order to gain deeper insights into the final amalgamation of Gondwana, the spatial and temporal trends of magmatism need to be investigated and compared to neighboring areas in central Dronning Maud Land situated to the west and the Yamato-Belgica complex situated to the east. Therefore, it is intended to obtain new U-Pb and Lu-Hf zircon data from various granitoids distributed across all terranes of Sør Rondane.



***d) Study of the Phanerozoic shallow crustal dynamics of Sør Rondane***

The application of low-temperature thermochronological methods (apatite fission track and apatite (U-Th-Sm)/He analyses) are applied in order to reconstruct the exhumation and landscape evolution of Sør Rondane and its relation to the break-up of Gondwana.

**2) *Characterization of the subglacial basement by combined aerogeophysical and geological studies***

Airborne magnetic data were acquired across Sør Rondane during the “Soviet Antarctic Expedition 36” in 1990 (Golynsky et al., 1996). This survey was flown with a sparse flight line spacing at high altitude (20 km; 4000–4500 m) and does not provide any detailed geological correlation of magnetic anomalies. Therefore, systematic aerogeophysical surveys were realized in close cooperation with AWI by using the polar aircraft Polar 5 and 6. Following aspects are being investigated:

***a) The tectonic and structural framework of Sør Rondane***

To gain a better understanding of the structural framework of Sør Rondane, more detailed aeromagnetic data with a flight line spacing of 5 km and additional ground based susceptibility measurements are carried out and combined with geological findings to provide a projection of tectonic terranes into ice-covered areas.

***b) The spatial extent of the prominent SE DML province***

The SE DML province is characterized by a distinct magnetic anomaly pattern, which was first described by Mieth et al. (2014) with hitherto unknown geology. Geological investigations in and adjacent to Sør Rondane are intended to yield new information about the nature of this unit (see above, 1.c). The acquisition of continuing aeromagnetic data covering the southern and eastern regions of Sør Rondane provide a better image about its dimensions within East Antarctica.

***c) The presumed eastern extent of the East African-Antarctic Orogen***

Within western Dronning Maud Land, the Heimefront Shear Zone represents the westernmost exposed boundary of the East African-Antarctic Orogen. In combination with aeromagnetic data a more spacious picture of the extent of this border was revealed and projected into ice-covered region (Golynsky and Jacobs, 2001). Therefore, aeromagnetic studies within the region of Sør Rondane potentially provide additional information about the eastern extent of the East African-Antarctic Orogen.

***d) Detailed image of the present subglacial bedrock topography and the gravimetric signatures of Sør Rondane***

In order to gain comprehensive data of the dimension of the East Antarctic Ice Sheet, today's bedrock topography, and geological processes that formed the subglacial landscape, the polar aircraft was equipped with additional geophysical measurement instruments to collect radar and gravity data.



# Chapter 2

## 2. Methods

Different methods have been used to investigate the geodynamic evolution of eastern Dronning Maud Land. Within this thesis, main emphasis was placed on structural geology, geophysics, and geochronology, as well as subordinately geochemistry and petrology in and adjacent to Sør Rondane. Each method was used to investigate the area of interest from a different perspective and was applied to address a specific scientific question. This chapter gives a brief introduction into main concepts of methods used in this study and presented within Chapters 4 to 6.

Within the GEA project, a wide range of techniques was used investigating the geodynamic and landscape evolution of Sør Rondane. Detailed descriptions of additionally applied methods or different setups are given in the respective Chapters 7 to 12 and within their associated ‘Electronic Appendix’ (e.g. U-Pb analyses, Sm-Nd isotope analyses, Lu-Hf isotopic analyses, apatite fission track (AFT) and AHe dating, (U-Th-Sm)/He dating).

### 2.1 Structural Geology

Geologic field work was realized during GEA II expedition (2011/12) with its main focus on structural geology. Roughly 500 measurements of ductile and brittle structures in different lithological units were documented, and additional 250 readings from the former GEA I expedition in 2010/11 (unpublished report by D. Damaske and J. Jacobs) were integrated into the analyses as well. The datasets contain the strike and dip of the foliation plane of different rock types and the dip and dip direction of lineaments on this plane measured along the Main Shear Zone and adjacent regions. Asymmetric structures derived from non-coaxial deformation in the xz-plane of the finite strain ellipsoid (main tension- and main pressure axis) and provide important information in ductilely deformed rocks regarding e.g. the sense of movement (Meschede, 1994). Multiple and different kinematic indicators at one locality can provide more reliable evidence for shear sense. Therefore, kinematic indicators, like SC-structures, porphyroclasts, folds etc., were documented during field work and verified by microscopy on thin sections.

Brittle deformation was recorded from 8 localities in the area of Sør Rondane and include measurements of fault planes and striations. The sense of movement of the hanging wall block is indicated by kinematic indicators like fiber steps or Riedel shears on the slickensides and classified according to four confidence levels (1=certain, 2=reliable, 3=unreliable to 4=very unreliable (e.g. Sperner et al., 1993). These data were intended to provide further evidence for Phanerozoic shallow crustal dynamics in combination with thermochronological methods (AFT and apatite (U-Th-Sm)/He) (Krohne, 2017).

Moreover, 34 oriented samples were collected in Sør Rondane Mountains over a distance of 150 km during the expedition GEA II. To keep track of all the samples a terminology for every outcrop was defined: e.g. 1214A1 indicate the year (12), day (14) outcrop (A), and the number of samples (1). Stereographic equal-area lower hemisphere plots were computed by using the Win-Tensor software by Delvaux and Sperner (2003). Structural data presented in Chapter 4 are listed in the ‘Electronic appendix’ A.1 Structural measurements.



## 2.2 Aeromagnetics

### 2.2.1 Platform and Measurement Systems

Airborne geophysical data were collected by using the AWI Basler aircraft Polar 5 and 6. The acquisition of magnetic data was carried out with a Scintrex Cs-3 cesium vapor magnetometer. The total magnetic field sensors were mounted at the ends of the nose and tail booms (Figure 2.1a, b). A fuselage-mounted three-component Billingsley TFM 100 fluxgate magnetometer was used for magnetic compensation.

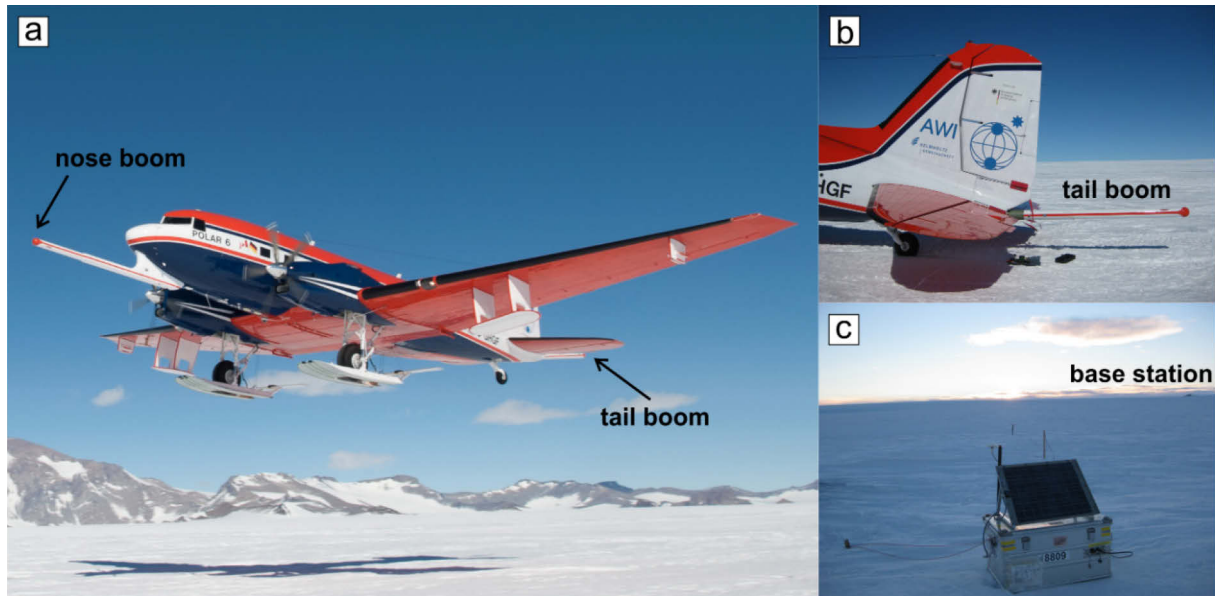


Figure 2.1: Setup for aeromagnetic measurements. a) Polar 6 aircraft showing its survey configuration with mounted nose and tail booms. b) Cesium vapor magnetometers are mounted in the tips of both booms, here the tail boom is shown. c) Magnetic base station used for monitoring diurnal variations.

### 2.2.2 Temporal Variations of the Earth Magnetic Field

In a simplified view, the earth is considered to be composed of three parts: core, mantle, and crust. The dipolar magnetic field results from convection processes in the liquid part of the iron core and accounts for approximately 98 % of the entire geomagnetic field. The mantle plays a minor role in earth magnetism, whereas the interaction of the core field with rocks of the Earth's crust produces magnetic anomalies that are of major interest for e.g. geology, geodynamics and resource exploration.

The core magnetic field exhibits variations of longer time-scale over years and decades (e.g. polarity reversal of the geomagnetic field). In Dronning Maud Land the total intensity is decreasing at 0.1 to 0.2 % per year and in addition the inclination/declination parameters change by a few arc minutes per year. The International Geomagnetic Reference, a mathematical model of the Earth's magnetic field, can describe these long-period variations (Thébault et al., 2015). The Earth's magnetic field changes with time. Therefore, a new model is released every five years with corrected fitting parameters for the mathematical model that is based on field data, observatories, and satellite observations.

Short-period variations are e.g. diurnal variations or magnetic storms and account for 2% of the magnetic field. Diurnal variations follow a daily cycle and are related to the rotation of the earth



with respect to the sun within the range of a few nanotesla. In contrast, magnetic storms are related to variable sunspot activity and measurements can exceed thousands of nanotesla. In order to account for the short-period variations of the magnetic field, magnetic base stations were utilized for their monitoring (Figure 2.1c).

For airborne surveys, the effects of the permanent magnetization of the aircraft itself and the induced magnetization which changes e.g. with the survey location or the direction of the flight can be corrected by active magnetic compensation. Therefore, a calibration flight in absence of major magnetic anomalies is necessary to attribute the magnetic variations arising from changes in heading and/or maneuvers of the aircraft. For Polar 5 and 6 aircraft this can be done in real time by flying a compensation box with five rolls ( $\pm 10^\circ$ ), five pitches ( $\pm 5^\circ$ ), and five yaws ( $\pm 5^\circ$ ) in each cardinal direction (Figure 2.2). AWI uses an AADC-II control unit from RMS-Electronics Limited for recording aeromagnetic data. This system implements a scheme for online compensation for such magnetic aircraft effects, which is based on the equations of Leliak (1961).

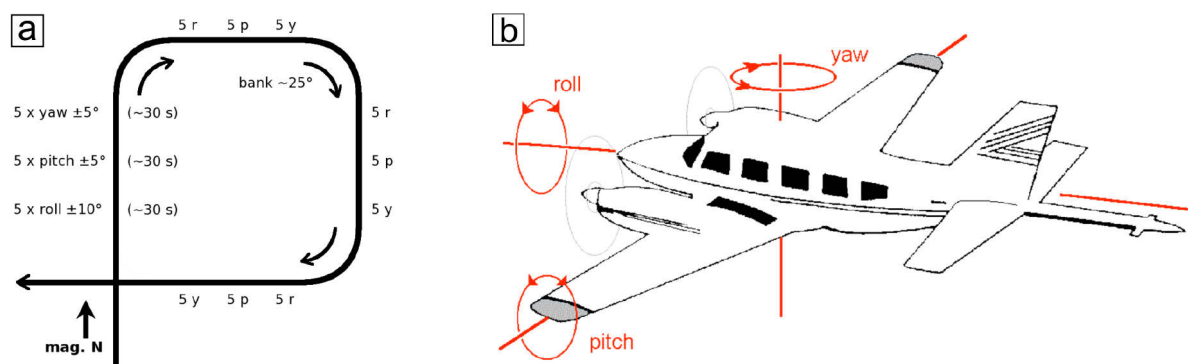


Figure 2.2. Magnetic compensation (modified after Reeves, 2005; Mieth, 2014). a) Schematic outline of the flight path for a compensation box with subsets of manoeuvres in each cardinal direction. b) Illustration of pitch, roll and yaw maneuvers of an aircraft.

### 2.2.3 Processing

Processing of airborne magnetic data was realized with the software ‘Oasis Montaj’ from GEOSOFT. The work flow included de-spiking, core-field and diurnal variation corrections as well as statistical and micro-levelling procedures (Figure 2.3). The final data were gridded with a grid cell size of 3 km. In order to simplify the interpretation of magnetic anomalies, the magnetic pattern was transformed by a grid-based reduction to the pole (Figure 2.3).



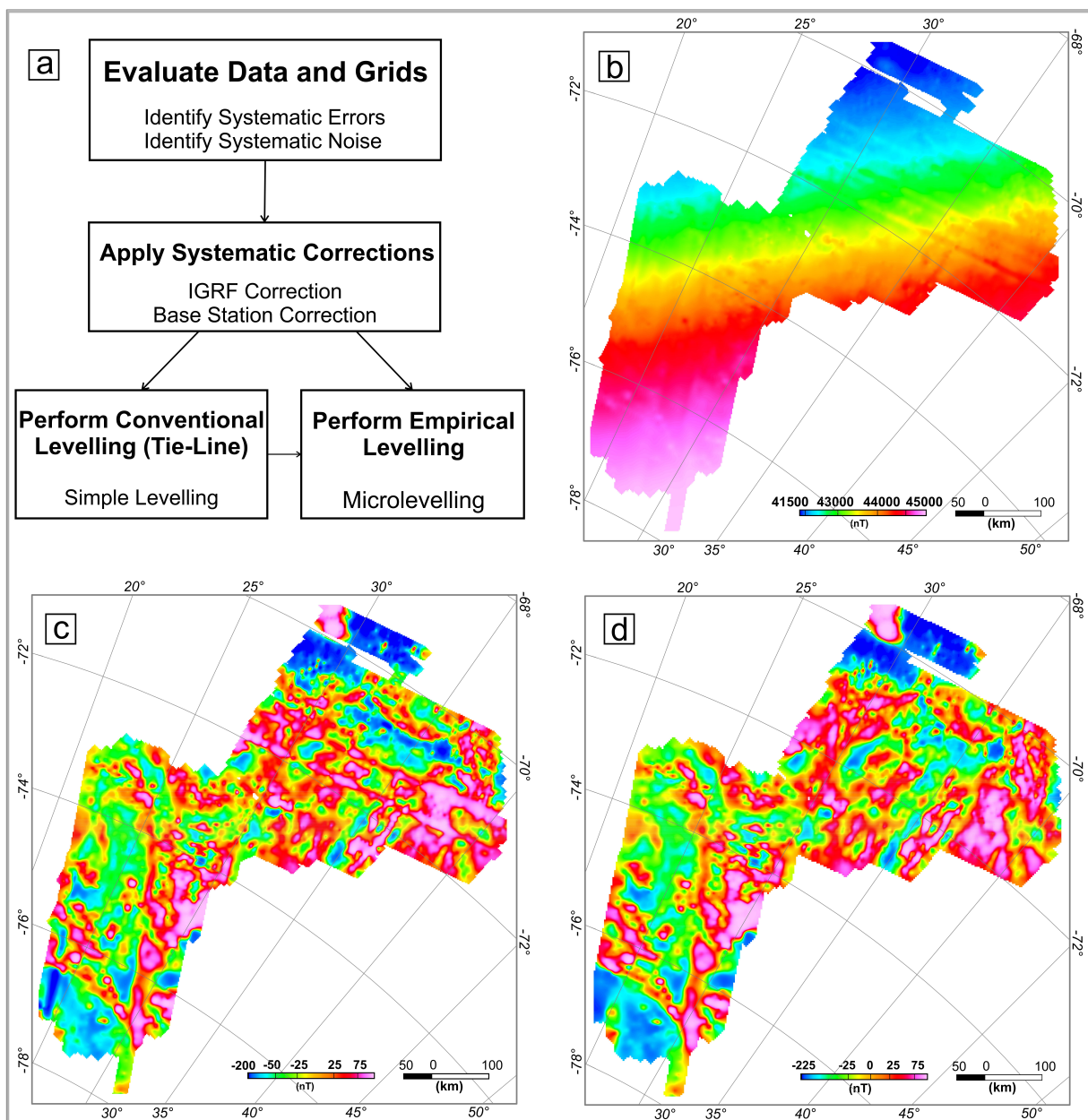


Figure 2.3: Processing steps for magnetic data. a) Standard levelling workflow for magnetic data. b) Raw data indicating the major influence of the earth's core field. c) Magnetic anomaly data after systematic corrections that includes the subtraction of the International Geomagnetic Reference Field and diurnal variations. d) Final magnetic anomaly map after simple and microlevelling.

## 2.2.4 Ground-Based Geophysics

Simultaneous with geologic field work (GEA I and GEA II) magnetic properties on all accessible rock exposures of different lithological units were measured (Figure 2.4). A total of 231 site measurements were collected with a hand-held KT-6 kappameter. For each site 12 single readings with the highest and lowest values considered outliers, resulted in one averaged value based on 10 readings. The measurements were taken within an area of up to 10 m<sup>2</sup> at each site. Ground based measurements were realized to define exposed magnetic units that can help to better understand and interpret airborne magnetic measurements and combines geology and geophysics. Ground control can be further helpful for mapping geologic units and structural features beneath the ice, which are not accessible to geological methods.



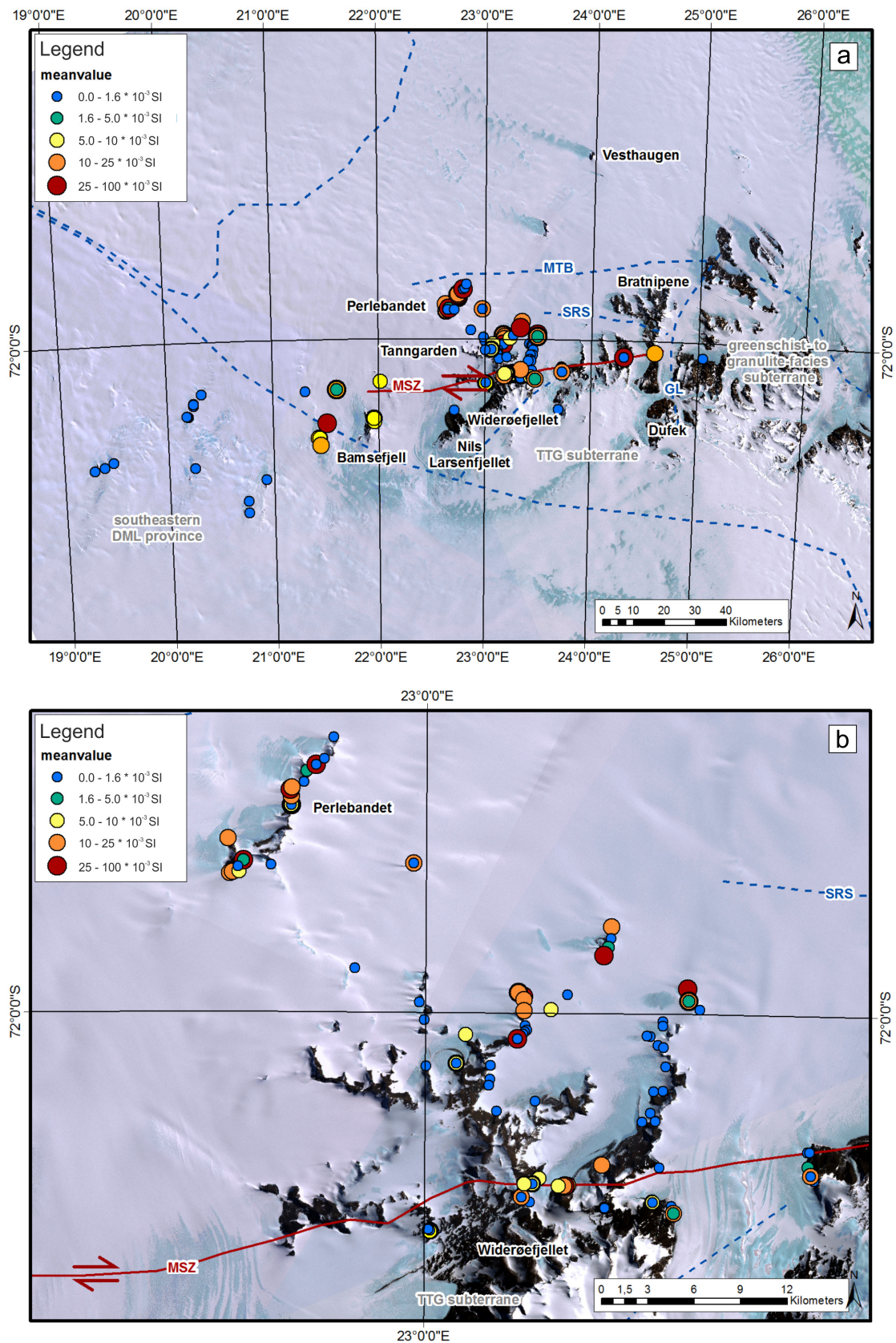


Figure 2.4: Susceptibility readings in Sør Rondane. a) Overview map with all readings. b) Close-up map for the Vikinghøgda and Widerøefjellet. Landsat Image Mosaic of Antarctica (LIMA) as backdrop.



## 2.3 Geochronology

### 2.3.1 $^{40}\text{Ar}/^{39}\text{Ar}$ Geochronology

#### Principles of the $^{40}\text{Ar}/^{39}\text{Ar}$ method

In general, the  $^{40}\text{Ar}/^{39}\text{Ar}$  dating technique is applied to date K-bearing rocks (e.g. basalts, meteorites) and minerals (e.g. biotite, muscovite, hornblende, K-feldspar or plagioclase). Therefore, the technique is used to determine the time since radiogenic argon became trapped in the mineral or rock which is produced by decay of  $^{40}\text{K}$ . The naturally occurring radioactive potassium isotope  $^{40}\text{K}$  exhibits a dual decay with a half-life of  $1.25 \cdot 10^9$  years (1.25 Ga) into the stable isotopes  $^{40}\text{Ar}$  and  $^{40}\text{Ca}$ .

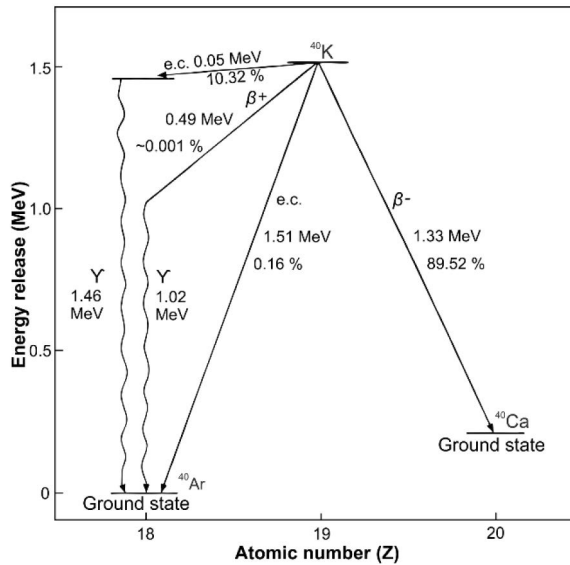


Figure 2.5: Dual decay scheme of  $^{40}\text{K}$  with 89.5 % of the decay yielding  $^{40}\text{Ca}$  by electron emission and 10.5 % producing  $^{40}\text{Ar}$  dominated by electron capture. Both daughter products being stable isotopes. The branch of decay of interest is the decay of  $^{40}\text{Ar}^*$  (radiogenic) from  $^{40}\text{K}$  (McDougall and Harrison, 1999).

In contrast to the conventional K-Ar method mass spectrometry  $^{40}\text{Ar}/^{39}\text{Ar}$  dating requires only the measurement of isotope ratios between naturally occurring isotopes ( $^{36}\text{Ar}$ ,  $^{38}\text{Ar}$ ,  $^{40}\text{Ar}$ ) and reactor produced isotopes ( $^{39}\text{Ar}$ ,  $^{37}\text{Ar}$ ). For the  $^{40}\text{Ar}/^{39}\text{Ar}$  method, potassium is measured by transmutation of the stable isotope  $^{39}\text{K}$  to  $^{39}\text{Ar}_K$

by irradiation (neutron bombardment) in a nuclear reactor. The ratio of  $^{39}\text{K}$  to  $^{40}\text{K}$  is constant and thus the critical  $^{40}\text{Ar}^*/^{40}\text{K}$  ratio is proportional to the ratio of the two argon isotopes  $^{40}\text{Ar}^*/^{39}\text{Ar}_K$ .

$$(1) \quad \frac{^{40}\text{Ar}^*}{^{39}\text{Ar}_K} \sim \frac{^{40}\text{Ar}^*}{^{39}\text{K}} \sim \text{age of mineral or whole rock}$$

The amount of produced  $^{39}\text{Ar}_K$  from  $^{39}\text{K}$  is dependent on the duration of the neutron irradiation, neutron flux, and neutron capture cross section and expressed in the  $J$ -value. To exactly determine the  $J$ -value a mineral of accurately known age (standard) is irradiated together with the unknown one to monitor the dose.

$$(2) \quad J = \frac{e^{\lambda t} - 1}{^{40}\text{Ar}^*/^{39}\text{Ar}_K}$$

With the known age of the standard sample the parameter  $J$  can be determined by measuring the  $^{40}\text{Ar}^*/^{39}\text{Ar}_K$  ratio in the gas extracted from the standard sample after irradiation. The  $J$ -value is then used together with the measured  $^{40}\text{Ar}^*/^{39}\text{Ar}_K$  ratio of the unknown sample which is irradiated at the same time to determine the sample age.

$$(3) \quad t = \frac{1}{\lambda} \ln\left(1 + J \frac{^{40}\text{Ar}^*}{^{39}\text{Ar}_K}\right)$$



### Age spectra, isochron plots and inverse isochron plots

The following subsection gives a short overview about the most common formats used for graphical representation of argon data.

In most cases, the argon is not produced purely by radiogenic decay within a geological sample and therefore it is subdivided into two types of argon: radiogenic and non-radiogenic. Radiogenic argon includes  $^{40}\text{Ar}$  accumulated from the decay of  $^{40}\text{K}$  in the mineral or rock of interest. In addition, relic  $^{40}\text{Ar}$  is also radiogenic argon that remains in the sample after e.g. a partial resetting. In contrast, Ar that does not accumulate during radioactive decay within the sample is referred to as non-radiogenic argon and comprises blank, trapped (excess and/or atmospheric), cosmogenic, and neutron-induced argon (Dalrymple and Lanphere, 1969; McDougall and Harrison, 1999).

To understand the history of the sample the progressive outgassing during incremental heating steps facilitate to identify argon loss or the presence of non-radiogenic Ar. In general, it can be said that, e.g. within a crystal, the rim is more susceptible to diffusional argon loss and should outgas at relatively low temperatures, whereas domains with tightly bound Ar should outgas at higher temperatures. Results are presented in either an age spectrum plot, isochron or inverse isochron plot (Figure 2.6). For a step heating spectrum the assumption is made that non-radiogenic argon has atmospheric composition and is therefore used for correction of all steps ( $^{40}\text{Ar}/^{39}\text{Ar} = 295.5$ ). A saddle shaped pattern was found to be characteristic of samples when excess Ar is present (Lanphere and Brent Dalrymple, 1976). The advantage of isochron or inverse isochron plots is that excess  $^{40}\text{Ar}$  in addition to atmospheric argon, can be detected (Kuiper, 2002).

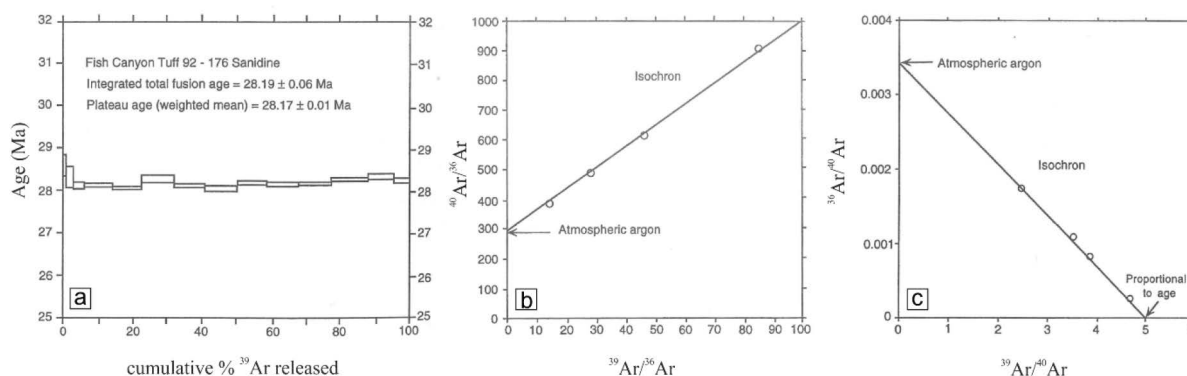


*Figure 2.6: Illustration of age spectrum plot, isochron, and inverse isochron plot. a) Age spectrum for sanidine sample. Spectrum illustrates the cumulative percentage of  $^{39}\text{Ar}_K$  released from the sample over the course of the entire step-heating analysis against the apparent age in millions of years (Ma), this can be taken as evidence that the radiogenic argon is distributed uniformly within the crystal. b) Schematic isochron plot. Here, the sample age is proportional to the slope of correlation line. c) Schematic inverse isochron plot. Here, the two intercepts correspond to the pure trapped (y-axis) and pure radiogenic (x-axis) components of the sample. All three plots are taken from (McDougall and Harrison, 1999).*

For this study, 24 samples were selected for  $^{40}\text{Ar}/^{39}\text{Ar}$  biotite and amphibole dating and were collected (i) along the Main Shear Zone, (ii) the SW-Terrane including the central Sør Rondane corridor, (iii) NE-Terrane, and (iv) nunataks to the W of Sør Rondane (Chapter 6). Identification of suitable samples was based on transmitted light microscopy. Major criteria were size, shape, and intergrowth of biotite and amphibole.



High-voltage electrical pulses, called electrical fragmentation were used for the fragmentation of rock samples. This method causes a disaggregation of minerals along grain boundaries and minimizes broken grains, which are expected to be more frequent by mechanical fracturing. A commercial lab-size machine (developed by SELFRAG AG) at the Technical University (TU) Freiberg was used for electrical fragmentation.

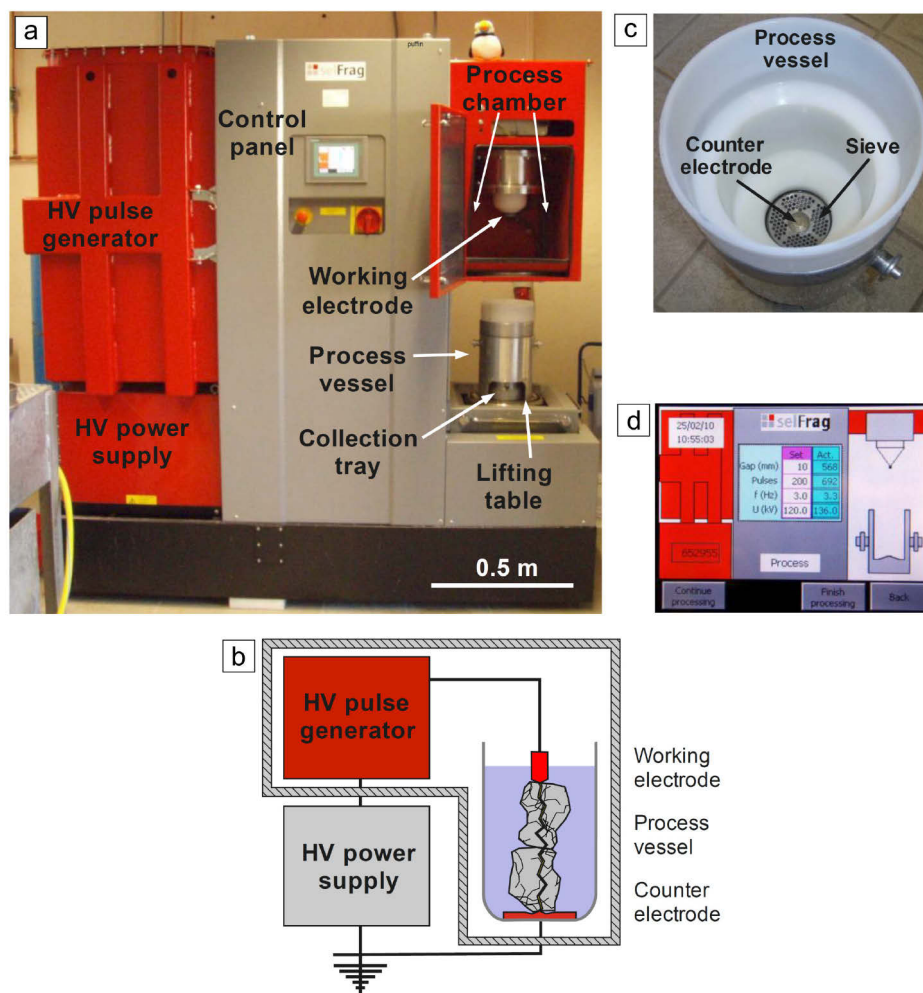


Figure 2.7: Overview of the SELFRAG lab and its mode of operation (taken from Sperner et al., 2014). a) SELFRAG lab with high-voltage (HV) power supply and HV pulse generator on the left side, and process chamber and process vessel on the right side. b) Principle of the SELFRAG lab. c) Process vessel with sieve and counter electrode at the bottom. Liberated minerals and small aggregates fall through the sieve into the collection tray. d) Control panel.

Figure 2.7 presents an overview of the SELFRAG lab and its mode of operation. A volume of ca. 1 dm<sup>3</sup> was precrushed with a jaw crusher and processed with the SELFRAG system. After fragmentation, the samples were sieved through different mesh sizes. Sieved material was inspected with a binocular and the suitable grain size fraction containing clean and idiomorphic minerals was chosen. The ferromagnetic minerals were removed with a hand magnet. The separation of paramagnetic and diamagnetic minerals was carried out with a Frantz magnetic barrier separator. Finally, optically inclusion-free crystals (biotite and amphibole) were handpicked from the largest possible magnetic grain-size fraction. Handpicked samples were handed over to the Argonlabor Freiberg (ALF) at TU Freiberg where <sup>40</sup>Ar/<sup>39</sup>Ar analyses were carried out (Pfänder et al., 2014). Further details regarding the methodology are given in Chapter 6.



### 2.3.2 U-Pb Zircon Data

U-Pb analyses on zircons were realized as contract work at the Senckenberg Naturhistorische Sammlungen Dresden, Germany. For this purpose, 1-2 kg of sample material (rock sample) was provided for further zircon separation and Laser Ablation combined with Inductively-Coupled-Plasma Mass-Spectrometry (LA-ICP-MS) techniques. For this work, three intrusive rock samples which were deformed by the Main Shear Zone were selected to gain an upper age limit for the shearing event. Cathodoluminescence images and measured ablation spots were evaluated and concordia diagrams ( $2\sigma$  error ellipses) and concordia ages (95 % confidence level) were produced using ISOPLOT 4.15 (Ludwig, 2012). Further details regarding the methodology are given in Chapter 6.

## 2.4 Geochemistry and Petrography

### 2.4.1 XRF Analyses

Major and trace element chemistry of all samples was analyzed by X-ray fluorescence (XRF) at BGR, Hannover. Therefore, the sample powders were mixed with lithium metaborate at a ratio of 1:5, fused at 1200 °C for 20 min, and analyzed using two different XRF spectrometers: a Philips PW 2400 (Rh tube) for the elements Si, Al, Fe, Mn, Mg, Na, P, S, F, As, Bi, Ce, Co, Cr, Cu, Ga, Hf, La, Mo, and a PW 1480 (Cr tube) for the elements Ti, Ca, K, Cl, Ba, Cs, Sb, Sc, and Sn. The trace element detection limits are as follows: 20 ppm for Ce and La, 10 ppm for Cu, 5 ppm for Ba, Cs, Hf, Ta, Th, and V, 4 ppm for Pb, 3 ppm for Co, Cr, Ga, Ni, U, Y, Zn, and Zr, and 2 ppm for Nb, Rb, Sc, and Sr. The calibrations are validated by reference material analysis. ‘Monitor’ samples and 130 certified reference materials (CRM) are used for the correction procedures. Loss on ignition (LOI) was determined by heating the sample powder to 1030 °C for 10 min. Figure 2.8 shows the chemical characterization of intrusive rocks, which were selected for age dating.

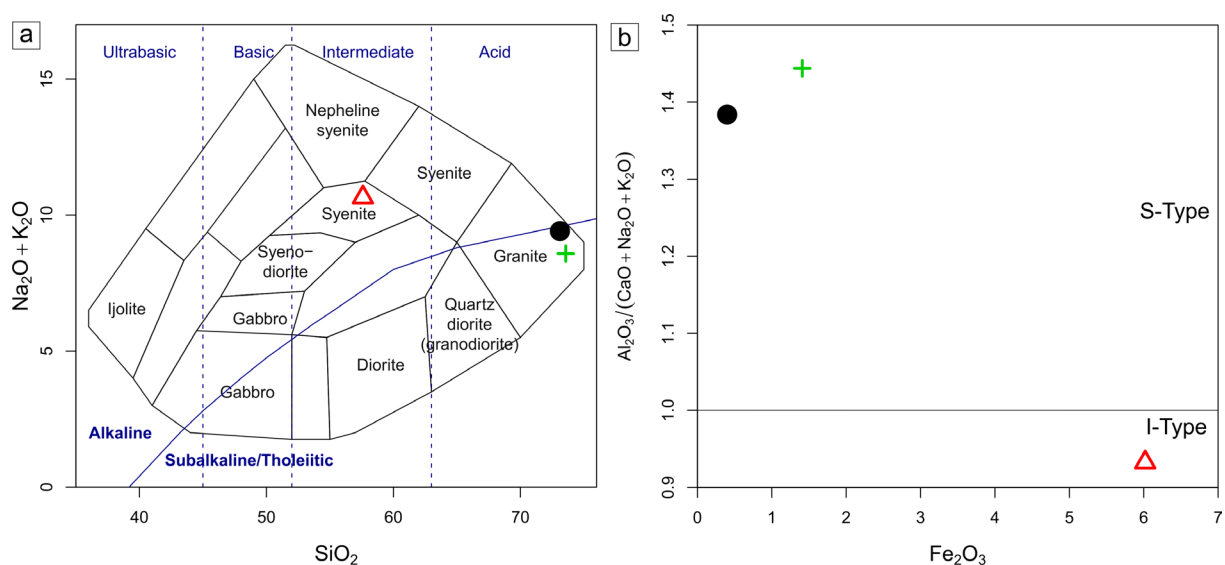


Figure 2.8: Plot of chemical data from three intrusives selected for zircon U-Pb dating. a) TAS classification diagram after Cox et al. (1979) and b) Discrimination diagram for I and S-type granites after Pearce et al. (1984). Diagrams are compiled with the Geochemical Data Toolkit GCDkit (Janoušek et al., 2006).



## 2.4.2 Petrographical Studies

Besides polarizing microscopy, analysis of geological thin sections were performed with  $\mu$ -Energy Dispersive X-Ray Fluorescence ( $\mu$ -EDXRF) for elemental analysis (Figure 2.9). This was realized with Bruker's M4 TORNADO spectrometer combined with hyperspectral analysis software ENVI.

Aim of this 'side study' was (i) the detailed mineralogical and petrographic analyses of strongly deformed mylonitic rocks of a dextral shear zone (Main Shear Zone) and (ii) mapping of minerals suitable for further geochronological analyses (zircon, titanite, apatite etc.). This topic was investigated by Katarzyna Krasniqi (M.Sc) during the main project phase and integrated into further studies (e.g. Chapter 6).

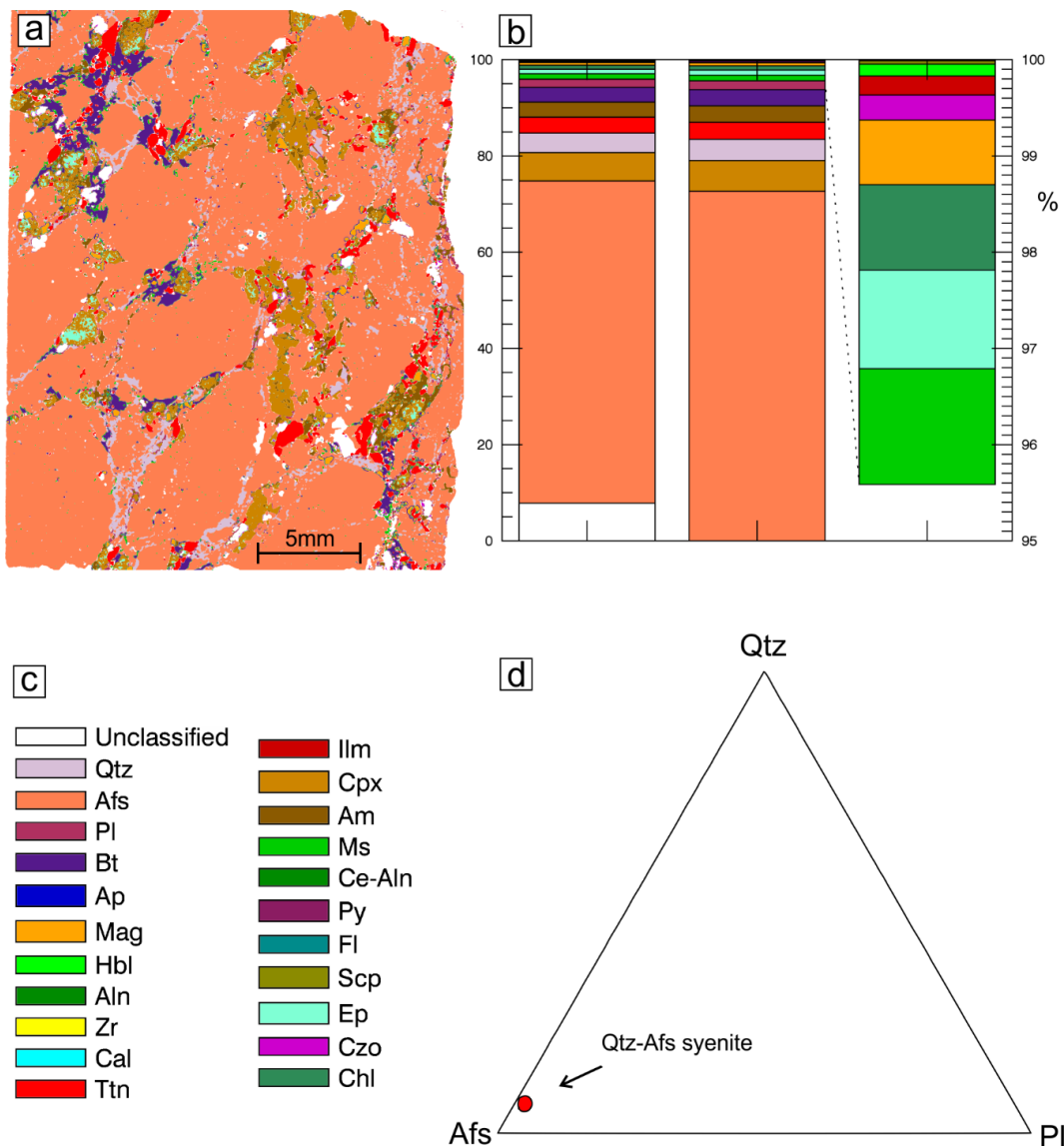


Figure 2.9: Data analysis a) Distribution of elements for a polished rock slab. b) Phase ratio of classified minerals for polished rock slab shown in a). c) Corresponding legend. d) Ternary plot for analyzed sample indicating a Qtz-Afs syenite.



# Chapter 3

## 3. Contributions to Scientific Journals

This chapter summarizes the titles, submission histories, contents and applied methods of scientific articles published as ‘first author’ and ‘co-author’ and elucidates the contributions of the individual authors. The chronological publication history of all submissions differs from the contributions made as ‘first author’. Here, presented publications do not follow a chronological order but are listed in a sequence that mentions ‘first author’ prior to ‘co-author’ contributions. ‘First-author’ contributions are presented in Chapters 4 to 6 and ‘co-author’ contributions in Chapters 7 to 12. This is schematically illustrated in Figure 3.1.

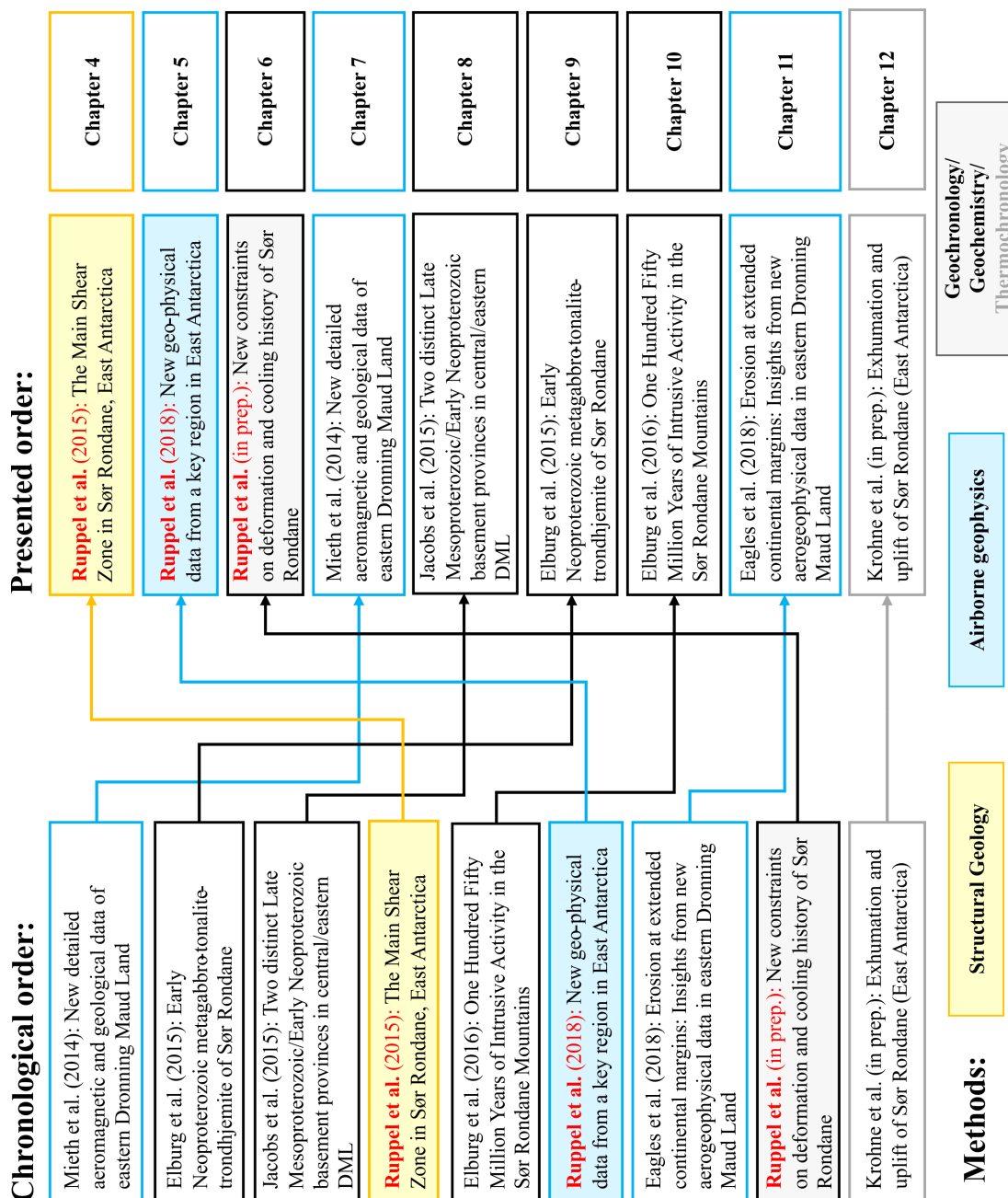


Figure 3.1: Flow chart indicating the chronological order of scientific contributions compared to the here presented order rearranged according to ‘first-author’ and ‘co-author’ contributions. Colors of rectangles indicate the applied methods.



# The Main Shear Zone in Sør Rondane, East Antarctica: Implications for the Late Pan-African Tectonic Evolution of Dronning Maud Land

Antonia S. Ruppel<sup>1</sup>, Andreas Läufer<sup>1</sup>, Joachim Jacobs<sup>2,3</sup>, Marlina Elburg<sup>4</sup>, Nicole Krohne<sup>5</sup>, Detlef Damaske<sup>1</sup>, and Frank Lisker<sup>5</sup>

<sup>1</sup>Federal Institute for Geosciences and Natural Resources, Hannover, Germany,

<sup>2</sup>Department of Earth Science, University of Bergen, Bergen, Norway,

<sup>3</sup>Norwegian Polar Institute, Tromsø, Norway,

<sup>4</sup>Department of Geology, University of Johannesburg, Johannesburg, South Africa,

<sup>5</sup>Department of Geosciences, University of Bremen, Bremen, Germany

Tectonics 34 (2015), pp. 1290–1305

<http://dx.doi.org/10.1002/2014TC003763>

Received 23 October 2014

Accepted 14 May 2015

Accepted article online 19 May 2015

In this article, we report on structural investigations carried out in the western Sør Rondane Mountains, Dronning Maud Land, which shed new light on the geodynamic evolution of East Antarctica regarding the formation of Gondwana. The over 120 km long and km-wide Main Shear Zone (MSZ) represents a prominent structural element in the SRM, of which only little was known with regard to its kinematics, extent, timing and role during the Pan-African orogenic cycle. Our new data demonstrate that the geodynamic significance of the MSZ has been widely underestimated and that it represents an important late-tectonic strike-slip boundary, which was active in Ediacaran to Early Palaeozoic times.

Field work for this study was realized during the first and second stage of the GEA project during austral summers 2010/11 and 2011/12. Structural data and rock samples were measured and collected by myself during the second field season in Sør Rondane. Additional structural readings were integrated from the first field season (unpublished report by D. Damaske and J. Jacobs). I produced, evaluated, and illustrated the structural datasets and performed thin section analyses to gain detailed structural and petrological information. I generated the figures and wrote the manuscript. Andreas Läufer, Joachim Jacobs, Marlina Elburg, Nicole Krohne, and Detlef Damaske were members of the geological field party in 2011/12 and contributed to discussions during field work. All co-authors contributed to the results and discussions of the manuscript.



# New Geophysical Data from a Key Region in East Antarctica: Estimates for the Spatial Extent of the Tonian Oceanic Arc Super Terrane (TOAST)

Antonia Ruppel<sup>1</sup>, Joachim Jacobs<sup>2,3</sup>, Graeme Eagles<sup>4</sup>, Andreas Läufer<sup>1</sup>, Wilfried Jokat<sup>4</sup>

<sup>1</sup>Federal Institute for Geosciences and Natural Resources (BGR), Stilleweg 2, 30655 Hannover, Germany.

<sup>2</sup>University of Bergen, P.O.Box 7800, 5020 Bergen, Norway.

<sup>3</sup>Norwegian Polar Institute, Fram Centre, 9296 Tromsø, Norway.

<sup>4</sup>Alfred Wegener Institute (AWI), Helmholtz Centre for Polar and Marine Research, Am Alten Hafen, 27568 Bremerhaven, Germany.

Gondwana Research 59 (2018), pp. 97-107  
<http://dx.doi.org/10.1016/j.gr.2018.02.019>

Received 27 September 2017

Revised in revised form 9 January 2018

Accepted 14 February 2018

Available online 28 March 2018

We investigated the area south and east of Sør Rondane with the research aircraft Polar 5 and 6 and report on a large new aeromagnetic data set acquired during the austral summers 2013/14 and 2014/15. The survey was realized during the fourth stage of the GEA project. The combination of surface geology from sparse exposures with new and existing aeromagnetic data provide a powerful tool to characterize the sub-ice geology and demonstrate that East Antarctica probably hosts extensive juvenile early Neoproterozoic crustal additions. We estimated the spatial extent of juvenile Neoproterozoic crust in Dronning Maud Land to at least ca. 500000 km<sup>2</sup> that probably represents major remnants of the Mozambique Ocean.

I processed the aeromagnetic data and compiled them with existing data from earlier campaigns. I used advanced filtering and transformation techniques to enhance prominent magnetic anomaly patterns. Further, the calculation of located Euler depth was calculated to estimate the depth of magnetic source bodies. I generated all figures other than Figure 5.2 and wrote the manuscript. Joachim Jacobs supported me in the geological interpretation of the magnetic data, contributed to the results in several discussions, wrote the principal part of the section 'Introduction'. Graeme Eagles (chief scientist of both field campaigns) was responsible for the acquisition of the data and contributed together with Andreas Läufer and Wilfried Jokat to the results in discussions.



# New Constraints on Deformation and Cooling History of Sør Rondane, East Antarctica, with Implications on the Final Assembly of Gondwana from $^{40}\text{Ar}/^{39}\text{Ar}$ and U-Pb Geochronology

Antonia Ruppel<sup>1</sup>, Joachim Jacobs<sup>2</sup>, Andreas Läufer<sup>1</sup>, Lothar Ratschbacher<sup>3</sup>, Jörg A. Pfänder<sup>3</sup>, Benita-Lisette Sonntag<sup>3</sup>, Katarzyna Krasniqi<sup>1</sup>, Marlina Elburg<sup>4</sup>, Nicole Krohne<sup>5</sup>, Detlef Damaske<sup>6</sup>, Frank Lisker<sup>5</sup>

<sup>1</sup>Federal Institute for Geosciences and Natural Resources (BGR), Stilleweg 2, 30655 Hannover, Germany

<sup>2</sup>University of Bergen, P.O.Box 7800, 5020 Bergen, Norway

<sup>3</sup>TU Bergakademie Freiberg, 09599 Freiberg, Germany

<sup>4</sup>University of Johannesburg, P.O. Box 524 Auckland Park 2006 Johannesburg, South Africa

<sup>5</sup>University of Bremen, Klagenfurter Str.2, 28359 Bremen, Germany

<sup>6</sup>Norderneystraße 21, 31303 Burgdorf, Germany

Manuscript ready for submission

Main emphasis of this study was on the dating of the Main Shear Zone by using the Ar/Ar technique on syngenetic minerals, such as mica. Further, spatial data contributed to an improved understanding of the cooling history of the distinct terranes of Sør Rondane itself as well as adjacent remote areas west and east of Sør Rondane.

Field work for this study was realized during the second stage of the GEA project during austral summer 2011/12. I planned and conducted field work in Sør Rondane in close cooperation with Andreas Läufer. I performed thin section analyses to gain detailed petrological information, which was necessary for selecting promising rock samples. I accomplished the mineral processing of rock samples with high-voltage electrical pulses (SEFRAG) at the TU Bergakademie Freiberg and prepared the mineral separates, which were analysed by Jörg Pfänder and Lothar Ratschbacher at the ‘Argonlabor Freiberg’ (ALF), TU Bergakademie Freiberg. The Senckenberg Naturhistorische Sammlungen Dresden carried out U-Pb analyses on zircon as commissioned work, which was performed by Benita-Lisette Sonntag. The Ar/Ar and U-Pb zircon data were illustrated and interpreted by myself. Katarzyna Krasniqi performed thin sections analyses with  $\mu$ -Energy Dispersive X-Ray Fluorescence ( $\mu$ -EDXRF) for elemental analysis and supported me with the final evaluation. Joachim Jacobs supported me in the geological interpretation of the geochronological data and contributed to the results in several discussions. Andreas Läufer, Marlina Elburg, Nicole Krohne were members of the geological field party in 2011/12 and contributed to discussions during field work. All co-authors contributed to the results and discussions of the manuscript.



# New Detailed Aeromagnetic and Geological Data of Eastern Dronning Maud Land: Implications for Refining the Tectonic and Structural Framework of Sør Rondane, East Antarctica

Matthias Mieth<sup>1</sup>, Joachim Jacobs<sup>2</sup>, **Antonia Ruppel**<sup>3</sup>, Detlef Damaske<sup>3</sup>, Andreas Läufer<sup>3</sup>, and Wilfried Jokat<sup>1</sup>

<sup>1</sup>*Alfred-Wegener-Institut Helmholtz-Zentrum für Polar- und Meeresforschung (AWI)  
Columbusstrasse, D-27568 Bremerhaven, Germany*

<sup>2</sup>*University of Bergen, P.O.Box 7800, 5020 Bergen, Norway*

<sup>3</sup>*Federal Institute for Geosciences and Natural Resources (BGR), Stilleweg 2, 30655 Hannover, Germany*

Precambrian Research 245 (2014), pp. 174-185  
<http://dx.doi.org/10.1016/j.precamres.2014.02.009>

Submitted 11 November 2013

Revised 12 February 2014

Accepted 17 February 2014

Available online 28 February 2014

This article is part of the PhD thesis of M. Mieth:  
<https://elib.suub.uni-bremen.de/peid=D00103761>

This article reports on aeromagnetic data that are correlated with magnetic susceptibility measurements and geological findings in the Sør Rondane Mountains and enable the projection of tectonic terranes into ice-covered areas. Geological and geophysical data agree reasonably well and support new mapping and the refinement of several tectonic boundaries.

Data were collected with the Alfred Wegener Institute's two Basler aircraft, Polar 5 and Polar 6, flying out of the Belgian research station Princess Elisabeth in the 2010/11, 2011/12 and 2012/13 seasons. The survey flights were realized during the first three stages of the GEA project.

This contribution was mainly composed by Matthias Mieth who contributed to the aerogeophysical data acquisition as member of the scientific flight crew (2010/11 and 2011/12) and as expedition leader (2012/13). Data processing and compilation as well as modelling of the aeromagnetic data was accomplished by Matthias Mieth whereas Joachim Jacobs supported in the geological interpretation of the magnetic data, contributed to the results in several discussions, wrote the section 'Geological overview of Sør Rondane'. I joined the geological field party in 2011/2012 and conducted the geophysical measurements as member of the scientific flight crew 2012/13. I processed and summarized the magnetic land-based susceptibility measurements, wrote the subsection 'Magnetic susceptibility measurements' and contributed to the results in discussions. Detlef Damaske, Andreas Läufer, and Wilfried Jokat contributed to the results in discussions.



## Two Distinct Late Mesoproterozoic/Early Neoproterozoic Basement Provinces in Central/Eastern Dronning Maud Land, East Antarctica: the Missing Link

Joachim Jacobs<sup>1,2</sup>, Marlina Elburg<sup>3</sup>, Andreas Laeuffer<sup>4</sup>, Ilka C. Kleinmanns<sup>5</sup>, Friedhelm Henjes-Kunst<sup>4</sup>, Solveig Estrada<sup>4</sup>, **Antonia Ruppel**<sup>4</sup>, Detlef Damaske<sup>4</sup>, Pilar Montero<sup>6</sup>, Fernando Bea<sup>6</sup>

<sup>1</sup>*Department of Earth Science, University of Bergen, PB 7803, N-5020 Bergen, Norway*

<sup>2</sup>*Norwegian Polar Institute, Fram Centre, N-9296 Tromsø, Norway*

<sup>3</sup>*Department of Geology, University of Johannesburg, Auckland Park 2006, Johannesburg, South Africa*

<sup>4</sup>*Bundesanstalt für Geowissenschaften und Rohstoffe (BGR), Stilleweg 2, D-30655 Hannover, Germany*

<sup>5</sup>*FB Geowissenschaften, Eberhard Karls-Universität Tübingen, Wilhelmstraße 56, D-72074, Tübingen, Germany*

<sup>6</sup>*Departamento de Mineralogía y Petrología. Campus Fuentenueva, 18002 Granada, España*

Precambrian Research 265 (2015), pp. 249-272

<http://dx.doi.org/10.1016/j.precamres.2015.05.003>

Received 22 October 2014

Revised 3 April 2015

Accepted 6 May 2015

Available online 15 May 2015

This paper introduces the existence of Late Mesoproterozoic/Early Neoproterozoic fragments between central DML and Sør Rondane based on field geology, geochronology and geochemistry. Small nunataks facilitated the characterization and ground-truthing of a large and mostly ice-covered region. SHRIMP/SIMS zircon analyses and geochemical data lead to the definition of a large Tonian Oceanic Arc Super Terrane (TOAST) that consists mainly of ca. 1000-900 Ma juvenile rocks. Based on this findings published in 2014/15, the question of its dimension in the ice-covered regions was raised and investigated with aerogeophysical methods during subsequent expeditions within the GEA project (see Chapter 5).

Field work for this study was realized during the first (2010/11) and second stage (2011/12) of the GEA project. This contribution was mainly composed by Joachim Jacobs who collected the rock samples and accomplished geochronological as well as geochemical data analyses. I was a member of the field party during the second stage of the GEA project and contributed to the petrographic description of rock samples by applying polarizing microscopy on thin sections, the results in discussions, and proofreading.



# Early Neoproterozoic Metagabbro-Tonalite-Trondhjemite of Sør Rondane (East Antarctica): Implications for Supercontinent Assembly

Marlina Elburg<sup>1,2</sup>, Joachim Jacobs<sup>3,4</sup>, Tom Andersen<sup>5</sup>, Chris Clark<sup>6</sup>, Andreas Läufer<sup>7</sup>,  
**Antonia Ruppel**<sup>7</sup>, Nicole Krohne<sup>8</sup>, Detlef Damaske<sup>7</sup>

<sup>1</sup>*Discipline of Geology, SAEES, UKZN, Westville, South Africa*

<sup>2</sup>*Department of Geology, University of Johannesburg, PO Box 524, Auckland Park 2006, South Africa*

<sup>3</sup>*Department of Earth Science, University of Bergen, Allégaten 41, 5007 Bergen, Norway*

<sup>4</sup>*Norwegian Polar Institute, Fram Centre, 9296 Tromsø, Norway*

<sup>5</sup>*Department of Geosciences, University of Oslo, PO Box 1047 Blindern, N-0316, Norway*

<sup>6</sup>*Department of Applied Geology, Curtin University, GPO Box U1987, Perth, WA 6845, Australia*

<sup>7</sup>*Federal Institute of Geosciences and Natural Resources (BGR), Stilleweg 2, 30655 Hannover, Germany*

<sup>8</sup>*Department of Geosciences, University of Bremen, PF 330 440, 28334 Bremen, Germany*

Precambrian Research 259 (2015), pp. 189-206

<http://dx.doi.org/10.1016/j.precamres.2014.10.014>

Received 6 March 2014

Revised 1 October 2014

Accepted 15 October 2014

Available online 25 October 2014

This article provides new evidence for the age and the geochemical composition of meta-igneous rocks from the SW-Terrane of Sør Rondane by integration of zircon U–Pb, Lu–Hf and trace element data with whole rock geochemical data. This study contributes to former investigations and adds data and discussion about the ca. 1 Ga meta-igneous rocks (Kamei et al., 2013). Further, data are compared with neighboring areas in Antarctica as well as its Gondwana neighbours and are used to assess the tectonic implications for the supercontinent-cycles of Rodinia and Gondwana.

Field work for this study was realized during the second stage of the GEA project (2011/12) aiming to characterize the southern part of the SW-Terrane S (PI: M. Elburg), which is separated by the a major structural feature (Main Shear Zone; Chapter 4) from the SW Terrane N. Geochronological/geochemical studies were interconnected with structural investigations (PI: A. Ruppel) to gain an understanding about the tectonic evolution and juxtaposition of the SW Terrane S related to adjacent terranes as well as neighbouring areas. This contribution was mainly composed by Marlina Elburg. I accomplished structural field work, contributed to the results in discussions, and proofreading.



# One Hundred Fifty Million Years of Intrusive Activity in the Sør Rondane Mountains (East Antarctica): Implications for Gondwana Assembly

Marlina A. Elburg<sup>1</sup>, Tom Andersen<sup>1,2</sup>, Joachim Jacobs<sup>3,4</sup>, Andreas Läufer<sup>5</sup>, **Antonia Ruppel**<sup>5</sup>, Nicole Krohne<sup>6</sup> and Detlef Damaske<sup>5</sup>

<sup>1</sup>*Department of Geology, University of Johannesburg, Auckland Park 2006, Johannesburg, South Africa*

<sup>2</sup>*Department of Geosciences, University of Oslo, PO Box 1047 Blindern, N-0316 Oslo, Norway*

<sup>3</sup>*University of Bergen, Department of Earth Science, PB 7803, 5020 Bergen, Norway*

<sup>4</sup>*Norwegian Polar Institute, Fram Centre, 9296 Tromsø, Norway*

<sup>5</sup>*Bundesanstalt für Geowissenschaften und Rohstoffe, Stilleweg 2, D-30655 Hannover, Germany*

<sup>6</sup>*Department of Geosciences, University of Bremen, PF 330 440, 28334 Bremen, Germany*

The Journal of Geology 124 (2015), pp. 1-26  
<http://dx.doi.org/10.1086/684052>

Received 13 April 2015

Accepted 1 September 2015

Available online 21 December 2015

This article presents new zircon U-Pb ages of igneous rocks from Sør Rondane and combines them with previously published igneous and metamorphic zircon ages. Additionally, data from the neighboring Yamato-Belgica Mountains in the east and the central and western Dronning Maud Land in the west are integrated to document spatial and temporal magmatic trends aiming to build a better picture of the final amalgamation of Gondwana.

New data from the Sør Rondane Mountains yield evidence for at least four thermal pulses between 650 Ma and 500 Ma and documents a prolonged history of magmatism and metamorphism. One of the magmatic and metamorphic periods (575-550 Ma) can most likely be associated with the final stages of ductile deformation resulting from dextral deformation by the Main Shear Zone (Chapter 4).

Overarching goal of geochronological sampling during the second stage of the GEA project (2011/12) was to gather samples for U-Pb zircon geochronology (PI: M Elburg), Ar-Ar geochronology (PI: A.Ruppel), and thermochronological methods (apatite fission track and apatite (U-Th-Sm)/He analyses; PI: N.Krohne) for a detailed geodynamic reconstruction of the study area. Therefore, base of this study was a common sampling strategy during field work followed by coordinated laboratory investigations. This study also combines new U-Pb zircon data with structural investigations, which were carried out by myself and feed into the interpretation of the sequence of events. This contribution was mainly composed by Marlina Elburg who accomplished the geochronological data analyses. I further contributed to the results in discussions and proofreading of the manuscript.



# Erosion at Extended Continental Margins: Insights from New Aerogeophysical Data in Eastern Dronning Maud Land

Graeme Eagles<sup>1</sup>, Nanna Karlsson<sup>1#</sup>, **Antonia Ruppel**<sup>2</sup>, Daniel Steinhage<sup>1</sup>, Wilfried Jokat<sup>1</sup>, and Andreas Läufer<sup>2</sup>

<sup>1</sup>*Alfred-Wegener-Institut Helmholtz-Zentrum für Polar- und Meeresforschung (AWI) Am Alten Hafen 26, 27568 Bremerhaven, Germany*

<sup>2</sup>*Federal Institute for Geosciences and Natural Resources (BGR), Stilleweg 2, 30655 Hannover, Germany*

<sup>#</sup>*Now at: Geological Survey of Denmark and Greenland, Øster Voldgade 10, 1350 Copenhagen, Denmark*

Gondwana Research 63 (2018), pp. 105-116  
<http://dx.doi.org/10.1016/j.gr.2018.05.011>

Received 6 November 2017

Revised in revised form 15 May 2018

Accepted 16 May 2018

Available online 02 July 2018

This article describes an extensive new aerogeophysical dataset of ca. 40.000 km of new gravity and radar data in eastern Dronning Maud Land. Data were collected with the Alfred Wegener Institute's two Basler aircraft, Polar 5 and Polar 6, flying out of the Belgian research station Princess Elisabeth in the 2013/14 and 2014/15 seasons. The survey was planned based on previous scientific investigations and results gained from the Sør Rondane Mountains (Chapter 7) and was realized during the fourth stage of the GEA project. Here, I contributed to evaluation of the former magnetic datasets and conception of the subsequent campaigns. The aerogeophysical dataset includes radar, gravity and magnetic data whereas latter are evaluated and presented in Chapter 6. Here, I contributed to parts of the interpretation related to magnetic data and provided the processed grid for the two-dimensional modelling.

The radar and gravity data document first-time details of the topography of the East Antarctic Ice Sheet and its bed topography. Their analyses revealed indications for a subglacial pre-existing fluvial landscape and an imposing subglacial canyon at the eastern margin of Sør Rondane. Special attention was paid to a sediment volume balance exercise. Combined new aerogeophysical and sediment thickness data sets offshore the continent (Leitchenkov et al., 2008) were used to test ideas about the pattern, timing and amount of erosion that lead to the formation of the Sør Rondane escarpment situated at an extended continental margin.

This contribution was mainly composed by Graeme Eagles who was responsible for the acquisition of the data and preformed the processing of the gravity data. Nanna B. Karlsson mainly accomplished processing of radar data. Beyond my contributions listed above I further took part in discussions and proofreading.



## Exhumation and Uplift of Sør Rondane (East Antarctica) – Inversion of an East Gondwana Triple Junction

Nicole Krohne<sup>1</sup>, Frank Lisker<sup>1</sup>, Andreas Läufer<sup>2</sup>, **Antonia S. Ruppel**<sup>2</sup>, Joachim Jacobs<sup>3</sup>,  
Marlina A. Elburg<sup>4</sup>, Detlef Damaske<sup>5</sup> and Cornelia Spiegel<sup>1</sup>

<sup>1</sup>*University of Bremen, Department of Geosciences, P.O. Box 330440, D-28334 Bremen, Germany*

<sup>2</sup>*Federal Institute for Geosciences and Natural Resources (BGR), Stilleweg 2, D-30655 Hannover, Germany*

<sup>3</sup>*University of Bergen, P.O.Box 7800, 5020 Bergen, Norway*

<sup>4</sup>*University of Johannesburg, PO Box 524 Auckland Park 2006, Johannesburg, South Africa*

<sup>5</sup>*Norderneystraße 21, 31303 Burgdorf, Germany*

Manuscript ready for submission to Tectonics

This article is part of the PhD thesis of N. Krohne:  
<https://elib.suub.uni-bremen.de/peid=D00106698>

This manuscript deals with the reconstruction of the Phanerozoic geological and long-term landscape evolution of western Sør Rondane. The combination of new thermochronological data (apatite fission track ages and apatite (U–Th–Sm)/He ages) and structural data were used for thermal history modeling.

Field work for this study was realized during the second stage of the GEA project. This contribution was mainly composed by Nicole Krohne. Nicole Krohne conducted thermochronological field work, thermochronological analysis, integration and interpretation of the data set. Andreas Läufer and I conducted the structural measurements during GEA II expedition, contributed to the section ‘Brittle fault-slip data’ and provided structural data as equal-area lower hemisphere projections. I further contributed to the results in discussions, and proofreading.



## Chapter 4

# 4. The Main Shear Zone in Sør Rondane, East Antarctica: Implications for the Late Pan-African tectonic evolution of Dronning Maud Land

Antonia S. Ruppel, Andreas Läufer, Joachim Jacobs, Marlina Elburg, Nicole Krohne, Detlef Damaske, and Frank Lisker

Key findings:

- **The Main Shear Zone is a major late Pan-African dextral lithotectonic boundary**
- **It is close to the eastern front of the East African-Antarctic Orogen (EAAO)**
- **It belongs to the NE directed branch of bilateral tectonic escape of the EAAO**

### 4.1 Abstract

Structural investigations in western Sør Rondane, eastern Dronning Maud Land (DML), provide new insights into the tectonic evolution of East Antarctica. One of the main structural features is the approximately 120 km long and several hundred meters wide WSW-ENE trending Main Shear Zone (MSZ). It is characterized by dextral high-strain ductile deformation under peak amphibolite-facies conditions. Crosscutting relationships with dated magmatic rocks bracket the activity of the MSZ between late Ediacaran to Cambrian times (ca. 560-530 Ma). The MSZ separates Pan-African greenschist- to granulite-facies metamorphic rocks with “East African” affinities in the north from a Rayner-age early Neoproterozoic gabbro-tonalite-trondhjemite-granodiorite complex with ‘Indo-Antarctic’ affinities in the south. It is interpreted to represent an important lithotectonic strike-slip boundary at a position close to the eastern margin of the East African-Antarctic Orogen (EAAO), which is assumed to be located farther south in the ice-covered region. Together with the possibly coeval left-lateral South Orvin Shear Zone in central DML, the MSZ may be related to NE directed lateral escape of the EAAO, whereas the Heimefront Shear Zone and South Kirwanveggen Shear Zone of western DML are part of the south directed branch of this bilateral system.

### 4.2 Introduction

The continuation of the East African Orogen (Stern, 1994) into Dronning Maud Land (DML) in East Antarctica is of major importance for the reconstruction of the final amalgamation of Gondwana during the Late Proterozoic and early Palaeozoic, including the number of crustal fragments involved. It is generally assumed that multiphase collision of various crustal blocks of proto-E and proto-W Gondwana led to at least two more or less continuous and apparently crossing Pan-African orogenic belts in late Neoproterozoic to early Palaeozoic times ca. 650 – 490 Ma ago (Meert, 2003; Boger, 2011; Satish-Kumar et al., 2013). In this scenario, the East African-Antarctic Orogen (EAAO) or Mozambique Belt (Stern, 1994; Jacobs et al., 1998;



2003c) was formed by the accretion of multiple arc terranes and continental collision of the African plate assembly and the Antarctic Coats Land Block at ca. 650-540 Ma followed by late-stage extension at ca. 530-490 Ma (Figure 4.1a); it stretches from the Arabian Peninsula along the margin of East Africa into western DML in East Antarctica. The Kuunga Orogen (Figure 4.1b), extending from Australia across eastern India, the Prince Charles Mountains-Prydz Bay region and eastern DML in East Antarctica and further into Mozambique and beyond, is the result of the collision of Indo-Antarctica and Australo-Antarctica, with its main phase, depending on the author, at either ca. 570-530 Ma (e.g. Meert, 2003), ca. 550-500 Ma (e.g., Fitzsimons, 2003), or ca. 530-490 Ma (e.g., Boger et al., 2001; Boger and Miller, 2004). Here, Sør Rondane in eastern DML holds a key position since it appears to be located close to the likely crossing-point of the EAAO and the Kuunga Orogen (Satish-Kumar et al., 2013; Mieth and Jokat, 2014).

The structure of the EAAO changes significantly along its length. Its northern part is to a large extent characterized by middle Late Proterozoic accretion of juvenile volcanic arc terranes separated by ophiolitic sutures that are sinistrally sheared and metamorphosed under low- to medium-grade conditions; the southern part experienced up to granulite-facies metamorphism and polyphase deformation of late Neoproterozoic-Cambrian age, which overprinted an Archean-Mesoproterozoic basement and was followed by late-tectonic voluminous high-temperature plutonism and collapse tectonics (Jacobs and Thomas, 2004). Evidence for a slightly younger Kuunga orogenic event (Figure 4.1b) in the Antarctic region is observed as significant high-grade regional metamorphic overprint in the Lützow-Holm Bay region around ca. 530-500 Ma (U-Pb zircon ages; Shiraishi et al., 1994) and in the Prince Charles Mountains at ca. 530-490 Ma, representing the collision between Indo-Antarctica and W Gondwana (Boger, 2011). The final collision phase of the Australo-Antarctic plate with W Gondwana is thought to have occurred around 530-490 Ma (Boger, 2011). To the W, similar ages of ca. 530-500 Ma were reported for peak deformation/metamorphism in the Damara Belt in the African part of W Gondwana (e.g. Gray et al., 2008).

A major question in reconstructing the amalgamation of Gondwana is the location of the suture zone between proto-E and proto-W Gondwana and the margins of the EAAO. Figure 4.1a presents four different scenarios of the proposed E/W Gondwana suture in DML. One of these scenarios suggests the suture to pass through the target region between central and eastern DML (Moyes et al., 1993). The western margin of the EAAO is represented by the Heimefront Shear Zone, an approximately 20 km wide major dextral transpression zone in western DML (e.g. Jacobs et al., 1997; 1998). The Heimefront Shear Zone separates Grenville-age rocks unaffected by Pan-African overprint to the W from Mesoproterozoic rocks that suffered widespread and intense polyphase high-grade deformation and metamorphism of Pan-African age to the E (e.g. Jacobs et al., 1996b; 1998) and is characterized by a prominent magnetic anomaly pattern (Golynsky and Jacobs, 2001). However, the position of the eastern margin of the EAAO remains unclear. In this regard, structural investigations in Sør Rondane may help to answer the question if a possible suture zone is preserved in the main mountain range or may provide evidence for the location of an eastern boundary of the EAAO. Therefore, a combined structural and geophysical survey was carried out over three consecutive Antarctic seasons in the Sør Rondane region between 2010 and 2013. One of the main targets was the Main Shear Zone (MSZ), which represents a prominent structural element in Sør Rondane.



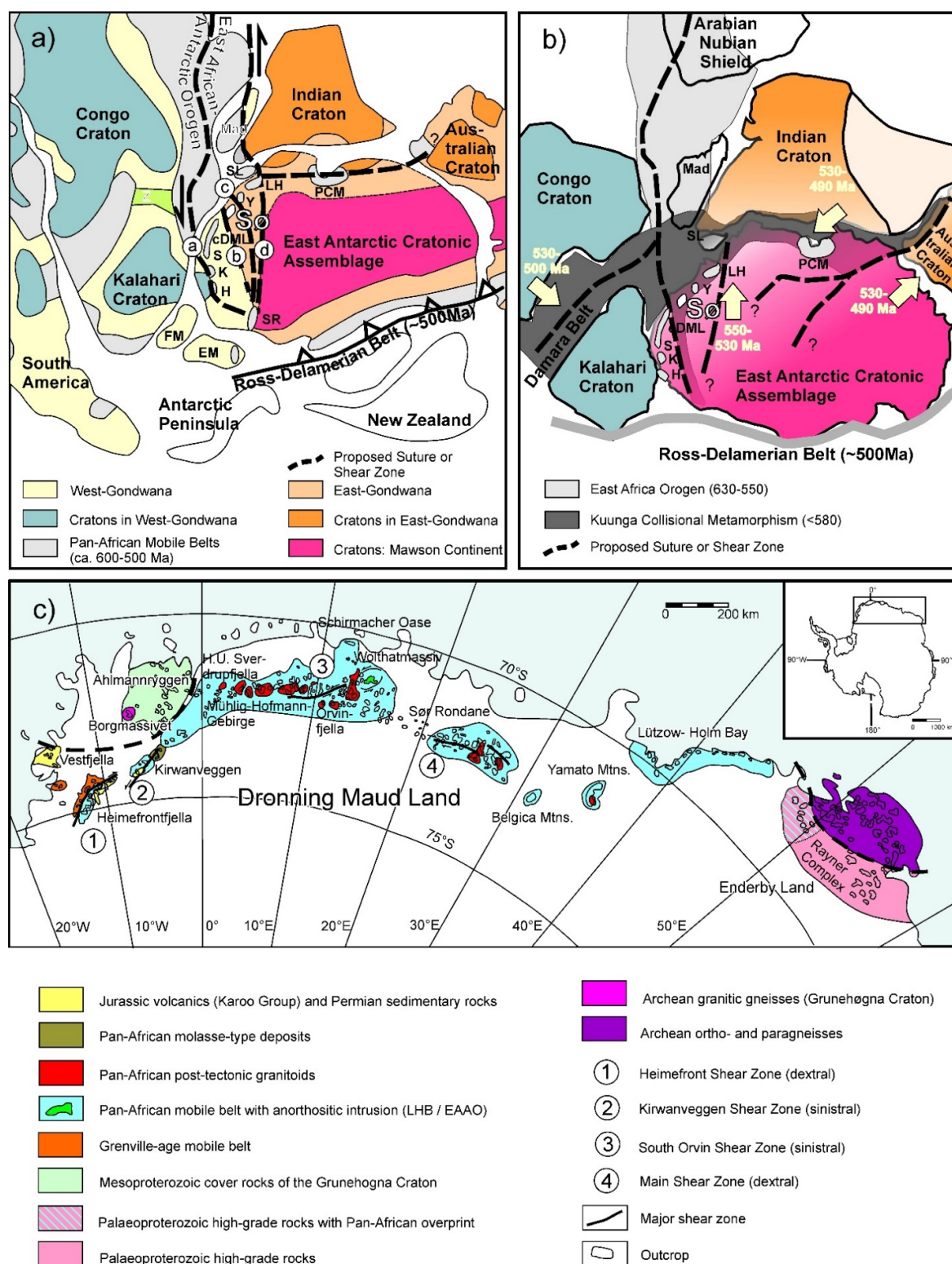


Figure 4.1: Overview of late Neoproterozoic to early Palaeozoic plate tectonic reconstructions indicating the position of Dronning Maud Land and Sør Rondane (Sø) within two apparently crossing Pan-African orogenic belts. East Antarctica, formerly considered to represent a stable entity (the “East Antarctic Craton”), consists of several separate cratons welded together during Proterozoic and early Palaeozoic orogenies (e.g. Boger, 2011). Therefore, we use the term “East Antarctic Cratonic Assemblage” here. a) Continuation of the East African-Antarctic Orogen (ca. 630-550 Ma) from the Arabian Peninsula in the N through East Africa into Dronning Maud Land in the S (modified after Grunow et al., 1996; Jacobs et al., 1998). Labels a)-d) indicate four different scenarios of where the E-W Gondwana suture has been proposed to be located (a) Shackleton, 1996; b) Jacobs et al., 1998; c) Moyes et al., 1993; d) Grunow et al., 1996). b) Slightly younger Pan-African metamorphic ages are observed e.g. in the Damara Belt, Lützow-Holm Belt, Prince Charles Mountains and in the Denman



*Glacier region and are referred to as the Kuunga Orogen (< 580 Ma) (modified after Meert, 2003). c) Geological map of Dronning Maud Land indicating the presence of four major shear zones (labeled 1-4) (adapted from Bauer et al., 2003, topographic base from Antarctic Digital Database, Grunehogna Craton boundary after Bauer et al., 2003 and Marschall et al., 2013). DML, Dronning Maud Land; EM, Ellsworth-Whitmore Mtns.; FM, Falkland Microplate; H, Heimefrontfjella; K, Kirwanveggen; LH, Lützow-Holm Bay; PCM, Prince Charles Mtns.; S, Sverdrupfjella; SL, Sri Lanka; Sør, Sør Rondane; SR, Shackleton Range; Z, Zambezi Belt.*

So far only little is known about the kinematics along the MSZ, and a modern structural characterization, its extent, timing, and role during the Pan-African orogenic cycle is largely lacking.

Here, we present a first-time detailed structural and kinematic analysis of the MSZ combined and integrated with the main geophysical and petrological/geochemical results of our expeditions (Mieth and Jokat, 2014; Jacobs et al., 2015; Elburg et al., 2015). The paper addresses the main questions: (1) which kinematics are involved and what is the geodynamic significance of the MSZ within the EAAO; (2) does the MSZ represent an important regional structure of the EAAO, or is it rather of minor significance as presumed so far; and (3) are there any hints for the location of the eastern front and thus the width of the EAAO in Sør Rondane?

### 4.3 Geological Overview of Sør Rondane

Sør Rondane is divided into a granulite-facies northeastern terrane (NE terrane) and an amphibolite- to greenschist-facies southwestern terrane (SW terrane), separated by the Sør Rondane Suture (Osanai et al., 1992, 1996a, b). This structure was interpreted as a large fault or shear zone with unknown kinematics along which the NE and SW terranes collided in Late Proterozoic times. Peak metamorphism of the NE terrane occurred around 650-600 Ma (SHRIMP U-Pb zircon ages, Shiraishi et al. 2008; LA-ICP-MS U-Pb zircon ages, Osanai et al. 2013). Collision was followed by subsequent retrograde metamorphism, orogenic collapse, and exhumation, which was dated at ca. 590-530 Ma in both terranes (Shiraishi et al., 2008; Osanai et al., 2013).

Osanai et al. (2013) refined the terranes and lithotectonic units of Sør Rondane (Figure 4.2), mainly based on new petrological and geochronological data, namely contrasting PTt-loops of different types of granulite-facies rocks (Adachi et al., 2013; Baba et al., 2013) and detrital zircon provenances in the NE and SW terranes. The newly defined Main Tectonic Boundary is interpreted to represent the suture between the NE and SW terranes, apparently associated with SW directed reverse ductile shearing around 650-600 Ma (Osanai et al., 2013). In this scenario, the former Sør Rondane Suture does not represent a suture but is part of the frontal fold zone of the Main Tectonic Boundary.

The amphibolite to granulite-facies NE terrane is mainly composed of metasupracrustal rocks deposited after 750 Ma but before Pan-African high-grade metamorphism at ca. 650-600 Ma or, alternatively, on a postulated ca. 1.1-1 Ga basement before or at ca. 800-750 Ma, based on detrital zircon data (Shiraishi et al., 2008). Mafic and locally ultramafic metavolcanic rocks indicate a formation in oceanic and island-arc to continental margin environments (Osanai et al., 1992; Ikeda and Shiraishi, 1998). The northern part of the SW terrane consists of metasedimentary and meta-igneous rocks, which reached granulite-facies conditions in the N and amphibolite- to greenschist-facies conditions in the S, both units separated by the Sør



Rondane Suture (Figure 4.2). The southern part of the SW terrane is represented by a gabbro-tonalite-trondhjemite-granodiorite (GTTG) complex. Kamei et al. (2013) determined two different geochemical series with different ages of emplacement for the GTTG complex that is interpreted to have formed along a juvenile oceanic arc. SHRIMP U-Pb zircon ages of ca. 998-995 Ma were derived for the intrusion of tholeiitic tonalites and of ca. 945-920 Ma for calc-alkaline tonalites. The GTTG complex shows evidence of tectono-thermal overprint under greenschist- to lower amphibolite-facies conditions at ca. 590-530 Ma (Osanai et al., 2013). However, our own observations show that the GTTG rocks still preserve igneous textures on a mesoscopic scale apparently without indications of strong deformation except close to the MSZ (e.g. Mieth and Jokat, 2014; Elburg et al., 2015).

The transection of the SW terrane along the MSZ (Kojima and Shiraishi, 1986) in an approximately E-W direction separates the low-grade to granulite-facies rocks in the N from the GTTG complex in the S. Toyoshima et al. (1995) presented an overview of the structural evolution for the central part of Sør Rondane and reported E-W to ENE-WSW striking mylonitic foliation with NE-SW to N-S trending mineral lineations dipping to the S. A top-to-the-SW to S displacement is interpreted to be associated with retrograde mylonitization and tonalite intrusion at ca. 950 Ma. Recent structural work of Toyoshima et al. (2013) revises the deformation history of Sør Rondane into multiple stages. They propose that the SE dipping detachment fault in Balchenfjella, which is thought to have formed in an extensional regime after ca. 600 Ma (Ishikawa et al., 2013), possibly represents the eastern continuation of the MSZ.

Two late to post- tectonic phases of Pan-African age can be recognized in Sør Rondane. Metamorphic U-Pb zircon ages between ca. 570-530 Ma (e.g. Picciotto et al., 1964; Pasteels and Michot, 1970; Shiraishi et al., 2008; Adachi et al., 2013; Grantham et al., 2013; Osanai et al., 2013) are interpreted to represent a post-collisional retrograde hydration event caused by regional magmatic activity, which affected the granulite- facies rocks in the NE terrane. This event is thought to be associated with extensional tectonics as well as the development of the Balchen detachment fault in easternmost Sør Rondane (Ishikawa et al., 2013). Post-peak-metamorphic plutonism is documented by the intrusion of late- to post-tectonic granitoids that are classified into three groups based on ages and magnetic signatures (Mieth and Jokat, 2014 and references therein). Plutonism is recorded for both terranes and is related to a major extensional phase (Li et al., 2003; 2006; Shiraishi et al., 2008). Mafic lamprophyre dykes and high-K dolerite dykes intrude the entire area with no systematic orientation and are interpreted as post-kinematic and possibly linked to the extensional stage after Pan-African collision (Kojima and Shiraishi, 1986; Takigami et al., 1987; Owada et al., 2008).

New detailed aeromagnetic measurements refine the geological framework of Sør Rondane based on geological information (Mieth et al., 2013). Seven distinct magnetic domains were identified and correlated with distinct tectonic domains. The data suggest an E-W division of Sør Rondane, possibly related to extensional tectonics. Main Shear Zone, Main Tectonic Boundary, and Sør Rondane Suture have a significant magnetic expression and can be traced underneath the ice cover. However, the geologic and magnetic boundaries differ in some places (cf. Figure 4.2 and Figure 4.3). The magnetic anomalies of the GTTG complex are collinear to the general SW-NE foliation trend in this unit. Additionally, it is suggested that a curvilinear agnetic anomaly within the GTTG complex developed as the result of major dextral shear strain.



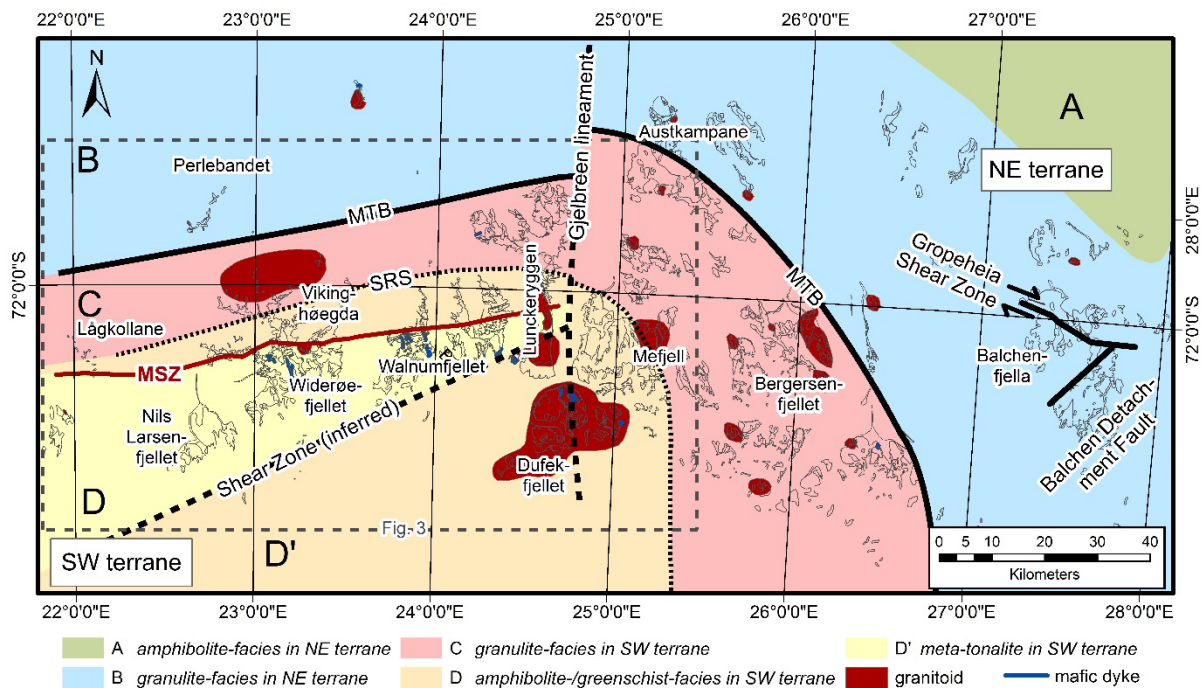


Figure 4.2: Geological overview of Sør Rondane indicating the subdivision of tectonic terranes and units (modified after Osanai et al., 2013) including representative place names. Units A and B belong to the NE terrane and units C, D, and D' to the SW terrane. The Main Tectonic Boundary (MTB) separates NE and SW terranes. The previously assumed boundary between these terranes, the Sør Rondane Suture (SRS), is redefined as part of a frontal fold zone of the MTB within the SW terrane (Osanai et al., 2013). The GTTG complex is separated from the northern greenschist- to granulite-facies rocks by the Main Shear Zone (MSZ). An inferred shear zone is indicated in the S of the GTTG complex (Shiraishi et al., 1992c; Osanai et al., 1996c). Another structural feature trending N-S with as yet unknown characteristics is termed the Gjelbreen lineament (Mieth et al., 2014). Age relation of Groppeheia Shear Zone and Balchen Detachment Fault based on aerogeophysical data (Mieth et al., 2014).

## 4.4 Structural Geology

The MSZ (Kojima and Shiraishi, 1986), which measures up to several hundreds of meters in width by roughly 120 km in length, represents a high-strain ductile shear zone of intense mylonitic deformation between Lågkollane in the west and Lunckeryggen in the east (Figure 4.3). It divides the SW terrane in a northern subterrane consisting of greenschist- to granulite-facies metamorphic and plutonic rocks and a southern subterrane dominated by a gabbro-tonalite-trondhjemite-granodiorite (GTTG) complex. The general strike direction of the MSZ is WSW-ENE, but locally its strike changes to a more south-westerly direction. The mylonitic foliation dips steeply to moderately to the S or SE with angles between 45°- 89°. Mineral stretching lineations plunge either shallowly E or W, less frequently they are moderately to steeply inclined and oriented down-dip (Figures 4.3, 4.4). Kinematic indicators both in the field and on polished rock slabs and in thin sections (Figure 4.5, Figure 4.6) indicate a dextral sense of shear with either transpressive or subordinate transtensive components suggested by foliation/lineation dip directions (cf. Figure 4.4). The main deformation zone of the MSZ is characterized by a large variety of mylonitic rocks, ranging from protomylonites to ultramylonites, apparently largely depending on original composition and grain size of the rocks. Microstructural analyses of rocks of the GTTG subterrane show mylonitic textures with plagioclase and K-feldspar porphyroclasts that have been ductilely deformed (undulose



extinction, deformation twins, grain boundary migration, dynamic recrystallization mainly along the margins of larger grains) with no brittle component, which points to deformation temperatures of 450-600 °C (Passchier and Trouw, 2005). Plagioclase porphyroclasts are partially replaced by clinozoisite and epidote, which is, however, independent of the deformation event (Elburg et al., 2015). Asymmetric pressure shadows are composed of dynamically recrystallized quartz, greenish-blue hornblende, and minor chlorite. Most frequently,  $\sigma$ -clasts and minor  $\delta$ -clasts can be observed confirming the right-lateral sense of movement observed in the field (Figure 4.6a, b). Quartz is to a large extent dynamically recrystallized and individual grains show undulose extinction, subgrain formation and grain-boundary migration. Ribbon quartz is very common. These fabrics are typically found in low- to medium-grade mylonitic rocks (Passchier and Trouw, 2005).

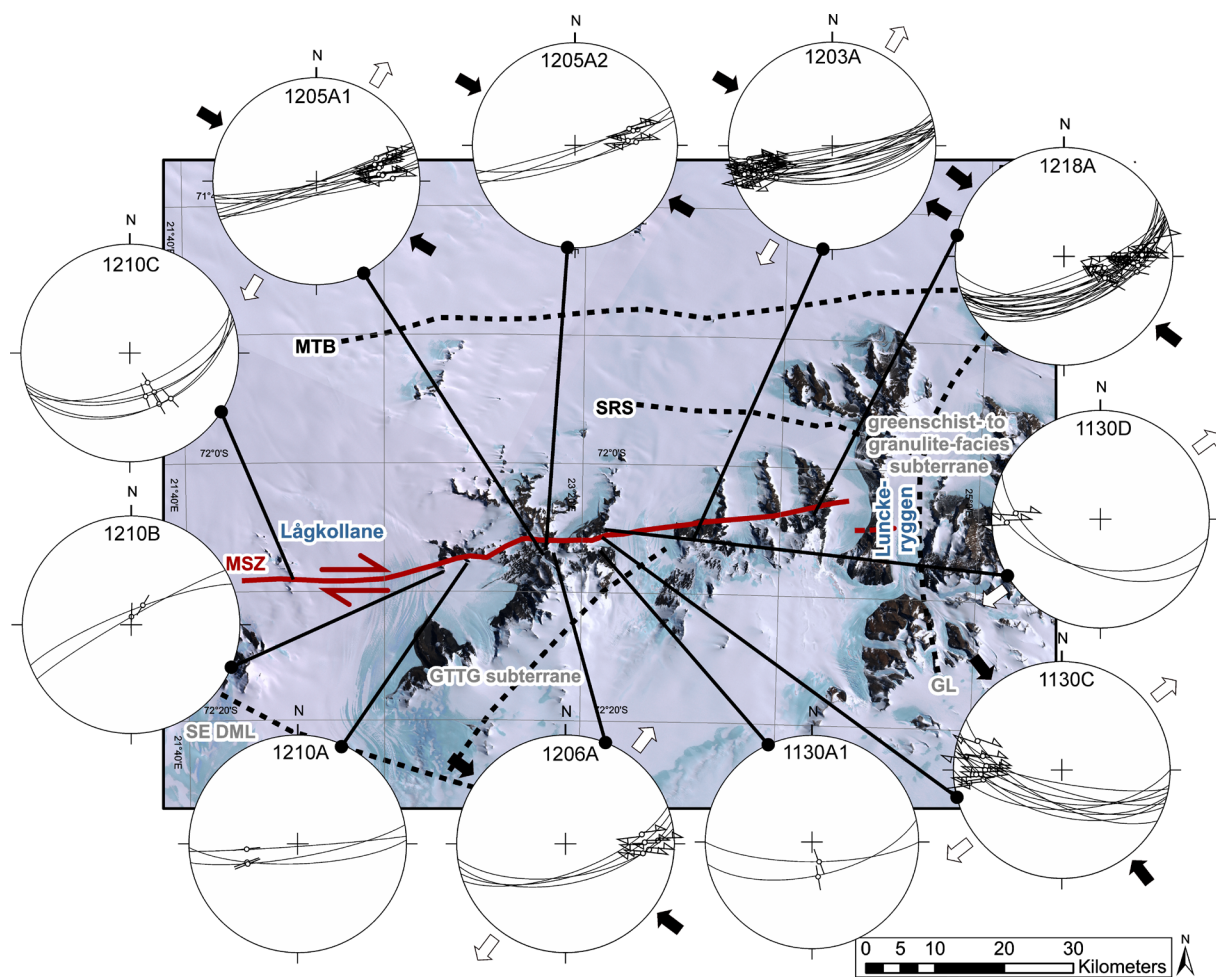


Figure 4.3: Map with equal-area lower hemisphere projections of kinematic analyses of mylonites along the MSZ. Foliation planes are plotted as great circles, and lineations and shear senses are marked as arrows. Thick arrows indicate horizontal stress directions: black = maximum horizontal stress, white = minimum horizontal stress. Dashed lines represent magnetic boundaries, based on aerogeophysical data and field observations (Mieth et al., 2014). Stereoplots were computed by using the Win-Tensor software by Delvaux and Sperner (2003). Abbreviations: GL Gjelbreen, lineament; GTTG, gabbrotonalite-trondhjemite-granodiorite; MSZ, Main Shear Zone; MTB, Main Tectonic Boundary; SE DML, southeastern Dronning Maud Land province; SRS, Sør Rondane Suture.



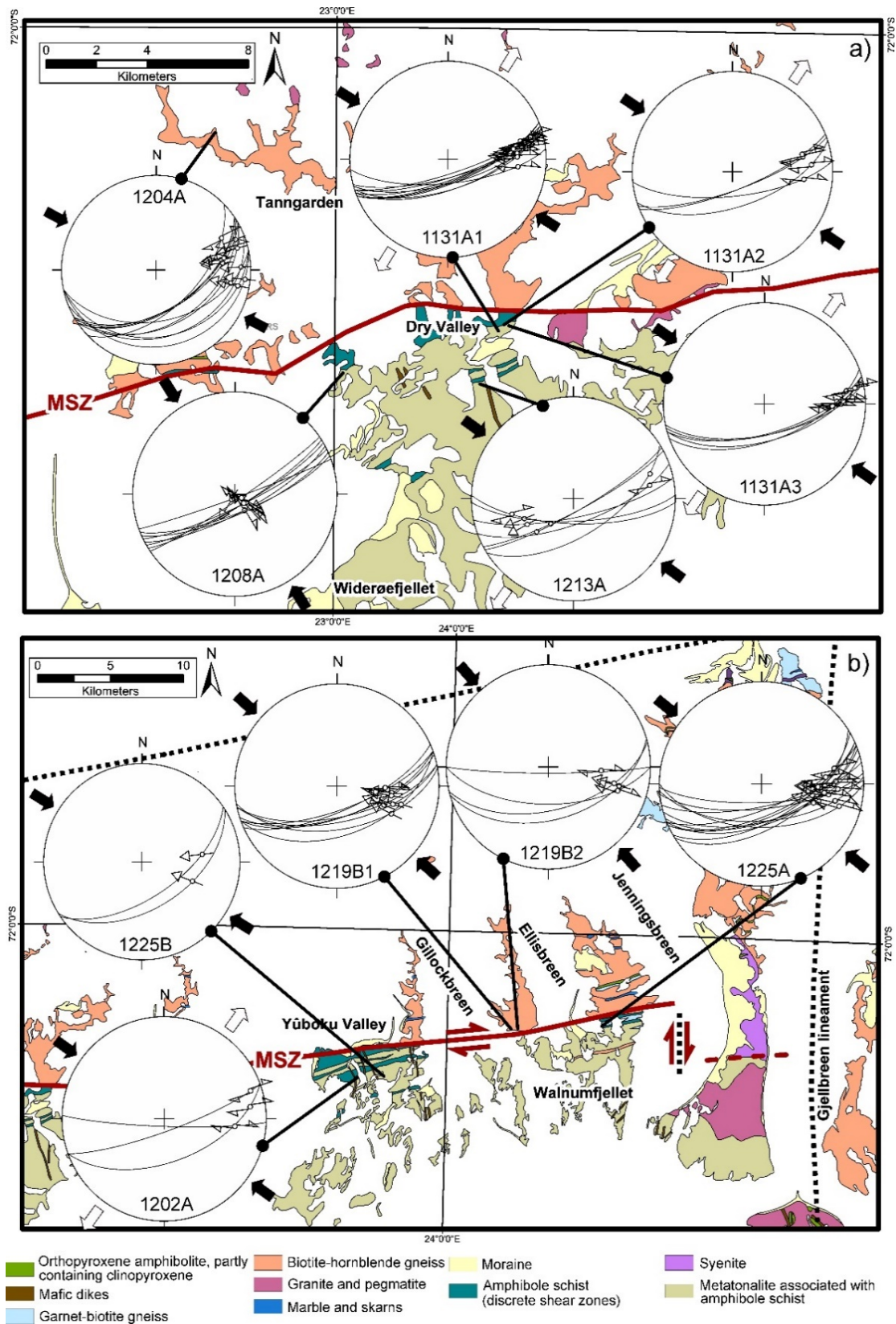


Figure 4.4: Geological map showing the position of additional structural measurements along the MSZ comprising foliation and lineation datasets characterized by a dextral sense of movement with apparent transpressive component for the regions a) Dry Valley, Tanngarden and b) Yüboke Valley, Ridges between Gillockbreen and Jenningsbreen. Amphibol schists represent discrete dextral shear zones following MSZ related fabrics. Stereoplots were computed by using the Win-Tensor software by Delvaux and Sperner (2003).



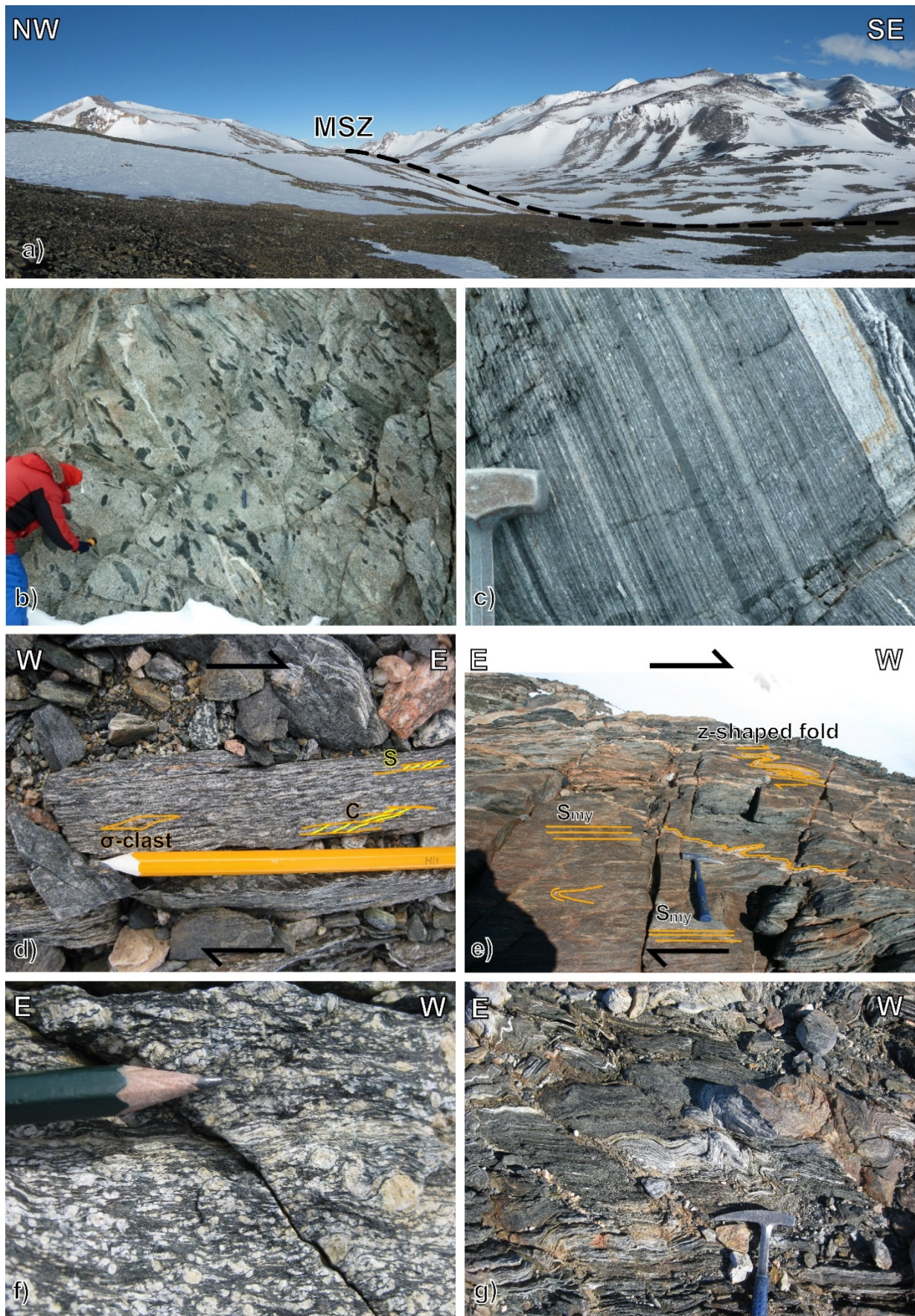


Figure 4.5: Photographs of key locations and examples of shear sense indicators of the MSZ in western Sør Rondane. a) The MSZ along the valley between Vikinghøgda in the N and Widerøefjellet in the S with the typical appearance of the MSZ as a depression due to the diminished competence of the mylonitic rocks. b) Example of a metatonalite with mafic enclaves from the GTTG complex ca. 3 km to the S of the MSZ. c) Mylonitized metatonalite of the GTTG complex shown in b), but close to the MSZ.



*Dark streaks are interpreted as transposed enclaves. d) S-C fabrics and  $\sigma$ -clasts point to a right-lateral sense of movement for mylonitic rocks at location 1205A. e) Right-lateral sense of movement indicated by z-shaped quartz veins in grey gneisses at Wallnumfjellet (ridge between Gillockbreen and Ellisbreen). f) Protomylonite from the central part of the MSZ at Yûboku Valley (1203A). g) Kink bands in the central part of the MSZ in mylonitic rocks E of Ellisbreen (1218A).*

Large garnet porphyroclasts were observed in ultramylonitic rocks in the main deformation zone. The clasts are ductilely deformed and elongated within the main foliation and show asymmetric, mostly  $\sigma$ -like geometries (e.g. locations 1203A, 1218A, Figure 4.3 and Figure 4.6e, f). Some smaller euhedral grains, show an internal straight  $S_i$  rotated in the main foliation and are interpreted as intertectonic porphyroblasts (c.f. Passchier and Trouw, 2005).

North of the principal deformation zone, MSZ-related mylonitic textures with right-lateral shear senses are preserved in both meta-igneous and metasedimentary rocks of the greenschist- to granulite-facies subterrane, as well as in late-tectonic granitoids that intruded along the MSZ (e.g. Vengen granite, unnamed granitic intrusion E of Gillocksbreen). Thin sections of mylonitic rocks show right-lateral plagioclase  $\sigma$ -clasts and SC- fabrics (Figure 4.6c, d). With increasing distance from the main deformation zone, grey gneisses of the SW terrane show decreasing grades of ductile deformation towards the N. Weak S-C fabrics and poorly developed plagioclase  $\sigma$ -clasts again indicate a dextral sense of shear. The mylonitic foliation is formed mainly by biotite and hornblende. Epidote occurs as an accessory mineral.

The late-tectonic Vengen granite, which was dated at ca. 560 Ma (SHRIMP U-Pb zircon; Shiraishi et al., 2008) intruded along the MSZ but also shows dextral ductile deformation and late-stage brittle off-sets, particularly visible along the western margin of Ketelersbreen. This may indicate that the Vengen granite intruded during the waning stages of shearing. The northern margin of the GTTG subterrane is strongly deformed by the MSZ, where the plutonic protoliths are transformed to mylonitic greenish epidote-hornblende±biotite±garnet schists and orthogneisses (Figure 4.5c). South of the MSZ, mylonitic deformation gradually decreases, and only right-lateral discrete shear zones consisting of low-grade schists with general trends (sub)parallel to the MSZ occur in certain domains of apparently rather undeformed GTTG rocks (Figure 4.5b). Discrete shear zones show sigmoidal internal foliation and phacoid bodies again indicating a right-lateral shear sense. Several ductile-brittle transitional and brittle structures can be observed along the MSZ. These chevron folds and kink bands (Figure 4.5g) and conjugated fault systems with MSZ-parallel dextral displacement of both aplitic and mafic dykes occur along brittly reactivated mylonitic foliation planes. Furthermore, MSZ-parallel slickensides with subhorizontal striations and fibers composed of feldspar and hornblende were recorded in the late-tectonic syenite stock at Lunckeryggen, which gave U-Pb zircon crystallization ages of ca. 560 Ma (Elburg et al., 2016). These slickensides occur in the direct extension of the MSZ further to the W (see also Osanai et al., 1996a) and may be interpreted as brittle activity of the shear zone overprinting the syenitic intrusion (Figure 4.7). In addition, negative flower structure-like arrays linked to MSZ-parallel faults are visible at the northern end of Lunckeryggen, again indicative of dextral strike-slip tectonics (e.g., Figure 4.7b).



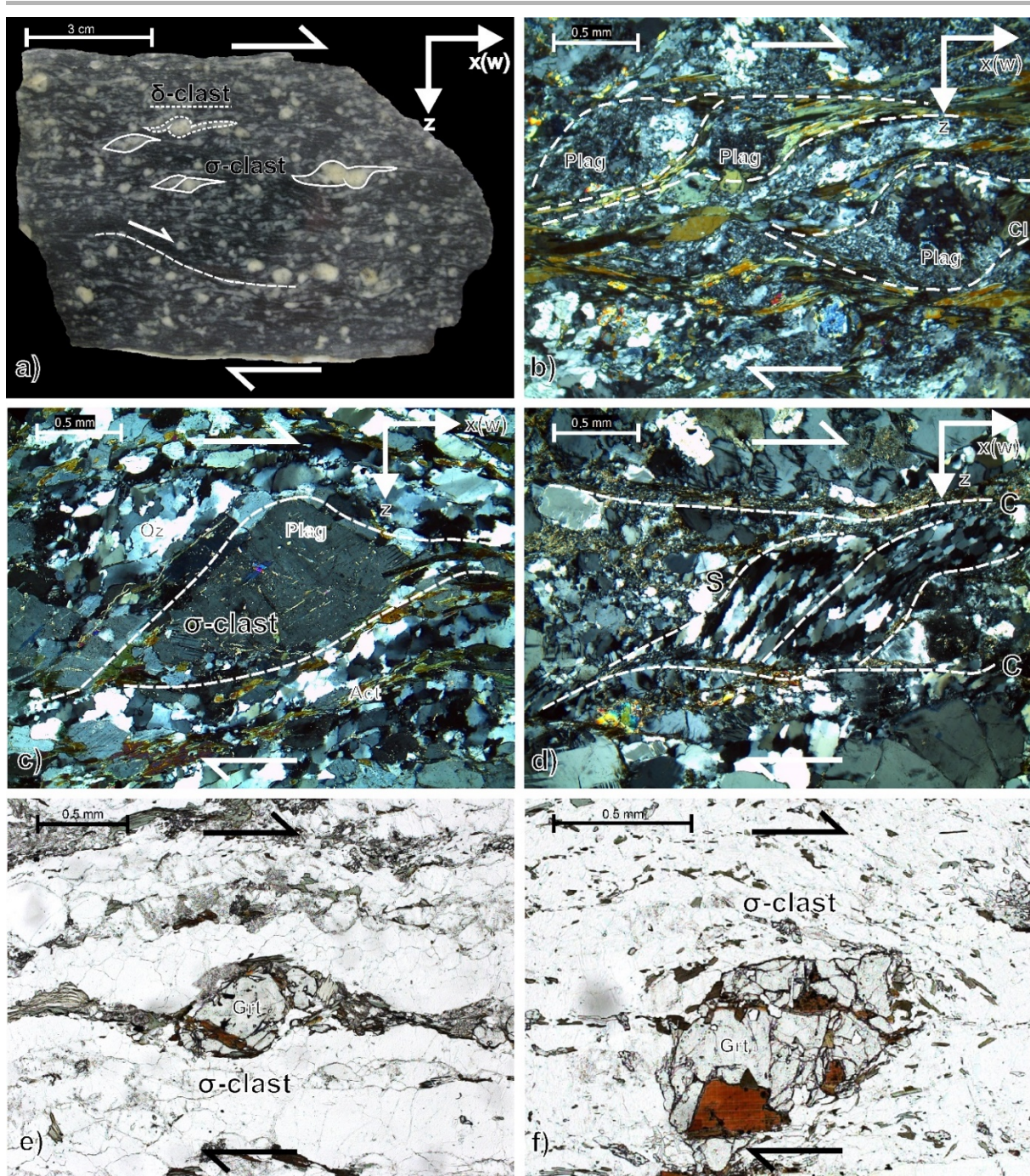


Figure 4.6: Polished rock slabs and photomicrographs of selected samples. a) Polished rock slab of an orthomylonite showing right-lateral sense of shear indicated by  $\sigma$ -clasts,  $\delta$ -clasts and shear bands (1203A). b) Photomicrograph of an orthomylonite with saussuritized plagioclase porphyroclasts (Plag) and asymmetric pressure shadow tails composed of actinolite (Act) and chlorite (Cl). These  $\sigma$ -clasts are evidence of a right-lateral sense of movement (1203A). c) Photomicrograph of a mylonitic rock with asymmetric plagioclase porphyroclasts indicating dextral shear sense (1205A). d) Photomicrograph of a mylonitic rock. Quartz is dynamically recrystallized, shows sutured grain boundaries, and is elongated. Elongated quartz grains form the S-surface and micas the C-surface of a right-lateral S-C fabric (1130C). Cl, chlorite; Plag, plagioclase; Qz, quartz. e + f) Mylonitic bt-hbl-gneiss with ductilely deformed and elongated garnet  $\sigma$ -clasts within the main foliation from the ridge between Ellisbreen and Jenningsbree indicating dextral shearing (1218A).



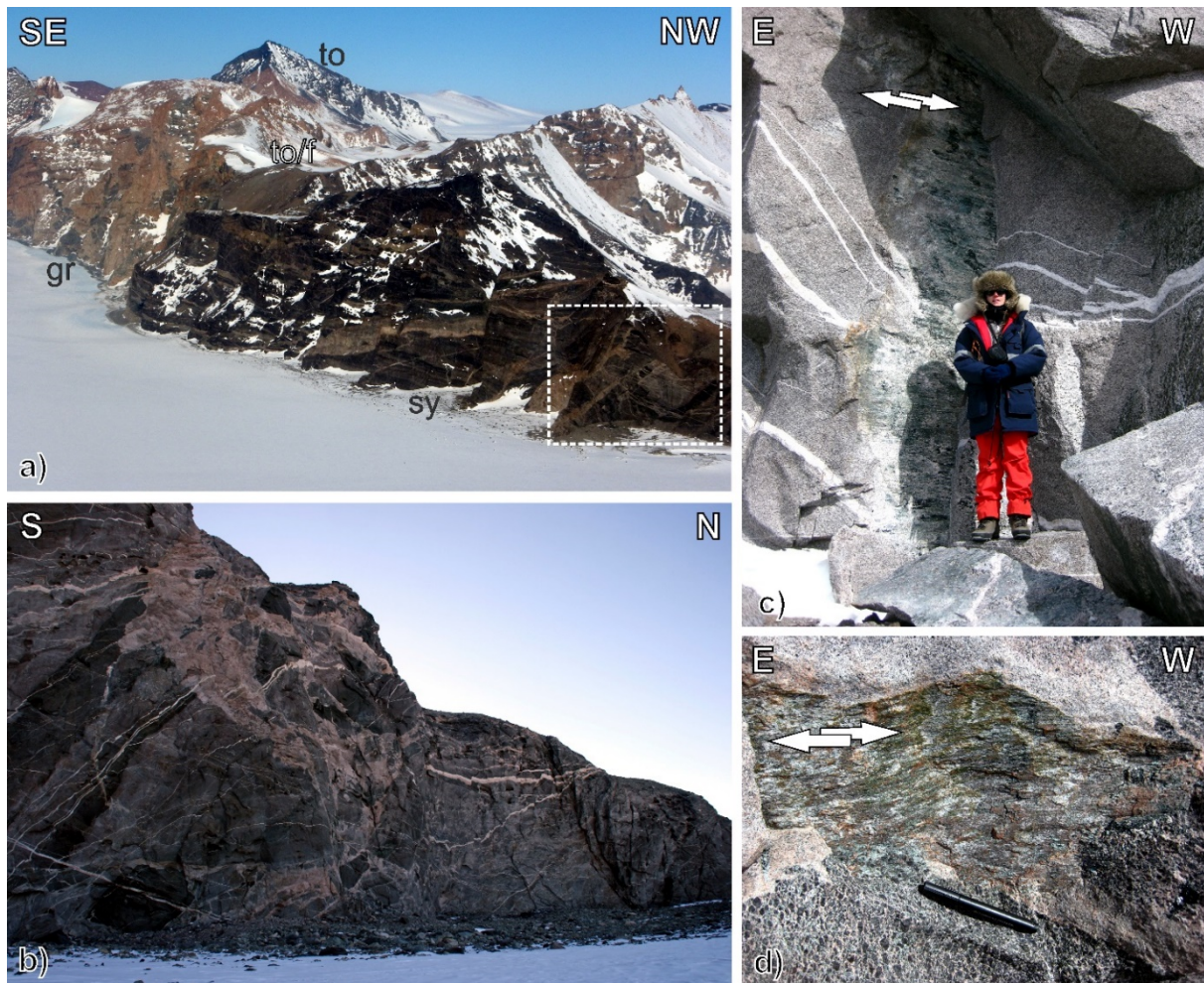


Figure 4.7: Photographs of MSZ-related brittle structures in the syenite of northern Lunckeryggen. Main rock types are melanocratic and quartz syenites, both intruded by granites. a) View to SW across the eastern face of Lunckeryggen. The stippled rectangle shows the position of the outcrop in photo b). The Lunckeryggen Syenite (sy) is located in the front. Lunckeryggen Granite (gr) and GTTG complex (to) are visible in the background. The granite intrudes the GTTG complex as well as the syenite and contains xenoliths of both. The morphological depression between granite and syenite (labeled to/f) represents the foliated and mylonitized contact zone of syenite and GTTG complex (Osanaï et al., 1996a) and is interpreted as the eastern continuation of the MSZ from Ellisbreen into Lunckeryggen dextrally offset by a postulated N-S oriented fault along Jenningsbreen. b) Eastern wall of northern Lunckeryggen. The wall shows subvertical and steeply inclined brittle faults with an approximate E-W strike direction parallel to the MSZ. The flower-like structure visible on the right side of the picture suggests strike-slip movements along the faults. c) Large E-W striking slickenside with subhorizontal striations along one of the faults seen in photo b). A right-lateral movement is indicated by fiber-steps on the fault plane. d) Example for slickensides in the syenite with kinematic indicators showing a dextral movement.

## 4.5 Discussion

### 4.5.1 The Main Shear Zone of Sør Rondane

The MSZ is characterized by a right-lateral sense of movement with a suggested transpressional and minor transtensional character along strike. The activity of the MSZ caused upper low- to medium-grade high-strain ductile to late stage brittle deformation, affecting both the Pan-African metamorphic rocks of the greenschist- to granulite-facies subterrane N of it and the early Neoproterozoic GTTG subterrane to the S. Low-grade schists reflect foliation-parallel,



discrete high-strain dextral shear zones in the GTTG complex. Shiraishi et al. (1992a) specify these rocks as greenschists or amphibole schists with mineral assemblages being identical with that of the tonalite, which is confirmed by our own observations (Elburg et al., 2015). The schists contain epidote, zoisite, and chlorite as secondary products and are characteristic for at least greenschist-facies conditions during activity of the MSZ. On a larger scale, these schists, as they are mapped in the Japanese Antarctic Geological Map Series in the vicinity of the MSZ, show a sigmoidal trend, which may indicate a strain increase toward the internal parts of the MSZ leading to a rotation of the pre-existing fabric of the rock into the general trend of the MSZ. These macro-structures swinging into the MSZ and the corresponding curvilinear magnetic anomalies are observed for the GTTG complex and may tentatively be interpreted as a result of major dextral shear strain along the MSZ (Mieth and Jokat, 2014). One major curvilinear magnetic anomaly continues along the schists at Walnumfjellet and finally meets the E trending MSZ. This may indicate that the western region of Sør Rondane records deformation caused by dextral shearing and this is supported by a general ENE-WSW trend of magnetic anomalies in the western part of the NE terrane (Mieth and Jokat, 2014). Since robust age determinations of the mylonites are lacking so far, the activity of the MSZ can only be narrowed down based on cross-cutting relationships with dated magmatic rocks. The lower age limit for the activity of the MSZ is provided by the youngest group of granitoid intrusions, which gave an age of ca. 530-510 Ma (Tainosho et al., 1992; Li et al., 2003, 2006; Shiraishi et al., 2008; Elburg et al., 2016) and appear to be unaffected by dextral ductile shearing. The intrusion of the Vengen granite at ca. 560-550 Ma (U-Pb zircon; Shiraishi et al. 2008, Elburg et al., submitted) which has undergone ductile deformation, gives an upper age constraint for the time of shearing. This is also supported by slickensides with the same orientation and kinematics as the MSZ and fibers composed of feldspar and hornblende, which were observed in the syenite complex at Lunckeryggen also dated to ca. 560 Ma (U-Pb zircon; Elburg et al., 2016) in direct extension of the MSZ W of it. The mineral association on the slickensides implies that brittle deformation occurred under elevated temperatures of up to approximately 300 °C and likely increased fluid activities during faulting. These slickensides may represent late-stage activities of the shear zone within the syenite. However, the syenite is intruded by and included as angular xenoliths in the Lunckeryggen granite, the main body of which is located further to the S (e.g. Li et al., 2003). Both syenite and granite may tentatively be regarded to be of roughly the same age. Based on U-Pb zircon age data of  $564 \pm 2$  Ma of a post-kinematic lamprophyre dyke and cross-cutting relationships of this dyke with other magmatic rocks, Owada et al. (2010, 2013) assume that both lamprophyre dykes and Lunckeryggen granite are roughly coeval and may be attributed to the same age group as the Vengen granite. Also, Li et al. (2003) interpret both syenite and the Vengen-type granite group to have evolved from the same magma source by crystal fractionation processes. The granites of this age group plot in the volcanic-arc and collisional field in Y-Nb discrimination diagrams, and can be classified as A-types on the basis of their Ga/Al ratios (Jacobs et al., 2015). The syenites have a similar geochemical signature, and resemble the lamprophyre dykes in terms of their Sr and Nd isotopic signature (Elburg et al., 2016). The geochemical coherence between all these rock types suggest mantle melting with subsequent crystal fractionation with or without crustal contamination.



Another possibility is that the MSZ is offset along a roughly N-S striking fault underneath Jenningsbreen, paralleling the Gjelbreen lineament (Figure 4.4b). The slickensides at Lunckeryggen would then represent brittle equivalents of the mylonitic MSZ located at some distance away from the principle deformation zone. Taking into account the simple approximation that the MSZ follows the boundary between the GTTG subterrane and the greenschist- to granulite-facies subterrane, the location of the mylonitic principle deformation zone may be assumed to be located in central Lunckeryggen possibly close to or within the boundary of the syenite and the northernmost tonalitic rocks of the GTTG subterrane (Figure 4.4b). In this regard, Osanai et al. (1996c) report that the syenite “shows remarkable mylonitic structures which are parallel to the contact plane of the mass”. This consequently suggests a considerable apparent right-lateral offset of a postulated fault underneath Jenningsbreen of several 10s of kilometres.

Further structural features are marked in the Japanese Antarctic Geological Map Series N and S of the MSZ as the “Sør Rondane Suture” and “Shear zone (inferred)”, respectively (Figure 4.2). Osanai et al. (2013) describe the Sør Rondane Suture as a feature that separates areas of different metamorphic grades but preserves no evidence of significant thrusting or fault movement as it would be expected within a collision boundary. The SRS rather seems to define a simple shear zone as part of the frontal fold zone of the overthrusting NE terrane over the SW terrane along the Main Tectonic Boundary. Since age and kinematics of the Sør Rondane Suture remain unknown, it might also be possible that it represents a dextral shear zone of late Pan-African age, similar to the MSZ. This is supported by our own field observations at the southern outcrops of Perlebandet, where steeply dipping, approximately E-W oriented foliation planes contain a prominent subhorizontal stretching lineation. However, this does not exclude that this structure has an older contractional increment. Another enigmatic shear zone is inferred to the S of the MSZ, however, this structure is ice-covered and structural data are missing (Figure 4.2). Furthermore, there is no evidence in the aeromagnetic data for the existence of this shear zone (Mieth and Jokat, 2014).

In any case, our data show that the MSZ can be interpreted as a large-scale, at least 120 km long late-Pan-African strike-slip structure of most likely late Ediacaran to Cambrian age. In this regard, Ishikawa et al. (2013) suggests that the eastern Balchenfjella area underwent the most intensive dextral and normal sense shear strain in Sør Rondane. According to the authors, the Groppeheia Shear Zone in this region results from high-grade dextral transpression during late Neoproterozoic times. These and our own observations from the MSZ may indicate that the whole area of Sør Rondane was affected by widespread, significant dextral shear in Pan-African times.

#### 4.5.2 Geodynamic Significance of the MSZ in the EAAO

Major questions regarding the geodynamic evolution of the EAAO in Gondwana concern the location of the suture(s) and the width of this mobile belt. Possible locations of the E/W Gondwana suture in DML (Figure 4.1) were proposed by Moyes et al. (1993), Grunow et al. (1996), Shackleton (1996), Jacobs et al. (1998). Kleinschmidt et al. (2000, 2002) and Helderich et al. (2004) assume that the suture runs from the Shackleton Range into eastern DML passing southern Kirwanveggen to its SE and reaching the Southern Ocean at about 20°E. In agreement with this hypothesis, Riedel et al. (2013) describe a pronounced set of NE trending magnetic



anomalies E of Jutulstraumen, which separates two areas with fundamentally different magnetic signatures. The authors interpreted the Forster Magnetic Anomaly as a major tectonic block boundary and/or suture zone within the EAAO, possibly between E and W Gondwana. Therefore, it is likely that a suture zone may be located W of Sør Rondane, possibly outcropping in the area of Wohlthat Massiv. However, there seems to be no continuation of the Forster Magnetic Anomaly further to the NE of Wohlthat Massiv. It either terminates in this region or is cut off by a yet unknown structure. Further support for this idea are reported by Shiraishi et al. (2008) who describe various types of mafic dykes linked to Pan-African orogenesis in central and eastern DML. Analyses of Sr and Nd isotopic signatures of mafic dykes show different crustal sources for the Mühlig-Hofmann-Gebirge and Sør Rondane (Owada et al., 2008). This indicates a different geologic history for the underlying crust of the Mühlig-Hofmann-Gebirge in central DML and Sør Rondane. Thus, these authors suggest a crustal boundary, potentially related to the suture zone of E and W Gondwana, passing between the Mühlig-Hofmann-Gebirge and Sør Rondane. Furthermore, discrepancies between the timing of magmatic and metamorphic activity in (i) Sør Rondane (Shiraishi et al., 2008; Osanai et al., 2013), the Schirmacher Oasis (Ravikant, 2006; Ravikant et al., 2007) and Yamato-Belgica Mountains (e.g. Shiraishi et al., 2003; 2008) against (ii) central DML for Pan-African (Jacobs et al., 2003b) as well as Grenvillian events (Elburg et al., in press) support the hypothesis that a possible suture zone that resulted from oblique collision is located between central and eastern DML.

The MSZ separates the SW terrane into (i) a northern subterrane with ca. 650-600 Ma greenschist- to granulite-facies peak metamorphism and 590-530 Ma retrogression (Shiraishi et al., 2008; Osanai et al., 2013) and (ii) a southern GTTG subterrane consisting of juvenile rocks with early Neoproterozoic protolith ages of ca. 995-920 Ma (Kamei et al., 2013; Elburg et al., 2015) and greenschist to lower amphibolite-facies thermal overprint at ca. 590-530 Ma (Osanai et al., 2013). The northern subterrane shows in many aspects close similarities to the area of Schirmacher Oasis, where Pan-African high-grade metamorphism is not younger than ca. 600 Ma and has thus clear “East African” affinities (e.g., Ravikant et al., 2007; Boger, 2011; Osanai et al., 2013). In contrast, the rocks of the GTTG subterrane are interpreted to have formed in an intra-oceanic arc environment with affinities to the Indo-Antarctic Rayner complex further to the E rather than the central and western DML basement (Elburg et al., 2015). On a mesoscopic scale, the GTTG subterrane contains large domains with apparently completely undeformed igneous textures, whereas strain seems to concentrate at its northern border along the MSZ and in discrete shear zones paralleling MSZ-related fabrics. So far, our observations do not provide any proof of pervasive deformation and high-grade >600 Ma old reworking of the GTTG subterrane. The rather weak tectonic overprint of the main body of the TTG subterrane could be explained by strong strain partitioning due to rheology contrasts between the plutonic rocks and the neighboring metasedimentary units. Therefore, the MSZ marks the boundary between two major lithotectonic units and separates “East African”-type crust in the N from Rayner-age, Indo-Antarctic crust in the S. The MSZ does, on the other hand, not represent the eastern margin of the EAAO as previously speculated (e.g. Mieth and Jokat, 2014). This is indicated by new geological evidence and geochronological data from previously unvisited nunataks W of Sør Rondane proving the presence of similar Rayner-age, ca. 1000-900 Ma old juvenile arc and metasedimentary cover rocks, however, with intense medium- to high-grade reworking at ca. 630-520 Ma and abundant felsic melt injections (Jacobs et al.,



2015). This region is characterized by a pronounced NW-SE trending magnetic pattern, namely the SE DML Province (Mieth and Jokat, 2014), which terminates at the Forster Magnetic Anomaly to the NW and continues into the ice-covered region S of Sør Rondane (Mieth et al., 2014). The SE DML Province may thus represent the westward extension of Rayner-age crust of accretionary origin, which has suffered protracted Pan-African overprint and abuts at the Foster Magnetic Anomaly (Jacobs et al., 2015). The north-eastern margin of the SE DML Province marks the boundary between its typical weak magnetic anomaly pattern with elongated positive anomalies to the SW and a pronounced magnetic low to the NE. This line can tentatively be traced from NE of Schirmacher Oasis (Mieth and Jokat, 2014) to the region S of Sør Rondane (Mieth et al., 2014) and may thus be referred to as the Schirmacher-Rondane Lineament (Figure 4.8). Due to the close similarities in the geology of the Schirmacher Oasis and Sør Rondane metamorphic basement N of the MSZ, it may be assumed that the Schirmacher-Rondane Lineament coincides with a major NW-SE striking shear zone with considerable dextral off-set. Consequently, the MSZ may be regarded to be part of this major shear system transecting the eastern DML basement. The high-grade metamorphic basement of DML is characterized by a number of large-scale shear zones of likely late Pan-African age, which are shown in the tectonic diagram of Figure 4.8b. These shear zones include from W to E the dextral Heimefront Shear Zone (e.g. Jacobs et al., 1998; 2009) and the sinistral South Kirwanveggen Shear Zone in western DML (e.g. Helferich et al., 2004), the sinistral South Orvin Shear Zone in central DML (e.g. Bauer and Siemes, 2004), and the dextral MSZ in eastern DML.

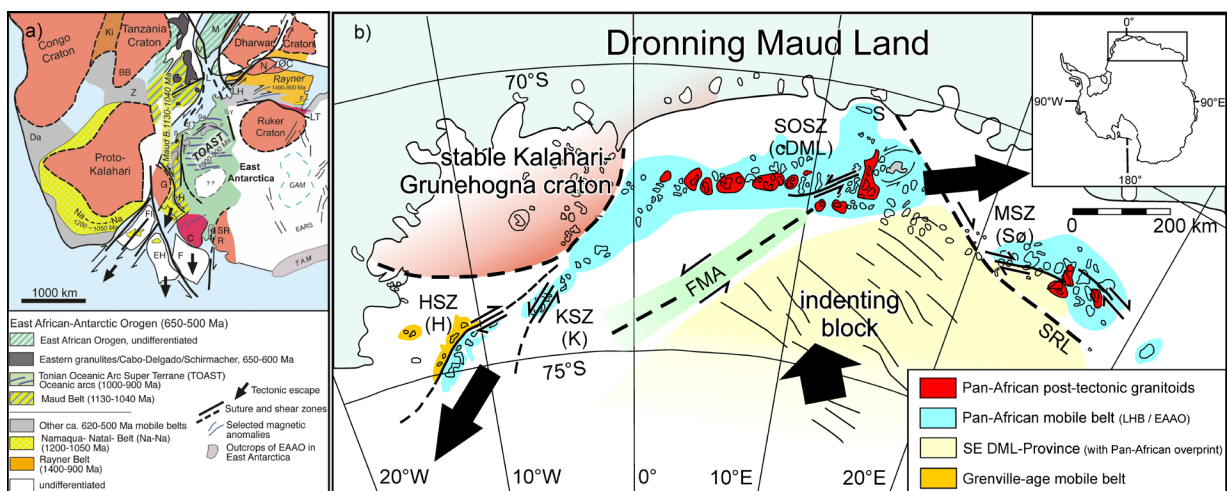


Figure 4.8: Lateral tectonic escape model for the southern and north-eastern terminations of the East African-Antarctic orogen (EAAO) within a) Gondwana configuration (modified after Jacobs et al. 2015) and within b) Dronning Maud Land. The dextral MSZ and the sinistral South Orvin Shear Zone are interpreted in terms of NE directed escape of the EAAO (geographic NE is related to the relative positions of Africa and Antarctica within Gondwana). For further explanations see text.

The MSZ may be interpreted in terms of an important strike-slip zone probably related to NE-directed lateral escape of the EAAO, possibly together with the presumably coeval South Orvin Shear Zone. The geographic direction “NE” is related to the relative positions of Africa and Antarctica within the supercontinent Gondwana. This model would fit well to the bilateral tectonic escape of the EAAO proposed by Jacobs and Thomas (2004; Figure 8a). We suggest that the Heimefront Shear Zone together with the South Kirwanveggen Shear Zone represents

part of the S-directed and the South Orvin Shear Zone and the MSZ with the Schirmacher-Rondane Lineament part of the NE-directed branch of this bilateral system. The SE DML Province may be regarded as the indenting block, while the Grunehogna-Kalahari Craton acted as its stable counterpart on the opposite side of the EAAO, forcing the S- and NE-ward translation of various tectonic blocks.

Focussing on our target area, in particular, NE-directed escape of crustal blocks and the accommodation of space may have been facilitated by (i) subduction and ocean closure between Indo-Antarctica and Australo-Antarctica between 560 and 520 Ma (e.g. Boger and Miller, 2004; Boger, 2011), (ii) a late Neoproterozoic to early Cambrian passive continental margin setting along N and NE Indo-Antarctica (e.g. Jiang et al., 2003; Boger and Miller, 2004), and (iii) the presence of several crustal blocks and fragments to the N and NE of the greater Sør Rondane region, which formed during previous collisional events of Grenville and Pan-African age (Figure 4.8a; Boger, 2011; Jacobs et al., 2015). Large numbers of late- to post-collisional igneous rocks are found in central DML, decreasing in amount towards western and eastern DML. Jacobs et al. (2008b) presume that these ca. 510 Ma high temperature A2-type granitoids result from a delaminated thickened lithosphere, followed by the influx of asthenospheric mantle material and subsequent orogenic collapse. The most frequent occurrences of these granitic intrusions may represent the central part of the collapsing EAAO. This in turn is accompanied by the development of the late tectonic Pan-African shear systems and bilateral escape tectonics in western and eastern DML.

## 4.6 Conclusions

- i) The MSZ is characterized by dextral high-strain ductile deformation under mostly upper low- to medium-grade metamorphic conditions. Except for its northern margin, MSZ-related deformation in the GTTG subterrane is limited to discrete low-grade shear zones.
- ii) The activity of the MSZ can be narrowed down based on relative age constraints with dated magmatic rocks between an upper age around 560 Ma and a lower age of ca. 530 Ma. Therefore, the MSZ can be interpreted as a large-scale late-Pan-African strike-slip structure of late Ediacaran to Cambrian age.
- iii) The MSZ represents an important lithotectonic boundary separating “East-African” from “Indo-Antarctic” Rayner-age crust presumably close to the eastern margin of the EAAO, which is assumed to be located further S in the ice-covered region.
- iv) Together with the Heimefront, Kirwanveggen and South Orvin shear zones, the MSZ may be related to bipolar lateral escape of the EAAO towards the NE and S. In this scenario, the central part of this orogen, preserved today in central DML, is characterized by the delamination of thickened lithosphere and followed by the influx of asthenospheric mantle material and subsequent orogenic collapse associated with late Pan-African opposite-directed tectonic escape along major regional shear zones.



## 4.7 Acknowledgements

This study was part of the collaborative research program ‘Geodynamic Evolution of East Antarctica’ (GEA) of the German Federal Institute of Geosciences and Natural Resources (BGR) and the Alfred Wegener Institute Helmholtz Centre for Polar and Marine Research (AWI). J. Jacobs, M. Elburg and N. Krohne are indebted to BGR for the invitation to participate in the expeditions and to AWI for providing polar clothing.

We would like to express our sincere thanks to Alain Hubert and his team at the Belgian Princess Elisabeth station for the wonderful time there and support in the field. Many thanks go also to the crew of Sky Heli, Germany, who took the geological party safely to the field and back to the station. This study was supported by the Deutsche Forschungsgemeinschaft (Grants LA1080/9 to A. Läufer and LI 745/15 to F. Lisker) in the framework of the priority programme 1158 ‘Antarctic Research with comparative investigations in Arctic ice areas’. M. Elburg was the recipient of an NRF-SANAP grant SNA2011110200002, which is gratefully acknowledged. J. Jacobs received funding through NFR-NARE, which is equally gratefully acknowledged. Finally, we thank Robert Thomas and Wilfried Bauer for the critical and helpful reviews. Data can be provided on request by contacting A. Ruppel or A. Läufer (BGR).



## Chapter 5

# 5. New Geophysical Data from a Key Region in East Antarctica: Estimates for the Spatial Extent of the Tonian Oceanic Arc Super Terrane (TOAST)

Antonia Ruppel, Joachim Jacobs, Graeme Eagles, Andreas Läufer, Wilfried Jokat

Key findings:

- New aerogeophysical data reveal subglacial nature of a key region in East Antarctica
- Structure and extent of Neoproterozoic juvenile arc terranes (TOAST) revealed
- Island arc boundaries/major shear zone recognized as major magnetic lineaments
- Spatial extent of the TOAST comparable in size with Antarctic Peninsula

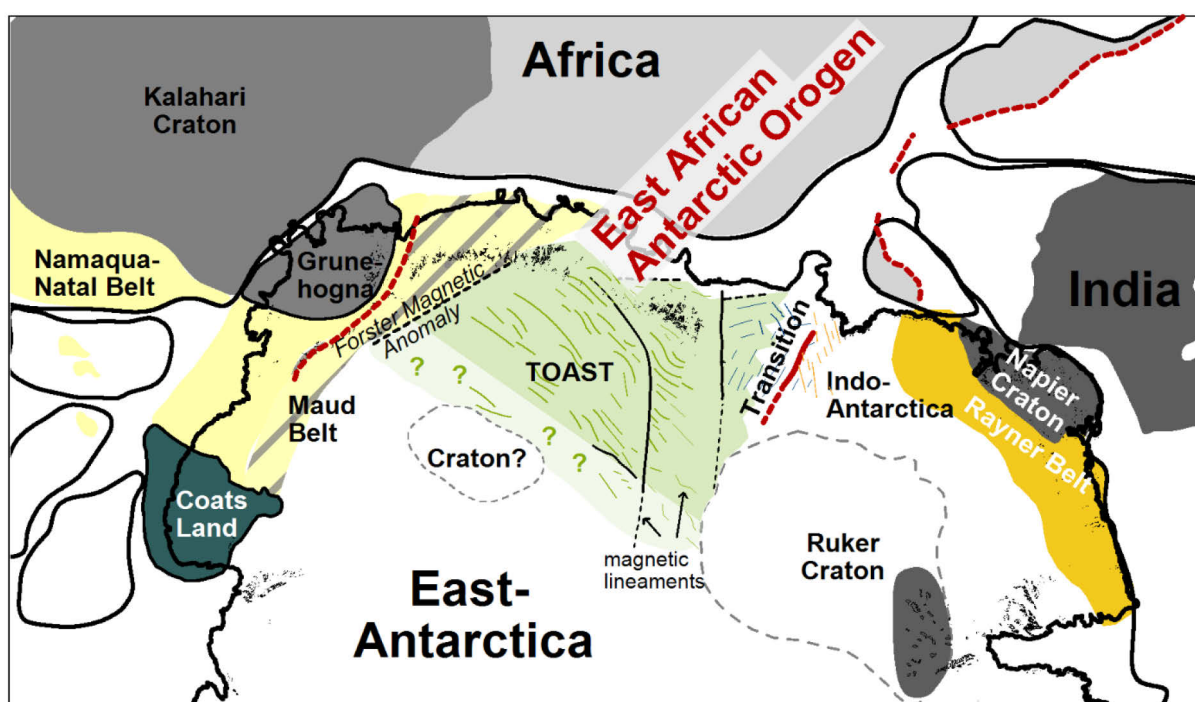


Figure 5.1: Graphical abstract

## 5.1 Abstract

Within Antarctica, eastern Dronning Maud Land (DML) represents a key region for improving our understanding of crustal fragments that were involved in the amalgamation and breakup histories of Rodinia and Gondwana. An aerogeophysical survey was flown during the austral summers 2013/14 and 2014/15 to explore the largely ice-covered region south and east of Sør Rondane. Here, we present 40000 new line kilometer of aeromagnetic data gathered across an area of ca. 295000 km<sup>2</sup> with a 10 km line spacing. Magnetic domains, major lineaments,



locations, and depths of magnetic source bodies are detected from total field data, their tilt derivative, pseudo-gravity, and analytical signal transformations, and from Euler Deconvolution maps. These data are integrated with exposure information from the Sør Rondane, Belgica and the Yamato mountains in order to identify the eastern spatial extent of a major juvenile Early Neoproterozoic crustal province, the Tonian Oceanic Arc Super Terrane (TOAST). Magnetic data reveal a characteristic pattern with NW-SE trending elongated magnetic anomalies to the south of Sør Rondane. This area is interpreted as the eastward continuation of the distinct SE DML Province and therefore of the TOAST. Major curvilinear magnetic anomalies of several hundreds of kilometers length dissect the region south and southwest of Sør Rondane. These may represent boundaries of individual oceanic arc terrane or alternatively major Pan-African shear zones. A significant change of the magnetic anomaly pattern ca. 800 km inland of Sør Rondane may indicate the southern minimum extent of the TOAST. Magnetic anomalies of varying size, amplitude, and orientation suggest a complex transitional area between the Belgica and Yamato Mts., which appears to separate the TOAST from an Indo-Antarctic craton to the east. The new data suggest that the TOAST is comparable in size with the Antarctic Peninsula and therefore represents a significant piece of Neoproterozoic crustal addition. It originated at the periphery or outboard of Rodinia and is a remnant of the Mozambique Ocean.

## 5.2 Introduction

East Antarctica amalgamated along a network of Late Neoproterozoic/Early Palaeozoic mobile belts during the formation of Gondwana (e.g. Shiraishi et al., 1994; Jacobs et al., 1998; Fitzsimons, 2000b; Meert, 2003). Prior to the Neoproterozoic, these fragments were variously attached to Kalahari, India and Australia (e.g. Dalziel, 1991; e.g. Moyes et al., 1993; Boger et al., 2001; Fitzsimons, 2003; Jacobs et al., 2008a). However, the geometries of these blocks and the outlines of mobile belts and suture zones between them are poorly known because of the mostly ice-covered nature of Antarctica. In Antarctica, systematic aerogeophysical surveys have proven to be very valuable for characterizing the subglacial basement, by integration with surface geology from the continent's scarce outcrops (e.g. Golynsky et al., 2007; Riedel et al., 2013; Mieth and Jokat, 2014; Mieth et al., 2014).

Dronning Maud Land (DML) is a key region for better understanding the amalgamation of various parts of East Antarctica during the reassembly of Rodinia into Gondwana (Figure 5.2). DML is dissected by the major ca. 650-500 Ma East African-Antarctic Orogen, which is part of the trans-Gondwana network of Late Neoproterozoic/Early Palaeozoic mobile belts (Jacobs et al., 1998; 2003a; Jacobs and Thomas, 2004). Various parts of east and west Gondwana collided along the East African-Antarctic Orogen, forming a long (>8000 km) mobile belt that displays a variety of tectonic styles along its length (e.g. Stern, 1994; Shackleton, 1996; Jacobs et al., 1998; Fritz et al., 2013). Significant portions of the East African-Antarctic Orogen are interpretable as products of an early accretionary tectonic stage between juvenile arc terranes, i.e. the Arabian-Nubian Shield (e.g. Stern, 1994; 2002; Johnson and Woldehaimanot, 2003; Johnson et al., 2011). Other parts are dominated by evidence for continent-continent collision (e.g. Muhongo and Lenoir, 1994; Kröner, 2001). The East African-Antarctic Orogen in Antarctica was long interpreted as a typical Himalayan-style continent-continent Himalayan-style continent-continent collision orogeny (Jacobs et al., 1998; Jacobs and Thomas, 2004).



However, evidence for significant Tonian juvenile oceanic arc terranes, the so-called Tonian Oceanic Arc Super Terrane (TOAST), were recently recognized in eastern DML. The TOAST has similarities to the Arabian-Nubian Shield and is interpreted to represent remnants of the Mozambique Ocean (Elburg et al., 2015; Jacobs et al., 2015; 2017).

In this contribution, we present a new large aeromagnetic data set to the south and east of Sør Rondane, eastern DML, surveyed during the austral summers 2013/14 and 2014/15 as part of GEA / WEGAS, a long-term joint project of the German Federal Institute for Geosciences and Natural Resources (BGR) and the Alfred Wegener Institute, Helmholtz Centre for Polar and Marine Research (AWI). The survey returned 40000 line kilometers of new aerogeophysical data covering an important region in the eastern part of the TOAST and its transition to cratonic Indo-Antarctica. The main objective of this study was to better constrain the eastern and southern extent of the TOAST and to provide estimates for its spatial extent by integrating the new data with existing aerogeophysical data.

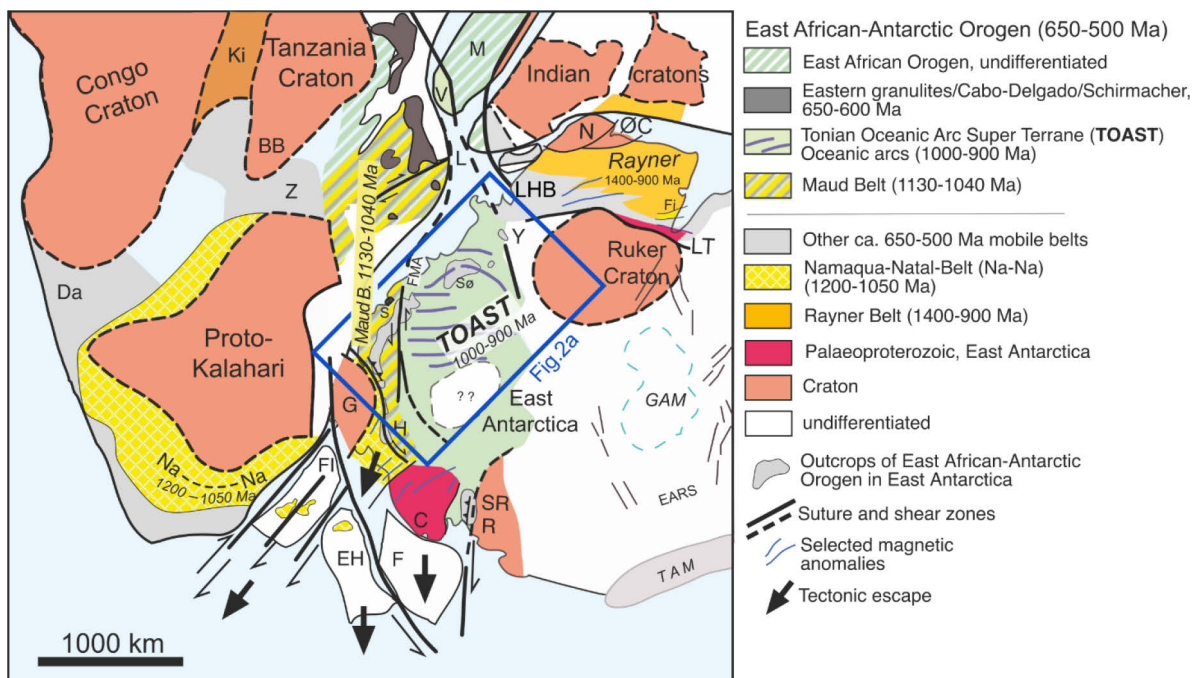


Figure 5.2: Study area in East Antarctica and within Gondwana at ca. 500 Ma after Jacobs and Thomas (2004) and Jacobs et al. (2015) and references therein. Blue outline indicates the position of the study area within DML. Africa is shown fixed to its present-day coordinates, the other continents are re-arranged accordingly. Abbreviations: C, Coats Land; DML, Dronning Maud Land; Da, Damara belt; EH, Ellsworth-Haag; F, Filchner block; FI, Falkland Islands; G, Grunehogna; H, Heimefrontfjella; L, Lurio Belt; LT, Lambert Terrane; N, Napier Complex; Na-Na, Namaqua-Natal; ØC, Øygarden Complex; S, Schirmacher Oasis; Sør, Sør Rondane, SR, Shackleton Range; TAM, Transantarctic Mts., LHB, Lützow-Holm Bay; M, Madagascar; R, Read Block; V, Vohibori; Y, Yamato Mts.; Z, Zambesi belt.

### 5.3 Geological-Geophysical Background of the Study Area and Adjacent Regions (from W to E)

The study area lies in eastern DML, immediately to the south and east of the Sør Rondane Mts. The Sør Rondane Mts. and small scattered nunataks to the west (Figure 5.3a) represent the most extensive and relatively well studied outcrops in the region. In the central and eastern part of



the study area, the remote Belgica Mts. and Yamato Mts. are much more poorly investigated. Just east of the Yamato Mts., a much better data base exists for the coastal Lützow-Holm Bay region. Most of the excellent geological work in these regions has been completed by the Belgian and Japanese Antarctic Research Programs (e.g. Van Autenboer and Loy, 1972; Shiraishi et al., 2008). The geology of the exposed regions is briefly summarized in the following.

### 5.3.1 Sør Rondane

The Sør Rondane Mts. are subdivided into three major tectonic units, separated by two major structural discontinuities. The units comprise the NE Terrane and the northern and southern parts of the SW Terrane (e.g. Osanai et al., 2013; Mieth et al., 2014). The NE Terrane is separated from the SW Terrane by the Main Tectonic Boundary, whilst the subdivision of the SW Terrane is achieved across the Main Shear Zone.

The southern part of the SW Terrane consists mainly of a little deformed gabbro-tonalite-trondhjemite-granodiorite complex, which is U-Pb zircon dated at ca. 1000-900 Ma (Kamei et al., 2013; Elburg et al., 2015). Their geochemistry, Sm-Nd and zircon Hf-signature, as well as the lack of older inheritance characterizes these gabbro-tonalite-trondhjemite-granodiorite complex as part of a juvenile oceanic arc complex (Elburg et al., 2015). Together with similar rocks in small nunataks to the west, these rocks represent the type locality for the TOAST (Jacobs et al., 2017). Minor crustal additions are still recorded at ca. 770 Ma (Kamei et al., 2013). The northern part of the SW Terrane consists of greenschist to granulite facies metasedimentary and meta-igneous rocks, with youngest detrital zircon ages of ca. 700 Ma (Otsuji et al., 2013; Owada et al., 2013). Peak metamorphic conditions are dated at ca. 640-600 Ma and are associated with an anticlockwise PT-path (Adachi et al., 2013). The northern SW Terrane and the gabbro-tonalite-trondhjemite-granodiorite complex are separated by the dextral Main Shear Zone, which represents an important lithospheric structure of Ediacaran to Cambrian age (Ruppel et al., 2015).

The amphibolite- to granulite facies NE Terrane is predominantly composed of metasupracrustal rocks with youngest detrital zircon ages of ca. 750 Ma; no basement to these rocks is recognized so far (Shiraishi et al., 2008). U-Pb zircon dating indicates granulite-facies metamorphic overprint associated with a counterclockwise PT-path at ca. 640-600 Ma and retrograde metamorphism at ca. 590-530 Ma, the latter of which is related to orogenic collapse. Contrasting PT-paths on either side of the Main Tectonic Boundary are interpreted to result from thrusting of the NE Terrane over the SE Terrane (Osanai et al., 2013). Rare inherited zircons with Archean and late Mesoproterozoic ages may suggest proximity to a continental source (Elburg et al. (2015). In general, the Sør Rondane Mts. show long-lasting tectono-metamorphism and associated magmatism between ca. 650 and 500 Ma, which is related to protracted accretion and collision in this part of the East African-Antarctic Orogen (Elburg et al., 2016).



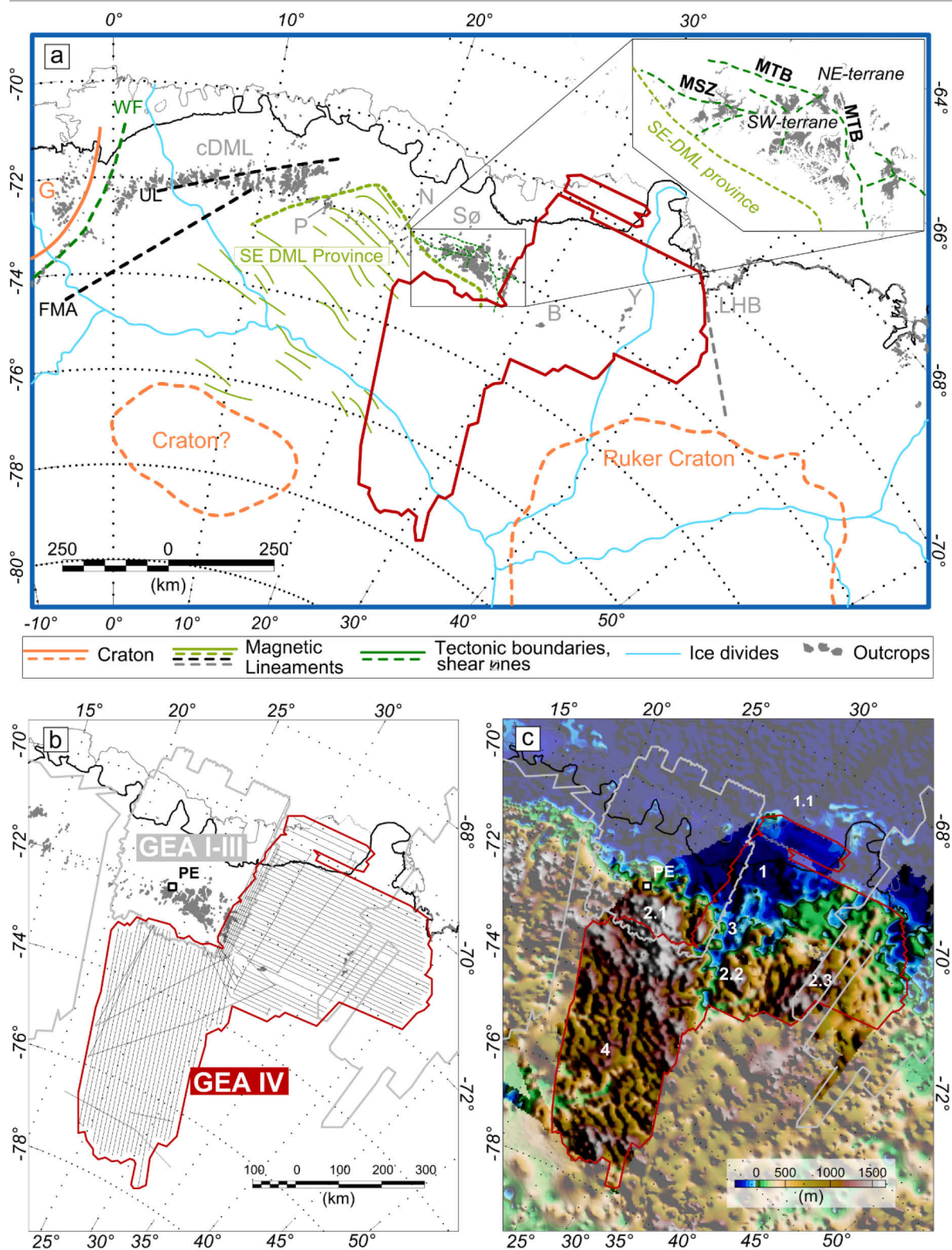


Figure 5.3: Overview and location of the study area within eastern DML. New geophysical survey area is outlined (red), grounding line (thick black), ice shelf edge (thin grey). a) Hitherto identified magnetic lineaments, tectonic boundaries, and major ice divides adjacent to the survey area. Magnetic anomalies/lineaments / boundaries after Riedel et al. (2013); (Nogi et al., 2013); Mieth et al. (2014); Mieth and Jokat (2014); ice divides after Rignot et al. (2011). Inset indicates the tectonic subdivision of Sør Rondane in a NE and SW Terrane separated by the Main Tectonic Boundary (MTB). The SW Terrane is further separated by the dextral Main Shear Zone (MSZ) in a northern and southern part. b) Location of new GEA IV aerogeophysical survey and indicated geophysical flight lines with a line separation of 10 km (thin black), adjacent surveys (thick grey). c) New bed topography (Eagles et al., 2018) superimposed on Bedmap 2 topography (Fretwell et al., 2013). The numbers (1-4) are discussed in the



*text. Abbreviations: B, Belgica Mts.; cDML, central Dronning Maud Land; FMA, Forster Magnetic Anomaly; G, Grunehogna; LHB, Lützow-Holm Bay; N, nunataks; P, Payerfjellet; Sør, Sør Rondane; WF, western front of the EAAO; Y, Yamato Mts..*

### 5.3.2 Belgica Mts. and Yamato Mts.

The Belgica and Yamato Mts. are located in the eastern survey area and represent an overall poorly studied region within DML. The geology of Belgica Mts. was first described by Van Autenboer and Loy (1972) as a small isolated mountain massif consisting of migmatized biotite-hornblende gneisses intercalated with marbles. The gneisses are intruded by coarser grained granite and two generations of younger dyke systems, which are also of granitic composition. The authors note the close correlation with Sør Rondane. The Yamato Mts. are characterized by metamorphic rocks, mainly composed of amphibolite-facies quartzo-feldspathic and intermediate gneisses, intermingled with low-pressure granulite facies rocks (cf. Hiroi et al., 1991; Shiraishi et al., 2003). Two thermal events at ca. 620 Ma and ca. 535 Ma may be associated with granulite facies metamorphism and amphibolite facies metamorphism, respectively (Shiraishi et al., 1982; Shiraishi et al., 2003). These ages indicate a similar history as in the Sør Rondane Mts. (Shiraishi et al., 2003). Metamorphic rocks are intruded by voluminous syenites which are considered to have been emplaced during the waning stage of granulite facies metamorphism (Zhao et al., 1995).

Based on sparse protolith age data ( $T_{DM}$  model ages), Shiraishi et al. (2008) suggest that the Belgica and Yamato Mts. may represent the easternmost parts of the ‘Sør Rondane Terrane’.

### 5.3.3 Lützow-Holm Bay

The Lützow-Holm Bay Complex in the easternmost part of the study area consists of high-grade metamorphic rocks with increasing metamorphic grade from upper amphibolite-facies in the east to granulite-facies in the southwest (Hiroi et al., 1991). Ultrahigh-temperature metamorphism in the Lützow-Holm Bay Complex was U-Pb zircon dated at ca. 550-520 Ma. (Motoyoshi and Ishikawa, 1997; Shiraishi et al., 1992b; 1994; 2003). The southeastern part of the Lützow-Holm Bay Complex is interpreted to have involved the collision of several volcanic arcs and oceanic components with Archean-Palaeoproterozoic crust, as evidenced by  $T_{DM}$  model ages (Shiraishi et al., 2008). Recent studies suggest a subdivision of the Lützow-Holm Bay Complex into three units (i) a Neoproterozoic–Early Palaeoproterozoic (ca. 2.5 Ga) unit in the southern Lützow-Holm Bay Complex, (ii) a Neoproterozoic (ca. 1.0 Ga) unit of juvenile character in the northern Lützow-Holm Bay Complex, and (iii) a supracrustal unit with fragments of Neoproterozoic to Neoproterozoic (ca. 2.5, 1.8, and 1.0 Ga) magmatic arc in the central Lützow-Holm Bay Complex (Tsunogae et al., 2015, 2016; Takahashi et al., 2017).

### 5.3.4 Tonian Oceanic Arc Super Terrane (TOAST)

The Tonian Oceanic Arc Super Terrane (Jacobs et al., 2015) was recognized by integrating geology and geophysics of the region to the west of the study area. First geophysical evidence for a major discrete crustal block was provided by aeromagnetic data from central DML (Mieth and Jokat, 2014). These authors identified a major distinct magnetic province (SE DML province) east of the Forster Magnetic Anomaly and to the south of central DML. This province is characterized by NW-SE trending, narrow (10-20 km) and elongated (120-200 km) positive,



small amplitude anomalies (50-100 nT) within a rather weak magnetic anomaly field/background (grey lines). This newly identified block was then interpreted as an orogenic belt of unknown age, whereas the structures were inferred to predate the Forster Magnetic Anomaly (Mieth et al., 2014).

The first geological evidence for the history of the TOAST documents a main phase of subduction in the form of juvenile magmatic rocks from around 995-975 Ma, followed by a younger phase around 960-925 Ma in the SW Terrane of Sør Rondane (Kamei et al., 2013; Elburg et al., 2015). Study of the mostly ice-covered area between central DML and Sør Rondane also revealed geochronological ages of ca. 1000-900 Ma for juvenile basement and new geochemistry data that are very similar to the SW Terrane of Sør Rondane (Elburg et al., 2015; Jacobs et al., 2015). The geological findings from between central DML and Sør Rondane correlate spatially with the aeromagnetic SE DML province (Mieth and Jokat, 2014) and suggest that the latter represents an extensive region of Neoproterozoic oceanic arcs, interpreted as remnants of the Mozambique Ocean (Elburg et al., 2015; Jacobs et al., 2015).

Further evidence for the extent of the TOAST and the geologic nature of its distinct magnetic domains has been obtained indirectly, by analyses of moraine material drained from the interior of East Antarctica. The north-directed ice flow in the region occurs within a catchment that is limited by a major ice divide ca. 800 km to the south of the Sør Rondane Mts. (Rignot et al., 2011; Jacobs et al., 2017). Analyses of a large detrital U-Pb zircon data set from glacial drift sourced out of this catchment strengthens the interpretation that the TOAST extends at least as far as the ice divide (Jacobs et al., 2017). A significant Stenian age peak correlates with juvenile grey granodioritic gneisses that represent a precursor of the TOAST. A few Palaeoproterozoic zircon grains from the easternmost samples may indicate the vicinity to a craton farther to the east, e.g. the Ruker Craton (Figure 5.3a).

The western extent of the TOAST is delineated by the Forster Magnetic Anomaly, at which it is juxtaposed with Grenville-aged rocks of the Maud Belt (Riedel et al., 2013; Jacobs et al., 2015). The southern and eastern extents of the TOAST are so far very speculative.

## 5.4 Data Acquisition and Processing

Airborne geophysical data were collected by using the AWI Basler aircraft Polar 5 and 6. Two target areas south (73°S/21°E to 77.5°S/32°E) and east (70.5°S/28°E to 72°S/40°E) of Sør Rondane were surveyed from the Belgian Princess Elisabeth Station (PE). These areas are attached to previous surveys of the GEA I-III campaigns covering Sør Rondane and the ice shelves north of it (Mieth et al., 2014). The survey lines were flown with a flight line spacing of 10 km in N-S direction south of Sør Rondane and in an E-W direction east of it (Figure 5.3b). In total, close to 40000 line kilometers of radar, gravity and magnetic data were collected. Radar and gravity data are presented and interpreted in detail (Eagles et al., 2018).

The acquisition of magnetic data was carried out with a Scintrex Cs-3 caesium vapour magnetometer mounted in a tail boom. A fuselage-mounted three-component Billingsley TFM 100 fluxgate magnetometer was used for magnetic compensation. Diurnal variations of the magnetic field were recorded with a magnetic base station deposited near the airfield of Princess Elisabeth station. Records from a year-round magnetic base station at Syowa were used for correction of data gaps and comparison. Processing of magnetic data was carried out using the geophysical software Oasis Montaj by Geosoft. The work flow included de-spiking, core-field



and diurnal variation corrections as well as statistical and micro-levelling procedures. The final data were gridded with a grid cell size of 3 km. In order to simplify the interpretation of magnetic anomalies, the magnetic pattern was transformed by a grid-based reduction to the pole.

Advanced filtering and transformation techniques including upward continuation, tilt derivative, pseudo-gravity and the analytical signal were applied to the magnetic data to enhance prominent magnetic anomaly patterns. Upward continuation attenuates high wavenumber anomalies associated with shallow magnetic sources and enhances regional magnetic anomalies resulting from deeper sources (Blakely, 1995). The upward continuation was calculated to an observation level of 10 km above sea level. Calculation of the tilt derivative was completed using the pole reduced magnetic anomaly grid, and can be used to enhance positive magnetic lineaments and to map structural trends (Miller and Singh, 1994; Verduzco et al., 2004). Peaks in the maximum horizontal gradient of pseudo-gravity are helpful in locating the edges of magnetic source bodies and magnetic lineaments (Cordell and Grauch, 1982; Blakely and Simpson, 1986). Further, the analytic signal and calculation of located Euler depth can be used to locate the edges and corresponding depths of magnetic source bodies (Roest et al., 1992).

## 5.5 Results

### 5.5.1 Bed Topography

The bed topography is subdivided into a northern and southern part, separated by a seawards-facing escarpment (Figure 5.3c, Eagles et al., 2018). A deep flat subglacial plain characterizes the northern part whereas the southern part hosts a south dipping low-relief subglacial landscape. Coastal areas (1) are characterized by topographic elevations below sea level (bsl) reaching down to 3000 m bsl (1.1). The E-W trending mountain range, whose seawards-facing escarpment hosts Sør Rondane (2.1) exhibits an average altitude of 2000 m above sea level (asl) with highest peaks reaching ca. 3000 m asl. Further subglacial topographic highs surround the outcropping Belgica Mts. (2.2) and Yamato Mts. (2.3). Sør Rondane and the Belgica Mts. are separated from one another by a NNW-SSE trending trough (3) underlying the West Ragnhild glacier. The hinterland topography of eastern DML (4) has an average altitude of 900 m asl. and is characterized by deeply incised v-shaped valleys reaching up to 110 m asl. This WSW-directed structures are interpreted as a pre-glacial fluvial landscape only lightly modified and preserved underneath a cold-based ice sheet (Eagles et al., 2018).

### 5.5.2 Airborne Magnetics

By combining the new magnetic data with those from the first three GEA campaigns (GEA I-III, Mieth et al., 2014), we generated new aeromagnetic anomaly maps and enhancements for the area across and adjacent to Sør Rondane in the south and east (Figures 5.4, 5.5, 5.6). Magnetic data and their enhancements were used to identify magnetic domains, major structural trends and possible magnetic sources. The continuation of the observed magnetic anomaly pattern is indicated in Figure 5.7. Here, data of this study and the former GEA I-III surveys over Sør Rondane are superimposed on the VISA magnetic data compilation of DML in the west



(Mieth and Jokat, 2014), and the lower-resolution ADMAP dataset (Golynsky et al., 2007) in the east. The magnetic anomaly pattern south and east of Sør Rondane is characterized by moderate amplitudes between  $-225$  and  $+390$  nT (Figure 5.4a). The highest anomaly values can be observed offshore, to the far east of Yamato Mts. and to the SSE of Sør Rondane. Negative magnetic anomalies occur close to the coast as well as in the southernmost part of the survey area.

The analyses of aeromagnetic data and their enhancements, together with their correlations to magnetic anomaly data from adjacent areas, lead to the identification of four magnetic domains ('I-IV'), separated by three major boundaries/lineaments ('a-c'), as labeled in Figure 5.4: Domain 'I' is characterized by positive and elongated NW-SE trending magnetic anomalies with amplitudes of ca. 50-100 nT. This domain is further subdivided in a northern subdomain 'Ia' with positive magnetic anomalies reaching up to 300 nT and a southern subdomain 'Ib' with maximum values of only 40 nT. The division into two subdomains is apparent in the long wavelength anomaly pattern indicated by the upward-continued magnetic anomaly data (Figure 5.4b), whereas the tilt derivative map emphasizes the subdomains' short wavelength trend similarities (Figure 5.4c). The magnetic low of subdomain 'Ib', with minimum values of  $-200$  nT, is also observable in the older low-resolution data compiled for ADMAP (Golynsky et al., 2007). The northeastern extent of domain 'I' is well confined by boundary 'a', which is characterized by a curved, approximately NNW-SSE directed, and partly discontinuous positive magnetic anomaly. This lineament can be traced in the survey area over ca. 550 km. Upward continued magnetic anomaly data support the definition of boundary 'a', which is indicated by a change from low (domain 'I') to higher magnetic values (domain 'II'). The curvilinear trend of this major lineament can be well observed in the tilt derivative map (Figure 5.4c), which highlights how its orientation changes from NW-SE in the northern part to NNW-SSE in the southern part. Magnetic anomalies west and east of boundary 'a' appear to be dragged into the curvilinear boundary, indicating a dextral sense of shear.

Domain 'II' is located east of boundary 'a' and shows similar curved, elongated positive NW-SE directed magnetic anomalies with amplitudes of 50-150 nT and values up to 380 nT. This domain is characterized by higher frequency magnetic anomalies than those in domain 'I'. Elongated (30-50 km), positive magnetic anomalies show a NW-SE orientation within domain 'II'. Further, the upward continuation of magnetic anomaly data reveals a distinct ENE directed magnetic low to the SE of Sør Rondane (L4). Boundary 'b' is the western boundary of domain 'II' with domain 'III' (Figure 5.4d). This boundary is characterized by a positive NE-SW trending magnetic lineament that is approximately parallel to that of the southern part of boundary 'a'. This lineament is very apparent in the tilt derivative map (Figure 5.4c). The ADMAP data suggest that boundary 'b' can be traced beyond the survey area to continue significantly farther inland (Figure 5.7).

Examination of the magnetic anomaly data, their upward continuation and tilt derivative, reveals a complex anomaly pattern with varying amplitudes, intensities, and trend directions in magnetic domain 'III'. High frequency, negative magnetic anomalies dominate the coastal area. Magnetic lows seem to be well defined in the upward continued anomaly data (L2, L3). Positive magnetic anomalies (up to 240 nT) are dominated by a N-S directed trend in Figure 5.4a, but SW-NE and NW-SE directed trends are also indicated by the tilt derivative. Boundary 'c' is



located between domains 'III' and 'IV' east of two distinct, parallel N-S trending positive magnetic anomalies parallel to the outcrop of the Yamato Mts.

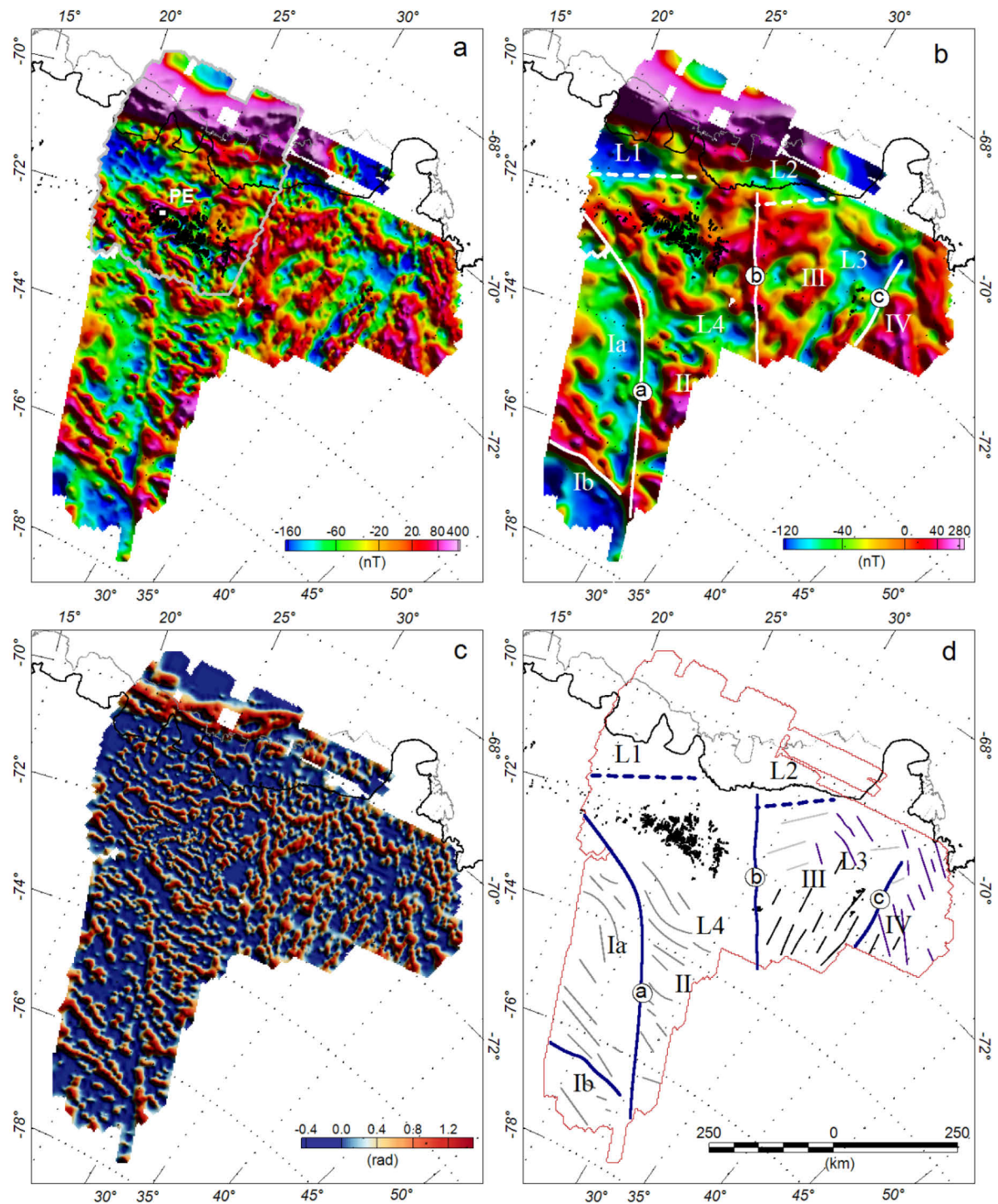


Figure 5.4: Magnetic data of Sør Rondane (GEA I-IV). a) Total magnetic intensity map. Abbreviations: PE, Princess Elisabeth Station. b) Upward continuation of magnetic anomaly data to enhance signatures from deeper crustal sources. White lines show boundaries (a-c) of magnetic domains (I-III). c) Positive tilt derivative map to enhance lineaments and shallow sources. d) Interpretation of magnetic data with same boundaries and magnetic domains compared to b). Trends within the domains are picked along the maxima of the positive tilt derivative. Outcrops (black dots), and the location of the survey (red outline) are indicated. All maps show the grounding line (thick black), and the shelf ice edge (thin grey).



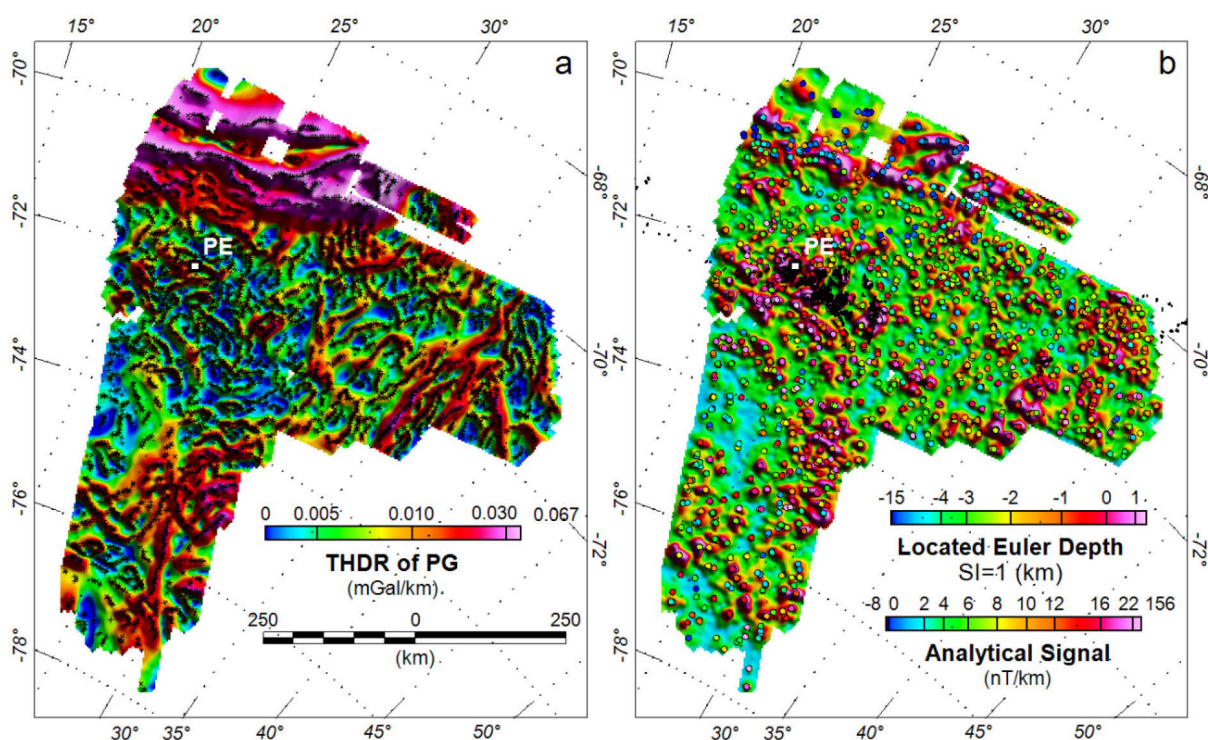


Figure 5.5: Analyses and enhancement of the magnetic anomaly pattern (GEA I-IV). a) Maximum horizontal gradient of pseudo-gravity and indicated peak solutions (+); this analyses is helpful to detect edges of magnetic source bodies and magnetic lineaments. Note the prominent N-S oriented structures in the eastern part of the survey area b) Analytical Signal overlain by Located Euler Depth solution with  $SI=1$  (dyke and sill structures).

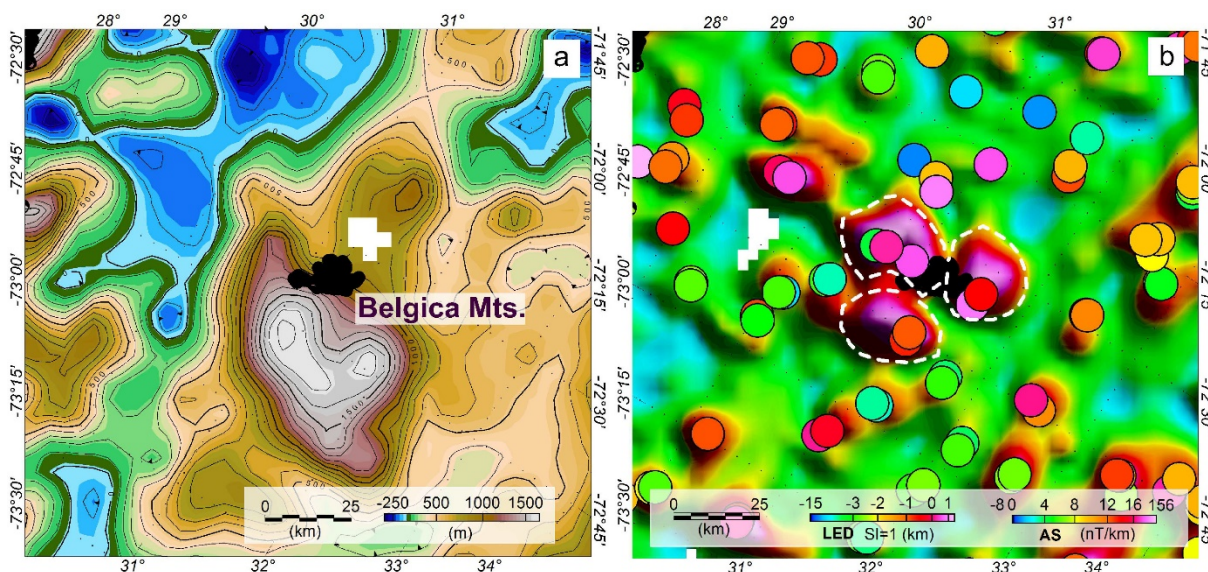


Figure 5.6: Detailed map of Belgica Mts.. a) Bed topography. Contour lines are shown in black, and contour interval is 100 m. b) Analytical Signal overlain by Located Euler Depth solution with  $SI=1$  (dyke and sill structures). Analytical Signal indicates three circular shaped structures with shallow sources most likely related to intrusive bodies.



Domain 'IV', east of boundary 'c', is dominated by positive magnetic anomaly values reaching up to 200 nT. The long wavelength anomaly pattern in the upward continued map indicates a distinct area of high values (Figure 5.4b). The tilt derivative map indicates mainly NNW-SSE directed trends of positive magnetic anomalies. Similar trends are subordinately present in domain 'III'.

Figure 5.5 illustrates further enhancements of the magnetic anomaly data, enabling depth estimates of magnetic source bodies. The maximum horizontal gradient of the pseudo-gravity enhances boundaries 'a'-'c' and indicates similar trends within the individual domains as the tilt derivative. As such, NW-SE oriented structures are present in domains 'I' and 'II', with the trends in domain II more subdued. The map significantly enhances the N-S oriented structures of domain 'III' and suggests a continuous magnetic source along boundary 'c' in the east. The change to a NNE-SSW orientation of possible magnetic source bodies is also evident within domain 'IV'. Located Euler depths are calculated and superimposed on the calculated analytical signal in Figure 5.5b. Relatively shallow depth solutions highlight the areas across and to the SW of Sør Rondane (within domain 'II'), Belgica Mts. and Yamato Mts. In contrast, the coastal area is dominated by deep seated depth solutions for possible source bodies (up to -15 km).

## 5.6 Interpretation and Discussion

The analyses of new aeromagnetic data and their enhancements provide new evidence for the structural architecture of eastern DML. In this section, the new data are correlated with adjacent aeromagnetic data and integrated with exposure information from Sør Rondane and the Belgica and Yamato Mts.. The correlation and integration of geophysical and geological data and their presumed extrapolation provides new evidence for the subglacial tectonic framework and improves knowledge of the spatial extent of the TOAST in eastern DML (Figure 5.7).

### 5.6.1 Spatial Extent of the SE DML Province (Subdomain 'Ia', Boundary 'a', Domain 'II')

Subdomain 'Ia' is characterized by positive, moderate-amplitude, elongate, NW-SE trending magnetic anomalies within an overall subdued magnetic anomaly field. The same characteristics account for the SE DML province. Based on this, subdomain 'Ia' is interpreted as the eastward continuation of the SE DML province (Mieth and Jokat, 2014). Ground-truthing of subdomain 'Ia' is possible at Payerfjellet (Steingarden). Here, U-Pb zircon dating of grey gneiss with igneous protolith (gabbro-tonalite-trondhjemite-granodiorite complex) revealed a crystallization age of ca. 980 Ma and two metamorphic ages of ca. 630 Ma and 560 Ma. The gabbro-tonalite-trondhjemite-granodiorite complex is interpreted to be part of a juvenile oceanic arc complex (part of the TOAST) with a protracted metamorphic overprint (Jacobs et al., 2015). Subdomain 'Ia' is bound to the east by boundary 'a', which is represented by a 700 km long, curvilinear, partly broken positive magnetic lineament (Figure 5.7b, c; including adjacent areas). Domain 'II' has generally higher magnetic values at long wavelengths than domain Ia. Domain 'II' also shows shorter (30-50 km) positive magnetic anomalies at higher frequencies. Despite this, the trend direction of the magnetic anomalies is similar to those in subdomain Ia. Sør Rondane and scattered nunataks to the west crop out at the northern tip of domain 'II'.



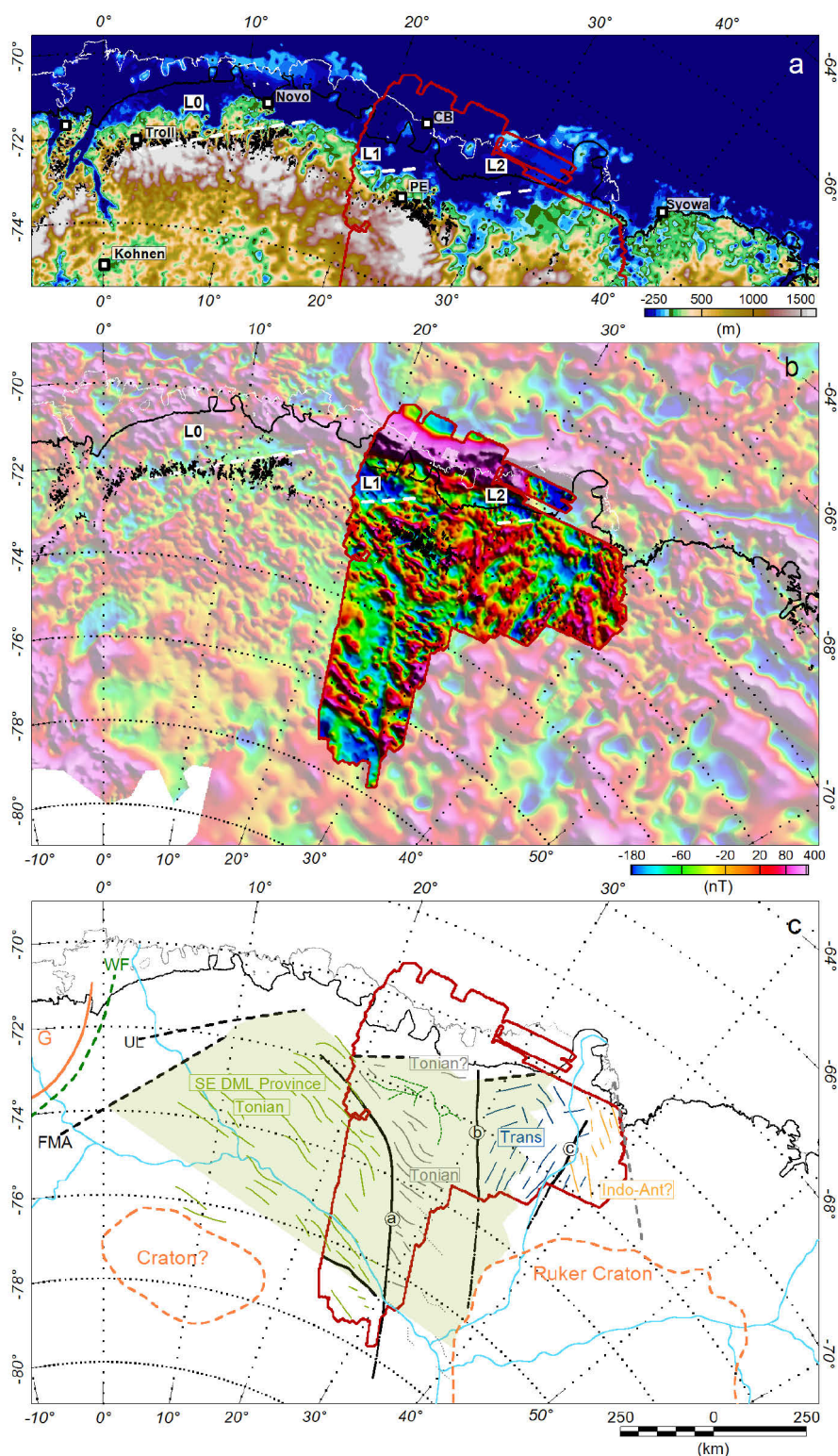


Figure 5.7: Interpretation of geophysical data. a) Bed topography alongshore of DML after (Fretwell et al., 2013). Note the correlation of topographic low plain and distinct magnetic lows (L0-L2); b) Magnetic data and its continuation beyond the survey area. GEA I-IV survey is superimposed on a compilation of magnetic data from the AWI-DML compilation in the west (Mieth and Jokat, 2014) and from ADMAP data (Golynsky et al., 2007) in the east. White lines show boundaries (a-c) of magnetic domains (I-III). c) Interpretation of combined magnetic and geological data. Main structural trends of magnetic domains are indicated within the domains with thin lines. Black lines show boundaries (a-c) of magnetic domains (I-III). Colors refer to individual domains. Boundaries are extrapolated based on magnetic compilation, shown in c). Green region indicates the minimum anticipated extent of the TOAST as discussed in the text. For abbreviation and legend see Figure 5.3.



Southwest Sør Rondane is mainly composed of a gabbro-tonalite-trondhjemite-granodiorite complex of Tonian age and clearly indicates juvenile crust that has evolved within an oceanic arc system (Jacobs et al., 2015). The northeastern part of Sør Rondane consists of high-grade metasedimentary rocks with no exposed basement. Detrital zircons of the metasedimentary rocks provide only minor evidence for an older, pre-Mesoproterozoic provenance (e.g. Shiraishi et al., 2008; Kitano et al., 2016). This is in line with U-Pb zircon analyses of glacial drift from the southern side of Sør Rondane, which also give no evidence for any pre-1100 Ma basement. However, the glacial drift shows an oldest Stenian age peak (1100-1000 Ma) that is largely unknown from exposures and which is the only evidence for pre-Tonian rocks in this region (Jacobs et al., 2017).

Based on the lack of pre-Stenian age components of exposed rocks in domain 'II' and the similarities in magnetic anomaly pattern, we suggest that domain II represents a further eastern continuation of the TOAST. The similarity of U-Pb zircon ages either side of boundary 'a' may indicate that it separates either two different Tonian arc complexes or different crustal levels of a single arc complex. Therefore, boundary 'a' may represent either a terrane boundary or a major shear zone. The anomaly patterns of subdomains 'Ia' and 'II' can be interpreted in terms of dextral simple shear along boundary 'a'. Major dextral transcurrent shearing is also recorded along the Main Shear Zone in the SW Sør Rondane Mts.

### 5.6.2 Southern Extent of the TOAST (Subdomain ,Ib')

The magnetic anomaly pattern of subdomain 'Ib' is significantly different than that in subdomain 'Ia' because of its overall negative anomaly pattern. Despite this, at shorter wavelengths its SE trend directions are very similar to those in subdomain 'Ia'. The lack of exposures prevents ground-truthing of subdomain 'Ib'. Since this region is located south of the ice divide, it is unlikely that domain 'Ib' is represented in samples of the glacial drift analysed by Jacobs et al. (2017). Interpretations of subdomain 'Ib' are thus speculative. Among many possibilities, it may represent (1) a continuation of the TOAST, whose different magnetic signature may be attributed to the contrasting composition of a probably older oceanic arc complex, or (2) a different crustal province of possibly older or cratonic nature, consistent with its negative magnetic anomaly pattern (cf. Grunehogna Craton).

### 5.6.3 Minimum Eastern Extent of the TOAST (Boundaries 'b' & 'c', Domain 'III' & 'IV')

The Belgica Mts. appear to crop out along the newly defined boundary 'b', which separates domains 'II' and 'III'. Boundary 'b' can be traced for ca. 450 km in the present dataset. On the regional ADMAP compilation this magnetic lineament appears to continue for another 300 km and to the proposed western rim of the Ruker Craton Golynsky et al. (2007) (Figure 5.7b, c). The magnetic anomaly pattern of domain 'III' differs clearly from the typical TOAST signature and exhibits a more complex structure with differently oriented magnetic structures. The calculated positive tilt derivative revealed three major trend directions. N-S directed trends are also significantly present in the THDR of pseudo-gravity at the eastern side of domain 'III', which may indicate elongated source bodies or structures. Additionally, the N-S trends are also observed in the bed topography as elevated ridges close to the Yamato Mts. and may suggest a major topographic influence on the geometry of the magnetic anomaly source.



Geological observations in the Belgica Mts. indicate similarities with the Teltet-Vengen Group in the northern portion of the SW-Terrane of Sør Rondane (Van Autenboer and Loy, 1972). The Belgica Mts. reveal migmatitic bt-hbl-gneisses of mainly granitic composition. They are intruded by lenses and streaks of coarse grained granite. Here, the calculated analytical signal indicates three major circular shaped magnetic complexes (Figure 5.6). Euler depth solutions show it is likely that these anomalies represent intrusive bodies with relatively shallow sources at levels between approximately 1000 m below and 800 m above sea level. Geochronological investigations at the Belgica Mts. have revealed one Nd-model age of approximately 0.94 Ga. This age correlates reasonably well with the average  $T_{DM}$  ages of 1.08 Ga observed in Sør Rondane. Amphibolite facies metamorphism was U-Pb zircon dated at ca. 660 Ma (Shiraishi et al., 2008). Similar metamorphic ages of ca. 640–600 Ma are also observed in the Sør Rondane region. Although these similarities are based on very sparse data, this may indicate that the Belgica Mts. and domain ‘III’ are both underlain by juvenile Neoproterozoic crust. Similarly, only very sparse geological information is available from the Yamato Mts. ca. 200 kilometers further east. Here, the Late Neoproterozoic/Early Palaeozoic metamorphic rocks are intruded by major granitoids dated to 620 Ma and 530 Ma and provide one Nd-model age of 1.3 Ga. This model age is transitional between the slightly younger model ages in Sør Rondane to the west and the usually significantly older model ages in the Lützow-Holm Bay region to the east. Samples of the Lützow-Holm Bay region show two groups of  $T_{DM}$  values between 0.87–2.70 Ga, with a major mode at 1.0–1.25 Ga and a smaller mode at 2.29–2.70 Ga (Shiraishi et al., 2008). The older mode is not evident to the W of Yamato Mts. Beyond this hint, there are no further indications of the age or origin of older crust in the basement underlying the Yamato Mts.

A significant change of the magnetic anomaly pattern and trend of magnetic structures can be observed east of the Yamato Mts. and boundary ‘c’. This N-S trending boundary can be traced farther S in the ADMAP data and, like boundary ‘b’, appears to terminate at the margin of the Ruker Craton (Figure 5.7b, c). The same structure has previously been interpreted in the ADMAP data as the western limit of the Indo-Antarctic craton by Osanai et al. (2013). If this interpretation is correct, the domain ‘III’ could represent a transition zone from Tonian arc terranes into the Indo-Antarctic continent. This interpretation is supported by the complex magnetic anomaly pattern, which may be expected in a complicated contact zone.

Domain ‘IV’ is located at the eastern margin of the survey area and is characterized by SSE directed magnetic anomalies of higher amplitudes, which coincide with elevations in the bed topography. This domain correlates with the geologically characterized southern Neoproterozoic–Early Palaeoproterozoic (ca. 2.5 Ga) unit of the Lützow-Holm Bay Complex, also referred to as Shirase microcontinent (Tsunogae et al., 2016; Takahashi et al., 2017). It is therefore different to domain ‘III’ and may well represent the western margin of Indo-Antarctica. The edge of the survey area coincides with a major NW-SE directed negative magnetic lineament (Nogi et al., 2013).



### 5.6.4 Coastal Magnetic Low (L0-L2)

The coastal region between the escarpment and the continental margin is characterized by prominent long-wavelength magnetic lows, labeled L0, L1 and L2 from west to east (Figure 5.7a). Field variation within the lows is relatively subdued, suggesting deep and/or weak magnetic sources. Each of the anomalies is offset dextrally from its neighbours along zones that trend SE, parallel to the very earliest fracture zones in the oceanic crust offshore (Mueller and Jokat, 2019; Tuck-Martin et al., 2018). These observations raise the possibility that the magnetic lows and their offsets represent the basement of a chain of sedimentary basins and crustal-scale transfer zones, consistent with their locations at the extended continental margin formed during Gondwana breakup. Looking further inland, however, it is clear that the two proposed transfer zones also coincide with the marginwards projections of boundaries ‘a’ and ‘b’, both of which are suggested above to have accommodated dextral shear in Pan-African escape tectonics (Ruppel et al., 2015). With this observation, therefore, it is possible to interpret the influence of pre-existing (Pan-African and TOAST) structures on the location and segmentation of the plate boundary formed during Gondwana break-up.

### 5.6.5 Spatial Extent of the TOAST

Integrating geology and geophysics in this region allows to estimate the geographical range of the TOAST. To the west, the Forster Magnetic Anomaly is thought to mark the TOAST’s minimum western extent (Figure 5.3; Jacobs et al., 2017). West of the Forster Magnetic Anomaly, typical Late Mesoproterozoic Maud Belt type crust with equivalents in the African Namaqua-Natal Belt is juxtaposed against Early Neoproterozoic juvenile crust of the TOAST. The southern extent of the TOAST is less well constrained. We consider the boundary between domains ‘Ia’ and ‘Ib’ to be the minimum southern extent of the TOAST. However, as speculated above it is possible that domain ‘Ib’ may still represent components of the TOAST, and the further southern extent of ‘Ib’ is difficult to interpret in the ADMAP compilation, which is based on very sparse data.

To the east, domain ‘II’ can be confidently assigned to the TOAST and lineament ‘b’ thus forms its minimum eastern boundary. Alternatively, the TOAST could well continue into a transitional zone in domain ‘III’. The rarely-visited and sparsely-studied Belgica and Yamato Mts. allow for ground-truthing of domain ‘III’, making them a key region for further geological and geochemical studies.

The minimum northern extent of the TOAST is considered as the Main Tectonic Boundary with the SW-Terrane as its type locality. Based on the lack of pre-Neoproterozoic basement and minor pre-Neoproterozoic detrital zircon provenance, we suggest to also include the NE-Terrane as part of the TOAST. Therefore, the northern extent is most likely defined by the southern boundaries of the coastal magnetic lows (L1 and L2). The typical anomaly pattern of the TOAST with its SE-striking parallel positive magnetic anomalies differs clearly from the coastal magnetic lows. If we restore the region by reverting the dextral shear component, then the southern margin of L1 and L2 would line up with the Ulvetanna Lineament (L0). At this stage, it is highly speculative what the coastal magnetic lows represent.

Considering the boundaries described for the TOAST above, its minimum extent can be estimated as 475000 km<sup>2</sup>. Including the proposed transitional areas, this might be enlarged to



550000 km<sup>2</sup>. This area represents approximately 5 % of East Antarctica and is comparable to the area of the Antarctic Peninsula with ca. 525000 km<sup>2</sup> (including Graham and Palmer Land), a major composite arc terrane that represents accretion and amalgamation of juvenile crust at the margin of Antarctica over a period of at least 200 Myrs, comparable in duration to the Tonian period and proposed (1100-900 Ma) amalgamation of both the TOAST and its Stenian precursor.

## 5.7 Summary and Conclusion

40000 line kilometers of new aeromagnetic data from southern and eastern Sør Rondane and their integration with surface geology provide new insights about the southern and eastern extents of the Tonian Oceanic Arc Super Terrane (TOAST).

- Interpretation of new and existing aeromagnetic data from DML under constraints from surface geology reveals the TOAST to consist of two or more major arc complexes separated across lineaments, one of which we interpret as a major shear zone with a probable dextral sense of movement and a possible Pan-African age.
- We identified an area of ca. 500000 km<sup>2</sup> to be the minimum extent of the TOAST, corresponding to at least 5 % by area of East Antarctica. This area is comparable to that of the Antarctic Peninsula, a juvenile composite arc that amalgamated over a similar duration during Phanerozoic times. The TOAST thus represents significant crustal addition during the assembly of East Antarctica.
- Our data suggest an eastward continuation of the TOAST at least until the Belgica Mts.. The magnetic anomaly pattern can be interpreted to imply the presence of a transitional area between Belgica Mts. and the Lützow-Holm Bay region, separating the TOAST from the Indo-Antarctic craton.
- The southern minimum extent of the TOAST lies ca. 800 km inland of Sør Rondane at the boundary to a region of strongly negative magnetic anomalies.

## 5.8 Acknowledgements

This study was part of the collaborative research program ‘Geodynamic Evolution of East Antarctica’ (GEA) of the German Federal Institute of Geosciences and Natural Resources (BGR) and ‘West/East Gondwana Amalgamation and Separation’ (WEGAS) of the Alfred Wegener Institute Helmholtz, Centre for Polar and Marine Research (AWI).

We thank the science and flight crews of AWI-Polar aircraft for their scientific and technical support. Many thanks to Tobias Binder, Veit Helm, the technicians of AWI and FIELAX, Wayne Hewison of Canadian Microgravity, and the pilots and crew of Kenn Borek Ltd. We would like to express our sincere thanks to Alain Hubert and his team at the Belgian Princess Elisabeth station and the crews at Novo Runway for their logistic support.

Parts of this study was financially supported by Deutsche Forschungsgemeinschaft (DFG) within the frame of the Collaborative Research Programme SPP 1158 (grants LA1080/9 to A. Läufer and LI 745/15 to F. Lisker) in the framework of the priority programme 1158 ‘Antarctic Research with comparative investigations in Arctic ice areas.’

Finally, we thank Sergei Pisarevsky and Toshiaki Tsunogae for the critical and helpful reviews.





## Chapter 6

# 6. New Constraints on Deformation and Cooling History of Sør Rondane, East Antarctica, with Implications on the Final Assembly of Gondwana from $^{40}\text{Ar}/^{39}\text{Ar}$ and U-Pb Geochronology

Antonia S. Ruppel, Joachim Jacobs, Andreas Läufer, Lothar Ratschbacher, Jörg A. Pfänder, Benita-Lisette Sonntag, Katarzyna Krasniqi, Marlina Elburg, Nicole Krohne, Detlef Damaske, Frank Lisker

Key findings:

- **Ar/Ar and U-Pb dating reveals protracted magmatism and cooling of a key region in East Antarctica**
- **Magmatism and cooling are correlated between 660–480 Ma across Sør Rondane**
- **SW Terrane S represents a structurally distinct tectonic block interpreted as a megaboudin**
- **Main Shear Zone activity terminated at ca. 525 Ma**
- **Gradual younging of cooling ages to the NE correlates with increasing distance to the East African-Antarctic Orogen**
- **Ar/Ar cooling ages in Sør Rondane are ca. 20–40 Ma older than in western Dronning Maud Land**

## 6.1 Abstract

This study investigates the Late Neoproterozoic–Early Paleozoic tectono-thermal history of the eastern part of the East African–Antarctic Orogen in Sør Rondane with  $^{40}\text{Ar}/^{39}\text{Ar}$  and U-Pb data from five structural domains. Twenty-eight new and a few published Ar/Ar ages span 660 to 480 Ma, roughly corresponding to the age range of at least three generations of syn- to post-tectonic granitoids. The ages are distinct for the five structural domains recognised. The oldest cooling ages come from the weakly-deformed SW Terrane S, a megaboudin and the root of a Tonian island arc, which escaped much of the Late Neoproterozoic accretionary deformation. This terrane is intruded by the oldest and largest granitoid of Sør Rondane at ca. 630 Ma. The oldest Ar/Ar amphibole and biotite ages of 570–525 Ma are from the Main Shear Zone, along the northern margin of the megaboudin. It hosts ca. 570–560 Ma granites strung out along the shear zone. A third granitoid phase is recorded in the adjacent four terranes to the W, N, and E of the megaboudin and correlates with the youngest group of Ar/Ar biotite ages spanning 510–480 Ma. An E-ward younging Ar/Ar age trend may record the outward growth of the orogen. We interpret the >150-Ma-long magmatic and cooling history to reflect repeated phases of accretion, magmatism, and reactivation, i.e. collage-style tectonism, pre-dating the incorporation of Sør Rondane into the Gondwana supercontinent. The study area first accreted



to the cryptic Valkyrie Craton and then was sandwiched between the Kalahari and Indo-Antarctica cratons, resulting in today's East Antarctica. We draw analogies with the Arabian-Nubian-Shield along the other end of the East African-Antarctic Orogen.

**KEYWORDS:**  $^{40}\text{Ar}/^{39}\text{Ar}$  geochronology, U-Pb zircon geochronology, Gondwana, accretionary orogen, Pan-African, Sør Rondane, Dronning Maud Land

## 6.2 Introduction

Sør Rondane in Dronning Maud Land (DML), East Antarctica, lies in the eastern part of the Late Neoproterozoic–Early Paleozoic East African-Antarctic Orogen (EAAO). There, the Tonian Oceanic Arc Super Terrane (TOAST) is sandwiched between Kalahari (Namaqua-Natal Belt, Proto-Kalahari, Maud Belt) and Indo-Antarctica (Indian cratons, Napier Craton, Lützow-Holm Belt, Rayner Belt, Madagascar, Sri Lanka) (Figure 6.1). Extensive rock exposures at 1000–3300 m elevation follow a continental margin-parallel escarpment ca. 200 km inland of the coast line.

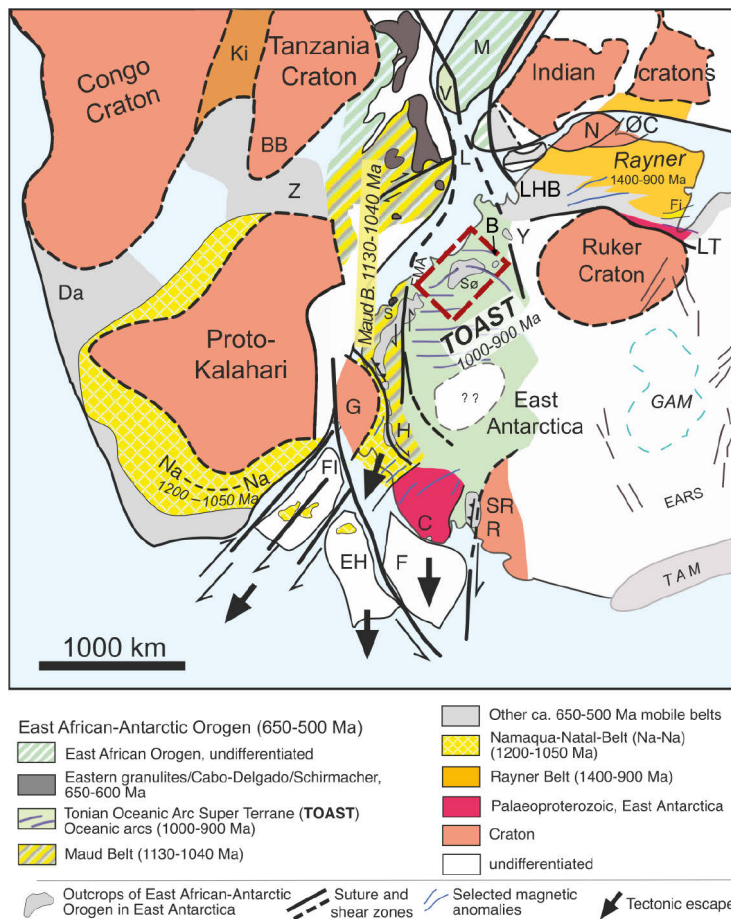


Figure 6.1: Study area (red outline) within Gondwana at ca. 500 Ma after Jacobs et al. (2015). Africa is fixed to its present-day coordinates; the other continents are re-arranged accordingly. Abbreviations: B, Belgica Mts.; C, Coats Land; DML, Dronning Maud Land; Da, Damara Belt; EH, Ellsworth-Haag block; F, Filchner block; FI, Falkland Islands; G, Grunehogna; GL, Gjellbreen Lineament; H, Heimefrontfjella; L, Lurio Belt; LHB, Lützow-Holm Belt; LT, Lambert Terrane; N, Napier Complex; Na-Na, Namaqua-Natal; ØC, Øygarden Complex; S, Schirmacher Oasis; Sør, Sør Rondane, SR, Shackleton Range; TAM, Transantarctic Mts., LHB, Lützow-Holm Bay; M, Madagascar; R, Read Block; V, Vohibori; Y, Yamato Mts.; Z, Zambesi Belt.

Previous geological studies by Belgian (e.g. Picciotto et al., 1964; Van Autenboer et al., 1964; Van Autenboer, 1969) and Japanese (e.g. Shiraishi et al., 2008; Grantham et al., 2013; Higashino et al., 2013; Osanai et al., 2013) expeditions focused on orogenic processes related to the final amalgamation of Gondwana. Ca. 490–420 Ma K/Ar and  $^{40}\text{Ar}/^{39}\text{Ar}$  (short Ar/Ar) whole rock and biotite ages from igneous and metamorphic rocks of eastern Sør Rondane were interpreted to indicate cooling following the latest metamorphism (Takigami et al., 1987; Takahashi et al., 1990; Takigami and Funaki, 1991; Osanai et al., 2013).



Recent geological and geophysical studies provided insights into the Meso- to Early Neoproterozoic history of the region (Hokada et al., 2013; Elburg et al., 2015; Jacobs et al., 2015; Ruppel et al., 2018), the intrusive activity during Gondwana assembly (Elburg et al., 2016), the structural and tectonic framework (Osanai et al., 2013; Owada et al., 2013; Mieth et al., 2014; Ruppel et al., 2015), and the Gondwana disintegration (Krohne, 2017). To better understand the final assembly of Gondwana during the Late Neoproterozoic–Early Paleozoic, we analyzed samples across Sør Rondane geochronologically to trace the geodynamic evolution during and after the formation of the EAAO (Stern, 1994; Shackleton, 1996; Jacobs et al., 1998; Nakano et al., 2013). In addition, we aim to test the hypothesis of collage-style accretion tectonics for the Sør Rondane region (Jacobs et al., 2015; Elburg et al., 2016). We present Ar/Ar cooling ages from five distinct terranes of Sør Rondane, including the little-studied region between Sør Rondane and central DML (western SR), and the eastern remote areas of Sør Rondane (Figure 6.2). Additional U-Pb zircon ages from syn- to post-tectonic granitoids constrain the timing of deformation along the Main Shear Zone (MSZ), the boundary between two major terranes of Sør Rondane.

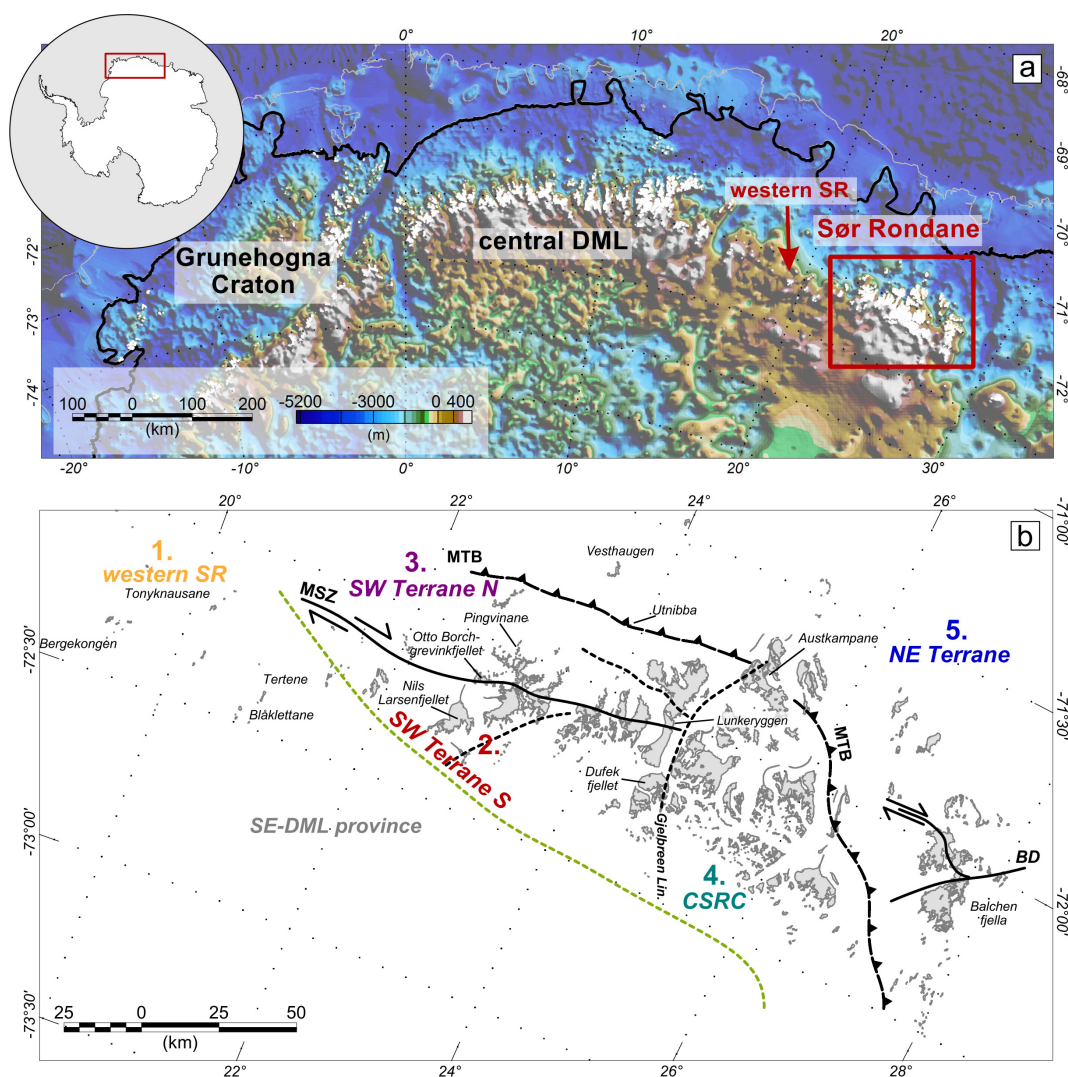


Figure 6.2: Study area in East Antarctica. a) Subsurface topography of Dronning Maud Land (DML) with indicated study area (Bedmap2, Fretwell et al., 2013). b) Exposed rocks (grey) and subdivision of Sør Rondane into five distinct tectonic terranes/units: Boundaries are from Mieth et al. (2014). Abbreviations: CSCRC = Central Sør Rondane Corridor MSZ, Main Shear Zone; MTB, Main Tectonic Boundary; SR= Sør Rondane.



## 6.3 Regional Geology of Sør Rondane

Sør Rondane's Late Mesoproterozoic–Early Neoproterozoic juvenile basement rocks lack significant remnants of Archaean or Palaeoproterozoic continental crust (e.g. Shiraishi et al., 2008; Jacobs et al., 2017; Elburg et al., 2016). Since the Late Mesoproterozoic, the region has undergone oceanic arc/terrane accretion, probably related to tectonics outboard of Rodinia (ca. 1100–900 Ma). The spatial extent of this so-called Tonian Oceanic Arc Superterrane (TOAST) was estimated to ca. 500000 km<sup>2</sup>, including the area to the south and southeast of central DML and Sør Rondane; it likely continues to the Belgica Mts. (Figure 6.1 Takigami and Funaki, 1991; Ruppel et al., 2018). The TOAST experienced metamorphism from ca. 850 to 580 Ma, resulting from ocean closure and the final amalgamation of Gondwana (Jacobs et al., 2017).

The southern part of the SW Terrane of Sør Rondane, the SW Terrane S, and a few scattered nunataks to the west represent the type locality of the TOAST (Figure 6.2; Jacobs et al., 2017). It consists mainly of a gabbro-tonalite-trondhjemite-granodiorite complex (GTTG), dated at ca. 1000–900 Ma; Nd whole rock and Hf-in-zircon isotopic signatures indicate that this complex represents a juvenile oceanic arc (Kamei et al., 2013; Elburg et al., 2015). The Main Shear Zone delimits the SW Terrane S from the SW Terrane N (Figure 2b); the latter is dominated by greenschist- to granulite-facies metasedimentary and metaigneous rocks with the youngest detrital zircon ages at ca. 700 Ma (Otsuji et al., 2013; Owada et al., 2013). Peak metamorphic conditions with an anticlockwise pressure-temperature (P-T) path were dated at ca. 640–600 Ma (Adachi et al., 2013; Osanai et al., 2013).

To the northeast, the SW Terrane is separated from the amphibolite- to granulite-facies metamorphic NE Terrane by the Main Tectonic Boundary (MTB) (Figure 6.2b; Osanai et al., 2013). The NE Terrane comprises metasupracrustal rocks with the youngest detrital zircon ages at ca. 750 Ma; metamorphism followed a clockwise P-T path and peaked at ca. 640–600 Ma (Shiraishi et al., 2008). The two contrasting P-T paths on either side of the MTB were interpreted to result from thrusting of the NE Terrane over the SE Terrane during the Pan-African orogeny (Adachi et al., 2013; Osanai et al., 2013). The former Sør Rondane Suture is interpreted here as part of the frontal fold zone of the MTB rather than a suture zone between the NE and SW Terranes. So far, pre-750 Ma basement has not been recognized in the NE Terrane; thus, it remains unclear if the NE Terrane is part of the TOAST or is a separate tectonic unit.

Intrusive rocks record at least four thermal pulses between ca. 650 and 500 Ma in Sør Rondane (e.g. Elburg et al., 2016). These authors suggested that the long-lasting magmatism and tectono-metamorphism between ca. 650 and 500 Ma likely represents protracted accretion and collision in this part of the EAAO. One particular igneous group is represented by the Vengen type-granitoids of ca. 560 Ma. They intruded along the MSZ and are weakly foliated, indicating a late syn- to post-tectonic emplacement (Shiraishi et al., 2008; Ruppel et al., 2015; Elburg et al., 2016). Metamorphic U-Pb zircon ages of ca. 570–530 Ma were reported across the entire region and were interpreted as recording post-collisional retrograde metamorphism and/or hydration after peak amphibolite-facies metamorphism at ca. 580–570 Ma (Shiraishi et al., 2008; Elburg



et al., 2016 with references therein). Data obtained from Rb-Sr, K-Ar and Ar/Ar span between ca. 660–420 Ma (Osanai et al., 2013 with references therein). The K-Ar and Ar/Ar data indicate an age trend across Sør Rondane. The SW Terrane S yielded one ca. 660 Ma age from a gneiss at Nils Larsenfjellet (Takigami and Funaki, 1991), and 500–480 Ma ages from granitic and syenitic rocks at Lunkeryggen and a gneiss at Otto Borchgrevinkfjellet. The SW-Terrane N (Pingvinane) provided one ca. 500 Ma K-Ar biotite age (Takigami and Funaki, 1991). The NE Terrane yielded the youngest cooling ages: ca. 470 Ma K-Ar biotite ages at Austkampane, and 430–420 Ma whole rock ages at Utnibba; metadolerites yielded 490–440 Ma K-Ar and Ar/Ar biotite dates (Takigami et al., 1987). Osanai et al. (2013), interpreted the ca. 490–420 Ma range of Rb-Sr, K-Ar, and Ar/Ar dates as cooling ages post-dating metamorphism.

Mieth et al.'s (2014), combining aeromagnetic and geological studies, refined the subdivision of Sør Rondane into distinct terranes. The general subdivision into the NE and SW Terranes remained, whereas major lineaments were confirmed or redefined (e.g. MSZ, MTB, Sør Rondane Suture). The magnetic anomaly pattern prompted a subdivision of the SW Terrane S into a western more tholeiitic and an eastern more calc-alkaline portion of the GTTG complex (Kamei et al., 2013; Mieth et al., 2014). Furthermore, the Central Sør Rondane Corridor (CSRC) was introduced as a distinct tectonic domain, separating Sør Rondane in an eastern and western part (Figure 2b). The CSRC was interpreted to be related to late Pan-African extensional tectonics (Mieth et al., 2014). It is characterised by more enriched Hf-isotopic signatures (Elburg et al., 2016).

## 6.4 Samples and Methods

### 6.4.1 Samples

We analyzed 23 samples for Ar/Ar biotite, 6 for Ar/Ar amphibole, and 3 for U-Pb zircon. Samples were collected during the 'Geodynamic Evolution of East Antarctica' (GEA) expeditions I and II in the austral summers of 2010/2011 and 2011/2012. They represent all major terranes/units previously identified by integrated geological-aerogeophysical studies. From southwest to northeast, our study includes (Figure 6.3):

- (i) Six samples from scattered nunataks west of Sør Rondane in the magnetically distinct SE-DML province; one is from a moraine. These samples include Stenian/Tonian GTTGs (J1211B\_2, J1221D\_1), Ediacarian to Cambrian garnet-bearing migmatites and orthogneiss sheets (J1211B\_1, J1213C, J1213D), and a late- to post-tectonic granitoid (J1212C). The Ar/Ar dating used the same samples as a previous U-Pb zircon study (Jacobs et al., 2015).
- (ii) Nine samples from the SW Terrane. In the SW Terrane S, we sampled in the vicinity of the MSZ in the GTTG complex. The lithologies include mylonitic rocks of tonalitic composition (27C\_1, 1208A1), gneisses (1131A1, 1131A2, 27A\_1), biotite and amphibole schist (1205A2, 1218A1, J1224B), and a late- to post-tectonic granitoid (1130D\_1).
- (iii) Three samples from the SW Terrane N, north of the MSZ. They comprise an orthogneiss (06A-1), a granitic gneiss (J1224C), and a metavolcanic rock (10A3).



- (vi) Three samples from the central Sør Rondane corridor (CSRC). They include two gneisses (1219C1, 1219D1) and a late- to post-tectonic granitoid from the easternmost CSRC (J1225D).
- (v) Two samples from the easternmost NE Terrane. They comprise a migmatitic gneiss (J1225C) and a diorite (J1225A).

#### 6.4.2 $^{40}\text{Ar}/^{39}\text{Ar}$ Analyses

Ar/Ar analyses were carried out at ALF, TU Bergakademie Freiberg, Germany. Mineral processing used the electrical-discharge SELFRAG® facility that yields grain sizes corresponding closely to the true crystal size; it also minimizes the proportion of broken grains (Spener et al., 2014). We used the largest grain-size fraction from which it was possible to handpick optically inclusion-free crystals. The mineral separates were washed repeatedly in deionised water using an ultrasonic bath. After drying, the mineral separates were wrapped in Al foil and loaded into wells on Al discs (33 mm diameter) for irradiation. Irradiation was done for 3.8 hours without Cd-shielding at the LVR-15 research reactor of the Nuclear Research Institute in Řež, Czech Republic. The thermal neutron fluence was in the order of  $6 \times 10^{13}$  n/cm<sup>2</sup>s at a thermal to fast neutron ratio of ~1.1 (~7.6 MW reactor power; for detailed irradiation geometry and reactor specifics see Rutte et al. (2015)). Irradiated micas were unwrapped and loaded into 3 x 1 mm (diameter x depth) wells on oxygen-free copper discs (30 samples per disc). Hornblende separates were loaded into Mo-crucibles for furnace degassing. Step-wise heating of micas was performed using a power controlled floating 30W New Wave CO<sub>2</sub> laser system, with a defocused beam with a 3 mm diameter. The heating time was 5 min per step. Stepwise heating of hornblende separates was performed using a Createc high-temperature cell (HTC; for details see Pfänder et al. (2014)), with a heating time of 10 min per step. Two GP50 getter pumps, one at room temperature, and one at 400° C, achieved gas purification. Cleaning time per step was 5 minutes for laser degassing, and 10 min for furnace degassing. Argon isotope compositions were measured in static mode on a GV Instruments ARGUS noble gas mass spectrometer equipped with five faraday cups and 10<sup>12</sup> Ohm resistors on mass positions 36–39 and a 10<sup>11</sup> Ohm resistor on mass position 40. Typical blank levels are  $2.5 \times 10^{-16}$  mol <sup>40</sup>Ar and  $8.1 \times 10^{-18}$  mol <sup>36</sup>Ar. Measurement time was 7.5 minutes per step acquiring 45 scans at 10 seconds integration time each. Mass bias was corrected assuming linear mass dependent fractionation and using an atmospheric <sup>40</sup>Ar/<sup>36</sup>Ar ratio of  $298.6 \pm 0.3$  (Lee et al., 2006; Mark et al., 2011). For raw data reduction and time-zero intercept calculation an in-house developed Matlab® toolbox was used. Isochron, inverse isochron, and plateau ages were calculated using ISOPLOT 4.15 (Ludwig, 2011). All ages were calculated using Drachenfels sanidine (DRF1) as fluence monitor ( $25.682 \pm 0.030$  Ma). This in-house standard was calibrated against Fish Canyon Tuff sanidine applying an age of  $28.305 \pm 0.036$  Ma (Renne et al., 2010), and using the decay constants given in Renne et al. (2010). Supporting information Figure B.1 show age-spectrum and isochron plots of all samples. Interference correction factors are given in Table B.2 of the supporting information along with the raw data of the Ar isotope measurements. (cf. ‘Electronic Appendix’).



### 6.4.3 U-Pb Zircon Analyses

Zircon concentrates were separated from 1–2 kg sample material using standard methods. Final selection of the zircon grains for U-Pb dating was achieved by hand-picking under a binocular microscope. Zircon grains of all sizes and morphological types were selected, mounted in resin, and polished to half their thickness. Zircons were analysed for U, Th, and Pb isotopes by the LA-ICP-MS technique, using a Thermo-Scientific Element 2 XR sector field ICP-MS coupled to a NewWave UP-193 Excimer Laser System at the Senckenberg Naturhistorische Sammlungen Dresden, Germany. A teardrop-shaped, low volume laser cell constructed by Ben Jähne (Dresden) and Axel Gerdes (Frankfurt/M.) was used to enable sequential sampling of heterogeneous grains (e.g., growth zones) during time-resolved data acquisition. Each analysis consisted of approximately 15 s background acquisition followed by 30 s data acquisition, using a laser spot-size of 25 or 35  $\mu\text{m}$ . A common-Pb correction, based on the interference-corrected and background-corrected  $^{204}\text{Pb}$  signal and a model Pb composition (Stacey and Kramers, 1975), was carried out if necessary. The necessity of the correction was judged on whether the corrected  $^{207}\text{Pb}/^{206}\text{Pb}$  lies outside of the internal errors of the measured ratios. Discordant analyses were generally interpreted with care. Raw data were corrected for background signal, common Pb, laser induced elemental fractionation, instrumental mass discrimination, and time dependent elemental fractionation of Pb/Th and Pb/U using an Excel® spreadsheet program developed by Axel Gerdes (Institute of Geosciences, Goethe University Frankfurt/M., Germany). Reported uncertainties were propagated by quadratic addition of the external reproducibility obtained from the standard zircon GJ-1 ( $\sim 0.6$  and  $0.5\text{--}1.0\%$  for  $^{207}\text{Pb}/^{206}\text{Pb}$  and  $^{206}\text{Pb}/^{238}\text{U}$ , respectively) during individual analytical sessions, and the within-run precision of each analysis. Concordia diagrams (2-sigma error ellipses) and concordia ages (95 % confidence level) were produced using Isoplot/Ex 4.15 (Ludwig, 2012). The  $^{206}\text{Pb}/^{238}\text{U}$  age was taken for interpretation. For further details on the analytical protocol and data processing, see Gerdes and Zeh (2006) and Frei and Gerdes (2009). The complete LA-ICP-MS zircon data are presented as supporting information (Table B.3 ‘Electronic Appendix’).

## 6.5 Results

### 6.5.1 $^{40}\text{Ar}/^{39}\text{Ar}$ Dating on Biotite and Amphibole

The results are presented and described in a regional order from southwest to northeast and grouped based on their geographical position within the distinct terranes. Table 6.1 summarizes the analytical results. In many samples, most of the steps are extremely radiogenic ( $\%^{40}\text{Ar}^* > 99\%$ ); therefore, most data points cluster close to the  $^{39}\text{Ar}/^{40}\text{Ar}$  axis in the inverse isochron plots and provide poor fits to the  $^{36}\text{Ar}/^{40}\text{Ar}$  vs.  $^{39}\text{Ar}/^{40}\text{Ar}$  data (Figure B.1 and Table B.2 ‘Electronic Appendix’). Whereas most biotite separates yielded flat sections in the age versus cumulative  $^{39}\text{Ar}$  diagrams with weighted mean ages (WMA) with MSWD values around 1 and probabilities of fit  $> 5\%$ , the amphibole spectra are commonly U-shaped patterns and do not permit the calculation of a WMA for the majority of analyses. Our preferred age interpretation includes age uncertainties of  $\pm 2\sigma$  or  $\geq 1\%$  of the age to account for sample complexities, in particular the uncertainties in the calculated initial  $^{40}\text{Ar}/^{36}\text{Ar}$ .



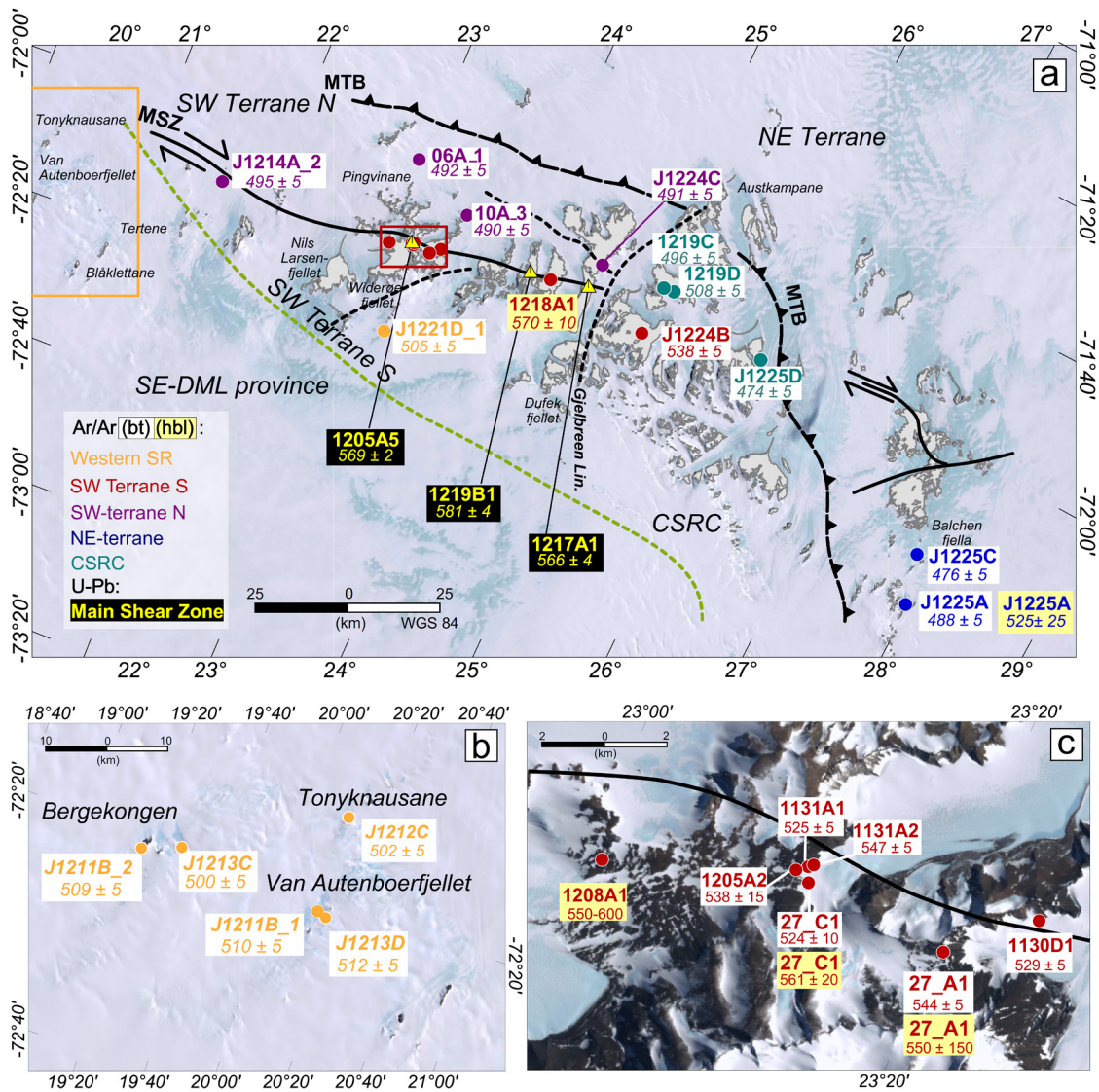


Figure 6.3: Summary and overview of new ages. Localities with sample number and corresponding geochronological ages in million years [Ma]. Colours refer to samples taken within distinct terranes and according to their interpretation, e.g. J1221D-1 moraine sample probably originated from the S. a) Preferred cooling ages of  $^{40}\text{Ar}/^{39}\text{Ar}$  data are indicated by white backdrop for biotite and yellow for hornblende; U-Pb zircon ages underlain by black backdrop. Orange rectangle indicates the region of the westernmost samples shown in detail in b). A close-up of the region adjacent to the MSZ is marked with the red rectangle and illustrated in detail in c).



Table 6.1:  $^{40}\text{Ar}/^{39}\text{Ar}$  Ar data.

Sample	Laboratory/ Device	Mineral	Weight [mg]	Grain Size [ $\mu\text{m}$ ]	WMA $\pm 1\sigma$ [Ma]	MSWD (WMA)	IIA $\pm 1\sigma$ [Ma]	MSWD (IIA)	$^{40}\text{Ar}/^{39}\text{Ar}$ (IIA)	% $^{39}\text{Ar}$ (Total)	Steps (Total)	Preferred Age Interpretation ( $\pm 2\sigma$ respectively $\geq 1\%$ [Ma])	Location
J1211_B1	ALF laser	Bt	2,97	250-500	510.8 $\pm$ 1.1	0.16	510.5 $\pm$ 2.2	0.72	450 $\pm$ 170	82.5	5-19 (19)	510 $\pm$ 5	
J1213C	ALF laser	Bt	2,72	250-500	501.8 $\pm$ 1.3	1.20	499.3 $\pm$ 2.7	0.71	943 $\pm$ 290	87.4	6-21 (21)	500 $\pm$ 5	
J1211B_2	ALF laser	Bt	2,23	250-500	509.6 $\pm$ 1.6	0.55	508.2 $\pm$ 2.8	1.6	409 $\pm$ 45	71.8	7-16 (18)	509 $\pm$ 5	western Sør Rondane
J1213D	ALF laser	Bt	2,76	250-500	513.0 $\pm$ 1.0	0.74	†			91.5	5-20 (20)	513 $\pm$ 5	
J1212C	ALF laser	Bt	2,72	160-250	502.7 $\pm$ 1.0	1.03	500.2 $\pm$ 4.6	0.69	1476 $\pm$ 910	75.2	6-21 (21)	501 $\pm$ 5	
J1221D_1	ALF laser	Bt	2,78	250-500	505.3 $\pm$ 1.5	0.86	501.8 $\pm$ 4.7	2.3	904 $\pm$ 440	80.4	6-19 (20)	503 $\pm$ 10	moraine
1205A2	ALF laser	Bt	2,24	80-250	542.7 $\pm$ 1.2	0.86	535.5 $\pm$ 8.2	0.59	987 $\pm$ 490	70.8	7-16 (16)	538 $\pm$ 15	
27C_1	ALF laser	Bt	2,72	80-250	534.6 $\pm$ 3.3	4.1	523.2 $\pm$ 4.1	1.07	1145 $\pm$ 230	56.3	8-18 (20)	524 $\pm$ 10	
27C_1	ALF laser	Amp	2,25	80-250	561.5 $\pm$ 2.8	0.25	560.2 $\pm$ 4.1*	1.6	552 $\pm$ 240	96.4	4-5 (5)	561 $\pm$ 20	
1131A1	ALF laser	Bt	2,23	160-250	526.0 $\pm$ 1.3	0.77	522.0 $\pm$ 6.3	1.5	900 $\pm$ 470	78.3	6-18 (18)	525 $\pm$ 5	
1131A2	ALF laser	Bt	2,24	160-250	547.4 $\pm$ 1.7	0.29	548.1 $\pm$ 3.3	3.5	287 $\pm$ 110	80.5	6-18 (18)	547 $\pm$ 5	
27A_1	ALF laser	Bt	2,25	80-250	543.4 $\pm$ 1.2	0.08	543.9 $\pm$ 2.7	0.81	332 $\pm$ 170	68.7	7-17 (17)	544 $\pm$ 5	SW Terrane S
27A_1	ALF furnace	Amp	40,46	80-250	†		550 $\pm$ 75	0.50	8349 $\pm$ 5500	30	12-15 (18)	550 $\pm$ 150	
1130D1	ALF laser	Bt	2,25	80-160	528.9 $\pm$ 1.3	0.07	528.4 $\pm$ 4.4	0.17	617 $\pm$ 490	84.9	6-18 (18)	529 $\pm$ 5	
1218A1	ALF furnace	Amp	29,44	<160-250	571.1 $\pm$ 1.6	1.5	570.2 $\pm$ 2.6	0.20	320 $\pm$ 17	19.6	15-18 (18)	570 $\pm$ 20	
1203A4	ALF furnace	Amp	40,97	<160	†		605 $\pm$ 300	1.11	40768 $\pm$ 7800	47	8-15 (20)	†	
1208A1	ALF furnace	Amp	28,97	<160-250	†							550-600	
J1224B	ALF laser	Bt	2,73	80-250	538.3 $\pm$ 1.2	0.04	539.0 $\pm$ 2.1	0.39	283 $\pm$ 63	90.9	7-22 (22)	539 $\pm$ 5	SW Terrane S ?
J1214_A2	ALF laser	Bt	2,71	80-250	494.9 $\pm$ 1.1	0.77	493 $\pm$ 12	2.6	493 $\pm$ 420	80.3	7-20 (20)	495 $\pm$ 5	SW Terrane N ?
06A_1	ALF laser	Bt	2,30	80-250	493.4 $\pm$ 1.2	0.49	491.5 $\pm$ 7.5	2.6	660 $\pm$ 420	81.9	11-26 (26)	493 $\pm$ 5	
10A_3	ALF laser	Bt	2,22	80-250	490.4 $\pm$ 1.5	0.54	†			92.1	6-19 (19)	490 $\pm$ 5	SW Terrane N
J1224C	ALF laser	Bt	2,74	80-250	491.2 $\pm$ 1.1	0.38	†			76.8	6-20 (20)	491 $\pm$ 5	
1219C1	ALF laser	Bt	2,26	160-250	497.7 $\pm$ 1.1	0.47	494.9 $\pm$ 2.9	1.17	455 $\pm$ 100	57.3	7-15 (17)	496 $\pm$ 5	
1219D1	ALF laser	Bt	2,21	80-250	508.4 $\pm$ 1.6	0.79	505.3 $\pm$ 4.5	10.8	378 $\pm$ 100	66.7	9-15 (15)	508 $\pm$ 5	Sør Rondane corridor
J1225D	ALF laser	Bt	2,26	250-500	475.1 $\pm$ 1.0	0.38	473.5 $\pm$ 2.5	0.64	665 $\pm$ 350	74.7	6-20 (20)	474 $\pm$ 5	
J1225A	ALF laser	Bt	2,73	250-500	487.6 $\pm$ 1.5	0.30	488.0 $\pm$ 2.8	2.5	365 $\pm$ 71	98.2	5-21 (21)	488 $\pm$ 5	
J1225A	ALF furnace	Amp	24,17	160-250	†		525 $\pm$ 12	0.24	7295 $\pm$ 12000	80.5	9-19 (21)	525 $\pm$ 25	NE Terrane
J1225C	ALF laser	Bt	2,24	80-250	476.8 $\pm$ 1.1	0.85	475.9 $\pm$ 5.0	6.5	462 $\pm$ 270	85.1	6-20 (21)	476 $\pm$ 5	

WMA, weighted mean age, calculated by weighting each age analysis by their reciprocal variance. IIA, inverse isochron age. MSWD, mean square weighted deviation. All WMA were calculated for a  $^{40}\text{Ar}/^{39}\text{Ar}$  ratio of  $298.6 \pm 0.3$  (Lee et al., 2006; Mark et al., 2010). IIA and WMA are based on fraction of  $^{39}\text{Ar}$  and steps listed. Bt, biotite; Amp, amphibole. †No meaningful calculation possible.



## Western Sør Rondane

### *J1211B 1, garnet–migmatite [bt], Bergekongen (72.406267°S; 20.920250°E)*

This garnet-bearing migmatite from Bergekongen consists of quartz, K-feldspar, plagioclase, and biotite. A zircon-core  $^{206}\text{Pb}/^{238}\text{U}$  age range of 1100 to 600 Ma shows two clusters at ca. 1070 and 1000 Ma; zircon rims gave a  $^{204}\text{Pb}$ -corrected  $^{206}\text{Pb}/^{238}\text{U}$  Concordia age of  $546 \pm 3$  Ma (MSWD = 1.83), interpreted to date a metamorphic overprint (Jacobs et al., 2015). 82.5 % of the released  $^{39}\text{Ar}$  provides an Ar/Ar biotite WMA of  $510.9 \pm 1.1$  Ma (MSWD = 0.16); the inverse isochron age (IIA) at  $510.5 \pm 2.2$  Ma (MSWD = 0.72) is identical, however, with an initial  $^{40}\text{Ar}/^{36}\text{Ar}$  value of  $450 \pm 170$ , reflecting the high radiogenic yield (Figure 6.4). Our preferred age interpretation is  $510 \pm 5$  Ma, dating post-metamorphic cooling.

### *J1213C, pegmatite gneiss [bt], Bergtussen (72.337533°S; 19.472300°E)*

This coarse-grained pegmatite within a migmatitic gneiss from Bergtussen shows moderate deformation; it consists mainly of quartz, plagioclase, K-feldspar, and biotite. Zircons yielded a  $^{206}\text{Pb}/^{238}\text{U}$  Concordia age of  $597 \pm 7$  Ma (MSWD = 3.13), interpreted as the time of pegmatite crystallization (Jacobs et al., 2015). 87.4 % of the released  $^{39}\text{Ar}$  yielded an Ar/Ar biotite WMA of  $501.8 \pm 1.3$  Ma (MSWD = 1.2) and an IIA of  $499.3 \pm 2.7$  Ma (MSWD = 2.6), the latter with an imprecise, non-atmospheric initial  $^{40}\text{Ar}/^{36}\text{Ar}$  value of  $943 \pm 290$  (Figure 6.4). Our age interpretation is  $500 \pm 5$  Ma.

### *J1211B 2, metagabbro/enderbite [bt], Bergekongen (72.358167°S; 19.288833°E)*

This Bergekongen sample is mainly composed of plagioclase and coarse-grained orthopyroxene. Biotite and amphibole formed during amphibolite-facies retrogression. Zircons provided a  $^{206}\text{Pb}/^{238}\text{U}$  Concordia age of  $916 \pm 13$  Ma (MSWD = 1.85), interpreted as the crystallization age of the gabbro/enderbite (Jacobs et al., 2015). Biotite yielded a WMA age of  $509.6 \pm 1.6$  Ma (MSWD = 0.55) and an IIA of  $508.2 \pm 2.8$  Ma (MSWD = 1.6), comprising 71.8 % of the released  $^{39}\text{Ar}$ ; the the initial  $^{40}\text{Ar}/^{36}\text{Ar}$  value of  $409 \pm 45$  indicates extraneous  $^{40}\text{Ar}$  (Figure 6.4). The preferred age is  $509 \pm 5$  Ma.

### *J1213D, pegmatitic granitoid [bt], Van Autenboerfjellet (72.362983°S; 20.244717°E)*

This pegmatite is from a coarse-grained granite sheet, intruding into the migmatitic gneisses at Van Autenboerfjellet. The sample consists of quartz, plagioclase, K-feldspar, and biotite. Zircons gave a  $^{206}\text{Pb}/^{238}\text{U}$  Concordia age of  $582 \pm 5$  Ma (MSWD = 2.25), interpreted as a crystallization age (Jacobs et al., 2015). 91.5 % of the released  $^{39}\text{Ar}$  yielded a biotite WMA of  $503.0 \pm 1.0$  Ma (MSWD = 0.74); this sample did not provide a meaningful IIA. The hump in the central part of the spectrum indicates that these steps incorporated extraneous Ar (Figure 6.4). Our preferred age is  $513 \pm 5$  Ma.



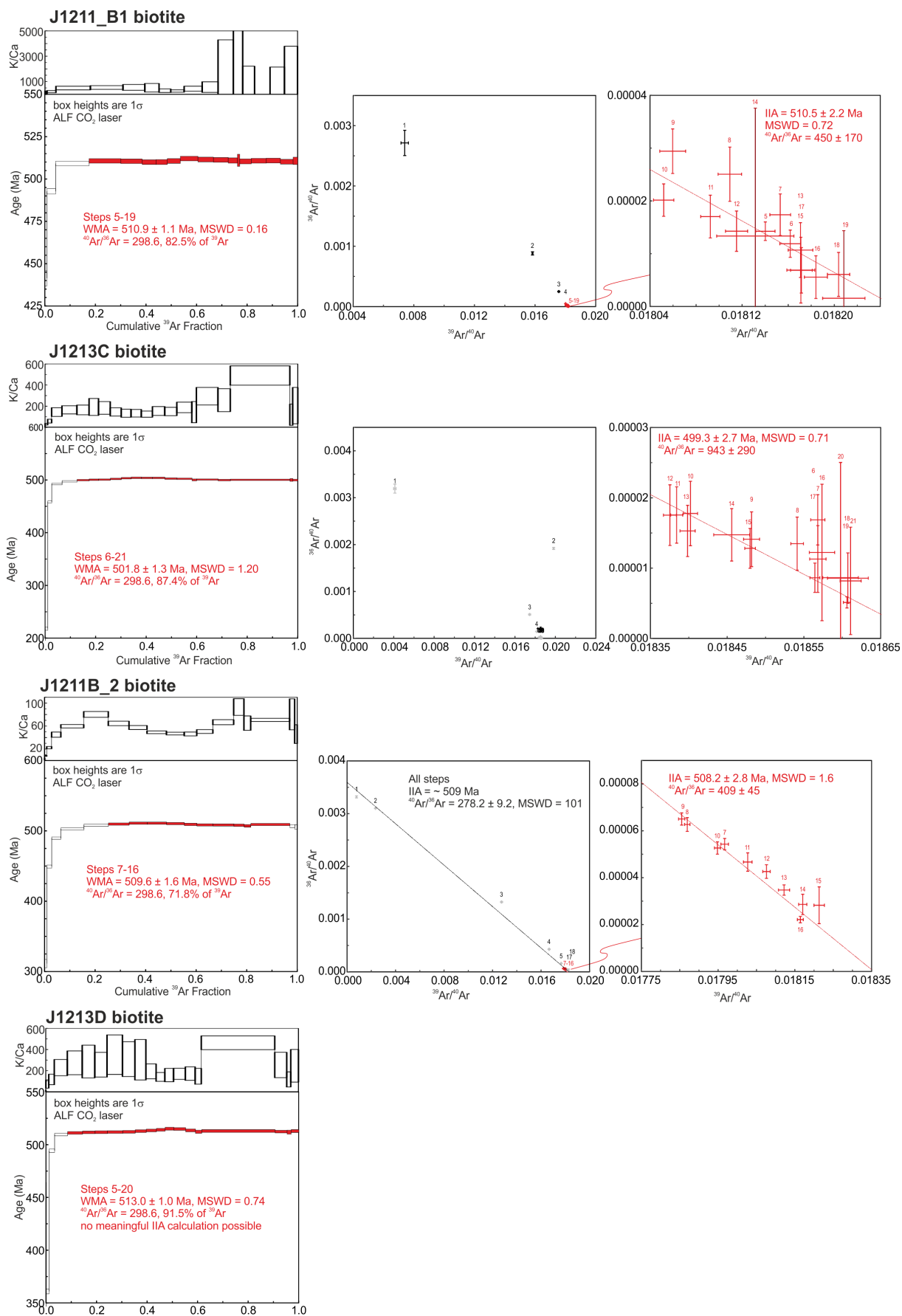


Figure 6.4:  $^{40}\text{Ar}/^{39}\text{Ar}$  age spectra and isochrons of samples from the western Sør Rondane. Ages are given with  $1\sigma$  uncertainties (including error in J).



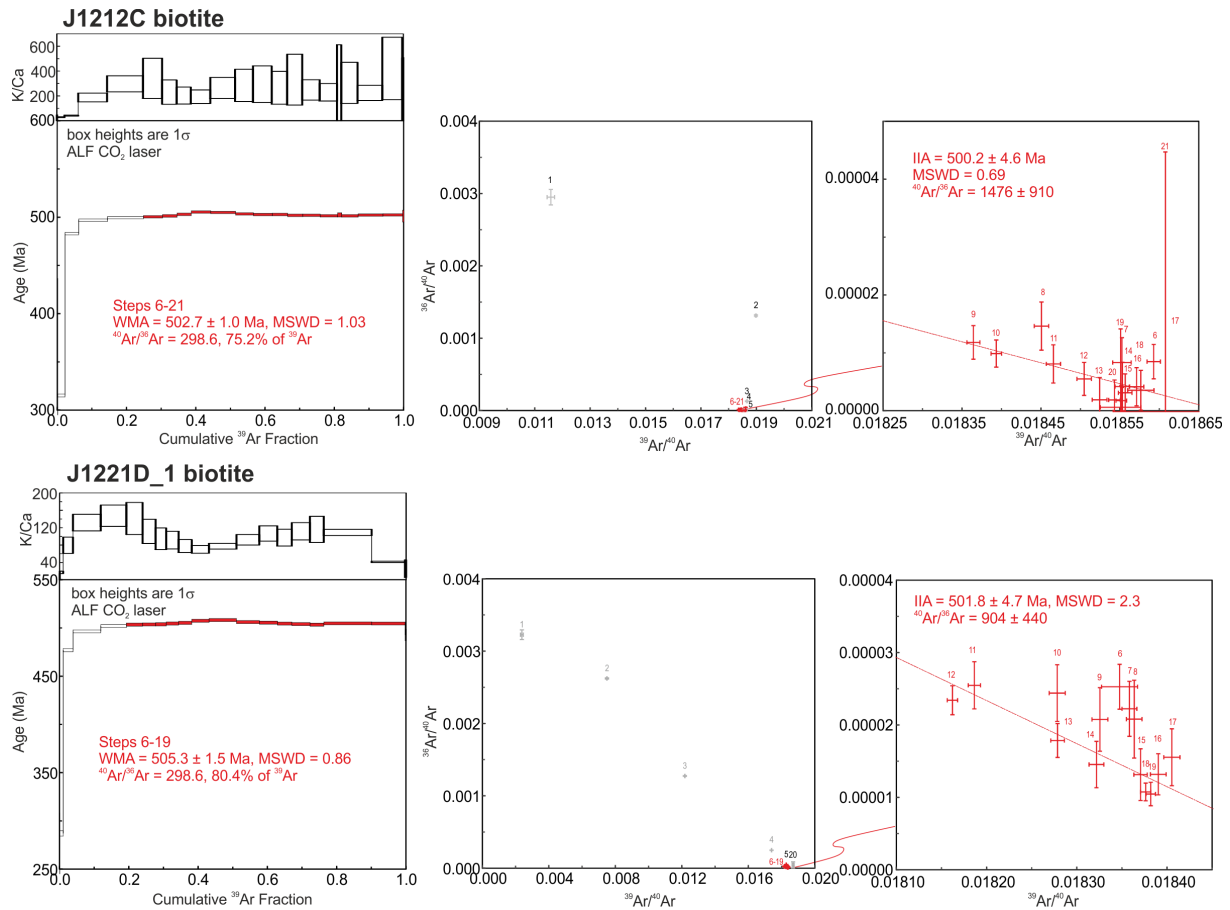


Figure 6.4: (continued)

J1212C, discordant granitic gneiss sheet [bt], Tonyknausane (72.212600°S; 20.182767°E)

Sample J1212C, a granitic gneiss sheet that cuts metasupracrustal gneisses at Tonyknausane, is mainly composed of quartz, plagioclase, K-feldspar, biotite, and titanite. Quartz and feldspar show undulose extinction; quartz also grain-boundary-migration recrystallization. Plagioclase has deformation twins and myrmekite; K-feldspar is altered. Dark brown biotite is idiomorphic to hypidiomorphic. The zircon  $^{206}\text{Pb}/^{238}\text{U}$  Concordia age of  $528 \pm 6$  Ma (MSWD = 3.63) is interpreted as a crystallization age of the granitic protolith (Jacobs et al., 2015). The biotite WMA of  $502.7 \pm 1$  Ma (MSWD = 1.03) and the IIA of  $500.2 \pm 4.6$  Ma (MSWD = 0.69) include 75.2 % of the released  $^{39}\text{Ar}$ ; the initial  $^{40}\text{Ar}/^{36}\text{Ar}$  value of  $1476 \pm 910$  reflects the high radiogenic yield (Figure 6.4). Our preferred  $501 \pm 5$  Ma age likely reflects post-crystallization cooling.

Sample J1221D\_1, grey gneiss [bt], moraine sample (72.33105°S; 23.25415°E)

This gneiss from a moraine between Swaabsteinen and Causinknappen consists mainly of quartz, plagioclase, microcline, myrmekite, and biotite. Quartz shows undulose extinction, subgrain-rotation and grain-boundary-migration recrystallization. Dark brown biotite with columnar habitus shows no preferred orientation. Accessory minerals are zircon and opaques. 80.4 % of the released  $^{39}\text{Ar}$  yielded a biotite WMA of  $505.3 \pm 1.5$  Ma (MSWD = 0.86) and a IIA at  $501.8 \pm 4.7$  Ma (MSWD = 2.3) with elevated  $^{40}\text{Ar}/^{36}\text{Ar}$  value of  $904 \pm 440$ , consistent with the hump in the central part of the spectrum, which indicates that these steps incorporated extraneous Ar (Figure 6.4). Our preferred age is  $503 \pm 10$  Ma.



## SW Terrane S Adjacent to the MSZ

### *Sample 1205A2, biotite-schist [bt], Dry Valley (72.10802°S; 23.18322°E)*

This hornblende-biotite schist from the northern part of Dry Valley (Figure 6.5a) consists of plagioclase, amphibole, chlorite, quartz, biotite, clinopyroxene, and epidote. Quartz shows grain-boundary-migration recrystallization. Dark brown biotite and greenish-blue hornblende define the foliation. Accessories are epidote, titanite, and rutile. 70.8 % of the released  $^{39}\text{Ar}$  defined at biotite WMA age of  $542.7 \pm 1.2$  Ma (MSWD = 0.86); the IIA is  $535.5 \pm 8.2$  (MSWD = 0.59) with an ill-defined initial  $^{40}\text{Ar}/^{36}\text{Ar}$  of  $987 \pm 490$  (Figure 6.6). The slightly hump-shaped spectrum indicates extraneous Ar in these oldest-age steps; our preferred age interpretation,  $538 \pm 15$  Ma, thus emphasizes the lower-age steps at the high-temperature degassing end of the spectrum.

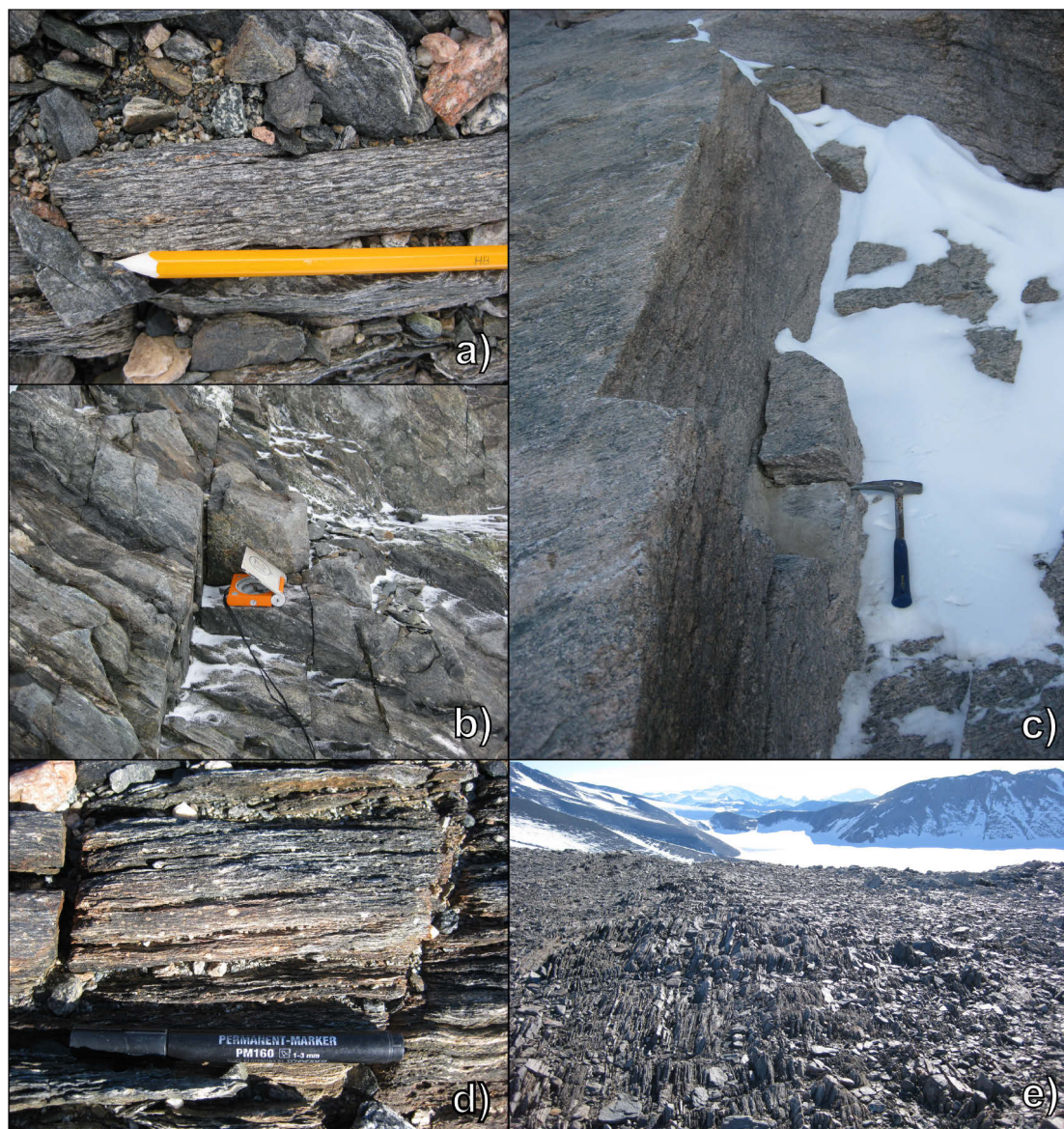


Figure 6.5: Field photographs of samples collected along the Main Shear Zone (MSZ). a) Dry Valley, mylonitic biotite-schist (1205A2); b) Ketelersbreen West, mylonitized diorite (1131A1); c) Gunnestadbreen West, Vengen/Vikinghøgda-type granite (1130D\_1); d+e) Ellis-/Jenningsbreen, view towards the west along strike of the MSZ and close up of mylonitic rock with tonalitic composition at this location (1218A1).



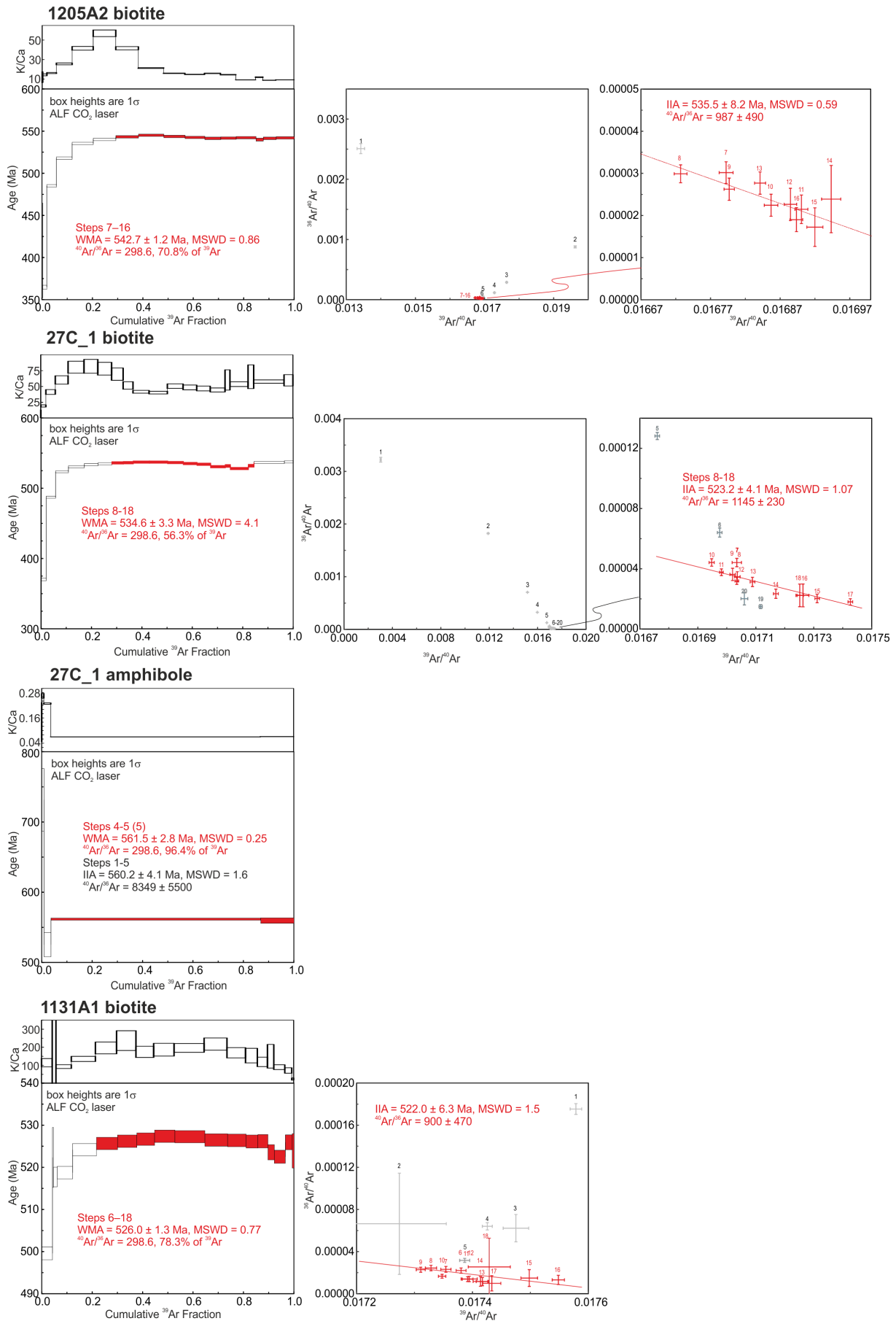


Figure 6.6:  $^{40}\text{Ar}/^{39}\text{Ar}$  age spectra and isochrons of samples along the MSZ. Ages are given with  $1\sigma$  uncertainties (including error in J).



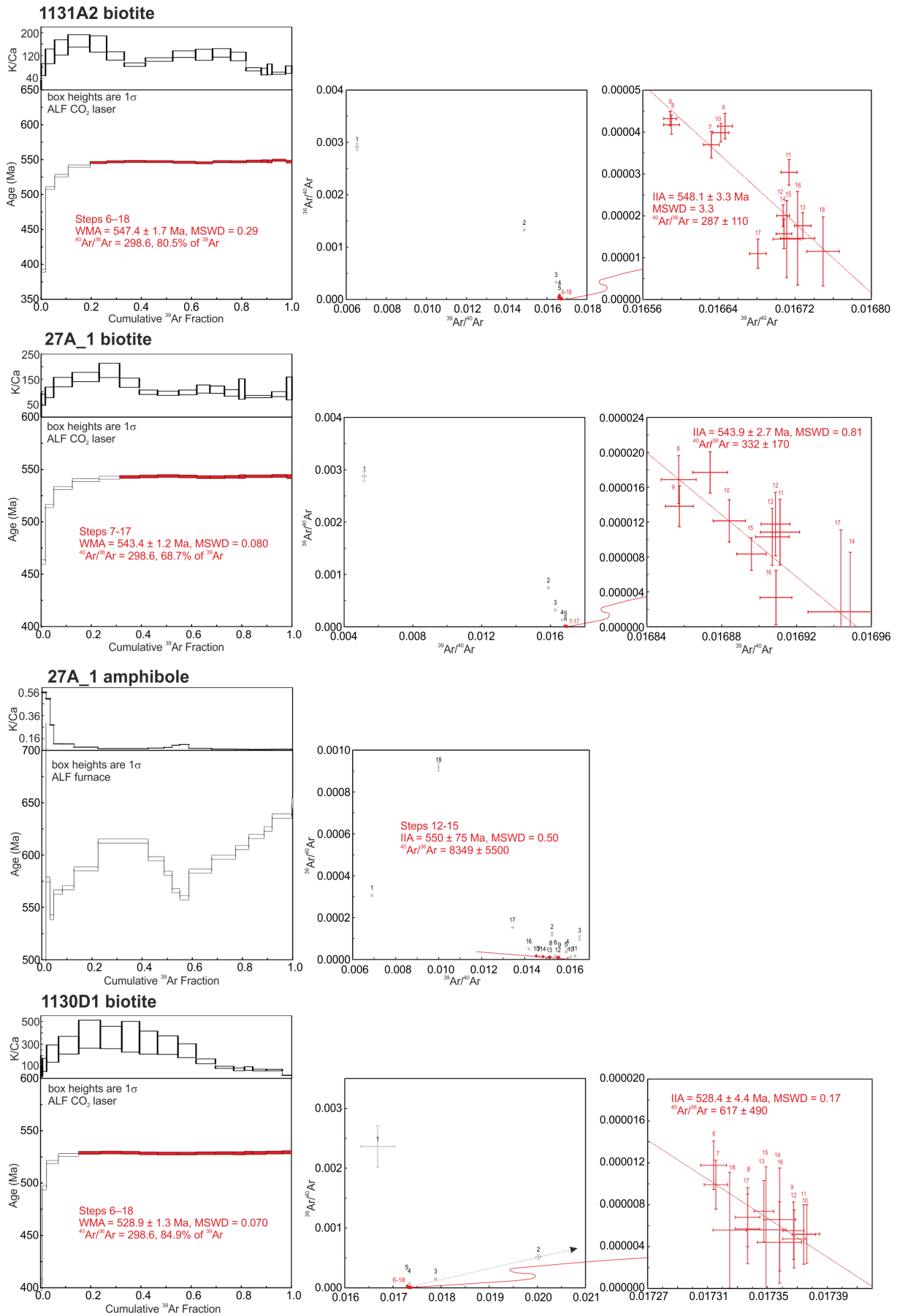


Figure 6.6: (continued)



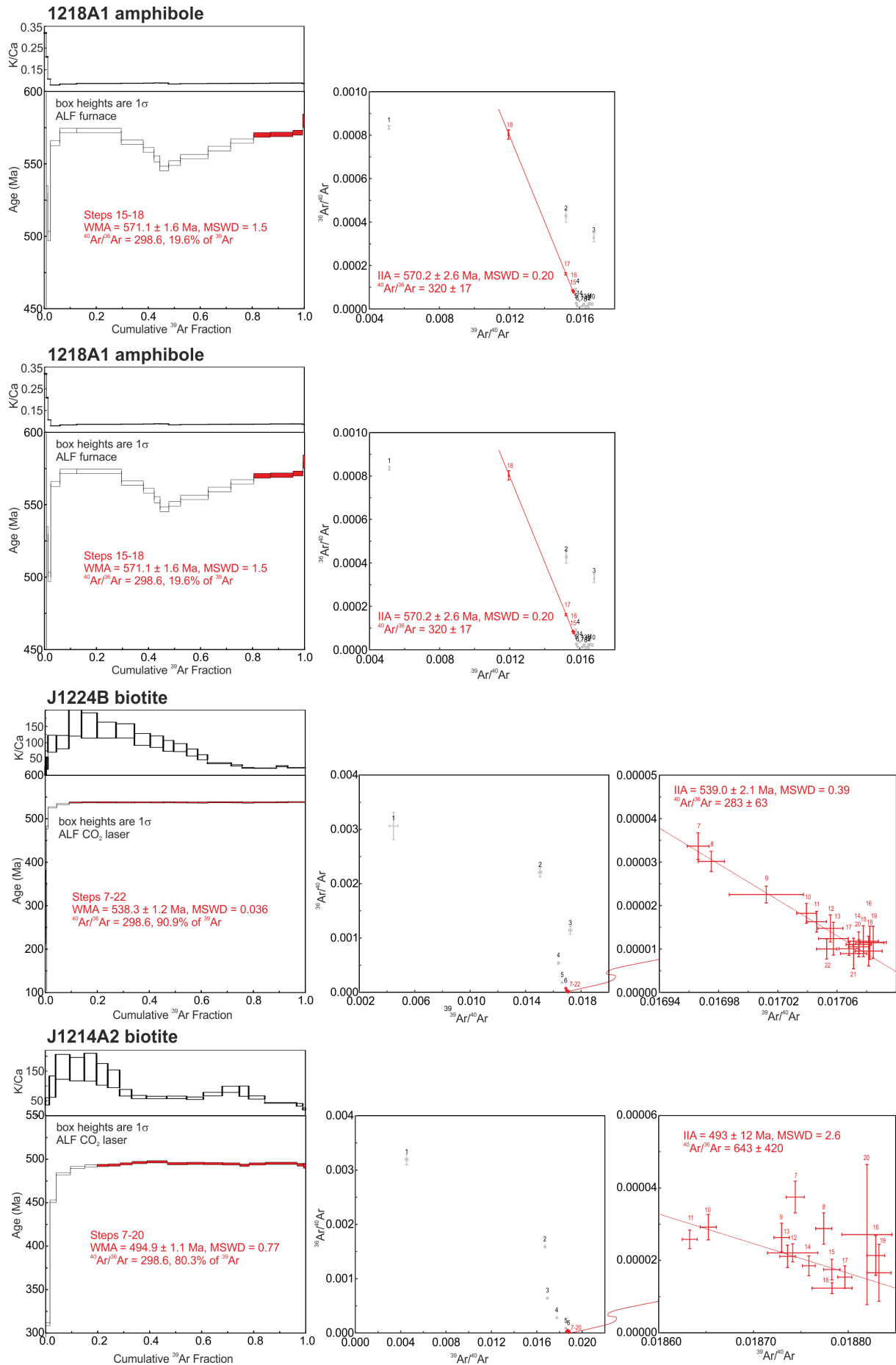


Figure 6.6: (continued)



Sample 27C\_1, mylonitic granodiorite gneiss [bt, hbl], Dry Valley (72.11°S; 23.1987°E)

This banded gneiss, composed of layers of recrystallized feldspar and quartz, was sampled at the western side of Ketelersbreen. Quartz shows both subgrain-rotation and grain-boundary-migration recrystallization. Plagioclase, K-feldspar, and hornblende form porphyroclasts with asymmetric pressure-shadow tails of recrystallized quartz, hornblende, and biotite. Dark brown biotite and greenish-blue hornblende occur within foliation. Epidote and opaque minerals are accessories. 56 % of the released  $^{39}\text{Ar}$  yielded a biotite WMA of  $534.6 \pm 3.3$  Ma; the high MSWD of 4.1 reflects the hump-shape of the spectrum (Figure 6.6). The IIA of  $523.2 \pm 4.1$  Ma (MSWD = 1.07) is younger with an initial  $^{40}\text{Ar}/^{36}\text{Ar}$  value of  $1145 \pm 230$ . Our preferred age interpretation of  $524 \pm 10$  Ma follows the youngest high-temperature steps and the IIA. 96.4 % of the released  $^{39}\text{Ar}$  yielded an amphibole WMA of  $561.5 \pm 2.8$  Ma (MSWD = 0.25). This date is based on only two steps; the IIA of all 5 steps (little material did not allow more steps to be measured) at  $560.2 \pm 4.1$  Ma (MSWD = 1.6;  $^{40}\text{Ar}/^{36}\text{Ar} = 8349 \pm 5500$ ; Figure 6.6) may indicate that this date has geological meaning. Our preferred age is  $561 \pm 20$  Ma.

Sample 1131A1, biotite-gneiss [bt], Ketelersbreen West (72.10577°S; 23.19255°E)

This fine-grained, foliated biotite-schist is from an outcrop west of Ketelersbreen close to the MSZ (Figure 6b). Quartz occurs as coarse-grained bands as well as recrystallized small grains. Plagioclase shows bulging recrystallization. Feldspar porphyroclasts show strong sericitization and are partly replaced by quartz. The porphyroclasts indicate a dextral sense of shear and have biotite in their pressure-shadow tails. Biotite, chlorite, and muscovite form the foliation. The mineral association, with quartz and plagioclase and minor amounts of chlorite, biotite, muscovite, and amphibole, suggests that this schist formed due to localized shearing of a tonalitic host rock under retrograde, greenschist-facies conditions.

78.3 % of the released  $^{39}\text{Ar}$  yielded a biotite WMA of  $526.0 \pm 1.3$  Ma (MSWD = 0.77) and an IIA of  $522 \pm 6.3$  (MSWD = 1.5; Figure 6.6). Again, the high radiogenic yield resulted in an ill-defined initial  $^{40}\text{Ar}/^{36}\text{Ar}$  value of  $900 \pm 470$ ; the hump-shaped spectrum reflects the extraneous Ar. Our preferred age is  $525 \pm 5$  Ma.

Sample 1131A2, mylonitic diorite gneiss [bt], Ketelersbreen East (72.10470°S; 23.19660°E)

This mylonitized diorite is from at the eastern side of Ketelersbreen. The main component is plagioclase, which forms asymmetric porphyroclasts (Figure 6.7a). Amphibole, chlorite, and biotite form the foliation. Quartz shows grain-boundary-migration and occurs in bands. 80.5 % of the released  $^{39}\text{Ar}$  provided a biotite WMA of  $547.4 \pm 1.7$  Ma (MSWD = 0.29) and an IIA age of  $548.1 \pm 3.3$  Ma (MSWD = 3.3; initial  $^{40}\text{Ar}/^{36}\text{Ar}$  value =  $287 \pm 110$ ; Figure 6.6). Our preferred age is  $547 \pm 5$  Ma.

Sample 27A\_1, mylonitic garnet-biotite-hornblende gneiss [bt, hbl], Dry Valley (72.113°S; 23.340083°E)

This gneiss from SE of Ketelersbreen consists of quartz, plagioclase, and minor K-feldspar, biotite, and amphibole. Quartz shows undulose extinction, subgrain-rotation and grain-boundary-migration recrystallization. Feldspar shows bulging recrystallization. Dark brown biotite and greenish-blue hornblende parallel the foliation; biotite occurs also in the pressure-shadow tails of feldspar porphyroclasts. Accessory minerals are garnet, zircon, epidote, and



opaque minerals. 68.7% of the released  $^{39}\text{Ar}$  provided a biotite WMA of  $543.4 \pm 1.2$  Ma (MSWD = 0.08) and an IIA of  $543.9 \pm 2.7$  Ma (MSWD = 0.81;  $^{40}\text{Ar}/^{36}\text{Ar}$  initial =  $332 \pm 170$ ; Figure 5). Our preferred age is  $544 \pm 5$  Ma. Amphibole of the same sample yielded a complex spectrum; the IIA, plagued by the high radiogenic yield, indicates an age overlapping with that of the biotite ( $550 \pm 150$  Ma; Figure 6.6).

*Sample 1130D\_1, monzogranite [bt], Gunnestadbreven West (72.09382°S; 23.41065°E)*

This Vengen/Vikinghøgda-type monzogranite, taken north of the MSZ, contains quartz, plagioclase, K-feldspar as major and biotite, muscovite, chlorite, titanite, and magnetite as minor components (Figure 6.5c, 6.7b). Asymmetric plagioclase and K-feldspar porphyroclasts, indicating dextral sense of shear, are surrounded by recrystallized plagioclase and bands of elongated quartz. Dark brown biotite occurs along the foliation and in the pressure shadows of plagioclase porphyroclasts. The Vengen/Vikinghøgda granite yielded crystallization ages of  $562 \pm 7$  Ma (Shiraishi et al., 2008) and  $551 \pm 8$  Ma (Elburg et al., 2016). 84.9 % of the released  $^{39}\text{Ar}$  provided a biotite WMA of  $528.9 \pm 3$  Ma (MSWD = 0.07) and a IIA of  $528.4 \pm 4.4$  Ma (MSWD = 0.17;  $^{40}\text{Ar}/^{36}\text{Ar}$  =  $617 \pm 490$ ; Figure 6.6). Our preferred age for the cooling of the Vengen/Vikinghøgda-type granite through biotite closure is  $529 \pm 5$  Ma.

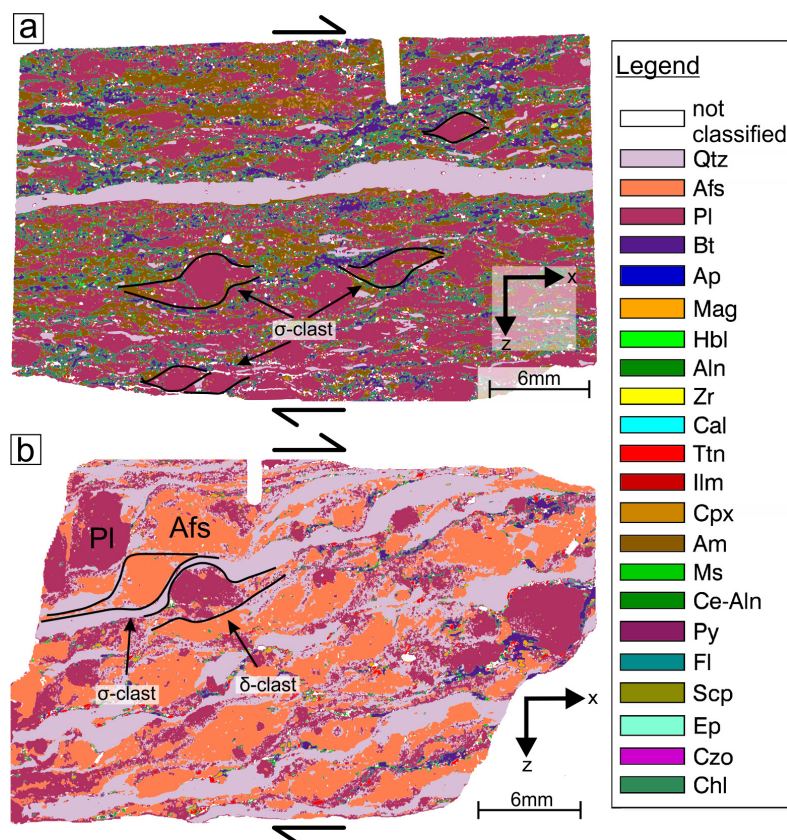


Figure 6.7: Composition of rock samples used for Ar/Ar dating located close to the MSZ. Rotated porphyroclasts within these thin sections indicate dextral shear sense. Thin sections were mapped with energy dispersive X-ray fluorescence with the M4 Tornado. a) Sample 1130D\_1, mylonitic monzogranite, b) Sample 1131A2, mylonitized rock of dioritic composition.



Sample 1218A1, mylonitic amphibole schist [bt], Ellis-/Jenningsbreen (72.05343°S; 24.29992°E)

This mylonite of tonalitic composition from a ridge between Ellisbreen and Jenningsbreen in the central part of the MSZ (Figure 6d, e) is strongly foliated and consists mainly of amphibole, plagioclase, quartz, scapolite, and clinopyroxene. Epidote, chlorite, clinozoisite, ilmenite, biotite, hornblende, and magnetite are accessories. Quartz in bands is elongated, shows subgrains and grain-boundary-migration recrystallization. Relictic plagioclase porphyroclasts are mostly recrystallized. Greenish-blue hornblende and fine grained biotite define the foliation. Just 19.6 % of the released  $^{39}\text{Ar}$  defined a amphibole WMA age of  $571.1 \pm 1.6$  Ma (MSWD = 1.5) and an IIA of  $570.2 \pm 2.6$  (MSWD = 0.2; initial  $^{40}\text{Ar}/^{36}\text{Ar} = 320 \pm 17$ ; Figure 6.6). Our preferred age is  $570 \pm 20$  Ma.

Sample 1203A4, orthomylonite [hbl], Ridge W of Ellisbreen, (72.0824°S, 23.0126°E)

This orthomylonite consists mainly of foliation-parallel greenish-blue hornblende, clinopyroxene, plagioclase, and minor quartz. Plagioclase porphyroclasts are altered to clinozoisite and epidote. Accessory minerals are epidote, opaque minerals and titanite. No meaningful age could be calculated for this sample but the amphibolite date is likely younger than ca. 600 Ma (Figure B.1, ‘Electronic Appendix’).

Sample 1208A1, mylonite of tonalitic composition [hbl], Widerøfjellet West (72.12718°S; 23.0126°E)

This mylonite from the western Dry Valley consists mainly of quartz, feldspar, greenish-blue hornblende, and dark brown biotite. Feldspar porphyroclasts have recrystallized mantles and asymmetric pressure shadows. Hornblende defines the foliation. Epidote appears as accessory. No precise age could be calculated; two isochrons through different steps may suggest an amphibole age between 600 and 550 Ma (Figure 6.6).

Sample J1224B, biotite-sillimanite-schist [bt], Meffell (72.07886°S; 25.13041°E)

This fine- to medium-grained gneiss consists of plagioclase, quartz, olive-green biotite, sillimanite, plenty of magnetite, and accessory apatite. 90.9 % of the released  $^{39}\text{Ar}$  provided a biotite WMA of  $538.3 \pm 1.2$  Ma (MSWD = 0.04) and an IIA of  $539.0 \pm 2.1$  Ma (MSWD = 0.39; initial  $^{40}\text{Ar}/^{36}\text{Ar} = 283 \pm 63$ , Figure 6.6); our preferred age is  $539 \pm 5$  Ma.

Sample J1214A\_2, granitic gneiss [bt], Ridge E of Taggen (72.14513°S; 21.6089°E)

This medium-grained orthogneiss from a ridge east of Taggen contains quartz of variable grain size with undulose extinction and grain-boundary-migration recrystallization; locally, recovery fabrics occur. Greenish-blue hornblende, K-feldspar, and plagioclase are rare, light- to dark-brown biotite with a columnar to radial texture is common but partly altered to chlorite. Accessories are zircon, epidote, and opaque minerals. U-Pb zircon dating yielded a crystallization age of  $980 \pm 8$  Ma (MSWD = 2.74) (Jacobs et al., 2015). 80.3 % of the released  $^{39}\text{Ar}$  provided a biotite WMA of  $494.9 \pm 1.1$  Ma (MSWD = 0.77) and an IIA of  $493 \pm 12$  Ma (MSWD = 2.6) with an initial  $^{40}\text{Ar}/^{36}\text{Ar}$  value of  $643 \pm 420$  due to the high radiogenic yield (Figure 6.6). Our preferred age is  $495 \pm 5$  Ma.



## SW Terrane N and CSRC

### Sample 06A-1, orthogneiss [bt], Fokknuten (71.9139°S; 22.97610°E)

This grey, foliated orthogneiss consists of quartz, feldspar, biotite, and hornblende. Quartz shows undulose extinction, subgrains, and grain-boundary-migration recrystallization. Plagioclase and microcline are common. Dark brown biotite with a columnar habitus and greenish-blue hornblende parallel the foliation. Accessory minerals are titanite, zircon, and opaques. 81.9 % of the released  $^{39}\text{Ar}$  yielded a biotite WMA of  $493.4 \pm 1.2$  Ma (MSWD = 0.49), and an IIA of  $491.5 \pm 7.5$  Ma (MSWD = 2.6; initial  $^{40}\text{Ar}/^{36}\text{Ar} = 660 \pm 420$ ). The weakly hump-shaped spectrum indicates extraneous Ar in the intermediate-temperature steps; WMAs calculated for parts of the spectrum yielded identical ages (Figure 6.8). Our preferred age is  $493 \pm 5$  Ma.

### Sample 10A3, grey gneiss [bt], Teltet (71.9924°S; 23.49375°E)

This gneiss is interpreted as a metavolcanic rock; it consists of coarse-grained quartz and plagioclase, set in a finer-grained groundmass of quartz, feldspar, and dark-brown biotite with accessory titanite. Calcite and muscovite are secondary minerals. 92.1 % of the released  $^{39}\text{Ar}$  provided a biotite WMA of  $490.4 \pm 1.5$  Ma (MSWD = 0.54; Figure 6.8). No IIA calculation was possible. Our preferred age is  $490 \pm 5$  Ma.

### Sample J1224C, granitic gneiss [bt], Bratnipene South (71.96869°S; 24.26387°E)

This well-foliated orthogneiss consists of quartz, feldspar, and biotite with accessory allanite, titanite, apatite, zircon, and opaques. Plagioclase is often saussuritised, and quartz sometimes forms bands. 76.8 % of the released  $^{39}\text{Ar}$  yielded a biotite WMA of  $491.2 \pm 3.3$  Ma (MSWD = 0.38; Figure 6.8); due to the high radiogenic yield, no meaningful IIA could be calculated. Our preferred age is  $491 \pm 5$  Ma.

### Sample 1219C1, garnet-biotite gneiss [bt], Menipa (71.95688°S; 25.13605°E)

This banded gneiss from the Sør Rondane corridor at Menipa is mainly composed of K-feldspar, plagioclase, quartz, biotite, and garnet. 57.3 % of the released  $^{39}\text{Ar}$  yielded a biotite WMA of  $497.7 \pm 1.1$  Ma (MSWD = 0.47) and an IIA of  $494.9 \pm 2.9$  Ma (MSWD = 1.17) with an initial  $^{40}\text{Ar}/^{36}\text{Ar}$  value of  $455 \pm 100$  (Figure 6.8). Our preferred age is  $496 \pm 5$  Ma.

### Sample 1219D1, garnet-sillimanite-biotite gneiss [bt], Menipa (71.95467°S; 25.21993°E)

This gneiss from Menipa consists mainly of microcline, plagioclase, quartz, and biotite with accessory sillimanite, garnet, and titanite. 66.7 % of the released  $^{39}\text{Ar}$  provided a biotite WMA of  $508.4 \pm 1.6$  Ma (MSWD = 0.79) and an IIA of  $505.3 \pm 4.5$  Ma with a MSWD of 10.8 that indicates the presence of non-analytical scatter given by the high radiogenic yield and reflected in the initial  $^{40}\text{Ar}/^{36}\text{Ar}$  value of  $378 \pm 100$  (Figure 6.8). This sample also shows pronounced Ar loss in the low-temperature steps. Our preferred age is  $508 \pm 5$  Ma.



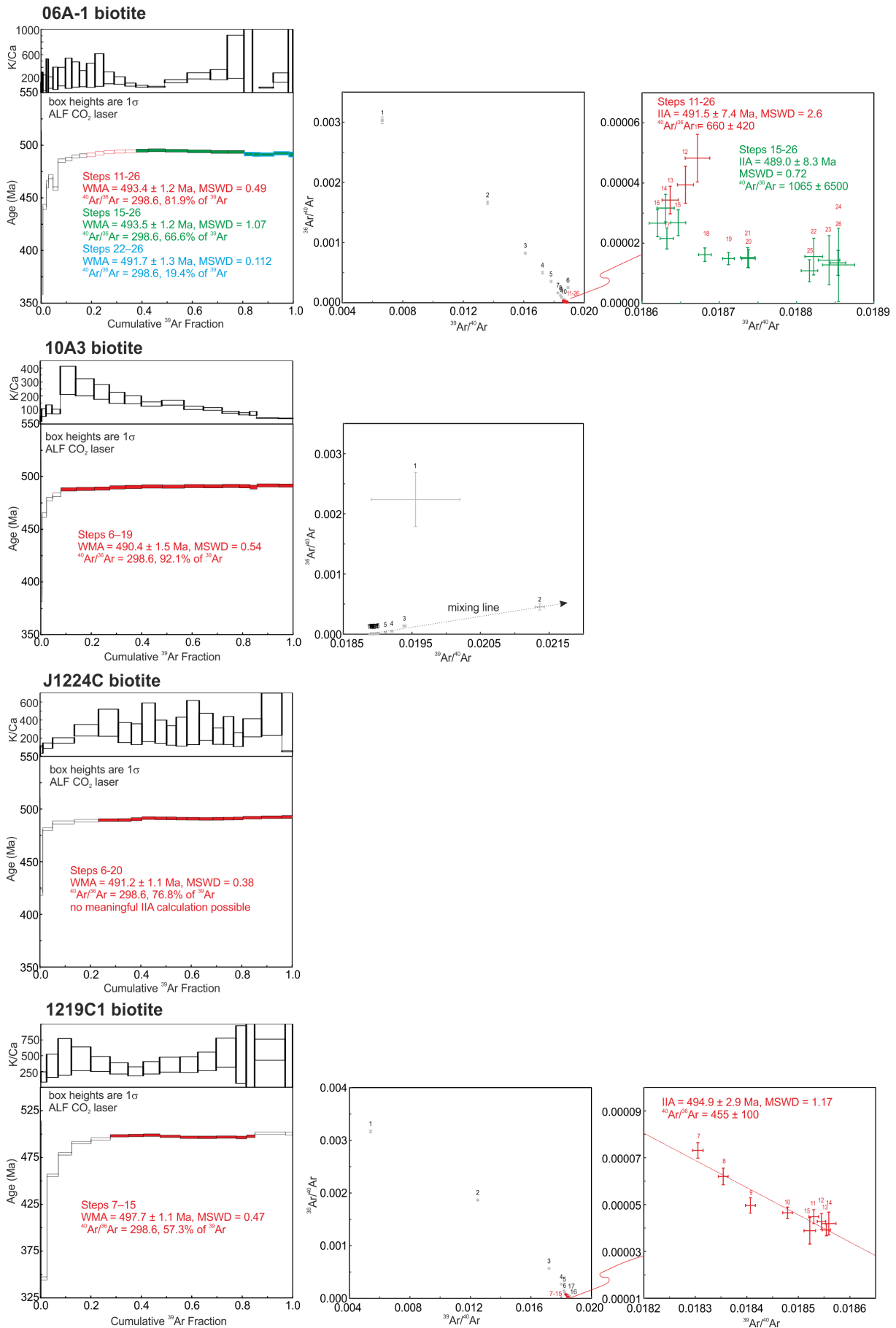


Figure 6.8:  $^{40}\text{Ar}/^{39}\text{Ar}$  age spectra and isochrons of samples from the SW Terrane N (06A-1, 10A3, J1224C) and the central Sør Rondane corridor (1219C1, 1219D1, J1225D). Ages are given with  $1\sigma$  uncertainties (including error in J).



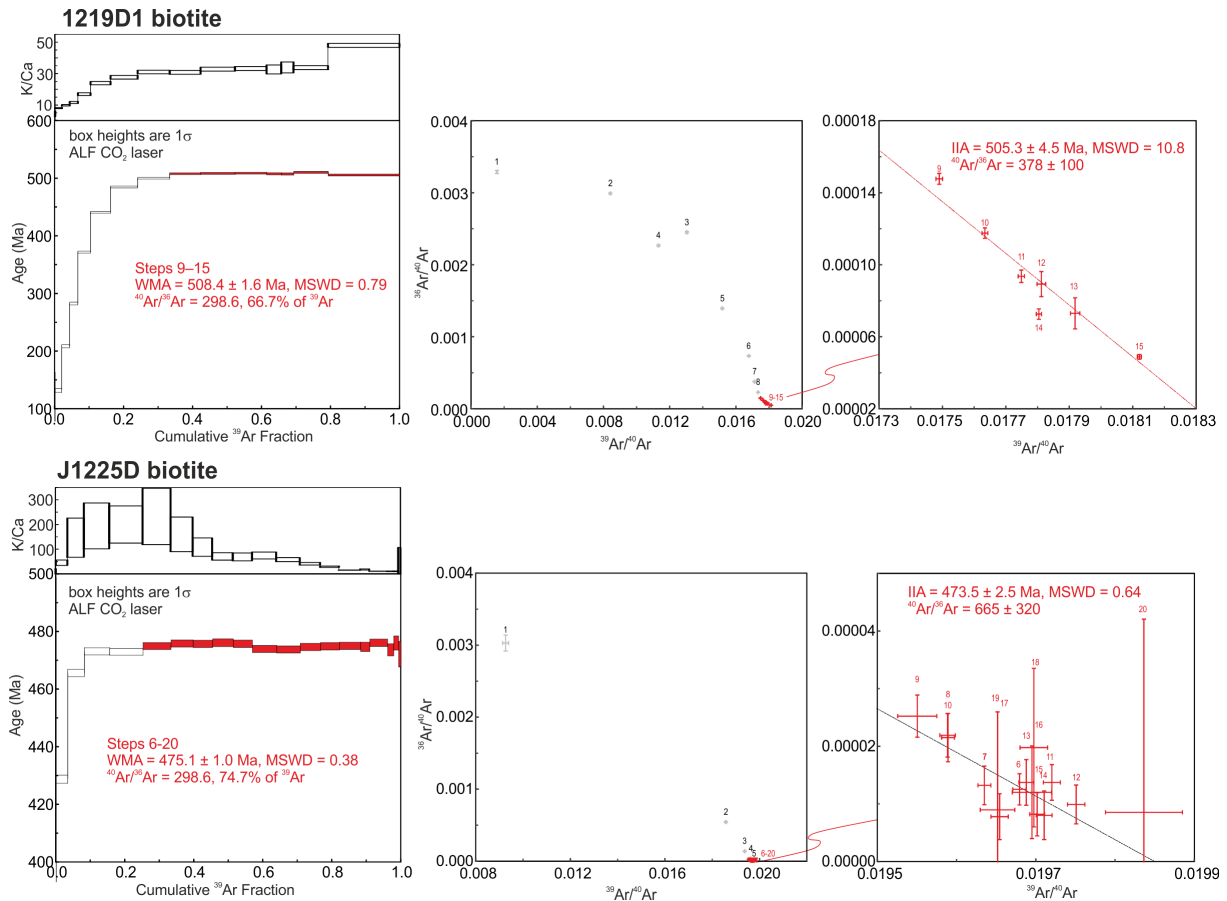


Figure 6.8: (continued)

Sample J1225D, granite [bt], Bautaen, (72.01281°S; 26.06616°E)

This granite gave a weighted mean  $^{206}\text{Pb}/^{238}\text{U}$  zircon age of  $532 \pm 3$  Ma, interpreted as its crystallization. It consists of quartz, plagioclase, microcline, and myrmekite. Biotite is weakly altered to chlorite, and titanite is associated with opaque minerals (Elburg et al., 2016). 74.7 % of the released  $^{39}\text{Ar}$  yielded a biotite WMA of  $475.1 \pm 1.0$  Ma (MSWD = 0.38) and an IIA of  $473.5 \pm 2.5$  Ma; the initial  $^{40}\text{Ar}/^{36}\text{Ar}$  value is  $665 \pm 320$ , again imprecise due to the high radiogenic yield (Figure 6.8). Our preferred age is  $474 \pm 5$  Ma.

**NE Terrane**Sample J1225A, diorite [bt, hbl], NE Terrane (72.38207°S; 27.97441°E)

This coarse-grained diorite has a U-Pb Concordia age of ca. 570 Ma for metamorphic zircon (unpublished, personal information J. Jacobs). 98.2 % of the released  $^{39}\text{Ar}$  provided a biotite WMA of  $487.6 \pm 1.5$  Ma (MSWD = 0.30) and an IIA of  $488.0 \pm 2.8$  Ma (MSWD = 2.5; initial  $^{40}\text{Ar}/^{36}\text{Ar}$  value =  $365 \pm 71$ ; Figure 6.9). Our preferred age is  $488 \pm 5$  Ma. The amphibole spectrum is complex. IIAs at ~525 and 500 Ma for the high- and low-temperature steps can be calculated; the low-temperature IIA may represent an amphibole-biotite mixture (Figure 6.9).



**Sample J1225C, migmatitic gneiss [bt], NE Terrane (72.26139°S; 27.86756°E)**

This coarse-grained gneiss consists of quartz, myrmekite, perthitic microcline, biotite, and minor olive-green hornblende. Feldspars are dynamically recrystallised. 85.1 % of the released  $^{39}\text{Ar}$  yielded a biotite WMA of  $476.8 \pm 1.1$  Ma (MSWD = 0.85); the IIA is  $475.9 \pm 5.0$  Ma (MSWD = 6.5; initial  $^{40}\text{Ar}/^{36}\text{Ar} = 462 \pm 270$ ; Figure 6.9). Our preferred age is  $476 \pm 5$  Ma.

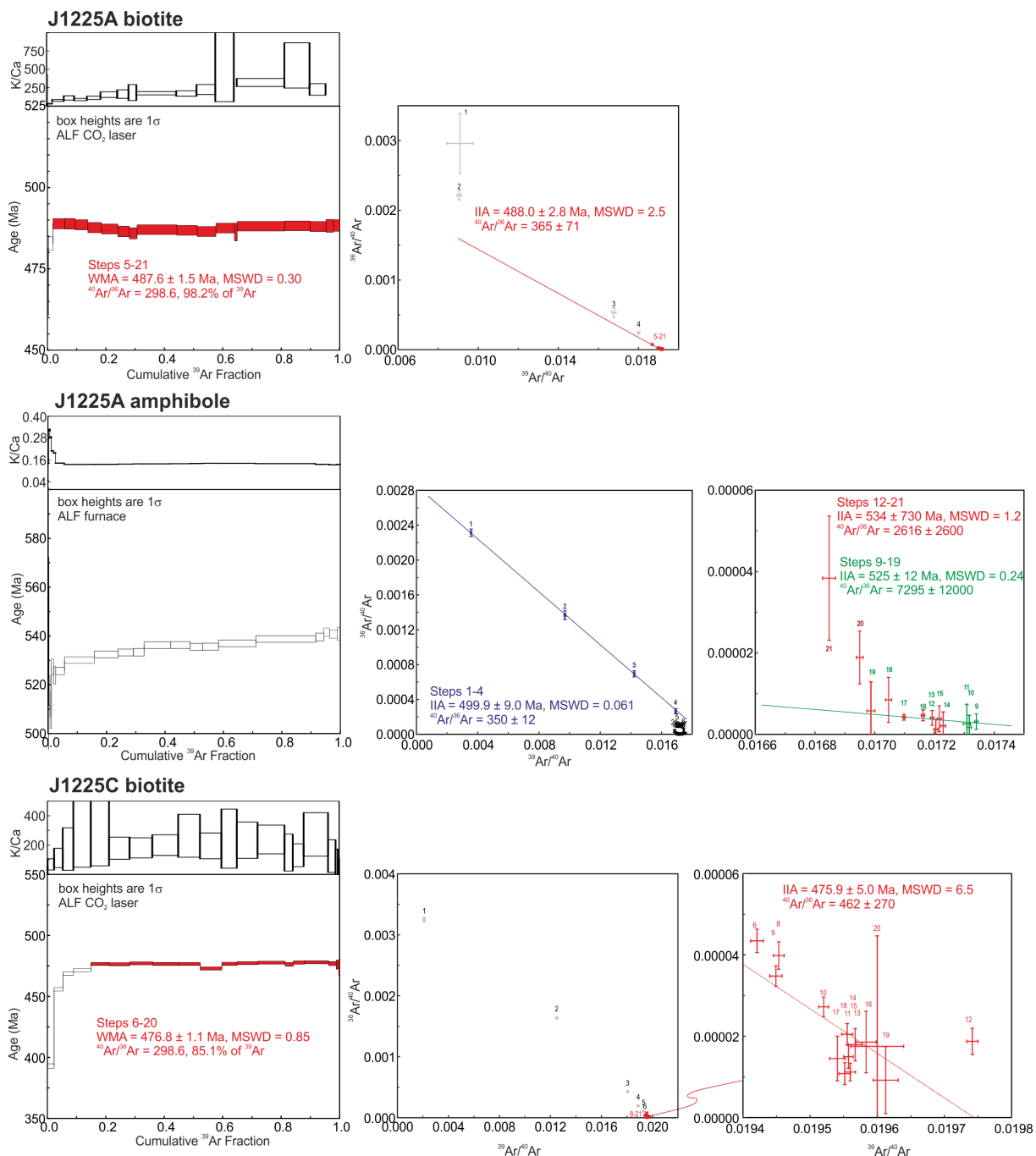


Figure 6.9:  $^{40}\text{Ar}/^{39}\text{Ar}$  age spectra and isochrons of samples from the NE Terrane. Ages are given with  $1\sigma$  uncertainties (including error in J).



## 6.5.2 U-Pb Age Data of Zircons

Zircon U-Pb data were acquired for three granitoids (Figure 6.10-6.12) that occur along the MSZ.

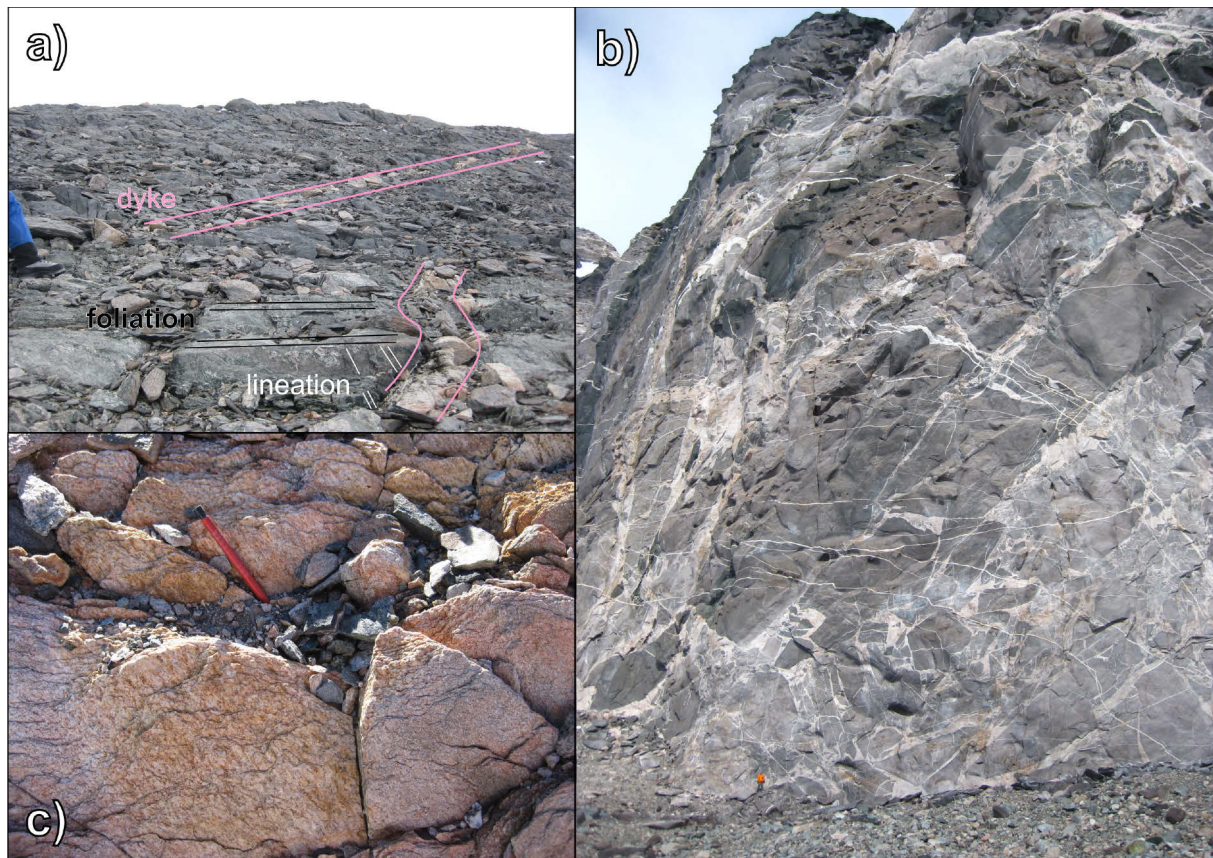


Figure 6.10: Field photographs of dated intrusive rocks. a) Dry Valley, deformed monzogranitic dyke cuts through mylonitic schist and is offset by a younger oblique reverse fault (1205A5); b) Lunckeryggen, syenite complex (1217A1) with human for scale; c) Ridge W of Ellisbreen, monzogranitic dyke with mylonitic texture, pencil indicates stretching lineation (1219B1).

Sample 1217A1, Syenite, Lunckeryggen E (72.03301°S; 24.59775°E); (U-Pb isotopic data, Table B.3 'Electronic Appendix')

This Lunckeryggen syenite is from its eastern flank in the eastward prolongation of the MSZ. It is mainly composed of K-feldspar, which shows oscillatory extinction and perthitic exsolution. Quartz, clinopyroxene, titanite, amphibole, biotite, and plagioclase occur subordinately. Elburg et al. (2016) obtained a weighted mean U-Pb zircon crystallization age of  $560 \pm 9$  Ma ( $2\sigma$ ) on a sample from the same area, with inherited age populations at ca. 617, 715, and 960 Ma. The syenite sample of this study contained only few zircons. They are mainly subhedral and rounded, some are anhedral or occur as fragments. All zircons are  $<200 \mu\text{m}$  in size. Twenty-nine analyses on 25 crystals were performed with 22 concordant analyses (level of  $^{206}\text{Pb}/^{238}\text{U}$ – $^{207}\text{Pb}/^{206}\text{Pb}$  concordance 90–110 %, Figure 6.11a, b). The U content of the concordant analyses varies between 15 and 2055 ppm. Three age populations with Concordia ages of  $590.3 \pm 4.1$  Ma ( $\text{MSWD}_{\text{C+E}} = 1.07$ ),  $562.8 \pm 3.6$  Ma ( $\text{MSWD}_{\text{C+E}} = 1.2$ ) and  $513.8 \pm 6.3$  Ma ( $\text{MSWD}_{\text{C+E}} = 1.9$ ) could be detected. The oldest population ( $n=8$ ) was measured on zircon cores with oscillatory zonation (e.g. Figure 6.11g 1) and sometimes low-luminescent rims. Its Th/U ratio spans 0.12–0.57 with a median at 0.37. The population at ca. 563 Ma ( $n=10$ ) has Th/U ratios of



0.11–0.72 with a median of 0.37. The measured zircon cores and rims are clearly oscillatory zoned (e.g. Figure 6.11g 2). The youngest age population is represented by only 4 concordant measurements on mostly dark structureless zircon cores. The Th/U ratio of this population is low (0.04–0.27, median 0.1). The oldest age population of ca. 590 Ma may reflect inheritance from a most likely igneous protolith. The Concordia age of  $562.8 \pm 3.6$  Ma is suggested to represent the time of crystallization. The youngest age population of ca. 510 Ma likely is geologically meaningless.

*Sample 1205A5, monzogranite, Dry Valley (72.10802°S; 23.18322°E); (U-Pb isotopic data, Table B.3 'Electronic Appendix')*

This foliated dyke crosscuts amphibolite- to greenschist-facies mylonites of the MSZ and is mainly composed of quartz, K-feldspar, plagioclase, with minor amounts of titanite, secondary scapolite, and epidote. Quartz shows undulatory extinction and grain-boundary-migration recrystallization. K-feldspar is recrystallized and contains deformation twins. The large plagioclase grains show sericitisation. The dyke's foliation is oriented parallel to the mylonitic foliation of the MSZ.

The sample contains small (up to 150  $\mu\text{m}$ ), mainly prismatic, euhedral, and slightly rounded zircons. Ninety-four out of 106 spots yielded concordant ages (Figure 6.11c, d). The U concentration varies from 97 to 851 ppm (with one exception of 2690 ppm) and the Th/U ratios vary from 0.14 to 0.97. Four main age populations were found with U-Pb ages of ca. 590 Ma, 570 Ma, 550–540 Ma and 500 Ma (Figure 6.11d). Two single grains with oscillatory zoning yielded  $^{206}\text{Pb}/^{238}\text{U}$  ages of ca. 700 Ma. The oldest population ( $588.1 \pm 2.5$  Ma,  $n = 22$ ) was measured on zircon cores and rims with oscillatory to patchy zoning and oscillatory to low-luminescent overgrowths, which yielded Th/U ratios of 0.19–0.77 (median 0.38, Figure 6.11g 3). The main age population ( $n = 36$ ) yielded a Concordia age of  $569.4 \pm 2.1$  Ma ( $\text{MSWD}_{\text{C+E}} = 1.3$ ). The analyses were conducted on oscillatory zoned zircon cores with sometimes low luminescent rims (Figure 6.11g 4). The Th/U ratios range from 0.23–0.86 with a median of 0.39. Zircons of the age population of ca. 550–540 Ma show dark and patchy cores and rims with sometimes no internal structure. This spot dates were sometimes measured in cores with older rims. Their Th/U ratios span 0.17–0.74 (median 0.38). The youngest population at ca. 500 Ma was measured on 4 spots of low luminescent cores and rims with a median Th/U of 0.27 (0.14–0.82). One core exhibits an older rim. The age population at ca. 590 Ma may record inheritance. The Concordia age of  $569.4 \pm 2.1$  Ma is interpreted as the time of crystallization; we consider the the two younger age populations as geologically meaningless.



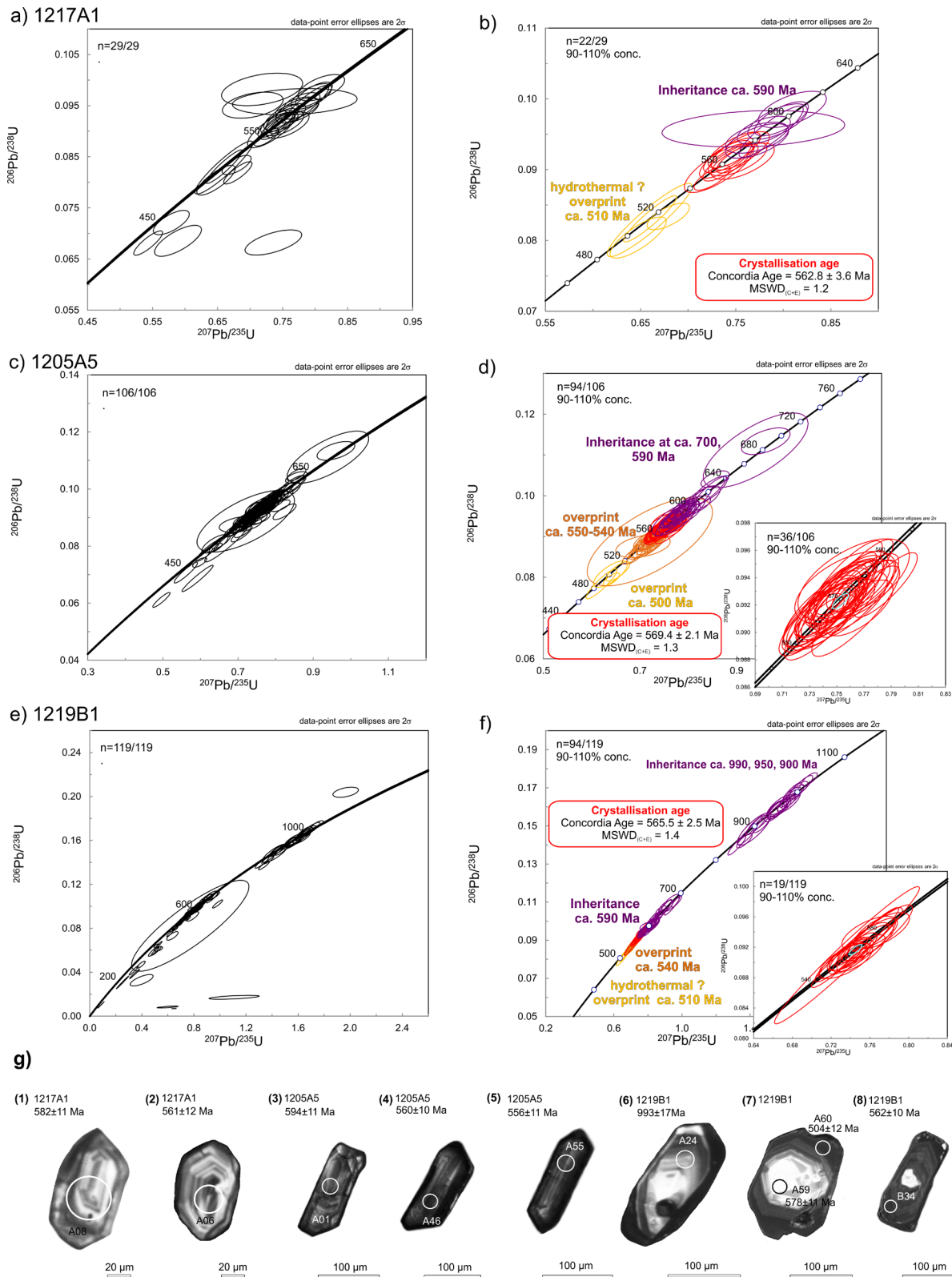


Figure 6.11: U-Pb zircon data. Concordia diagrams for all (a, c, e) and concordant (b, d, f) analytical spots. The diagrams indicate multiple age populations. The respective insets indicate the age population interpreted as the crystallization age. a, b) Sample 1217\_A1 reveals three age populations with concordant ages at ca. 590, 560 and 510 Ma. c, d) Sample 1205A5 reveals two age groups at ca. 700 and 590 Ma interpreted to reflect inheritance; the Concordia age at ca. 570 Ma is interpreted as the crystallization age. The younger spot dates at ca. 540 and 500 Ma may be geologically meaningless. e, f) Sample 1219B1 reveals five age groups with age populations at ca. 990, 950, 900, and 590 Ma, which reflect inheritance, and a Concordia crystallization age of ca. 566 Ma. Ellipses indicate  $2\sigma$  analytical uncertainties on single spot dates. g) Selected cathodoluminescence images of zircons with  $^{206}\text{Pb}/^{238}\text{U}$  dates of the marked ablation spot (circles).



*Sample 1219B1(3), monzogranite, ridge W of Ellisbreen, (72.05848°S; 24.13382°E) (U-Pb isotopic data, Table B.3 'Electronic Appendix')*

This dyke intruded a grey gneiss at a ridge west of Ellisbreen. It has a mylonitic texture orientated parallel to the MSZ. It consists mainly of quartz, K-feldspar, and plagioclase. Quartz shows undulose extinction, grain-boundary-migration recrystallization and foliation-parallel layers. Feldspar occurs as rotated asymmetric porphyroclasts with pressure shadows of muscovite and minor biotite. Chlorite, illmenite, magnetite, and titanite are accessories.

Zircons are subhedral, mainly long prismatic, sometimes rounded and reach up to 200  $\mu\text{m}$  in length. In cathodoluminescence images, many zircons show bright and oscillatory zoned cores, surrounded by dark rims, which are either oscillatory zoned or structureless (Figure 6.11d 6-8). Ninety-four of 119 ablation spots yielded concordant dates (Figure 6.11e, f). Four age populations at ca. 591, 566, 540, and 500 Ma were obtained. Additionally, 24 core measurements yielded concordant age populations of ca. 990, 950, and 900 Ma with median Th/U ratios of 0.33, 0.28, 0.29, respectively. Zircons of the oldest populations (990–900 Ma) are zoned and show high luminescent cores and rims. Eighteen analyses yielded a Concordia age of  $591 \pm 3.0$  Ma ( $\text{MSWD}_{\text{C+E}} = 1.4$ ) with Th/U ratios of 0.06–0.48 (median 0.19). A Concordia age of  $565.5 \pm 2.5$  Ma ( $\text{MSWD}_{\text{C+E}} = 1.4$ ,  $n = 19$ ) was obtained for the next younger age population. The measurements were conducted on oscillatory zoned zircon cores with dark luminescent rims. Their Th/U ratios range from 0.06–0.45 with a median of 0.15. The age of the 540-Ma population was obtained from rim analyses with Th/U ratios of 0.05–0.34 (median 0.08). The youngest population of ca. 500 Ma is represented by 4 analyses on dark structureless rims. The Th/U ratios are low with a range of 0.04–0.16 and a median of 0.11. We interpret the age populations at ca. 990, 950, 900, and 590 Ma as inheritance, and the Concordia age of  $565.5 \pm 2.5$  Ma as the crystallization age. The younger two age populations at 540 and 500 Ma may reflect overprinting events.

## 6.6 Interpretation and Discussion

In this study, we provide twenty-three new Ar/Ar biotite and two new Ar/Ar amphibole ages of ca. 570–480 Ma, complemented by three U-Pb zircon ages at 570–560 Ma of granitoid rocks exposed along the MSZ (Figure 6.12). Probability density and age histogram plots (Figure 6.13) summarize all available metamorphic and igneous U-Pb zircon ages (Li et al., 2006; Shiraishi et al., 2008; Adachi et al., 2013; Grantham et al., 2013; Higashino et al., 2013; Hokada et al., 2013; Nakano et al., 2013; Osanai et al., 2013; Owada et al., 2013; Jacobs et al., 2015; Elburg et al., 2016; this study) as well as the new and published Ar/Ar and K-Ar biotite cooling ages (Takigami et al., 1987; Takigami and Funaki, 1991, this study).

The large age spread of our new Ar/Ar ages together with the Ar/Ar and K-Ar mineral ages of the previous studies (Takigami et al., 1987; Takigami and Funaki, 1991) appear to reflect the protracted tectono-metamorphism and the similarly protracted igneous activity over 150 Ma in Sør Rondane (Elburg et al., 2016).



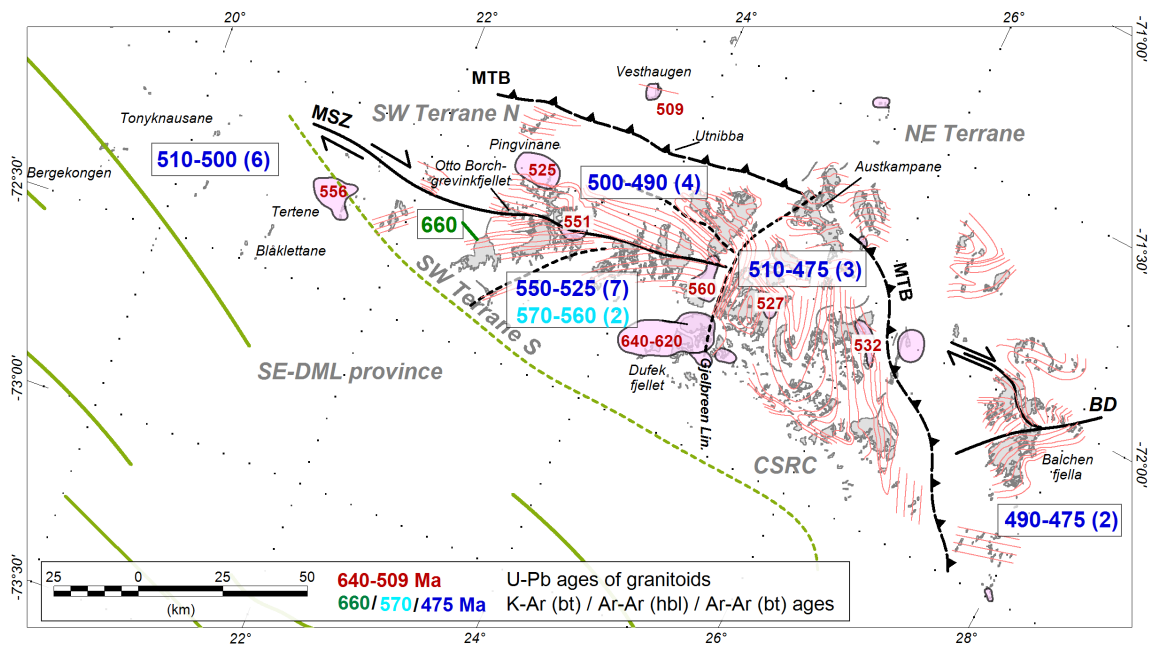


Figure 6.12: Summary and overview of new  $^{40}\text{Ar}/^{39}\text{Ar}$  ages (this study) and U-Pb zircon ages of major/voluminous granitoids (pink) available for Sør Rondane (Elburg et al., 2016). Dark Green: K-Ar age obtained from Nils Larsenfjellet (Takigami and Funaki, 1991). Black lines: Terrane boundaries interpreted based on combined aeromagnetic and geological findings modified after Mieth et al. (2014). Green lines: trend of magnetic anomalies within the SE-DML province, broken line southern boundary of the SE-Terrane S inferred from aeromagnetic data (Mieth et al., 2014). Red lines: Form line contours adapted from (Toyoshima et al., 2013). CSCRC = Central Sør Rondane Corridor; MSZ = Main Shear Zone; MTB = Main Tectonic Boundary.

In general, Sør Rondane was affected by two high-grade metamorphic events and voluminous and widespread igneous activity (e.g. Shiraishi et al., 2008; Elburg et al., 2016). Whilst the earlier granulite-facies metamorphism at 660–600 Ma is largely documented in the NE Terrane and along the contact to the SW Terrane N, the second amphibolite-facies metamorphism with a peak at ca. 580–570 Ma and subsequent regression until ca. 530 Ma is more widespread and is documented throughout Sør Rondane (e.g. Shiraishi et al., 2008). All Ar/Ar mineral ages of this study together with the available literature data post-date the main granulite-facies metamorphic event at ca. 640–600 Ma. Furthermore, our new Ar/Ar ages also post-date the second amphibolite-facies metamorphic event at ca. 580–570 Ma. Therefore, we interpret these ages to document cooling below the mineral-specific closure temperature of about 540–510 °C for a typical amphibole of 160  $\mu\text{m}$  with cooling rates between 25–5 °C/Myr (Harrison, 1982) and about 340–320 °C for a typical biotite of 250  $\mu\text{m}$  with cooling rates between 25–5 °C/Myr (Grove and Harrison, 1996).

The earlier granulite-facies metamorphism is interpreted to be related to the juxtaposition and overthrusting of the NE Terrane over the SW Terrane along the MTB (Osanaï et al., 2013). It is also contemporaneous with voluminous granitoid magmatism in the footwall of the MTB, namely the Dufek intrusion occurring at Dufekfjellet in the SW Terrane S and dated at ca. 640–620 Ma (Li et al., 2006; Elburg et al., 2016). The geochemistry of the Dufek granitoid shows a



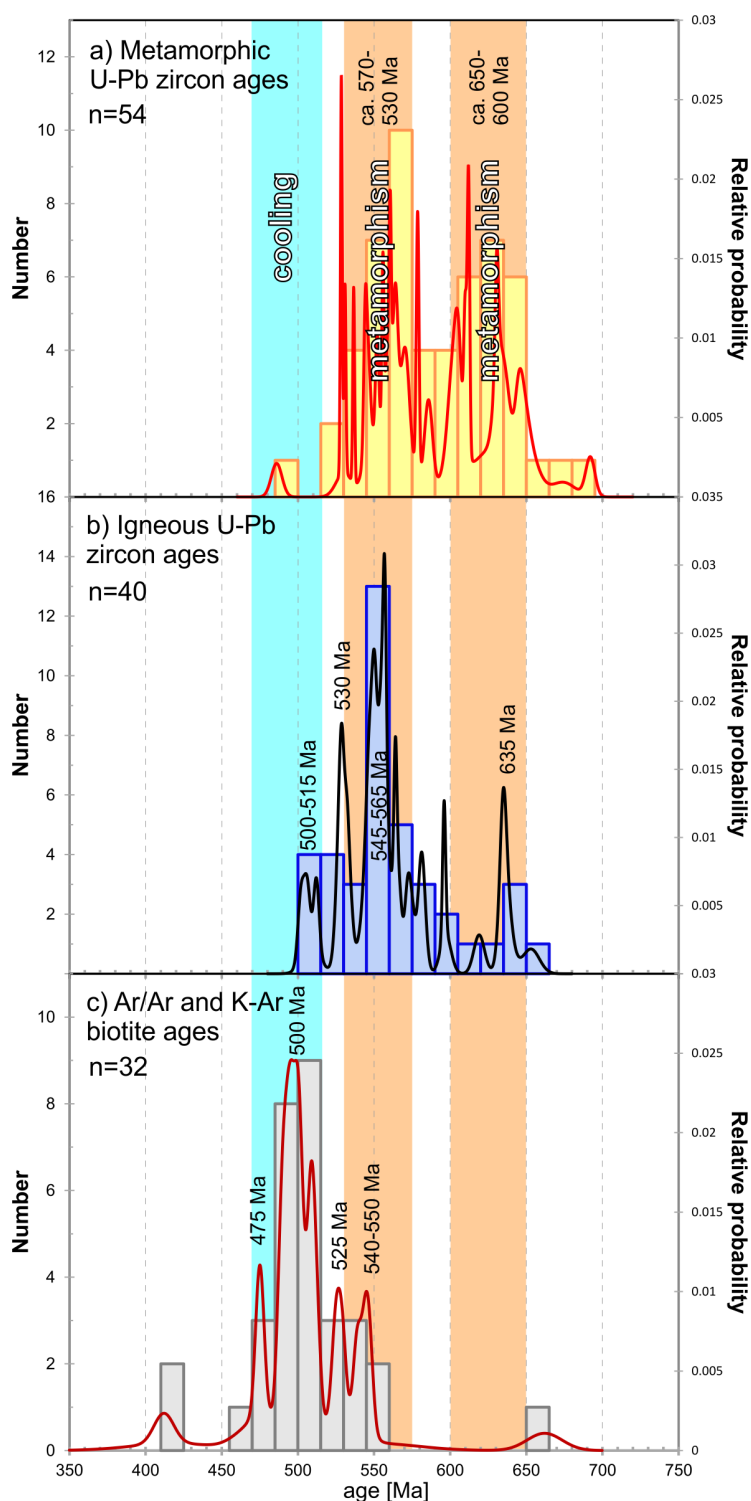


Figure 6.13: Metamorphic and igneous zircon U-Pb ages and Ar/Ar and K-Ar biotite cooling ages of Sør Rondane presented as probability density and age histogram plots. Source for U-Pb zircon ages: (Li et al., 2006; Shiraishi et al., 2008; Adachi et al., 2013; Grantham et al., 2013; Higashino et al., 2013; Hokada et al., 2013; Nakano et al., 2013; Osanai et al., 2013; Owada et al., 2013; Jacobs et al., 2015; Elburg et al., 2016; this study). Source for Ar/Ar and K-Ar biotite ages: (Takigami et al., 1987; Takigami and Funaki, 1991; this study).

volcanic-arc and/or collisional signature (Li et al., 2003), which may be explained by the crustal thickening.

At a regional scale, some parts of the SW Terrane S appear to be unaffected by the two high-grade tectono-metamorphic events. This terrane shows over large domains almost no or only weak deformation. The exception is its mylonitic to ultramylonitic contact to the SW Terrane N along the MSZ (e.g. Jacobs et al., 2015; Ruppel et al., 2015). Characteristically, the oldest K-Ar cooling age of  $662 \pm 23$  Ma comes from the weakly deformed core of the SW Terrane S at Nils Larsenfjellet (Takigami and Funaki, 1991). This terrane cooled below ca. 330 °C at that time, which is — within uncertainties — contemporaneous with the emplacement of the Dufek intrusion. The core of the SW Terrane S shows a broad NE-trending structural grain (Figure 6.12, form-line contours after Toyoshima et al., 2013). This is co-linear with the elongation of the Dufek intrusion and differs from the adjacent structural domains. Since the emplacement age of the Dufek intrusion and the cooling in the SW Terrane are nearly contemporaneous, it may be speculated that the NE-trending structural grain of the SW Terrane S originated at ca. 640 Ma. Therefore, this trend is probably a relatively old structural feature of Sør Rondane.



The oldest Ar/Ar mineral ages obtained in this study (ca. 570–525 Ma) are from the dextral, steeply south-dipping MSZ (Figure 12) which defines the northern margin of the SW Terrane S (Kojima and Shiraishi, 1986; Ruppel et al., 2015). The new Ar/Ar amphibole (570–560 Ma) and biotite ages (550–525 Ma) are similar or slightly younger than three U-Pb zircon crystallization ages of ca. 570–560 Ma of granitoid rocks, which occur along this shear zone (Shiraishi et al., 2008; Elburg et al., 2016, this study).

Two granitic dykes of ca. 570 Ma (1205A5, 1219B1) crosscut the main foliation of the MSZ but themselves show a foliation that parallels the MSZ fabric. Therefore, these dykes provide an upper age constraint for the timing of deformation in the central part of the MSZ. The third sample of ca. 560 Ma is from the Lunkeryggen syenitic complex, showing MSZ-parallel, late-stage ductile-brittle deformation (1217A1) (Ruppel et al., 2015). The new Ar/Ar amphibole ages of the mylonitic rocks of the MSZ are within the range of the granitoids; they are interpreted as dating the late-stage of shearing along the MSZ. The Ar/Ar biotite ages are interpreted as post-dating the ductile shearing. In general, our new granitoid crystallization ages coincide with the second main tectono-magmatic period in Sør Rondane that lasted from ca. 580 to 530 Ma (Figure 13) (e.g. Elburg et al., 2016).

The SW Terrane S is surrounded by three distinct tectonic domains to the north, east, and southwest, each with contrasting tectonic orientations compared to the SW Terrane S. All these domains record significant younger Ar/Ar cooling ages than the SW Terrane S. In the western nunataks (Figure 12), the structural grain is SE-trending, following the main trend of the magnetically distinct SE DML Province (Mieth et al., 2014). This area is interpreted to represent parts of the TOAST and is underlain by juvenile, ca. 1000–900 Ma old basement, tectonically interleaved with Neoproterozoic supracrustal rocks (Jacobs et al., 2015). Four Ar/Ar biotite ages derived from rocks of this region span 510–500 Ma. A fifth sample that gave an Ar/Ar biotite age of ca. 505 Ma was sampled from a moraine, which is interpreted to derive from the Antarctic interior to the S (J1221D-1, Jacobs et al., 2017). This indicates that TOAST-type rocks with ca. 500 Ma cooling ages are extensive and also occur significantly farther S. The closest larger pluton in the western Sør Rondane is at Tertene (Figure 12), which has a U-Pb zircon crystallization age of ca. 560 Ma (Elburg et al., 2016). Smaller late to post-tectonic granitoids provide evidence for igneous activity until 530 Ma (Jacobs et al., 2015). Granitoid magmatism as young as ca. 500 Ma is documented farther to the W at Steingarden (Jacobs et al., 2015). The Ar/Ar biotite cooling ages of the western Sør Rondane postdate the youngest phase (ca. 530 Ma) of tectono-metamorphism in the region. Furthermore, our new Ar/Ar ages indicate that the persistent SE-trend of the structural grain of the SE DML magnetic province is most likely younger than the NE-trend of the SW Terrane S; it probably originated relatively late in the structural evolution of the region, at ca. 530–500 Ma.

The SW Terrane N has an E-trending structural grain. This region records greenschist- to amphibolite-facies metamorphism at ca. 570–530 Ma, which is also documented in the CSRC and the NE Terrane (Osanai et al., 2013). It contains a major, ca. 530-Ma-old granitoid body at Utsteinen (Elburg et al., 2016). The sub-ice extent of this body has been mapped by aeromagnetic means and appears elongated E-W (Mieth et al., 2014). This orientation correlates



with the main E-trending structural grain of this domain. Four of our Ar/Ar biotite cooling ages derive from this domain and span 500–490 Ma; they are thus slightly younger compared to the ones from the western nunataks and post-date the metamorphic and magmatic activity.

In contrast, the CSRC to the E of the SW Terrane S has highly variable structural trends and shows large-scale folding at ca. 580–570 Ma (Toyoshima et al., 2013). Magnetic anomaly data indicate that the CSRC constitutes a discontinuity, disrupting the MTB into a western and an eastern part (Figure 6.12, Mieth et al., 2014). The CSRS may therefore represent a domain of major late-tectonic extension (Mieth et al., 2014). Two small granitoid bodies within the CSRC crystallized at ca. 530 Ma (Elburg et al., 2016) and two Ar/Ar biotite cooling ages are at 510 and 475 Ma. As for the SW Terrane N, the Ar/Ar biotite cooling ages post-date the late-tectonic magmatism by ca. 30 Ma.

The NE Terrane is largely dominated by an E-trending structural grain with the Balchen detachment, in Balchenfjella (Figure 6.12) possibly indicating large-scale extension between 600 and 550 Ma (Ishikawa et al., 2013). The NE Terrane exhibits only small granitoid intrusions that are mostly undated. One granitic dyke at Balchenfjella yielded a crystallization age of ca. 550 Ma (Shiraishi et al., 2008), whereas at Vesthaugen and the northern tip of Austkampane undeformed granitoid yielded crystallization ages of ca. 515–500 Ma (Adachi et al., 2013; Elburg et al., 2016). For the easternmost part of the NE Terrane, we obtained two Ar/Ar cooling ages of 490 and 475 Ma, the youngest ages of this study.

As indicated by Figure 13, the geochronological data record two major metamorphic events, which are accompanied by at least three magmatic pulses. A distinct age zoning of the emplacement of the larger granitoid bodies and of the Ar/Ar cooling occurs across Sør Rondane (Figure 6.12). The oldest and largest intrusion is the Dufek intrusion within the comparative weak deformed SW Terrane S (ca. 640–620 Ma). Ca. 530-Ma-old granitoids occur in the SW Terrane N and within the CSRC. The youngest igneous crystallization ages, ca. 515–500 Ma, are documented in the NE Terrane. This general crystallization age zoning correlates with the general younging of Ar/Ar mineral cooling ages. The systematic age trends correlate with the increasing distance to the central part of the EAAO and the assumed Late Neoproterozoic/Early Palaeozoic suture zone, which supports the hypothesis of a collage-style accretionary history in Sør Rondane (Elburg et al., 2016).

The SW Terrane S plays a special tectonic role, in that it (i) hosts the oldest and largest igneous intrusion, (ii) is comparatively little deformed, and (iii) appears to be surrounded by tectonic blocks, which are significantly more deformed and are characterised by younger intrusions and younger cooling ages. At the same time, the northern margin of the SW Terrane-S is confined by the MSZ, which syn- to post-tectonic granites at ca. 560 Ma, strung out along its length; it hosts the oldest Ar/Ar mineral ages of this study. We therefore interpret the SW Terrane S as a mega-boudin within a broad, rheologically weaker crust dominated by metasupracrustal rocks and overprinted by Late Neoproterozoic/Early Palaeozoic mobile belt(s), as suggested by Jacobs et al. (2015). The competent SW Terrane S appears exhumed along the tranpressive oblique MSZ (Ruppel et al., 2015) and experienced earlier cooling (with a higher estimated



cooling rate) than its surrounding regions. Further, the lack of younger granitoid intrusions and the higher rheological competence of the SW Terrane S, resulting in resistance to late-tectonic shearing. The adjacent structural domains may have remained at a deeper crustal levels, were accompanied by younger igneous pulses, and experienced later cooling, which kept these domains rheological weak and in turn led to strain concentration in them. This scenario may explain the up to 50 Ma younger Ar/Ar cooling ages adjacent to the SW Terrane S.

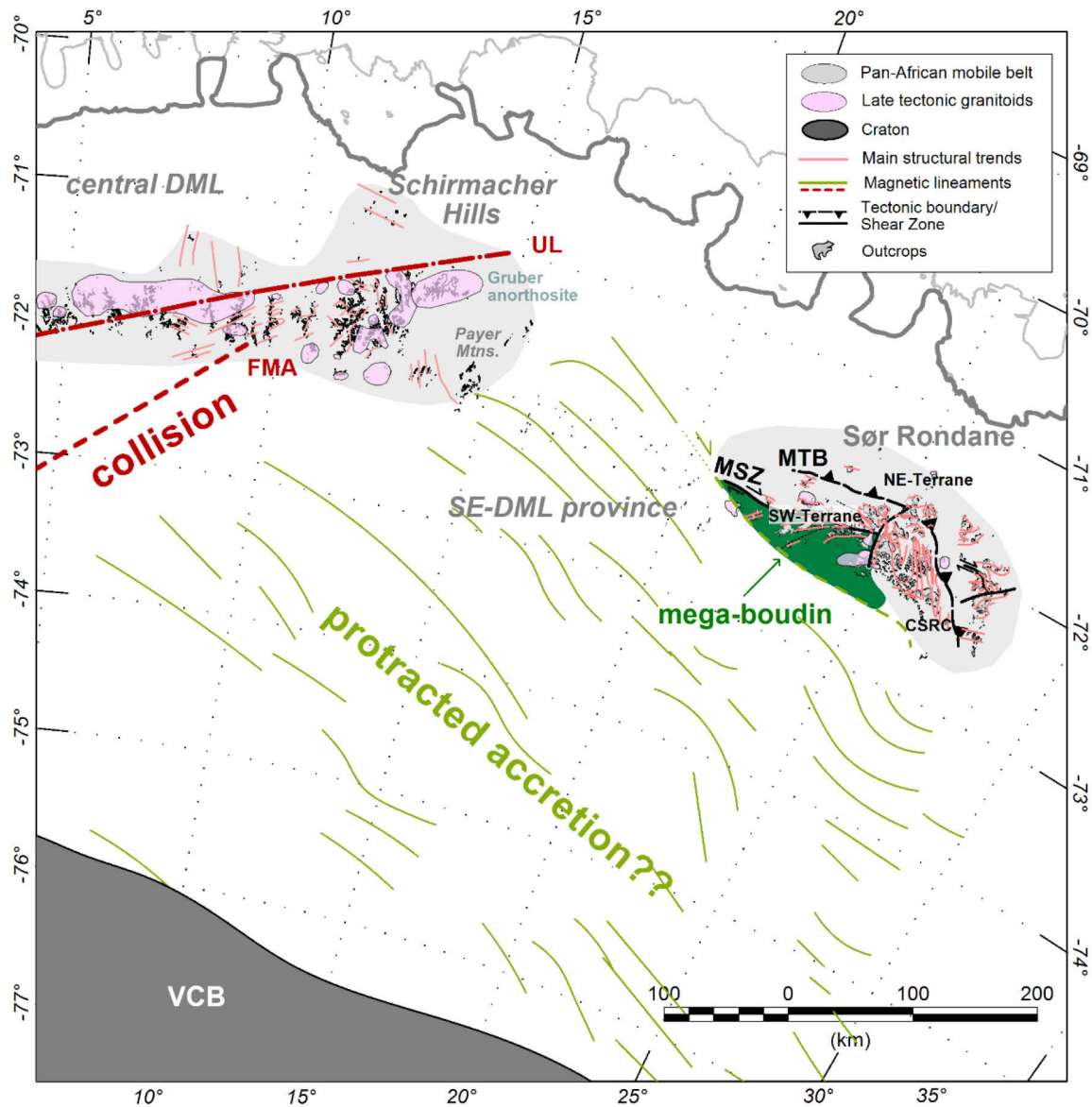


Figure 6.14: SW Terrane S of Sør Rondane is indicated as a mega-boudin within a rheologically weaker, Late Neoproterozoic-Early Paleozoic mobile belt. Black lines: Terrane boundaries interpreted based on combined aeromagnetic and geological findings modified after Mieth et al. (2014). Green lines: trend of magnetic anomalies within the SE-DML province, broken line southern boundary of the SE-Terrane S inferred from aeromagnetic data (Mieth et al., 2014). Red lines Sør Rondane: Form line contours adapted from (Toyoshima et al., 2013). CSRC = Central Sør Rondane Corridor; FMA= Forster Magnetic Anomaly (Riedel et al., 2013); MSZ = Main Shear Zone; MTB = Main Tectonic Boundary; UL= Ulvetanna Lineament (Damaske et al., 2005); VCB=Valkyrie Cratonic Block (Golynsky et al., 2018).



Our new  $\text{Ar}/\text{Ar}$  data appear systematically older by 20–40 Ma when compared to adjacent regions of the EAAO in DML, such as the western and central DML. In western DML, K-Ar and  $\text{Ar}/\text{Ar}$  hornblende and mica ages ( $n = 31$ ) span ca. 530–470 Ma, which are thought to reflect the post-tectonic cooling history of the Heimefront Shear Zone (western orogenic front of the EAAO) and areas to the east (e.g. Jacobs et al., 1995; 2003c). No correlation between  $\text{Ar}/\text{Ar}$  cooling and granitoid intrusion ages have been made in western DML, since late-tectonic intrusions are lacking there. In central DML, K-Ar and  $\text{Ar}/\text{Ar}$  hornblende and biotite ages ( $n = 5$ ) are reported for post-kinematic charnockitic rocks exposed in the eastern Mühlig-Hofmann-Gebirge. Ages of ca. 487 and ca. 466 Ma for amphibole and biotite, respectively, are interpreted to reflect cooling after crystallization at ca. 540 Ma (Markl and Henjes-Kunst, 2004). The apparent younging of the  $\text{Ar}/\text{Ar}$  ages towards the E in Sør Rondane and the young  $\text{Ar}/\text{Ar}$  ages along the western margin of the EAAO may reflect cooling following the progressive outward growth of the EAAO.

A peculiar feature of the study area is the persistent E- to SE-trending structural grain that is largely co-linear with magnetic anomalies of the TOAST (Figures 6.1, 6.14) This direction is approximately perpendicular to the Forster Magnetic Anomaly (Riedel et al., 2013). The latter is interpreted as the eastern limit of Kalahari and the boundary to the TOAST (Jacobs et al., 2015). If the persistent E- to SE-trending structure and magnetic anomaly trends of Sør Rondane and the TOAST, respectively, reflect the general along-strike trend of island arc terranes, then a primary accretion to the eastern Kalahari is unlikely. It would then be more likely that the island arc terranes first accreted to the cryptic Valkyrie Craton to the south (Figure 15, Golynsky et al., 2018), before this craton and the TOAST were sandwiched in between Kalahari and Indo-Antarctica. Alternatively, the island arc terranes could have accreted along a different place along blocks of E- or W-Gondwana and were only translated into the present location. In this respect, the study area and TOAST have similarities to the Arabian-Nubian Shield (ANS) at the other end of the EAAO. The ANS represents another accretionary part of the larger EAAO that is equally characterised by juvenile Neoproterozoic island arc accretion, although the ANS shows much lower metamorphic overprint (e.g. Stern, 1994; 2002; Johnson and Woldehaimanot, 2003; Johnson et al., 2011). As in the TOAST, the ANS terranes show similar oblique structural grains with respect to the general N-S elongation of the EAAO, which may relate to oblique accretion along the Sahara Metacraton.



## 6.7 Summary and Conclusions

Twenty-eight new Ar/Ar mineral and three U-Pb zircon ages of Sør Rondane yield a detailed perspective of the protracted late-tectonic cooling history of five distinct structural domains in Sør Rondane, with implications for the tectono-thermal evolution of this part of the EAAO and the assembly of East Antarctica in Late Neoproterozoic/Early Paleozoic times:

1. Metamorphic rocks of Sør Rondane document an Ar/Ar and K-Ar mineral age spectrum that spans 660–480 Ma and records the differential cooling history of the eastern East African-Antarctic Orogen. The large age range may be best explained by protracted collage-style accretion, differential reactivation, and strain localisation during collision related to the final stages of Gondwana assembly.
2. Strain localisation and Ar/Ar cooling ages correlate with lithotype and crystallization ages of late-tectonic granitoid intrusions. The SW Terrane S consists almost solely of competent GTTGs, whilst the surrounding structural domains have various proportions of metaigneous and Neoproterozoic metasedimentary rocks. Strain is concentrated in the metasedimentary rocks, which in turn may have focused the intrusion of syn- to post-tectonic granitoids. This may have led to later cooling of these weak structural domains that surround the more competent SW Terrane S.
3. The SW Terrane S is interpreted as a mag-boudin, consisting of rheologically competent GTTGs. It records the oldest K-Ar cooling age of ca. 660 Ma, and hosts the largest and oldest Late Neoproterozoic granitoid intrusions, the Dufek granitoid (ca. 640–620 Ma). It is characterised by a NE-trending structural grain that is most likely the oldest preserved structure in the region.
4. The northern contact of the SW Terrane S hosts several ca. 570–560 Ma granitoids, which are strung out along the mylonitic MSZ. The MSZ appears as a zone of strain concentration between the competent SW Terrane S and the rheologically weaker SW Terrane N. New Ar/Ar amphibole ages within the range of the granitoids are interpreted as dating the late-stage of shearing. The Ar/Ar biotite ages ranging from 550–525 Ma are interpreted as post-dating major ductile shearing.
5. The SW Terrane N, the NE Terrane, the CSRC and the western nunataks are intruded by younger granitoids with U-Pb zircon crystallization ages of ca. 530–500 Ma. All four domains are distinct in their structure and show much younger Ar/Ar mineral cooling ages (ca. 510–480 Ma) than the SW Terrane S.
6. A gradual younging of Ar/Ar cooling ages is documented from the western area of Sør Rondane across the SW Terrane N, the CSRC, and towards the NE Terrane. This younging correlates with the general age zoning pattern of late-tectonic granitoid intrusions. The younging of granitoid magmatism and Ar/Ar mineral cooling ages away from the centre of the EAAO may relate to a general outward growth and widening of the EAAO over time.
7. The Ar/Ar cooling ages of the Sør Rondane are ca. 20–40 Ma older than along the western margin of the EAAO in western DML. This difference in time is also apparent in the metamorphic, magmatic, and deformational histories of both regions and can be explained by a major tectonic boundary, most likely represented by the Forster Magnetic Anomaly.



## 6.8 Acknowledgements

This study was part of the collaborative research program ‘Geodynamic Evolution of East Antarctica’ (GEA) of the German Federal Institute of Geosciences and Natural Resources (BGR) and ‘West/East Gondwana Amalgamation and Separation’ (WEGAS) of the Alfred Wegener Institute Helmholtz, Centre for Polar and Marine Research (AWI). J. Jacobs, M. Elburg, and N. Krohne are indebted to BGR for the invitation to participate in the expeditions and to AWI for providing polar clothing. We would like to express our sincere thanks to Alain Hubert and his team at the Belgian Princess Elisabeth station for the wonderful time there and support in the field. Many thanks go also to the crew of Sky Heli, Germany, who took the geological party safely to the field and back to the station. B. Sperner and M. Ehrenfels are thanked for their contributions to Ar/Ar dating at Freiberg, and M. Hofmann and U. Linnemann gave access to the Senckenberg Laboratories. Parts of this study was financially supported by Deutsche Forschungsgemeinschaft (DFG) within the frame of the Collaborative Research Programme SPP 1158 (grants LA1080/9 to A. Läufer and LI 745/15 to F. Lisker) in the framework of the priority programme 1158 ‘Antarctic Research with comparative investigations in Arctic ice areas’. M. Elburg was recipient of an NRF-SANAP grant SNA2011110200002, which is gratefully acknowledged. J. Jacobs received funding through NFR-NARE, which is equally gratefully acknowledged.





## Chapter 7

# 7. New Detailed Aeromagnetic and Geological Data of Eastern Dronning Maud Land: Implications for Refining the Tectonic and Structural Framework of Sør Rondane, East Antarctica

Matthias Mieth, Joachim Jacobs, Antonia Ruppel, Detlef Damaske, Andreas Läufer, Wilfried Jokat

Key findings:

- **Magnetics and geology correlate quite well, revealing new structural insights.**
- **The new central Sør Rondane corridor separates the region into E and W parts.**
- **The prominent SE-DML province continues easterly into southern Sør Rondane.**
- **The TTG-subterrane in the SW is divided into two distinct magnetic domains.**
- **Strong high near Dufekfjellet is caused by a highly magnetised enigmatic body**

## 7.1 Abstract

The Sør Rondane Mountains (SRM) in eastern Dronning Maud Land (DML) are located in an area, where two apparent Pan-African (650-520 Ma) orogenic mobile belts appear to intersect, the East African-Antarctic Orogen and the Kuunga Orogen. Hence, a better understanding of the tectonic structure of the Sør Rondane region is an important key for unravelling the complex geodynamic evolution of the eastern DML and adjacent regions of East Antarctica during the Late Neoproterozoic/Early Palaeozoic amalgamation of Gondwana. The SRM were recently (2011-2012) aerogeophysically investigated with a 5 km flight line spacing, covering a total area of ~140000 km<sup>2</sup>. The aeromagnetic data are correlated with ground-based magnetic susceptibility measurements and geological field data and allow to project tectonic terranes and individual structures into ice-covered areas. Magnetic anomalies and basement foliation trends are collinear in areas dominated by simple shear deformation, whereas an area of large-scale refolding correlates with a subdued small-scale broken magnetic anomaly pattern. The latter area can be regarded as a distinct tectonic domain, the central Sør Rondane corridor. It magnetically separates the SRM into an eastern, a central, and a western portion. This subdivision is presumably related to late Pan-African extensional tectonics and suggests that such a tectonic regime may play a larger role than previously assumed. Voluminous late Pan-African granitoids, which are mainly undeformed, correlate with positive magnetic anomalies between +30 and +80 nT, while a strong magnetic high (+680 nT) near the granitic intrusion at Dufekfjellet is caused by a highly magnetised enigmatic body. The recently discovered prominent magnetic anomaly province of southeastern DML continues into the southern part of the Sør Rondane region, where only a few outcrops are exposed. Findings at these westernmost nunataks of the SRM indicate that the subdued magnetic anomaly pattern of this



southeastern DML province is most likely caused by the predominance of metasedimentary rocks of yet unknown age.

**KEYWORDS:** Aeromagnetism, Magnetic susceptibility, Gondwana assembly, Tectonics, Sør Rondane Mountains, Dronning Maud Land

## 7.2 Introduction

East Antarctica underwent a complex tectonic evolution since the Archaean, especially during the Pan-African (~650–520 Ma) assembly of Gondwana (e.g. Boger, 2011 and references therein). Our study area, the Sør Rondane region, is located within two apparently overlapping Pan-African mobile belts (e.g. Satish-Kumar et al., 2013), namely, the East African-Antarctic Orogen (Jacobs et al., 1998; Jacobs et al., 2003b; Jacobs and Thomas, 2004) and the Kuunga Orogen (Boger, 2011; Meert, 2003) as illustrated in Figure 7.1a. The former is thought to have formed a more or less continuous orogen extending from the Arabian Peninsula to the western DML, while the latter is thought to have formed an orogen extending from Australia through western India, the Prydz Bay region, and eastern DML into Mozambique and beyond. DML is, as most of Antarctica, widely covered with a thick ice sheet, and only a few outcrops provide scattered insights into the subglacial tectonic framework. Aerogeophysical investigations have allowed several large-scale crustal domains to be distinguished in DML (Golynsky and Aleshkova, 2000; Mieth and Jokat, 2014; Riedel et al., 2012; Riedel et al., 2013), while airborne data of higher resolution ( $\leq 5$  km flight line spacing) could be correlated with geological findings on a smaller scale (Damaske et al., 2005; Golynsky and Jacobs, 2001; Ferraccioli et al., 2005b; Ferraccioli et al., 2005a). During the ‘Soviet Antarctic Expedition 36’ in 1990, the Sør Rondane region was aerogeophysically investigated the first time with a flight line spacing of 20 km at an altitude of 4000–4500 m (Golynsky et al., 1996). However, the sparse flight line spacing and the high altitude above ground did not allow any geologically detailed interpretation of the aeromagnetic data. Therefore, the region was investigated in more detail during three geological-geophysical expeditions in the framework of the collaborative research programme “Geodynamic Evolution of East Antarctica” (GEA) of the German Federal Institute of Geosciences and Natural Resources (BGR) and the Alfred-Wegener-Institut Helmholtz-Zentrum für Polar- und Meeresforschung (AWI).

Here, we report on the newly acquired aeromagnetic data in the Sør Rondane region. Together with new ground-based susceptibility measurements and structural information, we use these data to extrapolate outcropping terrane boundaries and discontinuities into ice-covered areas to constrain the overall size of the mapped geological structures. This is a first step towards a better constraining of the geodynamic evolution of the SRM during the amalgamation of Gondwana in the Late Proterozoic and Early Palaeozoic.

## 7.3 Geological Overview of Sør Rondane

The broad geological framework of the Sør Rondane Mountains (SRM) was first established by Belgian researchers, who published the first geological map of the mountain range (Van Autenboer, 1969; Van Autenboer and Loy, 1972; Picciotto et al., 1964). This early work recognised two fundamentally different basement complexes, the Nils Larsenfjellet Group, a major (meta)-granitoid body in the SW part of the SRM, and the Teltet-Vengen Group (undiffe-



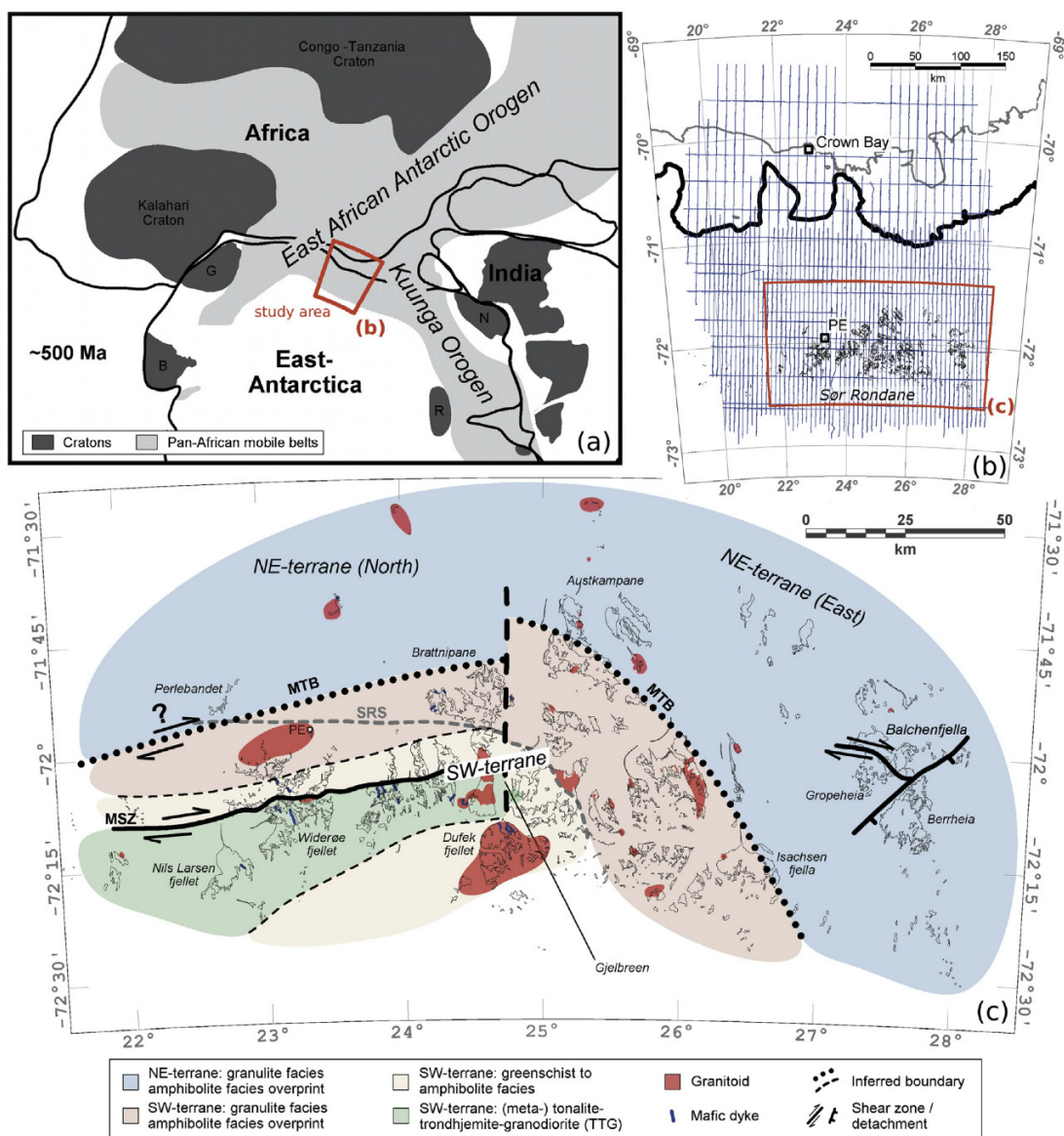


Figure 7.1: Overview of study area. Sketch of part of Gondwana (~500 Ma), showing the study area to be located close to the intersection of two Pan-African (650–520 Ma) mobile belts, abbreviations: B – BLM (Coats Land block), G – Grunehogna, N – Napier, R – Ruker. (b) Survey area with grounding line (thick black), ice shelf edge (grey), outcrops (thin black), and magnetic flight lines (blue). Measurement lines are 5 km separated in the onshore region, and 10 km over the ice shelf and beyond. Tie lines were flown every 30 km. Base stations for flight operation were Princess Elisabeth station (PE) and a temporary camp at Crown Bay. (c) Geological overview map of the SRM after Shiraishi et al. (2008) and Osanai et al. (2013). The SW-terrane is separated from the NE-terrane by the Main Tectonic Boundary (MTB). The SW-terrane is composed of a TTG subterrane (~995 Ma and 940–920 Ma) and a range of metamorphic rocks from greenschist to granulite facies, close to the MTB. The northern contact of the TTG subterrane is a major dextral shear zone, the Main Shear Zone (MSZ). The NE-terrane is predominated by granulite facies rocks, which were metamorphosed at ~640–600 Ma, similar to granulites within the SW-terrane, however with contrasting PTt-loops. Whilst metamorphic zircon ages of ~640–600 Ma are thought to indicate collision between the SW- and NE-terrane, metamorphic zircon ages of ~570 Ma are interpreted to indicate extensional exhumation and orogenic collapse following collision. The Sør Rondane Suture (SRS) is no longer considered an important boundary. Major volumes of late tectonic A-type granitoids and mafic dykes, dated at ~560–520 Ma, occur in the SW-terrane.



reniated metamorphic rocks), occupying the remaining major part of the mountain range. This early work was followed by extensive geological studies of the Japanese Antarctic Programme until today (e.g. Shiraishi et al., 2008; Satish-Kumar et al., 2013 and references therein). The Japanese teams published detailed geological maps of most of the mountain range and conducted detailed petrological, geochemical, and geochronological studies of the SRM (e.g. Asami et al., 1992; Asami et al., 1996; Asami et al., 1997; Asami et al., 2005; Osanai et al., 1992; Osanai et al., 2013; Owada et al., 2013; Satish-Kumar et al., 2008; Satish-Kumar et al., 2013; Shiraishi and Kagami, 1992; Shiraishi et al., 1991; Shiraishi et al., 1994; Shiraishi et al., 2008). Osanai et al. (1996b) and Shiraishi et al. (2008) subdivided the SRM into the distinct SW-terrane and the NE-terrane, separated by the so-called Sør Rondane Suture (Figure 7.1c; SRS). This subdivision was based on contrasting geochemical composition and metamorphic grades on either side of the Sør Rondane Suture. Whilst the NE-terrane is dominated by granulite facies rocks, the SW-terrane consists mainly of greenschist to amphibolite facies assemblages. In the granulite facies rocks of the NE-terrane, metamorphic U-Pb zircon ages of ~640–600 Ma were interpreted to represent collision tectonics, whilst slightly younger ages of ~570 Ma in both terranes were interpreted to represent retrograde metamorphism, orogenic collapse, and exhumation in both terranes postdating the collision (Shiraishi et al., 2008). In the western SRM, the structural grain, including the Sør Rondane Suture, trend roughly E-W, while it swings into a SE direction in its eastern portion (Figure 7.1c).

Different granulite facies rocks with contrasting PTt-loops within the NE-terrane were recently described close to the Sør Rondane Suture (Adachi et al., 2013; Baba et al., 2013; Osanai et al., 2013). Based on these different granulite facies rocks, the spatial extent of, and the boundary between, the SW- and NE-terranes were redefined. The boundary between the SW-terrane and the NE-terrane is called the Main Tectonic Boundary (MTB) by e.g. Osanai et al. (2013). The MTB is described as a high-strain zone with at present unknown kinematics. It separates granulites to the SW, which are characterised by a counter-clockwise PTt-path, and granulite facies rocks to the NE, which are characterised by a clockwise PTt-path, both dated at ~640–600 Ma (Osanai et al., 2013). The latter authors interpret the MTB as a suture with the NE-terrane thrust on top of the SW-terrane, which caused metamorphic zircon growth between ~640 and 600 Ma. Furthermore, they suggest that the Sør Rondane Suture has no great tectonic significance and it is no longer interpreted as a suture.

The SW-terrane after Osanai et al. (2013) consists of rocks with a wide range of metamorphic grades. Metamorphism increases towards the contact with the NE-terrane, where granulite facies is reached at Brattnipane (Baba et al., 2013). Generally, the SW-terrane is composed of two major rock units, a southern trondhjemite-tonalite-granodiorite (TTG) suite, metamorphosed under greenschist to amphibolite facies conditions (the Nils Larsenfjellet Group of Van Autenboer, 1969) and a northern greenschist to granulite facies metamorphic complex, predominated of a variety of metasedimentary and metaigneous rocks (Figure 7.1c). These are separated from each other by the several hundred metre wide dextral Main Shear Zone (Figure 7.1c; MSZ), first described by Kojima and Shiraishi (1986). To the south of the TTG subterrane, small exposures of metasupracrustal rocks crop out, similar to those north of the MSZ, hence, a southern boundary of the TTG subterrane is inferred (Figure 7.1c).

The TTG suite is subdivided into geochemically, petrologically, and geochronologically distinct domains with zircon crystallisation ages of ~995 Ma and 940–920 Ma (Ikeda and



Shiraishi, 1998; Kamei et al., 2013; Shiraishi et al., 2008; Takahashi et al., 1990). Whilst the earlier magmatism appears more tholeiitic in composition, the later formed more calc-alkaline adakites (Kamei et al., 2013). The two groups differ not only in their ages but also in the regional distribution. The western portion of the TTG subterrane is dominated by rocks with more tholeiitic affinity, whilst the eastern part is dominated by rocks with a tendency to calc-alkaline composition (Kamei et al., 2013). This plutonic complex is interpreted to have formed along a juvenile oceanic arc. A U-Pb titanite age of  $\sim 516$  Ma (Shiraishi et al., 2008) together with Rb-Sr and K-Ar mineral ages of  $\sim 510$ – $460$  Ma (Picciotto et al., 1964) indicate substantial Cambrian tectono-thermal overprint, although there appear also apparently undeformed portions of this igneous complex at the meso-scale. The TTG subterrane is laterally discontinuous.

To the north, the TTG subterrane is bounded by the ENE-trending MSZ. The MSZ is a steeply south-dipping, dextral mylonite zone with mostly subhorizontal and often shallowly easterly inclined stretching lineations (Ruppel, 2012). The MSZ separates the TTG subterrane from a variegated sequence of greenschist to granulite facies rocks. The area to the north of the MSZ is characterised by subordinate greenschist facies schists and a highly migmatitic sequence of volcano-sedimentary rocks. Metasedimentary rocks include quartzo-feldspathic gneisses interlayered with marbles. The metavolcanic rocks include grey homogenous gneisses, as well as finely banded plagioclase-hornblende gneisses, interpreted as metatuffites. Geochemically, these rocks have island arc to continental margin affinities (Shiraishi et al., 2008). This sequence is intruded by numerous small granitoids that were intensely transposed together with the metasupracrustal rocks. Both, isoclinal as well as open refolding occurs and two distinct foliations are recognised. Granulite facies rocks close to the MTB (Brattnipane) have metamorphic U-Pb zircon ages of  $\sim 640$ – $600$  Ma and are characterised by counterclockwise PTt-paths (Adachi et al., 2013; Baba et al., 2013; Osanai et al., 2013).

The granulite facies NE-terrane is dominated by metasupracrustal rocks that were deposited on a juvenile Late Mesoproterozoic basement. Mafic rocks are also recorded, and an oceanic affinity is documented (Shiraishi et al., 2008). Based on the age of detrital zircons, it is thought that sedimentary protoliths were deposited at least in part after 750 Ma (Shiraishi et al., 2008) and Neoproterozoic deposition ages are independently confirmed by a strontium isotope study on metacarbonate rocks (Otsuji et al., 2013). In contrast to the SW-terrane, granulites of the NE-terrane document a clockwise PTt-path at  $\sim 640$ – $600$  Ma (Shiraishi et al., 2008; Adachi et al., 2013; Osanai et al., 2013).

The contrasting PTt-paths on either side of the MTB are explained in a model, where the NE-terrane was thrust over the SW-terrane; granulite facies zircon growth at  $\sim 640$ – $600$  Ma is thought to date the collision (e.g. Shiraishi et al., 2008; Osanai et al., 2013). This infers that the MTB is a suture; note the difference to the Sør Rondane Suture (Shiraishi et al., 2008), of which some authors now believe that it is not a significant tectonic boundary within the SRM (e.g. Osanai et al., 2013).

Across the entire SRM, a number of metamorphic U-Pb zircon ages between  $\sim 570$  and  $530$  Ma are recorded (Adachi et al., 2013; Grantham et al., 2013; Osanai et al., 2013; Picciotto et al., 1964; Pasteels and Michot, 1970; Shiraishi et al., 2008). These ages are interpreted to represent a post-collision hydration event that affected many of the granulite facies rocks and is thought to be associated with extensional tectonics, following the main collision at  $\sim 640$ – $600$  Ma



(Shiraishi et al., 2008). In the NE-terrane, the NE-trending and extensional Balchen detachment (fault/shear zone) is interpreted to have evolved during this late-tectonic extension (Ishikawa et al., 2013). The Balchen detachment juxtaposes mafic and ultramafic rocks of the Gropeheia unit next to gneisses of the Berrheia unit.

Also late-tectonically, the SRM are intruded by in part large volumes of granitoids and a number of mafic dykes. The main volumes of melts occur in the SW-terrane. Late-tectonic granitoids include syenites and bi-granites, dated at ~620 Ma (group I), 570–560 Ma (group II), and 530–520 Ma (group III) (Li et al., 2006; Shiraishi et al., 2008). The largest granite, the Dufek granite, provided the oldest U-Pb zircon age of ~620 Ma. The late-tectonic Vengen granite, dated at ~560 Ma (U-Pb zircon) intrudes the MSZ, but is still deformed, which implies that the MSZ was active after ~560 Ma (Shiraishi et al., 2008). The mafic dykes are mainly lamprophyres and high-K dolerites and they are thought to have derived from a metasomatised mantle source (Owada et al., 2013).

A major inferred N-S trending fault dissects the SRM and separates the predominantly E-W trending western portion from the mainly NW-SE trending eastern part of the mountain range (e.g. Osanai et al., 2013). The fault follows the Gjelbreen (Figure 7.1c; along 24.7°E), and is probably collinear with a number of apparent lineaments, now occupied by major ice streams.

## 7.4 Data Acquisition and Processing

Airborne geophysical data of the GEA campaign have been acquired during three consecutive austral summer seasons in January/February 2011, January 2012, and November/December 2012 using the AWI Basler BT-67 aircraft Polar-5 in 2011 and Polar-6 in 2012. The target area over the SRM between 72.5°S/20°E and 71°S/28°E was surveyed from the Belgian Princess Elisabeth station as well as from a temporary base at Crown Bay. The survey area was extended northward across the ice shelf to 69.5°S during the third flight campaign, covering a total area of ~140000 km<sup>2</sup>. The measurement lines were flown in N-S orientation, with a spacing of 5 km in the main target area and 10 km in the northern extension. The E-W oriented tie lines were flown every 30 km. The length of all flights sums up to 37000 km. Data were acquired at a constant barometric flight altitude ensuring a minimum distance to the surface of 500 m.

Four Novatel global navigation satellite system (GNSS) receivers recorded the position of the aircraft with a sample rate of 50 Hz for scientific purposes. Two receivers were installed on the cabin roof and one on each aircraft wing. The GNSS positions were post-processed with Waypoint GPS software using the method of precise-point-positioning, which ensured the accuracy to be independent of distance to a GNSS base station.

The magnetic data were acquired using Scintrex Cs-2 Caesium magnetometers in 2011 and Cs-3 sensors in 2012 mounted in nose and tail booms of the aircraft. In both aircraft, a Billingsley TFM 100 fluxgate magnetometer was operated and used for magnetic compensation. Magnetic base station for recording the diurnal variations of the Earth magnetic field were deployed near the airfields of Novolazarevskaya, Princess Elisabeth, and during the second field season at Crown Bay. Magnetic data processing was carried out using Geosoft Oasis montaj software. The processing flow included de-spiking, core-field and diurnal variation corrections, upward continuation to 4600 m, and full levelling. The automatic full levelling reduced the cross-point error to  $0.1 \pm 0.8$  nT, without introducing artificial anomalies. However, more than 80 % of the



lines were flown at an altitude of 3200–3600 m, and many small wavelength anomalies became subdued due to the upward continuation. Therefore, the levelling process was repeated without applying an upward continuation beforehand. First, static shifts were applied to all lines flown significantly higher or deeper than 3400 m, followed by a careful low pass filtered tensioned spline levelling, resulting in a cross-point error of  $4.7 \pm 5.7$  nT. Thus, the higher frequencies of the recorded data were maintained, in particular in the region of the outcropping mountain range. Comparison to the upward continued full-levelled data ensured that no artificial anomalies had been introduced and that a similar levelling quality was reached. The final data were gridded with a grid cell size of 1.25 km (Figure 7.2a). Grid-based reduction-to-the-pole was performed with mean inclination of  $-62.8^\circ$  and mean declination of  $-38.2^\circ$  and, subsequently, the positive tilt derivative was calculated in order to enhance and to analyse the orientation of positive magnetic anomalies (Figure 7.2b).

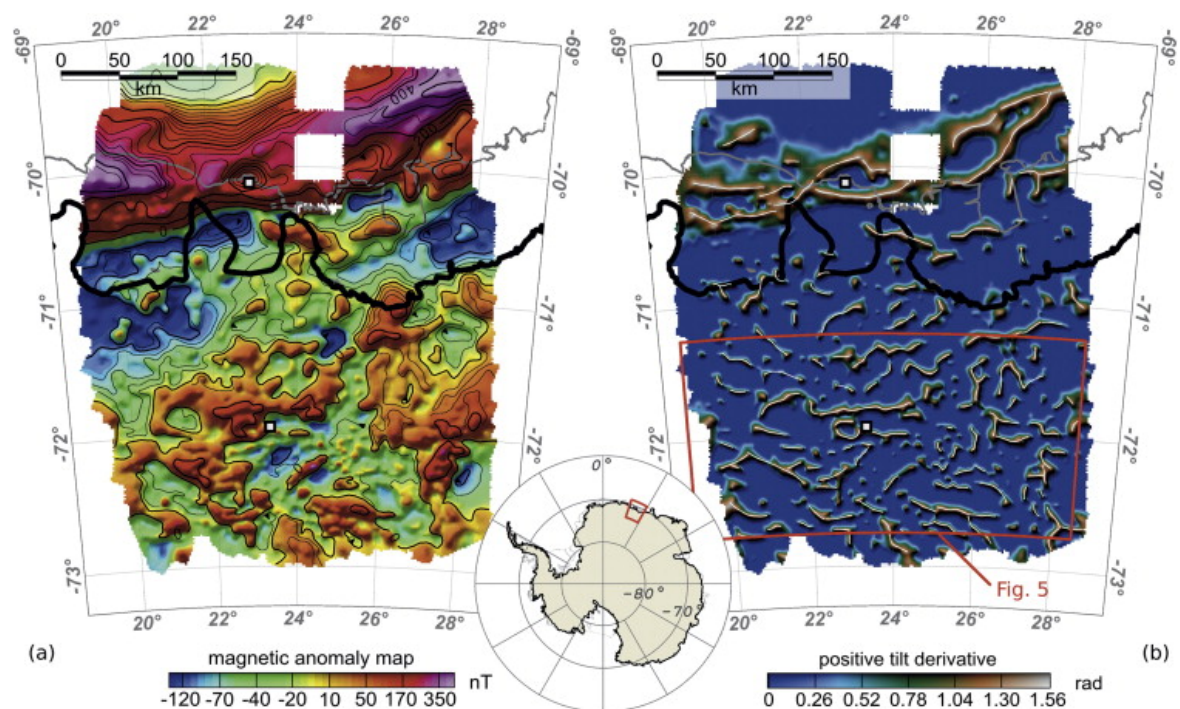


Figure 7.2: Magnetic data. Grounding line (thick black), ice shelf edge (grey) and location of base stations (squares) are shown for orientation. (a) Magnetic anomaly map with contour lines every 20/100 nT. The anomaly pattern can be described as moderate with values between  $-220$  and  $+350$  nT, except of the offshore region and one strong anomaly ( $+680$  nT) near Dufekfjellet ( $72.25^\circ\text{S}/24.41^\circ\text{E}$ ). (b) Positive tilt derivative, which indicates the strike of positive magnetic anomalies and support confining different magnetic domains. White lines are picked along the maxima.

## 7.5 Results

### 7.5.1 Airborne Magnetics

The gridded data are reduced-to-the-pole for interpretation (Figure 7.3), as we assume that induced magnetisation is predominant for most continental rock formations. The continuation of the anomaly pattern beyond the survey area is shown in the inset of Figure 7.3, where the dataset of this study is merged with the AWI magnetic data compilation of DML (Mieth and Jokat, 2014) in the west and with the ADMAP dataset (Golynsky et al., 2007) of lower spatial resolution in the east.



## 7.5.2 Magnetic Susceptibility Measurements

Magnetic susceptibility readings were carried out in the western part of the SRM using a Kappameter KT-6. Measurements were collected at 231 sites during the GEA campaign, consisting of 12 single readings for each site, taken within an area of up to 10 m<sup>2</sup>. The highest and lowest values were considered as outliers, thus 10 single measurements contributed to a mean value for each site. These mean values were grouped and averaged for each terrane and lithology. The results are presented in Table 7.1, including data from the westernmost SRM (SE-DML province) and from granitic intrusions. Relatively high values have been measured for grey gneisses, granulites, and amphibolites, while metasedimentary rocks show very low values in all terranes. Readings at granitoids show a wide range of magnetic susceptibilities, with a tendency to higher values for the older intrusions (group I and II).

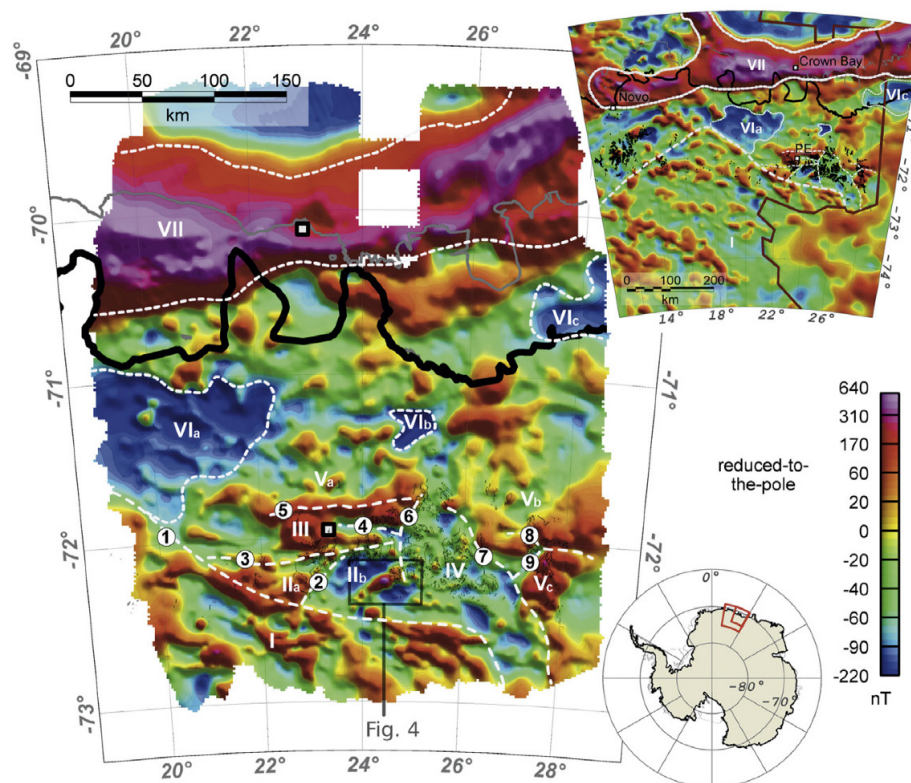


Figure 7.3: Magnetic anomaly data reduced-to-the-pole with inclination/declination of  $-62.8^{\circ}/-38.2^{\circ}$ . Grounding line (thick black), ice shelf edge (grey), and location of base stations (squares) are shown for orientation, white dashed lines are showing boundaries ('1–9') of magnetic domains ('I–VII'). The inset (top right) shows the continuation of the anomaly pattern beyond the survey area, based on a compilation of magnetic data from this study, from the AWI-DML compilation in the west (Mieth and Jokat, 2014) and from ADMAP data (Golynsky et al., 2007) east of the brownish line. Boundary '3' corresponds to the Main Shear Zone, lineament '4' to the Sør Rondane Suture, and lineament '9' to the Balchen detachment, while boundary '5' and '7' correspond to the Main Tectonic Boundary, and boundary '6' represents the Gjelbreen lineament. Domain 'I' corresponds to the SE-DML province, domain 'II', 'III', and 'IV' to the SW-terrane, domain 'V' to the NE-terrane, domain 'VI' to the transition zone, and domain 'VII' to the much larger Antarctic Continental Margin Magnetic Anomaly (Golynsky et al., 1996). Domain 'II' coincides with the TTG subterrane and domain 'Vc' with the Berrheia unit. The subdued and small-scale broken anomaly pattern of domain 'IV', the central Sør Rondane corridor, is conspicuous and separates magnetically the SRM into an eastern and a western portion.



### 7.5.3 Magnetic High Near Dufekfjellet Intrusion

The strong localised magnetic high (+680 nT) near Dufekfjellet is by far the highest magnetic anomaly observed in the entire Sør Rondane region. Figure 7.4a shows that this anomaly is located near, but not at an outcrop. Rocks of the labelled nunataks in Figure 7.4 are all granites. Mean magnetic susceptibilities measured on rock samples of Dufekfjellet range between 4.5 and  $12 \times 10^{-3}$  SI (Table 7.1). Attempts to model the observed strong anomaly with a large and thick granitic intrusion of similar magnetic susceptibility failed. The 2.75-D model displayed in Figure 7.4b rather demonstrates that a highly magnetised rock formation must be the source of the anomaly. The only constraints for the model, beside the magnetic anomaly data, are the outcropping granite at Rogerstoppane (Figure 7.4, R) and the bedrock elevation that was calculated from ice thickness radar measurements. Therefore, the degree of freedom in the modelling is rather high. We set the remanent magnetisation to zero and kept the magnetic susceptibility of the source body with  $150 \times 10^{-3}$  SI as low as possible. Note that a higher susceptibility value would directly lead to a smaller extent of the source body. The horizontal extension perpendicular to the profile is 8 km for the source body and 12 km for the granite. The vertical extent of the modelled source body is in good agreement with the result of a located 3D-grid based Euler deconvolution, which estimated a midpoint depth of  $\sim 800$  m below sea level for a sphere-shaped source.

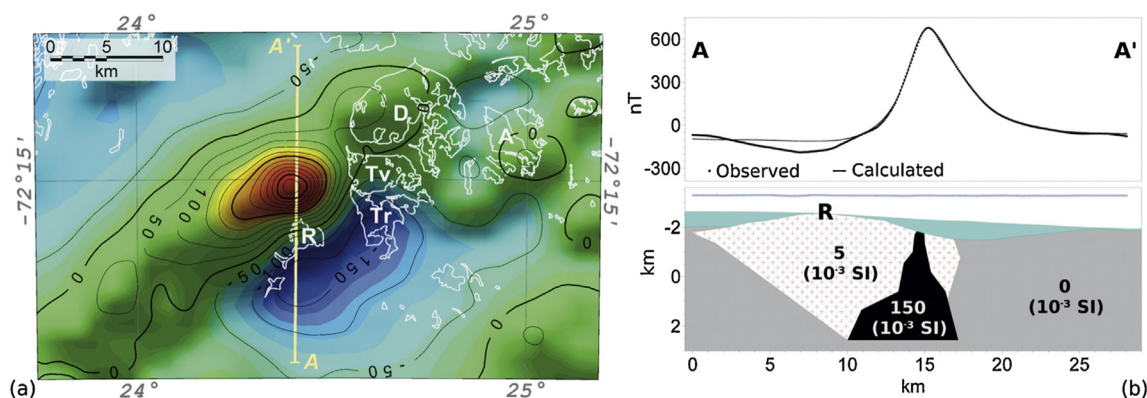


Figure 7.4: Strong magnetic high near Dufekfjellet. (a) Magnetic anomaly map with contour lines every 50/250 nT and outcrops in white. (b) 2.75-D model along a flight line profile from A to A' and the observed (dotted black line) and calculated magnetic anomaly (black line) at flight elevation (blue line). Displayed magnetic susceptibilities are homogeneous for each unit. Cyan represents the ice sheet (non-magnetic), red plus sign pattern the outcropping granite, black the highly magnetised source body, and grey the host rock. The granite body has an extension of 12 km perpendicular to the profile and the source body an extension of 8 km. No remanent magnetization was assumed and a DC shift of  $-60$  nT is applied to the calculated anomaly values. Abbreviation of nunataks: A – Arden, D – Dufekfjellet, Tr – Trerindane, Tv – Tvihøgda, R – Rogerstoppane.

The simplistic model demonstrates that even a large granitic intrusion itself cannot cause the observed strong magnetic high. A highly magnetised rock formation must be hidden under the ice (and possibly under a thin overlaying rock layer). Near Rogerstoppane, the discrepancy between observed and calculated values indicates a lower magnetisation of the granite and/or a much smaller extent as shown, but this discrepancy is related to the simplicity of the model as well. The magnetic susceptibility of the source body was chosen to be as low as possible. Note that a higher value would directly lead to a smaller extent of the body.



Near Rogerstoppane, the discrepancy between observed and calculated aeromagnetic values indicates an even lower magnetisation of the granite as the used  $5 \times 10^{-3}$  SI and/or a much small extent. However, this discrepancy is related to the simplicity of the model as well and, therefore, it is not investigated further. In addition, in order to estimate thicknesses of granitoids, we calculated the magnetic values of outcropping granitic intrusions modelled with a horizontal size of  $12 \text{ km} \times 12 \text{ km}$  and varying thicknesses at an altitude of 800 m above the surface. The resulting maximum anomaly values are given in Table 7.2 for a constant magnetic susceptibility of  $10 \times 10^{-3}$  SI for the intrusion body.

*Table 7.1: Summary of magnetic susceptibility readings in the western part of the SRM. Mean values of each location were grouped for lithology and tectonic terrane in Sør Rondane and subsequently averaged. Relatively high values have been measured for grey gneisses, granulites, and amphibolites, while metasedimentary rocks show very low values in all terranes. Readings at granitoids show a wide range of magnetic susceptibilities, with a tendency to higher values for the older intrusions (group I and II).*

Region	Lithology (No. of sites)	Mean ( $10^{-3}$ SI)	Range ( $10^{-3}$ SI)
<b>NE-terrane</b>	Grey gneiss (8)	26	8.3-95
Perlebandet	Qtz-Fsp gneiss, granulite (8)	12	0.1-57
	Augen gneiss (4)	1.2	0.2-2.5
	Metasedimentary rocks (5)	0.2	0.1-0.2
<b>SW-terrane</b>	Pyroxenite (1)	110	
TTG-subterrane	Mafic dyke (1)	19	
	Amphibolite, Enclave/ultramafic (6)	11	0.5-64
	Granite gneiss (8)	6.9	0.4-16
	(Meta)-granodiorite/tonalite (21)	3.0	0.1-11
	Myl. granodiorite/tonalite (7)	2.3	0.1-4.7
	(Meta)-gabbro (2)	0.5	0.4-0.6
	Grey (mig.) gneiss, metavolcanic? (22)	14	0.1-55
Other (north of MSZ)	Augen gneiss, orthogneiss, Qtz-Fsp gneiss, gneissic granite, migmatitic melt (24)	9	0-32
	Schist, meta-chert (5)	2.8	0.1-7.8
	Meta-sedimentary rocks (18)	0.1	0-0.9
<b>SE-DML province</b>	Gneiss, not classified (5)	0.3	0-0.3
	Metasedimentary rocks (8)	0.2	0-0.6
	Granitic gneiss (10)	0.1	0-0.3
<b>Granitoids</b>	Dufek, gneissic enclave* (1)	21	
Group I (~620 Ma)	Dufek granite* (5)	7.6	4.5-12
	Vengen granite (7)	20	8.6-44
Group II (570-560 Ma)	Tertene granite (2)	8.8	6.6-11
	Lågkollane granite (1)	8.4	
Group III (530-520 Ma)	Bamseungen granite (1)	5.1	
	Utsteinen granite (4)	0.6	0.1-1.7
	Pingvinane granite (3)	0.1	0.1-0.2
Age unknown	Lunckeryggen granite (1)	9.8	
	Mefjell granite (1)	0.2	

\* Measurements were carried out on rock samples instead of field exposures



## 7.6 Interpretations and Discussion

### 7.6.1 Magnetic Domains and Tectonic Terranes

The magnetic pattern over the SRM broadly supports the separation into a NE-terrane and a SW-terrane separated by the MTB, and most magnetic anomalies are co-linear with the general structural trend of the region (Osanai et al., 2013; Toyoshima et al., 2013). The new magnetic data reveal that both terranes can be roughly subdivided into western and eastern portions (Figure 7.5), separated by the N-S trending, curvilinear Gjelbreen lineament, which coincides with the magnetic boundary ‘6’ (Figure 7.3).

The eastern part of the NE-terrane is characterised by moderate to high magnetic anomalies, striking either NE-SW or E-W, and is divided into two magnetic subdomains ‘Vb’ and ‘Vc’. The latter matches with the geological Berrheia unit (quartzo-feldspathic gneisses), located SE of the Gropeheia unit (mafic and ultramafic rocks). The quartzo-feldspathic gneisses of the Berrheia unit are characterised by low magnetic values (Ishikawa et al., 2013). However, we have measured the highest magnetic values (up to +350 nT) in the Balchenfjella area over Berrheia. This unit, close to the SE-inclined Balchen detachment, must be rather thin and is probably underlain by the mafic- and ultramafic Gropeheia unit, which would explain the magnetic high. The NE-trending Balchen detachment coincides with a narrow distinct magnetic low (Figure 7.3, lineament ‘9’). In contrast to the geological interpretation of (Ishikawa et al., 2013), this magnetic lineament is truncated by the magnetic boundary ‘8’, which coincides in its NW-part with a dextral shear zone (Ishikawa et al., 2013) and continues to the SE into an ice covered area (Figure 7.5). Hence, we infer that either the NE continuation of the Balchen detachment is magnetically masked or that the dextral shear zone was reactivated during the tectonic extensional phase and only domain ‘Vc’ was displaced to the SE.

Thickness	Max. anomaly
1 km	32 nT
2 km	52 nT
3 km	70 nT
4 km	86 nT
5 km	99 nT
8 km	124 nT

*Table 7.2: Aeromagnetic response to 2.75-D forward models of a granitic intrusion into a non-magnetic host rock. The intrusion body reaches the surface and has a dimension of 12 km × 12 km, a varying thickness, and a magnetic susceptibility of  $10 \times 10^{-3}$  SI. Distance to the top of the anomaly is 800 m, which was the usual mean distance to the rock surface over the mountain range during flights of the GEA campaign.*

In the western part of the NE-terrane, the magnetic anomalies mainly trend ENE-WSW and the amplitude level is lower than in its eastern part. In general, the magnetic pattern tends to become lower frequency towards the coast, which reflects the increasing distance to the top of the bedrock due to the constant barometric flight altitude. Three prominent magnetic lows are mapped in this transition zone between the mountain range and the coast. They are similar to the large magnetic low found between the central DML mountain range and the Riiser-Larsen Sea (Damaske et al., 2005; Riedel et al., 2013). The meaning of these magnetic lows is thus far unresolved, as no outcrops constrain their origins. Another prominent magnetic low in the Grubergebirge (71.3°S/13.5°E), central DML, is correlated with a large anorthosite complex with a crystallisation age of ~600 Ma (Damaske et al., 2005; Jacobs et al., 1998). In contrast to the enigmatic magnetic lows, the interpretation of the magnetic high zone along the coastal



region (domain 'VII') is well constrained by seismic reflection data. This feature is part of the Antarctic Continental Margin Magnetic Anomaly, which extends from Enderby Land to central Dronning Maud Land (Golynsky et al., 1996). It is interpreted to reflect basaltic intrusions during Gondwana break-up (Leitchenkov et al., 2008). The higher resolution of the GEA aeromagnetic data reveals two ridges of magnetic highs along most parts of the continental margin. They probably indicate two distinct phases of basaltic intrusions during the Jurassic Gondwana break-up.

The magnetic expression of the boundary between the NE- and the SW-terrane (MTB) is different in its eastern and western part. In the east, the MTB is very well constrained between the high amplitude domain of the NE-terrane and the magnetically small amplitude domain ('IV') of the eastern portion of the SW-terrane. Here, the NE-trending anomalies of the NE-terrane appear clearly truncated by the MTB, which is refined in its location (Figure 7.5). In the west, the MTB is collinear with an E-W trending, 100 km long, linear magnetic high (boundary '5'). It is unclear, if this major anomaly is part of either the NE-terrane or the SW-terrane, or if it reflects the MTB itself. If this anomaly reflects the MTB, then the boundary of the NE- and SW-terrane would be to the north of Perlebandet (Figure 7.5) and not to the south of it (e.g. Osanai et al., 2013). Therefore, it remains to be tested, whether the granulite facies rocks of Perlebandet document a clockwise or counter-clockwise PTt-path and subsequently belong to either the NE- or SW-terrane. Field observations during the GEA campaign at the southern outcrop of Perlebandet revealed a high strain zone with subhorizontal stretching lineations but uncertain sense of shear. The vicinity of the western portion of the MTB is clearly characterised by substantial transcurrent shearing with parallel anomalies on either side. This parallelism might be the reason why the precise location of the MTB is difficult to describe based on our magnetic data.

The complex magnetic anomaly pattern of the SW-terrane reflects the geological complexity of this region. The TTG subterrane coincides with the magnetic domain 'II' (Figure 7.3). It is characterised by SW-NE trending magnetic anomalies, matching the foliation strike (Figure 7.5). The magnetic TTG domain can be subdivided into a positive amplitude subdomain ('IIa') and a negative amplitude subdomain ('IIb'). The older, ~995 Ma and more tholeiitic, western portion of the TTG subterrane (Kamei et al., 2013) might be associated with subdomain 'IIa', which is in good agreement with the magnetic susceptibility measurements in this area ( $0.5\text{--}110 \times 10^{-3}$  SI). On the other hand, the younger (940–920 Ma; Kamei et al., 2013), more calc-alkaline eastern part might correlate with subdomain 'IIb'. During our fieldwork, one location was visited within the subdomain 'IIb' at Verheyefjellet ( $72.2^{\circ}\text{S}/23.7^{\circ}\text{E}$ ), revealing corresponding low magnetic susceptibility values  $<0.8 \times 10^{-3}$  SI. In the north, the TTG subterrane is confined by the dextral, steeply south-dipping Main Shear Zone (MSZ), which coincides with the magnetic boundary '3'. The curvilinear magnetic anomalies of the TTG subterrane apparently swing into the east-trending MSZ, probably as a result of major dextral shear strain within the MSZ. The geologically inferred southern boundary of the TTG subterrane has not been identified by our data set. Hence, we assume that the TTG subterrane continues farther south to boundary '1'. The maximum E-W extension of the TTG subterrane is 130 km.



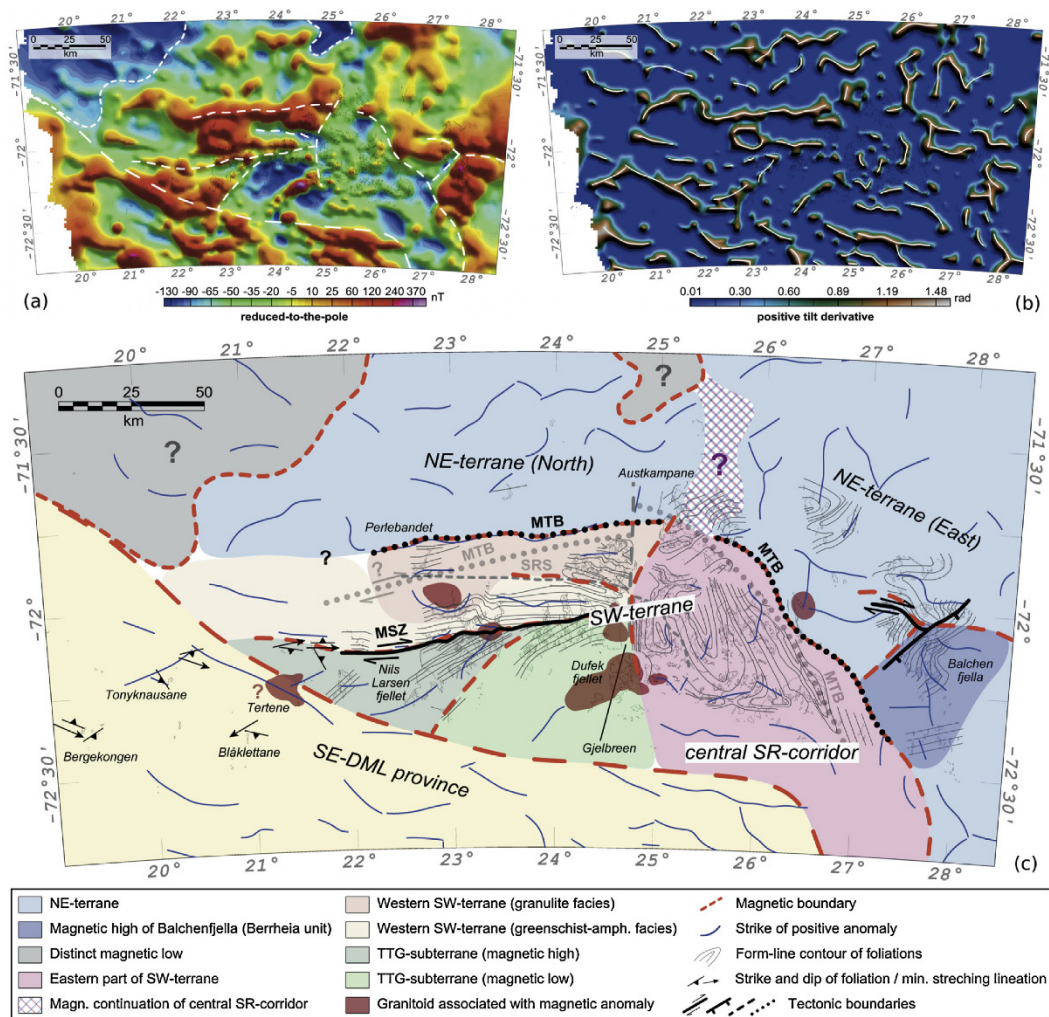


Figure 7.5: Interpretation of aeromagnetic data over Sør Rondane Mountains. (a) Magnetic anomaly map reduced-to-the-pole with inclination/declination of  $-62.8^{\circ}/-38.2^{\circ}$ . (b) Positive tilt derivative. (c) Combination of geological findings and interpretation of aeromagnetic data. The magnetic boundaries confirm, redefine, and reveal new tectonic lineaments and fault systems. Previously defined tectonic boundaries in grey (Osanai et al., 2013) are redefined by our interpretation in black. Form-line contour of foliations are based on Toyoshima et al. (2013). Abbreviations: central SR-corridor – central Sør Rondane corridor, MTB – Main Tectonic Boundary, MSZ – Main Shear Zone, SRS – Sør Rondane Suture. Strike of foliation and mineral stretching lineation in the westernmost nunataks of the study area are mainly collinear with the strike of elongated positive anomalies within the prominent magnetic SE-DML province. A ductilely undeformed granitoid was found at Tertene and coincides with an observed elongated magnetic high near the NE boundary of the SE-DML province. In contrast to previous interpretations, Perlebandet is magnetically interpreted to be part of the SW-terrane, which is supported by the occurrence of high magnetic grey gneisses at these nunataks and farther south. The MTB is magnetically not constrained within the central Sør Rondane corridor. Apparently, this corridor continues in the magnetic anomaly map farther north and separates magnetically the NE-terrane. Some granitoids could be associated with magnetic anomalies, others are either too small in extent or have magnetic susceptibilities similar to that of the host rock.

To the north of the MSZ, grey gneisses with high magnetic susceptibilities (up to  $55 \times 10^{-3}$  SI) are found and most likely cause the elongated magnetic high in the south of domain 'III'. This domain includes the greenschist to granulite facies units of the western SW-terrane, where magnetic anomalies as well as the E-W-trending foliation appear collinear (Figure 7.5). The narrow magnetic low (lineament '4') within domain 'III' coincides partly with what was previously considered the Sør Rondane Suture (Shiraishi et al., 2008). Extent, wavelength and



amplitude of this narrow magnetic low are conspicuously similar to the narrow low along the Balchen detachment zone within the NE-terrane (lineament '9'). Although the Sør Rondane Suture is not considered to be an important tectonic boundary by some authors (e.g. Osanai et al., 2013), it still has a significant magnetic expression. Higher amplitude anomalies in the northern part of domain 'III' can be correlated with high-grade metamorphic rocks of the SW-terrane. East of the Gjelbreen lineament (Figure 7.3; boundary '6'), the magnetic pattern changes abruptly to a diffuse and small amplitude pattern, without a dominant strike direction. Here, the tectonic structures appear complex and large-scale refolding is documented (Toyoshima et al., 2013). It is probably because of the large-scale refolding that no continuous, elongated magnetic anomalies are developed. There is a hint that this diffuse, small amplitude pattern continues to the north and it is speculative, whether this vague N-S trending belt of subdued anomalies may be related to large-scale extensional tectonics, separating the NE- and SW-terrane in a western and an eastern portion respectively.

The magnetic data reveal a southern boundary ('1') of the SW-terrane, which is located south of the mountain range and is accompanied by WNW-ESE striking elongated magnetic highs. We interpret this southwestern-most domain ('I') of the survey area as part of the prominent SE-DML province. Mieth and Jokat (2014) interpret this large magnetic province as an orogenic belt of unknown age, but inferred the structures to predate Pan-African ages (~650–520 Ma). A few nunataks of the southwestern-most SRM are located within the SE-DML province (Figure 7.5), some of which were visited during the Belgian expeditions in 1959/60 (Van Autenboer et al., 1964), others during our fieldwork. Both expeditions found a none-TTG basement predominated of metasedimentary rocks, including marbles, paragneisses and graphite schists. Typically, magnetic susceptibility data show very low values ( $\sim 0.2 \times 10^{-3}$  SI) on a variety of rock samples. Probably, the general subdued magnetic signature of the SE-DML province (except of the elongated highs) is caused by the predominance of metasedimentary rocks. The elongation of the magnetic anomalies in the SE-DML province correlates with the general foliation trend of the outcrops (Figure 7.5). The age of the foliation is thus far unresolved. Furthermore, ductilely undeformed granitoids are found within this province (Figure 7.4). These intrusions are similar in age and chemical composition to the late tectonic intrusions (group II and III) of the SW-terrane of the SRM (Kleinmanns et al., 2013).

## 7.6.2 Granitic Intrusions

Granitoids of various sizes crop out all over the mountain range, but mainly in the SW-terrane, whereas associated mafic dykes have been found only west of the Gjelbreen lineament (Figure 7.1c, along 24.7°E). The mafic dykes are in their extent too small to be identified and properly mapped by the 5 km flight line spacing. Similarly, some granitoid outcrops of small to moderate size (5–10 km) are often not well imaged by our data set. Magnetic susceptibility measurements revealed a broad range from 0.1 to  $44 \times 10^{-3}$  SI for samples of the granitoids. The group II intrusions (570–560 Ma; Li et al., 2006; Shiraishi et al., 2008) show usually higher susceptibilities above  $5 \times 10^{-3}$  SI, whilst most of the group III intrusions (530–520 Ma; Li et al., 2006; Shiraishi et al., 2008) show values below  $1 \times 10^{-3}$  SI with some exceptions (Table 7.1). Therefore, it is comprehensible that the granitoids cannot be identified in the magnetic anomaly map at the first glance. Larger granitoids can be identified in the magnetic anomaly map in the western portion of the SW-terrane and one in the eastern NE-terrane (Figure 7.5),



which are all characterised by anomalies between +30 and +80 nT. Forward modelling indicates that this anomaly range could be associated with thicknesses of the intrusions of 1–4 km (Table 7.2).

Two larger granitoids in the eastern part of the SW-terrane (Figure 7.1; at Mefjell 72.1°S/25.2°E and at Bergersenfjella 72.1°S/26.1°E) could not be correlated with a distinct magnetic anomaly pattern, which is in accordance with the low magnetic susceptibility ( $0.2 \times 10^{-3}$  SI) measured at Mefjell, though Tainosho et al. (1992) reported values of  $2\text{--}10 \times 10^{-3}$  SI for this granite. The granitoid at Pingvinane (SSE of Perlebandet) show low magnetic susceptibilities ( $0.1\text{--}0.2 \times 10^{-3}$  SI) as well, but it intruded into highly-magnetic granulite facies rocks, correlated with magnetic anomalies of up to +240 nT. Therefore, the granitoid appears as a zone of low amplitudes (+30 nT).

The most outstanding magnetic anomaly is that measured SW of Dufekfjellet. It is by far the highest value (+680 nT) measured in the SRM. The 2.75-D modelling (Figure 7.4) indicates that a highly magnetised body either within the granite body or at its rim causes the anomaly. Magnetic anomalies, similar in both spatial extent and anomaly values, in the vicinity of granitic intrusions have been reported from central DML within the Drygalskiberge and the A. v. Humboldt Gebirge at a slightly lower flight altitude of 2845 m (Damaske et al., 2005). Their origin is thus far unresolved. We speculate that ultra-mafic rocks or gabbro bodies are responsible for these anomalies. Contact metamorphism with ore formation can also not be ruled out. Notably, the granite of Dufekfjellet has not only a conspicuous magnetic signature within the SRM, its crystallisation age (620 Ma; Li et al., 2006) is also by far the oldest amongst the voluminous Pan-African granitoids. This would infer that the granite of Dufekfjellet intruded during a different tectonic phase and has probably a different magmatic source. A similar age for a Pan-African intrusion in DML is only reported from the anorthosite complex in the Grubergebirge (600 Ma; Jacobs et al., 1998).

A hitherto unknown granitoid was recorded at Tertene nunataks during our fieldwork (Figure 7.5). These 1800 m high nunataks were crossed at a flight altitude of 3150 m, and a local magnetic maximum of +256 nT had been measured over the southern outcrop. This local maximum corresponds to an elongated high along the boundary ('1') of the SE-DML province (Figure 7.3). Compared with the other magnetic anomalies over granitic intrusions in the SRM, this magnetic anomaly shows much higher amplitudes, while the magnetic susceptibility of the outcropping granite is in the same range than other intrusions in the SRM (Table 7.1). Either this granitoid is much larger in extent and thickness, or the outcropping intrusion is rather thin and underlain by higher magnetised rocks. A more detailed geochemical and mineralogical analysis of this granitoid and of another found at Sarkofagen and Urna (72.2°S/16.8°E) could reveal the differences or similarities to the granitoids of the SRM. Such a study might be crucial for understanding the meaning of the elongated parallel anomalies of the SE-DML province and, thereby, for constraining its geodynamic evolution.



### 7.6.3 Open Questions

Although the correlation between geological and geophysical data is reasonably good in large parts of the mountain range, there are areas, where detailed geological investigations as well as additional geophysical research would substantially enhance our understanding of the tectonic evolution of the SRM.

The significance of the central Sør Rondane corridor that apparently separates the SRM into an eastern and western part is not sufficiently well understood. This aeromagnetic domain ('IV') has characteristic low magnetic anomalies and coincides with an area of large-scale refolding (Toyoshima et al., 2013). It also coincides at least in parts with the assumed collision zone between the NE- and SW-terrane (e.g. Osanai et al., 2013). The question, however, is, whether the large-scale refolding is really related to compression tectonics during juxtaposition of the two terranes. Since the MTB does not appear to cross the central Sør Rondane corridor, it could well be of extensional nature and then it would be late-tectonic. A more detailed aeromagnetic survey acquired in an E-W direction across this zone should improve our understanding of the central Sør Rondane corridor. The MTB is exposed at Austkampane, however, very little is known about the kinematics along the MTB. Clearly, a better structural characterisation of the MTB, the central Sør Rondane corridor and its boundaries to the east and west is needed. If the central Sør Rondane corridor is of extensional nature, then the finite juxtaposition of the different granulite facies rocks (e.g. Adachi et al., 2013; Baba et al., 2013; Osanai et al., 2013) could be of extensional rather than compressional nature.

In the west, the aeromagnetic data suggest that Perlebandet could be part of the SW- and not the NE-terrane. A detailed PTt-path for Perlebandet is so far not available. It should therefore be tested, whether these granulite facies rocks really follow a clockwise PTt-path, as typical for the NE-terrane, or rather follow an anticlockwise PTt-path as would be typical for the SW-terrane. The geophysical interpretation that Perlebandet is part of the SW-terrane is supported by the occurrence of the same type of highly magnetic grey gneisses, the significance and origin of which is however not known at present. It should also be investigated whether these grey gneisses are absent from the NE-terrane and are typically found in the SW-terrane only. It should be tested, whether the two magnetically different parts of the TTG subterrane are exclusively a result of the more calc-alkaline and the more tholeiitic parts of the TTG suite. Whereas, the question why only the SW part of the Balchen detachment has a magnetic significant expression will probably remain unresolved due to limited outcrops at its NE continuation.

## 7.7 Conclusion

The careful correlation of aeromagnetic data together with susceptibility measurements and structural information allowed a reasonably good correlation of geological and geophysical information, despite a 5 km flight line spacing and the varying distance to top of the bedrock, varying from a few hundred metres to some kilometres. Magnetic susceptibility measurements proved important to link aeromagnetic and outcrop information and to trace and map major tectonic terranes and boundaries into ice-covered areas. The three-fold subdivision of the western SRM into a northern, a central, and the TTG subterrane is relatively well imaged by the aeromagnetic data. The eastern portion of the MTB is also well imaged in our new data.



However, our results also reveal certain discrepancies to the hitherto tectonic models, and therefore suggest a refinement and modification of the existing models. The main discrepancies can be summarised as follows. (a) Our data suggest the existence of the central Sør Rondane corridor, which separates the SRM into a western, a central and an eastern part, rather than into a NE- and a SW-terrane. Whilst the eastern portion of the MTB is well imaged with the aerogeophysical data, it does not appear to continue through the Sør Rondane corridor. Therefore, the central Sør Rondane corridor might reflect a late Pan–African tectonic structure, possibly related to extensional tectonics, similar to the Balchen detachment to the east. (b) The TGG subterrane is magnetically divided into two distinct parts, and its southern boundary is farther south as previously assumed. (c) The interpretation of the western portion of the MTB is ambiguous based on the magnetic data. Its magnetic signal differs from that of the eastern portion of the MTB, which might reflect a significant difference of them in their tectonic relevance. (d) The Sør Rondane Suture, which is no longer considered as an important boundary, can clearly be identified and its magnetic signal is very similar to that of the Balchen detachment (fault/shear zone).

Furthermore, we can conclude that late to post Pan-African tectonic granitoids show a significant varying magnetic signal, both in their magnetic susceptibility and in the aeromagnetic data. From a size of >10 km, granitoid bodies can be revealed underneath the ice, if their magnetic susceptibilities sufficiently differ from that of the host rocks. The boundary between the SE-DML province and the SRM could be mapped based on the aeromagnetic data, but its tectonic significance is uncertain. Although metasedimentary rocks have been found at a few outcrops within this province, its age and tectonic evolution remains thus far enigmatic.

## 7.8 Acknowledgements

We thank the flight and science crews of AWI-Polar aircraft for data acquisition and the visited research station in Dronning Maud Land for logistic support. Particularly, we would like to express our thanks to Alain Hubert and his team at the Belgian Princess Elisabeth station for the wonderful time there and support in the field. Many thanks go also to the crew of Sky Heli, Germany, who took the geological party safely to the field and back to the station. Last-not-least, we wish to thank the entire expedition team for cooperative fieldwork and stimulating discussions. J. Jacobs is indebted to BGR for the invitation to participate at GEA I and II and to AWI for providing polar clothing; support from NFR-NARE, and the Meltzer Fund during a research visit at AWI are gratefully acknowledged. This study was partly supported by the Deutsche Forschungsgemeinschaft (Grant LA1080/9 to A. Läufer) in the framework of the priority programme ‘Antarctic Research with comparative investigations in Arctic ice areas’.





## Chapter 8

# 8. Two Distinct Late Mesoproterozoic/Early Neoproterozoic Basement Provinces in Central/Eastern Dronning Maud Land, East Antarctica: The Missing Link

Joachim Jacobs, Marlina Elburg, Andreas Läufer, Ilka C. Kleinhanns, Friedhelm Henjes-Kunst, Solveig Estrada, Antonia S. Ruppel, Detlef Damaske, Pilar Montero, Fernando Bea

Key findings:

- **Extensive exposures of juvenile Early Neoproterozoic oceanic arcs found.**
- **Integrating geology with geophysics shows that oceanic arcs may be extensive.**
- **Tonian Oceanic Arc Super Terrane (TOAST) shows intense reworking from ca. 630 to 500 Ma.**
- **Forster Magnetic Anomaly is a major suture between TOAST and ca. 1.1 Ga Maud Belt.**
- **TOAST might correlate with Vohibori Terrane, Madagascar, and the Arabian–Nubian Shield.**

### 8.1 Abstract

This article highlights the field geology, geochronology and geochemistry of an important and previously unstudied region between eastern (Sør Rondane Mountains) and central Dronning Maud Land (DML). The area allows the characterisation and ground-truthing of a large and mostly ice-covered area that is geophysically distinct and which was previously interpreted as a potentially older cratonic block south of a Late Neoproterozoic/Early Paleozoic (LN/EP) mobile belt, as exposed in the Sør Rondane Mts. (SRM). SHRIMP/SIMS zircon analyses of 20 samples together with new geochemistry indicate that the exposed basement consists of a ca. 1000–900 Ma juvenile terrane that is very similar to the juvenile rocks of the SW-Terrane of the SRM, a characteristic gabbro–trondhjemite–tonalite–granite (GTTG) suite, with normalised trace element patterns typical for subduction-related magmas and mostly positive initial epsilon Nd values. The area shows strong LN/EP crustal reworking, migmatisation and melt production, including 560–530 Ma A-type magmatism. Therefore, this area is very similar to the SW-Terrane and differs only in the degree of LN/EP reworking. We interpret the SW-Terrane of Sør Rondane as a mega-boudin sandwiched in between rheologically weaker portions of similar oceanic arc terranes. Therefore, the study area, and thereby the aeromagnetically distinct SE DML province does neither represent the foreland of a LN/EP mobile belt, nor a craton, as speculated based on geophysical data alone. Instead, a large Tonian Oceanic Arc Super Terrane (TOAST) with significant extent emerges. Its western limit is represented by the Forster Magnetic Anomaly, which represents a suture to the Grenville-age Maud Belt. East of the TOAST, the Rayner Complex is similar in age but otherwise distinctly



different. The Rayner Complex has a much longer history of island arc accretions with continent–continent collision at ca. 950 Ma and it has markedly more evolved crust. In contrast, the TOAST has a pronounced juvenile character without significant inheritance and lacks metamorphic overprint immediately following crust formation. This indicates that it has not been an integral part of Rodinia. The eastern boundary of the TOAST is probably in the vicinity of the Yamato Mts., whilst its northern extension might be seen in the Vohibori Terrane (SW Madagascar), which in turn could correlate with the Arabian Nubian Shield. The LN/EP tectono-metamorphic overprint of the TOAST shows a slight decrease in ages from W to E, possibly indicating that it first amalgamated on its Kalahari side before it was attached to Rukerland/Indo-Antarctica.

**KEYWORDS:** Dronning Maud Land; SHRIMP zircon; Mesoproterozoic/Early Neoproterozoic; Magnetic anomaly; Oceanic arc terrane

## 8.2 Introduction

In its original Gondwana configuration, Dronning Maud Land (DML), East Antarctica, is framed by four known cratons or cratonic fragments, interleaved and amalgamated by different Palaeoproterozoic, Mesoproterozoic and Late Neoproterozoic/Early Palaeozoic mobile belts (Figure 8.1). In western DML, the Grunehogna Craton, shown to have geological affinities with the Kaapvaal Craton (e.g. Jacobs et al., 2008a), is fringed by the Mesoproterozoic Maud Belt. Easternmost DML and adjacent regions East and South include the Napier and Ruker cratons, which are interleaved by Palaeoproterozoic rocks of the Øygarden and Lambert terranes as well as the early Neoproterozoic Rayner Complex (1000–900 Ma) (e.g. Fitzsimons, 2003); this area has clearly Indo-Antarctic affinities. Large areas of DML show an intense Late Neoproterozoic/Early Palaeozoic (LN/EP) tectono-metamorphic overprint, reaching granulite facies in places. Therefore, besides the likely presence of Palaeoproterozoic and Mesoproterozoic suture zones in the area, the existence and position of a number of LN/EP suture zones have been debated (e.g. Moyes et al., 1993; Grunow et al., 1996; Shackleton, 1996; Wilson et al., 1997; Jacobs et al., 2003a; Jacobs and Thomas, 2004). One possible LN/EP suture zone has been recognised in the Shackleton Range (Talarico et al., 1999; Schmädicke and Will, 2006), which there separates a cratonic fragment represented by the Read Group from the Coats Land Block. Its eastern extent, however, is thus far unrevealed. In the Prince Charles Mts., the existence of a LN/EP suture zone between the Napier and Ruker cratons is still controversial (e.g. Boger et al., 2001; Fitzsimons, 2003; Meert, 2003). Another LN/EP suture zone has been suggested for central DML (Jacobs and Thomas, 2004), recently corroborated by geophysical techniques (Riedel et al., 2013; Mieth et al., 2014). The major Forster and Ulvetanna magnetic anomalies appear as significant tectonic lineaments, projecting into the so far poorly studied Kurze, Conrad and Humboldt Mts. of central DML (Figure 8.1 and Figure 8.2). The tectonic nature of this major magnetic lineament in the corresponding outcropping area is thus far unrevealed. Improved knowledge of the geological significance of the Forster Magnetic Anomaly has significant importance for the better understanding for both the eastern extent of the Mesoproterozoic Maud Belt and the western extent of the Early Neoproterozoic Rayner Belt. In eastern DML, basement rocks of the Sør Rondane Mts. (SRM) have protolith ages predominantly ranging from ca. 1000 to 900 Ma (e.g. Shiraishi et al., 2008; Elburg et al., 2015). These ages are similar to those of the Rayner Complex and differ from the Maud Province, the



latter of which are dominated by older protolith ages ranging from 1130 to 1040 Ma (e.g. Jacobs et al., 1998). This appears consistent with a LN/EP suture zone to the W of the SRM. A recent aerogeophysical survey over eastern DML has revealed an extensive tectonic block (SE DML province), characterised by low amplitude, elongate, SE-trending magnetic anomalies that bounds the SRM to the S (Mieth and Jokat, 2014; Mieth et al., 2014). To the NW, this block appears to terminate along the Forster Magnetic anomaly and it has been speculated whether this block represents the southern foreland of the western extension of the Rayner Province in the region. Consequently, one interpretation is that it could represent an older, possibly unknown cratonic block.

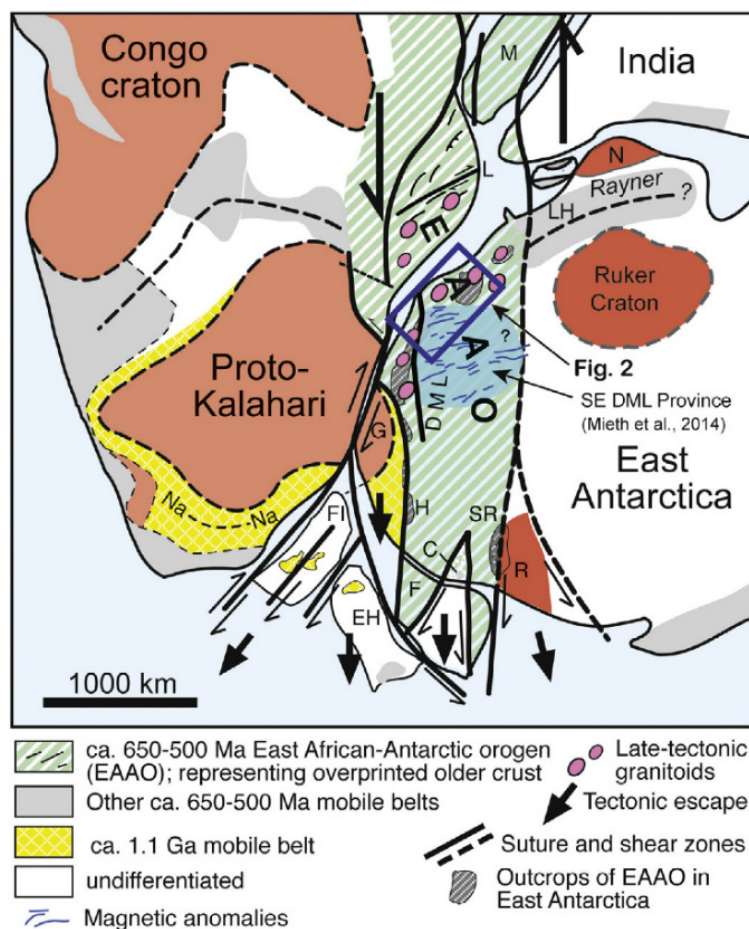


Figure 8.1: Position of the study area in a Gondwana reconstruction after Jacobs and Thomas (2004). The area is situated in a critical area where two late Mesoproterozoic/Early Neoproterozoic mobile belts meet, however, are highly reworked by the ca. 600–500 Ma East African–Antarctic Orogen. Thus far, the western extent of ca. 1000–900 Ma Rayner-type crust on the one hand and the eastern extent of ca. 1130–1000 Ma Maud Belt crust on the other are presently highly speculative. Abbreviations: C, Coats Land; DML, Dronning Maud Land; EH, Ellsworth-Haag; F, Filchner block; FI, Falkland Islands; G, Grunehogna; H, Heimefrontfjella; K, Kirwanveggen; L, Lurio Belt; N, Napier Complex; Na–Na, Namaqua–Natal; SR, Shackleton Range; M, Madagascar; R, Read Block.

The SE DML aeromagnetic province is exposed only in a number of small, so far undocumented nunataks between the Payerfjellet in central DML and the westernmost SRM, between 14 and 22°E. Because of their remote position to any stations, this group of ca. 30 nunataks has never been studied previously and therefore prevented ground truthing of the SE DML aeromagnetic province so far. The only exception is a petrographic description of rock samples from nunataks and moraines of the Steingarden area (around 16°E) collected during the QueenMET Expedition 2007/08 (Schlüter et al., 2011). During the International GEA-II Expedition (2011–12), more than half of these previously unvisited nunataks were visited, mapped and sampled. Following, we summarise our field findings and provide 16 SHRIMP and 4 SIMS zircon ages on different lithologies along with geochemical and Nd-isotope data. These new data are integrated and provide new constraints for Gondwana models in this so far poorly studied area of East Antarctica.



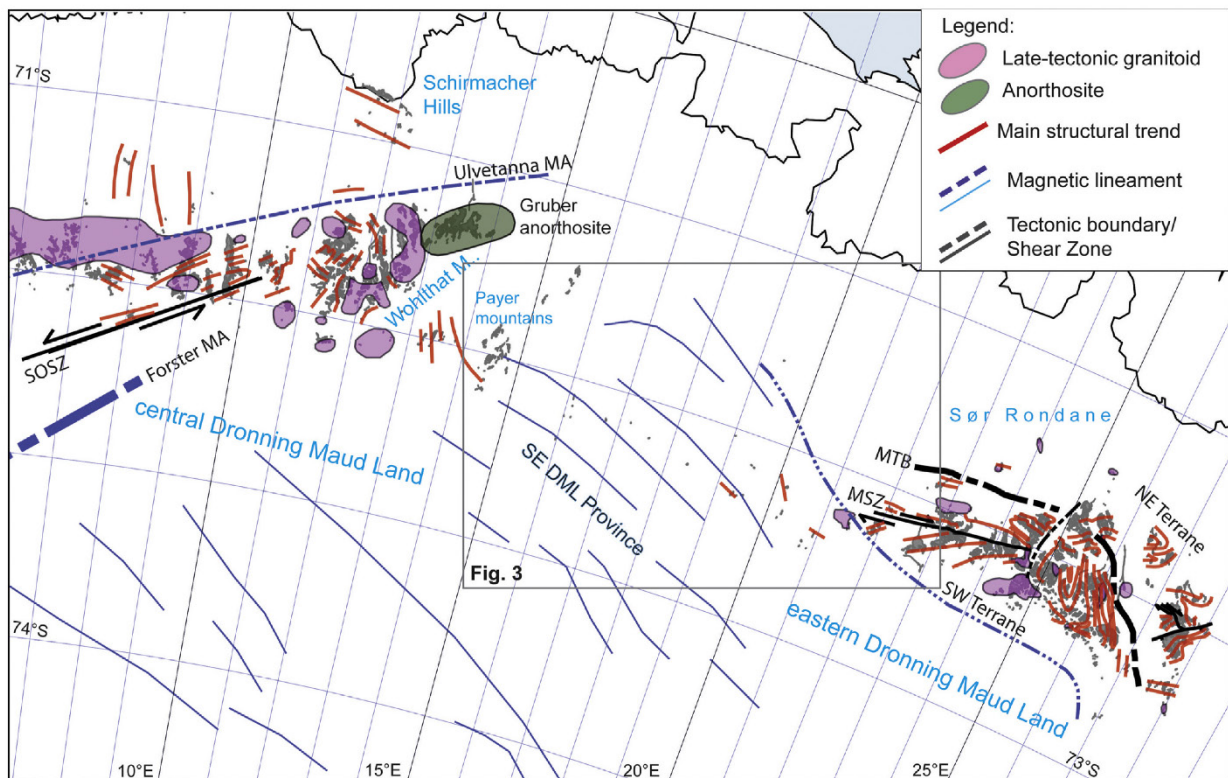


Figure 8.2: Study area of so far unvisited nunataks between Sør Rondane in the E and the Wohlthat massif in the W. Main structural trends (red) derived from field observations (Paech et al., 2004; Toyoshima et al., 2013) and aeromagnetic lineaments are derived from aerogeophysical observations (Mieth and Jokat, 2014; Mieth et al., 2014). (For interpretation of the references to color in this figure legend, the reader is referred to the web version of this article.)

## 8.3 Geological Background

### 8.3.1 Sør Rondane (22–28°E)

The present geological knowledge of the SRM and specifically the petrological evolution of at least two major medium to high-grade polymetamorphic terranes has been revealed by the extensive work of the Japanese National Antarctic Programme over several decades (e.g. Shiraishi et al., 2008; Osanai et al., 2013; Hokada et al., 2013; Satish-Kumar et al., 2013). Some of their most recent findings have lately been complemented and refined through an airborne magnetic survey (Mieth et al., 2014).

The SRM are subdivided into the distinct SW-Terrane and the NE-Terrane, separated by the Main Tectonic Boundary (MTB) (Osanai et al., 2013). The mainly granulite facies NE-Terrane is predominantly composed of metasupracrustal rocks with detrital zircon ages in part younger than 750 Ma, deposited on older basement of unknown, possibly Rayner-type, crust (Shiraishi et al., 2008). Granulite facies metamorphism has been dated by U–Pb on zircon dating at ca. 640–600 Ma and is associated with a clockwise PT-path (Osanai et al., 2013). Amphibolite-facies retrogression is widespread, has been U–Pb zircon dated at ca. 590–530 Ma and is thought to represent retrograde metamorphism and orogenic collapse (Osanai et al., 2013).

The SW-Terrane is separated into a northern and southern part by the km-wide dextral Main Shear Zone (MSZ) (Figure 8.2). South of the MSZ, a distinct gabbro–trondhjemite–tonalite–granodiorite (GTTG) suite is exposed, within what has been called the D'-sector of the SW-



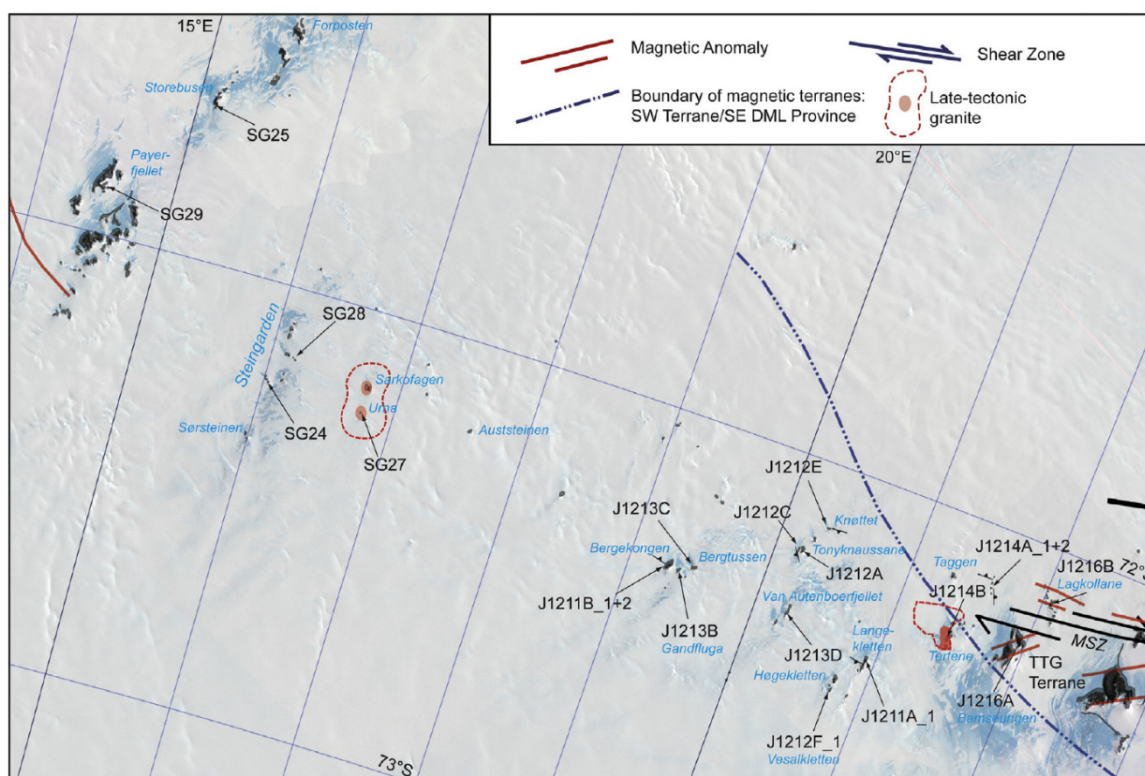


Figure 8.3: Localities of analysed samples. Significant late-tectonic granitoids are exposed at Sarkofagen/Urna and Tertene. Blue dashed line represents the southern boundary of the SW-Terrane as suggested by aerogeophysical studies (Mieth et al., 2014). (For interpretation of the references to color in this figure legend, the reader is referred to the web version of this article.)

Terrane (Osanai et al., 2013). The GTTG suite is subdivided into geochemically, petrologically, and geochronologically distinct domains with zircon crystallisation ages of ~995 Ma and 940–920 Ma (Elburg et al., 2015; Ikeda and Shiraishi, 1998; Kamei et al., 2013; Shiraishi et al., 2008; Takahashi et al., 1990). Whilst the earlier magmatism appears more tholeiitic in composition, the later event was geochemically more diverse with both high-Ti mafics and intermediate-felsic calc-alkaline intrusives with higher Sr/Y ratios (Kamei et al., 2013; Owada et al., 2013; Elburg et al., 2015). This plutonic complex is interpreted to have formed along a juvenile oceanic arc. This GTTG subterrane shows strong deformation partitioning, where some areas appear mesoscopically completely undeformed. Metamorphism does not exceed lower amphibolite facies grade, dated at ca. 590–530 Ma (Osanai et al., 2013).

To the north, the GTTG subterrane is bounded by the ENE-trending MSZ. The MSZ is a steeply south-dipping, dextral mylonite zone with mostly subhorizontal and often shallowly easterly inclined stretching lineations (Ruppel et al., 2015). The MSZ separates the GTTG subterrane from a variegated sequence of greenschist to granulite facies rocks with mostly volcano-sedimentary protoliths. Whilst metasedimentary rocks include quartzo-feldspathic gneisses and marbles, the metavolcanic rocks are represented by grey homogenous gneisses and banded gneisses, characterised by high magnetic susceptibilities. Geochemically, these rocks have island arc to continental margin affinities (Shiraishi et al., 2008). Granulite facies rocks close to the MTB (e.g. Brattnipane) have metamorphic U–Pb zircon ages of ~640–600 Ma, but in contrast to the granulites of the NE-Terrane have counterclockwise PTt-paths (Adachi et al., 2013; Baba et al., 2013; Osanai et al., 2013). Granulite facies rocks with contrasting PT-loops



and similar metamorphic ages on either side of the MTB have been explained by the thrusting of the NE over the SW-Terrane. Therefore, the MTB was interpreted as a suture zone.

Geophysically, the MTB is well imaged by aeromagnetic techniques and can be traced underneath the ice for some distance. However, the MTB appears discontinuous across central Sør Rondane (Mieth et al., 2013). In central Sør Rondane, the main structural grain changes from mainly E–W trending in western Sør Rondane to predominantly NW–SE-trending in the eastern part. It has been speculated whether central Sør Rondane represents a wide zone of late E–W directed extensional tectonics (Mieth et al., 2014).

The entire area is intruded by at least three phases of late- to post-tectonic granitoids. The oldest is the Dufek granite, dated at ca. 620 Ma (Li et al., 2003; 2006), followed by a suite of ca. 570 Ma old granites at e.g. Vengen (Shiraishi et al., 2008). The youngest granites are dated at ca. 530 Ma and are exposed at Utsteinen and Pingvinane (Tainosho et al., 1992; Li et al., 2003; 2006; Shiraishi et al., 2008). Post-kinematic mafic dykes represent the latest intrusions in the area (Owada et al., 2008).

### 8.3.2 Eastern Central Dronning Maud Land (11–14°E)

The geology of the eastern part of Central DML (A.v. Humboldtgebirge–Payerfjellet, 11–14°E) is much poorer understood than that of the SRM. The only published map of the area is at a scale of 1:500000, produced during a single reconnaissance expedition (GeoMaud 95/96; Paech et al., 2004). The area is characterised by large volumes of late-tectonic granitoids, including charnockites, anorthosites, gabbros and granites (e.g. Jacobs et al., 1998; Jacobs et al., 2008a). Only one basement rock was dated at Petermannketten, where a granitic gneiss provided a U–Pb zircon crystallisation age of ca. 1130 Ma (Jacobs et al., 1998). The volumes of late-tectonic granitoids are much larger than in the SRM, falling however into the same age range from ca. 620 to 500 Ma (Jacobs et al., 1998; 2008a). The older intrusions are typically charnockites and include a large anorthosite intrusion at Grubergebirge. The younger intrusions are predominantly granites with A-type characteristics (Roland, 2004).

### 8.3.3 Geology Between Taggen and Payerfjellet (15–21°E)

The previously unexplored nunataks consist of a range of greenschist to granulite facies rocks, predominated by amphibolite facies rocks. Both metasedimentary and meta-igneous rocks occur.

The metasedimentary rocks include highly deformed marbles, calc-silicates and migmatitic metapelites (Figure 8.4A). In the NE part of Bergtussen, major outcrops of marble with spectacularly boudinaged calc-silicate bodies occur (Figure 8.4B). Some mafic layers within the marble either indicate primary layering or several generations of foliation and deformation. The southern end of Bergekongen consists of highly migmatitic, coarse-grained gt-gneisses with very low magnetic susceptibility values, typical for metasedimentary rocks. The often stromatic leucosomes are particularly felsic and often lack mafic components. In central Tonyknausane, gt-sill gneisses occur that are intruded by large amounts of transposed gt-bearing granite melts. In the western part, very white marbles and calcsilicates crop out. The metasedimentary rocks are intruded by felsic melts and granodiorite sheets, which are still deformed together with the marble. At Høgekletten, migmatitic banded gt-bt gneiss, interlayered with boudinaged calc-silicate layers, crop out. At least two different felsic melts



intrude these metasupracrustal rocks. The central part of Langekletten is made up of bt-hbl gneiss interlayered with gt-gneisses and graphite schists. The coarse-grained graphite schists contain green V-bearing garnet. Low- to high-grade metamorphosed graphite schists are also present in moraines of the Steingarden area. They are rich in pyrite and some samples contain vanadium-rich green muscovite (Schlüter et al., 2011). Their protoliths are black shales.

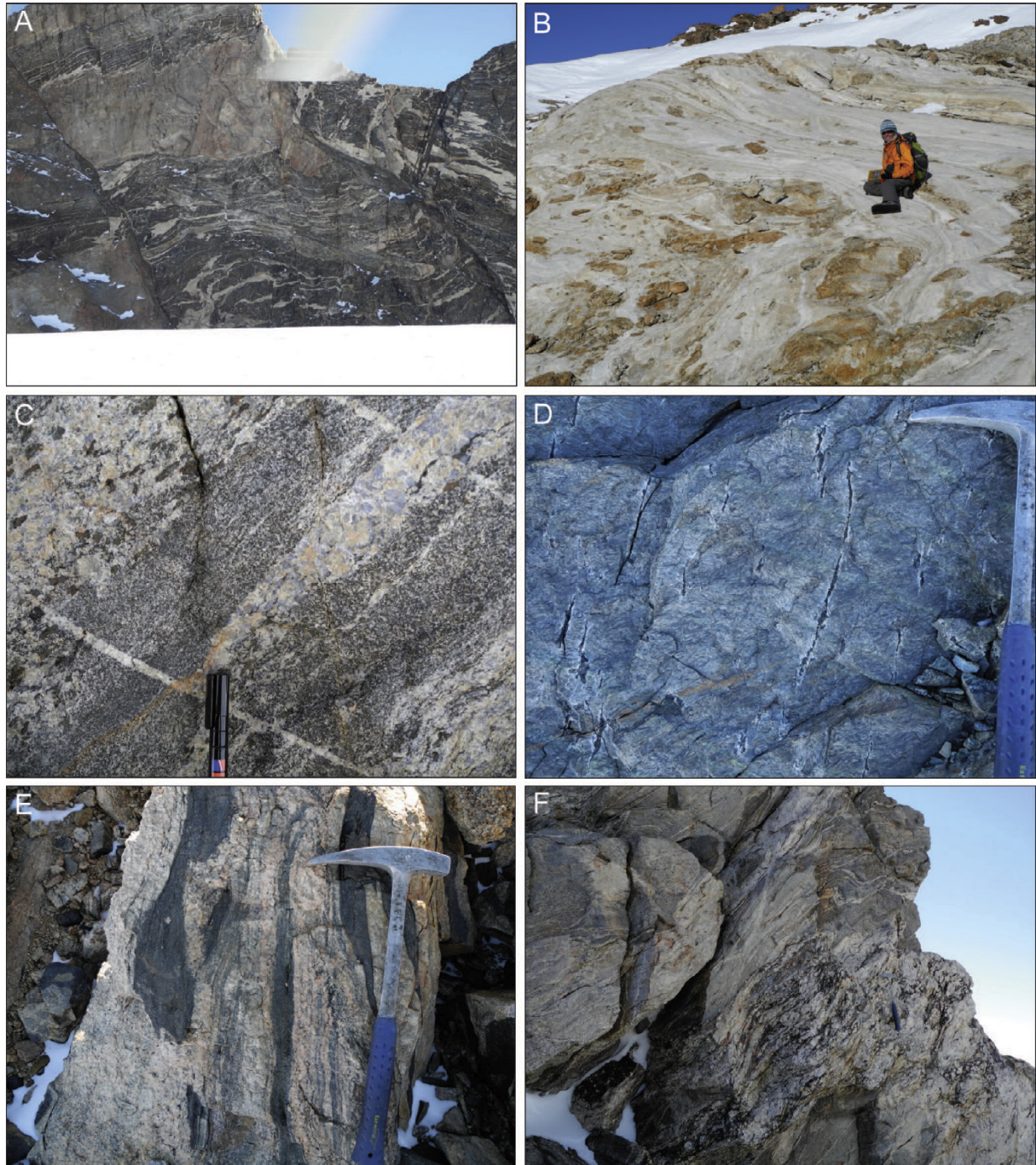


Figure 8.4: Field photographs. (A) Blåkletten, migmatitic bt-gneisses intruded by mafic dykes and major granite sheets, dissected by shear zones, height of wall ca. 100 m; (B) Bergtussen, marble with boudinaged calcsilicate layers; (C) Grandfluga, enderbitic gneiss with coarse-grained leucosome containing opx and blue qtz (J1213B); (D) Knøttet, amphibole gneiss (GTTG) with brittle-ductile tension gashes (J1212E); (E) Vesalkletten, granitic melt (A-type) with bt-gneiss enclaves (J1212F\_1); (F) Bergtussen, coarse-grained granite sheet intruded and folded with migmatitic gneisses (J1213C).



Garnet-bearing migmatites and gneisses are common lithologies at Bergekongen, Tonyknausane and Langekletten. It is often difficult to conclude what their protolith was. They typically contain garnet, biotite, quartz, plagioclase and K-feldspar with opaque minerals, and apatite and zircon as accessory phases. Muscovite is generally a secondary phase.

The meta-igneous rocks occur as amphibole gneisses, metabasics of likely volcanic origin, partly retrogressed orthopyroxene-bearing orthogneisses (enderbites) (Figure 8.4C), garnet-bearing migmatites and gneisses and late tectonic A-type granitoids.

Major outcrops of medium to coarse-grained amphibole gneisses with a granodioritic to tonalitic composition (Figure 8.4D), sometimes containing mafic enclaves are found at Knøttet, Taggen, Steingarden, Storebusen and Payerfjellet. They consist of amphibole, plagioclase (which may or may not be altered to epidote), quartz, titanite and/or an opaque phase, with or without garnet, biotite, chlorite and muscovite, plus accessory apatite and zircon. At Taggen, a plagioclase-rich cumulate occurs and would classify as an olivine norite based on its normative composition.

Well-foliated metabasic rocks are exposed at Tertene and at more northerly, unnamed nunataks. They are dominated by green-brown amphibole, with quartz and plagioclase and/or epidote as minor phases and have high values of magnetic susceptibilities. Opaque minerals, titanite, apatite and zircon occur as accessories. Several samples have an amygdaloidal texture. The samples are mostly gabbros in terms of normative composition.

Massive enderbitic gneisses crop out at Bergekongen, Bergtussen, Van Autenboerfjellet and Gandfluga, containing quartz, plagioclase, biotite, ortho- and clinopyroxene with accessory apatite and zircon. The pyroxenes are retrogressed to various degrees. The enderbites contain coarse-grained leucosomes consisting of blue quartz, pink feldspar and retrogressed orthopyroxene. The enderbites are intruded by various granitic veins.

Coarse-grained granites occur as up to several hundred metre wide outcrops at Bamseungen, Tertene, Urna and Sarkofagen. They consist of K-feldspar, quartz, plagioclase and biotite and occasionally amphibole. Most outcrops show at least a weak foliation. At Blåkletten late-tectonic granite sheets intrude migmatitic bt-gneisses. Here, the granites are in turn intruded by mafic dykes (Figure 8.4A).

## 8.4 Samples and Methods

### 8.4.1 Samples

We selected 20 samples for geochronological and geochemical studies (for sample locations, see Figure 8.3). Field evidence and petrography allows to discriminate three groups: (1) seven samples derive from a group representing amphibole gneisses/enderbite (J1211B\_2, J1212E, J1213B, J1214A\_1, J1214A\_2, SG28, SG29), including a fine-grained granodiorite gneiss, interpreted as a metavolcanic rock, amphibole gneisses, a metagabbro, migmatitic grey gneisses and an enderbite, (2) five samples form a group of gt-migmatites and foliated granitoid gneiss sheets (J1211B\_1, J1212A, J1212F\_1, J1213C, J1213D), which are considered syn-tectonic; this group of samples also includes coarse-grained, foliated pegmatitic granitoids. (3) Finally, eight samples belong to a group of late- to postorogenic granitoids (J1211A\_1, J1212C, J1214B, J1216A, J1216B, SG24, SG25, SG27). These include weakly foliated massive or sheet-like granites, granodiorites and diorites as well as massive granites and monzogranites.



## 8.4.2 U-Pb Zircon Geochronology and Whole Rock Sm–Nd Isotope Analyses

U/Pb zircon dating was carried out at the IBERSIMS laboratory, University of Granada (Spain) and at the NordSIM facility, Stockholm Museum of Natural History (Sweden). Analytical details are given in ‘Electronic Appendix C.1 and C.2’ (Black et al., 2003; Clauoué-Long et al., 1995; Jacobsen and Wasserburg, 1980; Ludwig, 2011; Raczek et al., 2003; Stacey and Kramers, 1975; Steiger and Jäger, 1977; Weis et al., 2006; Whitehouse and Kamber, 2005; Whitehouse et al., 1999; Wiedenbeck et al., 1995; Williams and Claesson, 1987; Williams and Herget, 2000; Williams, 1998). If common lead concentrations are low, we report uncorrected ages, otherwise we report common lead corrected ages. Presentation of the U–Pb results is largely regionally from E to W, from the known westernmost parts of Sør Rondane, across the geophysical boundary as defined by Mieth et al. (2014) into the SE DML Province.

Sm–Nd isotope data were acquired at the Federal Institute for Geosciences and Natural Resources (BGR, Germany) and the University of Tübingen (UniTueb, Germany). Analytical details of all analyses are given in ‘Electronic Appendix C.3’.

## 8.5 Results

### 8.5.1 U–Pb Zircon Geochronology

Tabulated analytical results are provided in ‘Electronic Appendix C.2’.

#### J1214A\_1, fine-grained granodioritic gneiss, ridge E of Taggen (–72.145133; 21.608900)

This rock from an unnamed ridge east of Taggen is a fine-grained granodioritic to tonalitic gneiss. It consists of quartz, feldspar (mostly plagioclase and subordinately K-feldspar), biotite and secondary muscovite. Quartz and feldspar are recrystallized, plagioclase shows deformed twin lamellae. Accessory minerals include epidote, titanite and opaque minerals. The rock was interpreted as a metavolcanic rock. It contains small, isometric, sub-idiomorphic, brown zircons. The grain size rarely exceeds 100 µm. The unusual zircons are intergrown with an opaque phase and resemble zircons in alkaline rocks. The zircons show low cathodoluminescent (CL) response (Figure 8.5A). Twenty-three areas in 23 grains were analysed (Figure 8.6A). The U concentration varies from 700 to 3900 ppm and Th/U from 0.3 to 1.3. Most analyses are concordant with low common lead abundance.

Two analyses are from younger outliers (12.1, 18.1). The remaining 21 analyses provide a  $^{207}\text{Pb}/^{206}\text{Pb}$ -age of  $961 \pm 4$  Ma (MSWD = 2.76). This age is interpreted as the crystallisation age of the volcanic protolith of the granodioritic gneiss.

#### J1214A\_2, granodioritic gneiss, ridge E of Taggen (–72.145133; 21.608900)

This medium-grained granodioritic gneiss was sampled at the same unnamed ridge east of Taggen. Quartz shows undulose extinction, sutured grain boundaries as well as in some parts recovery fabrics. Plagioclase has deformed twinning lamellae, K-feldspar is mainly microcline. Light to dark brown biotite with columnar to radial habit is common and partly altered to chlorite. Greenish-blue hornblende is rarely present. Accessory minerals are zircon, epidote, and opaque minerals.



The sample has small, up to 150  $\mu\text{m}$  long stubby, clear to light brownish zircons. In CL, many zircons show large high-U cores, which often appear metamict (Figure 8.5B). Cores are surrounded by an oscillatory-zoned component that again is sometimes rimmed by a thin high-U rim. Twenty-seven analyses from the three different zircon components are concordant and have low common lead abundance (Figure 8.6B).

Four core analyses have U from 900 to 3700 ppm (Th/U: 0.4–1.4), 18 oscillatory-zoned intermediate areas have U from 200 to 1000 ppm (Th/U: 0.3–0.7) and rims have U from 400 to 2600 ppm (Th/U: 0.3–1.1). The three different zircon components cannot be distinguished in their  $^{207}\text{Pb}/^{206}\text{Pb}$  ages and all 27 analyses together provide a weighted mean  $^{207}\text{Pb}/^{206}\text{Pb}$  age of  $980 \pm 8$  Ma (MSWD = 2.74). This age is interpreted as the crystallisation age of the granitic protolith of J1214A\_2.

#### J1212E, mylonitic amphibole gneiss, Knøttet (–72.150050; 20.321083)

This mylonitic amphibole gneiss consists of quartz, plagioclase, K-feldspar, biotite, hornblende, muscovite, and dispersely scattered secondary carbonate. Quartz is recrystallized and occurs as relict clasts with biotite in pressure shadow tails. Quartz aggregate layers locally form rootless folds associated with a pre-mylonitic foliation. The rock shows a complex history.

The sample has small, clear to yellowish, short prismatic to elongate zircons with length/width ratios up to 2. Most zircons do not exceed 100  $\mu\text{m}$  in length. In CL images, the zircons show oscillatory, probably magmatic growth zoning (Figure 8.5C). Some zircons have indistinct inner cores of similar luminescence and U-concentration as the main oscillatory zircon components. Many zircons have thin rims showing a more uniform CL response. The main oscillatory zircon components and the innermost cores were analysed in 20 areas, whilst the thin rims allowed analyses in only two cases (Figure 8.6C). All analyses are concordant and contain low amounts of common lead. U concentration in the zircon cores ranges from 100 to 430 ppm (Th/U: 0.24–0.53), whilst the two rim analyses have U of ca. 200 and 300 ppm (Th/U: 0.15, 0.22). The analyses show significant scatter, but rim analyses are indifferentially from core analyses. Twenty core analyses provide a  $^{206}\text{Pb}/^{238}\text{U}$  age of  $925 \pm 11$  Ma (MSWD = 5.52). This age is interpreted as the crystallisation age of the amphibole gneiss protolith. The significant scatter may be due to younger overprint.

#### J1211A\_1, granitic gneiss (syntectonic), Langekletten (–72.406267; 20.920250)

The granitic gneiss sample at Langekletten was collected from a homogeneous, medium- to coarse-grained granitic gneiss sheet. The sample contains quartz, K-feldspar, plagioclase, biotite, and secondary muscovite. Quartz shows undulose extinction, recrystallization, sutured grain boundaries as well as recovery fabrics. K-feldspar is characterised by undulose extinction, perthitic exsolution, and alteration. Microcline and plagioclase are common and generally appear recrystallized. Dark brown biotite occurs as mafic component.

The sample contains two distinctly different types of zircons. The first type consists of long prismatic zircons with aspect ratios up to 6 and a maximum length of 400  $\mu\text{m}$ . Larger, but more stubby zircons, make up the second type. They are characterised by many inclusions and being in part metamict. This is reflected in a contrasting CL response: the first type shows oscillatory zoning and the second type is very dark and structureless (Figure 8.5D). In total, 29 analyses were performed in 29 grains, 10 analyses in the oscillatory-zoned parts and 19 analyses in the



dark CL zircons (Figure 8.6D). Analyses in the oscillatory-zoned zircons have typical U of 300–800 ppm (Th/U: 0.37–0.47), whilst the dark CL zircons have much higher U, ranging from 1900 to 12,000 ppm (Th/U: 0.06–0.17). Of the 10 analyses performed on the oscillatory-zoned zircons, one analysis has a large error and two outliers occur. The remaining seven analyses provide a  $^{204}\text{Pb}$ -corrected  $^{206}\text{Pb}/^{238}\text{U}$  age of  $930 \pm 12$  Ma (MSWD = 0.72).

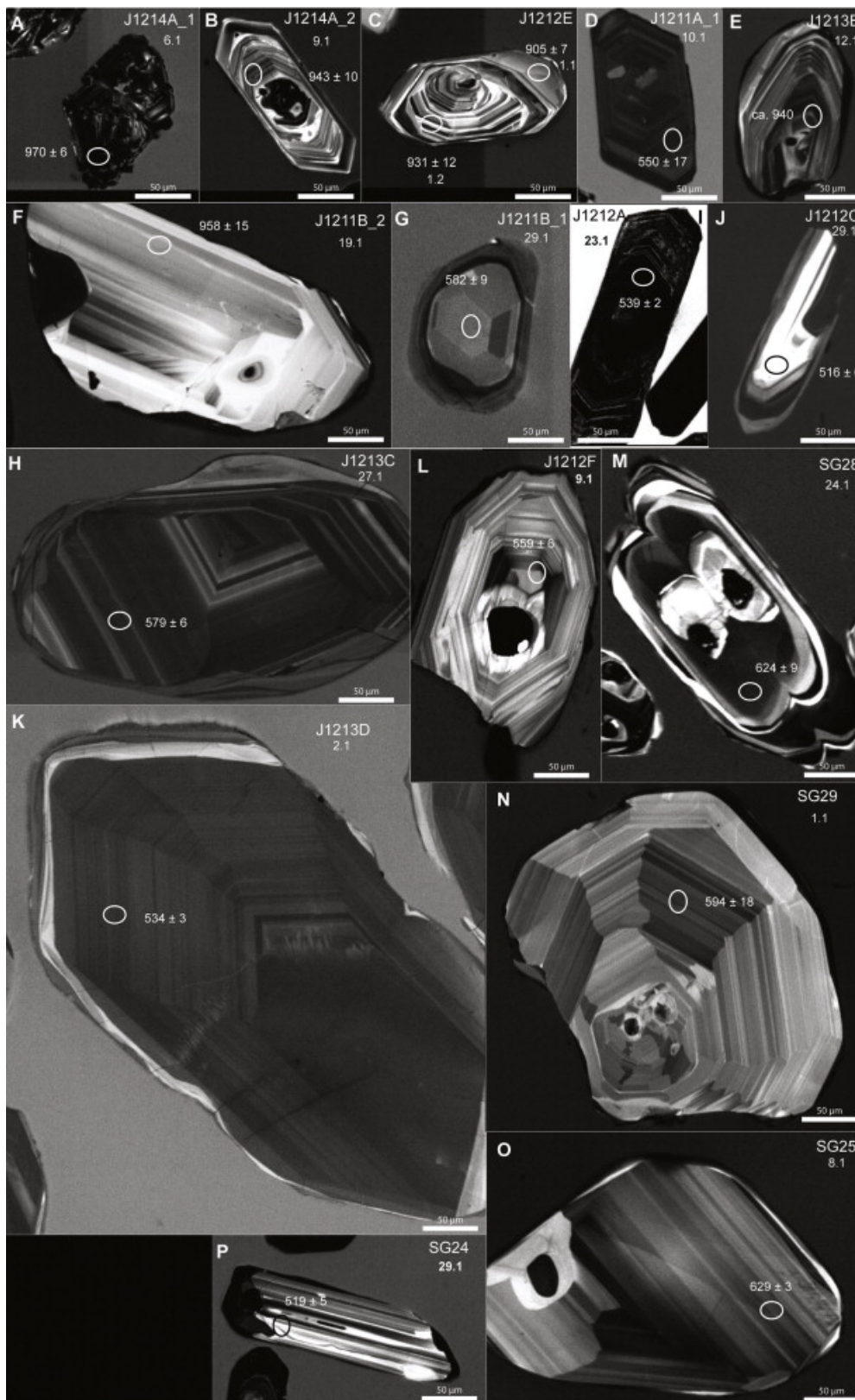


Figure 8.5: Selected cathodoluminescence images of most dated samples.



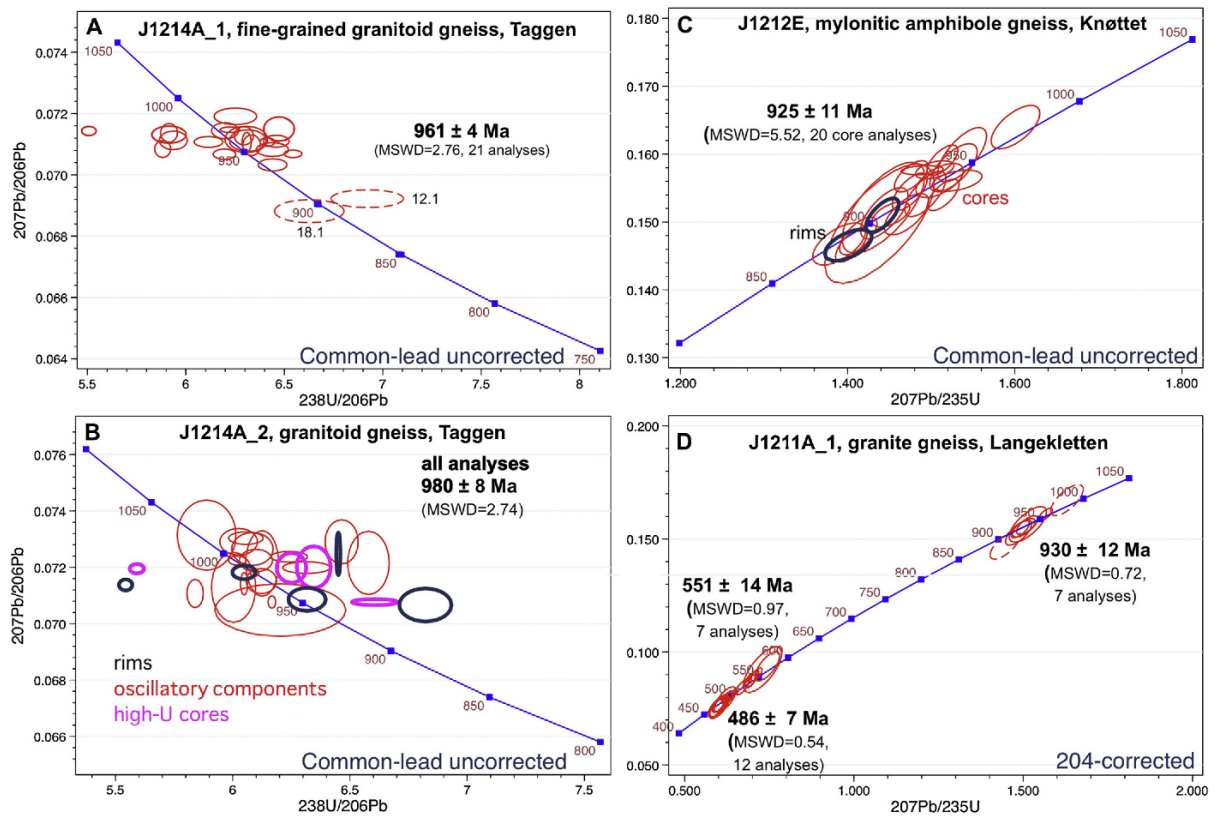


Figure 8.6: SHRIMP zircon geochronology of the easternmost part of the study area.

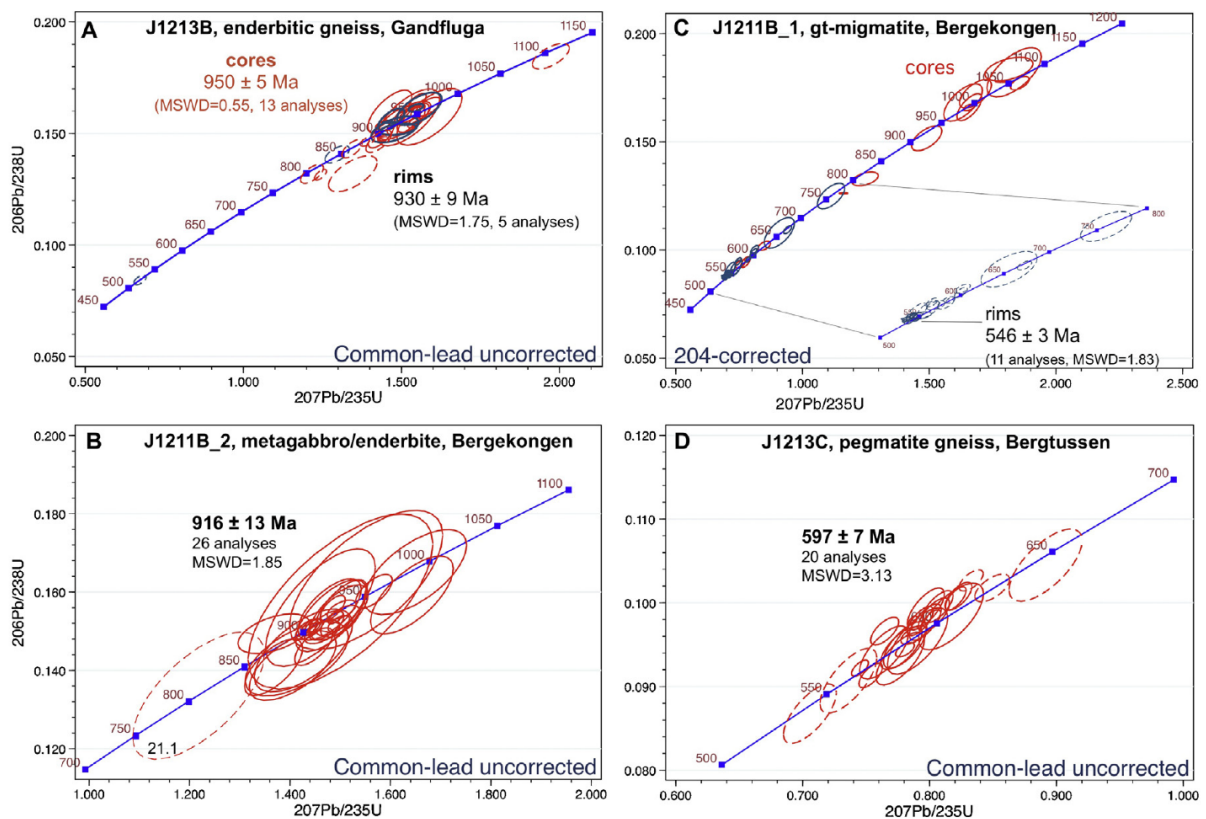


Figure 8.7: SHRIMP zircon geochronology of Bergekongen, Bergtussen and Grandfluga.



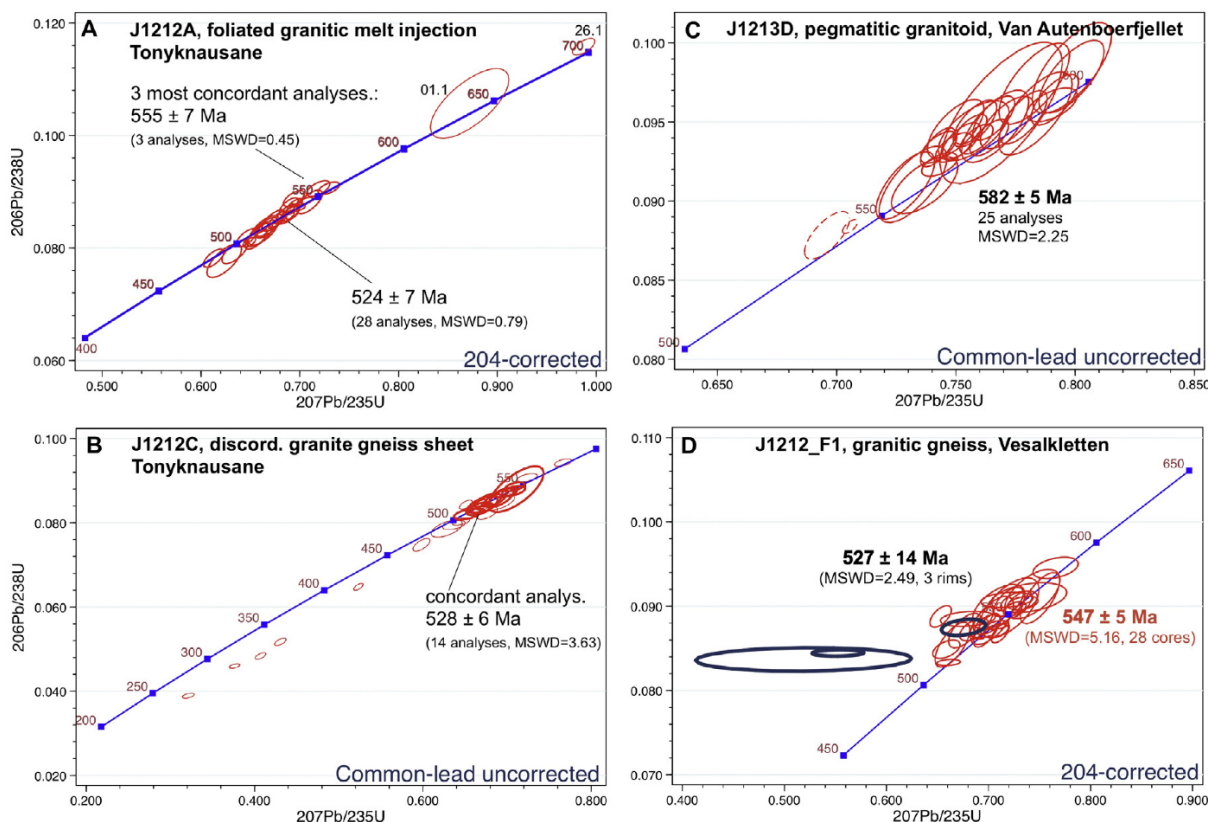


Figure 8.8: SHRIMP zircon geochronology of Tonyknausane, Van Autenboerfjellet and Vesalkletten.

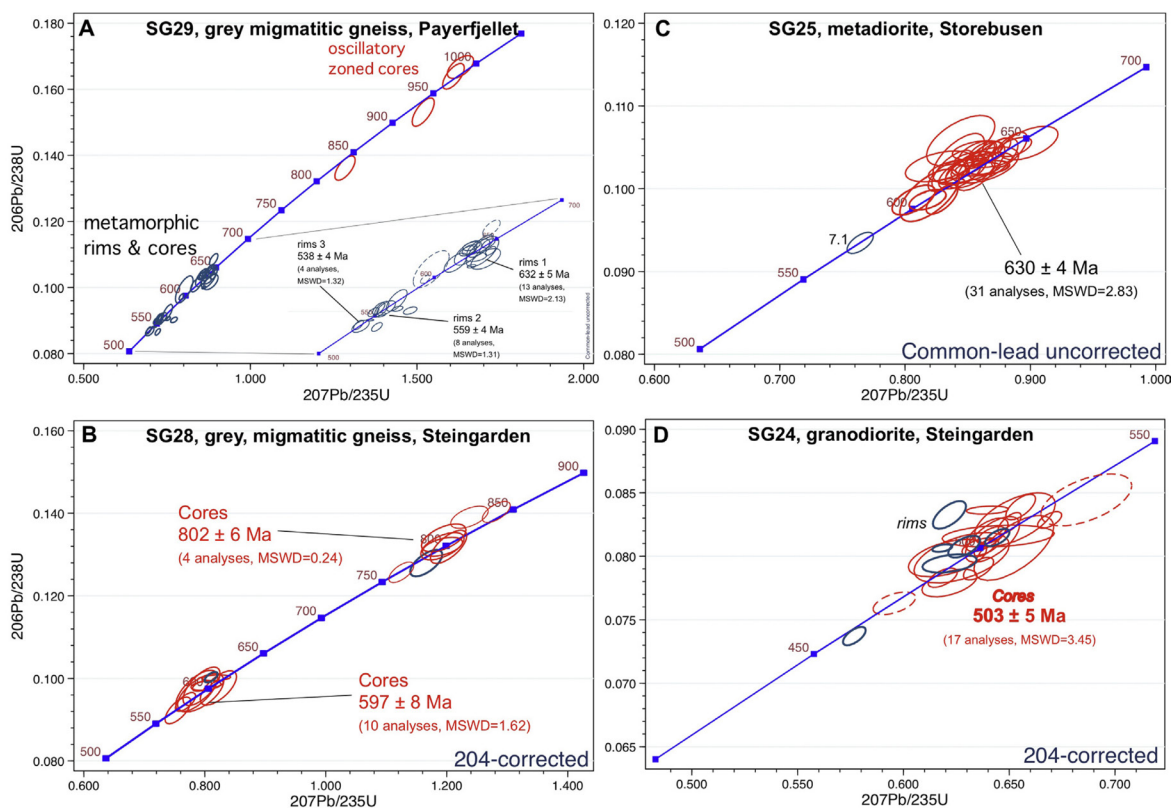


Figure 8.9: SHRIMP zircon geochronology of the westernmost part of the study area.



The 19 analyses performed in the dark CL zircons give younger ages, which fall into two distinct subgroups. The 7 older ages form a group with  $^{204}\text{Pb}$ -corrected  $^{206}\text{Pb}/^{238}\text{U}$  age of  $551 \pm 14$  Ma (MSWD = 0.97), whilst the 7 younger ages form a group providing a  $^{204}\text{Pb}$ -corrected  $^{206}\text{Pb}/^{238}\text{U}$  age of  $486 \pm 7$  Ma (MSWD = 0.54).

The interpretation of the data is difficult. We interpret the older age of ca. 930 Ma as inheritance, the age group of ca. 550 Ma probably indicates the igneous crystallisation age of the granite protolith, whilst the slightly younger age of ca. 490 Ma could indicate metamorphic overprint.

#### J1213B, grey, enderbitic gneiss, Grandfluga (-72.350917; 19.384233)

Sample J1213B was collected from a grey enderbitic gneiss that has opx-bearing melt patches. The sample has stubby to irregular elongate, clear to light brownish, up to 250  $\mu\text{m}$  long zircons with many inclusions. CL imaging reveals mostly oscillatory zoning of the zircons, whereby some have an up to 50  $\mu\text{m}$  wide, relatively homogeneous rim (Figure 8.5E). A number of zircons have small, CL-dark cores.

Thirty-five areas were analysed in 27 cores and 7 rims (Figure 8.7A). U concentration of the oscillatory zoned parts is in the range from 100 to 1400 ppm, with Th/U from 0.01 to 0.5, whilst rim analyses have U concentrations ranging from 170 to 640 ppm with Th/U from 0.14 to 0.24. Three core and one rim analyses are discordant or have large errors (9.1, 16.1, 18.2, 20.1). One core analysis is significantly older (16.2). The remaining core analyses fall into an older and a younger group. The older group of 13 analyses gave a  $^{206}\text{Pb}/^{238}\text{U}$  age of  $950 \pm 5$  Ma (MSWD = 0.55), whilst the remaining core analyses straddle the concordia or are slightly discordant. Five rim analyses give a  $^{206}\text{Pb}/^{238}\text{U}$  age of  $930 \pm 10$  Ma (MSWD = 1.75), whereas two other concordant rim analyses gave  $^{206}\text{Pb}/^{238}\text{U}$  ages of ca. 850 and 520 Ma.

The main group of core analyses are interpreted to represent the crystallisation age of the igneous protolith at ca. 950 Ma, whilst the rim analyses probably represent an only slightly younger metamorphic overprint at 930 Ma. This metamorphic overprint together with a younger phase of overprint at ca. 520 Ma probably led to Pb loss and resulted in a number of discordant analyses.

#### J1211B\_2, metagabbro/enderbite, Bergekongen (-72.358167; 19.288833)

This metagabbro/enderbite from Bergekongen consists mainly of plagioclase and coarse-grained orthopyroxene. Plagioclase shows well-developed deformation lamellae. Additionally, the rock contains biotite and large amphiboles, which formed due to amphibolites facies retrograde metamorphism.

The sample has up to 700  $\mu\text{m}$  large brownish zircons with irregular shapes and many inclusions. Zircons show irregular and occasionally sector-zoning in CL imaging (Figure 8.5F). Thirty areas were analysed in 30 grains, most of which are concordant and have low common lead abundances (Figure 8.7B).

Zircons are low in U, ranging from ca. 100 to 700 ppm with Th/U from 0.2 to 1.3. Two analyses are discordant (4.1, 16.1) and one analysis has a large error (12.1). Of the remaining 27 analyses, one analysis (21.1) forms a younger outlier, whilst the other 26 analyses provide a  $^{206}\text{Pb}/^{238}\text{U}$  age of  $916 \pm 13$  Ma (MSWD = 1.85). This age is interpreted as the crystallisation age of the metagabbro/enderbite protolith.



J1211B\_1, Gt–migmatite (syntectonic), Bergekongen (–72.406267; 20.920250)

Sample J1211B\_1 was collected from a gt–migmatite sheet that appears intrusive into the migmatitic bt–gt gneisses. The sample consists mainly of quartz, K-feldspar, plagioclase, and biotite. Garnet grains are 0.5–2 cm in size with inclusions of biotite and quartz. Quartz is characterised by undulose extinction, dynamic recrystallization, and sutured grain boundaries. K-feldspar and subordinate plagioclase show weak alteration/sericitization. Coarse grained and light to dark brown coloured biotite is common. The sample has rounded to elongate, light brownish typical metamorphic zircons, with clear core–rim relations and max. length of 200  $\mu\text{m}$ . Some zircon cores are metamict. Zircon cores appear in part oscillatory-zoned with high CL response, whilst broad zircon rims often have weak or no CL response (Figure 8.5G). Occasionally, these rims can contribute to more than 50 vol.% of the zircons.

Thirty-four areas were analysed in 32 grains, 14 core and 20 rim analyses (Figure 8.7C). U concentration in zircon cores varies between 100 and 1400 ppm, with Th/U of 0.17–0.54 (some outliers lower). Rim analyses have U of 370–1300 ppm and Th/U of 0.00–0.14. The 20 core analyses show a large range of  $^{206}\text{Pb}/^{238}\text{U}$  ages from ca. 1100 to 600 Ma with two small clusters at ca. 1070 and 1000 Ma. The 20 rim analyses also show a strong scatter between ca. 750 and 540 Ma, with a strong culmination at the lower age range. The youngest portion of the rim analyses (11 analyses) form a well-defined  $^{204}\text{Pb}$ -corrected  $^{206}\text{Pb}/^{238}\text{U}$  age of  $546 \pm 3$  Ma (MSWD = 1.83). The core analyses are interpreted as an older inherited zircon population. The rim analyses probably reflect a protracted metamorphic episode, culminating at ca. 540 Ma.

J1213C, pegmatite gneiss (syntectonic), Bergtussen (–72.337533; 19.472300)

Sample J1213C was collected from a very coarse-grained pegmatite gneiss that intrudes highly migmatitic gneisses. The pegmatite shows moderate deformation and contains mainly quartz, partly antiperthitic and sericitized plagioclase, K-feldspar and biotite. Quartz shows undulose extinction and grain boundary migration.

The sample contains large, irregular, often fragmented zircons, which are clear to brownish and frequently have mineral inclusions. Zircons reach 500  $\mu\text{m}$  in length. Zircons show moderate CL response, mostly with a wide oscillatory zoning (Figure 8.5H). Many grains show resorption and thin zircon overgrowth.

Thirty areas were analysed in 28 grains (Figure 8.7D). The U concentration ranges between 500 and 1200 ppm and Th/U ranges from 0.04 to 0.1. Of the 30 analyses, four analyses are discordant and one grain has a large error. The remaining 25 analyses have significant scatter. If the three oldest and the two youngest analyses are disregarded, the remaining 20 analyses give a  $^{206}\text{Pb}/^{238}\text{U}$  age of  $597 \pm 7$  Ma (MSWD = 3.13). This age is interpreted as the crystallisation age of the zircons in the pegmatite.

J1212A, foliated granite melt injection (syntectonic), Tonyknausane (–72.214100; 20.197967)

Tonyknausane is dominated by meta-supracrustal rocks that have large melt components. This foliated granitic melt injection consists mainly of quartz, plagioclase, subordinate K-feldspar and biotite altered to chlorite. Muscovite occurs as a secondary product. Quartz shows undulose extinction, sutured grain boundaries, and is recrystallized. Plagioclase shows signs of grain boundary migration, deformation lamellae as well as myrmekitization. Subordinate garnet occur as large grains.



The sample contains clear, light brownish and mostly long-prismatic zircons of up to 200  $\mu\text{m}$ . Many zircons are zoned with well-developed terminations, whilst some zircons appear less idiomorphic and have rounded terminations. A number of zircons have metamict cores and mineral inclusions are abundant. All zircons have very low CL response, but a faint oscillatory zoning is visible (Figure 8.5I).

Thirty areas were analysed in 30 grains (Figure 8.8A). U and Th are extremely high, with U ranging from 3500 to 23,000 ppm and Th/U from 0.02 to 0.11. Many analyses are highly discordant. Twenty-eight analyses form one age group, however with a notable age dispersion, giving a  $^{204}\text{Pb}$ -corrected  $^{206}\text{Pb}/^{238}\text{U}$  age  $524 \pm 7$  Ma (MSWD = 0.79). The three most concordant analyses give a  $^{204}\text{Pb}$ -corrected  $^{206}\text{Pb}/^{238}\text{U}$  age of  $555 \pm 7$  Ma (MSWD = 1.41). Two analyses form older outliers (01.1; 26.1). Grain 26.1 is a core analysis and could therefore represent inheritance. There is no apparent reason why analysis 01.1 is significantly older than the main age group. It is surprising that despite the high U, the grains are apparently clear with metamictisation confined to some cores. This could be due to young thermal event that led to annealing of the radiation damage. The interpretation of the age is difficult. The three most concordant analyses with an age of ca. 555 Ma might best represent the crystallization age of the granitic protolith.

#### J1212C, discordant granitic gneiss sheet, Tonyknausane (-72.212600; 20.182767)

Sample 1212C was collected from a granitic gneiss sheet that cuts the metasupracrustal gneisses. The sample consists of quartz, plagioclase, K-feldspar, biotite and titanite. Both quartz and feldspar show undulose extinction, recrystallization and sutured grain boundaries. Plagioclase has deformation twins and myrmekite is present. K-feldspars are generally strongly altered, whereas idiomorphic to hypidiomorphic dark brown biotite shows sparse inclusions. The sample has small stubby to highly elongate zircons and zircon fragments that seldom reach more than 100  $\mu\text{m}$  in length. Zircons are clear to light brownish with strong zonation and occasional metamict cores. In CL imaging, many zircons show light and oscillatory-zoned cores, surrounded by dark rims, which are either structureless or oscillatory-zoned (Figure 8.5J).

Twenty-eight areas were analysed in 22 cores and 6 rims (Figure 8.8B). Core analyses have a wide range of U (70–850 ppm) with Th/U ranging from 0.13 to 0.71. Rim analyses range from 360 to 600 ppm U and have a narrower range of Th/U (0.23–0.39). All analyses are low in common Pb abundance and no obvious age difference between cores and rims is observed. Some analyses are significantly discordant, especially those with high U (2.1, 5.1, 19.1, 24.1, 28.1), indicative for subrecent Pb-loss, but still preserve a similar apparent  $^{207}\text{Pb}/^{206}\text{Pb}$  age. All 28 analyses fall on a discordia line with an upper intercept at  $532 \pm 10$  Ma (MSWD = 2.40). The 14 most concordant analyses (<1 % discordance) give a  $^{206}\text{Pb}/^{238}\text{U}$  age of  $528 \pm 6$  Ma (MSWD = 3.63). This age is interpreted as the crystallisation age of the granitic protolith.

#### J1213D, pegmatitic granitoid (syntectonic), Van Autenboerfjellet (-72.362983; 20.244717)

Van Autenboerfjellet is dominated by highly migmatitic garnet–biotite-gneisses. Sample J1213D was collected from a very coarse-grained granite sheet, intruding these migmatites. The sample consists of quartz, plagioclase, K-feldspar, and biotite. Quartz and both feldspars show undulose extinction. Quartz has sutured grain boundaries.



The sample has stubby to rounded zircons with a maximum size of up to 400  $\mu\text{m}$ . The zircons are clear to light-brownish and usually have rounded terminations. Aspect ratios seldom exceed two. Some zircons have inclusions and cracking is common. Zircons show a low CL response, with thin rims of stronger CL (Figure 8.5K).

Twenty-nine areas were analysed in 29 grains (Figure 8.8C). The U concentration varies between 400 and 1900 ppm and Th/U between 0.13 and 0.17. Despite their low CL response, most analyses are concordant with very low common lead abundances. If one analysis with a large error (13.1), one highly discordant analysis (7.1), and two younger outliers are excluded, the remaining 25 analyses give a  $^{206}\text{Pb}/^{238}\text{U}$  age of  $582 \pm 5$  Ma (MSWD = 2.25). This age is interpreted as the crystallisation age of the pegmatitic granite.

#### J1212F\_1, granitic gneiss, Vesalkletten (-72.495433; 20.749850)

At Vesalkletten, massive pink granitic gneisses contain large schollen of biotite gneiss. Sample J1212F\_1 was collected from a medium-grained granitic gneiss. The sample consists mainly of quartz, K-feldspar, plagioclase, and biotite. Quartz grains reveal undulose extinction, sutured grain boundaries, and are strongly recrystallized. Both feldspars are strongly sericitized.

The sample has yellowish, small to medium-sized zircons with many inclusions and rounded tips. Most zircons are short-prismatic with maximum length of 400  $\mu\text{m}$ . Many zircons show core-rim relationships in CL images, with highly luminescent, often oscillatory-zoned cores and darker, often thin, high-U rims (Figure 8.5L). Thirty-one analyses from 28 cores and 3 rims were performed in 29 grains (Figure 8.8D). U concentration in core analyses varies between 140 and 500 ppm (Th/U: 0.18–0.43), whilst the three rim analyses have higher U (700–1300 ppm) and hence lower Th/U (0.09–0.25). Most analyses are concordant and have low common lead abundance, whilst three analyses are highly discordant (2 rims, 1 core). Twenty-eight core analyses give a  $^{206}\text{Pb}/^{238}\text{U}$  age of  $547 \pm 5$  Ma (MSWD = 5.16), which is interpreted as the crystallisation age of the granitic protolith. The three rim analyses are highly discordant and slightly younger (ca. 530 Ma).

#### SG29, migmatitic grey gneiss with mafic enclaves, Payerfjellet (-71.894200; 14.508200)

SG29 was collected from a migmatitic grey gneiss with abundant mafic enclaves and relatively high magnetic susceptibilities. Quartz shows undulose extinction, sutured grain boundaries, and abundant inclusion trails. Plagioclase reveals polysynthetic twinning. K-feldspar is represented in minor amounts and the mafic components are amphibole, biotite and titanite.

The sample has rounded to highly elongate zircons with maximum length of up to 400  $\mu\text{m}$ . Most zircons have metamict cores, many mineral inclusions and are highly cracked. The non-metamict areas are clear. In CL imaging, metamict zircon cores show wide homogeneous or zoned zircon rims with moderate to low CL response (Figure 8.5N).

Thirty-two areas were analysed in 30 grains, including 7 core and 25 rim analyses (Figure 8.9A). Four analyses are from non-metamict oscillatory-zoned cores; these have moderate U concentrations of 240–370 ppm with uni-form Th/U of ca. 0.2. These four core analyses have highly varying  $^{206}\text{Pb}/^{238}\text{U}$  ages between ca. 1000 and 800 Ma. Three further core analyses (2.1, 9.1, 16.2) are from clear areas, whose CL resemble the wide metamorphic rims of other zircons. These grains give scattered ages between ca. 600 and 530 Ma.



Metamorphic rims are highly variable in U (120–1900 ppm) with Th/U of 0.03–0.33. The 25 rim analyses have  $^{206}\text{Pb}/^{238}\text{U}$  ages ranging from 650 to 530 Ma with distinct populations at ca. 630, 560 and 540 Ma. These different populations cannot be distinguished in CL imaging. The oldest metamorphic rims are defined by 13 analyses, which provided a  $^{206}\text{Pb}/^{238}\text{U}$  age of  $632 \pm 5$  Ma (MSWD = 2.13). Eight rims form an intermediate group of rim ages with a  $^{206}\text{Pb}/^{238}\text{U}$  age of  $559 \pm 4$  Ma (MSWD = 1.31). The lowest age group is formed by four analyses, which provide a  $^{206}\text{Pb}/^{238}\text{U}$  age of  $538 \pm 4$  Ma (MSWD = 1.32). The protracted metamorphic overprint has to a large extent obliterated the crystallisation history of the igneous protolith, which is only recorded by a few core analyses of ca. 980 Ma.

SG28, grey, migmatitic gneiss, Steingarden (–72.200067; 16.151233)

Sample SG28 was collected from grey, migmatitic gneisses in Steingarden. The sample has strongly altered K-feldspar and plagioclase, the latter with deformation twins. Small amounts of fine-grained quartz occur, with undulose extinction and sutured grain boundaries. Biotite is dark-brown. The sample has stubby to elongate, clear to light brownish zircons with maximum length of 200  $\mu\text{m}$ . Most zircons appear zoned, have many inclusions and rounded tips. In CL imaging, zircons show pronounced oscillatory-zoned cores with strong CL response (Figure 8.5M); some zircons have rims with low CL-response.

Twenty-four areas were analysed in 24 grains, 19 cores and 5 rims (Figure 8.9B). Typical core analyses have 120–1200 ppm U, with Th/U of 0.16–0.66, whilst rim analyses have U from 860 to 1200 ppm, with Th/U of 0.05–0.09. Three rim and two core analyses with relatively high U are highly discordant.

Seven core analyses show ages of ca. 800 Ma with a significant scatter; if the two oldest and the youngest age in this group are excluded, the remaining four analyses form a well constrained  $^{206}\text{Pb}/^{238}\text{U}$  age of  $802 \pm 6$  Ma (MSWD = 0.24). In addition, further 10 core analyses yield a  $^{206}\text{Pb}/^{238}\text{U}$  age of  $597 \pm 8$  Ma (MSWD = 1.62). For both age clusters at least one concordant rim analyses accompanies the cores in age. The interpretation of the age distribution is difficult. The age group of ca. 600 Ma might date migmatisation of the grey gneiss, whilst the ca. 800 Ma age group might represent the crystallisation age of the igneous protolith.

SG25, metamonzodiorite, Storebusen (–71.645917; 15.120467)

Sample SG25 was collected from a massive, weakly foliated metadiorite at Storebusen. The sample contains mainly plagioclase with undulose extinction and deformation twins. Minor K-feldspar is present. Dark-brown biotite and coarse-grained greenish-brown amphibole occur as mafic components. The sample contains clear, xenomorphic and mostly isometric, irregular zircons, up to 400  $\mu\text{m}$  in size. Zircons display sector and complex zoning in CL (Figure 8.5O). A few zircons show thin rims.

Thirty-two areas were analysed in 27 grains, most of the analyses from zircon cores (Figure 8.9C). Zircons are low in common Pb abundance and have moderate U (160–460 ppm) with Th/U ranging from 0.06 to 0.49. Thirty-one core analyses from diversely zoned areas form a single age group with a weighted-mean  $^{206}\text{Pb}/^{238}\text{U}$  age of  $630 \pm 4$  Ma (MSWD = 2.83). This age is interpreted as the crystallisation age of the protolith of the metadiorite. One rim analysis (7.1) has a  $^{206}\text{Pb}/^{238}\text{U}$  age of ca. 580 Ma and is interpreted to have grown during metamorphic overprint.



SG24, granodiorite, Steingarden-S (-72.223950; 16.027433)

This weakly foliated granodiorite from Storebusen has a well preserved plutonic texture. The main mineral phases include quartz (with undulose extinction and inclusion trails), plagioclase (with deformation twinning), K-feldspar, and coarse-grained biotite as well as titanite.

The sample has clear to greyish, short prismatic to elongate zircons with aspect ratios up to 5. Zircons are up to 500  $\mu\text{m}$  long and have many inclusions. In CL, the zircons show irregular high-luminescent cores and in part wide, dark rims (Figure 8.5P). Some cores show oscillatory zoning, others are very irregular and indicate recrystallisation. The rims are structureless in CL. Thirty-one areas were analysed in 29 grains, most of which show low common lead abundance (Figure 8.9D). Three core analyses (2.1, 22.1, 24.1) have large errors, two analyses are discordant (1.1, 16.1), and two analyses (12.2, 28.1) are outliers and are not further considered. Seventeen core analyses have U ranging from 75 to 1300 ppm (Th/U: 0.06–1.05) and give a  $^{204}\text{Pb}$ -corrected  $^{206}\text{Pb}/^{238}\text{U}$  age of  $503 \pm 5$  Ma (MSWD = 3.45). Seven rim analyses have high U (570–5900 ppm), with Th/U of 0.1–0.8, and show significant age scatter, indistinguishable in age from the core analyses. The core analyses of ca. 503 Ma are interpreted as the crystallisation age of the granodiorite.

SG27, granite, Urna (-72.234169; 16.774981)

This granite is medium-grained and weakly foliated. It contains quartz, plagioclase, K-feldspar, amphibole and biotite. K-feldspar shows Carlsbad twinning and flame perthitic exsolution; microcline also occurs. Quartz shows undulose extinction with chessboard pattern. Plagioclase is recrystallized and has deformation twins. Plentiful zircon is present that shows strong radiation damage halos in amphiboles and biotites. The sample contains clear to brownish, euhedral, elongate, up to 400  $\mu\text{m}$  long zircon grains with aspect ratios up to 4. In CL, dark high-U rims of variable thickness and oscillatory zoning are observed. Two types of cores can be distinguished: (a) high luminescent low-U cores with broad oscillatory zoning; (b) dark high-U cores with irregularly placed inclusions and magmatic oscillatory zoning. Some cores of either type show very irregular zoning with embayments indicating recrystallization (Figure 8.5Q).

Thirty-four areas were analysed in 22 grains (Figure 8.10A). Of these, eight analyses (#4628-1e, 7d, 7d2, 12d, #4631-1d2, 5e, 3b, 7c2) are not further included either due to more than 5% discordance or large analytical uncertainties. Within the remaining 26 analyses, core analyses have a larger scatter in U concentration (50–5070 ppm, Th/U: 0.18–1.05) than rims (500–4700, Th/U: 0.14–0.47). Twenty-three analyses yield a concordia age of  $515 \pm 2$  Ma (MSWD 1.05) that agrees well with a weighted average  $^{206}\text{Pb}/^{238}\text{U}$  age of  $516 \pm 3$  Ma (MSWD 1.6). Three analyses point to a slightly older concordia age of  $532 \pm 5$  Ma (MSWD 0.85; #4628-6b, #4631-3b2, 5a2) or weighted average  $^{206}\text{Pb}/^{238}\text{U}$  age of  $534 \pm 6$  Ma (MSWD 0.105). One analysis (#4631-11c) indicates older zircon inheritance with an age of ca. 730 Ma. The age of  $515 \pm 2$  Ma is interpreted as crystallisation age whereby the four older analyses indicate minor zircon inheritance or assimilation.



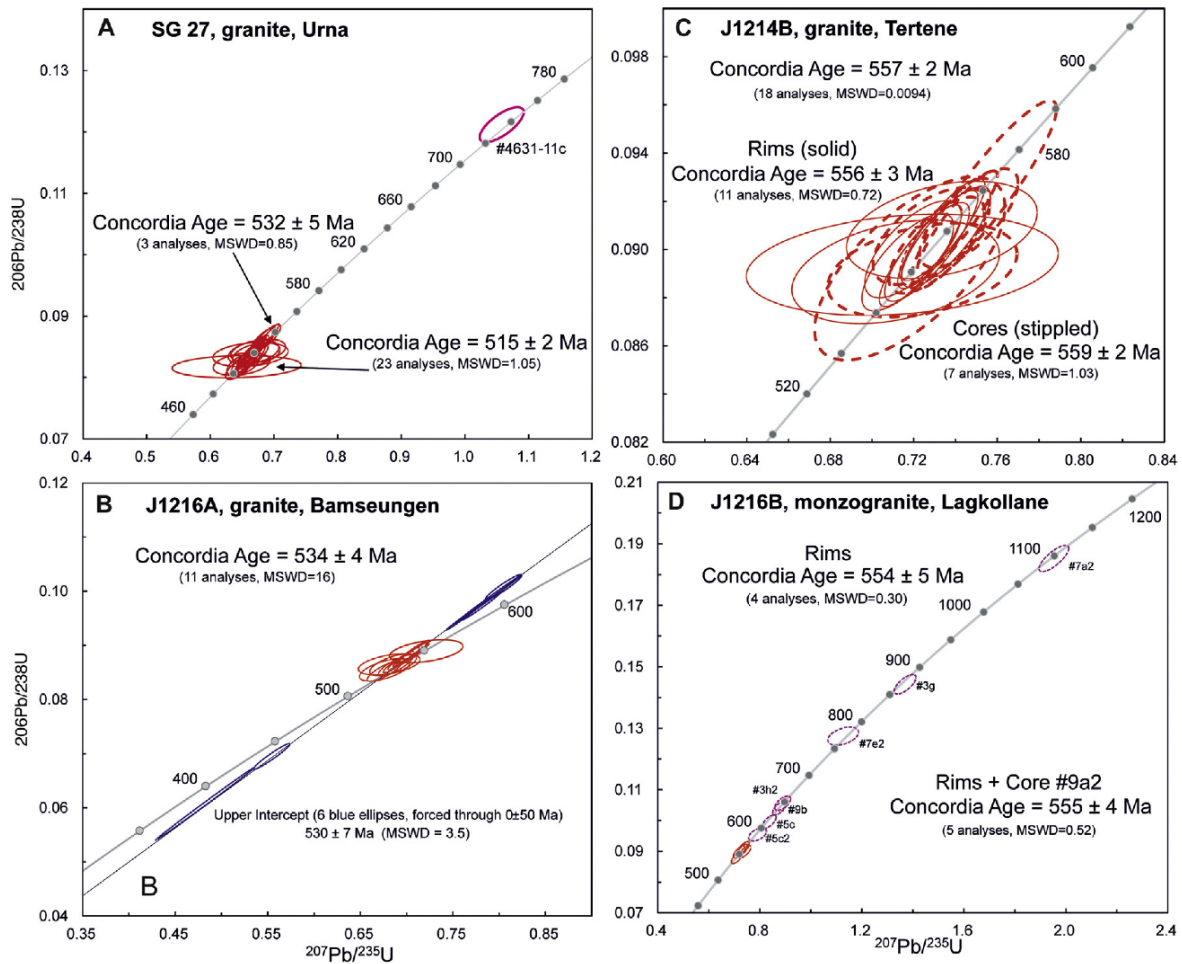


Figure 8.10: SIMS zircon geochronology of four late-tectonic granitoids.

#### J1216A, granite, Bamseungen ( $-72.228930$ ; $21.953620$ )

This granite is fine- to medium-grained and weakly foliated. The mineral assemblage consists of pinkish K-feldspar, plagioclase, quartz and minor biotite. Quartz has subgrains with a chessboard undulose extinction and bulging grain boundaries. Plagioclase shows in part deformation twinning with strong recrystallization and alteration. K-feldspar is microcline. Only few amphiboles are present that are in rare cases replaced by biotite.

The sample contains brown, stubby and euhedral zircon grains with aspect ratio from 1.5 to 3 and maximal length to  $350 \mu\text{m}$ . In CL, nearly all grains appear dark with oscillatory zoning accompanied by alteration. Altered rims are even darker and point to high-U concentration and hence possibly metamictisation in these zones. Only few grains show lighter core areas with typical unaltered oscillatory zoning (Figure 8.5R).

Twenty areas in 17 grains were analysed (Figure 8.10B). Core areas show relatively high U contents (750–5700 ppm) and a large range of Th/U ratios (0.17–1.34). Rims display even higher U concentrations (4000–20,000 ppm) and consequently lower Th/U ratios between 0.07 and 0.16. Three analyses (#4625-7b, 10d, #4635-8a) are excluded from further age calculation due to high analytical errors. Eleven of the remaining 17 analyses are concordant and yield a concordia age of  $534 \pm 4$  Ma (MSWD = 16) that agrees with a weighted average  $^{206}\text{Pb}/^{238}\text{U}$  age of  $538 \pm 5$  Ma (MWSD = 2.5). From the other six analyses ('Electronic Appendix C.2', U-Pb data table, supplementary material, marked "D") a discordia age of  $530 \pm 7$  Ma (MSWD = 3.5, lower intercept forced through  $0 \pm 50$  Ma) is calculated that supports the previously determined



concordia age. The obtained age of ca. 534 Ma is interpreted as the crystallisation age of this granite.

#### J1214B, granite, Tertene (-72.284683; 21.435233)

This granite is medium- to coarse-grained and has random texture. The mineral assemblage comprises pinkish K-feldspar, plagioclase, quartz, amphibole, biotite and titanite. Quartz shows subgrain formation with equilibrated grain boundaries and undulose extinction. K-feldspar shows microcline and Carlsbad twinning and occasionally flame perthitic exsolution. Amphibole is common as mafic phase, which in some cases is transformed to biotite.

Zircon grains are brown and euhedral with aspect ratio from 2 to 5 and a maximum length of 450  $\mu\text{m}$ . In CL images most grains show typical magmatic oscillatory zonings although some grains reveal cores with a diffuse pattern (Figure 8.5S).

Twenty-nine areas were analysed in 19 grains (Figure 8.10C). Core analyses have a wide range of U (130–2300 ppm) with Th/U ranging from 0.15 to 1.39. Rim analyses range from 250 to 2700 ppm U and have a narrower range of Th/U (0.33–0.67). Eleven analyses (#4627-2e2, 11f, 15d, 15d2, #4630-3c2, 7b, 8a, 11b, 14b, 15d2) show either more than 5 % discordance or large analytical errors and are not considered in any age calculation. Seven core analyses yield a concordia age  $559 \pm 2$  Ma (MSWD = 1.03) and 11 rim analyses give a concordia age of  $556 \pm 3$  Ma (MSWD = 0.72). Since both ages overlap within their uncertainties a combined concordia age is calculated with an age of  $557 \pm 2$  Ma (MSWD = 0.0094) that is perfectly consistent with a weighted average  $^{206}\text{Pb}/^{238}\text{U}$  age of  $557 \pm 3$  Ma (MSWD = 0.83). This age is interpreted as the crystallisation age of this granite.

#### J1216B, quartz-monzonite, Lågakollane (-72.121600; 22.018700)

This sheet-like granite is fine to medium-grained and has a number of up to 10 cm large xenoliths. A weak foliation is developed. The mineral assemblage comprises pinkish K-feldspar, plagioclase, quartz and biotite. Quartz shows subgrain formation with oriented c-axes and undulose extinction. Plagioclase is altered. K-feldspars show undulose extinction with both microcline and rare Carlsbad twinning occurring. Amphibole is the main mafic component, which is replaced by biotite along the grain boundaries.

Zircons of this sample are clear, euhedral, long-prismatic with maximum length of 350  $\mu\text{m}$  and aspect ratios between 2 and 5. Distinct core–rim relationships are visible in CL. Core areas generally are rounded and show oscillatory magmatic zoning. Overgrown rims usually are low in U in close contact to the core (a narrow, highly luminescent rim) that grades continually into normal oscillatory magmatic zoning with higher U concentrations. In some cases embayments of cores are observed that possibly indicate recrystallized areas during rim growth (Figure 8.5T).

Fourteen areas in seven grains were analysed (Figure 8.10D) and two of these (#46,263h, 7e) are not further considered due to high analytical error. U concentrations for the rims are uniform (250–280 ppm) and Th/U show a narrow range (0.12–0.26). Analysed core regions show a larger scatter in U concentration (170–560 ppm) and Th/U ratios (0.06–0.43). Four analyses were obtained in rim areas and a concordia age of  $554 \pm 5$  Ma (MSWD = 0.30) is obtained. One of the analysed core areas shows a similar apparent  $^{207}\text{Pb}/^{206}\text{Pb}$  age of  $551 \pm 17$  Ma. Combined reduction of this core and the rims yields a concordia age  $555 \pm 4$  Ma (MSWD = 0.52). This



age is interpreted as the crystallisation age of this monzogranite. Seven core areas show older zircon inheritance with apparent  $^{207}\text{Pb}/^{206}\text{Pb}$  ages varying from 606 Ma to 1100 Ma. The observed larger variations in U and Th concentrations and resulting U/Th ratios sustain the interpretation of mixed (i.e. inherited) zircon derivation.

## 8.6 Summary of Geochronological Data

The geochronology of the sample set is summarised in Table 8.1 with respective grouping as outlined earlier. The regional distribution of the data from E to W is presented in Figure 8.11 across the inferred geophysical boundary. Crystallisation ages of the group of GTTGs, enderbites and grey migmatitic gneisses range from ca. 980 to 910 Ma; one sample has a crystallisation age of ca. 800 Ma. Thus, no cratonic rocks were found. Most samples show a protracted tectono-metamorphic overprinting history between ca. 630 and 490 Ma. Metamorphic zircon growth of ca. 930 Ma might be recorded in sample J1213B, otherwise there is no evidence of major metamorphism immediately following early Neoproterozoic crust formation. Metamorphic overprint and intense melting is recorded by *gt*-migmatites and foliated syntectonic granitic sheets over a more or less continuous time from ca. 630 to 490 Ma. Some samples show a protracted metamorphic history with many phases of metamorphic zircon growth (J1211B\_1). Syn- to late-tectonic granitoids accompany tectono-metamorphic overprint during the entire period. Very little inheritance older than 990 Ma is recorded, inheritance older than 1.1 Ga is completely lacking. Two granitoid samples have inherited zircons with ages of ca. 750 Ma. In general, syn- to post-tectonic magmatism as well as the associated metamorphic overprint appears to decrease from W to E.

### 8.6.1 Geochemistry and Nd Isotope Composition

The meta-igneous rocks can be divided into (i) amphibole/biotite/garnet gneisses, which resemble the intrusive meta-igneous rocks of the GTTG subterrane of Sør Rondane; metabasic rocks of likely volcanic origin; orthopyroxene-bearing orthogneisses (enderbites), which may be partially retrogressed; (ii) syntectonic (garnet-bearing) migmatites and granitic gneisses; and (iii) potassium-rich late-tectonic or postorogenic granitoids and gneisses.

The amphibole/biotite/garnet gneisses of the first group, denoted as ‘GTTG gneiss’ in Figure 8.11–13 are granodioritic (e.g. dated samples J1212E) to tonalitic–trondhjemitic (J1214A\_1, J1214A\_2) in composition (Figure 8.12). These samples have undergone greenschist facies metamorphism, but there is no evidence for significant chemical alteration of these coarse-grained rock types. This is illustrated by their coherent normalised trace element patterns (Figure 8.14), characterised by prominent negative Nb and Ti anomalies, typical for subduction-related igneous rock, similar to the 900–1000 Ma GTTG samples from the D’ sector in Sør Rondane (Kamei et al., 2013; Elburg et al., 2015). Their Rare Earth Element (REE) patterns are slightly light (L)REE enriched (SG29) to LREE depleted (J1214A\_1; Figure 8.14F). Intermediate samples are classified as magnesian, while more felsic members are ferroan (following Frost et al., 2001), reflecting the samples’ low MgO content, typical for highly evolved rocks. The samples fall in the calcic field on the modified alkali-lime diagram of Frost et al. (2001) (Figure 8.13F) and broadly resemble the GTTG suite from the SW-Terrane of the Sør Rondane Mountains in terms of potassium, Zr and Sr. They mostly plot within the volcanic



arc to syn-collisional granitoid field on an Nb–Y classification diagram (Figure 8.13B). As has also been noted for the Sør Rondane GTTG suite (Elburg et al., 2015), the 900–1000 Ma amphibole gneisses are significantly different in geochemical signature to the slightly older orthogneisses of central Dronning Maud Land, which are more potassic and enriched in incompatible trace elements, and plot dominantly in the within-plate granite field in Figure 8.13B. Six out of the seven samples analysed from this group have an initial Nd isotopic signature that is indistinguishable from that of GTTG suite, with  $\epsilon_{\text{Nd}}$  values between +2 and +4 (Figure 8.15). Only sample J1214A\_1 has a negative initial value of  $\epsilon_{\text{Nd}}$  –2, despite its major and trace element signature being similar to the other samples. These marginally negative to positive values are broadly similar to those of the central Dronning Maud Land orthogneisses. Depleted mantle extraction ages are 1.0–1.7 Ga. No reliable Nd model age can be obtained for J1214A\_1 due to its depleted mantle-like LREE signature.

The metabasic volcanic samples of the first group are gabbros in terms of normative composition, apart from one sample with significant quartz veins, which causes the rock to plot as a tonalite. No samples of this group were dated or analysed for Nd isotopes. The samples show a broad geochemical coherence with the amphibole gneisses, and thereby also resemble the (quartz-)gabbros associated with the ca. 990 Ma tholeiitic metatonalites of the GTTG subterrane, although two samples have higher Zr concentrations. The latter two samples fall in the MORB to OIB field (Figure 8.12A) on the Ti–V diagram of (Shervais, 1982), whereas the other samples classify as arc basalt. Data for more mobile elements may not be very reliable as a result of metamorphic processes. This may also be the reason for the scattered normalised trace element diagrams, with many elements being close to or below detection limits.

The enderbitic gneisses of the first group dominantly have intermediate  $\text{SiO}_2$  contents (59–68 wt.%), and  $\text{K}_2\text{O}$  of 1–2 wt.%, giving them a granodioritic to quartz-monzodioritic composition in terms of normative mineralogy; only sample J1211B\_2 from Bergekongen has a gabbroic composition. They partially overlap with the more enriched amphibole gneisses in geochemical compositions, and are broadly similar to the enderbitic gneisses from the Brattnipene area (C sector of the SW-Terrane) analysed by Shiraishi and Kagami (1992).

Their normalised trace element signatures (Figure 8.14) are coherent, suggesting that metamorphism did not have a pronounced influence. The intermediate enderbitic samples are slightly more enriched in (fluid-immobile) incompatible elements such as Th, Nb and Ti than the GTTG gneisses but their initial Nd isotopic signature is similar to that of the amphibole gneisses with  $\epsilon_{\text{Nd}}$  values between +2 and +4 (Figure 8.15).



Table 8.1: Summary of geochronological data, age in Ma. Figure numbers correspond to this chapter e.g. Fig.6B is Figure 8.6B.

Metamorphic		Igneous		Inheritance
Inheritance				
<b>Amphibole/biotite/garnet gneisses (GTTG)</b>				
J1214A_2		<b>980 ± 8</b>		Granodiorite gneiss, E of Taggen (Fig. 6B)
J1214A_1		<b>961 ± 4</b>		Fine-grained granitoid gneiss with unusual zircons, E of Taggen (Fig. 6A)
J1212E		<b>925 ± 11</b>		Mylonitic amphibole gneiss, Knøttet (Fig. 6C)
J1213B	<b>930 ± 10</b>	<b>950 ± 5</b>		Enderbite, opx -bearing melt patches, Gandfluga (Fig. 7A)
J1211B_2		<b>916 ± 13</b>		Metagabbro/enderbite, Bergekongen (Fig. 6B)
SG29	<b>559 ± 4, 632 ± 5</b>	ca. 980		Grey, migmatitic gneiss, Payerfjellet (Fig. 9A)
<b>Gt-migmatites and foliated granitoid gneiss sheets</b>				
SG28		<b>597 ± 8</b>	802 ± 6	Grey, migmatitic gneiss, Steingarden (Fig. 9B)
J1211B_1	<b>546 ± 3</b>	ca. 1000, 1060		Gt-migmatite sheet, Bergekongen (Fig. 7C)
J1213C		<b>597 ± 7</b>		Pegmatite gneiss, Bergtussen (Fig. 7D)
J1213D		<b>582 ± 5</b>		Pegmatitic granitoid gneiss, Van Autenboerfjellet (Fig. 8C)
J1212A		<b>ca. 555</b>		Foliated, granite melt injection, very high-U, Tonyknausane (Fig. 8A)
J1211A_1	<b>486 ± 7 ?</b>	<b>551 ± 14</b>	930±12	Foliated granitic gneiss sheet, Langekletten (Fig. 6C)
J1212F_1	<b>ca. 530</b>	<b>547 ± 5</b>		Granite gneiss with large rafts of bt-gneiss, Vesalkletten (Fig. 8D)
<b>Late to post-orogenic granitoids</b>				
SG25		<b>630 ± 4</b>		Metadiorite, Storebusen (Fig. 9C)
J1214B		<b>557 ± 2</b>		Granite, Tertene (Fig. 10C)
J1216B	<b>555 ± 4</b>	ca. 600, 750, 850		Granite, Lågkollane (Fig. 10D)
J1216A		<b>534 ± 4</b>		Granite, Bamseungen (Fig. 10B)
SG27		<b>532 ± 5</b>	ca. 730	Granite, Urna (Fig. 10A)
J1212C		<b>528 ± 6</b>		Discordant granite gneiss sheet, cuts regional foliation, Tonyknausane (Fig. 8B)
SG24		<b>503 ± 5</b>		Granodiorite, foliated (Fig. 9D)

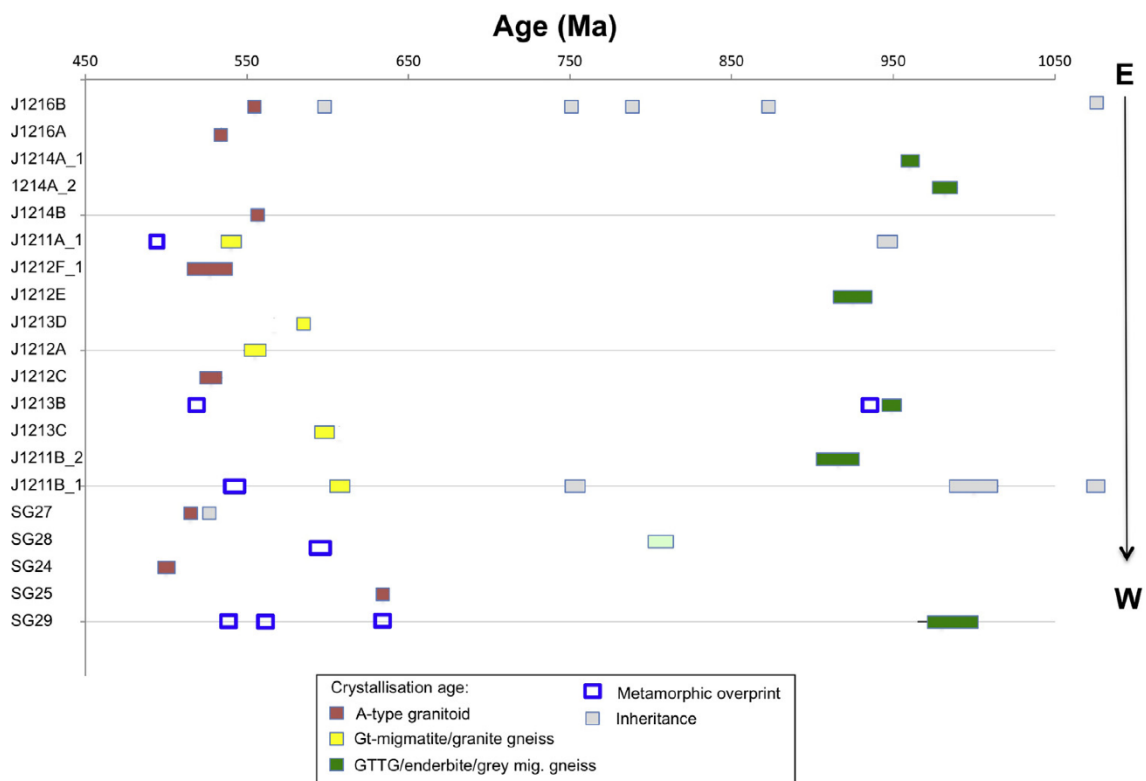


Figure 8.11: Summary of geochronological data.



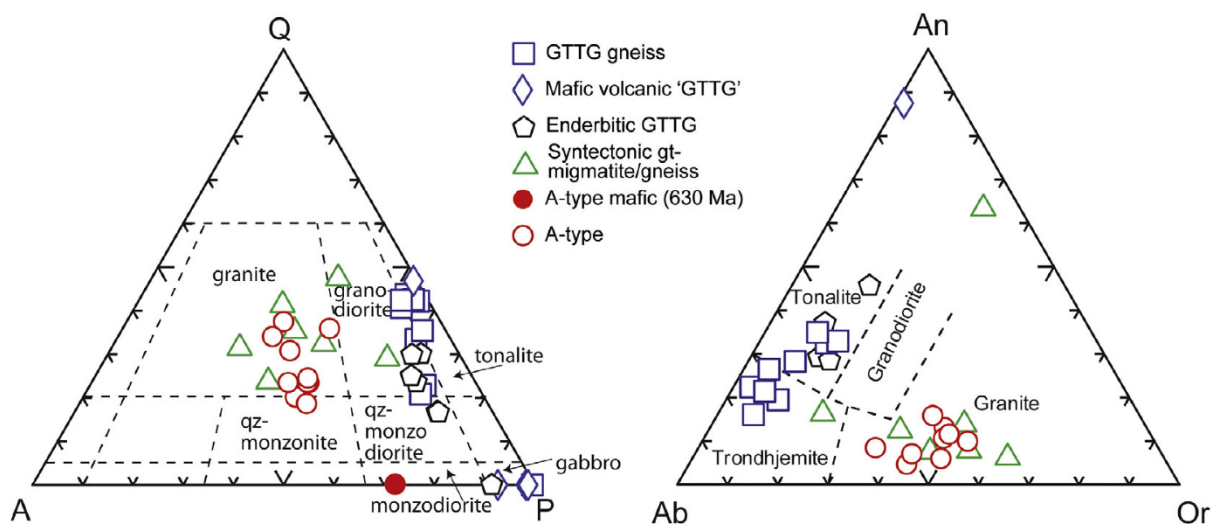


Figure 8.12: Quartz–alkali–feldspar–plagioclase (QAP) and anorthite–albite–orthoclase diagrams, based on the normative mineralogy. Only samples with >20% normative quartz are shown in the An–Ab–Or diagram.

The syn-tectonic garnet-bearing migmatites and gneisses of group 2, to which samples J1211A\_1 and J1212A belong, have potassium contents up to 7 wt.%, and thus extend to far higher concentrations than the older samples of group 1. They classify as granites to granodiorites in terms of QAP normative mineralogy, but one of the two ‘granodioritic’ samples classifies as a trondhjemite (SG28) in the Ab–An–Or triangular diagram (Figure 8.13). These syn-tectonic samples are peraluminous and dominantly calc-alkalic in terms of modified alkali-lime index as well as ferroan (Figure 8.13C, D, and F). They plot in the field for volcanic arc and syncollisional granites (Figure 8.13B). Normalised trace element patterns are more enriched in incompatible elements than for the older samples, and the REE pattern of sample SG28 is significantly enriched in LREE over HREE. Three samples (J1211A-1, J1211B-1, J1212A) have initial  $\epsilon_{Nd550}$  values of –1 to –3, while SG28 yields an  $\epsilon_{Nd800}$  value of +4. The late-tectonic or postorogenic granitoids (group 3) show A-type affinities through their Zr contents (Figure 8.13G) and/or Ga/Al ratios (Whalen et al., 1987; not shown), but plot dominantly in the field for volcanic arc and syncollisional granites in terms of Y and Nb (Figure 8.13B). Potassium contents are similar to the garnet-bearing migmatites, and the samples plot in the calc-alkalic, alkali-calcic and alkalic fields at high silica contents (69–75 wt.%; Figure 8.13C). They extend from the metaluminous into the peraluminous fields, and from the magnesian to the ferroan.

Hence, according to the classification scheme of Frost et al. (2001), Frost and Frost (2011) and Eby (1990), they may not be true A-type granitoids, but certainly show affinities to this group. A notable feature is the extreme Sr and Ba contents for some of the samples (>1000 and >2500 ppm respectively). They share these characteristics with the Pan-African syenites of Lunkeryggen, within the GTTG subterrane and also with the A-type granites of central Dronning Maud Land (Roland, 2004). Samples SG24 and 27 from Steingarden and Urna, respectively, reveal similar geochemical signatures, but do not show these enrichments in Sr and Ba. These two samples are also younger (500–530 Ma) than the more easterly (530–560 Ma) samples, so it remains unclear whether the distinction is related to geographical position or age. Normalised trace element diagrams show even greater enrichment in the incompatible



elements than for the syntectonic samples, and the available REE patterns suggest strong LREE over HREE enrichments, with absent to negative Eu-anomalies. Nd isotope data were obtained for seven granite samples (Table 8.2) and yield  $\epsilon_{\text{Nd}}$  values consistently between +2 and -2 at the time of their respective intrusion ages (Figure 8.14), indicating involvement of material with a low time-integrated Sm/Nd ratio. All samples plot close to the border between the fields defined for SRM and cDML A-type granites and thus, no simple classification to either crustal domain is possible. SG 27 shows an affinity with the cDML field as was speculated already due to the westerly geographic location and younger intrusion age of this sample.

Sample SG25, with a ca. 630 Ma age has been interpreted to be a mafic rock with affinities to A-type granitoids, and classifies as a monzodiorite. It has high  $\text{K}_2\text{O}$  (3.3 wt.%) for its low  $\text{SiO}_2$  concentration (48.4 %). It also shows extreme enrichment in Sr and Ba (1400 and 3500 ppm) and an alkalic signature (Figure 8.13F and H). Within V–Ti space, however, it falls in the MORB-BABB field and therefore shows an association with the GTTGs of the Sør Rondane D' sector, thus rendering a final classification of this sample difficult.

## 8.6.2 Interpretation and Discussion

Neither older basement nor cratonic rocks were found in the “missing link” between Sør Rondane and central Dronning Maud Land. Ground-truthing of the geophysically outlined SE DML province (Mieth et al., 2014) indicates that the oldest rocks are of Early Neoproterozoic age (980–910 Ma), consisting of GTTGs, mafic volcanics and enderbites with gabbroic to trondhjemitic composition. These resemble the GTTGs from the D'-sector of the Sør Rondane SW-Terrane. They have low concentrations of incompatible elements, and mostly show slightly positive initial  $\epsilon_{\text{Nd}}$  values. The more mafic samples fall within the arc-field on a V–Ti diagram. These characteristics all indicate that the most likely setting in which they were formed was an oceanic arc, also based on the significant negative Nb and Ti anomalies observed, as has also been proposed for the GTTGs further east (Kamei et al., 2013; Elburg et al., 2015). Although the initial  $\epsilon_{\text{Nd}}$  value for one of the samples yields subchondritic values around -2, an aberrant lower zircon Hf isotopic signature was also recorded for one of the GTTGs from the D'-sector of Sør Rondane (Elburg et al., 2015), so this value does not sever the link between the two terranes. There is very little evidence for major metamorphic overprint immediately following crust formation. Only sample J1213B shows evidence for metamorphic zircon overgrowth dated at ca. 930 Ma. The GTTGs are intimately associated with sedimentary rocks including abundant metacarbonates, which in the SRM have a Tonian-Cryogenian age (Otsuji et al., 2013).



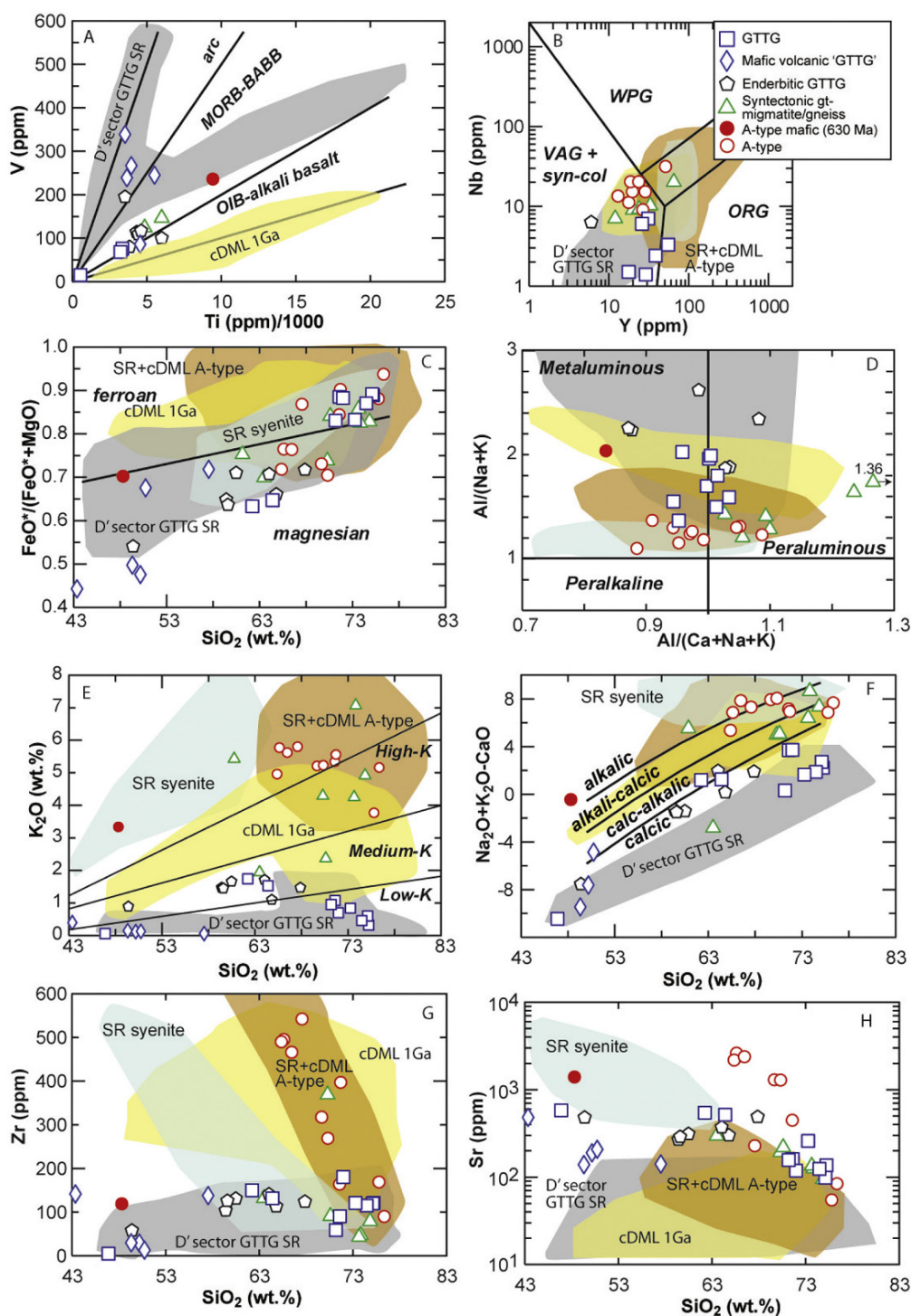


Figure 8.13: Variation diagrams for the samples analysed. SR = Sør Rondane; cDML = central Dronning Maud Land. Coloured fields are based on literature data. Data sources: D' sector: Kamei et al. (2013); (Owada et al., 2013; Elburg et al., 2015); cDML 1 Ga: Mikhalsky and Jacobs (2004); Pan-African granites and syenites cDML and SR: Roland (2004); Li et al. (2001, 2003), own data. (A) Diagram of V versus Ti, after Shervais (1982). (B) Nb versus Y classification diagram for granites, after Pearce et al. (1984). (C) Granitoid classification diagram based on  $FeO^*/(MgO + FeO^*)$  ratio after Frost et al. (2001). (D) Granitoid classification diagram based on aluminium saturation index and peralkalinity. (E)  $K_2O$  versus  $SiO_2$ . (F) Modified alkali-lime diagram after Frost et al. (2001). (G) Zr versus  $SiO_2$ . (H) Sr versus  $SiO_2$  (note log scale).



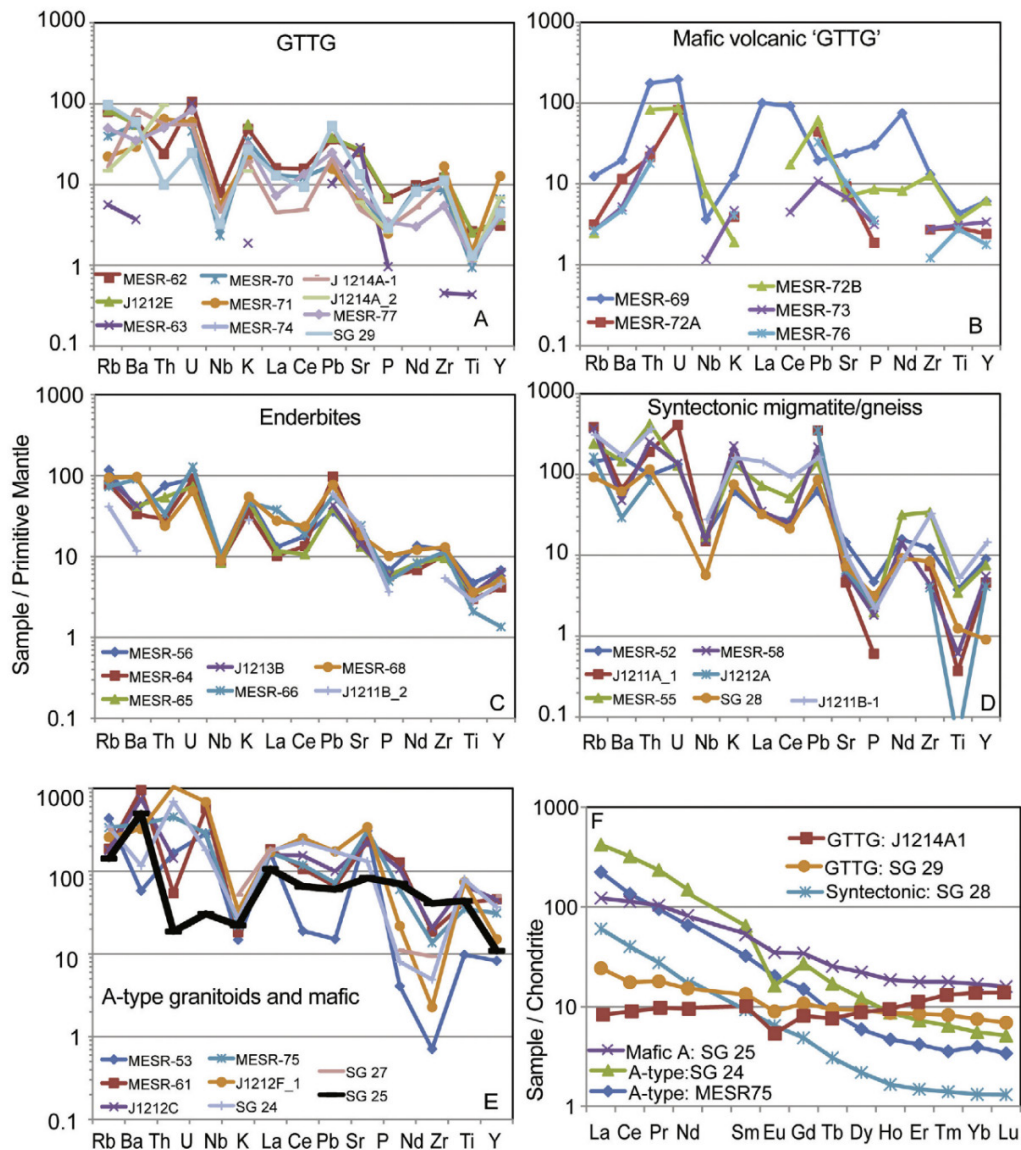


Figure 8.14: Normalised trace element diagrams. (A–E) Primitive mantle normalised diagrams for the different subgroups. Normalising values from Palme and O'Neill (2003). (F) Chondrite normalised Rare Earth Element diagram for available samples. Normalising values from Evensen et al. (1978).

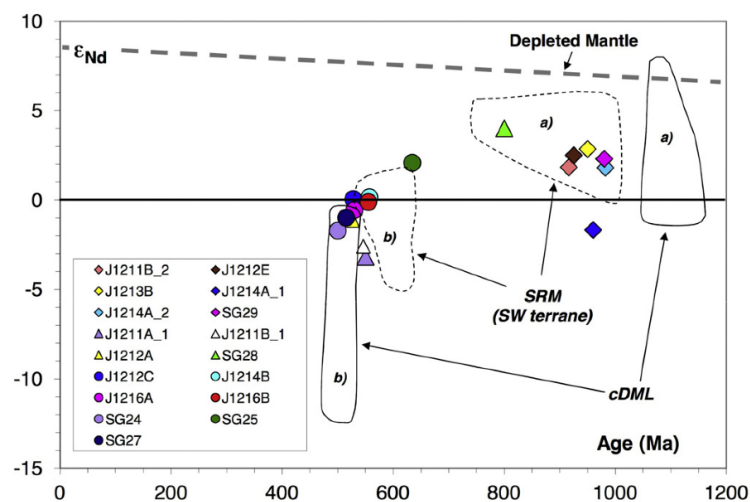


Figure 8.15: Initial  $\epsilon_{Nd}$  versus age for selected samples, compared to data for the D'-sector of the SW-Terrane of Sør Rondane (b) (Kamei et al., 2013; Owada et al., 2013; Elburg et al., 2015) and central Dronning Maud Land (a) (Jacobs et al., 1998; Markl and Henjes-Kunst, 2004).



Table 8.2: Sm–Nd concentration and isotope data for metamorphic and igneous rocks from easternmost Central Dronning Maud Land.

Lithological group <sup>a</sup> Sample ID	Rock	Location	Area	Age <sup>b</sup> (Ma)	Lab <sup>c</sup>	Sm (ppm)	Nd (ppm)	<sup>147</sup> Sm/ <sup>144</sup> Nd	<sup>143</sup> Nd/ <sup>144</sup> Nd <sup>d</sup> Present day	$\epsilon_{Nd}$ Present day	$\epsilon_{Nd}(f)^e$	$t_{DM}$ (Ga)
(1)												
J1211B.2	Metagabbro	Bergekongen	New nunataks	916	BGR	3.16	13.44	0.1421	0.512405	-4.5	1.8	1.48
J1212E	Mylonitic amphibole gneiss	Knøttet	New nunataks	925	BGR	3.37	16.01	0.1272	0.512346	-5.7	2.5	1.33
J1213B	Grey enderbitic gneiss	Gandfluga	New nunataks	950	BGR	4.14	18.68	0.1340	0.512395	-4.7	2.9	1.35
J1214A.1	Granodioritic gneiss	Ridge E of Taggen	New nunataks	961	BGR	2.33	7.14	0.1974	0.512557	-1.6	-1.7	-
J1214A.2	Granodioritic gneiss	Ridge E of Taggen	New nunataks	980	BGR	3.22	12.68	0.1536	0.512454	-3.6	1.8	1.65
SG29	Grey migmatic gneiss	Payerfjellet	Eastern Wohlthat massiv	ca. 980	BGR	3.00	10.73	0.1690	0.512579	-1.2	2.3	1.79
(2)												
J1211A.1	Granitic gneiss	Langekletten	New nunataks	550	BGR	5.73	23.80	0.1457	0.512292	-6.7	-0.6	1.82
J1211B.1	Garnet migmatite	Bergekongen	New nunataks	546	BGR	17.06	90.52	0.1139	0.512210	-8.3	-2.6	1.36
J1212A	Foliated granitic injection	Tonyknausane	New nunataks	ca. 555	BGR	2.00	7.53	0.1602	0.512459	-3.5	-1.1	1.84
SG28	Grey migmatic gneiss	Steingarden	New nunataks	802	BGR	2.65	16.20	0.0990	0.512333	-5.9	4.0	1.01
(3)												
J1212C	Granitic gneiss sheet	Tonyknausane	New nunataks	528	BGR	14.78	90.97	0.0982	0.512301	-6.6	0.1	1.05
J1214B	Granite	Tertene	New nunataks	557	UniTueb	5.83	36.92	0.0970	0.512283	-6.9	0.2	1.06
J1216A	Granite	Bamseungen	New nunataks	534	UniTueb	12.09	60.51	0.1235	0.512356	-5.5	-0.6	1.25
J1216B	Quartz-monzonite	Lågkollane	New nunataks	555	UniTueb	11.03	71.59	0.0951	0.512264	-7.3	-0.1	1.07
SG24	Metagranodiorite	Steingarden-S	New nunataks	503	BGR	16.54	119.89	0.0834	0.511855	-8.9	-1.7	1.07
SG25	Metamonzodiorite	Storebusen	New nunataks	630	BGR	12.20	59.11	0.1248	0.512447	-3.7	2.1	1.11
SG27	Granite	Urna	New nunataks	532	UniTueb	16.58	87.51	0.1169	0.512319	-6.2	-1.0	1.23

<sup>a</sup> Compare text for details.

<sup>b</sup> According to the zircon crystallisation ages deduced for the individual samples.

<sup>c</sup> BGR, Federal Institute for Geosciences and Natural Resources; UniTueb, University of Tübingen.

<sup>d</sup> Relative to <sup>143</sup>Nd/<sup>144</sup>Nd = 0.511845 for the La Jolla Nd standard.

<sup>e</sup>  $\epsilon_{Nd}(f)$  calculated using the zircon crystallisation ages deduced for the individual samples.



The late Neoproterozoic to early Palaeozoic syntectonic granitoids and migmatites are geochemically distinct from the GTTGs in being granitic in composition, despite showing strong evidence for intracrustal reworking of this older material, as evidenced by the presence of ca. 930 Ma zircons in sample J1211A\_1, and its lower  $\epsilon\text{Nd}$  isotopic signature of  $-1$ . The high Alumina Saturation Index and low sodium content for some samples (e.g. MESR55, J1211B\_1) suggest that melt loss may have occurred, and that the samples have a restitic character. On the other side of the spectrum, sample SG28 shows significant HREE depletion, indicative of garnet retention during partial melting. Linking their geochemistry to a specific source is therefore difficult. In general, an age trend of these melts is recognised, decreasing to the W.

For the late-tectonic to postorogenic A-type granitoids an interesting distinction in Sr and Ba concentrations is seen between the two slightly younger samples from Steingarden (SG24) and Urna (SG 27), and those from further east, with the latter showing a far greater enrichment, resembling the Sør Rondane syenites in this respect. Interestingly, the sample from Bamseungen (J1216A) has an intermediate age, and a very low Ba and Sr content, even though it is the most easterly sample. Unfortunately, its very evolved composition makes it hard to decide whether it belongs to the high- or low-Sr + Ba clan, since the concentrations of these elements decrease with increasing differentiation. Since this sample shows low  $\text{K}_2\text{O}$ , a high degree of differentiation seems unlikely as reason and thus, a different source region or involvement of material seems probable. This is, however, not reflected in a different Nd isotope signature for this sample (Figure 8.14). The observed Nd isotopic signatures of these A-type granites point towards a source with a low time-integrated Sm/Nd ratio. This source could ultimately be seated in the mantle as the incorporation of older basement would be expected to be visible in older zircons of these samples. However, crustal reworking may have contributed to the granitoids as well, considering the evidence for inheritance in sample J1216B. Since the age of initial crust formation (ca. 1000–900 Ma) is similar to the age of inheritance (ca. 1000–600 Ma), the isotopic signature of crustal reworking and melting of enriched mantle is not expected to differ significantly. Magmatism in this time-period is therefore likely to reflect melting of the lithospheric mantle, combined with crustal assimilation. This may reflect asthenospheric upwelling or delamination of the lithospheric mantle around this time period. In addition, an older (ca. 630 Ma) mafic sample with A-type affinities (SG25) is present showing the highest initial  $\epsilon\text{Nd}$  (+2) within the group of late-tectonic to postorogenic A-type granitoids. Considering the age difference with the granites, it seems unlikely that this older “A-type-affinity” sample is part of the same event. More data are needed to establish whether this older event is typical for the more northerly area of DML, from which this sample was taken. When the Sm–Nd data of the ca. 630–500 Ma age group are considered as a whole, a decrease in the epsilon Nd values with age is visible, which suggests tapping of a different source component. As there is no obvious correlation between the isotopic signature and any index of differentiation, or the amount of inheritance (see below) this is unlikely to reflect progressive amounts of crustal contamination. We propose that this source with a low time-integrated Sm/Nd ratio may be located in the mantle.

With a few exceptions, there is very little evidence of inherited material older than 1000 Ma, just recorded in one sample. Striking absence of older material was also noted for the SW-Terrane of Sør Rondane (Osanai et al., 2013). Rare evidence of detrital 750 Ma components is



similar to those occasionally found elsewhere in SRM and also in the NE-Terrane. These ages are broadly similar to those reported by Kamei et al. (2013) for some calc-alkaline GTTGs from the Sør Rondane D'-sector.

This supports interpretation that typical lithologies of the SW-Terrane continue for a significant distance further W. The difference is the degree of LN/EP tectono-metamorphic overprint and the accompanying melt addition. Whilst the southern part of the SW-Terrane shows limited LN/EP reworking, often confined to discrete shear zones and typically not exceeding greenschist facies conditions, the area W of Bamseungen shows medium- to high-grade metamorphism and significant amounts of LN/EP syn- and post-tectonic felsic melt additions, similar to the northern part of the SW-Terrane (Osanai et al., 2013). The structural grain of the region appears co-linear with the trend of SE-trending magnetic anomalies of the SE DML Province between Payerfjellet and the southern SRM (Mieth et al., 2014). The mostly low-amplitude magnetic anomalies are probably linked to the GTTG rocks that are interleaved with metasedimentary cover rocks, with the latter likely the magnetic lows. Since the area has undergone LN/EP medium to high-grade metamorphism, the magnetic fabric of SE DML should also have a LN/EP age.

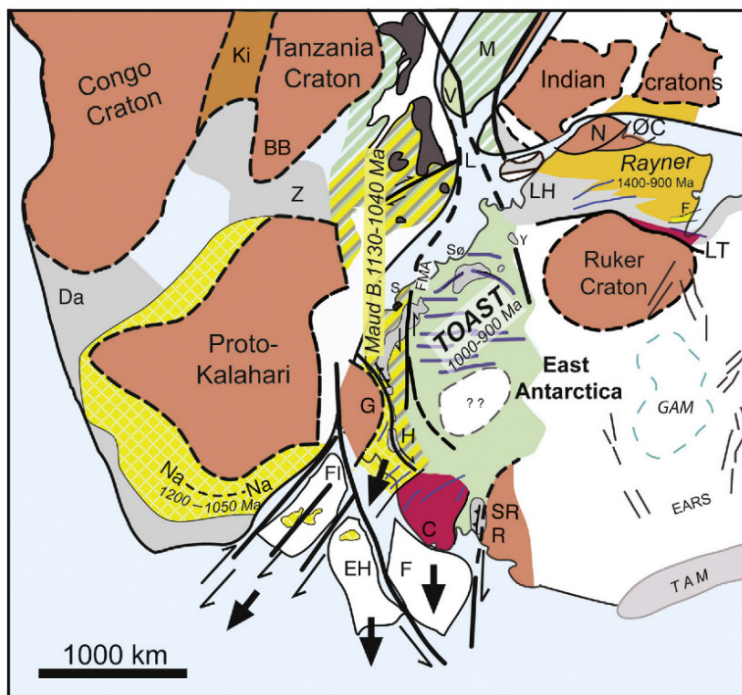
This indicates that the southern part of the SW-Terrane probably forms an arrested block within a larger zone of LN/EP deformation on either side. It might represent a mega-boudin within a rheologically weaker crust, the latter of which might be represented by a larger percentage of metasedimentary rocks. The SE DML Province of Mieth et al. (2014) can therefore not represent the southern foreland or a craton to a LN/EP mobile belt as has previously been speculated. The magnetic anomaly on the S-side of the SW-Terrane is probably a rheological boundary, separating highly deformed rocks to the S from much less deformed similar rocks in the SW-Terrane.

## 8.7 Regional Implication

The juvenile Early Neoproterozoic rocks of our 'missing link' together with those of Sør Rondane appear to form one major Tonian Oceanic Arc Super Terrane (TOAST). Part of this terrane is represented by the aeromagnetically defined SE DML Province (Mieth et al., 2014), which in the W terminates along a wide zone of WSW- to SW-trending co-linear shear zones and magnetic anomalies that appear to separate typical Maud Belt crust from the EDML oceanic arc terrane (Figure 8.2 and Figure 8.16). The wide boundary zone includes the Forster Magnetic Anomaly, the South Orvin Shear Zone and the Ulvetanna Magnetic Anomaly. This zone probably represents the suture zone between the TOAST and the Grenville-age Maud Belt.

To the E of the TOAST, rocks with similar ages are exposed in the Rayner Complex. However, although age similarities between the two regions can be drawn, there are also significant differences between the two. The Rayner Complex formed during a more protracted period of time between ca. 1400 and 900 Ma as a result of convergence between the Napier Craton and the Lambert Terrane (e.g. Fitzsimons, 2000b; Kelly et al., 2002; Boger, 2011; Grew et al., 2012; Liu et al., 2014). It incorporates a number of island arc terranes with final collision and high-grade deformation recorded at ca. 950 Ma. In contrast, there is very little evidence for high-grade metamorphism immediately following crust formation in our study areas.





#### East African-Antarctic Orogen (630-500 Ma)

East African Orogen, undifferentiated

Eastern granulites/Cabo-Delgado/Schirmacher

Tonian Oceanic Arc Super Terrane (TOAST)  
Oceanic arcs (1000-900 Ma)

Maud Belt (1130-1040 Ma)

Other ca. 620-500 Ma mobile belts

Namaqua-Natal Belt (Na-Na)  
(1200-1050 Ma)

Rayner Belt  
(1400-900 Ma)

undifferentiated

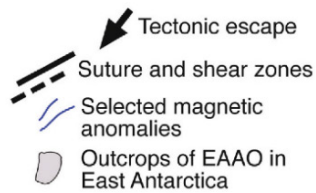


Figure 8.16: Revised geodynamic map of part of East Antarctica in a Gondwana reconstruction, based on Jacobs and Thomas (2004), singling out the combined East African–Antarctic Orogen (650–500 Ma). This compilation is based on integrating new geology with existing geophysics for the Antarctic part. The eastern part of the EAAO in DML is represented by a major Tonian oceanic arc terrane (Tonian Oceanic Arc Super Terrane, TOAST, 1000–900 Ma) that shows a protracted overprinting history from 630 to 500 Ma, whilst a general decrease of overprinting ages is recognised towards the E. We speculate that the TOAST collided with Kalahari first, after which Rukerland and/or Indo-Antarctica emplaced on the other side, toasting the TOAST. The western boundary of the TOAST is represented by the Forster Magnetic Anomaly (FMA). To the

S, the TOAST appears to terminate against a possibly cryptic craton. Its northern extension could be the Vohibori Terrane, SW Madagascar (Boger et al., 2015), which in turn might connect with similar oceanic arc terranes of the Arabian–Nubian Shield (Stern, 1994; Fritz et al., 2013). The eastern limit of the TOAST might run somewhere close to the Yamato Mts. (Y). The E side of Proto-Kalahari might therefore represent a long lasting margin of accretionary tectonics, starting with the addition of the Maud Belt (1130–1040 Ma), followed by the TOAST. The Eastern Granulites/Cabo Degado Nappes in Tanzania–Mozambique might have their counterpart in the Schirmacher Oasis (S). These early granulite facies rocks are exposed along the boundary between the Maud Belt and the TOAST and might represent hot, thinned continental crust that underwent W-directed overthrusting (e.g. Fritz et al., 2013) during the early collision with the TOAST. Outline of Ruker Craton, Coasts Land Block and a number of magnetic anomalies are from (Golynsky and Jacobs, 2001). Differentiation of Namaqua–Natal (1200–1050 Ma) vs. Maud Belt (1130–1040 Ma) after Mendonidis et al. (2015, this volume). Trend of Tonian Oceanic Arc Super Terrane (TOAST), its southern boundary, as well as the western boundary (Forster Magnetic Anomaly, FMA) are from Mieth and Jokat (2014); Mieth et al. (2014) and Riedel et al. (2013). Gamburtsev Mts. (GAM) and East Antarctic Rift System (EARS) from Bedmap2 (Fretwell et al., 2013) and Ferraccioli et al. (2011). Outline of major African tectonic domains after Bingen et al. (2009); Fritz et al. (2013); Ksienzyk and Jacobs (2015). Abbreviations: C, Coats Land; DML, Dronning Maud Land; Da, Damara belt; EH, Ellsworth-Haag; F, Filchner block; FI, Falkland Islands; G, Grunehogna; H, Heimefrontfjella; L, Lurio Belt; LA, Lambert Terrane; N, Napier Complex; Na–Na, Namaqua–Natal; ØC, Øygarden Complex; S, Schirmacher Oasis; Sø, Sør Rondane, SR, Shackleton Range; TAM, Transantarctic Mts., LH, Lützow–Holm Bay; M, Madagascar; R, Read Block; V, Vohibori; Y, Yamato Mts.; Z, Zambesi belt



The Rayner Complex also derived from markedly more evolved crust with TDM of 1.5–2.2 Ga (Liu et al., 2014). The formation of the TOAST coincides in age with the formation of major syn-tectonic plutonic rocks in the Rayner Complex during the final amalgamation of the Napier Craton and Lambert Terrane. The Ruker Craton probably attached later to the Indo-Antarctica along a Cambrian suture zone, resulting in significant reworking of the southern part of the Rayner Complex at ca. 530–500 Ma (e.g. Boger, 2011; Grew et al., 2012). The Lützow-Holm Complex shows still evolved crust, so that the boundary between the TOAST and the Rayner Complex probably lies close to the Yamato Mts., a so far little studied area in easternmost DML (Zhao et al., 1995). Therefore, the TOAST is distinct for its juvenile character and has clear differences to the Maud Belt on the one side and the Rayner Complex on the other. It is likely bound by suture zones on either side (Figure 8.16). To the S, the SE DML province is bound by a crustal block with a distinct flat aeromagnetic signature (Mieth and Jokat, 2014) (Figure 8.16), which probably indicates the southern termination of the TOAST. It is unclear whether this block represents a cryptic craton. At the northern end, similar juvenile rocks with oceanic arc affinities are recognised in SW Madagascar, the Vohibori Terrane (Boger et al., 2015), the latter of which may be linked in turn with the Arabian–Nubian Shield farther N (e.g. Stern, 1994; Fritz et al., 2013).

It is unclear when the TOAST amalgamated to Kalahari and to Indo-Antarctica. In the W, the area of the Forster Magnetic Anomaly has only been studied at the reconnaissance level and this area is certainly a key area to understand the amalgamation processes of the TOAST with the Maud Belt. There is very little evidence of major metamorphism following crust formation of the TOAST. Later LN/EP metamorphic overprinting is very heterogeneous throughout the TOAST ranging from greenschist to granulite facies. The distribution of metamorphic ages is also heterogeneous, however, appear to increase from E to W in the study area (Figure 8.11). The protracted metamorphism of the TOAST is similar to metamorphic ages found throughout the Maud Belt (e.g. Jacobs et al., 1998; Baba et al., 2015), indicating a common long collision history. This probably indicates that the TOAST collided with Kalahari first at ca. 630–600 Ma, after which it was attached to Indo-Antarctica on the other side at ca. 530–500 Ma. Therefore, the metamorphic overprint of the TOAST resulted from accretion and toasting in between the Kalahari and an Indo-Antarctic/Ruker Craton over some 150 Ma. The western boundary of the TOAST is marked by granulite facies nappes (Eastern Granulites in Tanzania, Cabo-Delgado Nappes in Mozambique, Schirmacher granulites). These rocks might have evolved as the result of early overthrusting of hot and thinned continental margin rocks onto the margin of the larger Tanzania and Kalahari Cratons (e.g. Fritz et al., 2013).



## 8.8 Summary and Conclusions

The poorly known nunataks between Sør Rondane and central Dronning Maud Land have juvenile basement with crystallisation ages of ca. 1000–900 Ma that resembles that of the SW-Terrane of Sør Rondane. Therefore, the SE DML Province does not represent the foreland of a LN/EP mobile belt as has been previously speculated (Mieth et al., 2014).

The oldest rocks found are GTTGs, which probably originated along juvenile oceanic arcs, and which are in turn overlain by various sedimentary units. There is very limited evidence of older inheritance. The difference to the relatively pristine SW-Terrane is solely the higher degree of LN/EP reworking in our study area. The southern part of the SW-Terrane probably represents a mega-boudin within a broad, rheologically weaker, LN/EP mobile belt. Therefore, the SE DML Province is neither a craton nor the foreland of a LN/EP mobile belt as has been previously speculated. Together with the main outcrops of the Sør Rondane, the SE DML Province likely represents one large Tonian Oceanic Arc Terrane. The TOAST is similar in age with the Rayner Complex in the E, however has also many differences, and probably represents a separate entity.

The TOAST underwent a protracted overprinting history between ca. 630 and 500 Ma, including polyphase reworking and granitoid magmatism. In general, metamorphic overprinting ages decrease from W to E. This is taken as evidence that the TOAST collided with Kalahari first, after which it amalgamated with Rukerland and/or Indo-Antarctica on its eastern side.

Late-tectonic to postorogenic granitoids with A-type affinities across the region may represent two different groups, namely high and low Ba–Sr–granites. However, these differences are not reflected in either absolute ages (Figure 8.10) or initial Nd isotope signatures (Figure 8.13). The available U–Pb zircon ages, however, seem to be slightly younger in the east (Figure 8.10) although the source region remains similar as evidenced by homogenous Nd isotope signatures between 0 and –1 at the time of intrusion. Therefore, the contrasting trace element contents are likely related to the assemblage of residual minerals stable during partial melting of the source. Our study refines previous interpretations that the zone between the Forster and Ulvetanna magnetic anomalies is a major tectonic feature that forms the eastern limit of the Grenville-age Maud Belt and therefore forms a suture to what has been identified as the TOAST in this study. The TOAST probably correlates with similar rocks in SW Madagascar (Vohibori Terrane) and it has similarities with the Arabian–Nubian Shield.

The TOAST overlaps age-wise with the collisions history of the Rayner Complex to the E, however, apart from this there are major differences. The Rayner Belt has a long history of island arc accretions between the Napier Craton and Lambert Terrane/Rukerland (1400–900 Ma) culminating in continent–continent collision at ca. 950 Ma; it involves markedly more evolved crust. The TOAST in contrast has a pronounced juvenile character without significant inheritance and lacks metamorphic overprint immediately following crust formation. This indicates that it has not been an integral part of Rodinia. The eastern boundary of the TOAST and the Rayner Belt probably is in the vicinity of the Yamato Mts.



## 8.9 Acknowledgements

J. Jacobs and M. Elburg greatly appreciate the invitation to participate in the GEA II expedition conducted by the Federal Institute for Geoscience and Natural Resources (BGR). The whole GEA II team would like to thank the helicopter pilots Knut Wagner, Florian Tauber and Jörn Hergenröder of Sky Heli, Germany, for their flying skills, and Alain Hubert, Gigi Johnson-Amin and the whole crew of the Belgian 'Princess Elisabeth' Station for their hospitality and support during the field season. J. Jacobs wishes to thank Alfred-Wegener-Institute for Polar and Marine Research (AWI) and M. Elburg International Polar Foundation (IPF) and BELARE for providing polar clothing. J. Jacobs acknowledges funding through NFR-NARE. M. Elburg acknowledges funding from the SANAP programme of the South African National Research Foundation. A. Läufer acknowledges funding through Deutsche Forschungsgemeinschaft. I. Kleinhanns acknowledges financial support by the Carl-Zeiss-Foundation. Martin Whitehouse, Kerstin Lindén and Lev Ilyinsky are thanked for analytical support at the Natural History Museum in Stockholm and Monika Bockrath and Siegrid Gerlach are thanked for analytical support at the BGR. We are very thankful for informal reviews and advice by T. Abu-Amal, P. I. Myhre and R.J. Thomas. Thoughtful reviews by S. Boger and S. Elvevold significantly helped to improve our ms. This is Nordsim contribution number 401 and IBERSIMS publication N° 24.





## Chapter 9

# 9. Early Neoproterozoic Metagabbro-Tonalite-Trondhjemite of Sør Rondane (East Antarctica): Implications for Supercontinent Assembly

Marlina Elburg, Joachim Jacobs, Tom Andersen, Chris Clark, Andreas Läufer, Antonia Ruppel, Nicole Krohne, Detlef Damaske

Key findings:

- **The ca. 1 Ga meta-igneous rocks of the Sør Rondane Mountains (E. Dronning Maud Land, Antarctica) were generated in an oceanic arc setting.**
- **Subduction halted around 950 Ma, giving rise to more diverse magmatism.**
- **Igneous ages and isotopic characteristics suggest a pre-Gondwana connection to India-Sri Lanka-Madagascar.**

## 9.1 Abstract

New data for intrusive meta-igneous rocks from the Southwest terrane of the Sør Rondane Mountains confirm the view that this is a juvenile oceanic arc terrane, with the main phase of subduction-related magmatic activity around 995–975 Ma. Younger magmatism (960–925 Ma) is more varied: a high Sr/Y ('adakitic') suite is present, as well as high-Ti mafic dykes, and one sample of A-type granite. This is interpreted as reflecting the end of subduction. The occasional presence of Archaean inherited zircons suggests proximity of Sør Rondane to an older continental nucleus from which detritus was shed. Although the 'meta-igneous sector' appears to be unique in representing a juvenile oceanic arc terrane, igneous ages and isotopic compositions around 1000–900 Ma suggest a broad coherence between outcrops ranging from Schirmacher Oasis (11°E) to Yamato Mts (35°E). This area seems unrelated to the slightly older, and isotopically and geochemically more enriched Mesoproterozoic rocks of central and western Dronning Maud Land. A closer relation appears to exist with Sri Lanka-India-Madagascar during the earliest Neoproterozoic than with southern Africa.

**KEYWORDS:** Antarctica; Rodinia; Gondwana; Oceanic arc; Zircon U–Pb Lu–Hf

## 9.2 Introduction

The Sør Rondane Mountains, located in the eastern part of Dronning Maud Land, have been subjected to an appreciable amount of geological research recently, as they have been proposed to lie in an area where several fold belts, related to the amalgamation of Gondwana, interact (Boger, 2011; Jacobs et al., 1998; Meert, 2003; Osanai et al., 2013). To correctly interpret Gondwanan events it is important to characterise the fragments involved in amalgamation, and their similarities and distinctions to neighbouring areas. In this context, interesting differences



between the ca. 1 Ga meta-igneous samples from Sør Rondane and those from the more westerly parts of Dronning Maud Land were noted recently (Kamei et al., 2013; Owada et al., 2013; Shiraishi et al., 2008). With the present contribution, we want to add to the data and discussion provided by previous authors on the 1.0–0.9 Ga meta-igneous rocks (the ‘metatonalite suite’ of Kamei et al., 2013) in the southwestern part of Sør Rondane. We will focus on the integration of zircon U–Pb, Lu–Hf and trace element data with whole rock geochemical data to assess the models proposed for the tectonic setting in which the magmas were generated. A comparison with data from neighbouring areas in Antarctica and its Gondwana neighbours will be used to assess the tectonic implications for the Rodinia as well as Gondwana supercontinent.

### 9.3 Geological Background

The first geological investigations of the Sør Rondane Mountains were carried out by Belgian expeditions in the 1950–60s, who recognised that an older series of metamorphic rocks (metatonalites and related lithologies) was intruded by younger (now known to be Pan-African) granites (Van Autenboer et al., 1964). More recent mapping has been done by Japanese expeditions, who also published a geological map of the area (Shiraishi et al., 1997), and whose most recent efforts were described in a special issue of *Precambrian Research* (volume 234, 2013).

The Sør Rondane Mountains have been divided into two areas of different metamorphic affinities, the granulite-amphibolite-facies Northeast (NE) terrane and amphibolite-greenschist-facies South-west (SW) terrane. The boundary between the two areas, first named the ‘Sør Rondane Suture’ (Shiraishi et al., 1997) has recently been redefined as the ‘Main Tectonic Boundary’ (Osanai et al., 2013), and shifted slightly northwards compared to its location inferred previously. What will be referred to as the ‘meta-igneous sector’ is part of the SW-terrane, located between the Main Shear Zone (MSZ; with a dextral sense of shear (Ruppel, 2012)) in the north and another, inferred, shear zone north of Dufekfjellet in the south (Figure 9.1), where the rocks consist almost wholly of meta-igneous rocks, at amphibolite-greenschist-facies. The part of the SW-terrane located north of the MSZ consist largely of metasedimentary, rather than meta-igneous rocks, and has experienced granulite- to amphibolite-facies metamorphism (Osanai et al., 2013).

Data on the meta-igneous suite have been provided by the reports to the individual geological maps of Sør Rondane (Shiraishi et al., 1992a), and by Ikeda and Shiraishi (1998), but a more detailed study was done by Kamei et al. (2013), and additional data, focused on the mafic end member, were presented by Owada et al. (2013). The work by Kamei et al. (2013) divides the area in several suites: a 998–995 Ma (SHRIMP U–Pb zircon) gneissose Bt-Hbl metatonalite, with tholeiitic affinities in terms of (elevated)  $\text{FeO}^*/\text{MgO}$  ratios, with associated mafic enclaves; and four suites of calc-alkaline rocks (hbl-bt metatonalite, hbl metagabbro, hbl-bt tonalitic gneiss, and bt metatonalite), which yielded ages of 945–920 Ma, apart from a sample of bt metatonalite in Nils Larsenfjellet, which gave an age of 772 Ma. On the basis of the geochemical characteristics of the two suites, Kamei et al. (2013) proposed a juvenile oceanic arc setting for the tholeiitic suite, and interpreted the calc-alkaline suite as having formed by an ‘adakite scenario’, i.e. melting of a subducted oceanic slab with residual garnet, also in a subduction setting.



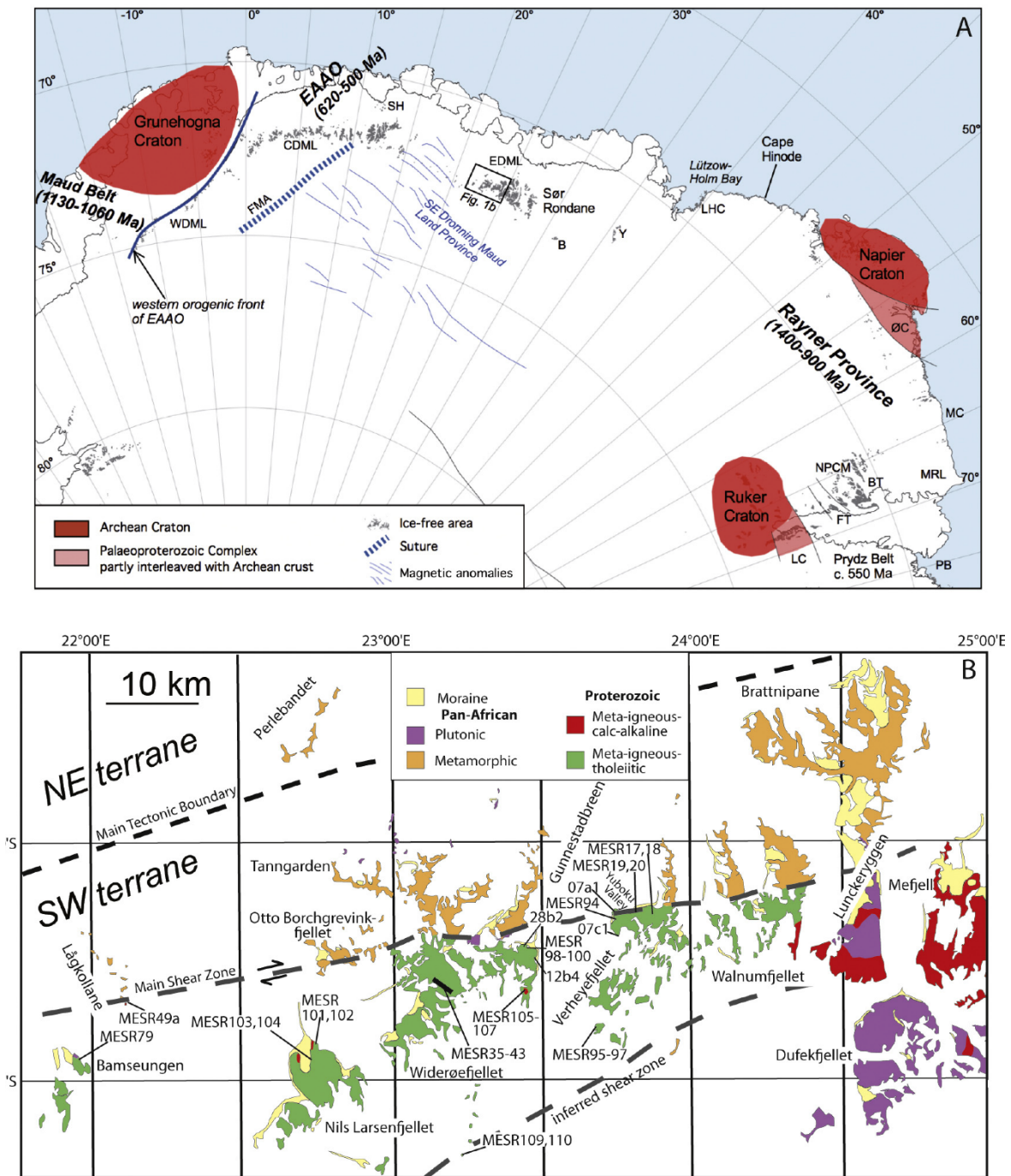


Figure 9.1: A) Regional tectonic framework of the Sør Rondane Mountains, eastern Dronning Maud Land. Sør Rondane is located halfway between the Grunehogna and the Napier cratons. The Grunehogna Craton is surrounded by the Mesoproterozoic Maud Belt with African (Kalahari) affinities, whilst the Napier Craton, which is fringed by the ca. 1.4–0.9 Ga Rayner Complex, has affinities to greater India. The Forster Magnetic Anomaly (FMA) has been recognised as a significant Late Neoproterozoic suture zone. The area may be dissected by additional Late Neoproterozoic suture zones that are, however, less well defined. Abbreviations: B, Belgica Mts.; BT, Beaver Terrane; CDML, central Dronning Maud Land; EAAO, East African-Antarctic Orogen; FT, Fischer Terrane; LC, Lambert Complex; LHC, Lützow-Holm Complex; MC, Mawson Coast; MRL, Mac. Robertson Land; NPCM, northern Prince Charles Mts.; PB, Prydz Bay; SH, Schirmacher Hills; WDML, western Dronning Maud Land; Y, Yamato Mts; ØC, Øygarden Complex. B) Geological map of the Sør Rondane mountains after Kamei et al. (2013), Osanai et al. (2013), Shiraishi et al. (1997) and our own data, indicating the location of the samples analysed in this study.



In contrast, Owada et al. (2013) focussed on the mafic rocks associated within the meta-igneous sector, and divided them into a ca. 995 Ma low-Ti ( $\text{TiO}_2 < 1.2$  wt.%) suite of mafic enclaves and a ca. 945 Ma high-Ti ( $\text{TiO}_2 > 1.2$  wt.%) suite of dykes. Owada et al. (2013) also interpreted the low-Ti samples to have formed in a juvenile arc terrane, but the younger, high-Ti group was, interpreted to have been formed in a back-arc setting, contrasting with the subducted slab-melt scenario of Kamei et al. (2013).

## 9.4 Sample Description

### 9.4.1 Field Appearance

A total of thirty-four samples was collected from the outcrops occurring to the south of the ‘Main Shear Zone’ (Shiraishi et al. (1997); Figure 9.1) during the German-led ‘Geodynamic Evolution of East Antarctica’ (GEA) expeditions I and II in the Austral summer of 2010–2011 and 2011–2012. The rocks are dominantly coarse-grained and mesocratic in appearance, with a distinctly green tinge. More melanocratic rocks can be fine- or coarse-grained. The melanocratic rocks occur as discrete mappable bands or as mafic enclaves or dykes within the more mesocratic rocks (Figure 9.2A–F). In some cases, the mafic enclaves can be seen to originate from mafic dykes. Leucocratic dykes of up to 5 m width have also been observed. There is plenty of evidence of ductile deformation in the field, especially close to the ‘Main Shear Zone’, but the intensity of this deformation is variable. In some instances, it is possible to recognise textures that can be interpreted to be of igneous origin, such as the presence of (subvolcanic) quartz phenocrysts (Figure 9.3A) and larger feldspar crystals that are likely to have been phenocrysts before becoming porphyroclasts.

### 9.4.2 Petrography

All samples analysed are, essentially, metamorphic rocks, with epidote and chlorite as the most obvious metamorphic minerals, but the extent to which they have been metamorphosed is variable. In some samples, plagioclase crystals are wholly replaced by finer-grained epidote, while in other samples igneous oscillatory zoning may still be visible within the plagioclase (Figure 9.3B). Because of the metamorphic overprint, the samples have been classified (Figure 9.4) on the basis of their normative mineralogy and intrusive QAPF classification (Le Maitre, 2002), with the additional category of trondhjemite based on the Ab-An-Or diagram of Barker (1979) (see Geochemistry section, and ‘Electronic Appendix D.2’, which also gives data on the modal mineralogy). The texture of the meta-(quartz-) gabbros is variable: it can be foliated, porphyroclastic, coarse- or fine-grained equigranular, meta-porphyratic, meta-ophitic, or poikilitic, with large oikocrysts of amphibole. In some cases, amphibole is zoned from cores with amore olive-green colour to rims where the green has a more bluish tinge. Plagioclase in variable stages of epidotisation is present in all samples, as is minor quartz. Chlorite is more common in the sheared samples. Opaque minerals are present in most samples, and titanite in some. Apatite is an accessory phase, apart from sample MESR109, in which it occurs at the percent level; this sample also contains more abundant oxides than other meta-gabbros. Intermediate samples mainly classify as metatonalites, and contain lower modal amounts of amphibole, while chlorite and quartz increase in abundance, with biotite in more potassium-



rich samples. Accessory minerals are apatite, zircon, titanite, and opaque minerals, and more rarely rutile. In some samples, the opaque minerals are partially replaced by titanite. Amphibole is sometimes riddled with small inclusions of opaque minerals and/or rutile, often elongated in certain orientations with respect to the host crystal, suggesting they were formed by exsolution. Garnet occurs as eu- to subhedral crystals in samples with higher  $\text{FeO}^*/\text{MgO}$  ratios.

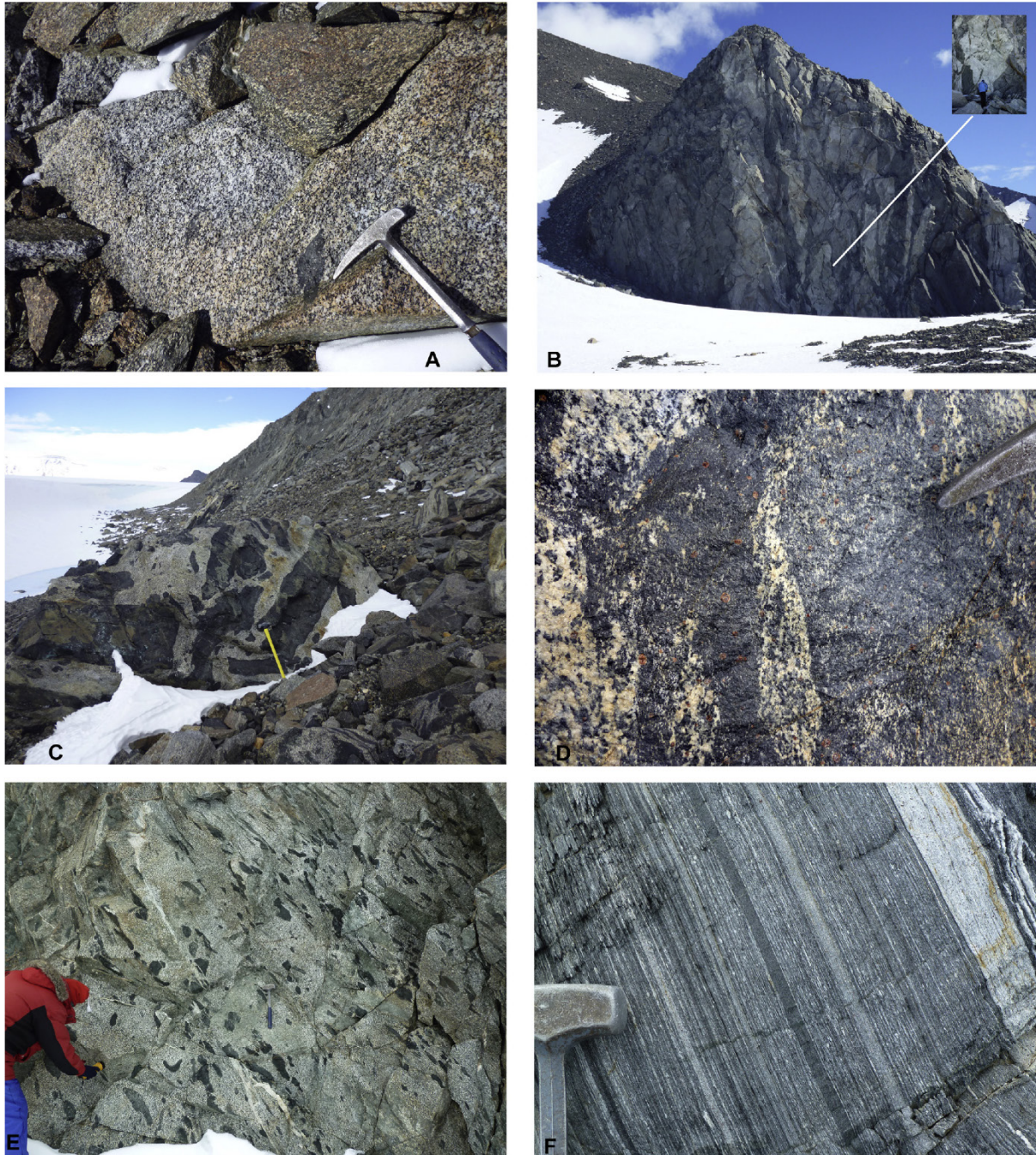


*Figure 9.2: Field photographs of the sampled lithologies. A) Metatonalite with quartz-gabbroic enclave on central Widerøefjellet (sample MESR38). B) Outcrop at the east side of Widerøefjellet. Sample MESR99 was taken from the most leucocratic material. Inset shows person for scale. C) Enclave-bearing metatonalite on the east side of Nils Larsenfjellet (MESR101-102). Note the scalloped rims of the mafic enclaves, indicative of an origin by magma mingling. D) Causinknappen nunatak, showing intermingling of mafic and felsic (MESR110) material, and the presence of garnet. E) Undeformed enclave-bearing metatonalite from which sample 07C1 was taken. F) Area from which sample 07A1 originates, interpreted to be the deformed equivalent of panel E.*



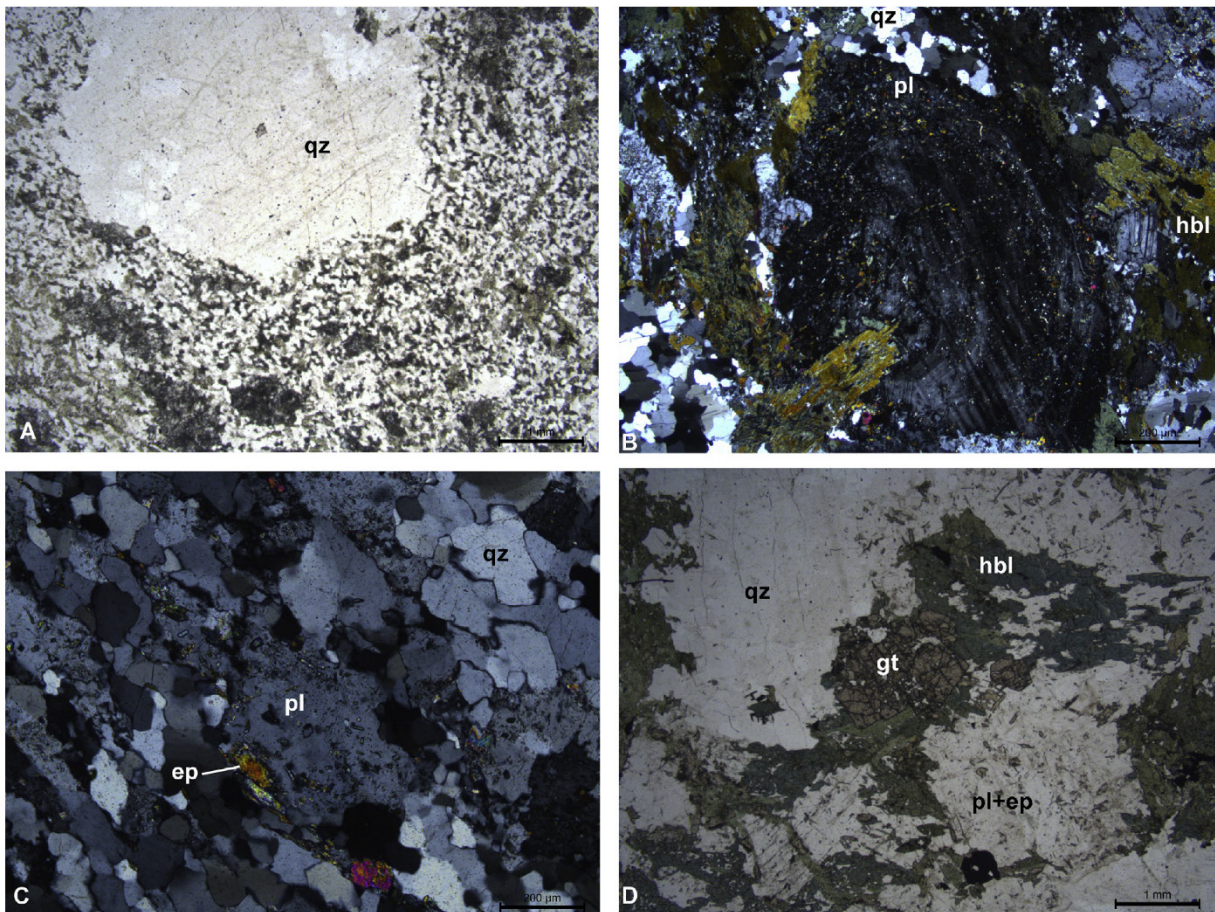


Figure 9.3: Photomicrographs of selected samples. A) Sample MESR97, with quartz phenocrysts in a fine-grained matrix, interpreted to represent a shallow-intrusive origin of the sample. B) Sample MESR100, showing broad oscillatory zoning in the plagioclase crystal, interpreted to be a relict of the igneous protolith. C) Sample MESR99, the oldest sample analysed, consisting predominantly of quartz and plagioclase, partially altered to epidote. This sample could either be a felsic cumulate, or a crystal-rich tuff; the texture is clearly metamorphic, and does not permit a choice between the two options. D) Sample MESR104, containing subhedral garnet, interpreted to be of metamorphic origin.

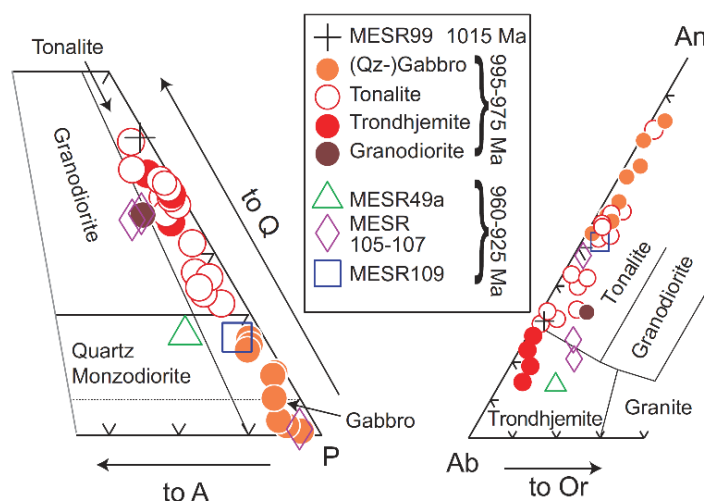


Figure 9.4: Relevant parts of QAPF (Le Maitre, 2002) and Ab-An-Or normative diagrams (Barker, 1979) on which the classification of the samples has been based.



It can contain inclusions of opaque minerals, and does not display reaction rims; it is therefore interpreted to be formed during pro-grade metamorphism of the tonalites. Calcite occurs as a secondary mineral in some samples. Sample MESR99 classifies as a tonalite, but is extremely low in mafic minerals (leucotonalite). The metatondhjemites mainly differ from the meta tonalites in their lower modal amount of amphibole, the absence of titanite and higher quartz contents, but the distinction between tonalite (modal An% >30) and trondhjemite (modal An% <30) is gradual. One sample (MESR49a) is an only slightly metamorphosed quartz-monzodiorite, and, unlike all the other samples, contains microcline. Samples MESR97, 105 and 106 are classified as meta-granodiorites, and contain white mica. All samples show some signs of deformation, varying from undulose extinction of the quartz, to sutured grain boundaries and a porphyroclastic texture, whereby larger plagioclase crystals are enveloped by ribbons of quartz, amphibole, epidote and chlorite defining an S-C fabric. Neither the intensity of metamorphism, as evidenced by the extent of epidote formation, nor the intensity of deformation appears to be related to the age (varying between ca. 1015 and 925 Ma, see below) of the samples.

## 9.5 Analytical Techniques

A more detailed description of the analytical techniques used is given in ‘Electronic Appendix D.1’. Major and trace elements were analysed at the Discipline of Geological Sciences, University of KwaZulu-Natal, by X-ray fluorescence (XRF) spectrometry on fused discs and pressed pellets respectively, using a PANalytical Axios–minerals sequential XRF spectrometer. Lower-level trace elements were analysed by laser ablation (LA) inductively coupled plasma mass spectrometry (ICPMS) of the XRF fused discs using an NWR UP-213 laser and Perkin-Elmer Nexion quadrupole ICPMS. Trace elements in zircon were also analysed using the latter set-up.

Laser-ablation U–Pb and Lu–Hf isotopic analyses were performed at the Department of Geosciences, University of Oslo, using an NWR UP-213 laser and a Nu Instruments multi-collector ICPMS, following techniques described by Elburg et al. (2013). Four samples were dated by U–Pb on zircon using a Sensitive High Resolution Ion-Microprobe (SHRIMP) at Curtin University (Perth, Western Australia; ‘Electronic Appendix D.1’). Two samples were analysed for Sr and Nd isotopes at the Department of Geological Sciences of the University of Cape Town.

## 9.6 Zircon U-Pb and Lu-Hf Data

Zircon U-Pb data were acquired on a total of twelve samples, spanning the geographic area from which the samples were obtained. Eight of these were analysed by LA-MC-ICPMS (sample identifiers starting with ‘MESR’) and four by SHRIMP (sample identifiers starting with a number). The full data set can be found in ‘Electronic Appendix D.2’. All uncertainties are quoted at the 2-sigma level (Table 9.1). The zircons that were dated by LA-ICPMS were also analysed for their Lu–Hf isotope systematics to determine the initial  $^{176}\text{Hf}/^{177}\text{Hf}$  ratios and assess the degree of homogeneity within the samples.

Sample 07C1 comes from a mesoscopically undeformed tonalite, containing abundant mafic enclaves (Figure 9.E). This locality is ca. 1 km S of the MSZ (Figure 9.1). The up to 400  $\mu\text{m}$



large zircons are clear to light brownish with few inclusions. In cathodoluminescence (CL) imaging, zircons show irregular sector zoning, and sometimes a faint oscillatory zoning. Eighteen spots were analysed on eighteen crystals. Typical U-concentrations range from 100 to 900 ppm (Th/U: 0.15–0.28). The 18 analyses define a concordia age of  $986 \pm 3$  Ma (Figure 9.5A), which is interpreted as the crystallisation age of the tonalite. This is indistinguishable of the weighted average  $^{207}\text{Pb}/^{206}\text{Pb}$  age of  $987 \pm 6$  Ma.

Table 9.1: Summary of zircon U-Pb ages and Hf isotopes.

Sample	Age type	Age (Ma)	2 $\sigma$ (Ma)	n	Interpretation	$\epsilon\text{Hf}_i$	2 $\sigma$
07A1	Concordia	979	5	15	Igneous		
	$^{207}\text{Pb}/^{206}\text{Pb}$ wtd. av.	987	13				
07C1	Concordia	986	3	18	Igneous		
	$^{207}\text{Pb}/^{206}\text{Pb}$ wtd. av.	987	6				
12B4	Concordia	984	6	12	Igneous		
	$^{207}\text{Pb}/^{206}\text{Pb}$ wtd. av.	994	8				
	Upper intercept	1024	14				
28B2	Concordia	991	5	11	Igneous		
	$^{207}\text{Pb}/^{206}\text{Pb}$ wtd. av.	990	6				
MESR99	Concordia	1015	4	20	Igneous	+6.5	2.6
	$^{207}\text{Pb}/^{206}\text{Pb}$ wtd. av.	1010	5				
MESR43	Concordia	991	4	25	Igneous	+6.5	2.0
	$^{207}\text{Pb}/^{206}\text{Pb}$ wtd. av.	986	4				
MESR104	Concordia	986	6	14	Igneous	+6.3	1.7
	$^{207}\text{Pb}/^{206}\text{Pb}$ wtd. av.	984	7				
MESR79	Concordia	986	7	15	Igneous	+7.3	2.4
	$^{207}\text{Pb}/^{206}\text{Pb}$ wtd. av.	990	18				
MESR110	Upper intercept	979	18	8	Igneous	+4.2	1.2
	$^{207}\text{Pb}/^{206}\text{Pb}$ wtd. av.	979	15				
MESR106	Concordia	957	8	11	Igneous	+7.5	2.1
	$^{207}\text{Pb}/^{206}\text{Pb}$ wtd. av.	957	5				
	$^{207}\text{Pb}/^{206}\text{Pb}$	1006–1070		4	Inherited	+7.9	0.8
	$^{207}\text{Pb}/^{206}\text{Pb}$	2910–2966		1	Inherited?	+3.6	0.9
MESR49a	Concordia	947	8	10	Igneous	+7.7	1.8
	$^{207}\text{Pb}/^{206}\text{Pb}$ wtd. av.	960	7				
MESR109	Upper intercept	927	+37/–22	2	Igneous	+6.9	5.2
	$^{207}\text{Pb}/^{206}\text{Pb}$ wtd. av.	929	14				
	Upper intercept (with MESR106)	2970	+32/–30	1	Inherited	–2.1	

n, number of analyses on which the age is based. Samples 07A1, 07C1, 12B4 and 28B2 analysed by SHRIMP, others by LA-MC-ICPMS.

**Sample 07A1** represents the mylonite equivalent of the metatonalite (Figure 9.F), as exposed in the southern part of the MSZ, west side of Yuboku Valley (Figure 9.1). It contains zircons that appear as anhedral fragments up to 200  $\mu\text{m}$  in size. Zircons are clear to light brownish and have numerous inclusions. In CL images, they show oscillatory or sector zoning. Some zircons have high-U rims, which are too thin to be analysed. Eighteen crystals were analysed with one spot each. The zircons are low in U (70–210 ppm) with Th/U from 0.13 to 0.24. Two spots yielded discordant ages, and one spot gave an age that was ca. 50 Ma younger than the other analyses. The remaining fifteen analyses yielded a concordia age of  $979 \pm 5$  Ma (Figure 9.5B), which is interpreted to be the age of the tonalitic protolith to the mylonite. The weighted average  $^{207}\text{Pb}/^{206}\text{Pb}$  age is similar at  $987 \pm 13$  Ma. The discordant analyses probably reflect Pb-loss as the result of deformation.

**Sample 12B4** comes from the east side of Widerøefjellet and is a heterogeneous, fine-grained felsic gneiss of trondhjemitic composition. The zircons are mostly small and clear, often not exceeding 100  $\mu\text{m}$  in size. In CL imaging, the zircons show moderate zoning. Some zircons have metamict cores others have thin high-U rims. Sixteen grains were analysed from the main weakly oscillatory- zoned parts, which have typical U concentrations of 250–500 ppm (Th/U: 0.36–0.48). Fourteen analyses define a concordia age of  $984 \pm 6$  Ma (Figure 9.5C), albeit with



a slightly high MSWD of concordia of 4.5. This age is the best estimate of the igneous crystallisation age of the sample, and within error of the weighted average  $^{207}\text{Pb}/^{206}\text{Pb}$  age of  $994 \pm 8$  Ma. The remaining four analyses can be used to give a discordia with a very poorly defined lower intercept and an upper intercept of  $1024 \pm 14$  Ma (weighted average  $^{207}\text{Pb}/^{206}\text{Pb}$  age is  $1039 \pm 13$  Ma). The MSWD of this discordia is 0.58, and its relevance will be discussed in conjunction with the LA-MC-ICPMS data for sample MESR99 from the same general area. **Sample 28B2** comes from an area to the northwest of 12B4 and is a foliated metatonalite. The zircons are stubby, light brownish and mostly anhedral. In CL, the zircons show a core-rim relationship, with dark cores and very bright irregular rims. Twelve crystals were analysed, targeting eight cores and 4 rims. One core yielded a strongly discordant analysis. Whilst the high-U cores have U from 500 to 2200 ppm (Th/U: 0.14–0.52), the rim analyses have much lower U ranging from 60 to 150 ppm (Th/U: 0.38–0.41). However, the seven core and four rim analyses are indistinguishable in age and yield a concordia age of  $991 \pm 5$  Ma (Figure 9.5D), which is interpreted as the crystallisation age of the protolith, indistinguishable from the weighted average  $^{207}\text{Pb}/^{206}\text{Pb}$  age of  $990 \pm 6$  Ma.

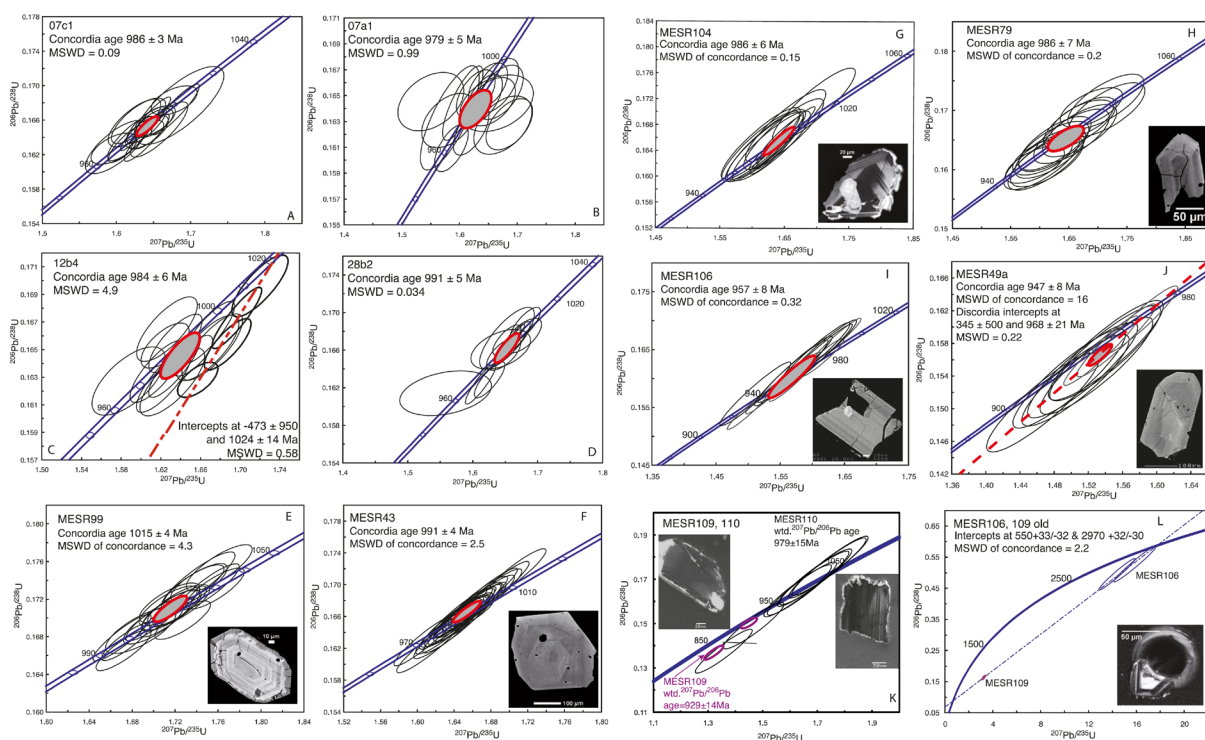


**Figure 9.5:** Zircon U–Pb data. Only the analytical points that were used for age calculation are shown; full analyses are given in the ‘Electronic Appendix D.2’. All uncertainties are  $2\sigma$ . A–D) Sample analysed by SHRIMP (Curtin University, W. Australia); E–L) samples analysed by LA-MC-ICPMS (Oslo University, Norway), which were also analysed for Lu–Hf and trace elements. Zircon portraits are BSE images, apart for panels G, H, K and L (CL). The ca. 3 Ga zircon in sample MESR106 (panel L) was only imaged after ablation, hence the crater.

**Sample MESR99** comes from an area between 12B4 and 28B2 on the east side of Widerøefjellet (Figure 9.1 and Figure 9.B). The outcrop consists of a variety of undeformed rock types, ranging from mesocratic to leucocratic metatonalite. The most mafic compositions are represented as mafic enclaves within an intermediate fairly coarse-grained intrusive. The most leucocratic material is present as 10 m-sized semi-angular patches with equidimensional to elongate shapes. The geological relationships between the different phases is unclear from field observations, as



no chilled contacts were observed. The dated sample is of the leuco-tonalite, which is homogeneously fine-grained. Its zircons are euhedral, with aspect ratios  $<2:1$  and typically only 100–150  $\mu\text{m}$  in their longest dimension. Many of them have a turbid brown appearance, but clear ones are found as well. Back-scattered electron (BSE) imaging shows that some zircons display well-defined oscillatory zoning (Figure 9.5E), but others have more patchy zoning; the latter crystals typically yielded discordant analyses with significant common Pb. Many zircons have a thin, darker rim, which was not of sufficient size to be analysed. Thirty-six crystals were analysed, and yielded U-contents of 600–1200 ppm, with Th/U ratios (determined by LA-Q-ICPMS) of 0.4–1. Sixteen analyses yielded discordant and/or common-Pb influenced analyses. The remaining twenty analyses had  $^{206}\text{Pb}/^{204}\text{Pb}$  ratios  $>8000$  and yielded a concordia age of  $1015 \pm 4$  Ma, with an MSWD of 4.3 (weighted average  $^{207}\text{Pb}/^{206}\text{Pb}$  age is  $1010 \pm 5$  Ma). The somewhat high MSWD reflects a range in the ages of the individual points between 1031 and 998 Ma (Figure 9.5E). The homogeneity in crystal size and shape, and their oscillatory zoning indicates that this is a single population of igneous zircons, and the age is interpreted to be the crystallisation age of the zircons. A similar age is found from the discordia of four zircons in sample 12B4, from slightly further north. However, the main igneous age there is younger at  $984 \pm 6$  Ma. This may reflect a next phase of magmatism, which may also have been responsible for the (undated) thin rims on the zircons in MESR99.

The average initial  $^{176}\text{Hf}/^{177}\text{Hf}$  ratio of the 29 zircons analysed is  $0.282334 \pm 0.000089$  (2 sigma; Figure 9.6). The scatter is slightly outside that expected from analytical uncertainty, based on the repeated analyses of the Temora standard. The two lowest analyses might be outliers, and if these are left out the average comes to  $0.282341 \pm 0.000074$ , which translates to an  $\epsilon\text{Hf}_i$  of  $6.5 \pm 2.6$ .

Sample MESR43 was taken near the bottom of a traverse down the south-central part of Widerøefjellet (Figure 9.1), and it is a moderately deformed, coarse-grained metatonalite. Its zircons are generally clear, with a light-purple colour and aspect ratios  $<2:1$ . Their size is around 200–350  $\mu\text{m}$ . Zoning is only poorly visible in BSE images, but appears to be oscillatory (Figure 9.5F). Twenty-six crystals (with U concentrations of 200–500 ppm; Th/U ratios around 0.25) were analysed, of which only one is discordant. The other twenty-five analyses define a concordia age of  $991 \pm 4$  Ma, albeit with a slightly elevated MSWD of 2.5. This age is within error of the weighted average  $^{207}\text{Pb}/^{206}\text{Pb}$  age of  $986 \pm 4$  Ma, and is interpreted as the crystallisation age of the intrusion.

The twenty-six Lu–Hf analyses constitute a homogeneous population, with the spread in data within that expected from analytical uncertainty. The average initial  $^{176}\text{Hf}/^{177}\text{Hf}$  ratio is  $0.282360 \pm 0.000056$ , or  $\epsilon\text{Hf}_i$  of  $6.5 \pm 2.0$ .

Sample MESR104 comes from Nils Larsenfjellet and is a moderately deformed metatonalite, which in places contains mafic enclaves. Zircons in this sample are about 200  $\mu\text{m}$  and have aspect ratios from 1:1 to 3:1. Cathodoluminescence (CL) imaging shows well-defined oscillatory zoning in most crystals. Nineteen grains (U contents 200–600 ppm, Th/U = 0.25–0.5) were ablated, of which five gave discordant analyses. The other fourteen gave a concordant age of  $986 \pm 6$  Ma (Figure 9.5G; weighted average  $^{207}\text{Pb}/^{206}\text{Pb}$  age is  $984 \pm 7$  Ma), with an MSWD of 0.15, and this age is most likely to reflect the igneous crystallisation age of the sample.



Twenty zircons yielded a homogeneous Hf isotope population with an initial  $^{176}\text{Hf}/^{177}\text{Hf}$  ratio of  $0.282353 \pm 0.000049$ , or  $\epsilon\text{Hf}_i$  of  $6.3 \pm 1.7$ .

**Sample MESR79** is a coarse-grained metatrandhjemite from Bamseungen. Its zircons are between 100 and 200  $\mu\text{m}$ , with aspect ratios up to 3:1, and show oscillatory zoning, which is poorly defined in BSE images, but clearly visible in CL. Some featureless cores are present too. Twenty-five ablations were performed on 23 grains. U concentrations were variable, from 50 to 200 ppm, but with spikes up to 3000 ppm; Th/U ratios were 0.4–1, with the higher values for the U-enriched grains. Some grains caused problems, because of elevated count rates for  $^{206}\text{Pb}$  (>1 Mcps) causing dead-time problems and deviation from ion-counter linearity, resulting in reversely discordant analyses. Only fifteen analyses could therefore be used to obtain the igneous age of this sample, which is a concordia age of  $986 \pm 7$  Ma (MSWD = 0.2; Figure 9.5H), within error of the weighted average  $^{207}\text{Pb}/^{206}\text{Pb}$  age of  $990 \pm 18$  Ma.

Twenty-seven zircons were analysed for Lu–Hf systematics, of which two gave values that were significantly lower than the main population, and the CL image of one of these zircons showed the presence of a core, with a slightly discordant  $^{207}\text{Pb}/^{206}\text{Pb}$  age of  $1043 \pm 32$  Ma. Without these two analyses, the average initial  $^{176}\text{Hf}/^{177}\text{Hf}$  ratio is  $0.282380 \pm 0.000067$ , or  $\epsilon\text{Hf}_i$  of  $7.3 \pm 2.4$ .

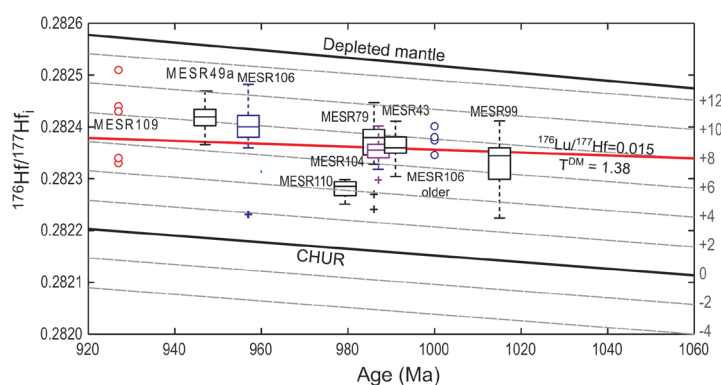


Figure 9.6: Box-and-whisker plot of initial zircon Hf isotopic composition versus age, with labelled contour lines for epsilon Hf. Because of the limited number of zircons analysed for MESR109, only the data points are shown. Other data points shown are outliers from the main population. The reference line with  $^{176}\text{Lu}/^{177}\text{Hf} = 0.015$  indicates the typical evolution of crust with a depleted mantle extraction age of ca. 1.4 Ga, which passes through most of the ca. 995–975 samples.

**Sample MESR106** was taken from the southeastern side of Widerøefjellet in an area with both felsic and mafic intrusives. It is a fine-grained granodiorite, with zircons of 100–200  $\mu\text{m}$ . They are euhedral with aspect ratios from 2:1 to 5:1, and show concentric zoning, generally mimicking the outline of the crystal, in BSE images. Slightly brighter cores, with cracks around them, are present in some crystals. Twenty-six spots were ablated, with U contents typically 200–800 ppm, and Th/U between 0.25 and 0.45. One crystal gave an age of ca. 3 Ga, and four crystals yielded ages of 1050–995 Ma. Eleven other analyses gave concordant analyses, which together defined an age of  $957 \pm 8$  Ma (Figure 9.5I; weighted average  $^{207}\text{Pb}/^{206}\text{Pb}$  age is  $957 \pm 5$  Ma), which is likely to be the crystallisation age of the intrusion.

The igneous population ( $n = 21$ ) gave an initial  $^{176}\text{Hf}/^{177}\text{Hf}$  ratio of  $0.282406 \pm 0.000059$ , or  $\epsilon\text{Hf}_i$  of  $7.5 \pm 2.1$ . The four grains that are slightly older give a marginally lower initial  $^{176}\text{Hf}/^{177}\text{Hf}$  ratio of  $0.282374 \pm 0.000049$ . The initial  $^{176}\text{Hf}/^{177}\text{Hf}$  ratio of the ca. 3 Ga grain was  $0.28096 \pm 0.000028$  or  $\epsilon\text{Hf}_i$  of  $3.6 \pm 0.9$ .

**Sample MESR49a** comes from the southernmost nunatak of the Lågakollane group, which consists of moderately deformed coarse-grained quartz-monzodiorite, intruded by undeformed finer-grained granitoid and a pegmatite dyke. The sample is of the deformed quartz-monzodiorite. It contains numerous euhedral zircons between 200 and 400  $\mu\text{m}$  in length and



aspect ratios around 3:1. Cracks and inclusions are quite common. Several contain cores that are very bright and patchy in BSE images, but the majority of crystals displays fine-scale oscillatory zoning. Thirty-six spots were analysed, but many of them were discordant and rich in common Pb, probably as a result of the many cracks and inclusions. U contents are 200–500 ppm, and Th/U ratios around 0.35. Only twelve analyses were of sufficient quality to be retained, and ten of these yielded a concordia age of  $947 \pm 8$  Ma (Figure 9.5J). However, since most analyses plotted below the concordia, the MSWD of concordance is as high as 14. A discordia through the same sample set gives an upper intercept of  $968 \pm 21$  Ma, which is within error of the concordia age, and the weighted average  $^{207}\text{Pb}/^{206}\text{Pb}$  age of  $960 \pm 7$  Ma. The other two analyses gave significantly younger ages at 880–910 Ma. The ca. 950 Ma age is taken as the best estimate of the igneous age for this sample. MESR49a yielded a homogeneous Hf-isotope population of zircons ( $n = 34$ ), with an average of  $^{176}\text{Hf}/^{177}\text{Hf} = 0.282419 \pm 0.000050$ , or  $\epsilon\text{Hf}_i$  of  $7.7 \pm 1.8$ .

Sample MESR109 and 110 both come from the very small Causinknappen nunatak, which consists of tonalite (MESR110) with garnet-bearing mafic enclaves and schlieren (Figure 9.D). Garnet-free mafic material is also present, which has a sharper contact with the host rock and which we interpret to being a (poorly exposed) dyke; this constitutes sample MESR109.

MESR110 contains clear, virtually colourless zircons, typically with prismatic shape, and up to 300  $\mu\text{m}$  in their longest dimension. Aspect ratios are typically 3:1. They show fine oscillatory zoning in CL imaging. Ten crystals were ablated, and gave U contents of 200–800 ppm. Two zircons are discordant and give  $^{207}\text{Pb}/^{206}\text{Pb}$  ages of 940–950 Ma, and may have been affected by partial resetting by the magma that yielded MESR109 (see below). The other eight spots gave a weighted average  $^{207}\text{Pb}/^{206}\text{Pb}$  age of  $979 \pm 15$  Ma (MSWD = 0.06), and intercept ages at  $979 +19/-18$  and  $66 +280/-60$  Ma (Figure 9.5K).

This sample yielded a very homogeneous Hf isotopic population: 12 grains gave an average initial  $^{176}\text{Hf}/^{177}\text{Hf}$  ratio of  $0.282283 \pm 0.000034$ , or  $\epsilon\text{Hf}_i$  of  $4.2 \pm 1.2$ .

Zircons in MESR109 are rare and small (100  $\mu\text{m}$ ), and elongated in shape. Small zircons have aspect ratios up to 4:1, but larger ones are generally 2:1. They are typically cloudy brown in colour, and give a very poor CL response. Only nine crystals could be ablated, of which one grain is clearly older ( $^{207}\text{Pb}/^{206}\text{Pb}$  age  $>2$  Ga). Of the seven other grains, only two show less than 15% discordance; the other five show a combination of Pb-loss and common Pb, yielding  $^{207}\text{Pb}/^{206}\text{Pb}$  ages between 950 and 1570 Ma, and  $^{206}\text{Pb}/^{204}\text{Pb}$  ratios as low as 300. The two least discordant grains, with the highest  $^{206}\text{Pb}/^{204}\text{Pb}$  ratios define a two-point isochron with an upper intercept of  $927 +37/-22$  Ma (Figure 9.5K), which is within error of the weighted mean  $^{207}\text{Pb}/^{206}\text{Pb}$  age of  $929 \pm 14$  Ma, which we take as the best estimate of the igneous age. When the older grain is combined with the two analyses of the old crystal in MESR106, a discordia with intercepts at  $550 +33/-32$  and  $2970 +32/-30$  Ma (MSWD 2.2) can be constructed (Figure 9.5L).

Only 6 grains were suitably large for Hf isotope analysis, and one of them was the inherited grain. The five igneous grains give a scattered distribution (Figure 9.6) with an average of  $^{176}\text{Hf}/^{177}\text{Hf}$  of  $0.282408 \pm 0.000147$ , or  $\epsilon\text{Hf}_i$  of  $6.9 \pm 5.2$ . If an age of 2.97 Ga is taken for the inherited grain, its initial Hf isotopic composition is 0.280821 or  $\epsilon\text{Hf}_i$  of  $-2.1$ .



## 9.7 Geochemistry

In order to facilitate the presentation and discussion of the data, three main groups of samples are defined on the basis of their age: one sample, MESR99, with an age of ca. 1015 Ma; the main group of samples with ages between 995 and 975 Ma; and the younger samples (960–925 Ma). The main group has been subdivided on the basis of their mineralogy (Figure 9.4) into (quartz-)gabbros (nine samples), tonalites (fifteen samples), trondhjemites (four samples), and a single granodiorite (MESR97). The younger samples are quartz-monzodiorite MESR49a from Lågakollane, the quartz-gabbro MESR109 from Causinknappen, and the two granodiorites and a gabbro from the SE of Widerøefjellet (MESR105–107). Note that the samples are referred to by their igneous name from now on, although all are strictly speaking metamorphic rocks.

### 9.7.1 Major and Trace Elements

Figure 9.7 shows selected Harker variation diagrams of major and trace elements (all analyses can be found in the ‘Electronic Appendix D.2’), while Figure 9.8 and Figure 9.9 show normalised rare earth element (REE) and trace element diagrams. The main age (995–975 Ma) group of samples shows coherent trends that broadly conform to those expected from a consanguineous group of igneous rocks, related to each other by the fractionation of plagioclase and ferromagnesian mineral phases: CaO (as well as  $\text{Fe}_2\text{O}_3^*$ , MnO and MgO) decrease, whereas  $\text{Na}_2\text{O}$  and to a lesser extent  $\text{K}_2\text{O}$  increase with increasing  $\text{SiO}_2$  content. The tonalite sample from Causinknappen (MESR110) is unusual in its low sodium and high calcium content. Data for  $\text{TiO}_2$  are somewhat scattered on the low- $\text{SiO}_2$  side of the diagram, but decrease from tonalite to trondhjemite. For the trace elements, V (as well as Cr, Ni, Sc and Co) decrease with increasing  $\text{SiO}_2$  content, Y and Zr (as well as Rb, Ba and REE) show a scattered increase, while Sr contents remain more or less constant after an initial increase. REE patterns are typically flat to slightly LREE-enriched for the (quartz-)gabbros, while LREE concentrations increase in tonalitic and trondhjemitic samples. Both positive and negative Ce- and Eu-anomalies occur, unrelated to the modal composition of the samples. Two (undated) samples show somewhat aberrant behaviour: quartz-gabbro MESR18 has higher  $\text{TiO}_2$ ,  $\text{P}_2\text{O}_5$ , Y and REE contents than other samples of this group, while granodiorite MESR97 has higher  $\text{K}_2\text{O}$ , Rb and Ba concentrations.



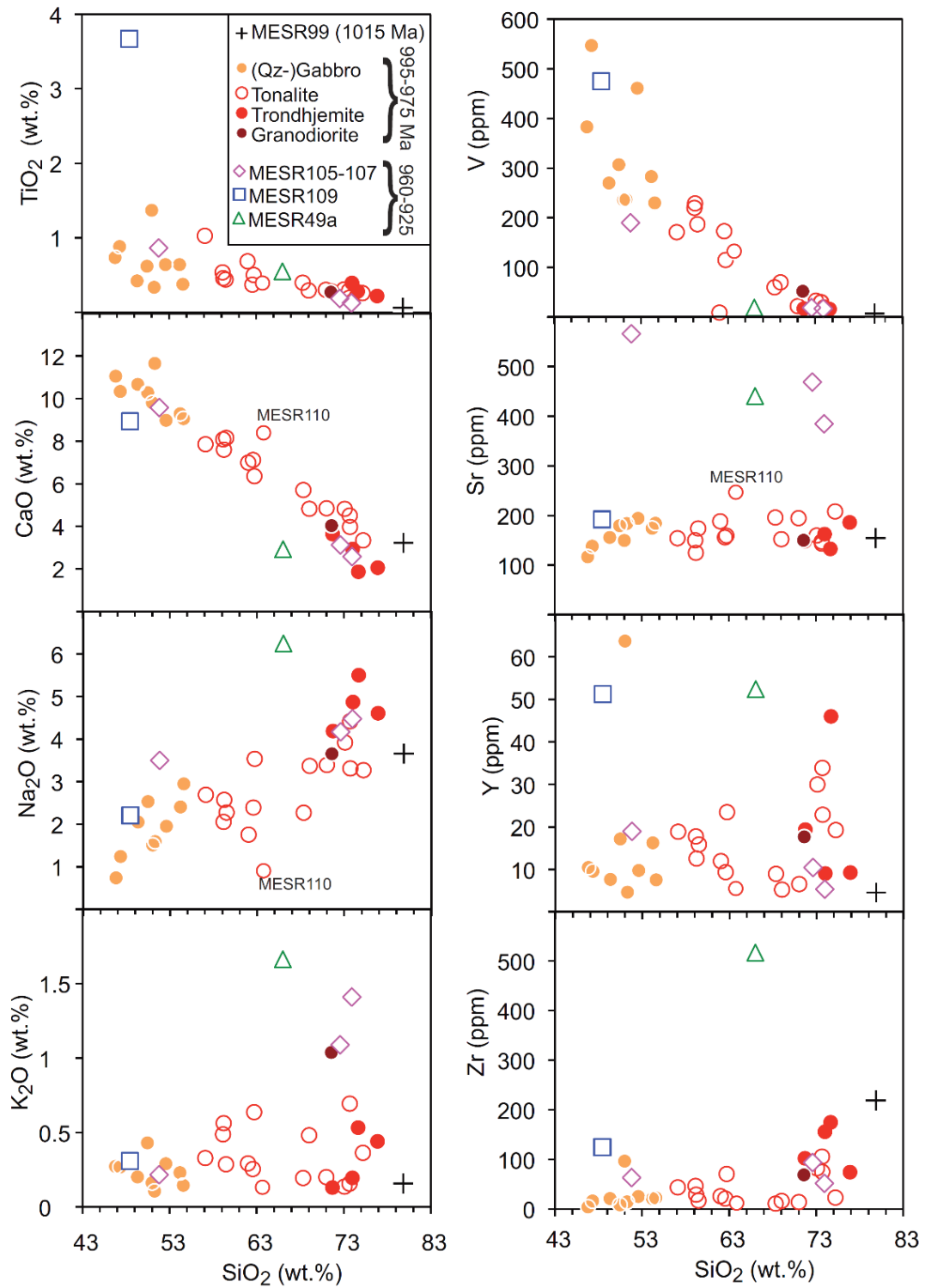


Figure 9.7: Harker variation diagrams for selected oxides and elements. Legend is given in the figure.



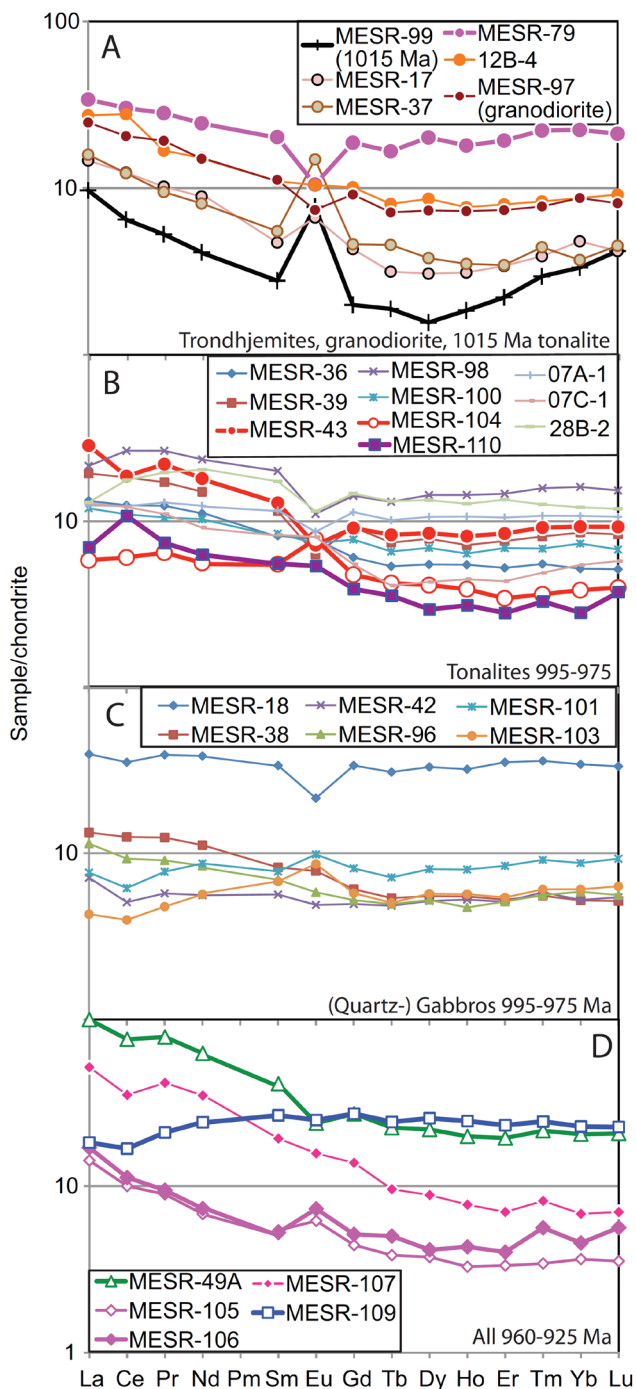


Figure 9.8: CI-normalised Rare Earth Element diagrams. Normalising values from Evensen et al. (1978). Dated samples given in bold lines. A) Patterns for the 995–975 Ma trondhjemites, granodiorite and the one older, high-SiO<sub>2</sub> tonalite MESR99. B) Patterns for the 995–975 Ma tonalites. C) Gabbroic samples assumed to belong to the 995–975 Ma age group. D) Mafic and felsic samples 960–925 Ma.



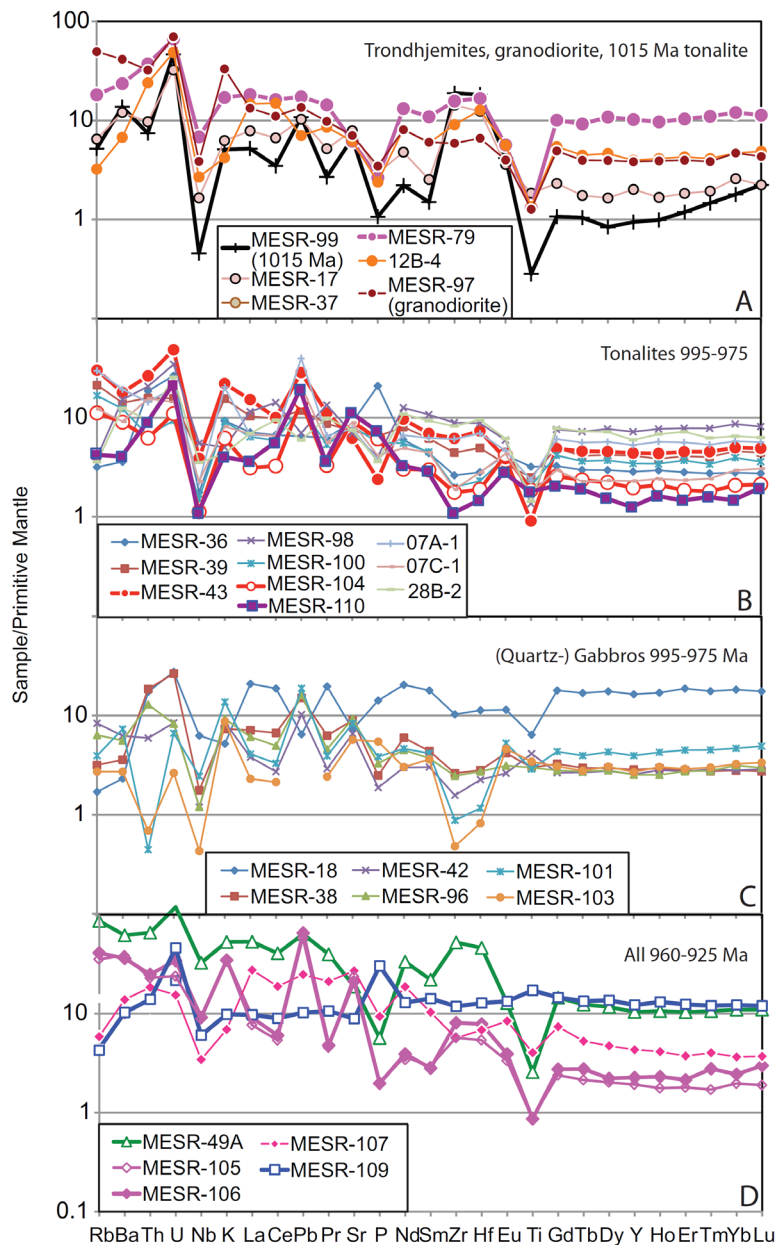


Figure 9.9: Primitive mantle-normalised trace element patterns. Normalising values from Palme and O'Neill (2003). Legend and panels as for Figure 9.8.

The one sample that gave a marginally older age at ca. 1015 Ma has the highest  $\text{SiO}_2$  content, and lies on the extension of the trend for the 995–975 Ma age group for most variation diagrams. Its REE pattern shows MREE depletion and a very pronounced positive Eu-anomaly ( $\text{Eu}/\text{Eu}^* = 3.3$ ), but is not too dissimilar to that of some of the trondhjemitic samples (Figure 9.8A). Of the younger (960–925 Ma) samples, MESR105–107 as well as MESR49a stand out with respect to their high Sr, and for the felsic samples also high  $\text{K}_2\text{O}$ , Rb and Ba concentrations. Additionally MESR49a also has high Zr, Y, Nb, Ga and REE concentrations compared to the 995–975 age group. The qz-gabbro from Causinknappen, MESR109, has very high  $\text{TiO}_2$  (and  $\text{P}_2\text{O}_5$ ) contents, and is the only sample to show LREE depletion. Most samples, apart from some of the most felsic ones, are metaluminous (Figure 9.10). They classify as calcic in the modified alkali-lime diagram of Frost et al. (2001), apart from MESR49a, which is alkali-calcic and MESR109 which comes up as marginally calc-alkalic.



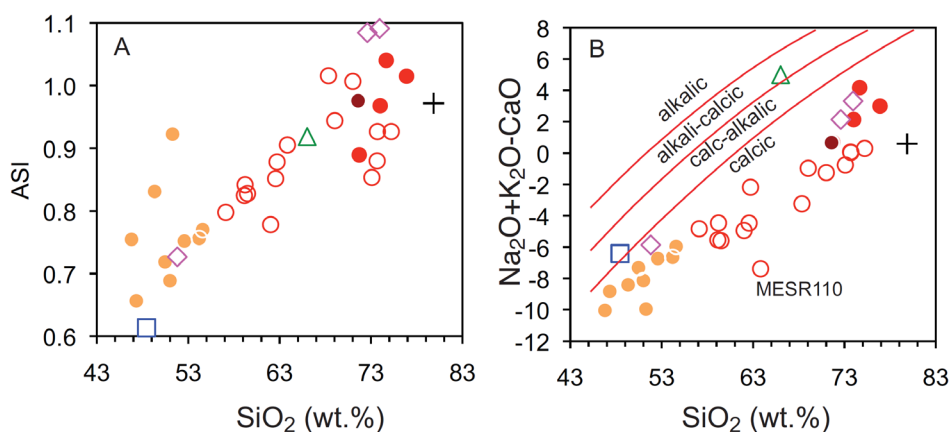


Figure 9.10: Classification diagrams. A) Aluminium-saturation index ( $ASI = \text{molar } Al_2O_3 / (Na_2O + K_2O + Na_2O)$ ) versus  $SiO_2$ . B) Modified alkali-lime diagram (Frost et al., 2001). Most data classifies as being calcic, with MESR49a being a notable exception.

### 9.7.2 Sr and Nd Isotopic Systems

Only two samples were analysed for Sr and Nd isotope ratios, since a major body of data on these systems was already presented by Kamei et al. (2013) and Owada et al. (2013). Sr isotopic ratios may be affected by metamorphism, and are therefore less reliable than the Nd isotopic values. The initial  $^{87}Sr/^{86}Sr$  ratios are around 0.7033 for both MESR106 and MESR43 (Table 9.2), which is more or less the value for the Bulk Earth at that time. The  $^{143}Nd/^{144}Nd$  ratios are, however, decidedly superchondritic (initial  $\epsilon Nd$  +3 to +4), with a somewhat higher value for MESR106 than for MESR43.

### 9.7.3 Zircon Trace Element Data

Trace element analyses were performed on some of the zircons for which Hf data were obtained in order to compare them to the whole rock analyses and assess whether the latter could represent liquid compositions, or that they are influenced by cumulate or alteration processes. Since the analyses were quite homogeneous only average data are shown and discussed.

The chondrite-normalised REE patterns (Figure 9.11A) show the features expected for zircon, with very low LREE/HREE ratios and a positive Ce-anomaly. There is slightly less than an order of magnitude variation in the absolute concentration of the REE between the samples, with MESR43 having the lowest, and MESR79 the highest concentrations. Most samples display negative Eu-anomalies, but these are much reduced for MESR106 and MESR104, which both show positive Eu-anomalies in their whole rock REE pattern too. MESR99, which has a very noticeable positive Eu-anomaly in its whole rock REE pattern, shows a clear negative anomaly in its zircon REE pattern.

When the zircon REE-patterns are normalised over the whole rock patterns (Figure 9.11B), the results can be interpreted to represent the zircon/liquid distribution coefficient (K<sub>d</sub>), provided the whole rock compositions represent liquid compositions. All samples have a steeply sloping K<sub>d</sub> pattern, with positive Ce- and negative Eu-anomalies, as is expected from zircon's crystal structure (Belousova et al., 2002). MESR99 displays the strongest Eu-anomaly in its K<sub>d</sub> pattern, being as low as 0.04. This lies outside the range found experimentally for varying conditions of temperature and oxygen fugacity (Trail et al., 2012), and outside the trend seen for the other samples (Figure 9.11B inset).



Table 9.2: Representative whole rock analyses.

Sample name	MESR43 Widerøefjellet C	MESR49A Lågkollane	MESR79 Bamseungen	MESR99 Widerøefjellet E	MESR104 Nils Larsenfjellet W	MESR106 Widerøefjellet SE	MESR109 Causinknappen	MESR110 Causinknappen
SiO <sub>2</sub>	73.70	66.01	74.66	79.85	68.34	72.59	48.43	63.77
TiO <sub>2</sub>	0.19	0.55	0.28	0.06	0.40	0.19	3.67	0.39
Al <sub>2</sub> O <sub>3</sub>	12.43	15.97	13.54	11.70	14.54	14.87	12.39	15.30
Fe <sub>2</sub> O <sub>3</sub> *	3.57	4.61	2.85	0.85	6.25	2.22	17.18	7.67
MnO	0.08	0.11	0.03	0.02	0.15	0.05	0.27	0.16
MgO	0.51	0.73	0.83	0.22	1.26	0.58	4.80	1.84
CaO	3.97	2.92	1.86	3.22	5.71	3.12	8.93	8.41
Na <sub>2</sub> O	3.31	6.25	5.50	3.66	2.27	4.17	2.21	0.90
K <sub>2</sub> O	0.69	1.66	0.53	0.16	0.20	1.09	0.31	0.13
P <sub>2</sub> O <sub>5</sub>	0.05	0.11	0.05	0.02	0.12	0.04	0.60	0.15
LOI	1.05	0.45	1.59	0.73	1.36	1.18	0.36	0.31
Sum	98.59	99.14	100.22	99.83	99.29	99.02	99.33	98.81
Sc	11	9	9	5	17	4	46	27
V	30	19	16	7	60	19	475	132
Zn	45	83	26	7	62	34	128	70
Ga	12	24	17	10	15	15	25	13
LA-ICPMS								
Rb	18.3	52.3	11.0	3.1	6.8	24.9	2.7	2.6
Sr	126	381	125	134	186	433	181	231
Y	19.3	45.6	44.6	4.1	8.6	9.9	53.4	5.5
Zr	66.9	567	169.2	203.5	19.1	87.4	128.1	11.9
Nb	2.3	19.6	4.1	0.3	0.7	5.5	3.6	0.7
Cs	1.0	1.9	0.5	0.2	0.3	0.5	0.1	0.2
Ba	121.6	418.7	158.7	92.3	61.0	244.2	69.4	27.7
La	10.5	36.6	12.5	3.6	2.1	6.2	6.7	2.5
Ce	17.9	72.8	29.0	6.2	5.8	10.8	16.1	10.1
Pr	3.0	10.8	3.9	0.7	0.9	1.3	2.9	1.0
Nd	12.9	44.5	17.5	2.9	4.0	5.2	17.2	4.4
Sm	3.0	9.5	4.7	0.6	1.3	1.2	6.1	1.3
Eu	0.63	2.08	0.92	0.67	0.68	0.64	2.17	0.46
Gd	2.79	8.30	5.74	0.61	1.47	1.57	8.32	1.18
Tb	0.48	1.30	0.97	0.11	0.25	0.29	1.41	0.20
Dy	3.24	8.33	7.68	0.60	1.58	1.58	9.73	1.10
Ho	0.69	1.69	1.54	0.16	0.33	0.37	2.09	0.26
Er	2.11	4.84	4.81	0.55	0.86	1.00	5.77	0.69
Tm	0.33	0.77	0.79	0.11	0.13	0.20	0.87	0.12
Yb	2.31	5.08	5.55	0.83	0.96	1.13	5.65	0.69
Lu	0.35	0.79	0.81	0.16	0.15	0.21	0.86	0.14
Hf	2.21	13.88	5.01	5.47	0.57	2.36	3.84	0.44
Ta	0.19	1.09	0.32	0.04	0.05	0.63	0.31	0.08
Pb	8.22	13.42	3.72	4.79	1.76	15.13	1.89	4.56
Th	2.21	5.51	3.11	0.62	0.52	2.08	1.16	0.76
U	1.06	2.61	1.45	1.01	0.24	0.75	1.00	0.47
<sup>87</sup> Sr/ <sup>86</sup> Sr	0.708200					0.705215		
2se	0.000012					0.000012		
<sup>87</sup> Rb/ <sup>86</sup> Sr	0.3489					0.1289		
<sup>87</sup> Sr/ <sup>86</sup> Sr <sub>i</sub>	0.703256					0.703452		
εSr <sub>i</sub>	-1.25					0.97		
<sup>143</sup> Nd/ <sup>144</sup> Nd	0.512412					0.512588		
2se	0.000009					0.000012		
<sup>147</sup> Sm/ <sup>144</sup> Nd	0.1364					0.1577		
<sup>143</sup> Nd/ <sup>144</sup> Nd <sub>i</sub>	0.511525					0.511598		
εNd <sub>i</sub>	3.24					3.81		

LOI, loss on ignition; Fe<sub>2</sub>O<sub>3</sub>\*, all Fe as Fe<sub>2</sub>O<sub>3</sub>.

The positive Eu-anomaly of the whole rock pattern for MESR99 is therefore highly likely to be an accumulative feature. The whole rock patterns for MESR106 and MESR104, with their positive Eu-anomaly, might be a reflection on the liquid composition, since their Kd Eu-anomaly is 0.4, and thereby higher than for the samples without a WR positive Eu-anomaly, and within the experimentally determined range.

Sample MESR43 displays a, potentially metamorphism- or alteration-related, negative Ce-anomaly in its WR REE pattern. The value for the Ce-anomaly in the zircon/WR REE pattern is 5.7, and thereby lower than those for MESR99 or 79, and within the range of experimentally determined values. The question whether this WR Ce-anomaly is a primary feature can therefore not be answered unambiguously, but we think it is related to metamorphism and/or alteration.

Apart from REE, the zircons analysed also contain quantifiable amounts of Th and Nb. High Th/Nb ratios are a feature of subduction-related magmas, and the WR analyses show quite a range of Th/Nb ratios (Figure 9.9). Zircon Th/Nb ratios also vary strongly, with a more systematic variation of Nb than Th on a per-sample basis (Figure 9.12). There is a broad correlation between Nb contents of the zircons and of the whole rock, in that the sample with



the highest WR Nb contents (MESR49a) also has the higher zircon Nb concentrations and lower Th/Nb ratios than, for instance MESR104 with low Nb concentrations and high Th/Nb ratios for both zircon and whole rock. The exception is again MESR99, which has very high WR Th/Nb ratios, and the lowest Nb concentrations, whereas the zircon data are similar to those for MESR79. Calculated zircon/WR ratios for MESR99 are 43 for Nb and 1290 for Th, whereas literature values are 0.3–27 and 11–69 respectively (Nardi et al., 2013). So this confirms the non-liquid composition of the WR sample, as already deduced from the REE patterns. The Nb zircon data for the other samples appears to be compatible with a cogenetic crystal-liquid relationship between zircon and whole rock, since calculated zircon/WR ratios for Nb are 0.5–4.4, while the results for Th are less convincing, with an apparent average Kd of 27–630.

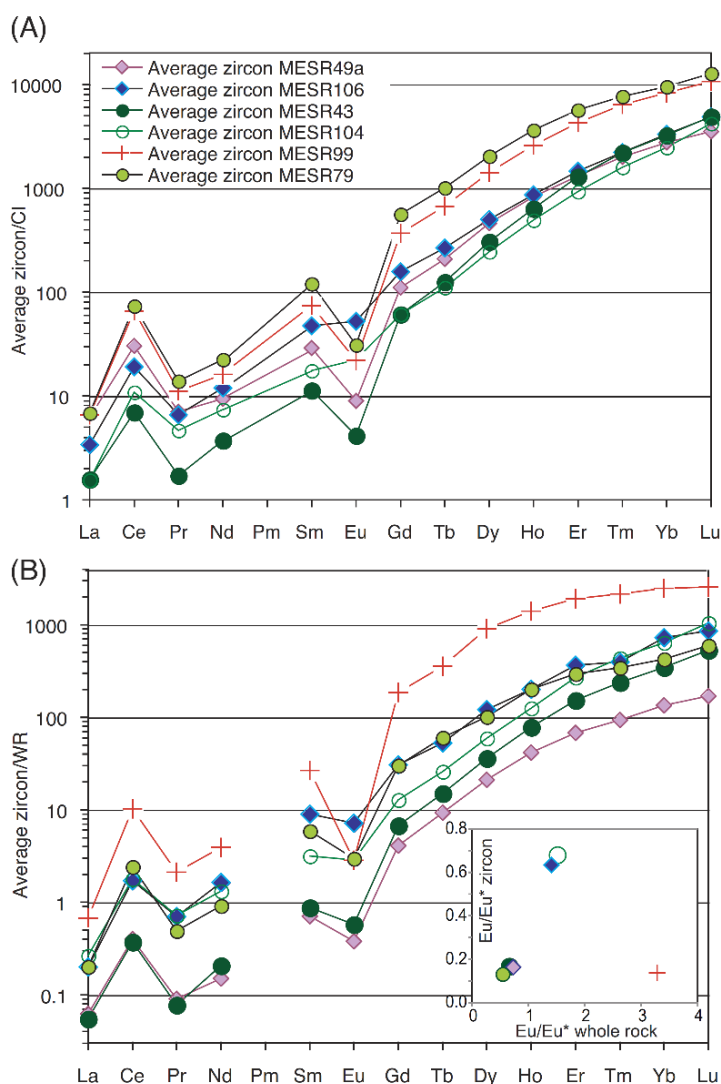


Figure 9.11: Zircon trace element data, averaged per sample. A) Chondrite-normalised REE patterns for average zircons from the different sample, showing the positive Ce- and negative Eu-anomalies expected from the zircon's crystal chemistry. Samples MESR104 and 106 display a reduced negative Eu-anomaly compared to the other samples. B) Whole rock-normalised zircon REE patterns. The very low zircon/whole rock Eu ratio for MESR99 indicates that the whole rock composition is unlikely to represent a liquid. Samples MESR104 and 106 have a Eu-anomaly within the range expected for zircon/liquid distribution coefficients, indicating that the positive Eu-anomaly in the whole rock samples is unlikely to be a cumulate effect.



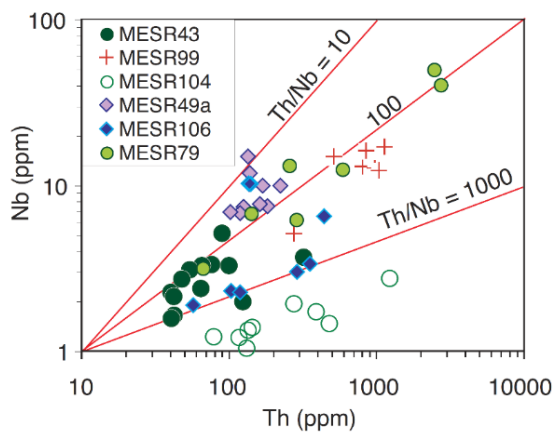


Figure 9.12: Nb versus Th concentrations for zircons. Note log scale on both axes. Although not highly systematic, there is a relationship between whole rock and zircon data, with sample MESR104 also showing a pronounced negative Nb anomaly for the whole rock, whereas this anomaly is very much reduced for MESR49a.

## 9.8 Discussion

### 9.8.1 U-Pb Zircon Age Groups

Our U–Pb zircon dating shows that the majority of samples have an igneous crystallisation age between 975 and 995 Ma, independent of the analytical technique used for dating (SHRIMP or LA-MC-ICPMS); these ages are similar to, but slightly younger than those reported by Kamei et al. (2013) and Owada et al. (2013) for the main group of (tholeiitic/low-Ti) meta-igneous rocks (998–995 Ma).

Our three younger ages of  $957 \pm 8$ ,  $947 \pm 8$  and  $929 \pm 14$  Ma are similar to up to marginally higher than the SHRIMP dates reported previously. Shiraishi et al. (2008) obtained an igneous age of  $920 \pm 8$  Ma for a metatonalite sample from Mefjell, and this age could correspond to the one obtained for our more mafic sample MESR109. Kamei et al. (2013) dated three (CA, high-Sr) samples at 945–930 Ma, while Owada et al. (2013) obtained a single zircon from a high-Ti mafic dyke with an age of  $945 \pm 9$  Ma. An igneous age of  $951 \pm 17$  Ma, so within the time frame of our analyses, has been reported by Shiraishi et al. (2008) for an enderbitic gneiss from northern Brattnipene; this is located north of the Main Shear Zone, but still south of the Main Tectonic Boundary (Figure 9.1), and is thus part of the SW terrane. The slightly older ages from sample MESR106 at 1070–1060 Ma are likely to represent inherited zircons. A similar age of  $1048 \pm 12$  Ma was reported by Osanai et al. (2013) for garnet-biotite gneiss from Mefjell South, within the SW-terrane. The ca. 3 Ga single zircons in MESR106 and MESR109 are quite remarkable. Although laboratory cross-contamination can never be completely excluded, no rocks of a similar age were treated in the laboratory at the same time. Also, old ages are not completely unknown from the Sør Rondane Mountains, but only north of the Main Tectonic boundary: Shiraishi et al. (2008) reports a single ca. 3260 Ma grain within a paragneiss from northern Austkampane while Pasteels and Michot (1968) report zircon fractions from granitoids to the SW of Austkampane that yielded an ca. 2700 Ma upper intercept. Within the broader Antarctic context, igneous activity around 2990 Ma has been reported in the Napier Craton (Kelly and Harley, 2005) and similar ages also exist in the Ruker Complex (see overview in Liu et al., 2013). Whether it is statistically relevant that we only found Archaean zircons in the younger intrusions is unclear.

One of our samples, MESR99, yielded an older age of  $1015 \pm 4$  Ma. Four zircons from a nearby sample, 12B4, give a similar upper intercept age. Similar, inherited U–Pb zircon ages of 1014



$\pm 15$  and  $1009 \pm 13$  Ma have been reported by Shiraishi et al. (2008) from gneiss samples in the NE terrane (Perlebandet and Utnibba), while Osanai et al. (2013) report inherited ages of 1030–1040 Ma from Bamseungen within the meta-igneous sector of the SW terrane.

The ages presented here strengthen the connection between the SW- and NE-terrane of Sør Rondane. The two areas show different P–T–t paths related to the amalgamation of Gondwana, and were also thought to differ in the maximum age of inherited zircon, with ages older than 1100 Ma previously unreported for the SW terrane (Osanai et al., 2013). If we accept the validity of the two ca. 3 Ga inherited zircons presented here, then this distinction has ceased to exist. However, 900–1000 Ma ages are noticeably scarcer in the NE- than the SW-terrane (Shiraishi et al., 2008; Osanai et al., 2013), which could be related to the difference in crustal level between the two terranes, as the NE-terrane is dominated by metasedimentary rocks.

Our ages, together with those published previously, reinforce the idea that Meso-Neoproterozoic magmatism in the Sør Rondane Mountains occurred significantly later than in Central and Western Dronning Maud Land where it has been dated at 1130–1060 Ma (Jacobs et al., 1998; 2003c), similar to ages found in the South African Natal Belt (McCourt et al., 2006). The area furthest west from Sør Rondane in Antarctica where 900–1000 Ma (Sm–Nd isochron) ages are found is the Schirmacher Hills (Rao et al., 2000; Ravikant, 2006), although these are interpreted to reflect metamorphism, rather than a magmatic event. Towards the east, there is a scarcity of data for the Yamato-Belgica complex, but Shiraishi et al. (1994) present a U–Pb zircon protolith age of ca. 1000 Ma. From the Lützow-Holm to the Rayner Complex ca. 1000 Ma ages are quite common (Shiraishi et al., 2008; Liu et al., 2013), e.g. in the Cape Hinode metatrandhjemites ( $1017 \pm 13$  Ma, Shiraishi et al., 2008) and Mawson Coast charnockites (Halpin et al., 2012). This is most widely interpreted as reflecting a connection between this part of Antarctica and Sri Lanka–India–Madagascar prior to Gondwana amalgamation (e.g. Boger et al., 2014). In this reconstruction, the Vijayan Complex of Sri Lanka would be closest to Sør Rondane, and ages of 900–1100 Ma are indeed found there (Kröner et al., 2013).

## 9.8.2 Comparative Geochemistry

In the following section we compare our data to those published by others to interpret the likely tectonic setting in which the magmas were generated and their similarity to similarly-aged (meta-) igneous rocks within Sør Rondane, neighbouring areas in Antarctica (central Dronning Maud Land and Schirmacher Hills; Mikhalsky and Jacobs, 2004; Rao et al., 2000; Ravikant, 2006) and the Vijayan Complex in Sri Lanka (Milisenda et al., 1994; Kröner et al., 2013). Connections between the Sør Rondane Mountains, the Namuno block of Mozambique and the Central Highlands Complex of Sri Lanka have been proposed by Grantham et al. (2008), based on the available geochronological and structural data. The SHRIMP U–Pb zircon ages for a charnockite from the Ocuca and a tonalitic gneiss from the Marupa complex in Mozambique of  $994 \pm 61$  and  $951 \pm 44$  Ma respectively (Grantham et al., 2008) are indeed similar to the ages reported here, but no geochemical data are available to further investigate the connection.

### **Relationships within SW-terrane Sør Rondane: tectonic interpretation**

The one sample (MESR99) that gave the older, ca. 1015 Ma, age is more SiO<sub>2</sub>-rich than any of the other samples. The homogeneity of the age and Hf isotopic composition of the zircons composition demonstrates that it is an igneous rock. However, its whole rock composition is



unlikely to represent a liquid composition, as indicated by the zircon/whole rock trace element ratios, which do not fall within the range for published distribution coefficients. The sample is very rich in quartz and plagioclase (partially replaced by epidote), and has unusually high zirconium and hafnium concentrations compared to its REE contents; we therefore interpret it to be a felsic cumulate or crystal-rich tuff. Considering the similarity in zircon Hf isotope ratios and trace element contents to some of the 995–975 Ma samples, its parental magma must have shown a strong geochemical resemblance to the magmas of this age group, and we will therefore consider it together with these samples. Because of its aberrant whole rock composition and unknown age, qz-gabbro MESR18 may not belong to this group. Although the ca. 980 Ma age of Causinknappen tonalite MESR110 falls into the 995–975 Ma age group, its geochemical (low sodium, high calcium) and isotopic characteristics (lower Hf isotopic composition) are aberrant; this could be related to its position further south than the other samples. It lies close to an inferred shear zone (Figure 9.1A), and the boundary with the SE Dronning Maud Land Province of Mieth et al. (2014).

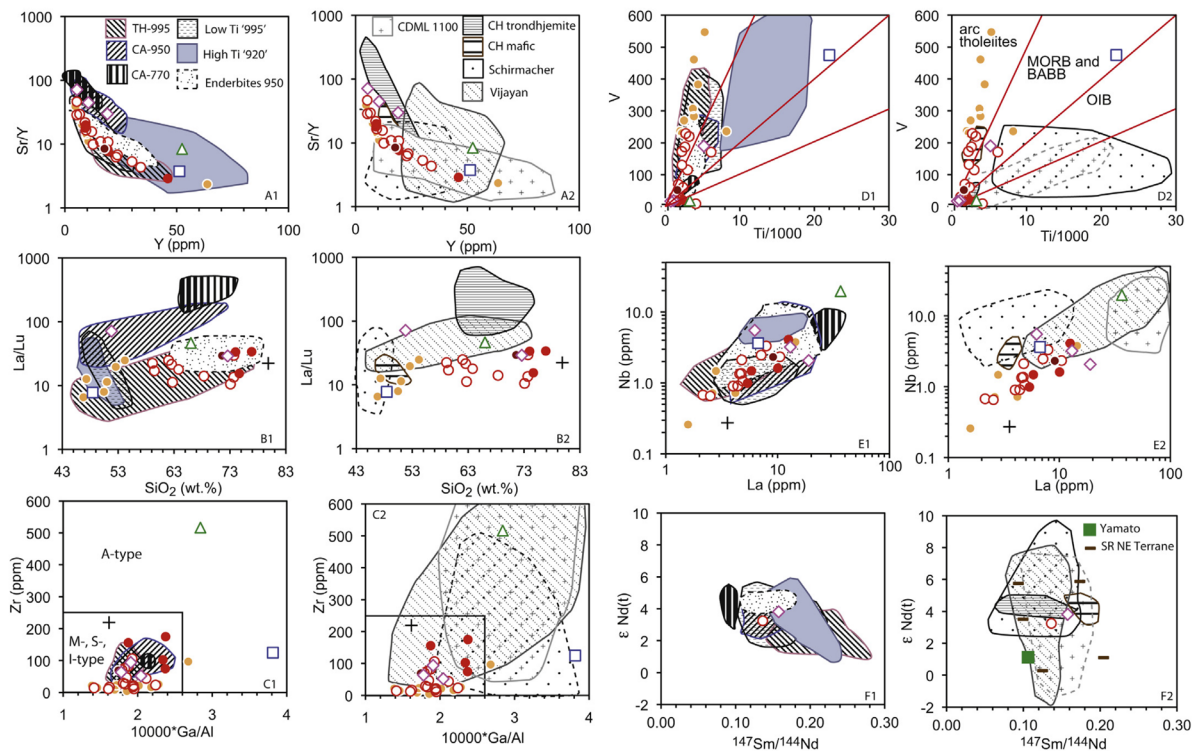


Figure 9.13: Comparison between samples analysed in the present study and published data; symbols as in Figure 9.7 and given in diagram. Panels on left show data from the SW-terrane of Sør Rondane: ca. 995 Ma tholeiites, 920–945 and ca. 770 Ma calc-alkaline: Kamei et al. (2013); low-Ti enclaves (ca. 995 Ma) and high-Ti dykes (ca. 920 Ma): Owada et al. (2013); ca. 950 Ma enderbites: Shiraishi and Kagami (1992). Panels on right show data from the broader region: Central Dronning Maud Land: Jacobs et al. (1998), Mikhailsky and Jacobs (2004); Cape Hinode trondhjemite: Ikeda et al. (1997); Cape Hinode mafics: Suda et al. (2008); Schirmacher Hills: Rao et al. (2000), Ravikant et al. (2007); Vijayan Complex, Sri Lanka: Milisenda et al. (1994), Kröner et al. (2013). A) Sr/Y versus Y (note log scale for y-axis); B) La/Lu (log scale) versus SiO<sub>2</sub>; C) Zr versus 10,000 × Ga/Al with fields for different granite types from Whalen et al. (1987); D) V versus Ti/1000 with fields for different types of basalts from Shervais (1982); E) Nb versus La (double log scale); F) initial εNd value versus <sup>147</sup>Sm/<sup>144</sup>Nd, with additional data from Shiraishi et al. (2008) for Yamato Mts, and Grew et al. (1992) for NE-terrane gneisses.



Our samples that are interpreted to belong to the main 995–975 Ma age group have low  $\text{TiO}_2$  (<0.6 wt.%), Sr (<200 ppm) and Zr (<200 ppm) concentrations. They have flat to slightly LREE-enriched rare earth element patterns (at CI-normalised values between 40 and 4), and their zircons show an average  $\epsilon\text{Hf}$  of 6.3–7.3. They closely resemble the ‘main lithotype’ (tholeiitic biotite-hornblende metatonalite and associated enclaves) of Kamei et al. (2013) and the low-Ti microgabbros of Owada et al. (2013) in terms of Sr/Y, La/Lu, Ga/Al, V/Ti ratios and initial epsilon Nd ratios (Figure 9.13), but also the ca. 950 Ma enderbritic gneisses from the Brattnipene area, north of the Main Shear Zone (Shiraishi and Kagami, 1992).

In common with Kamei et al. (2013) and Owada et al. (2013), we interpret the samples from this age group to have formed in an oceanic arc environment. All the hallmarks for a subduction setting are present in the normalised trace element diagrams: negative Nb anomalies, positive Sr anomalies in the gabbros and enrichment in REE relative to Zr and Hf. The interpretation of an oceanic rather than continental arc is based on the flat REE patterns for the gabbros and the low absolute concentrations of incompatible trace elements. In this respect, our samples resemble data for e.g. the mid-crustal section of the Jurassic Talkeetna oceanic arc (Greene et al., 2006). There is a strong chemical coherence between the mafic, intermediate and felsic samples which is interpreted as a cogenetic relationship. The dominance of intermediate samples (tonalites) is typical for arc terranes (e.g. Reubi and Blundy, 2009). The occurrence of the (quartz-)gabbros as enclaves within the more felsic intrusives, and the crenulated margins on these enclaves (Figure 9.C), implies that both were (partially) liquid at the same time, and it is therefore likely that the intermediate to felsic magmas were derived from the more mafic magmas by crystal fractionation. The presence of a small positive Eu-anomaly in some samples, of which the zircon trace element data show that it is likely to be a feature of the magmatic liquid could be related to the fractionation sequence being dominated by amphibole rather than plagioclase; this is in line with the concave REE patterns for the felsic samples, and the fairly constant Sr concentrations with increasing  $\text{SiO}_2$  content. In the less fractionated (quartz-)gabbro samples, it could be a result from preferential mobilisation of divalent Eu during dehydration of the slab in the sub-arc mantle (Bau and Knittel, 1993).

Our samples that have been dated as at 960–925 Ma have variable geochemical characteristics and do not form a coherent group. They are enriched in Sr compared to the older group (leading to higher Sr/Y ratios), and can have high  $\text{TiO}_2$  and  $\text{P}_2\text{O}_5$  contents (MESR109) or high Zr concentrations (MESR49a). REE patterns vary from LREE depleted (MESR109) to LREE-enriched (MESR107). The Nd and Hf isotopic characteristics are marginally more depleted (i.e. higher values) than for the older age group. These characteristics indicate that high-Sr samples MESR105–107 are most closely related to the 920–950 Ma calc-alkaline group of Kamei et al. (2013), while high-Ti sample MESR109 resembles the ca. 950 Ma high-Ti dykes of Owada et al. (2013). Sample MESR49a has uniquely high Nb and Zr concentrations, but could potentially be related to the high-Ti clan of rocks by fractionation processes.

Considering the geochemical variety of magmas present between 960 and 925 Ma, the interpretation of the tectonic setting is more difficult. Kamei et al. (2013) interpreted their calc-alkaline series as adakites, based on the Sr/Y ratios, reflecting slab melting; Owada et al. (2013) suggested a back-arc environment based on the V versus Ti diagram for his high-Ti dykes. The evidence for an adakitic signature in the felsic samples of this time period is not as strong as for the Cape Hinode metatondhjemites (Ikeda et al., 1997), which have a much higher La/Lu and



Sr/Y ratios (Figure 9.13A and B), but a geochemical shift is nevertheless noticeable, also towards slightly more depleted isotopic characteristics. The high-Ti samples are characterised by LREE-depleted patterns and low La/Nb ratios (Figure 9.13E), atypical for arc-related magmatism, and also have Ti–V characteristics more typical for Mid-Ocean Ridge (MORB) or Back-Arc Basin Basalt (BABB) than for arc-related magmas (Figure 9.13D). However, samples with HFSE enrichments compared to ‘classical’ arc rocks are found both in back-arc basins (Sinton et al., 2003; Sorbadere et al., 2013) and arc settings (Gazel et al., 2011; Kratzmann et al., 2009; Kuritani, 2001; Peate et al., 1997; Sorbadere et al., 2013). In both environments, the geochemical signature can be explained by a small contribution from the subducted slab and a more important role for adiabatic melting of asthenospheric mantle compared to typical arc settings, where melting is mainly induced by a hydrous flux from the slab. Since the degree of melting is smaller than for flux-melting, or for the more extensive adiabatic upwelling at Mid-Ocean Ridges, fluid-immobile incompatible trace elements are more enriched than in either arc or MOR magmas. In an arc setting, this type of high-HFSE magma is typically found when there are heterogeneities within the subducting slab, such as a ridge (Kratzmann et al., 2009; Peate et al., 1997), a seamount chain (Peate et al., 1997) or a hotspot track (Gazel et al., 2011), which can lead to slab tear or break-off, and enhanced mantle upwelling compared to a classical subduction situation. This is also an environment in which adakites can form (Yogodzinski et al., 2001).

The fact that this diverse group of magmas intruded after the typical arc-type magmas at 995–975 Ma indicates that a profound change in tectonic regime has occurred. This is most likely the end of a real subduction scenario, either due to collision with a microcontinent or oceanic plateau, or slab break-off. A limited number of samples with similar geochemical characteristics to the 960–925 Ma adakite-like materials was dated at ca. 770 Ma by Kamei et al. (2013). Whether this reflects resumption of subduction or reworking of pre-existing crust is not clear; the isotopic data permit either interpretation.

### **Relationships within wider Antarctica and Gondwana**

Comparing the geochemistry of 900–1200 Ma samples from different areas in Antarctica, and the Vijayan Complex of Sri Lanka, to those from the SW-terrane of Sør Rondane, there are some clear differences and similarities.

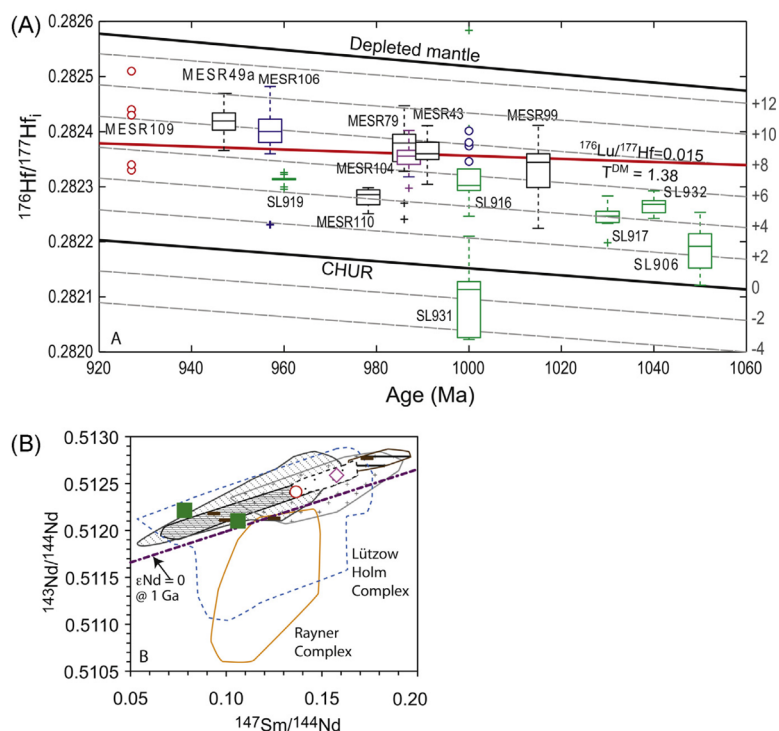
The biotite- and pyroxene-bearing gneisses from the NE-terrane analysed by (Grew et al., 1992) for Nd isotopes, and the one gneiss sample from the Yamato Mountains (Shiraishi et al., 2008) extend to marginally lower initial ratios (Figure 9.13F); however, major and trace element characteristics were not given, apart from Sm and Nd concentrations, which are similar to the 960–925 Ma samples from the SW-terrane.

The mafic and felsic samples from Cape Hinode (Ikeda et al., 1997; Suda et al., 2008) are very similar in terms of Nd isotopes to the meta-igneous samples from the SW-terrane. The felsic samples are slightly more typically trondhjemitic in trace element composition, as described before. The mafic samples are similar to the (quartz-)gabbros.

The orthogneisses from Central Dronning Maud Land (Jacobs et al., 1998; Mikhalsky and Jacobs, 2004) overlap with, but extend to lower values for initial Nd isotopic ratios, similar to the gneisses from the NE-terrane. However, they are geochemically very different, and have much higher contents of (relatively immobile) incompatible elements, such as the REE, Zr, Th



and Nb (Figure 9.13A, C and E). Similarly, the granulites from Schirmacher Hills show a clear overlap in Nd isotopes (Rao et al., 2000; Ravikant, 2006), but Ti, Nb and Zr contents are significantly enriched. The granitoid gneisses of the Vijayan Complex (Sri Lanka) largely overlap with the gneisses from Central Dronning Maud Land, rather than with our Sør Rondane samples, in geochemistry and isotopic composition. The Hf isotopic composition of the Vijayan zircons is also typically lower than that of the Sør Rondane samples (Figure 9.14A). Although



our sample MESR49a shows similarly enriched trace element characteristics to CDML, Schimacher and Vijayan, it distinguishes itself with its depleted Hf isotopic signature for the zircons (Figure 9.14A).

Figure 9.14: A) As Figure 9.6, but with data for the Vijayan Complex of Sri Lanka (SL sample numbers) from Kröner et al. (2013). B) Present-day  $^{143}\text{Nd}/^{144}\text{Nd}$  versus  $^{147}\text{Sm}/^{144}\text{Nd}$ ; data sources and symbols as for Figure 9.13, with additional data from the compilation by Shiraishi et al. (2008). Reference line for  $\epsilon_{\text{Nd}} = 0$  at 1000 Ma shown for comparison. Data for the Lützow-Holm and Rayner Complex extend to far lower  $^{143}\text{Nd}/^{144}\text{Nd}$  ratios than the Sør Rondane samples, indicative of an old crustal component in their source.

So the meta-igneous sector of the SW-terranes compares poorly to the Central Dronning Maud Land orthogneisses in both age (younger) and geochemical composition (more depleted). Despite the overlapping ages and Nd isotopic composition, the samples from Schirmacher Hills do not match in geochemical composition, while the Vijayan complex is both marginally older (up to 1100 Ma), and more enriched in Nd and Hf isotopic signature as well as trace element composition. A reasonably good match exists with the mafics and metatrandhjemites from Cape Hinode, although the latter are ca. 1015 Ma rather than <960 Ma for the Sør Rondane samples that most closely match them in geochemical composition. Not only this age difference is problematic in proposing a match between the two areas, but also the fact that samples from the Lützow-Holm Complex that lie geographically between Cape Hinode and Sør Rondane have Nd isotopic compositions that point towards a more significant role for crustal reworking (Shiraishi et al., 2008; Figure 8.14B) – and the presence of the Main Tectonic Boundary, which separates the SW- and NE-terranes. Rocks from the Rayner Complex (Figure 9.1A), where ca. 900–1000 Ma ages are common too (Boger et al., 2000; Corvino et al., 2008; Mikhalsky and



Sheraton, 2011; Grew et al., 1992; Halpin et al., 2012) extend to even more isotopically enriched values (Figure 9.14B), reflecting a much longer crustal prehistory.

### 9.8.3 Timeline of Events and Possible Tectonic Scenarios

The data and comparison shown here have implications for both the Rodinia and Gondwana supercontinents. The disparity in igneous ages between Central Dronning Maud Land and Sør Rondane clearly shows that the latter was more closely related to the Indo-Antarctic Craton (Sri Lanka–India–Madagascar) whereas the former shows strong ties with the Kalahari Craton, being a close match to the South African Natal Belt.

Our data confirms that the meta-igneous sector of the SW-terrane was formed in an oceanic arc setting around 995–975 Ma, and we interpret the signature of the younger rocks to reflect stalling subduction from 950 Ma onwards. No deformation or metamorphism has been recognised in the area around this time, so the halting of the subduction process may be a far-field effect of a collision elsewhere. The dimensions of the meta-igneous sector of the tonalite terrane are more in keeping with either N- or S-dipping subduction in present-day coordinates (rather than E or W), but we have no constraints on the vergence. The rare occurrence of Archaean inherited zircons within the <960 Ma intrusives suggests the proximity to an older craton, which may have been the collider that halted subduction. This could have been part of the aeromagnetically defined Southeast-Dronning Maud Land (SE-DML) Province of Mieth et al. (2014), located directly southwest of the meta-igneous sector. However, it could also be the craton from which the sediments, which are now found in the NE-terrane, have been shed, in which case a more easterly location seems more plausible – although it is unclear what the relative positions of the SW- and NE-terranes were at this stage.

The northern, dominantly supracrustal, sector of the SW-terrane seems related to the meta-igneous terrane in terms of ages and geochemical composition, even though the two sectors are separated by the much younger dextral Main Shear Zone of Pan-African age (Ruppel, 2012). The ca. 770 Ma ages for calc-alkaline magmatism in the SW-terrane reported by Kamei et al. (2013) can be interpreted to reflect resumption of subduction. This age and type of magmatism is also known from Sri Lanka (Wanni Complex, Willbold et al., 2004) and Madagascar (see overview by Boger et al., 2014). However, Central and Western Dronning Maud Land were part of Rodinia (Powell and Pisarevsky, 2002), which was in the process of splitting up around this time, and do not appear to record this phase of magmatism. Zircons with 800–700 Ma ages are also found in Schirmacher Hills (Mikhalsky et al., 2011) and within a metadiorite in the NE-terrane of Sør Rondane (Osanai et al., 2013).

The next event is the 650–600 Ma high-grade metamorphism in Sør Rondane (see overview of geochronology in Osanai et al., 2013), which has also been recognised in the Yamato Mountains (Asami et al., 2005) as well as Schirmacher Hills (Ravikant et al., 2004), but not in the Lützow-Holm area (Asami et al., 2005; Shiraishi et al., 2008). This may point towards a crustal boundary between the Yamato Mountains and Lützow-Holm area, as also proposed on the basis of magnetic anomalies (Osanai et al., 2013). For Sør Rondane, the ca. 600 Ma metamorphic event has been linked to the collision between the SW- and NE-terrane, as the downgoing and overthrust blocks respectively. The Dufekfjellet granite (Li et al., 2006; Figure 8.1) intruded at the same time (ca. 620 Ma) into the SW-terrane, so into the low-grade portion of the downgoing block, which seems somewhat mysterious from a tectonic point of view, unless another block



was being underthrust underneath the SW-terrane from the south. This could then be the SE-DML Province.

The final event is wide-spread intrusion of granitoids and minor syenites (570–510 Ma) in both the SW- and NE-terrane, which were amalgamated at this stage, and associated retrograde metamorphism.

On a larger scale, the juxtaposition of terranes with both ca. 630 and ca. 550 Ma metamorphic ages has also been noted by Boger et al. (2015) for the Vohibory-Androyen and Anosyen domains of SW Madagascar, has been and connected to the events in Antarctica and eastern Africa. Collision between the Vohibory and Androyen terrane was interpreted to have occurred around 630 Ma, so at a similar time to the inferred collision between the NE- and SW-terrane in Sør Rondane. It was followed by collision with the Androyen Terrane, connected to greater India, at ca. 550 Ma. Boger et al. (2015) extend this scenario into Antarctica with the Sør Rondane-Yamato domain (containing ca. 630 Ma ages) colliding with the Lützow-Holm area around 550 Ma during the final amalgamation of Gondwana. Although the Madagascan Vohibory Domain resembles the meta-igneous sector of the SW-terrane of Sør Rondane in being a juvenile oceanic arc terrane, the Vohibory protoliths were formed at 850–700 Ma (Jöns and Schenk, 2008), rather than around 980 Ma. Also, the inferred vergence of the ca. 630 Ma collision in Madagascar is opposite to what has been suggested for the SW- and NE-terrane of Sør Rondane, so a simple one-to-one correlation between SW Madagascar and Sør Rondane does not exist. However, it confirms the idea that Sør Rondane holds an important place in the final amalgamation of Gondwana.

## 9.9 Conclusion

- The meta-igneous sector of the SW-terrane of Sør Rondane was the mid-crustal part of a juvenile oceanic arc terrane around 1020–975 Ma, as indicated by whole rock trace element patterns typical for subduction-related magmas (negative Nb anomalies in mantle-normalised diagrams, positive LREE/HFSE ratios), combined with a high (typically ca. +7) zircon initial epsilon Hf and fairly flat REE patterns. Comparison of zircon and whole rock REE patterns suggest that some of the moderately positive Eu-anomalies may be a feature of the magmatic liquid rather than reflecting cumulate processes.
- Younger igneous samples (960–920 Ma) are more variable: they are either characterised by high Sr/Y ratios ('adakitic' signature) or have a reduced to absent subduction signature in terms of trace element patterns; all have higher zircon Hf isotopic ratios. This is interpreted as signifying the end of subduction, and magmatism related to adiabatic upwelling of subduction-modified or unadulterated depleted mantle, and/or slab melting.
- Rare inherited zircons with Archaean and late Mesoproterozoic ages in the <960 Ma intrusives could indicate increasing proximity to a cratonic area, potentially the fragment that caused subduction to halt.
- Compared to neighbouring areas in Antarctica and in a wider Gondwanan context, the meta-igneous sector of the SW-terrane is unique with respect to the combination of protolith age, geochemical and isotopic signature.



- The 1000–900 Ma ages are younger than those of the classic ‘Grenville’ orogeny (as seen in central and western Dronning Maud Land and the South African Natal Belt) that formed Rodinia, and more similar to ages observed in India–Sri Lanka–Madagascar. This supports the idea that greater India was not part of or was located in a peripheral position to the Rodinian supercontinent (Powell and Pisarevsky, 2002).
- The ca. 630 and 550 Ma metamorphic and igneous history of Sør Rondane documented by other workers reflects the progressive amalgamation of Gondwana, and may be connected to events in SW Madagascar and eastern Africa (Boger et al., 2015).

## 9.10 Acknowledgements

The whole GEA II team would like to thank the helicopter pilots Knut Wagner, Florian Tauber and Jörn Hergenröder of Sky Heli, Germany, for their flying skills, and Alain Hubert, Gigi Johnson-Amin and the whole crew of the Belgian ‘Princess Elisabeth’ Station for their hospitality and support during the field season. The analytical work was funded by grant # 90036 from the South African National Research Foundation to MAE; Carishma Ramchurran and Pat Suthan are thanked for their help with the analytical work at UKZN, and Christel Tinguely, Phil Janney and Petrus Le Roux at UKZN. Siri L. Simonsen and Magnus Kristoffersen helped with the analyses at the University of Oslo. J. Jacobs, N. Lucka and M. Elburg are indebted to BGR for the invitation to participate at the GEA expeditions. J. Jacobs wishes to thank Alfred-Wegener-Institute for Polar and Marine Research (AWI) and M. Elburg International Polar Foundation (IPF) and BELARE for providing polar clothing. The study was partly supported by the Deutsche Forschungsgemeinschaft (Grants LA 1080/9 to A. Läufer, BGR, and LI 745/15 to F. Lisker, Univ. Bremen) in the framework of the priority programme ‘Antarctic Research with comparative investigations in Arctic ice areas’. J. Jacobs work was funded in part by NFR-NARE. The manuscript benefited greatly from reviews by A. Kamei and S. Boger; their considerable efforts have been very much appreciated.



## Chapter 10

# 10. One Hundred Fifty Million Years of Intrusive Activity in the Sør Rondane Mountains (East Antarctica): Implications for Gondwana Assembly

Marlina A. Elburg, Tom Anders, Joachim Jacobs, Andreas Läufer, Antonia Ruppel, Nicole Krohne, Detlef Damaske

### 10.1 Abstract

New U-Pb zircon ages for the younger phase of magmatism in the Sør Rondane Mountains (East Antarctica) are combined with published igneous and metamorphic zircon ages and show evidence for at least four thermal pulses: at 650–600 Ma, 580–550 Ma, ca. 530 Ma, and a magmatic tail between 510 and 500 Ma. No igneous U-Pb ages younger than 500 Ma have been found, in contrast to the situation in central and western Dronning Maud Land. Zircon Lu-Hf isotopic data are best explained as reflecting both crustal reworking and juvenile input, with the latter more obvious during the 580–550 Ma period. The Hf isotopic data, together with the presence of mafic and silica-undersaturated intrusives, argue against purely intracrustal melting as a petrogenetic process. Apart from the observed temporal trend, there is also a geographic trend in Hf isotopic compositions, with lower initial  $\epsilon_{\text{Hf}}$  values toward the northeast. However, the Hf isotopic shifts are gradual and do not show evidence for a dramatic change between the two previously defined metamorphic terranes. This observation, together with the long duration of magmatism, suggests that the Sør Rondane Mountains may be a collage of several different (sub-)terrane that were amalgamated over a longer period of time.

### 10.2 Introduction

The geology of the Sør Rondane Mountains (East Antarctica) has been the focus of intensive research for the past few years, as it was interpreted to be the locus where two orogens - the ca. 660–600 Ma East African-Antarctic Orogen (EAAO; Figure 10.1A) and the later (ca. 560–530 Ma) Kuunga Orogen - crossed (e.g. Satish-Kumar et al., 2008; 2013). This has led to a wealth of new data, especially high-quality U-Pb zircon age data, with a strong focus on the metamorphic history of the area. With this contribution, we want to emphasize the magmatic development during these orogenic periods in terms of not only ages and their relationship to deformational events but also the Hf isotopic composition of the dated zircons. For this, we obtained U-Pb and Lu-Hf zircon data on 13 samples that span most of the area and the known Pan-African age range of the Sør Rondane Mountains. Our new data are integrated with previous zircon U-Pb ages on the Sør Rondane Mountains - as well as the neighboring Yamato-Belgica Mountains in the east and the central and western Dronning Maud Land in the west - to document spatial and temporal magmatic trends, which will help to build a better picture of





*terrane, the Sør Rondane Suture (SRS), is shown as a thin dashed line. MSZ, Main Shear Zone. C) Location of the Sør Rondane Mountains within Antarctica. D) Map with the magnetic boundaries (black and blue dashed lines) and structural trendlines (in red) following Mieth et al. (2014), and sample locations (prefix MESR omitted for clarity). Smaller italic sample numbers refer to samples from Elburg et al. (2015). Pink areas indicate the extent of granitoid bodies, as interpreted from aeromagnetic data and ground truthing.*

## 10.3 Regional Geology

The Sør Rondane Mountains have been the subject of a considerable number of studies, first in the frame of the Belgian Antarctic Research Expeditions following the International Geophysical Year in 1957–1958 and later mainly reflecting the results of the Japanese Antarctic Research Expeditions. The current understanding of the area has been detailed in a special issue of *Precambrian Research* (vol. 234), with Osanai et al. (2013) giving the most comprehensive overview of the tectonic development of the area. The existence of two terranes - the southwest (SW) and northeast (NE) terranes - has been known for a longer time (Shiraishi et al., 1997), but the boundary between the two has now been shifted to what has been called the Main Tectonic Boundary (Figure 10.1B) from a more southerly position for what used to be the Sør Rondane Suture. The SW terrane, in its most recent definition, consists of both greenschist-amphibolite (D and D') and granulite-facies (C) sectors, with a counterclockwise PTt path; while the NE terrane consists of amphibolite- and granulite-facies sectors (sectors A and B, respectively), with a clockwise PTt path (Osanai et al., 2013). Within the SW terrane, the D' sector consists of a suite of amphibolite to greenschist facies meta-intrusives (Kamei et al., 2013; Owada et al., 2013; Elburg et al., 2015), separated from the D sector to the north by the Main Shear Zone, a dextral strike-slip fault with a length of ca. 120 km (Ruppel et al., 2015). The southern boundary of the D' sector may be another shear zone hidden under the ice (Shiraishi et al., 1997), although magnetic anomalies appear to define a different trend (Mieth et al., 2014).

The D' sector consists of greenschist- to amphibolite-grade gabbro, tonalite, trondhjemite, and minor granodiorite, with ages ranging from 920 to 1015 Ma. The trace element and isotopic signature of the samples have been interpreted to reflect magmatism in an oceanic arc setting until ca. 975 Ma (tholeiitic signature), after which magmatism became somewhat more variable (calc-alkaline signature), which could be interpreted as reflecting a postsubduction stage, perhaps linked to slab break-off (Elburg et al., 2015). Only very sparse zircons with ages older than ca. 1040 Ma were found in this area, in the form of two ca. 3 Ga grains in the 970–920 Ma intrusives (Elburg et al., 2015). Kamei et al. (2013) also described a spatially limited occurrence of calc-alkaline intrusives with ages around 770 Ma in the Nils Larsenfjellet area.

The other sectors consist mainly of metamorphosed supracrustal rocks intruded by Pan-African granitoids. The depositional ages of these supracrustals has been established as being Late Tonian–Early Cryogenian (880–790 Ma) on the basis of the isotopic composition of marbles found in both the SE and the NW terrane (Otsuji et al., 2013). This agrees with the youngest U-Pb zircon ages found in detrital rocks, which are around 780 Ma, for both the NW and the SE terranes (Osanai et al., 2013). Zircons with ages older than ca. 1 Ga are more common in the NE than in the SW terrane. The oldest detrital age recorded within the C and D sectors of the SW terrane are ca. 1200 Ma, whereas detrital ages in the NE terrane include Paleoproterozoic



and Archaean (up to ca. 3.3 Ga) components (Shiraishi et al., 2008; Kamei et al., 2013; Osanai et al., 2013; Elburg et al., 2015).

An inferred large-scale tectonic feature is an NS lineament (Figure 10.1), which offsets the boundary between the two terranes (Osanai et al., 2013) but which is hidden under the ice. A magnetic boundary has been observed in roughly the same location (Mieth et al., 2014). The latter authors tentatively relate this central Sør Rondane corridor to late-stage extensional tectonics following the main collisional event.

Previous workers have divided the Pan-African granitoids into four different groups, on the basis of their geochemical characteristics (Li et al., 2001; 2003). The group 1 granites comprise the Dufek and Lunkeryggen granites, with an arc-type trace element signature located within the SW terrane, whereas the group 2 granites (Austkampane, Pingvinane, Rogerstoppane, and Vikinghøgda; both SW and NE terrane) were classified as having a within-plate signature. The Lunkeryggen Syenite Complex was classified as a separate group, as were the syenitic and granitic rocks from the Mefjell Plutonic Complex (both SW terrane). The ages of the different granites are, however, poorly known, since most dates were obtained by K-Ar, Ar-Ar, and Rb-Sr dating, which yielded (closure) ages between 530 and 460 Ma. Only the ages of the Vikinghøgda ( $562 \pm 7$  Ma; Shiraishi et al., 2008) and Dufek granite ( $619 \pm 7$  Ma; Li et al., 2006) have been obtained by U-Pb zircon dating, and they are notably older than the earlier ages reported. The uncertainty in the age of the granitoids also hampers the interpretation of their isotopic signature, since the initial Sr isotopic signature for these rather high Rb/Sr samples changes significantly when ages shift tens of millions of years. This may explain why the initial  $^{87}\text{Sr}/^{86}\text{Sr}$  ratios appear to vary between 0.703 and 0.73 within a single group (see compilation in Li et al., 2003).

## 10.4 Samples and Methods

Thirteen samples were collected from a wide area of the Sør Rondane Mountains (Figure 10.1) during the German-led expedition Geodynamic Evolution of East Antarctica II in the Austral summer of 2011–2012. Unfortunately, the sampling was done on the basis of the previous interpretation of the Sør Rondane Suture (e.g. Shiraishi et al., 2008) as the boundary between the SW and NE terrane rather than the new interpretation of the more northerly Main Tectonic Boundary (Osanai et al., 2013); thus, the SW terrane is now overrepresented with 11 samples (Figure 10.1), while only one sample comes from the NE terrane (MESR113 from Vesthaugen) and one sample on the boundary between the two terranes (MESR121). The position of the latter sample is, however, still to the west of the magnetic boundary that Mieth et al. (2014) propose to represent the Main Tectonic Boundary.

Analytical techniques employed were identical to those described by Elburg et al. (2013), using the LA-MC-ICPMS laboratory at the Department of Geosciences of Oslo University. Zircons used for U-Pb standardization were GJ-1 ( $^{207}\text{Pb}/^{206}\text{Pb}$  age  $608 \pm 1$  Ma; Jackson et al., 2004), 91500 ( $^{207}\text{Pb}/^{206}\text{Pb}$  age  $1065 \pm 1$  Ma; Wiedenbeck et al., 1995), and A382 (concordia age =  $1877 \pm 2$  Ma; Huhma et al., 2012). Internal structures of zircons were obtained with backscattered electron (BSE) imaging at the Geology Division of the School of Agricultural, Earth, and Environmental Sciences at the University of KwaZulu-Natal.

For the U-Pb data, common Pb-affected analyses were not corrected but were either used for an intercept age in a Tera-Wasserburg diagram or not used for age calculations. All data are



provided in Table E.1 ('Electronic Appendix'). Ages were calculated using the ISOPLOT add-in for Microsoft Excel 2003 (ver. 3.71; Ludwig, 2008). Errors are quoted at the  $2\sigma$  level and at a 95 % confidence level for weighted average ages. The MSWD for the concordant ages are for combined concordance and equivalence. For some of the samples, the spread in concordant dates is larger than can be explained by the uncertainty of the individual measurements. This could reflect the presence of different age groups within the population, the presence of (minor) common Pb, or Pb loss. In these instances, the age spread has been visualized by sorting the concordant analyses in order of ascending  $^{206}\text{Pb}/^{238}\text{U}$  age, with error bars representing the uncertainty of each analytical point. This approach is based on the treatment proposed for  $^{207}\text{Pb}/^{206}\text{Pb}$  ages obtained from zircon evaporation dating (Dougherty-Page and Bartlett, 1999). Because analyses with high  $^{206}\text{Pb}/^{204}\text{Pb}$  ratios are less likely to be influenced by common Pb, this ratio has also been shown in the diagrams and is represented by the size of each data point. This way of representing the data facilitates identifying the presence of different age groups by visual inspection.

For the Hf isotopic compositions, the homogeneity of the zircons can be assessed by comparison to the statistics of the standards that were measured during the analytical period (table 1). The Mud Tank standard yielded an initial  $^{176}\text{Hf}/^{177}\text{Hf}_{732}$  of  $0.282510 \pm 0.000036$  ( $2\sigma$ ;  $n = 65$ ), which translates into an uncertainty of 1.3  $\epsilon$  units. Since this zircon is extremely low in heavy rare earth elements (HREEs) ( $^{176}\text{Yb}/^{177}\text{Hf} < 0.003$ ), both interference and age corrections are minimal, so this is the best possible uncertainty we can obtain with the method. For the Temora 2 standard ( $^{176}\text{Yb}/^{177}\text{Hf} = 0.03\text{--}0.1$ ), the  $2\sigma$  uncertainty on the initial ratio increases to 0.000068 (2.4  $\epsilon$  units), and the high-HREE standard LV-11 ( $^{176}\text{Yb}/^{177}\text{Hf} = 0.1\text{--}0.35$ ) yields 0.000083 (3  $\epsilon$  units). Most zircons analyzed in this study had a  $^{176}\text{Yb}/^{177}\text{Hf}$  ratio similar to that of Temora 2, so the expected  $2\sigma$  uncertainty on a homogeneous population is around 2.5  $\epsilon$  units, unless the zircons were exceptionally rich in Hf, which typically improves the statistics. A few analyses with  $^{176}\text{Yb}/^{177}\text{Hf} > 0.35$  ( $^{176}\text{Lu}/^{177}\text{Hf} > 0.005$ ) were discarded, since we noted a change in the initial ratios for the LV-11 standard above this value, casting doubt on the efficiency of our interference correction at these high Yb/Hf ratios.

## 10.5 Results

The data are presented in order of their U-Pb zircon ages, from older to younger. The full data set can be found in Table 10.1. Field photographs are given in Figure 10.2 and photomicrographs in Figure 10.3.

TC43 is an unfoliated, medium-grained sample from the Dufek granite. This pluton is located within the amphibolite-greenschist-facies D sector of the SW terrane, stitching an N-S running shear zone with apparent sinistral displacement (Osanaï et al., 2013). The main minerals are quartz, K-feldspar (typically perthitic microcline), and plagioclase, with lesser amounts of biotite. Myrmekite is quite common (Figure 10.3A). Plagioclase shows minor sericitization, and some of the biotite has been altered to chlorite. Quartz shows undulose extinction or has undergone dynamic recrystallization. Accessory minerals are opaque minerals, titanite, apatite, and zircon.

Zircons are colorless and clear, and they vary from equidimensional to elongated, with aspect ratios up to 3 and a typical length of 150  $\mu\text{m}$ . Equidimensional crystals often have an anhedral shape. Internal structures, as viewed in BSE imaging, are variable (Figure 10.4).





*Figure 10.2: Field photographs. A) Vertical granite dyke (with hammer) from which MESR12 was taken, crosscutting gneisses but also showing a steep foliation itself. B) Granite dyke (labeled) from which sample MESR82 originates, clearly discordant to host gneisses and calc-silicates. C) Pink syenites, similar to sample MESR89, intruding more melanocratic rocks of the Lunkeryggen complex. D) Vertical granite dyke (sample MESR113) with a scalloped contact against host diorite at Vesthaugen. E) Contact between Utsteinen granite and host gneisses at Princess Elisabeth Antarctica Station. F) Pegmatite veins (MESR88) with amazonitic feldspar crosscutting other syenitic phases at Lunkeryggen. G, Red granite (MESR75) with small mafic enclave.*



Table 10.1: Zircon U-Pb and Hf Isotope Data for Samples and Standards Analyzed

Sample/ standard	Latitude S	Longitude E	Type age	n	Age $\pm 2\sigma^a$	Recommended <sup>b</sup>	MSWD <sup>c</sup>	Type age	$\varepsilon\text{Hf}_i \pm 2\sigma$	$^{176}\text{Hf}/^{177}\text{Hf}_i \pm 2\sigma$	Recommended <sup>b</sup>	n	
TC43	72°10.360'	24°38.454'	$^{206}\text{Pb}/^{238}\text{U}$ wtd. av.	2	950 $\pm$ 18		1.6	Inherited, igneous prot.	+3.9 $\pm$ 2.4	.28228 $\pm$ 3		2	
			$^{206}\text{Pb}/^{238}\text{U}$	6	664–800			Inherited	Ca. +6	.28247 –252		4	
			$^{206}\text{Pb}/^{238}\text{U}$ wtd. av.	7	637 $\pm$ 6		1.0	Preferred igneous	+4.3 $\pm$ 1.7	.28250 $\pm$ 5		10	
MESR12	71°59.889'	23°14.360'	$^{206}\text{Pb}/^{238}\text{U}$	1	603 $\pm$ 7		1.6	Metamorphic?	+2.5 $\pm$ .9	.28247 $\pm$ 3		1	
			Concordia	9	577 $\pm$ 6		.75	Igneous					27
			$^{206}\text{Pb}/^{238}\text{U}$ wtd. av.	8	575 $\pm$ 5		5.4	Preferred igneous	+5.0 $\pm$ 1.0	.28256 $\pm$ 3		1	
MESR82	72°7.296'	22°1.122'	$^{206}\text{Pb}/^{238}\text{U}$	1	644 $\pm$ 3		1.9	Inherited	+2.7	.28246		1	
			$^{206}\text{Pb}/^{238}\text{U}$ wtd. av.	21	572 $\pm$ 4		1.9	Preferred igneous	+2.4 $\pm$ 2.2	.28249 $\pm$ 6		32	
			$^{206}\text{Pb}/^{238}\text{U}$	1	960			Inherited, igneous prot.	+8.4 $\pm$ 1.2	.28241 $\pm$ 4		2	
MESR89	72°1.981'	24°35.865'	$^{206}\text{Pb}/^{238}\text{U}$	1	715		1.5	Inherited, igneous prot.	+5.6 $\pm$ .3	.28249 $\pm$ 1		2	
			$^{206}\text{Pb}/^{238}\text{U}$ wtd. av.	4	617 $\pm$ 14		1.9	Inherited, metam. prot.	+2.6 $\pm$ .7	.28247 $\pm$ 2		4	
			$^{206}\text{Pb}/^{238}\text{U}$ wtd. av.	6	560 $\pm$ 9		1.5	Preferred igneous	+3 $\pm$ 2.8	.28244 $\pm$ 8		11	
MESR88	72°1.981'	24°35.865'	Assumed	5	556 $\pm$ 4		1.5	Assumed	+1.3 $\pm$ 1.0	.28247 $\pm$ 3		15	
			Concordia	2	Ca. 1000			Preferred igneous	+2.4 $\pm$ 1	.28250 $\pm$ 3		21	
			$^{206}\text{Pb}/^{238}\text{U}$	2	Ca. 1000			Inherited	+7 to +8.5	.28241 $\pm$ 2		3	
MESR75	72°17.081'	21°26.114'	$^{206}\text{Pb}/^{238}\text{U}$	1	803 $\pm$ 8		1.0	Inherited	+6.5 $\pm$ 1	.28246 $\pm$ 3		6	
			$^{206}\text{Pb}/^{238}\text{U}$ wtd. av.	3	742 $\pm$ 7		.4	Inherited	+2 to +8	.28239–56		5	
			$^{206}\text{Pb}/^{238}\text{U}$	1	669 $\pm$ 5		6.1	Inherited	+3.1 $\pm$ 1.0	.28245 $\pm$ 3		1	
MESR121	72°3.970'	26°0.769'	$^{206}\text{Pb}/^{238}\text{U}$ wtd. av.	11	551 $\pm$ 8		2.2	Preferred igneous	.0 $\pm$ 2.9	.28244 $\pm$ 8		44	
			$^{206}\text{Pb}/^{238}\text{U}$ wtd. av.	19	532 $\pm$ 3		2.9	Preferred igneous	+2.1 $\pm$ 1.2	.28246 $\pm$ 5		1	
			$^{206}\text{Pb}/^{238}\text{U}$ wtd. av.	9	529 $\pm$ 3		1.6	Preferred igneous	–5.9 $\pm$ 1.6	.28228 $\pm$ 5		23	
MESR123	71°56.824'	23°20.813'	Concordia	43	528 $\pm$ 4		1.5	Preferred igneous	+1.3 $\pm$ 1.4	.28249 $\pm$ 4		30	
			$^{206}\text{Pb}/^{238}\text{U}$ wtd. av.	12	527 $\pm$ 5		1.7	Preferred igneous	–1.8 $\pm$ 1.6	.28240 $\pm$ 5		47	
			$^{206}\text{Pb}/^{238}\text{U}$ wtd. av.	3	600–535			Preferred igneous	–4.4 $\pm$ 2.9	.28233 $\pm$ 8		42	
MESR118	72°2.810'	25°3.449'	$^{206}\text{Pb}/^{238}\text{U}$	12	527 $\pm$ 5		1.1	Inherited	–8 $\pm$ 1.0	.28238 $\pm$ 3		1	
			$^{206}\text{Pb}/^{238}\text{U}$ wtd. av.	4	509 $\pm$ 12		2.2	Preferred igneous	–2.5 $\pm$ 1.6	.28239 $\pm$ 4		18	
			$^{206}\text{Pb}/^{238}\text{U}$ wtd. av.	12	340.2 $\pm$ 1.4		1.1	Preferred igneous	–1.3 $\pm$ 2.1	.28243 $\pm$ 6		36	
MESR22	72°2.309'	22°50.998'	Concordia	12	506 $\pm$ 4		1.1	Preferred igneous				65	
			$^{206}\text{Pb}/^{238}\text{U}$ wtd. av.	12	340.2 $\pm$ 1.4		1.1	Preferred igneous				27	
			$^{207}\text{Pb}/^{206}\text{Pb}$ wtd. av.	61	560.7 $\pm$ 1.4		1.1	Preferred igneous				73	
Plesovice	C	Initial <sup>d</sup>	Initial <sup>d</sup>	732			.9					63	
			Initial <sup>d</sup>	414									
			Initial <sup>d</sup>	290									
Mud tank	Temora	LV11	Initial <sup>d</sup>	290			.9					65	
			Initial <sup>d</sup>	290								27	
			Initial <sup>d</sup>	290								73	
LV11	LV11	Initial <sup>d</sup>	Initial <sup>d</sup>	290			.9					63	
			Initial <sup>d</sup>	290									
			Initial <sup>d</sup>	290									

Note. All ages are in Ma. Preferred igneous ages are in bold.  $^{206}\text{Pb}/^{238}\text{U}$  wtd. av. = weighted average of the  $^{206}\text{Pb}/^{238}\text{U}$  ages; prot. = protolith; metam. = metamorphic.

<sup>a</sup> Weighted average  $^{206}\text{Pb}/^{238}\text{U}$  quoted at the 95% confidence level.

<sup>b</sup> MSWD of the concordia ages is for combined concordance and equivalence.

<sup>c</sup> Recommended ages and initial Hf isotopic compositions from (Woodhead and Hergt, 2005), Sláma et al. (2008); (Heinonen et al., 2010a); Kristoffersen et al. (2013).

<sup>d</sup> Analyzed for only Lu-Hf isotope systematics; age used for calculation of initial Hf isotope ratio.

<sup>e</sup> Only analyses with  $^{176}\text{Yb}/^{177}\text{Hf} < 0.35$ .



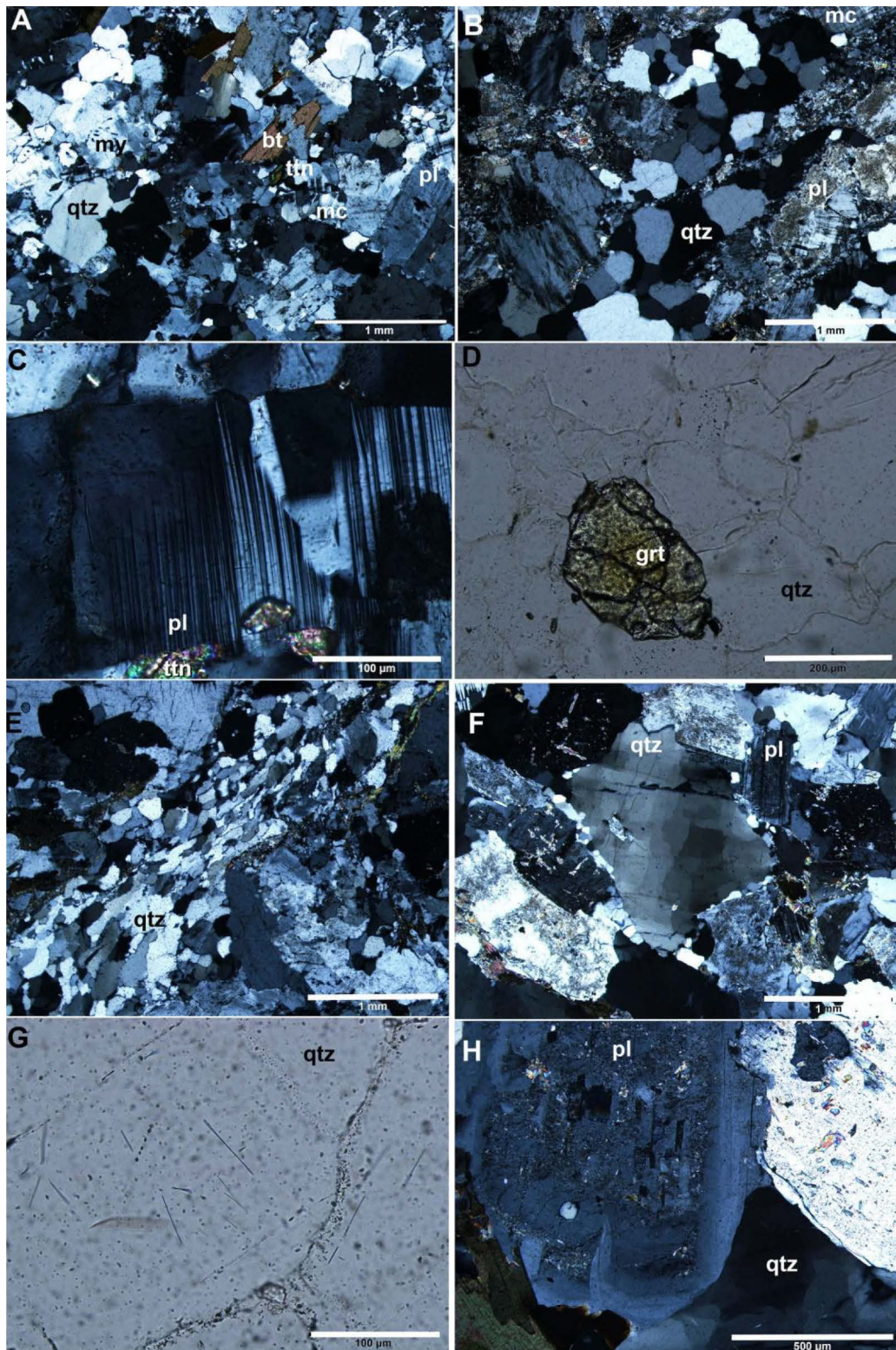


Figure 10.3: Photomicrographs of selected samples. Abbreviations following Kretz (1983): *my*, myrmekite; *xpl*, crossed polars; *ppl*, plane polarized light. A) Sample TC 43 from Dufek, with little evidence for deformation; *xpl*. B) MESR12, showing fine-grained bands defining the foliation and recrystallized domains of quartz; *xpl*. C) Bent plagioclase twins as the only evidence for deformation in syenite sample MESR89. D) Yellow garnet in pegmatitic sample MESR88 within the Lunkeryggen syenite complex; *ppl*. E) Sample MESR30 from the sheared Vengen/Vikingshøgda granite, showing elongate and serrated quartz grains; *xpl*. F) Sample MESR80 from Bamseungen, showing compositionally zoned plagioclase and chessboard deformation in quartz; *xpl*. G) Putative rutile needles within quartz of sample MESR123; *ppl*. H) Sample MESR22, the youngest granite analyzed, with zoned plagioclase and undulose quartz; *xpl*.



Some crystals show indistinct oscillatory zoning, sometimes surrounding a euhedral, BSE-bright patchy core; others have a homogeneous, rounded core and BSE-bright rim; while others are homogeneous or patchy throughout. A total of twenty-four spots were analyzed on 21 grains, yielding unsystematic variations in U concentrations between 200 and 3000 ppm.  $^{206}\text{Pb}/^{204}\text{Pb}$  ratios varied between 60 and 80000, with the lower ratios in strongly discordant analyses. The unfiltered data give intercepts in a Tera-Wasserburg plot at  $645 \pm 54$  and  $1995 \pm 900$  Ma, but the MSWD of 79 indicates the severity of scatter, supported by the presence of different textures in the zircons. Two near-concordant grains (2, 12) yield a combined weighted average  $^{206}\text{Pb}/^{238}\text{U}$  age of  $950 \pm 18$  Ma and are thought to represent an inherited component from an igneous protolith, since both zircons show oscillatory zoning in the analyzed areas.

One grain (14) with a homogenous, rounded, BSE-dark core and BSE-bright rim gives a concordant  $664 \pm 10$  Ma  $^{206}\text{Pb}/^{238}\text{U}$  date for the core and ca. 750 Ma - but strongly reversely discordant (and likely meaningless) - for the rim. Four more grains (8, 15, 21 and 22) with patchy to absent zoning yield near-concordant to (reversely) discordant dates around 750 Ma. Of the remaining analyses, eight are (near-) concordant, of which one (13) gives a slightly younger date of  $603 \pm 7$  Ma. This is a homogeneous, rounded, BSE-dark core, with a low U content (180 ppm) surrounded by a BSE-light rim (Figure 10.4). The other seven analyses on weakly oscillatory-zoned parts of crystals are tightly clustered (Figure 10.5A) and give a weighted average  $^{206}\text{Pb}/^{238}\text{U}$  age of  $637 \pm 6$  Ma (concordia age  $636 \pm 8$  Ma), which we interpret to reflect the crystallization of the granitic magma. The one zircon with the ca. 600 Ma age may reflect metamorphic resetting.

The 10 Lu-Hf analyses on igneous grains with a ca. 640 Ma age give an  $\epsilon\text{Hf}_{637}$  value of  $+4.3 \pm 1.7$ , or  $^{176}\text{Hf}/^{177}\text{Hf}$   $637 = 0.282500 \pm 0.000049$  (Table 10.1; Figure 10.6; Figure 10.8). The one grain that gave a younger age around 600 Ma also has a slightly lower  $\epsilon\text{Hf}_i$  at  $2.5 \pm 0.9$ . The two inherited grains with ca. 950 Ma ages have initial values between +3 and +5, while the 750 Ma analyses have an average around +6.  $^{176}\text{Yb}/^{177}\text{Hf}$  ratios vary unsystematically between 0.04 and 0.18.

MESR12 is a fine-grained leucocratic granite sheet (ca. 1.5 m wide) that crosscuts the foliation defined by the grey gneisses in the area (Figure 10.2A), which is the granulite-facies section of the SW terrane. The sample itself is also foliated, mainly defined by anastomosing bands of more fine-grained materials (predominantly quartz and feldspar). Somewhat coarser quartz seems to contain very thin needles, which may be rutile. Quartz crystals often display  $120^\circ$  triple junctions (Figure 10.3B). Microcline and plagioclase are the next most abundant minerals, with the latter often sericitized. Biotite is scarce, often altered to chlorite. Accessory minerals are opaques and zircon.

The sample contains mostly turbidly brown zircons up to 300  $\mu\text{m}$  long, with typical aspect ratios of 3. Quite a few show spongiform areas, often surrounded by radial cracks (Figure 10.4). Zoning outside of those areas is typically oscillatory.

Thirty-nine spots were analyzed on 32 grains, with U contents varying between 300 and 3000 ppm. Most points were discordant as a result of high common Pb content, with  $^{206}\text{Pb}/^{204}\text{Pb}$  ratios down to 60. Nine concordant analyses yielded a concordia age of  $577 \pm 6$  Ma (MSWD = 1.6; Figure 10.5), which is within the uncertainty of the weighted average  $^{206}\text{Pb}/^{238}\text{U}$  age of  $575 \pm 5$  Ma (MSWD = 0.75; one analysis rejected on statistical grounds). This is deemed to be the best estimate of the igneous age of this dyke. The 27 Lu-Hf analyses define a tightly clustered



population at an  $\epsilon\text{Hf}_{575}$  value of  $+5.0 \pm 1$ , or  $^{176}\text{Hf}/^{177}\text{Hf}_{575} = 0.282563 \pm 0.000029$  (Figure 10.6).  $^{176}\text{Yb}/^{177}\text{Hf}$  ratios are around 0.05.

MESR82 is a medium-grained granite from the western side of Sør Rondane (Lågkollane), located within the D sector of the SW terrane, if the sector boundaries - as defined by (Osanai et al., 2013) - are extended westward. The cream-colored granitoid body crosscuts the main layering of the outcrop and intrudes gneisses and calc-silicate rocks (Figure 10.2B). Deformation of the granite is evidenced by the dynamically recrystallized quartz and a weak foliation defined by the preferential alignment of biotite. K-feldspar is typically perthitic. Plagioclase is often slightly sericitized, but biotite is only rarely altered to chlorite. Titanite is a minor phase, and allanite is found sporadically, often overgrown by or associated with biotite. Apatite, opaque minerals, and zircon are relatively abundant accessory phases. Muscovite and calcite also occur but appear to be secondary phases.

Zircons are colorless and clear and typically 100–200  $\mu\text{m}$  long, with aspect ratios up to 5. Elongated grains are often euhedral, while more stubby ones are generally sub- to anhedral. Zoning is typically faint and can be oscillatory or patchy. Forty spots were analyzed on 22 grains, with U contents varying between 80 and 1300 ppm but most within the 200–300 ppm range. Common Pb is a problem for a number of grains, but 23 analyses gave concordant dates. Of these, one core (22c) was clearly older at  $644 \pm 3$  Ma, although BSE imaging did not reveal a striking difference between core and rim at the level of exposure. The remaining analyses give a spread in dates that is greater than can be explained by analytical uncertainty and therefore do not provide a concordia age. A weighted average  $^{206}\text{Pb}/^{238}\text{U}$  age is  $572 \pm 4$  Ma (with the youngest age rejected on statistical grounds) but with an MSWD of 5.4. When the individual  $^{206}\text{Pb}/^{238}\text{U}$  dates are put in ascending order, a plateau is visible from 572–575 Ma (Figure 10.5C), which includes the analyses with the highest  $^{206}\text{Pb}/^{204}\text{Pb}$  ratios (up to 110,000, indicated by the bubble size) and thus the least influence of common Pb. We therefore propose that the ca. 572 Ma weighted average  $^{206}\text{Pb}/^{238}\text{U}$  age reflects the crystallization of the granitoid. Using the unmixing function of IsoPlot gives the same result, with a dominant age population at  $575 \pm 3$  Ma and a subordinate one at  $554 \pm 4$  Ma.

The one grain of ca. 644 Ma is similar to the other zircons in terms of Lu-Hf, with an  $\epsilon\text{Hf}_{644}$  value of +2.7 ( $^{176}\text{Hf}/^{177}\text{Hf}_{644} = 0.282456$ ). Of the other 33 analyses, one BSE-bright undated core has an  $\epsilon\text{Hf}_{572}$  value of  $-2.5$  ( $^{176}\text{Hf}/^{177}\text{Hf}_{572} = 0.282355$ ). The remaining 32 analyses give an average  $\epsilon\text{Hf}_{572}$  value of  $+2.4 \pm 2.2$ , or  $^{176}\text{Hf}/^{177}\text{Hf}_{572} = 0.282492 \pm 0.000062$ .  $^{176}\text{Yb}/^{177}\text{Hf}$  ratios are low, around 0.02.

MESR89 is a pink syenite from the complex at Lunkeryggen, within the amphibolite-greenschist-facies D sector of the SW terrane. The pink syenite crosscuts the more melanocratic rocks of the complex (Figure 10.2C) but is itself crosscut by pegmatites similar to sample MESR88 (below). The sample is rich in K-feldspar, typically with coarse patchy perthitic exsolution. Plagioclase and quartz occur in subordinate amounts; the former occasionally shows bent twins (Figure 10.3C), while the latter can show  $120^\circ$  triple junctions between individual crystals. Sericitization of the feldspars is very minor. The dominant ferromagnesian phase is amphibole, with greenish-blue to brown pleochroism. Greenish-brown biotite is a minor phase. Titanite and apatite are relatively abundant, and an opaque phase occurs as equant crystals. Zircon and allanite are accessory phases. Fluorite and calcite occur interstitially, while rare epidote is found as larger, anhedral crystals.



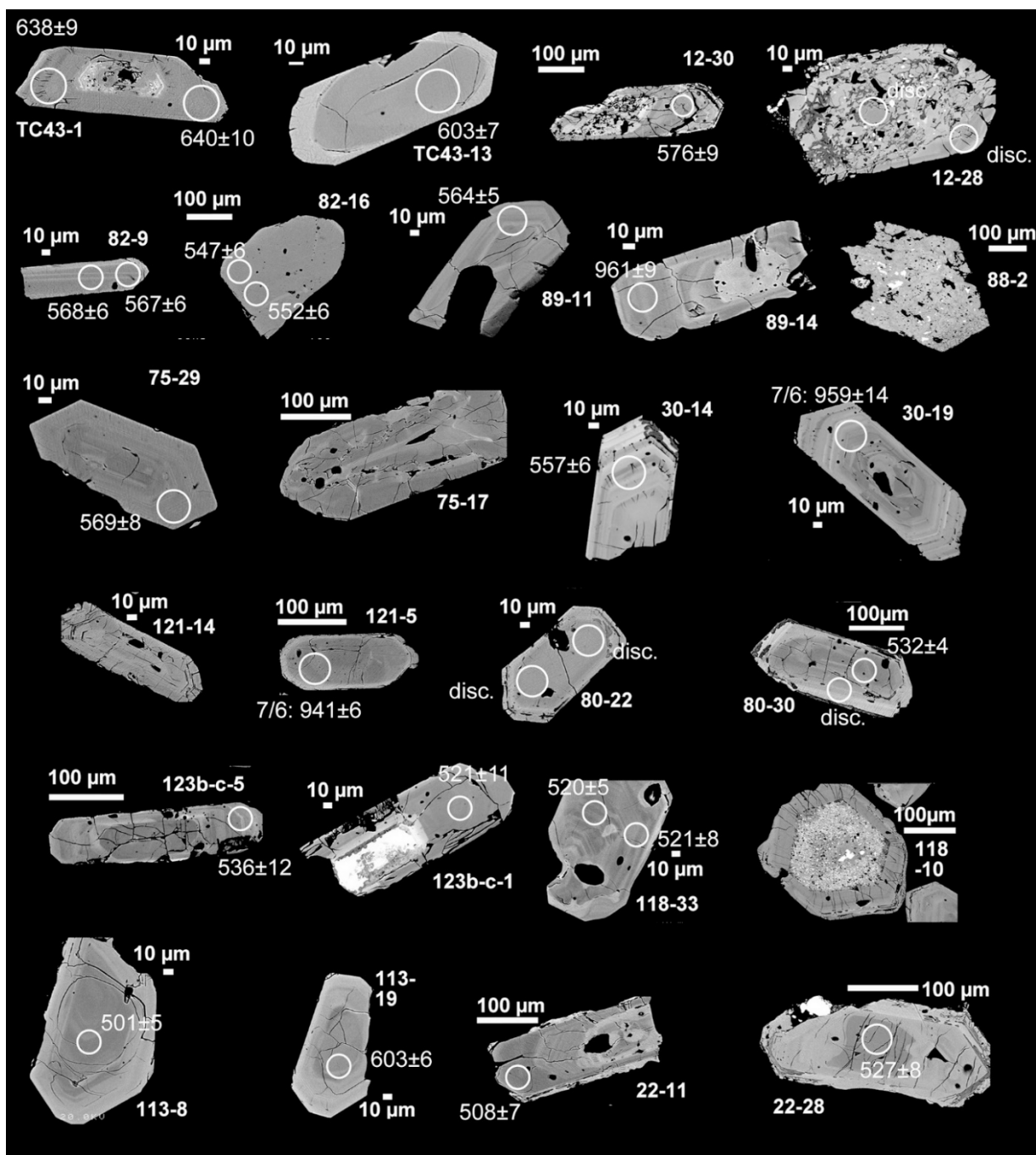


Figure 10.4: Typical zircon backscattered electron images for the samples analyzed. The first number is the sample without the prefix MESR, and the second is the number of the individual zircon, as also used in the text and table S1.  $^{206}\text{Pb}/^{238}\text{U}$  dates (in Ma) are given next to the indicated ablation spots, unless badly discordant because of common Pb (disc.); for slightly discordant analyses, the  $^{207}\text{Pb}/^{206}\text{Pb}$  date is given.



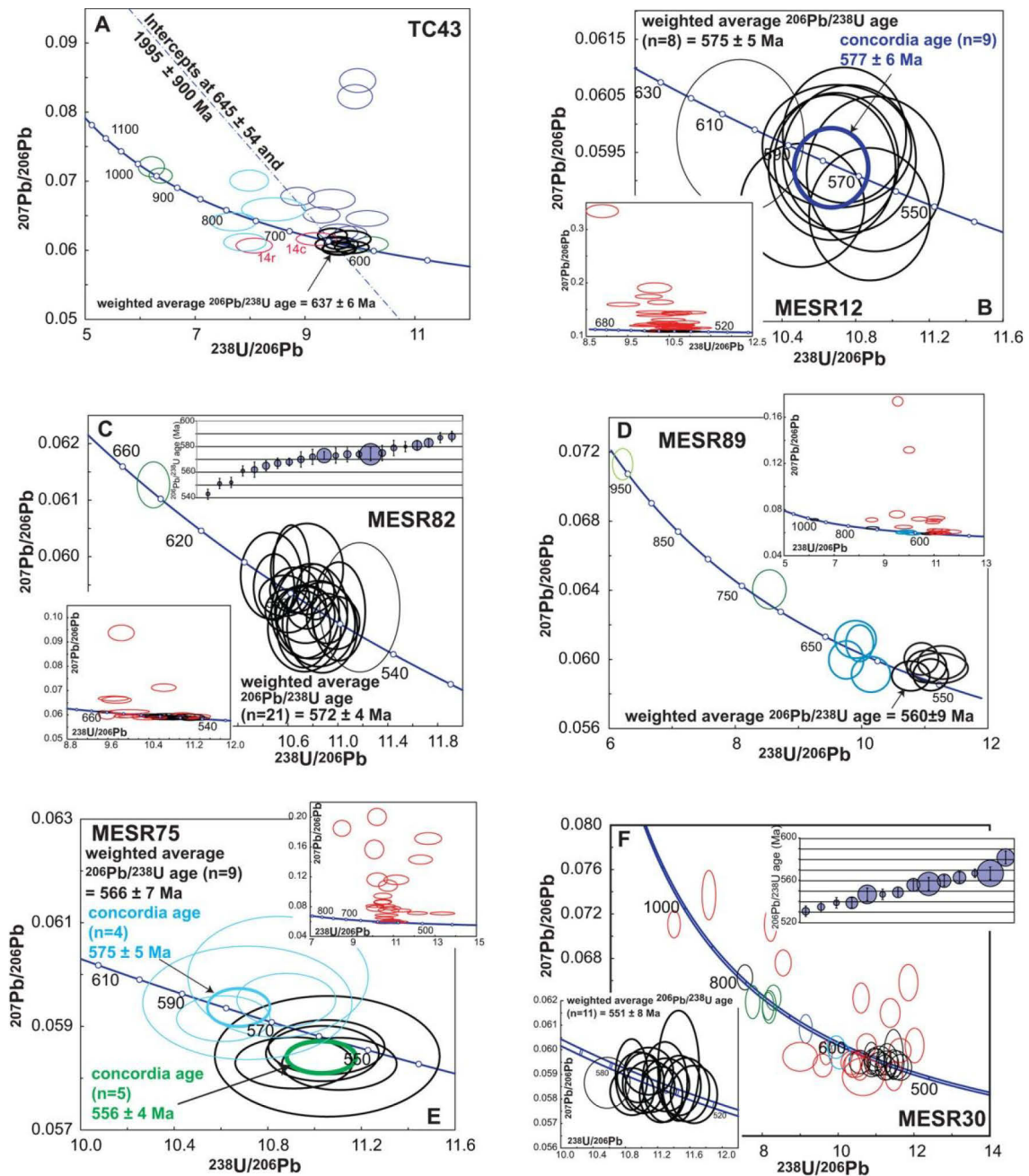


Figure 10.5: Tera-Wasserburg diagrams for all dated samples. All error ellipses are  $2\sigma$ . Thick black circles are the analyses used for establishing the igneous age of the sample. A) Sample TC43 from Dufek. B) Sample MESR12 from northern D sector of the SW terrane. Inset includes discordant data points (in red), not used for igneous age calculation. C) Sample MESR82 from the Lågkollane group. Insets show Tera-Wasserburg diagram for all data and the concordant  $^{206}\text{Pb}/^{238}\text{U}$  ages in ascending order, with bubble size proportional to the  $^{206}\text{Pb}/^{204}\text{Pb}$  ratio. D) Sample MESR89 from the Lunkeryggen syenite complex; red data points (inset) show discordant points, blue and green circles are interpreted as inherited components. E) MESR75 from the western part of the SW terrane, with two apparent age populations of zircons that show identical internal structures and Hf isotopic compositions. The youngest age group is provisionally taken as representing the igneous age of the sample. Inset shows discordant points in red. F) MESR30 of the northern side of the sheared Vengen/Vikinhøgda granite, with discordant points in red. Inset shows close-up of data for igneous zircon; blue and green colors represent inherited components. G) MESR121 from the boundary between the NE and the SW terranes. H) MESR80 from Bamseungen. I) MESR123 from Utsteinen (Princess Elisabeth Antarctica Station). J) MESR118 from Meffell. K) MESR113 from Vesthaugen (NE terrane). L) MESR22 from the northern D sector of the SW terrane.



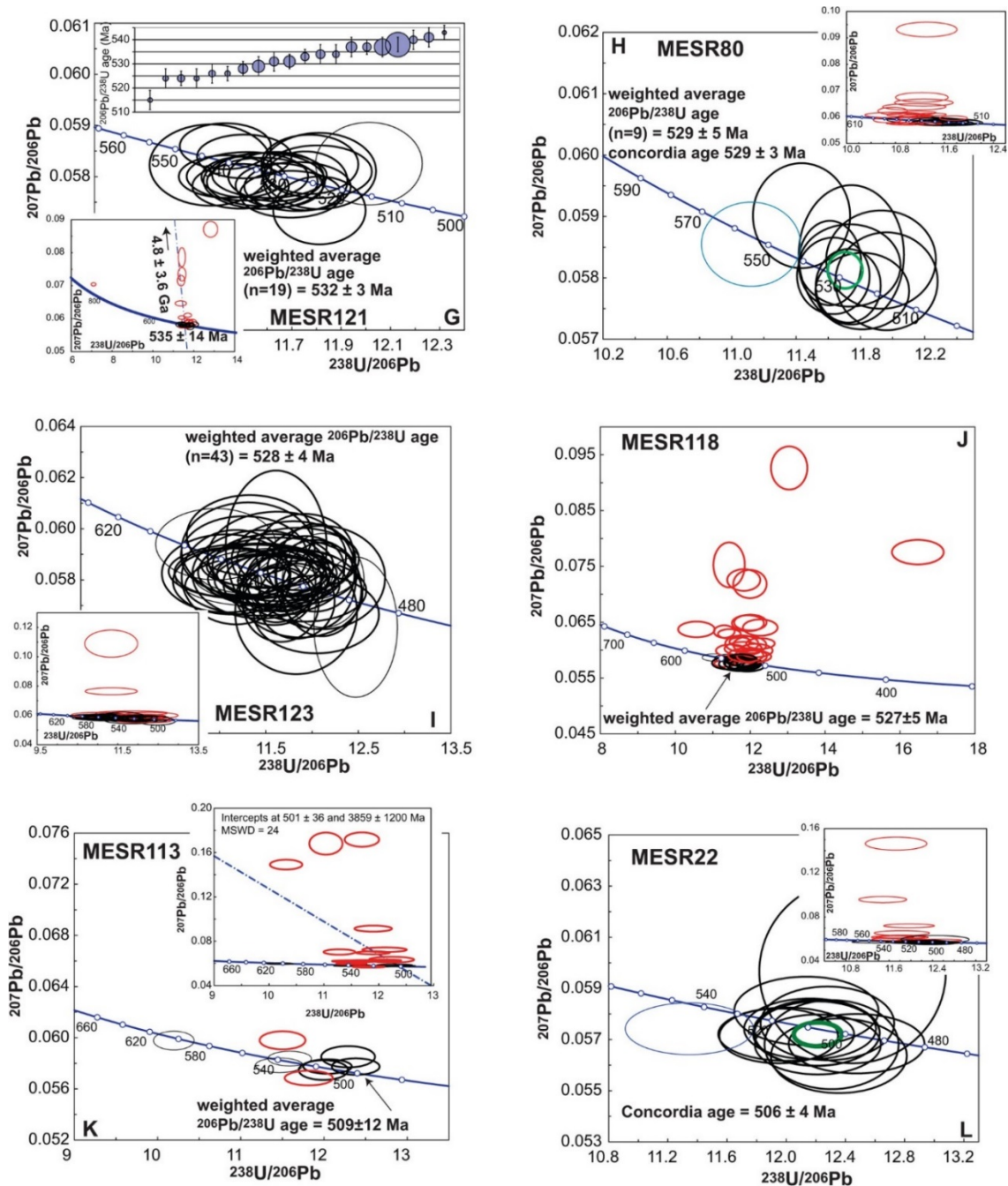


Figure 10.5 (Continued)

The sample contains a small number of zircons, varying from colorless to brownish-pink, of variable sizes and shapes. The largest ones are fragments of more than 400  $\mu\text{m}$  in their longest dimension, whereas most crystals are no longer than 200  $\mu\text{m}$  and have aspect ratios up to 4. The zoning visible in BSE images varies from oscillatory to patchy. Twenty-four analyses were performed on 16 crystals. Uranium content varied between 70 and 2000 ppm. About half of the crystals contained appreciable common Pb, with  $^{206}\text{Pb}/^{204}\text{Pb}$  ratios between 100 and 44000, resulting in a significant number of discordant analyses. The 12 (near-)concordant analyses yielded a spread of dates (Figure 10.5D). The core of grain 14 yielded a  $^{206}\text{Pb}/^{238}\text{U}$  date of  $961 \pm 9$  Ma, and oscillatory zoned crystal 02a gave  $714 \pm 9$  Ma, while four analyses on homogeneous-looking parts of three grains (6, 16, 20) gave a weighted average  $^{206}\text{Pb}/^{238}\text{U}$  age of  $617 \pm 14$  Ma. These ages are interpreted to reflect inheritance from igneous (961, 714 Ma) or metamorphic (617 Ma) protoliths. The remaining six analyses (on oscillatory zoned or



homogeneous crystals) yielded a weighted average  $^{206}\text{Pb}/^{238}\text{U}$  age of  $560 \pm 9$  Ma (MSWD = 1.9), and a concordia age of  $564 \pm 9$  Ma (MSWD = 2.8).

Two analyses on the ca. 961 Ma grain yielded an  $\epsilon\text{Hf}_{960}$  value of  $+8.4 \pm 1.2$ , or  $^{176}\text{Hf}/^{177}\text{Hf}_{961} = 0.282414 \pm 0.000035$ , while the ca. 714 Ma grain yielded an  $\epsilon\text{Hf}_{714}$  value of  $+5.6 \pm 0.3$  ( $^{176}\text{Hf}/^{177}\text{Hf}_{714} = 0.282492 \pm 0.000008$ ). Four analyses of the ca. 617 Ma age group yielded  $\epsilon\text{Hf}_{617} = +2.6 \pm 0.7$  ( $^{176}\text{Hf}/^{177}\text{Hf}_{620} = 0.282469 \pm 0.000021$ );  $^{176}\text{Yb}/^{177}\text{Hf}$  ratios are around 0.03. The values for the 11 grains with igneous ages of ca. 560 Ma yielded an average  $\epsilon\text{Hf}_{560}$  of  $+0.3 \pm 2.8$ , or  $^{176}\text{Hf}/^{177}\text{Hf}_{560} = 0.282441 \pm 0.000078$  (Figure 10.6), with  $^{176}\text{Yb}/^{177}\text{Hf}$  ratios around 0.06. The spread in initial ratios is slightly high for a homogeneous population with these Yb/Hf ratios.

MESR88 is a leucocratic late pegmatite dyke from the Lunkeryggen syenite complex, of which the K-feldspar has an amazonitic color (Figure 10.2F). In thin section, it can be seen to have microcline twinning and only limited exsolution. Granophyric intergrowths occur around some of the larger microcline crystals. Plagioclase and quartz are the other common minerals. There is hardly any sericitization of the feldspars. Ferromagnesian minerals are green clinopyroxene and a yellow garnet (Figure 10.3D). Titanite and opaque minerals are additional subordinate phases. Fluorite occurs interstitially.

The sample contains zircons up to 700  $\mu\text{m}$  long with a milky brown to gray color. BSE imaging showed bright patchy zoning with many U-rich inclusions (Figure 10.4). No dates could be obtained from these zircons because of their extreme uranium contents and metamict nature. The age of the sample was assumed to be within error of the ca. 560 Ma age for MESR89.

Despite the uncertainty in age, the 15 zircons analyzed form quite a tight population in terms of their Hf isotopic composition, with an  $\epsilon\text{Hf}_{560}$  of  $+1.3 \pm 1.0$ , or  $^{176}\text{Hf}/^{177}\text{Hf}_{560} = 0.282469 \pm 0.000027$ , with  $^{176}\text{Yb}/^{177}\text{Hf}$  ratios around 0.05. The good statistics on this sample reflect the high intensities of LA-MC-ICPMS signal for the Hf isotopes, which is a reflection of high Hf contents in pegmatitic zircons (Elburg et al., 2013). The Hf isotope array overlaps with and lies toward the high side of that for MESR89 (Figure 10.6).

MESR75 is a sample of a bright red granite from the far western side of the study area, of which the macroscopically visible deformation appears to be limited to minor brittle features. No contacts with host rocks were observed. More mafic enclaves occur sporadically (Figure 10.2G) and are interpreted as evidence for mingling between mafic and felsic magmas (Elburg and Nicholls, 1995). The sample contains K-feldspar with coarse perthitic exsolution lamellae, plagioclase (with some sericitization), and quartz. The latter can show  $120^\circ$  triple junction with neighboring quartz crystals. Plagioclase twins are occasionally bent. Blue-green amphibole and green-brown biotite occur in subequal proportions; titanite, opaque minerals, and apatite are common. Minor fluorite occurs interstitially.

Zircons can be clear and colorless or murky yellowish brown. They are typically 200  $\mu\text{m}$  long and have aspect ratios up to 4, but most are around 2. The majority of the crystals is cracked, and inclusions are common. Oscillatory zoning is observed in most crystals, and only few have developed patchy zoning. Thirty-five spots were ablated on 22 grains, which have U contents between 200 and 1500 ppm. Most grains contained appreciable common Pb and gave very discordant dates. Nine analyses were concordant. Together, they define a weighted average  $^{206}\text{Pb}/^{238}\text{U}$  age of  $566 \pm 7$  Ma but with an MSWD of 3.1. The dates are not equivalent, so a concordia age cannot be calculated.



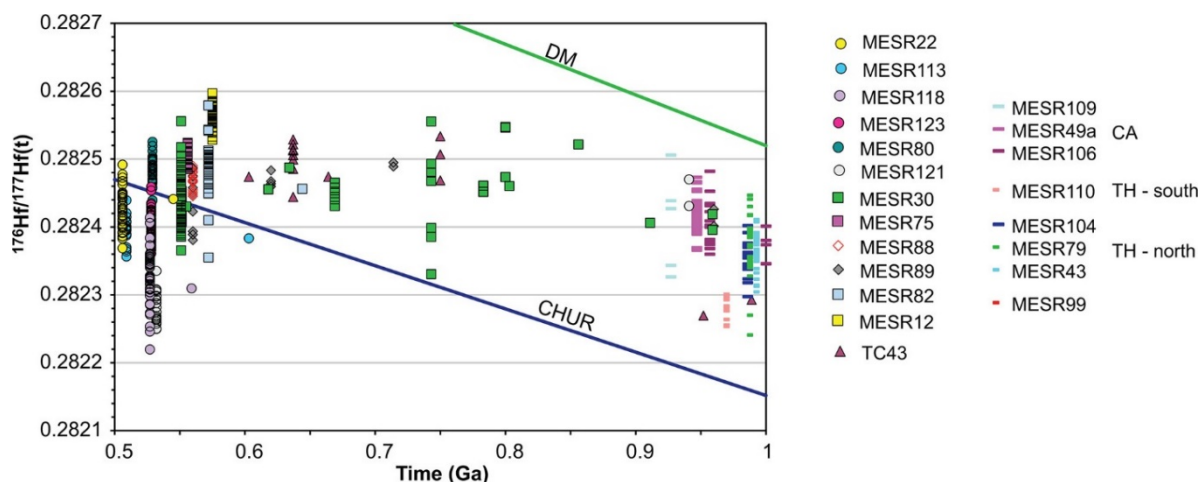


Figure 10.6: Initial  $^{176}\text{Hf}/^{177}\text{Hf}$  isotopic ratio versus age for all samples analyzed in this study, plus those from Elburg et al. (2015) for the 0.9–1.0 Ga meta-igneous rocks from the D' sector of the SW terrane. Errors on individual data points not shown for clarity. The line of  $^{176}\text{Lu}/^{177}\text{Hf} = 0.015$  gives the evolution curve for a typical crustal reservoir.  $^{176}\text{Lu}/^{177}\text{Hf} = 0.00$  is the limiting case of a Lu-free reservoir, similar to the evolution curve for a zircon. CHUR, Chondritic Uniform Reservoir; DM, depleted mantle; TH, tholeiitic; CA, calc-alkaline.

Visual inspection of the data points in the concordia diagrams suggest the existence of two clusters, with four points defining a concordia age of  $575 \pm 5$  Ma (MSWD = 1.5) and five others an age of  $556 \pm 4$  Ma (MSWD = 1.5). The areas analyzed look similar in BSE imaging in terms of zoning patterns and have similar  $^{206}\text{Pb}/^{204}\text{Pb}$  ratios, but the older areas have higher U contents (600–900 vs. 200–500 ppm). On the basis of the presence of mafic enclaves, it seems possible that there are different intrusive phases present, and we tentatively take the age of the younger cluster as the most likely representative for the igneous age.

Despite the spread in dates, the 21 analyzed zircons define a very tight cluster in terms of Hf isotopic composition. The average  $\epsilon\text{Hf}_{556}$  is  $+2.4 \pm 1.0$ , or  $^{176}\text{Hf}/^{177}\text{Hf}_{556} = 0.282502 \pm 0.000027$ . The  $^{176}\text{Yb}/^{177}\text{Hf}$  ratios are around 0.03.

MESR30 is a sample from the Vengen/Vikingshøgda granite, taken just north of the Main Shear Zone. The granite is located within the amphibolite-greenschist facies D sector of the SW terrane and is hosted by a series of metasedimentary rocks, including calc-silicates and chlorite-garnet schists. The granite sample has a tectonic foliation, mainly defined by bands of a finer grain size, consisting largely of white mica or deformed quartz (Figure 10.3E). Plagioclase (with some sericitization), quartz, and microcline, with flame perthite, are the main minerals. Larger quartz crystals display undulose extinction, while patches of finer-grained quartz typically show mutual  $120^\circ$  triple junction. The main ferromagnesian mineral is dark-brown biotite (sometimes with minor alteration to chlorite), but patches of finer-grained epidote, interpreted to be secondary, are also present.

The sample contains zircons of variable shapes and sizes, with the majority being euhedral, about 200  $\mu\text{m}$  long, and with an aspect ratio of 2, but more rounded or equidimensional grains are found as well. Their colors vary from colorless and pinkish to yellowish brown. Zoning patterns can be oscillatory or patchy, but some grains do not display any zoning apart from core-rim structures. Some have BSE-bright high-U cores, with radial cracks in the mantling zones. Forty-four spots were analyzed on 32 grains, with widely varying U contents between 100 and 3000 ppm. Common Pb and discordance are a problem in some grains, but 21 spots yielded concordant dates. Inheritance is pronounced, with a number of different age groups.



Two spots (19, 6) yielded discordant dates around 1 Ga, and the oscillatory zoning of those zircons suggests an igneous protolith. One core with oscillatory zoning (21c) gave a concordant date of  $803 \pm 8$  Ma, another one (24c, with less distinct zoning) at  $783 \pm 7$  Ma, and three analyses on two zircons (both with oscillatory zoning) yielded a combined weighted average  $^{206}\text{Pb}/^{238}\text{U}$  age of  $742 \pm 7$  Ma. One grain with wavy zoning is concordant at  $669 \pm 5$  Ma, and two other analyses (17, 24r, both with oscillatory zoning) combine to give a date of  $616 \pm 9$  Ma. Fourteen grains give dates between 531 and 582 Ma but do not constitute a single concordant population. A weighted average  $^{206}\text{Pb}/^{238}\text{U}$  age is  $551 \pm 8$  Ma (with the oldest date rejected on statistical grounds) but with a high MSWD of 6.1. The zircons with the clearest oscillatory zoning are those in the 556–557 Ma age bracket (e.g., grain 14), while the three youngest analyses (<540 Ma) have somewhat lower  $^{206}\text{Pb}/^{204}\text{Pb}$  ratios; we therefore take this ca. 550 Ma age as the best estimate of igneous crystallization. Some of the younger dates could be a result of resetting during late shearing in the granite.

Because of the complicated age pattern, a large number of Lu-Hf analyses were done, with 22 analyses representing inherited grains and 44 for the igneous age group (Figure 10.6). If the initial  $^{176}\text{Hf}/^{177}\text{Hf}$  ratios for the two groups are compared, the younger grains fall within the range observed for the older grains: the inherited grains range from 0.282331 to 0.282556, while the ca. 550 Ma age group gives a range in  $^{176}\text{Hf}/^{177}\text{Hf}_{551}$  of 0.282366–0.282517. The average for the igneous population is  $0.282438 \pm 81$ , or  $\epsilon\text{Hf}_{551}$   $0.0 \pm 2.9$ . The spread in the initial ratios for this group is not much greater than what can be expected from the analytical uncertainty, considering that the  $^{176}\text{Yb}/^{177}\text{Hf}$  ratios are on the high side, with values in the 0.03–0.25 range (average = 0.1).

Sample MESR121 comes from a granite in the border area between the granulite-facies area of the SW terrane and the NE terrane, as defined by Osanai et al. (2013), where it intrudes more mafic host rocks. The sample consists of quartz (with undulose extinction), plagioclase (which can be zoned, with sericitization mainly confined to the cores of the crystals), microcline (with flame perthite), and myrmekitic intergrowths. Biotite is dark brown to straw yellow in color and shows minor alteration to chlorite; it often contains zircon inclusions. Titanite is often associated with equant opaque minerals, and apatite is a conspicuous accessory phase.

Colorless to light yellow zircons are 100–200  $\mu\text{m}$  long and have aspect ratios varying from 2 to 5. More than half the grains are sub- to anhedral. Zoning, as observed in BSE imaging, varies from indistinct to oscillatory. Thirty-five points were analyzed on 22 grains, which typically yielded U concentrations of 300–600 ppm. One homogeneous, BSE-dark core (grain 5) gave a  $^{207}\text{Pb}/^{206}\text{Pb}$  date of  $941 \pm 6$  Ma, which constitutes the only obvious evidence for inheritance. A significant number of other grains also gave mildly to severely discordant dates, and the whole data set defines a discordia with a lower intercept at  $535 \pm 14$  Ma, albeit with an MSWD of 67. A total of 20 points are concordant, but their spread is greater than can be explained by analytical error, frustrating attempts to obtain a concordant age. The weighted average  $^{206}\text{Pb}/^{238}\text{U}$  age is  $532 \pm 3$  Ma (with the youngest age rejected on statistical grounds; MSWD = 2.9). There is no obvious plateau within the spread of ages between 524 and 543 Ma, and the ca. 530 Ma age is therefore taken to represent the intrusive age of the granitoid.

The one zircon with the ca. 941 Ma age yielded two Hf isotope points around  $\epsilon\text{Hf}_{941} +9$  ( $^{176}\text{Hf}/^{177}\text{Hf}_{941} = 0.28245$ ). The remaining 23 analyses define a homogeneous population, with



an average  $\epsilon\text{Hf}_{532}$  of  $-5.9 \pm 1.6$ , or  $^{176}\text{Hf}/^{177}\text{Hf}_{532} = 0.282282 \pm 0.000045$ . The  $^{176}\text{Yb}/^{177}\text{Hf}$  ratios are around 0.03.

Sample MESR80 is a fine-grained red granite sample from Bamseungen in the D' sector of the SW terrane, with ca. 1 Ga metatonalites (Elburg et al., 2015) as host rocks. Quartz displays a chessboard pattern (Figure 10.3F) and rarely contains very thin needles of presumably rutile. Both plagioclase (which can be zoned) and microcline have undergone some alteration, and secondary muscovite has formed. Biotite is dark brown to very light brown in color and shows only minor alteration to chlorite. Allanite and fluorite are found as accessories. Calcite is a rare secondary phase.

The sample contains colorless to yellow-brown zircons with largish sizes (up to 400  $\mu\text{m}$  length), aspect ratios around 2, and zoning patterns that are typically oscillatory, sometimes partly replaced by patchy areas. Twenty-two spots were ablated on 17 grains. Uranium concentrations vary between 100 and 5000 ppm, but the latter zircons typically give discordant analyses. Ten analyses were concordant, of which one, with U contents close to 5000 ppm, gave a slightly older age of  $578 \pm 5$  Ma, which we interpret to reflect an analytical artifact, resulting from nonlinearity of the ion counters at high intensities. The other nine points yielded a concordia age of  $529 \pm 3$  Ma (MSWD concordia and equivalence = 1.6), which is in excellent agreement with the weighted average  $^{206}\text{Pb}/^{238}\text{U}$  age of  $533 \pm 4$  Ma (MSWD = 1.8). This ca. 530 Ma age is taken to date the crystallization of the granite.

The zircon population ( $n = 30$ ) is very homogeneous in its Hf isotopic composition, with an average  $\epsilon\text{Hf}_{529}$  of  $+1.3 \pm 1.4$  ( $^{176}\text{Hf}/^{177}\text{Hf}_{532} = 0.282486 \pm 0.000039$ ) and a relatively high  $^{176}\text{Yb}/^{177}\text{Hf}$  ratio of ca. 0.11.

MESR123 comes from the pink Utsteinen granite at the Belgian Princess Elisabeth Antarctica Station within the D sector of the SW terrane. The granite intrudes gneissic host rocks with sharp contacts (Figure 10.2E). Quartz displays undulose extinction and contains putative rutile needles (Figure 10.3G), while microcline has coarse to lamellar perthitic exsolution. Plagioclase is somewhat sericitized, and microcline to a lesser extent. Biotite is more abundant than amphibole and shows very dark brown to light brown pleochroism. Amphibole is very dark green to olive green. Apatite, titanite, fluorite, and metamict allanite are accessory minerals. Minor calcite is also present. Zircon crystals can already be seen to contain cores in thin section.

The zircons obtained are typically 200  $\mu\text{m}$  long and vary from equidimensional to elongated, with aspect ratios up to 4. However, most grains are fragmented and/or riddled with cracks. Rims are typically colorless and cores brown and cloudy. Many grains have very high uranium contents (up to 3000 ppm), and different settings were used between sessions to analyze both low- and high-U spots. High uranium contents are often found in euhedral cores, which give a characteristic BSE-bright response (Figure 10.4). Oscillatory zoning is commonly seen in the BSE-dark rims. Because of the range in U contents, a large number of spots (54) were analyzed on 43 grains. Rims have U contents from <100 to ca. 600 ppm, while BSE-bright cores vary between 1500 and 9000 ppm. Despite the variable U contents, there is no evidence that different age groups are present. Forty-five analyses are concordant, and with the rejection of one high and one low outlier, the weighted average  $^{206}\text{Pb}/^{238}\text{U}$  age came out at  $528 \pm 4$  Ma (MSWD = 1.5), which agrees with the concordia age of  $529 \pm 3$  Ma. This is interpreted to be the age of igneous crystallization.



Of the 51 analyses performed for Lu-Hf, four had to be discarded because of  $^{176}\text{Yb}/^{177}\text{Hf}$  ratios  $>0.35$ . The remaining 47 analyses form a well-defined homogeneous population, without a distinction in isotopic ratios between cores and rims. The  $\epsilon\text{Hf}_{528}$  is  $-1.8 \pm 1.6$  ( $^{176}\text{Hf}/^{177}\text{Hf}_{528} = 0.282399 \pm 0.000045$ ). Cores and rims differ in their  $^{176}\text{Yb}/^{177}\text{Hf}$  ratio, with an average of 0.04 for the rims and 0.2 for the cores.

MESR118 comes from Mefjell, located just within the granulite-facies C sector of the SW terrane. The granite is light colored and fine grained, and it crosscuts a more mesocratic intrusive with a sharp contact. The sample is very fresh and is dominated by quartz, plagioclase, and perthitic K-feldspar, which all contain exceedingly thin needles, similar to those seen in the quartz crystals in several other samples. Quartz shows undulose extinction, and myrmekite is abundant. Biotite is very dark brown to light brown in color and is often associated with opaque minerals. Accessories are zircon, apatite, and metamict allanite.

The sample contains colorless to yellow or brown zircons that vary from equidimensional to elongated, with aspect ratios up to 5. Lengths can be up to 500  $\mu\text{m}$  but are more typically in the 200–300  $\mu\text{m}$  range. About one-third of the zircons have large euhedral cores that are riddled with BSE-bright inclusions, show patchy zoning, and have very high U contents, which made it impossible to obtain dates from these cores with the setup used. Oscillatorily zoned rims around these cores often display radial cracks. Another third of the zircons mounted have patchy or indistinct zoning, and the remainder displays oscillatory zoning. A total of 32 points were measured on 32 grains, but many analyses displayed high common Pb contents, with  $^{206}\text{Pb}/^{204}\text{Pb}$  ratios varying between 500 and 48000. Measured U contents range between 75 and 1300 ppm. Thirteen analyses are concordant and have  $^{206}\text{Pb}/^{204}\text{Pb}$  ratios  $>6000$ . One of these analyses (29) has a slightly older  $^{206}\text{Pb}/^{238}\text{U}$  date of  $559 \pm 6$  Ma, and the other 12 analyses yield a weighted average of  $527 \pm 5$  Ma, which we interpret to be the igneous age of the sample.

The 41 analyses done on the ca. 527 Ma zircons show a spread in Hf isotope ratios that is slightly larger than what can be expected from analytical error, considering that the  $^{176}\text{Yb}/^{177}\text{Hf}$  ratios are around 0.08. The average  $\epsilon\text{Hf}_{527}$  is  $-4.4 \pm 2.9$ , or  $^{176}\text{Hf}/^{177}\text{Hf}_{527} = 0.282327 \pm 0.000082$ . The one zircon with the apparently slightly older age of 559 Ma does not differ from the main group, with  $^{176}\text{Hf}/^{177}\text{Hf}_{559} = 0.282310 \pm 0.000070$ .

MESR113 comes from a granite from Vesthaugen in the B sector of the NE terrane, well north of the Main Tectonic Boundary. It crosscuts a diorite with a sharp but scalloped contact and is rather inhomogeneous in appearance, with coarser- and finer-grained patches (Figure 10.2D). The sample appears undeformed but has undergone extensive alteration, with chloritization of the biotite, growth of secondary muscovite at the expense of feldspars, and interstitial calcite. Quartz contains thin needle-like inclusions. Accessory phases are opaque minerals, titanite, apatite, and zircon.

The zircons are colorless to light pink, with aspect ratios up to 4 and a typical length of 200  $\mu\text{m}$ . Many crystals are cracked. Most crystals show clearly visible zoning in BSE images, which can be either oscillatory or more patchy. Nineteen spots were analyzed on 18 crystals. Uranium contents vary between 100 and 1000 ppm, and most crystals contain significant common Pb, resulting in widely varying  $^{206}\text{Pb}/^{204}\text{Pb}$  ratios of 100–35000. When all data are plotted on a Tera-Wasserburg diagram, they yield an age of  $501 \pm 36$  Ma, but the MWSD of 24 indicates that this is not a meaningful age. The seven (almost) concordant analyses from zircons with oscillatory zoning and high  $^{206}\text{Pb}/^{204}\text{Pb}$  ratios give scattered dates. One (19) is clearly older,



with a  $^{206}\text{Pb}/^{238}\text{U}$  date of  $603 \pm 6$  Ma. Two high-U (ca. 1000 ppm) analyses yield  $^{206}\text{Pb}/^{238}\text{U}$  dates of 534 and 539 Ma, and the other four spots range between 501 and 516 Ma. The latter four give a weighted average  $^{206}\text{Pb}/^{238}\text{U}$  age of  $509 \pm 12$  Ma (95% confidence level), with an MSWD of 2.2. Since the ca. 539 Ma age was measured on a rim (grain 8), of which the core gave a concordant age of ca. 501 Ma, we think that the two high-U analyses with slightly older dates are an artifact related to nonlinearity of the ion counters at high count rates. We therefore take the ca. 510 Ma age as the best estimate for the crystallization age of the granite.

The 18 analyses performed for Hf isotopes yielded a homogeneous population, with an average  $\epsilon\text{Hf}_{509}$  of  $-2.5 \pm 1.6$  ( $^{176}\text{Hf}/^{177}\text{Hf}_{509} = 0.282393 \pm 0.000043$ ) and an unremarkable  $^{176}\text{Yb}/^{177}\text{Hf}$  ratio of 0.06. The one older grain has a very similar initial Hf isotopic ratio, with  $^{176}\text{Hf}/^{177}\text{Hf}_{603} = 0.282383 \pm 0.000070$ .

MESR22 is derived from an ca. 5-m-thick white granite dyke with large K-feldspar crystals from Tanngarden, just within the granulite facies C sector of the SW terrane. It is macroscopically undeformed and intruded subparallel to the bedding of the metamorphic country rocks (calc-silicates and gneisses). Quartz displays equant subgrains and irregular grain boundaries. K-feldspar is largely microcline and shows coarse perthitic exsolution lamellae. Plagioclase displays discontinuous normal zoning (Figure 10.3H); some crystals appear to be fractured. Slight sericitization is observed in the feldspars. Biotite has dark brown to light brown pleochroism and can be altered to chlorite. Secondary muscovite is present in many feldspar crystals. Fluorite, apatite, and zircon are accessory phases.

Zircons are numerous and large, with lengths up to 400  $\mu\text{m}$  and aspect ratios varying between 2 and 4. Most crystals display well-defined oscillatory zoning in BSE, but some have dark featureless cores, with low U contents of <200 ppm compared with the 400–2000 ppm of the other areas. These cores have a brownish color, contrasting with the colorless appearance of the rest of the zircons. Some crystals have started to develop patchy zoning that partly obliterates the oscillatory zoning. Twenty-two analyses were performed on 17 grains, and 13 are concordant. Of these, grain 26 - with the highest U contents of ca. 2000 ppm - yields a slightly older date at  $545 \pm 8$  Ma, which may reflect an analytical problem at these high U concentrations. The other 12 analyses define a concordia age of  $506 \pm 4$  Ma, which is indistinguishable from the weighted average  $^{206}\text{Pb}/^{238}\text{U}$  age of  $507 \pm 4$  Ma and defines the age of igneous crystallization.

The 36 Lu-Hf analyses gave an average  $\epsilon\text{Hf}_{506}$  of  $-1.3 \pm 2.1$  ( $^{176}\text{Hf}/^{177}\text{Hf}_{507} = 0.282428 \pm 0.000059$ ) at a  $^{176}\text{Yb}/^{177}\text{Hf}$  ratio of 0.09 (one analysis was discarded because of its high Yb/Hf ratio). The one grain that had given a slightly older age has an indistinguishable initial ratio of  $0.282441 \pm 0.000022$ .



## 10.6 Discussion

### 10.6.1 Comparison with Published Pan-African Zircon U-Pb Ages

#### Sør Rondane

Our data complement previous U-Pb ages from the Sør Rondane Mountains, which were mainly obtained in the framework of the Japanese Antarctic program. The oldest Pan-African intrusive we dated is Dufekfjellet ( $637 \pm 6$  Ma), for which a somewhat younger SHRIMP U-Pb zircon age of  $619 \pm 7$  Ma was published by Li et al. (2006). Although apparently broadly similar in mineralogy, the sample analyzed by Li et al. (2006) came from the western side of the intrusion and contained garnet, while ours was from the north, and no garnet was observed. Another distinction is that our analyses show a prominent inherited component, which was not reported by the previous authors. It is therefore possible that the  $\geq 5$  Ma difference in age represents different phases within the intrusive, or it could represent an underestimate of the uncertainty on the age. The fact that our sample yielded one zircon with a younger age ( $603 \pm 7$  Ma) could indicate a prolonged magmatic history for the intrusion.

A U-Pb SHRIMP zircon age on the Vengen/Vikinghøgda granite, from which our sample MESR30 is derived, was given by Shiraishi et al. (2008) as  $562 \pm 7$  Ma (sample 9091405A); their titanite age is similar at  $568 \pm 11$  Ma. Both are within error of our age of  $551 \pm 8$  Ma. Inherited, xenocrystic zircon was also described by the previous authors, with ages around 1100, 1000, and 600 Ma, of which the latter two compare well with the age fractions present in our sample.

Three SHRIMP U-Pb zircon ages were provided by Jacobs et al. (2015) for samples from three locations in the west from the same outcrops where MESR75, 80, and 82 were taken (Jacobs's samples of J1214B, J1216A, and J1216B, respectively). For MESR75, the younger age cluster compares very well ( $556 \pm 4$  vs.  $557 \pm 2$  Ma), as is the case for MESR80 ( $529 \pm 3$  vs.  $534 \pm 4$  Ma). However, sample MESR82 yields an igneous age of  $572 \pm 5$  Ma, whereas J1216B yields  $555 \pm 4$  Ma; moreover, the former yielded only a single inherited zircon, whereas the latter gave as many inherited as igneous ages. Because the outcrop consists of a significant number of different intrusive phases, the presence of distinct age components can be expected. The dominant age population in J1216B appears as a minor population in MESR82 (Figure 10.5C), pointing toward a prolonged thermal history for this area. Note that the choice of age has a minimal influence on the initial Hf isotopic composition of the zircons, which would change from +2.4 at 572 Ma to +1.9 at 555 Ma.

No other samples that are close equivalents to the ones analyzed in this study have been dated previously, but a significant body of igneous and metamorphic U-Pb zircon ages already exists on Pan-African metamorphism and magmatism in the Sør Rondane Mountains (Li et al., 2006; Shiraishi et al., 2008; Adachi et al., 2013; Grantham et al., 2013; Higashino et al., 2013; Nakano et al., 2013; Osanai et al., 2013; Owada et al., 2013; Elburg et al., 2016) as well as for older intrusives (Shiraishi et al., 2008; Kamei et al., 2013; Owada et al., 2013; Elburg et al., 2015). Focusing on Pan-African ages ( $\leq 700$  Ma), we compiled the existing U-Pb zircon data, which have been plotted in order of decreasing age (Figure 10.7). This representation has the advantage over a histogram that age peaks are not influenced by the choice of bin sizes or boundaries; it also permits showing the error on individual analyses. The diagram shows that metamorphism in the NE terrane was contemporaneous with magmatism (such as the Dufek



granite) and metamorphism in the SW terrane between ca. 660 and 600 Ma, with perhaps a short hiatus in activity around 630 Ma. This period of zircon formation has been related to the EAAO, whereby the NE terrane was thrust over the SE terrane (Osanai et al., 2013). The next magmatic-metamorphic period peaked between 580 and 550 Ma, which also involved rare magmatism in the NE terrane. This age group was not explicitly mentioned by Osanai et al. (2013), but Grantham et al. (2013) equate this with the thrusting event. Magmatism around 530 Ma is accompanied by minor (?retrograde) metamorphism in the NE terrane, and there is a tail of magmatism between 510 and 500 Ma. Although this last event is represented with few data points, three out of four are from the NE terrane, which is a noticeably higher proportion of igneous ages for the NE terrane than in any of the previous period, although it cannot be excluded that this just reflects the unreliable statistics of small numbers. Only one age, a metamorphic one, is younger than 500 Ma. Previous authors have viewed the ca. 530 and 500 Ma stages as representing magmatism and associated retrograde metamorphism resulting from intracrustal melting after crustal thickening (Grantham et al., 2008; 2013; Osanai et al., 2013). Our samples cover all age groups, with TC43 (Dufek, SW terrane) representing the oldest (>600 Ma) age group; MESR12, 82, 89 (Lunkeryggen syenite), 75, and 30 (Vengen/Vikinhøgda), which all come from the SW terrane, fall within the 550–580 Ma group; the ca. 530 Ma group is represented by MESR121 (just within the NE terrane), 80, 123, and 118 (SW terrane); while the two youngest granites are MESR113 from Vesthaugen in the NE terrane and MESR22, which hails from the SW terrane. Inherited zircon is found within granites of all age groups but is limited to ages  $\leq 1$  Ga and will be discussed further in the section on Hf isotopes (see below). Although the number of samples with a particular age may help to define the timing of metamorphic-igneous events, it is unlikely to give an accurate representation of the volumes of magma emplaced at any given time. This is most obvious for the Dufek granitoid, for which two ages are available but which appears to define the single largest intrusion in the area on the basis of the observed large positive magnetic anomaly (Figure 1; after Mieth et al., 2014). However, interpreting the magnetic anomalies as representing a single magmatic body is unlikely to be correct, as can be seen from the fact that samples MESR12 and 123 are from the same interpreted granitoid body, whereas their ages differ by approximately 50 million years, which is consistent with the observed differences in mineralogy and fabric between the two samples.

### **Neighboring Areas**

U-Pb zircon age data from the Yamato-Belgica Mountains bordering the Sør Rondane Mountains to the east are very scarce but point toward metamorphism around 660–600 Ma and magmatism in the ca. 530 Ma age bracket (Shiraishi et al., 2003). This overlaps with two of the age groups seen in Sør Rondane. Whether the other two age groups are also present within the Yamato-Belgica Mountains needs to be clarified by further dating studies.

In central and western Dronning Maud Land, U-Pb zircon evidence for the oldest period of magmatism and metamorphism (680–630 Ma) is found only in the Schirmacher Oasis (Baba et al., 2010), augmented by Sm-Nd isochrons and U-Pb data on titanite and monazite (Ravikant et al., 2004; 2007) and by U-Pb zircon ages from Hochlinfjellet (Baba et al., 2015). For the rest of the area, magmatism and metamorphism appear to start between ca. 610 and 550 Ma, with, for instance, the Gruber Anorthosite at ca. 600 Ma (Jacobs et al., 1998).



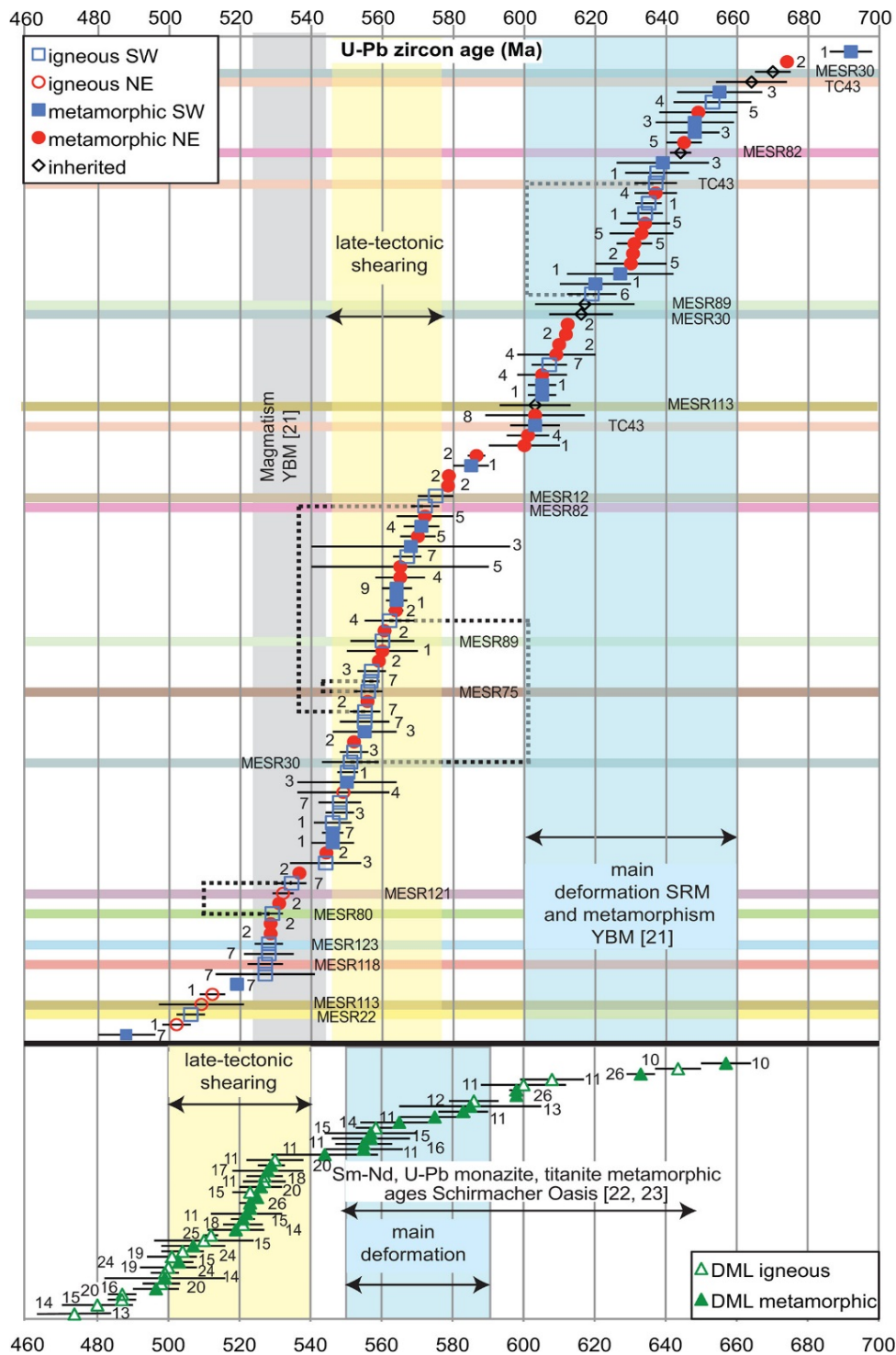


Figure 10.7: All available igneous and metamorphic U-Pb zircon ages for the NE and SW terrane of the Sør Rondane Mountains (top) and central and western Dronning Maud Land (bottom). Error bars are  $2\sigma$ . Our own data are highlighted by colored bars; the inherited components are only from our own data. Dotted lines connect samples from the same outcrops or intrusive bodies. YBM, Yamato-Belgica Mountains. Source: 1, Adachi et al. (2013); 2, Grantham et al. (2013); 3, Nakano et al. (2013); 4, Shiraishi et al. (2008); 5, Osanai et al. (2013); 6, Li et al. (2006); 7, Jacobs et al. (2015); 8, Higashino et al. (2013); 9, Owada et al. (2013); 10, Baba et al. (2010); 11, Jacobs et al. (1998); 12, Bauer et al. (2003b); 13, Harris et al. (1995); 14, (Board et al., 2005); 15, Jacobs et al. (2003a); 16, Jacobs et al. (2003c); 17, Jacobs et al. (2003d); 18, Jacobs et al. (2003b); 19, Paulsson and Austrheim (2003); 20, Bisnath et al. (2006); 21, Shiraishi et al. (2003); 22, Ravikant et al. (2004); 23, Ravikant et al. (2007); 24, Jacobs et al. (2008b); 25, Mikhalsky et al. (1997a); 26, Baba et al. (2015).



The next pulse of activity was between 530 and 520 Ma, and then another was between ca. 510 and 480 Ma (Mikhalsky et al., 1997a; Jacobs et al., 1998; 2003b; 2003a; 2003c; 2003d; 2008b; Bauer et al., 2003b; Paulsson and Austrheim, 2003; Board et al., 2005; Bisnath et al., 2006). A notable difference with the Sør Rondane Mountains is the evidence for magmatism younger than 500 Ma, for which no U-Pb zircon ages have been found in the Sør Rondane Mountains. The greater resemblance of the Sør Rondane Mountains with the Yamato-Belgica Mountains and Schirmacher Oasis than with the remainder of Dronning Maud Land was already noticed by Elburg et al. (2015) regarding the older phase of magmatism (1–0.9 Ga in Sør Rondane vs. 1.2–1.05 in Dronning Maud Land); the apparent absence of the older Pan-African metamorphic period within central and western Dronning Maud Land has been noticed by other workers (Grantham et al., 2008) and has been used for large-scale tectonic reconstructions of Gondwana amalgamation (Grantham et al., 2008; 2013; Boger et al., 2015; Jacobs et al., 2015). It must be noted that the geochronological data for central and western Dronning Maud Land are scarcer than for the Sør Rondane Mountains, so this apparent later start of magmatism and metamorphism could be a sampling artifact, as the most recent ages published by Baba et al. (2015) illustrate. However, the slightly younger age of postcollisional magmatism in central and western Dronning Maud Land appears to be a true difference between the two areas.

### 10.6.2 Age of Deformation

Only few of the samples studied show macroscopic evidence for deformation. The oldest granitoid (Dufek, TC43, at ca. 640 Ma) is largely undeformed, which could be a result of the relatively large size of this intrusion, which thereby behaved as a rigid block during deformation. It is located within the D sector, which as a whole displays little evidence for deformation, leading to the suggestion of Jacobs et al. (2015) that the area behaved as a megaboudin during deformation associated with Gondwana amalgamation.

Sample MESR12, an ca. 575 Ma granitoid dyke crosscutting the main foliation, is foliated itself, so deformation was still ongoing at that time. In sample MESR82, which has the same age within error, evidence for deformation is limited to the presence of dynamically recrystallized quartz and a weak alignment of the micas. The next younger samples (such as the syenite complex sample MESR89 and far western granite MESR75) show very limited evidence for ductile deformation, with rare bent plagioclase twins, although some brittle features were observed, and the contact between the syenites and the host rocks is sheared (Ruppel et al., 2015). Further evidence for the halting of regional deformation around this time comes from the U-Pb zircon age of undeformed and unmetamorphosed minette dykes (Owada et al., 2013) from the SW terrane at  $564 \pm 2$  Ma.

The dextral Main Shear Zone (Ruppel et al., 2015) was clearly active until at least ca. 550 Ma, which is the age of sheared Vengen/Vikingshøgda sample MESR30. Thus, deformation on this feature appears to have continued longer than the regional deformational event. Perhaps this shear zone also affected the granites at Bamseungen (MESR80), for which the chessboard quartz (Figure 10.3F) provides for high-temperature deformation (Kruhl, 1996). Because sample MESR123, representing the granite from Utsteinen, does not show any sign of dextral shear, its age of ca. 528 Ma may provide a lower limit for activities of the Main Shear Zone and related structures.



The age of deformation in central and western Dronning Maud Land has been inferred in a similar way by U-Pb zircon dating of intrusives affected and unaffected by deformation (Jacobs et al., 2008b and references therein). The main deformational event in central and western Dronning Maud Land appears to have taken place between 590 and 550 Ma, with late-tectonic shearing in the period of 540–500 Ma and posttectonic intrusives appearing only at 500–480 Ma. Therefore, not only magmatism but also deformation seems to have occurred slightly later in central and western Dronning Maud Land than in the Sør Rondane Mountains (Figure 10.7).

### 10.6.3 Lu-Hf Data

#### The Inherited Components

Hf isotope results for zircons from the Sør Rondane Mountains are appreciably scarcer than U-Pb age data, with only Elburg et al. (2015) providing data for the 0.9–1 Ga meta-gabbro/tonalite/trondhjemite/granodiorite from the SW terrane, which are shown in Figure 10.6 and Figure 10.8 for comparison. The locations are given in Figure 10.1. The oldest inherited component in the Pan-African granitoids analyzed yielded ages around 950 Ma (similar to the dominant groups of metatonalites of the SW terrane (Kamei et al., 2013; Owada et al., 2013; Elburg et al., 2015) and were found in TC43 (Dufek), MESR89 (Lunkeryggen syenite), and MESR30 (Vengen/Vikinhøgda granite), all from the SW terrane. The ca. 950 Ma zircons within the latter two intrusions match the age and average isotopic signature ( $\epsilon_{\text{Hf}_i}$  ca. +7.5) of samples MESR106 and 49a, interpreted to belong to a postsubduction calc-alkaline magmatic episode (Elburg et al., 2015). The ca. 950 Ma inherited component within TC43 has an isotopic signature ( $\epsilon_{\text{Hf}_i}$  ca. +4) that is most closely matched by sample MESR110, which comes from the metatonalite outcrop furthest south. However, the Hf isotopic composition of the Pan-African igneous zircons in sample TC43 is too high to be formed by reworking of this tonalite body and resembles the characteristics of the northern tholeiitic bodies more closely (see below).

Inherited zircons in the 700–800 Ma age bracket (in MESR30 [Vengen/Vikinhøgda] and MESR89 [syenite]) could possibly be related to another phase of calc-alkaline magmatism dated at ca. 770 Ma (Kamei et al., 2013). However, the ca. 750 Ma zircons from MESR30 show a large range in  $\epsilon_{\text{Hf}_i}$  values (+2 to +8), which may point toward a role for crustal reworking in addition to juvenile magmatic additions at 750 Ma. This period of magmatic activity in the Sør Rondane Mountains still needs further clarification. Zircons with similar ages are commonly the youngest igneous component in metasedimentary samples from the NE terrane. Within the SW terrane, only a single detrital age in this bracket (at  $784 \pm 2$  Ma) has been reported (Adachi et al., 2013) and was interpreted to represent igneous activity. The scarcity of these ages was interpreted to reflect a lack of igneous and metamorphic activity in the SW terrane between 650 and 950 Ma and/or an older depositional age for the SW terrane than the NE terrane (Osanai et al., 2013). Our new data and the evidence for calc-alkaline magmatism in the SW terrane given by Kamei et al. (2013) make the distinction between the NE and the SW terrane less pronounced, although the absence of inherited ages older than 1200 Ma within the SW terrane, as noted by Osanai et al. (2013), still stands.

Inherited zircons with ages  $\leq 700$  Ma overlap in age with the oldest phase of magmatism and metamorphism Figure 10.7. They often have an initial  $^{176}\text{Hf}/^{177}\text{Hf}$  ratio that is within error of the igneous population Figure 10.8.



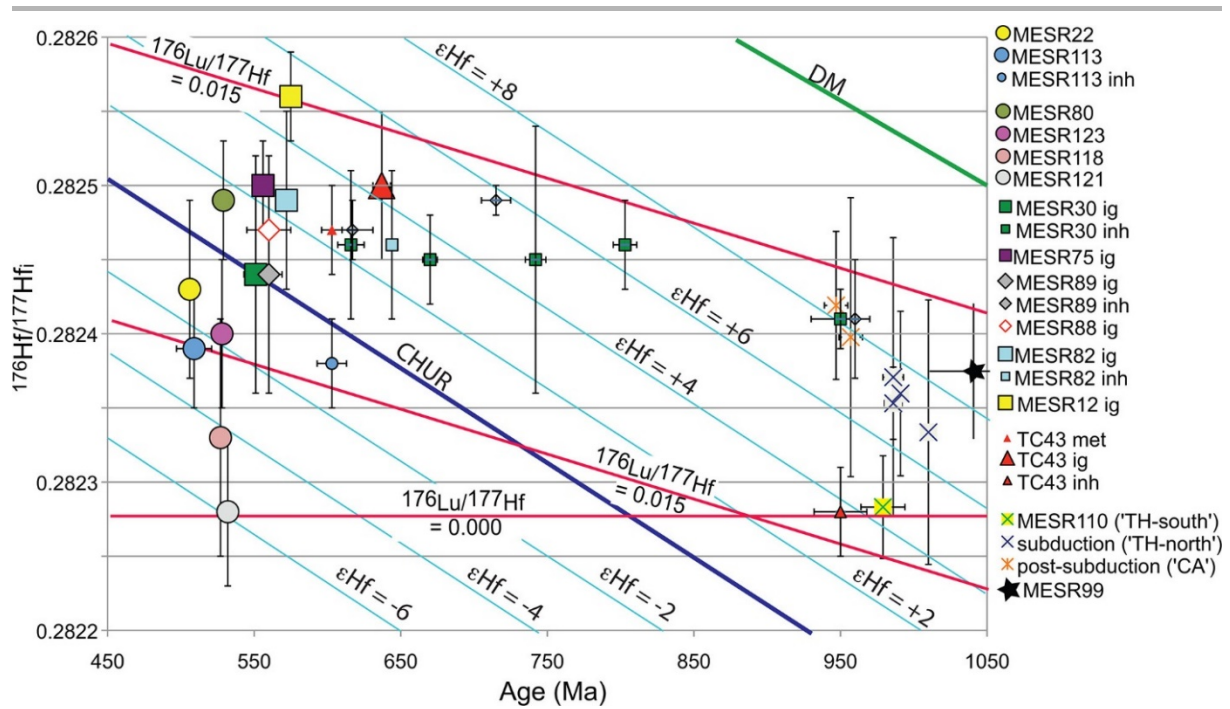


Figure 10.8: Initial  $^{176}\text{Hf}/^{177}\text{Hf}$  zircon isotopic ratio versus age, averaged per age group. Error bars are 2 SD. The line of  $^{176}\text{Lu}/^{177}\text{Hf} = 0.015$  gives the evolution curve for a typical crustal reservoir;  $^{176}\text{Lu}/^{177}\text{Hf} = 0.00$  is the limiting case of a Lu-free reservoir, similar to the evolution curve for a zircon. CHUR, Chondritic Uniform Reservoir ( $^{176}\text{Lu}/^{177}\text{Hf} = 0.0336$ ); DM, depleted mantle ( $^{176}\text{Lu}/^{177}\text{Hf} = 0.0388$ ). The 900–1015 Ma samples are from Elburg et al. (2015), with sample names as in Figure 10.6.

### The Igneous Populations

The igneous populations of zircons vary in average initial  $^{176}\text{Hf}/^{177}\text{Hf}$  ratios between ca. 0.28225 and 0.28257, or  $\epsilon\text{Hf}_i$  values of  $-6$  to  $+5$ . Most of the range of Hf isotopic values could potentially just be explained by reworking of the 0.9–1 Ga population of zircons, within a reservoir with a  $^{176}\text{Lu}/^{177}\text{Hf}$  ratio of 0.015 (Figure 10.8), which is commonly taken as the average ratio for continental crust (Griffin et al., 2004). Only samples MESR118 and 121 have Hf isotopic compositions that are lower and which would necessitate reservoirs with lower  $^{176}\text{Lu}/^{177}\text{Hf}$  ratios, whereby MESR121 can be modeled with only a ratio of 0; this would work only if the lowest Hf isotope population of the 0.9–1 Ga age group was reset in terms of U-Pb age but not in Hf isotopic composition. This seems an unlikely interpretation, also because the ca. 0.9–1 Ga metatonalites are restricted to the D' sector of the SW terrane at a distance of more than 40 km from the location of MESR121. The depleted mantle extraction ages of the zircons - assuming aging in a crustal reservoir with a  $^{176}\text{Lu}/^{177}\text{Hf}$  ratio of 0.015 before zircon formation - range from 1.15 Ga for MESR12 to 1.8 Ga for MESR121; assuming an upper crustal reservoir with a  $^{176}\text{Lu}/^{177}\text{Hf}$  ratio of 0.010 changes these numbers to 1 and 1.45 Ga, respectively. This is slightly older than the Nd model ages for the SW terrane given by Shiraishi et al. (2008), which range between 0.9 and 1.25 Ga.

For the samples of which the isotopic signature could potentially be explained by reworking of the ca. 1 Ga metatonalitic crust (i.e., excluding MESR118 and 121), there is a broad trend of decreasing initial  $^{176}\text{Hf}/^{177}\text{Hf}$  ratios from ca. 575 to 500 Ma. This seems somewhat coincidental if the zircon isotopic signature were a result of intracrustal reworking only, since there would not be an obvious reason why early stages of magmatism would have reworked preexisting crust with higher Hf isotopic compositions than later stages of magmatism. We therefore think that the isotopic signatures are better explained by a decreasing contribution of juvenile material



with time. Another observation that argues against intracrustal reworking only is the existence of the Lunkeryggen Syenite Complex, which dominantly consists of quartz-poor syenites to melasyenites that are unlikely to have been formed by remelting of preexisting continental crust. They could possibly be related to the undeformed high-potassium, silica-undersaturated minette dykes that were also dated at ca. 560 Ma by both K-Ar and U-Pb zircon dating and that were interpreted to reflected melting of the lithospheric mantle, modified by the subduction and collision processes at 600–660 Ma (Owada et al., 2013).

The older Dufek granite does not appear to conform to the trend of decreasing Hf isotopic compositions with time and could very well be explained by pure intracrustal reworking of the 0.9–1 Ga subduction-related metatonalites. This interpretation fits better with the tectonic scenario proposed by (Osanai et al., 2013), whereby the SW terrane is thrust underneath the NE terrane during peak metamorphism at 600–660 Ma than if the Dufek granite is interpreted to have formed in a subduction setting at this time. However, some question remains of how melting was initiated during the isothermal compressional event around this time that was deduced from the PTt path of the SW terrane (Osanai et al., 2013).

When looking at the four ca. 530 Ma granitoids only (which include MESR118 and 121), there is a huge spread in zircon Hf isotope ratios. This could potentially be related to the spatial distribution of the intrusives, whereby the ratios decrease from west to east (Figure 10.9). Sample MESR121, with the lowest value, is located close to the boundary of the SW and NE terranes. This does not mean that there is a significant difference in isotopic ratios between the SW and NE terrane, since the one (younger) sample that is located unambiguously within the NE terrane (MESR113 from Vesthaugen) has an average initial  $^{176}\text{Hf}/^{177}\text{Hf}$  ratio that is within error of that of the similarly aged sample MESR22 from the SW terrane and is higher than Mefjell sample MESR118 from the granulite (C) sector of the SW terrane (Figure 10.9). The tectonic scenario envisaged by Osanai et al. (2013), with the NE terrane having been thrust over the SW terrane, implies that the SW terrane could potentially underlie the NE at greater depth, which could explain the similarity between sample MESR113 from Vesthaugen with granitoids of the SW terrane; it cannot, however, explain why the Hf model ages for samples MESR118 and 121 are older than for other granitoids from the SW terrane. These older model ages point toward the involvement of older crust in their petrogenesis. This could mean that the SW terrane is not a single entity, with a mantle extraction age similar to that of the 0.9–1 Ga metatonalites, but that it is a collage of several domains, with contrasting geological histories. The area from which MESR118 and 121 are derived forms a distinct structural and aeromagnetic domain (Figure 10.1D), called the central Sør Rondane corridor by Mieth et al. (2014). The latter authors speculated that this area with complex tectonic structures might be an extensional corridor, but the distinction in isotopic signatures with the rest of the SW terrane could mean that it is a different crustal domain.

## 10.7 Recapitulation and Conclusions

Our new data and compilation of published U-Pb zircon ages show a prolonged history of magmatism and metamorphism in the Sør Rondane Mountains. The main metamorphic phase is at 660–600 Ma, recognized most clearly in the NE terrane, accompanied with minor magmatism, of which the Dufek granite is the most important example. This granite may have been formed by reworking of the 0.9–1 Ga metatonalites in the area, since its reported



geochemical arc signature (Li et al., 2003) is hard to reconcile with its position in the lower plate, according to the interpretation of the metamorphic terranes by Osanai et al. (2013). However, the timing of intracrustal melting in the supposed lower plate during isothermal decompression is also somewhat problematic. This period is also thought to be the main phase of deformation, although distributed inhomogeneously throughout the area. If this period of magmatism and metamorphism indeed represents the EAAO (Osanai et al., 2013), it seems a bit surprising that evidence for magmatism and metamorphism around this time is scarce in central Dronning Maud Land.

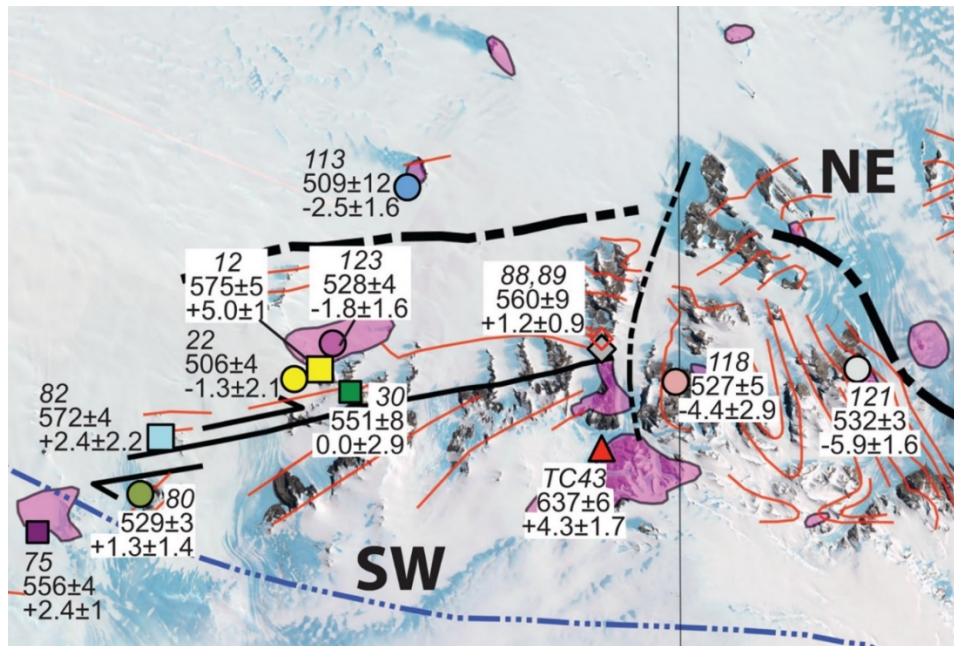


Figure 10.9: Overview of ages and  $\epsilon_{\text{Hf}}$  for the different granitoids analyzed.

The next magmatic and metamorphic period was from 575 to 550 Ma and may represent the final stages of ductile deformation, mainly focused on the Main Shear Zone, as evidenced by a sheared sample of the Vengen/Vikingshøgda granite at ca. 550 Ma. From 575 Ma onward, the zircon Hf isotopic compositions show a decreasing trend, in both absolute and  $\epsilon$  units, from an  $\epsilon_{\text{Hf}}_{575 \text{ Ma}}$  of +5. The Lunkeryggen syenite complex also falls within this magmatic period and could potentially be genetically linked to the minette dykes of the same ca. 560 Ma age (Owada et al., 2013). The variable Hf isotopic signature, the association of mafic and felsic magmas, and the presence of a syenite complex of which the rocks cannot be generated by crustal remelting suggest the involvement of mantle melts during this magmatic period.

The four samples from the ca. 530 Ma magmatic episode show a strong decrease in zircon Hf isotope ratios from west to east (Figure 10.9). It is noteworthy that one of the two least radiogenic samples (MESR118 from Mefjell), which fall outside of the isotopic range that could be explained by simple intracrustal reworking of the 0.9–1 Ga metatonalites, still lies within the SW terrane, as defined by Osanai et al. (2013), but on the eastern side of the N-S running lineament that offsets the boundary between the two terranes, within the aeromagnetically (Mieth et al., 2014) defined central Sør Rondane corridor. This could potentially be a slightly older crustal domain than the rest of the SW terrane. Metamorphism and magmatism around this time has been associated with the collision between the Kalahari Craton (to which the Sør Rondane Mountains had already been accreted) and the Indo-Antarctic Craton in the east (Osanai et al., 2013). The available data show that metamorphism in this age bracket is better



represented in central Dronning Maud Land than in the Sør Rondane Mountains, so it is somewhat surprising if this event represented a collision with a more easterly block.

Two granitoids, among which is a sample from Vesthaugen in the NE terrane, yielded ages between 510 and 500 Ma and  $\epsilon_{\text{Hf}_i}$  around  $-2$ . Magmatism of this age and younger is again more prevalent in central Dronning Maud Land.

The observed temporal and spatial isotopic trends in the Sør Rondane Mountains suggest waning importance of juvenile magmatic input over time and a control by the crust into which the granitoids intruded. Although crustal contamination may have played a role, this cannot have been very important for, for example, the silica-poor Lunkeryggen syenite complex, since crustal contamination would rapidly increase the magmas' silica content. It is therefore likely that the lithospheric mantle has had an important influence on the magmas' isotopic composition. This suggests that a process like lithospheric delamination (Jacobs and Thomas, 2004) or postcollisional extension is a more likely cause for the observed magmatism than intracrustal melting related to crustal thickening (Grantham et al., 2008). However, neither a single period of delamination nor crustal thickening can explain the ca. 150 Ma duration of magmatism.

The metamorphic, magmatic, and deformational history of the Sør Rondane Mountains appears to be shifted to an ca. 20–40 Ma older age bracket than what has been documented in central and western Dronning Maud Land (with the possible exception of Schirmacher Oasis). Although data from the Yamato-Belgica complex are scarce, they overlap in age with those for the Sør Rondane Mountains. This reinforces the idea put forward by previous studies (Riedel et al., 2013; Elburg et al., 2015; Jacobs et al., 2015) that an important tectonic boundary exists between the Sør Rondane Mountains and central and western Dronning Maud Land, which could be the Forster Magnetic Anomaly (Riedel et al., 2013). This is, however, unlikely to be the one and only large-scale boundary between eastern and western Gondwana, but it more likely represents one of a number of boundaries where different slices of the supercontinent came together. The variation seen within the Sør Rondane Mountains in terms of inherited zircons between the NE and SW terrane (Osanai et al., 2013; this work) as well as the difference in Hf isotopic composition between different sectors of the SW terrane may favor a collage-style accretionary history. Evidence for this style of accretion also comes from central Dronning Maud Land, where different geographic areas show contrasting metamorphic ages (Baba et al., 2015). Such a collage-style accretion may also be the cause of the extended duration of magmatism in the Sør Rondane Mountains. A modern analog may be the Indonesian area, which consists of a collage of fragments with contrasting geological histories (Hall, 2002; Leeuwen et al., 2007) and where magmatism has been semicontinuous during this assembly (e.g. Elburg et al., 2003).



## 10.8 Acknowledgements

The Geodynamic Evolution of East Antarctica II team would like to thank the helicopter pilots K. Wagner, F. Tauber, and J. Hergenröder of Sky Heli, Germany, for their flying skills and A. Hubert, G. Johnson-Amin, and the crew of the Belgian Princess Elisabeth Antarctica Station for their hospitality and support during the field season. The analytical work was funded by grant 90036 from the South African National Research Foundation to M. A. Elburg. C. Ramchurran and J. Reinhardt are thanked for their help with the analytical work at the University of KwaZulu-Natal, and we also thank S. L. Simonsen at Oslo University. J. Jacobs, N. Krohne, and M. A. Elburg are indebted to the Bundesanstalt für Geowissenschaften und Rohstoffe (BGR) for the invitation to participate at the Geodynamic Evolution of East Antarctica expeditions. J. Jacobs wishes to thank the Alfred-Wegener-Institute for Helmholtz Centre for Polar and Marine Research, and M. A. Elburg acknowledges the International Polar Foundation, the Belgian Federal Science Policy Office, and the Belgian Antarctic Research Expedition. The study was partly supported by the Deutsche Forschungsgemeinschaft (grants LA 1080/9 to A. Läufer, BGR, and LI 745/15 to F. Lisker, University of Bremen) in the framework of the priority program Antarctic Research with Comparative Investigations in Arctic Ice Areas. J. Jacobs's work was funded in part by Norges Forskningsråd–Norwegian Antarctic Research Expeditions. Helpful reviews by T. Adachi and A. Kamei are gratefully acknowledged.





## Chapter 11

# 11. Erosion at Extended Continental Margins: Insights from New Aerogeophysical Data in Eastern Dronning Maud Land

Graeme Eagles, Nanna B. Karlsson, Antonia Ruppel, Daniel Steinhage, Wilfried Jokat, Andreas Läufer

Key findings:

- Nearly 40000 km of new gravity and radar data in eastern Dronning Maud Land
- Paleo-fluvial drainage system behind escarpment saw short-lived phase of alpine glaciation preceding present cold-based era
- Erosion by balanced backwearing and downwearing seawards of a breakup-aged or older (i.e. Jurassic) inland drainage divide
- Paleo-fluvial drainage system may therefore be very ancient
- Longer-distance sediment transport in Jurassic river system via glacially-deepened Grand Canyon-sized trough

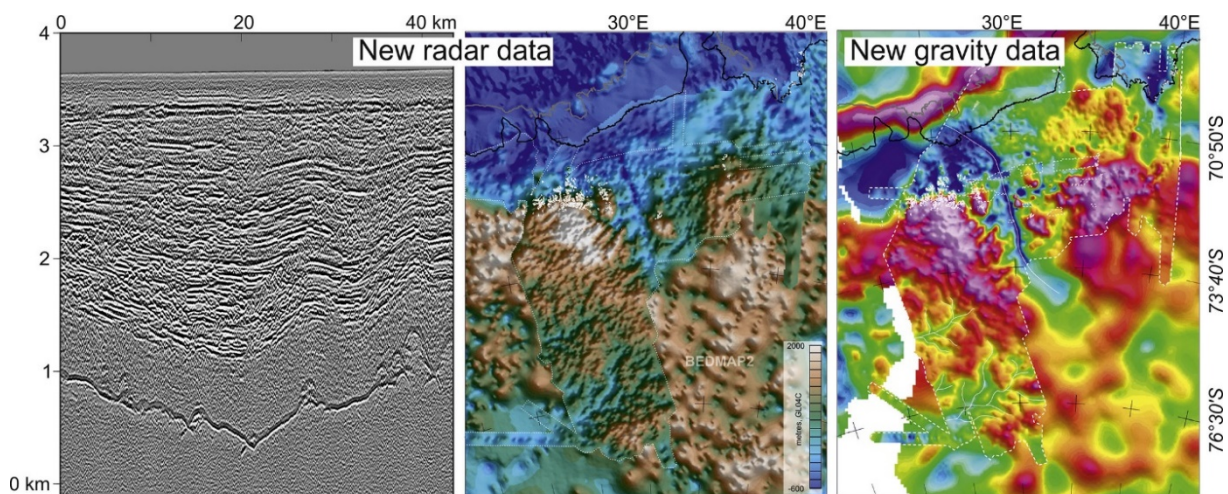


Figure 11.1: Graphical Abstract

### 11.1 Abstract

Modelling-, rock cooling-, sedimentation- and exposure-based interpretations of the mechanisms by which topography evolves at extended continental margins vary widely. Observations from the margin of Dronning Maud Land, Antarctica, have until now not strongly contributed to these interpretations. Here, we present new airborne gravity and radar data describing the eastern part of this margin. Inland of a tall (2.5 km) great escarpment, a plateau topped by a branching network of valleys suggests preservation of a fluvial landscape with SW-directed drainage beneath a cold-based ice sheet. The valley floor slopes show that this landscape was modified during a period of alpine-style glaciation prior to the onset of the current cold-based phase around 34 Ma. The volume of sediments in basins offshore in the



Riiser-Larsen Sea balances with the volume of rock estimated to have been eroded and transported by north-directed drainage from between the escarpment and the continental shelf break. The stratigraphy of these basins shows that most of the erosion occurred during the ~40 Myr following late Jurassic continental breakup. This erosion is unlikely to have been dominated by backwearing because the required rate of escarpment retreat to its present location is faster than numerical models of landscape evolution suggest to be possible. We suggest an additional component of erosion by downwearing seawards of a pre-existing inland drainage divide. The eastern termination of the great escarpment and inland plateau is at the West Ragnhild trough, a 300 km long, 15–20 km wide and up to 1.6 km deep subglacial valley hosting the West Ragnhild glacier. Numerous overdeepened (by >300 m) segments of the valley floor testify to its experience of significant glacial erosion. Thick late Jurassic and early Cretaceous sediments fanning out from the trough's mouth into the eastern Riiser-Larsen Sea betray an earlier history as a river valley. The lack of late Jurassic relief-forming processes in this river's catchment in the interior of East Antarctica suggests this erosion was related to regional climatic change.

## 11.2 Introduction

### 11.2.1 Background and Rationale

Facing the oceans, and several hundred metres to three kilometres in height, so-called great escarpments are known from numerous extended continental margins worldwide (e.g. southern Africa, Brazil, eastern Australia, the Red Sea, and western India). Their presence or absence appears not to correlate with margin age, attesting to their longevity (Gilchrist and Summerfield, 1990). This in turn is linked to the escarpments' roles as drainage divides, by which they sustain feedbacks between climate, erosion, tectonics and isostasy (e.g. Matmon et al., 2002; Sacek et al., 2012b). Ideas about the evolution of great escarpment relief vary based on modelling and observation but, as a starting condition, all require the presence or generation of high topography (Braun, 2018). The majority of studies, acknowledging the extended continental margin setting, relate this topography to tectonic processes. Some emphasise the role of normal faulting (e.g. King, 1953; Beaumont et al., 2000). Others focus on flexural-isostatic responses to rifting-related loading of the lithosphere (e.g. Ollier, 1984; Cockburn et al., 2000; Fleming et al., 1999; Gilchrist and Summerfield, 1994; Sacek et al., 2012b).

Long-term erosion rates increase strongly following the creation of relief and in response to changes in weathering regimes (e.g. Koppes and Montgomery, 2009). These factors may develop in feedback with one another, but weathering regimes can also alter independently as a consequence of regional or global climatic or tectonic changes. Consistent with the former, the fills of sedimentary basins offshore of the Gondwanan escarpments all seem to have experienced rapid sediment accumulation early on in their histories following the creation of relief by extensional tectonics (Rust and Summerfield, 1990; Gunnell and Fleitout, 1998; Campanile et al., 2008; Rouby et al., 2009; Guillocheau et al., 2012). In these studies, detailed interpretation of the processes by which extended continental margins are shaped by erosion is hampered by the recognition of later accumulation pulses, which can be related to drainage capture events and the evolution of dynamic topography in escarpment hinterlands.



Utilizing onshore evidence instead, geomorphological studies have long concluded that so-called backwearing dominates erosion at extended continental margins. Backwearing involves erosion to base level by intensive gorge incision into escarpments; the escarpments retreat without changing their slope. The observation of multiple regional escarpments and terraces at some margins has led to interpretations of backwearing occurring in cycles modulated by tectonic and climatic changes on geological timescales (e.g. Partridge and Maud, 1987). The idea of cyclicity is consistent with the variable escarpment retreat rates interpreted worldwide from low temperature geochronology and rock exposure dating, which in many instances are an order of magnitude slower than might be required to attain present-day escarpment-shelf distances by constant rates of post breakup retreat (e.g. Brown et al., 2002; Cockburn et al., 2000; Heimsath et al., 2006; Kounov et al., 2007; Mandal et al., 2015; Wildman et al., 2016). Despite this, the spatial and depth resolutions of many low temperature geochronology data sets cannot unequivocally depict rapid escarpment retreat, and alternative scenarios have been preferred where sufficient resolution does exist (Braun and van der Beek, 2004). In addition, numerical landscape evolution models have failed to produce very fast ( $>1$  km/Myr) retreat rates or large sustained changes in retreat rate as a response to any physical process (e.g. Braun, 2018).

Most of the types of studies described above remain to be applied for the continental margin of Dronning Maud Land, Antarctica. Low temperature geochronology data from both ends of the escarpment reveal periods of cooling that can be related to denudation shortly after continental breakup (Jacobs et al., 1992; Jacobs et al., 1995; Näslund, 2001; Krohne, 2017). As elsewhere in the world, however, the spatial and depth resolutions of these data are not sufficient to unequivocally support the idea of escarpment retreat by erosional backwearing. Using new aerogeophysical data sets, we describe the eastern end of the great escarpment and its surroundings at much higher resolution than possible with previous data sets. Based on our findings, we investigate independently the setting and pattern of erosion and sedimentation each side of the continental margin. We first present a volume-balancing test of the first-order idea that rocks were eroded from the eastern part of the great escarpment and transported as sediments over the shelf and into the deep Riiser-Larsen Sea (Figure 11.2). To this end, we combine our aerogeophysical observations with estimates of the volume of clastic material in sediments sampled by marine seismic data. Using the same offshore data set, we interpret the history of sediment accumulation in terms of the pattern and timing of erosion that would have been necessary onshore to produce it.

### 11.2.2 Geological History of Dronning Maud Land and the Riiser-Larsen Sea

Mountains of the Sør Rondane region provide the few rocks from which the geological history of eastern Dronning Maud Land has been interpreted (Figure 11.2). This history starts in the 1.0–0.5 Ga period with the accretion of multiple juvenile arc terranes between cratonic parts of Africa and East Antarctica (Jacobs et al., 2015; Ruppel et al., 2018). Accretion culminated in the amalgamation of Gondwana. The next major event was the supercontinent's breakup in Jurassic times. This is interpreted from magnetic, gravity and seismic evidence for igneous and volcanic rocks at the region's extended continental margin and in the deep ocean basins of the Lazarev and Riiser-Larsen seas (Riedel et al., 2013; Eagles and König, 2008; Leinweber and



Jokat, 2012). These rocks have not been dated directly, but magnetic anomaly isochrons offshore show that seafloor spreading was underway by 160 Ma at the latest, and conceivably earlier (Leinweber and Jokat, 2012). Following this, the only rock-based record of the region's geological history until the development of the East Antarctic ice sheet comes from the low temperature geochronology work of Krohne (2017). Paleotopographic modelling (Wilson et al., 2012) depicts high elevations in Dronning Maud Land around the Eocene-Oligocene transition at 34 Ma, so that it acted as a nucleation zone for the East Antarctic ice sheet as global climate cooled (DeConto and Pollard, 2003). In mid-Miocene times, further cooling led to an increase in ice thickness that has been maintained ever since (Shevenell et al., 2004; Holbourn et al., 2005).

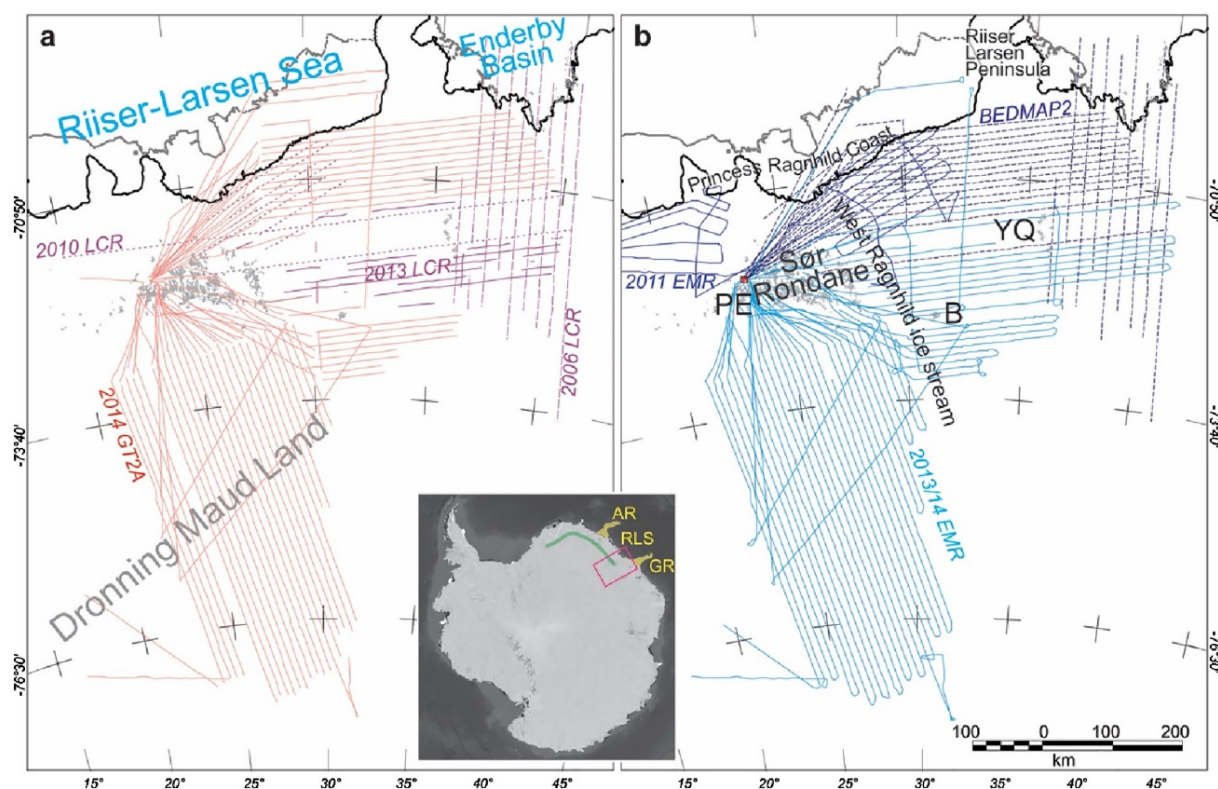


Figure 11.2: Study location and flight lines used. a) Data used for compilation of free-air gravity anomaly grid; GT2A: Gravimetric Technologies gravimeter; LCR: Lacoste & Romberg/ZLS AirSea gravimeter. b) Data used for compilation of sub-ice topography grid. B: Belgica Mountains; PE: Princess Elisabeth station; YQ: Yamato (Queen Fabiola) Mountains. Inset: Antarctica, the survey area (red box) and the great escarpment of Dronning Maud Land (green line). Yellow: basement ridges at the margins of the Riiser-Larsen Sea (RLS). AR: Astrid Ridge, GR: Gunnerus Ridge. (For interpretation of the references to colour in this figure legend, the reader is referred to the web version of this article.)

Ice streams flow over short distances towards the present-day continental shelf from the area north of Sør Rondane. Further east, longer-distance ice transport occurs via the West Ragnhild glacier, which originates inland of a gap between Sør Rondane and the Belgica Mountains (Figure 11.2, Figure 11.3) to drain a rectangular catchment of ~140,000 km<sup>2</sup> (Rignot et al., 2011; Callens et al., 2015). Based on sparse existing radar observations (Siegert et al., 2005) and thermomechanical ice-sheet models (Pattyn, 2010), the base of this part of the East Antarctic ice sheet is thought not to experience widespread pressure melting. The ice sheet south of Sør Rondane thus remains frozen to its bed, limiting its capacity to erode, and leaving open the possibility for landscape preservation. The subglacial topography and geology,



however, are only incompletely known from Soviet aerogeophysical data collected along widely spaced (25 - 50 km) flight lines flown without continuous satellite navigation. These data are widely known via their contributions to Antarctic radio echo sounding (BEDMAP2), gravity (AntGG) and magnetic anomaly (ADMAP2) compilations (Fretwell et al., 2013; Scheinert et al., 2016; Golynsky et al., 2018).

Besides these onshore observations and data, the post-breakup geological history is also recorded indirectly within the fills of sedimentary basins in the Riiser-Larsen Sea. These basins are isolated from their neighbours to the east and west by basement ridges. Astrid Ridge (Figure 11.2) is a magmatic and volcanic ridge whose construction accompanied continental breakup and early seafloor spreading and continued at its northern end until at least 145 Ma, the age of oceanic lithosphere on which it rests (Leinweber and Jokat, 2012). Gunnerus Ridge (Figure 11.2) formed in continental crust during relocation of a sheared segment of the Jurassic and early Cretaceous plate boundary from east to west Gondwana as the site of seafloor spreading between the two switched from the west Somali Basin to the Enderby Basin at around 133 Ma (Tuck-Martin et al., 2018).

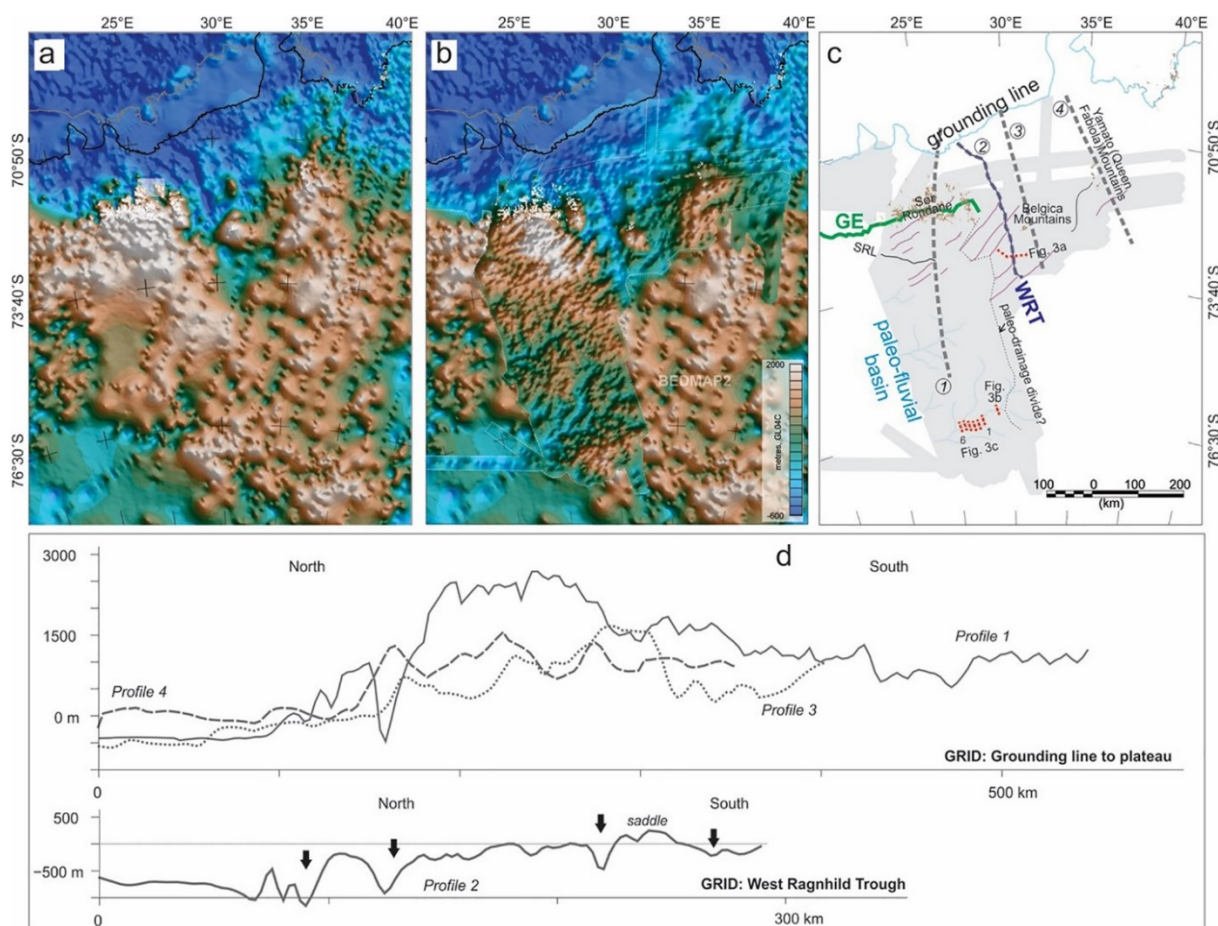


Figure 11.3: a) BEDMAP2 bed depth estimates; b) bed depth estimates from new EMR data set (inside the dotted outline) with BEDMAP2 in the background, c) interpretation (see text for details). Grey fill: area covered by new data at 10 km line spacing. Green line/GE: great escarpment (the gridded 2.2 km contour along the escarpment face); dark blue line/WRT: West Ragnhild trough; black line/SRL: valley associated with part of Schirmacher-Rondane Lineament; light blue lines: valley networks with fluvial branching characteristics; mauve lines: straight, NE-trending lineaments. Grey dashed lines: lines of grid profiles shown in (d). Red dotted lines: locations of radargrams of Figure 11.4. d) Profiles over the grid of bed elevation. Black arrows: overdeepened sections along valley profiles. (For interpretation of the references to colour in this figure legend, the reader is referred to the web version of this article.)



## 11.3 Aerogeophysical Data

Extensive new aerogeophysical datasets were collected with the Alfred Wegener Institute's two Basler aircraft, Polar 5 and Polar 6, flying out of the Belgian station Princess Elisabeth in the 2013–14 and 2014–15 seasons (Figure 11.2). The data were collected during the fourth stage of the GEA (Geodynamic evolution of East Antarctica) project, an ongoing collaboration between the Federal Institute for Geosciences and Natural Resources and the Alfred Wegener Institute, Helmholtz Centre for Polar and Marine Research. In total, close to forty thousand kilometres of gravity, radar, and magnetic data were collected for GEA-IV. Here, we present and discuss the gravity and radar data that are useful for evaluating the sources and transport pathways of sediments that are now preserved offshore in the Riiser-Larsen Sea. The magnetic data are presented and interpreted by Ruppel et al. (2018).

### 11.3.1 Radar

Large quantities of new radar data were collected using AWI's airborne EMR (Elektromagnetisches Reflexionssystem Nixdorf et al., 1999). The system sends signal bursts with a frequency of 150 MHz and amplitude of 1.6 kW, toggling between durations of 60 ns and 600 ns with the aim of returning high-resolution images of both the internal structure and the bed of ice as much as 4 km thick. After 7-fold stacking and conversion from two-way travel time to depth, the dataset can be used to calculate distances between the aircraft and the top surface of the ice and its subglacial interface. These can be used together to determine ice thickness, and, with GPS determinations of flight level, ellipsoidal heights of the ice sheet surface and subglacial interface.

A GPS equipment failure led to the loss of radar capability on one flight in the 2013–14 season, and recurrent EMR signal problems led to the collection of unusable data on a further seven flights to the region north of the Yamato (Queen Fabiola) Mountains during the 2014–15 season. To make up for these losses, in part of the study region we use data gathered with AWI's EMR instrument during a EUFAR-funded flight in the 2010–11 season (Callens et al., 2014). Elsewhere, we sampled values from BEDMAP2 along our flight lines (Fretwell et al., 2013). After adjusting our bed depths to the GL04C geoid (Förste et al., 2008) used for BEDMAP2, we then gridded the data set using minimum curvature rules for a regular 3 km grid spacing. The resulting basal topography is shown in Figure 11.3b. Example radargrams are shown in Figure 11.4.

### 11.3.2 Gravity

New free-air gravity data were collected as part of GEA-IV in 2013–14 with the Alfred Wegener Institute's LaCoste and Romberg/ZLS AirSea gravimeter (serial number S56) and in 2014–15 with the institute's Gravimetric Technology GT2A gravimeter (serial number 28). The International Gravity Standardization Net tie to Princess Elisabeth airfield (for the 2013–14 and 2014–15 data) was completed using AWI's LaCoste and Romberg portable gravimeters G744 and G877 via Novolazarevskaya Station (absolute measurement by Mäkinen, pers. comm. to Yildiz et al. (2017)), visited before and after both campaigns. The 2013–14 data were collected at constant elevations, constrained by the capabilities of the AirSea gravimeter. Unpredictable



broken and multi-level cloud in the 2013–14 season led to considerable data loss owing to multiple flight level changes on some profiles. Consequently, crossover errors within the AirSea data set are only determined along fragments of two tie lines and are not numerous enough to be statistically meaningful.

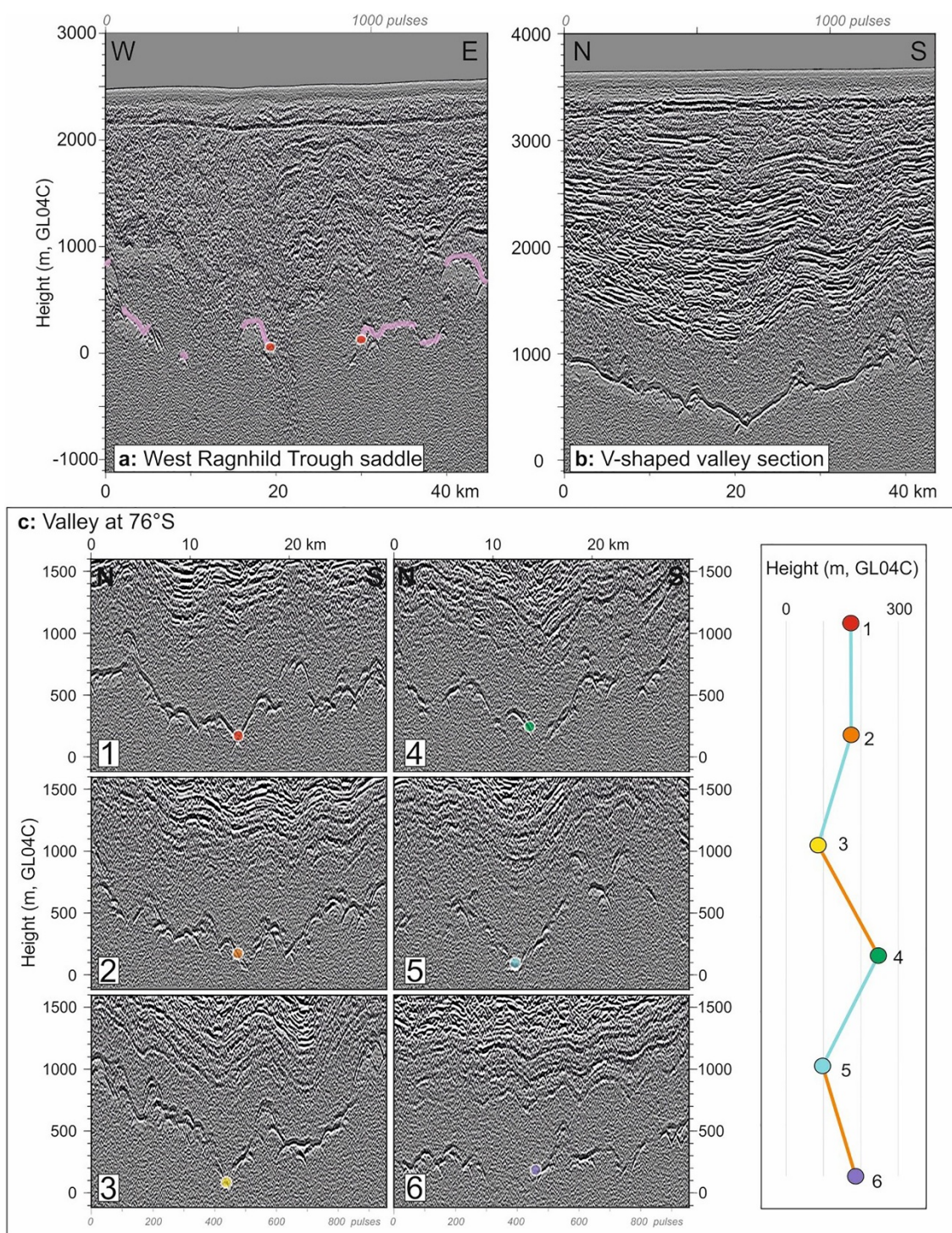


Figure 11.4: a) Radargram over the saddle in the West Ragnhild trough (at ~25 km distance) between Sør Rondane and Belgica Mountains. Pink lines are interpreted bed reflections, red discs show the deepest picks at the trough flanks between which the trough floor is not imaged but likely to lie below sea level; b) radargram over mid-stream section of a v-shaped valley south of Sør Rondane, c) Six radargrams showing valley floor picks (coloured discs) further downstream in the same valley as (b), and a height profile from those picks. Uphill-westwards segments are coloured orange.



At face value, these crossover values in the range 0–7 mGal suggest the instrument performed according to expectations. In contrast, along track reliably during climb and descent. A 100 s filter length and flight speeds of 120–140 knots simply along-track half-wavelength resolution in the range 3.0–3.6 km. Where weather conditions permitted, data with this instrument were collected at a constant ice separation of 600 m. Crossover determinations within the GT2A data set are more numerous (90 to tie lines), the raw data returning a mean crossover error of  $-0.15$  mGal and standard deviation of suggesting this gravimeter too performed satisfactorily. These data are combined with older data recovery with the GT2A gravimeter exceeded 95 % owing to its capability to operate 2.50 mGal, data acquired using S56 in 2006 and 2010 (Nogi et al., 2013; Mieth, 2014) to generate the grid in Figure 11.5b. After internal levelling, the S56 data were levelled to the GT2A data set. Simple Bouguer gravity anomalies (Figure 11.5c) were calculated using ice, seawater, and crustal densities of 900, 1020 and  $2670 \text{ kg m}^{-3}$  without any terrain correction.

## 11.4 Interpretation

### 11.4.1 Bed Topography

Figure 11.3 shows that the overall pattern in subglacial topography is one of strong contrast between a plateau in the south, with highland peaks in and around Sør Rondane exceeding 3000 m above sea level, and coastal plains reaching a maximum depth around 960 m below sea level.

West of the Belgica Mountains, the coastal plain lies at an average of 380 m below sea level and gives way to the inland plateau at 1000–1500 m above sea level via a 2000–3000 m high escarpment (e.g. Figure 11.3d, Profile 1). The mountains of Sør Rondane crop out on the seaward face and crest of the escarpment. A straight ESE-trending valley cuts the subglacial surface about 100 km south of the escarpment, coincident with part of the magnetically-defined Schirmacher-Rondane lineament of Ruppel et al. (2015). Hanging and overdeepened valleys can be interpreted from the grid in the areas between and immediately south of the mountains. These features record a phase of alpine glaciation and furthermore suggest that the escarpment relief hosting them was already in place at the time the ice sheet started to accumulate in the run-up to the Eocene-Oligocene transition.

The picture east of the Belgica Mountains is different (Figure 11.3d, Profile 4). Here, the coastal plain dips somewhat irregularly inland, starting close to sea level a short distance behind the grounding line, and eventually dropping to around 150 m below sea level just north of a  $\sim 100$  km length of east-striking escarpment. This escarpment, of around 1100–1500 m height, bends southwards at its western end to continue inland at lower elevations for at least another 150 km. The Yamato (Queen Fabiola) Mountains crop out from a north-striking spur to the north of the east-striking segment of escarpment. Together, this spur and the south-trending segment of the escarpment lie along strike from the Riiser-Larsen Peninsula (Figure 11.2) and its offshore continuation, the submarine Gunnerus Ridge, suggesting they share a deeper geological control.

The  $\sim 150$  km wide area between the Yamato (Queen Fabiola) Mountains and Sør Rondane presents a coastal plain with seaward and landward terraces at  $\sim 480$  m and  $\sim 180$  m below sea level (Figure 11.3d, Profile 3). Further inland, the subglacial topography rises up landwards to



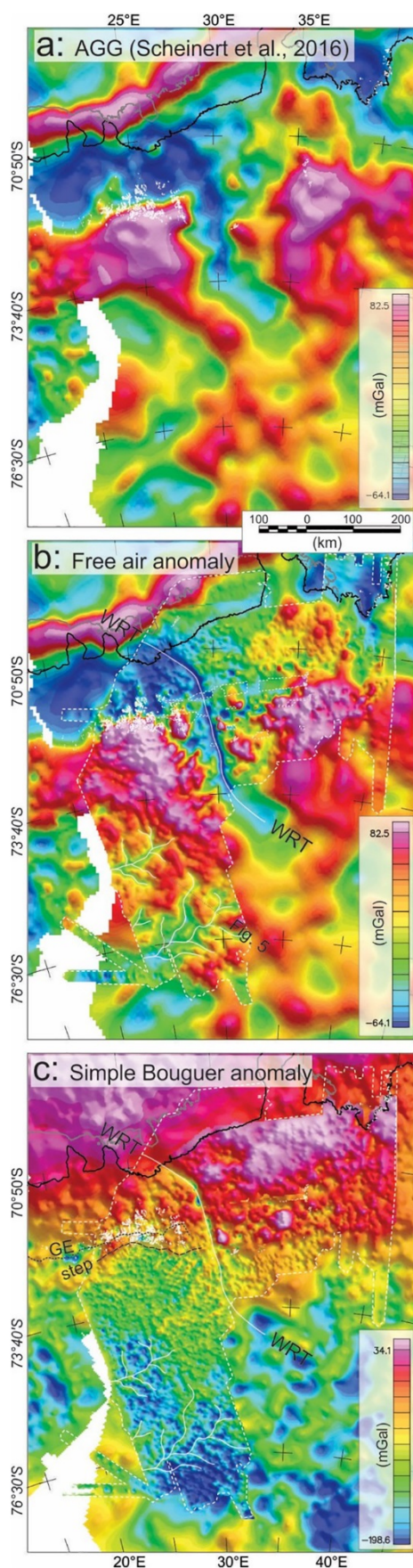


Figure 11.5: Free air anomalies in the AntGG free-air anomaly dataset of Scheinert et al. (2016). b) Newly compiled free-air anomaly data within the dotted outline, AntGG outside it. White lines: valleys interpreted from EMR data. WRT: West Ragnhild trough. c) new simple Bouguer anomalies overlain on complete Bouguer anomaly dataset of Scheinert et al. (2016). GE: gridded 2.2 km contour on escarpment face, from Figure 11.3; 'step': short wavelength marginwards increase of Bouguer anomaly at the escarpment crest.

1700 m via a series of isolated rises, the most prominent of which bears outcrop at the Belgica massif.

The Belgica massif is separated from Sør Rondane to the west by a 15–20 km wide trough beneath the West Ragnhild glacier, which we refer to as the West Ragnhild trough. BEDMAP2 (Fretwell et al., 2013) shows the trough as a continuous feature north of Belgica Mountains. Our new radio echo sounding data show it also to continue until at least 100 km south of the mountains (Figure 11.3c, Profile 2), where it passes out of the region of our survey. Along the way, the depth of the trough floor rises from its deepest point at least 1300 m below sea level (Callens et al., 2014) via a set of overdeepened sections, which the grid suggests to be individually 10–15 km long and between 150 and 350 m deep, to depths within a few hundred metres either side of sea level in a saddle near the Belgica Mountains. Averaging and smoothing of bed depths picked from the better-imaged trough flanks results in the narrow trough floor in the saddle being depicted at around 200 m above sea level in the grid (Figure 11.3b). However, inwards of the flanks numerous EMR picks are made below sea level, and the steep sides of the unimaged parts of the trough leave little doubt that a narrow swath of its floor lies well below sea level (Figure 11.4a). The current picture of the West Ragnhild trough is thus one of a canyon at least 350 km long, 15–20 km wide, and up to 1600 m deep, whose floor is likely to lie below sea level all along its length. The trough runs straight in a NNW orientation between 74°S and 71.2°S where, having passed the great escarpment on its western side, it bends sharply NW to continue to the grounding line. This section of the trough

may be related to a pre-existing tectonic grain, as its NW trend is repeated in a separate ridge and trough lying 50 km to the south. The bend at 71.2°S coincides with the deepest of the overdeepened sections, and marks the northwards change from a deep rough bed to a smoother shallower bed first observed by Callens et al. (2014). Side valleys feeding into the West



Ragnhild trough appear to be structurally controlled on the basis of their linearity and consistent northeasterly strike on both sides of the trough. Segments of the valleys at the western side of the trough are preserved as hanging valleys that permit ice drainage only along short (<100 km) tributaries to the West Ragnhild glacier (Rignot et al., 2011). The West Ragnhild trough and glacier at the present day thus drain only the eastern fringes of Sør Rondane and the plateau south of it.

Further west, inland of the great escarpment, very little about the bed was interpretable from BEDMAP2 (Figure 11.3a) in which elevations over a large area were based on very sparse radio echo sounding data and a low-resolution inverse gravity model (Fretwell et al., 2013). Mieth and Jokat (2014) interpreted magnetic anomaly data to suggest that this region's upper crustal structural grain is oriented NW-SE. Figure 11.3 shows that relief with this trend is present, but by no means dominant, in the subglacial landscape. More prominently, the new data reveal the presence of a network of subglacial valleys reaching depths as much as 600 m below the surrounding topography. These valleys are sinuous, and thus appear less strongly controlled by geological structures than the West Ragnhild trough and its tributaries. The valleys are 15–30 km wide and usually V-shaped in cross section (Figure 11.3b, Figure 11.4b). The valleys converge at acute angles that close towards the southwest. The overall slopes of the great majority of these valley floors are towards the southwest. Consistent with the possibility of landscape preservation outlined above, these observations support the interpretation of a fluvial landscape with southwest-directed drainage. In the easternmost ~50 km of the data set, the floors of some of the valleys slope towards the east, suggesting the presence of a south-trending drainage divide to the catchment of the West Ragnhild trough (Figure 11.3c). The apparent connectivity of these short east-sloping valley floor segments with the floors of the much longer southwest-sloping valleys suggest that this divide formed by local capture of southwest-flowing streams.

In more detail, the floors of the remaining parts of the valley system also do not slope monotonously downwards to the southwest, but instead feature local overdeepened (by ~100–150 m) segments (e.g. Figure 11.4c). These observations are consistent with the valleys' modification by glacial erosion and deposition processes. As none of the valleys presently correlates with any present-day ice stream, and their orientation is perpendicular to the coastward ice flow direction (Rignot et al., 2011), we conclude that this modification occurred during an alpine glaciation phase that pre-dated establishment of the modern state of the ice sheet.

### 11.4.2 Free-Air Gravity

The free-air gravity anomalies, as expected, display strong coherency with basal topography interpreted from the EMR data. This coherency is well evident over the great escarpment of Sør Rondane and in the branching pattern of valleys south of the mountains (Figure 11.5b). These valleys are not interpretable in the AntGG data set (Scheinert et al., 2016), which in this region is based on widely-spaced Soviet data (Leitchenkov et al., 2008). Free-air anomaly troughs are centred over the valley axes, their shapes mirroring those in the EMR bed topography, suggesting an origin by erosion into largely homogeneous rocks with no strong geological structural control.



The West Ragnhild trough anomaly is much sharper and deeper than in the AntGG dataset and, like the branching valleys south of Sør Rondane, its close mimicry of the EMR-based bed topography suggests its relief to be controlled dominantly by erosion. Its depth and shape through the saddle next to the Belgica Mountains are closely similar to those immediately north and south, supporting the interpretation that even in the saddle the trough floor lies below sea level. In the north, the free-air anomaly low associated with the trough continues for at least 30 km seawards of the grounding line. Beneath the ice shelf, it is likely therefore that the trough continues as a sediment-filled feature like that imaged immediately south of the grounding line by Callens et al. (2014). From the GT2A data set's southernmost crossings of the trough, the free-air anomaly low bends into a SE orientation, suggesting the trough may adopt a southeasterly strike just north of  $73^{\circ}40'$  S. This impression is consistent with the orientation of a broad free-air low in the AntGG data set (Figure 11.5a), whose greater extent also suggests that the SE-striking segment of the trough might continue towards  $75^{\circ}$ S,  $35^{\circ}$ E.

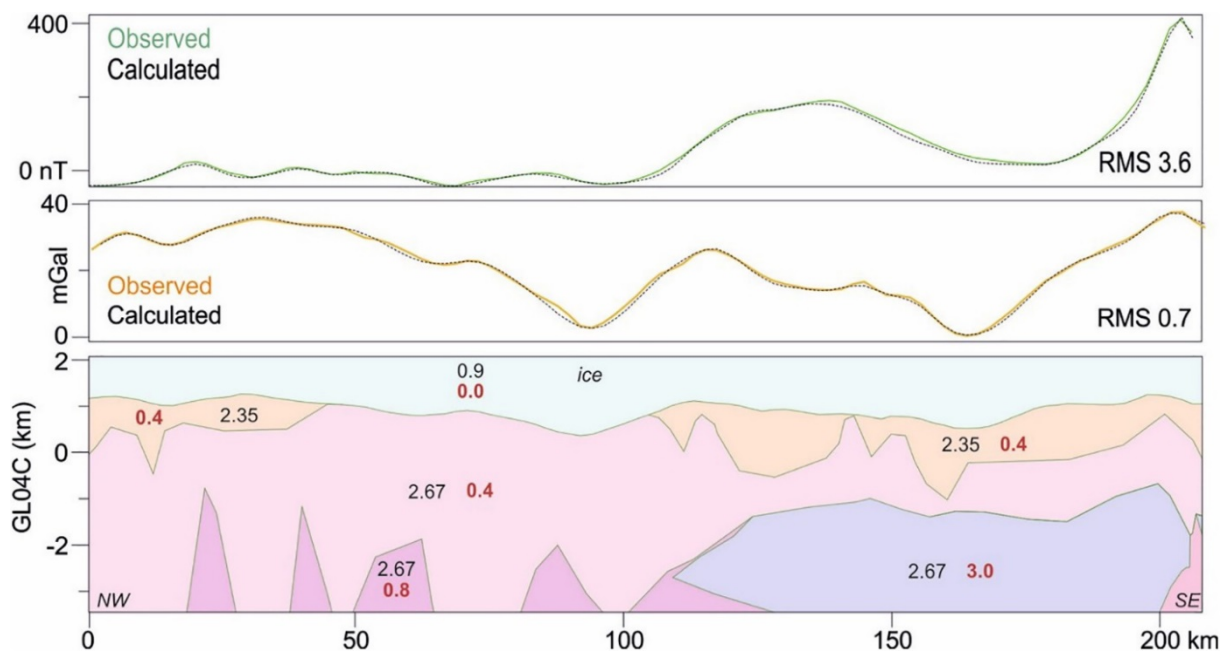


Figure 11.6: Two-dimensional gravity (centre) and magnetic (top) anomaly models for a profile running NW-SE, perpendicular to one of the main valleys (at 95 km) south of the Sør Rondane escarpment (see Figure 11.5 for location). Red numbers indicate SI magnetization values  $\times 10^{-3}$ . Black numbers indicate densities in thousands of  $\text{kg m}^{-3}$ . Given the very sparse regional outcrop constraints, model body variability is interpreted in the text only in terms of metamorphic grade.

### 11.4.3 Bouguer Anomaly

The long wavelength signal in the Bouguer anomaly data set is one of increasing values northwards, towards the extended continental margin of Antarctica (Figure 11.5c). This is consistent with increasing gravitational acceleration due to increasingly-shallow mantle rocks with densities exceeding  $2670 \text{ kg m}^{-3}$  beneath the crust, which we expect both to thin northwards as a result of tectonic extension, and to flex upwards in response to the reduced loading by the thinning ice sheet. At shorter wavelengths, this increase shows a sharp ( $\sim 30$  km) step at the crest of the great escarpment. This wavelength is not typical of flexural topography (Watts and Moore, 2017), but might still be seen as consistent with a step-like contrast in Moho depth across a crustal-scale basin-bounding fault coincident with the escarpment. Seismic



estimates of crustal thickness in the region are too sparse to reveal details of its Moho topography, but outcrop geology (e.g. Jacobs et al., 2015) and magnetic anomalies (Ruppel et al., 2018) do not permit the interpretation of any such fault near the surface. A more plausible interpretation is that the upper crust north of the escarpment crest has been thinned more by erosion than that further south. There is no comparable sharp contrast in Bouguer gravity values across the Yamato (Queen Fabiola) Mountains.

The West Ragnhild trough appears as a subdued linear low in the Bouguer anomaly data. North of the bend in the anomaly at 71.2°S, this low is confidently interpretable in terms of a trough fill of subglacial sediments of lower density than the rocks the trough is cut into. Further south, localised more strongly negative Bouguer values correlate to segments of the trough floor without radar reflections. We regard these negative anomalies as artefacts related to the erroneously shallow interpolated bed values in the EMR data grid.

In contrast, some of the larger valleys south of Sør Rondane are marked by ~20 mGal relative Bouguer highs. If these highs were consequences of systematically poorly-picked bed depths in the EMR data, then the valley floor picking error would be too large to have gone unnoticed, in the region of 200 m. A more plausible alternative interpretation is that the valleys are cut into an uppermost crustal layer with a density less than the crustal reduction density of 2670 kg m<sup>-3</sup> used for the Bouguer correction. A density of <2670 kg m<sup>-3</sup> could be characteristic of low-grade metasedimentary rocks like the greenschist-facies supracrustal rocks widely reported from Sør Rondane (Jacobs et al., 2015). Figure 11.6 illustrates such a scenario using a two-dimensional model of gravity anomalies sampled from the grid. The accompanying model of magnetic anomalies sampled from the data set of Ruppel et al. (2018) uses small susceptibilities in its uppermost layer that are also typical of metasedimentary rocks.

## 11.5 Erosion and Sedimentation Across the Continental Margin

### 11.5.1 Background

Before this study, retreat of the great escarpment of Dronning Maud Land has only been addressed in relation to interpretations of denudation from low temperature geochronology data. As at many other margins worldwide, the distribution of mineral cooling data from Dronning Maud Land means such interpretations are not unequivocal (Braun and van der Beek, 2004). Näslund (2001) interpretation of post-breakup denudation in western Dronning Maud Land (Jacobs et al., 1992; Jacobs et al., 1995) in terms of erosional retreat of an originally-tectonic fault scarp thus remains to be tested using complementary approaches.

At the escarpment's further eastern reaches, Krohne (2017) generated apatite fission track data from a small area of Sør Rondane to interpret its denudation history. Together with regional geological constraints, they interpreted cooling at 215–180 Ma in terms of the removal of 2.8 km fill from a Permo-Triassic intracontinental basin in response to tectonic uplift at the margins of extensional basins formed during Gondwana breakup. Following this, those authors interpret ongoing extensional tectonism leading to reburial of Sør Rondane in a local basin until 140 Ma, perhaps responding to landward migration of a flexurally-controlled drainage divide, followed by renewed denudation at 140–120 Ma, quiescence until 40 Ma, and localised



denudation accompanying strong rock cooling until present. Added to these ideas, in the previous sections we used our new datasets to interpret how at the time of ice sheet glaciation, >100 million years following the onset of seafloor spreading in the Riiser-Larsen Sea, a significant escarpment and drainage divide existed at the continental margin of eastern Dronning Maud Land. We build on these starting observations and ideas in the next section, which examines further products of erosion at the continental margin: the sediments deposited offshore of it.

### 11.5.2 Sedimentation and Basins of the Riiser-Larsen Sea

Leitchenkov et al. (2008) interpreted the stratigraphy revealed in a network of seismic reflection profiles from the Riiser-Larsen Sea (Figure 11.7a). The framework of their interpretation is a set of regional reflection surfaces. Below the seafloor, the uppermost of these surfaces is dated to the onset of regional glaciation at 34 Ma, because it marks the change from sub-parallel and parallel to more varied reflectivity patterns (Kuvaas et al., 2004). Ages are assigned to five deeper surfaces on the basis of their onlaps onto oceanic crustal basement. The age of the deepest, the top of acoustic basement, varies from place to place owing to its creation by extension of pre-existing continental crust (>160–164 Ma) or by seafloor spreading processes (<160–164 Ma). The age of the deepest sedimentary surface is assigned based on its interpretation by Leitchenkov et al. (2008) as a breakup unconformity marking the onset of seafloor spreading at 160–164 Ma, as determined from magnetic anomaly data from the conjugate Mozambique Basin (Leinweber and Jokat, 2012). The remaining three ages are more confidently applicable because the basement age is directly constrained by magnetic isochron interpretations at 144 Ma, 122 Ma, and 51 Ma. Total sediment thickness variation in the Riiser-Larsen Sea reveals the presence of two main basins on the continental rise. The western basin, labelled A in Figure 11.7a, lies between Astrid Ridge and the mouth of the West Ragnhild trough near 20°E. It is subdivided into western and eastern parts by an unnamed basement high near 16°E. Sediment fill is thickest in its eastern part. The lack of any major offshore sediment fan or long onshore feeder trough allows us to assume that sediments accumulated in basin A from two local sources. The first was the adjacent continental margin, which has been limited southwards by the great escarpment since Gondwana breakup. The second, in late Jurassic times only, was active volcanoes along the magmatic Astrid Ridge. In the eastern basin, B, the total sediment thickness increases from west to east, reaching maxima in excess of 6.5 km in two lobes that narrow towards the mouth of the West Ragnhild trough at 24°E on the continental slope. The lobes are suggestive of the trough having hosted sediment transport processes to basin B.

Castelino et al. (2016) presented estimates of sedimentation rate histories at two points in basin B and at one in the shallow part of basin A. All three reveal fast accumulation in late Jurassic and early Cretaceous times and in the run-up to post-Eocene perennial glaciation of East Antarctica. For a more wide-ranging picture of the sedimentation history, Figure 11.7b shows normalised accumulation histories that have been determined from 59 locations spaced at 25 km intervals along four of Leitchenkov et al.'s (2008) interpreted profiles. The majority of the profiles show a three-stage pattern, with an initial rapid phase of accumulation in late Jurassic through early Cretaceous times followed first by a long period of very slow accumulation, and



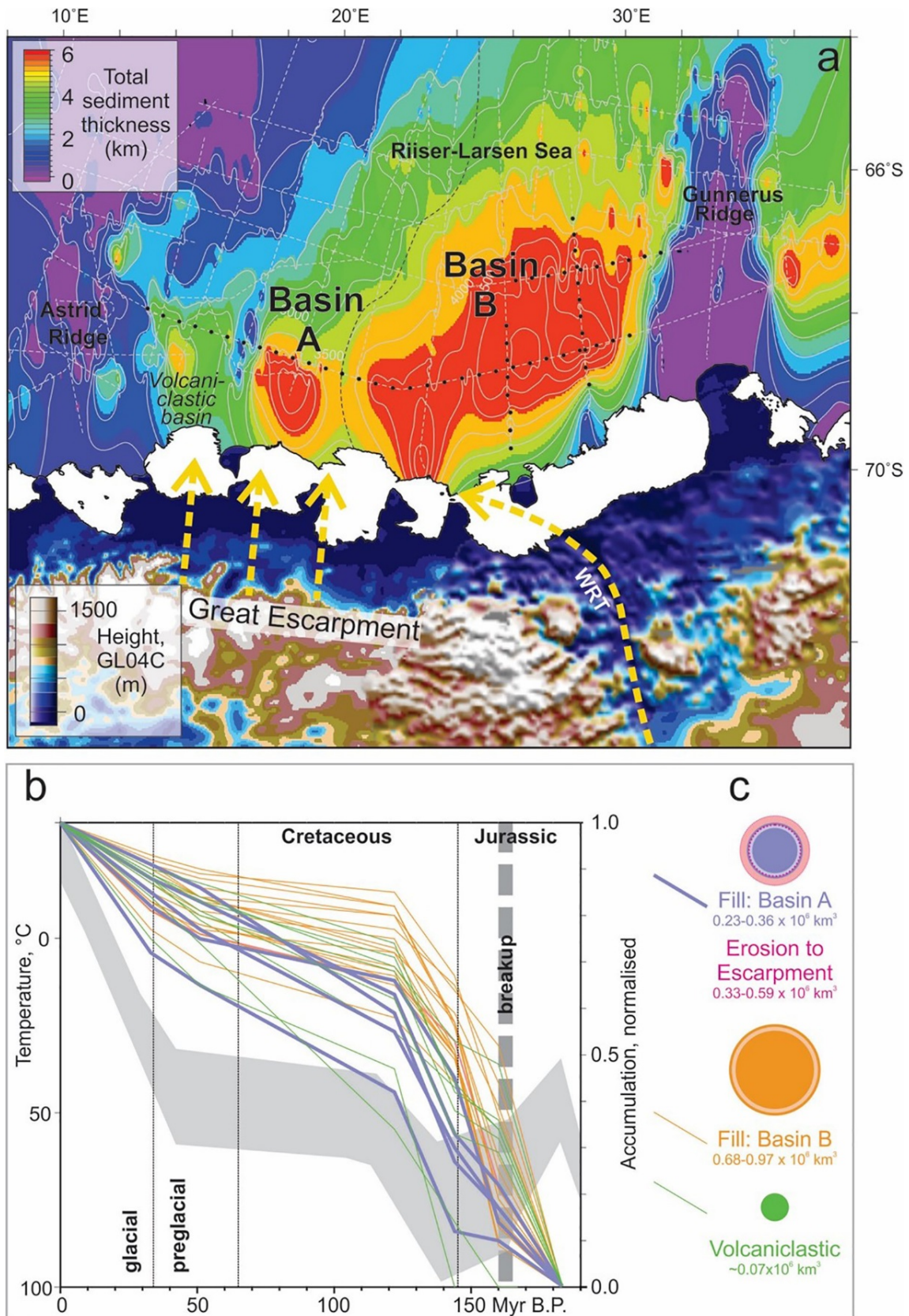


Figure 11.7: a) Total sediment thickness distribution in the Riiser-Larsen Sea (Leitchenkov et al., 2008) and bed topography of neighbouring Sør Rondane region. Dashed lines show locations of seismic data constraints. WRT: West Ragnhild trough. b) Sediment accumulation histories at sites spread throughout the Riiser-Larsen Sea (black discs in a) and low-temperature thermal history (background grey envelope) of Sør Rondane after Krohne (2017). c) Maximum and minimum estimated volumes of clastic component of Riiser-Larsen Sea sediments and of material eroded from seawards of the great escarpment.



later by accelerated sediment accumulation accompanying the onset of regional glaciation in Cenozoic times. Figure 11.7b shows that this pattern is broadly consistent with the conclusions of Krohne's (2017) cooling-based denudation study. In detail, however, whilst Leitchenkov et al.'s (2008) seismic stratigraphy should be finely enough resolved to test Krohne's (2017) interpretation of basin filling onshore at ~160–140 Ma, there is no obvious signal of such an event having stalled offshore accumulation. We propose an alternative interpretation of this reheating that draws on a lull in the rate of filling in the volcanoclastic basin east of Astrid Ridge at ~160–140 Ma (Figure 11.7b), at a time when the rest of basins A and B were filling rapidly. If this lull is interpreted to represent uplift and emergence of Astrid Ridge and the neighbouring part of basin A in response to activity of the Astrid Ridge mantle plume, then the accompanying increase of regional heat flow might be postulated as the cause of reheating at Sør Rondane.

### 11.5.3 Sediment Volume Balance Test of Great Escarpment Erosion History

As noted above, rapid late Jurassic sediment accumulation (Figure 11.7b) indicates extensional tectonics during Gondwana breakup led to the development and erosion of significant tectonic topography at the continental margin of the Riiser-Larsen Sea. Further to this, we expect the Riiser-Larsen Sea to be well suited for testing more detailed ideas about the great escarpment's role in this erosion because sediment transport to it has only ever been possible across the Princess Ragnhild Coast; along-slope transport is restricted by the Astrid and Gunnerus ridges. Figure 11.7c presents a gross check of this expectation by comparing estimates of clast volumes deposited in and sourced to the Riiser-Larsen Sea since 164 Ma.

To generate these estimates, we again used Leitchenkov et al.'s (2008) sediment thickness data set. The thicknesses are based on average interval velocities from sonobuoy records that enable a coarse depth migration of travel times in the network. Based on an error analysis of similar data sets further east around the East Antarctic margin, uncertainty in these thicknesses may reach 25 % of the calculated values (Whittaker et al., 2013), with possible extra unquantifiable uncertainty attached to the fact that the onlap-defined stratigraphy can only be indirectly verified by extrapolation of the DSDP/ODP-tied stratigraphy in the Weddell Sea (Rogenhagen et al., 2004; Lindeque et al., 2013; Huang and Jokat, 2016). Using the 25 % thickness uncertainty, and assuming average porosity to 7 km depth lies in the range 12–21 % (based on Bahr et al.'s, 2001 compaction coefficients for sand and mud) the volume of clasts in basin A sediments amounts to something in the range between  $2.9 \times 10^5$  and  $4.2 \times 10^5$  km<sup>3</sup>. Subtracting the proportion of volcanoclastic material in the sub-basin neighbouring Astrid Ridge, whose volume we estimate on the basis of its proportion of chaotic or transparent reflectivity to amount to about  $0.65 \times 10^5$  km<sup>3</sup>, we estimate that basin A contains a volume of  $2.25$ – $3.55 \times 10^5$  km<sup>3</sup> in clasts that can be assumed to have been eroded from the adjacent continental margin seaward of the great escarpment. We compare this volume to that of a now-eroded rock body that had been 600 km long and 150 km wide, the same as the present-day area between the shelf and Sør Rondane, whose bottom surface lay at around 0.4 km below sea level (Figure 11.3b) and whose top surface lay 2–3 km (cf. the denudation estimates of Jacobs et al. (1995) and Krohne (2017) above the present-day height (1.3–3.1 km) of the mountains, making it something in the range 3.7–6.5 km thick. Assuming negligible porosity prior to erosion, the volume of this eroded rock lay in the range  $3.3$ – $5.9 \times 10^5$  km<sup>3</sup>. In view of the expected loss of some of the eroded material by passage through basin A, to deposition on the continental shelf, or to dissolution, this volume



is consistent with the estimated total volume of clasts in basin A sediments (Figure 11.7c). The volume balance exercise thus enables us to conclude that continental margin topography developed during and soon after Gondwana breakup was eroded to form sediments that were subsequently deposited in the western Riiser-Larsen Sea. In the following section, we adopt this conclusion as an assumption that allows more detailed analysis of the erosion and sedimentation history.

## 11.6 Discussion

### 11.6.1 Great Escarpment Erosion: Mechanism and History

The slight increase in sedimentation rates after the Eocene (Figure 11.7b) and modest alteration of the fluvial landscape south of Sør Rondane suggest that the ice sheet facing basin A did not experience a long-lived or widespread warm-based phase of activity during its build up. Based on this, we assume that the escarpment is currently stationary and has been ever since 34 Ma. Immediately beforehand, the period 122–34 Ma saw very slow sediment accumulation in Basin A. Escarpment retreat in that period is thus likely to have been at modest rates, and not to have led to capture of any large drainage catchment. Similarly, the same observations for that period allow us to rule out that the region was affected by significant changes in dynamic topography, tectonic relief generation, or large climatic changes. The 165–122 Ma period, in contrast, saw the accumulation of around two-thirds of the fill of Basin A, suggesting an early period of more meaningful escarpment retreat. These conclusions are also consistent with the observation that the regional subglacial landscape is characterised by a single escarpment and plain (Figure 11.3), except perhaps in the narrow margin segment occupied by the Belgica mountains and West Ragnhild trough.

The present day great escarpment lies 150 km inland of the continental shelf break. To achieve this separation during a single phase of escarpment retreat starting with breakup at 165 Ma and ending with cold-based glaciation at 34 Ma would require a long-term backwearing rate of 1.1 km/Myr. This resembles both the long-term escarpment retreat rate estimated for the Namibian escarpment by Cockburn et al. (2000), and maximum plausible long-term backwearing rates in the landscape evolution model experiments presented by Braun (2018). However, the long-term retreat rate required to fill basin A by two-thirds in the 165–122 Ma period would be about 2.3 km/Myr. With reference to the results of Braun's (2018) one-dimensional landscape evolution modelling, achieving this by backwearing alone would require a physically unreasonable combination of conditions; an unusually long characteristic length, unusually high transport by hillslope processes, and unusually large lithospheric effective elastic thickness. Following Brown et al. (2002), Cockburn et al. (2000) and Fleming et al. (1999), an alternative to this implausibility is to accept the occurrence of a significant (that is, approximately equal in sediment yield) component of downwearing over an area between the escarpment and an inland drainage divide that existed prior its formation. The existence of such a divide raises the possibility that the fluvial valleys in the subglacial landscape south of Sør Rondane may have been draining towards the southwest since as long ago as early-to-middle Jurassic times.



## 11.6.2 Sediments Transported by the ‘Ragnhild River’

At something in the range  $6.8\text{--}9.7 \times 10^5 \text{ km}^3$ , the volume of clastic material in basin B is between one and a half and three times greater than that eroded from the margin in the west and now resting in basin A. Figure 11.7b shows that this material accumulated most rapidly during Callovian–Aptian times. Unlike in basin A, it is not possible to relate this signal to the erosion of breakup-related margin relief because of its size. Although the Belgica and Yamato (Queen Fabiola) mountains present fragments of escarpments that might testify to such a process, the short length of the margin segment they occupy mean that the expected volume material eroded from in front of them would be less, not more, than that west of the West Ragnhild trough. Instead, the accumulation of basin B sediments in lobes that fan out from the mouth of the West Ragnhild trough suggests they were transported to the margin by a river whose valley was later glacially altered to form the trough. The trough originates well inland of the Belgica and Yamato escarpment fragments, beyond which BEDMAP2 data, although sparse, suggest this ‘Ragnhild river’ catchment may have occupied much of western Enderby Land northwest of the older (Permo-Triassic; Thomson et al., 2013) tectonic relief of the East Antarctic rift system. Whilst the catchment's relatively large area potentially explains the volume of sediment encountered in basin B, there is a lack of evidence for Jurassic tectonic relief-forming processes that would explain the sediments' accumulation in the short period following Riiser-Larsen Sea breakup. This accumulation signal can instead be related to regional climate change, in which an arid pre-breakup continental interior became humid in response to the development of the new ocean between the Weddell and Riiser-Larsen seas. There is no available rock record from the Ragnhild river catchment to test such an idea. Paleocirculation modelling (Sellwood and Valdes, 2006) however raises the possibility of humidification in accompaniment to seaway development across Gondwana, albeit for an outdated plate kinematic model in which this seaway is considerably wider by Late Jurassic times than more modern studies show.

## 11.7 Conclusion

New aerogeophysical data reveal details of the topography of the East Antarctic Ice Sheet and its bed in the region south of Sør Rondane for the first time.

- Sør Rondane lies on a 2–3 km high escarpment. The subglacial topography of the plateau inland of this escarpment is interpretable as that of a pre-existing fluvial landscape. The fluvial drainage pattern shows that the escarpment existed as a drainage divide prior to ice sheet glaciation.
- The eastern margin of Sør Rondane is the West Ragnhild trough, an imposing subglacial canyon just 15–20 km wide but over 350 km long and exceeding 1.6 km deep in places. Almost the entire length of the trough floor in the new data lies below sea level.
- The relief of the great escarpment around Sør Rondane, the West Ragnhild trough, and the fluvial landscape southwest of them were locally enhanced by alpine glaciation at some time prior to the ice sheet glaciation of the region, which probably dates from 34 Ma.
- A volume balance exercise to assess erosion and deposition of sediments that were transported from continental East Antarctica to the western Riiser-Larsen Sea across the Princess Ragnhild Coast supports concepts of great escarpment formation during rapid



early erosion of topography formed by tectonic processes at the time of continental breakup.

- Compared to the results of published landscape evolution models, the Jurassic-early Cretaceous rate of escarpment retreat implied for this erosion to occur by backwearing alone is unfeasibly fast. Backwearing was likely accompanied by downwearing to such an extent that both may have yielded similar quantities of eroded material.
- The requirement for a pre-existing inland drainage divide to focus the coastal downwearing component suggests some features of the regional relief may be even older than late Jurassic.
- The concentration of sediments in the eastern Riiser-Larsen Sea in lobes fanning out from the West Ragnhild trough reveals the trough's pre-glacial history as the valley of a major river draining parts of the East Antarctic interior.
- Rapid accumulation of the sediment lobes in the immediate aftermath of continental breakup suggests the development of an ocean led to the late Jurassic onset of a wetter climate in the continental interior of East Gondwana.
- The first order relief of eastern Dronning Maud Land dates at least from the aftermath of Gondwana breakup in late Jurassic times. The region has been characterised by high topography ever since.

## 11.8 Acknowledgements

We gratefully acknowledge Kenny Matsuoka and EUFAR (<http://www.eufar.net>) for their roles in enabling the collection of EMR data in 2010/11. The GEA programme is jointly funded by the Alfred Wegener Institute, Helmholtz Centre for Polar and Marine Research (AWI), and the Federal Institute for Geosciences and Natural Resources (BGR). GEA-IV would not have been possible without the scientific, technical and logistical expertise of Tobias Binder, Veit Helm, the technicians of AWI and FIELAX, Wayne Hewison of Canadian Microgravity, the crews of Kenn Borek Air Ltd., Alain Hubert of the Polar Foundation, and the support crews at Novo Runway and Princess Elisabeth station. For further scientific and technical support at AWI, we are grateful to Rashpal Singh and Jude Castelino. Two anonymous reviewers provided generously detailed and constructive feedback for which we are extremely grateful.



## Chapter 12

# 12. Exhumation and Uplift of Sør Rondane (East Antarctica) – Inversion of an East Gondwana Triple Junction

Nicole Krohne, Frank Lisker, Andreas Läufer, Antonia S. Ruppel, Joachim Jacobs, Marlina A. Elburg, Detlef Damaske and Cornelia Spiegel

### 12.1 Abstract

Sør Rondane in eastern Dronning Maud Land (DML) is located near the junction of Africa/Madagascar and India/Sri Lanka, which separated during Gondwana break-up. The recent landscape represents a passive margin setting characterized by escarpment-bound, high massifs topped by plateau remnants or intensely ice-molded peaks 150 km off the present coastline. Here, we reconstruct the Mesozoic and Cenozoic geological and long-term landscape evolution of western Sør Rondane by means of thermochronological data supplemented with brittle fault-slip data and geomorphological observation. Apatite fission track (AFT) ages between 136 and 226 Ma are associated with mean track lengths of 11.6 – 13.5  $\mu\text{m}$  and broad track length spectra. Apatite (U–Th–Sm)/He (AHe) ages vary between 98 Ma and 237 Ma. Thermal history modeling of these data indicates at least two post-Permian long-term reheating phases to maximum temperatures of 110 °C, which were interrupted by cooling phases at ca. 215 Ma, ca. 140 Ma and ca. 40 Ma. The first reheating is related to the formation of a 2.0–3.5 km deep Permo-Triassic sag basin that was transiently uplifted at ca. 180 Ma possibly related to dynamic topography. Subsequent burial by up to 1.5 km thick sediments was likely due to the formation of a continental depression, its inversion started at ca. 140 Ma. Substantial exhumation, morphological modification, uplift, and latest faulting occurred in the last 30 Ma, most certainly superimposed by isostatic readjustments and crustal response to downwearing, bedrock incision, and adjacent glacial load.

**KEYWORDS:** Gondwana break-up, passive margin evolution, continental basin

### 12.2 Introduction

Dronning Maud Land (DML) constitutes the approximately 1500 km long coastal segment of the East Antarctic continental margin between Weddell Sea and Riiser-Larsen Sea. It is characterized by an almost continuous high-standing, escarpment-bound inland plateau in some distance to the passive/sheared margin that slopes down to a lowland plain towards the interior (Näslund, 2001; Bauer et al., 2003a) (Figure 12.1). The highland relicts are generally built up by Precambrian to Early Paleozoic basement rocks, either topped by remnants of a regional Paleozoic erosion surface or featured by alpine-type peaks. The sedimentary cover of DML is restricted to a few isolated and thin remnants of Cambrian/Ordovician or lower Permian sedimentary rocks and Jurassic magmatic rocks, whereas Mesozoic and Cenozoic deposits are not preserved or not accessible (Juckes, 1972; Kleinschmidt et al., 2000).



This poor sedimentary record does not allow to reconstruct the Phanerozoic geological history by means of traditional, stratigraphic and paleontological data. Instead, regional burial, exhumation and uplift has been derived during the last two decades from fission track and (U–Th–Sm)/He data. The combination of both low-temperature thermochronometers provides insights to the thermal history of the crust to temperatures between ca. 40–120 °C, and refers to exhumation from depths of 1–5 km.

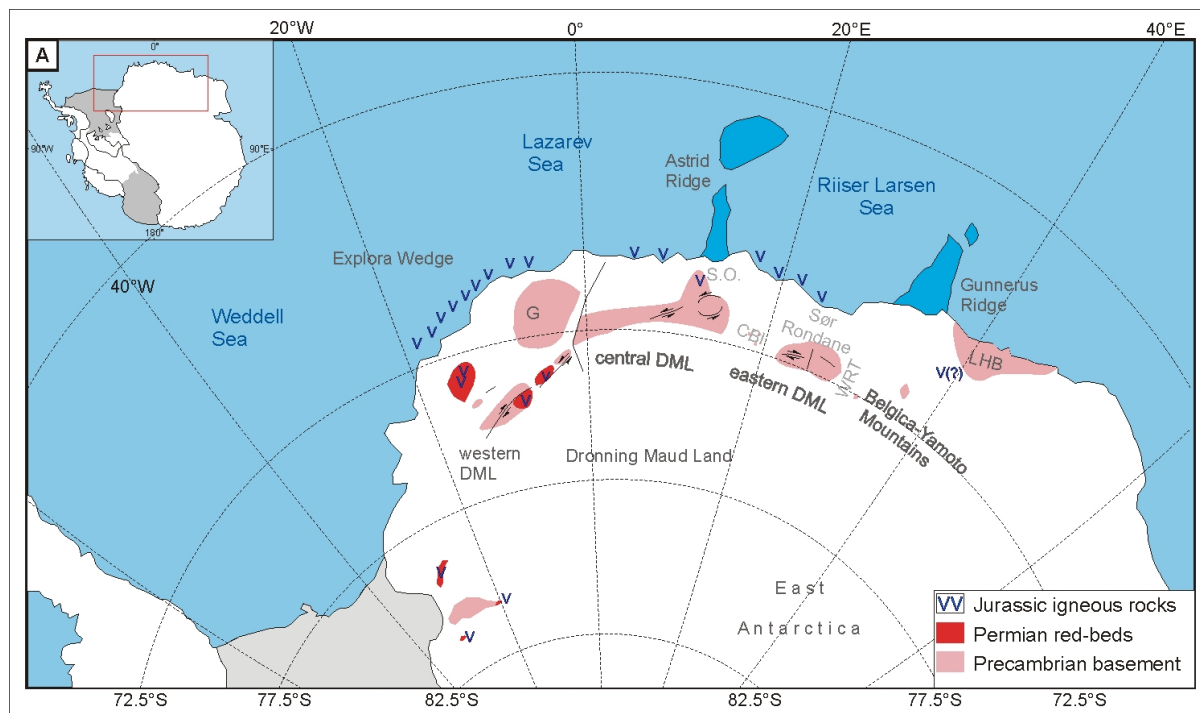


Figure 12.1: Geographic and geological overview of DML and adjacent regions redrawn after (Bauer et al., 2003a), offshore igneous rocks after Kristoffersen et al. (2014). Solid lines indicate major tectonic features. Abbreviations: CBI: Carsten-Borchgrevinck-Isen, G: Grunehogna Craton, LHB: Lützow-Holm Bay, S.O.: Schirmacher Oasis, WRT: West Ragnhild Trough.

A whole series of thermochronological studies in the mountain massifs of western and central DML produced AFT and AHe sample ages of ~90 – 310 Ma, respectively, with a general increase from western to central DML (Jacobs et al., 1996a; Jacobs and Lisker, 1999; Meier et al., 2004; Emmel et al., 2007; 2008; 2009; Sirevaag et al., 2018a; 2018b). Published thermal history models of these age data and associated proxies suggest up to three cooling stages since ~300 Ma, each followed by periods of stable and enhanced temperatures. These cooling stages were interpreted in terms of Late Carboniferous, Triassic-Early Jurassic, and Cretaceous-Paleogene exhumation episodes, mainly due to rifting and passive margin development. This scenario of long-term monotonous uplift and exhumation is supposed to have been interrupted only by one episode of locally varying shallow burial during Permo-Triassic times (Emmel et al., 2009). However, a common consideration of thermochronological data and thermal history models together with geological evidence and geomorphological patterns does challenge the published Mesozoic and Cenozoic exhumation history of the region.

Some of the thermochronological studies did not pay sufficient attention to the widely exposed late Paleozoic erosion surface that is often covered in western DML by patches of Permian sediments. These deposits in turn are intruded or topped by ~183 Ma Karoo mafic sills and flows. Such a constellation requires multiple exposure of the present surface at least during



Permian and Jurassic times. A significant portion of AFT ages <180 Ma, partially even <100 Ma, implies that the pre-Karoo (near-) surface section was heated from Early Jurassic (near-) surface temperatures to temperatures partly exceeding ~100 °C. Such a temperature increase can only be explained by burial beneath a pile of either volcanic rocks and lava flows (Jacobs and Lisker, 1999; Sirevaag et al., 2018a) or Mesozoic basin formation including volcanic activity as described from neighboring regions of central Gondwana (e.g. Thomson et al., 2013; Tinker et al., 2008; Lisker and Läufer, 2013; Krohne et al., 2016)

Regional basin development in the context of Gondwana breakup can be arguably best studied and tested in the hinge of the former supercontinent, at the triple junction between Antarctica, Africa/Madagascar and India/Sri Lanka. This crucial position has been occupied by Sør Rondane in easternmost DML, a group of mountains extending for ~160 km between 22–28°E and 71–72.5°S and rising up from sea level to an elevation of 3400 m (e.g. Yoshida et al., 1992) (Figure 12.1, Figure 12.2). Gondwana fragmentation there initiated in the Jurassic, associated with basin formation in Africa and India, and the emplacement of the Karoo Large Igneous Province between Africa and Antarctica at ~183 Ma (e.g. Kent, 1991; Jokat et al., 2003; Veevers, 2012). Sør Rondane hence represents a key locus for understanding intra-Gondwana extension and basin formation, the opening of the South Atlantic Ocean, the establishment of the present plate configuration, and the formation of a whole system of passive continental margins.

Here, we aim to reconstruct the exhumation and landscape evolution of western Sør Rondane and its relation to continental breakup. This is implemented by an integrated approach with combined thermal history modeling of AFT and AHe data, complemented with potential subaerial exposure times suggested by analogy to central and western DML and correlated with the offshore geophysical and stratigraphic record. Combined thermal history models provide timing, amount, velocity, and areal distribution of temperature changes within the uppermost 3 km in the crust. This will help to detect exhumation/burial stages and its geometry, and the evaluation and timing of relative uplift, related erosion rates and potential lag-times and on the comprehension of course, timing, processes, and amount of exhumation/burial. The stages may be complemented by brittle fault-slip data allowing their tectonic interpretation.

The results help to evaluate the landscape evolution history and paleogeographic setting of Sør Rondane prior, during and after breakup of Gondwana. Furthermore, they provide constraints into Gondwana breakup and passive margin evolution processes of DML, the paleogeographic and tectonic placement of Sør Rondane during Gondwana dispersal and the long-term landscape evolution of Sør Rondane since tectonic isolation of Antarctica.

## 12.3 Geologic Overview

### 12.3.1 Sør Rondane Basement

The basement of Sør Rondane is divided in two terranes that were juxtaposed during the Pan-African Orogeny (e.g. Osanai et al., 1988; Shiraishi et al., 1994) (Figure 12.2). The NE-Terrane is composed of amphibolite to granulite facies supracrustal rocks, whereas the SW-Terrane consists of amphibolite/greenschist facies supra- and infracrustal rocks and granulite metasedimentary and meta-igneous rocks. The two terranes are divided and transected by two



major tectonic structures. The so called ‘Sør Rondane Suture’ is postulated as part of the frontal fold zone between both terranes whereas the Main Tectonic Boundary is described as the main suture between the NE-Terrane and SW-Terrane (Osanai et al., 2013). The exact position of the Main Tectonic Boundary differs according to petrographic and aerogeophysical evidence (Osanai et al., 2013; Mieth et al., 2014).

Within the SW-Terrane, the WSW–ENE trending dextral Main Shear Zone (MSZ) divides amphibolite/greenschist facies supracrustal rocks in the north from a Gabbro-Tonalite-Tronthjemite-Granodiorite complex in the south (Mieth et al., 2014; Elburg et al., 2015; Ruppel et al., 2015; Figure 12.2). The MSZ appears to terminate at the N–S trending Gjølbreven Lineament, that likely represents a N–S trending fault zone (Kojima and Shiraishi, 1986; Mieth et al., 2014; Ruppel et al., 2015). However, the MSZ together with the likely synchronous dextral Grophelia Shear Zone in eastern Sør Rondane is indicative for widespread strike-slip movements in Sør Rondane (Ishikawa et al., 2013; Ruppel et al., 2015). Dextral strike-slip movement at the MSZ was most likely active between ca. 560 and ca. 530 Ma, including different deformation phases under ductile to late brittle conditions. Temperatures reached max. 600 °C to finally ca. 300 °C (Ruppel et al., 2015).

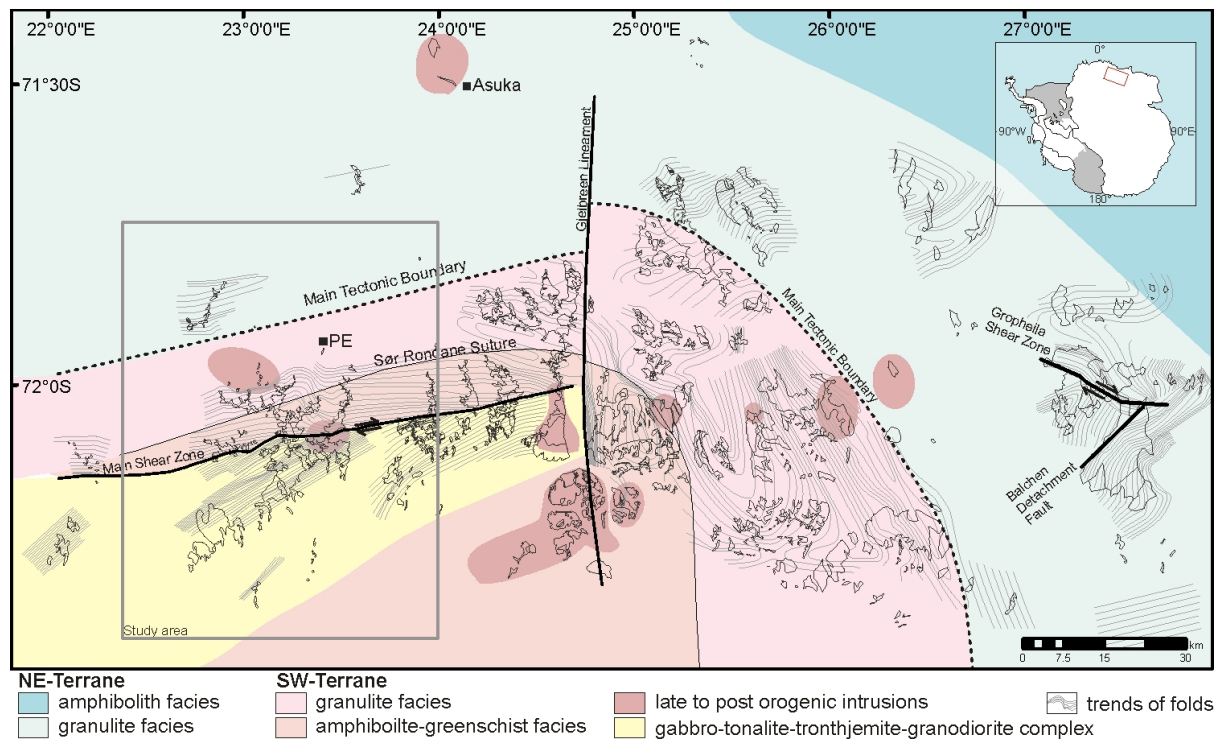


Figure 12.2: Geologic map of Sør Rondane with terranes and associated structures. Fine contour lines indicate the structural trends of the main foliation. Modified after Ishikawa et al. (2013); Osanai et al. (2013); Toyoshima et al. (2013); Mieth et al. (2014); Ruppel et al. (2015). Filled squares: Research Stations. PE: Princess Elisabeth Station. Grey rectangle outlines the study area.

Further possible strike-slip boundaries are proposed in southern Sør Rondane by geophysical observation or are inferred on the geological map (Shiraishi et al., 1992c; Mieth et al., 2014). A NE–SW trending magnetic anomaly boundary within the Gabbro-Tonalite-Tronthjemite-Granodiorite subterrane is proposed as a result of dextral strain related to the MSZ, whereas an inferred and ice-covered shear zone further south shown on the geological map cannot be confirmed by geophysical observation (Mieth et al., 2014). Indications of late-stage deformation at strike-slip boundaries, ductile detachment faults and late to post tectonic granite



and syenite intrusions and mafic dykes were related to episodes of lateral orogenic collapse at ca. 600–460 Ma and NW–SE extension (Shiraishi et al., 2008; e.g. Ishikawa et al., 2013). Post-orogenic cooling and ongoing exhumation is represented by whole rock K–Ar and Ar/Ar ages of 420–490 Ma (Takigami et al., 1987; Takigami and Funaki, 1991; Osanai et al., 2013).

### 12.3.2 Regional Phanerozoic Geological Evolution

The Precambrian basement of Sør Rondane contains several Cambrian to possibly earliest Ordovician late tectonic intrusions, while no further Phanerozoic stratigraphic record is preserved until the deposition of Quaternary moraines (Shiraishi et al., 1992c). Nevertheless, the general geological frame and the most relevant processes can be loosely constrained by evaluating the regional to supra-regional onshore and offshore record. At least five major geological and relief-forming processes affected DML during the Phanerozoic:

(i) *Exhumation and relief decay of the Pan-African Orogen.* Cambro-Ordovician deposition and compaction of molasse-type sediments in western DML and the Shackleton Range and on the African continent attest the ongoing exhumation of the Orogen (e.g. Jacobs and Thomas, 2004). At least during the Early Permian, the topography is completely leveled and characterized by regional planation surface(s) (Näslund, 2001).

(ii) *Karoo Ice Age (Permo-Carboniferous glaciation).* The Permo-Carboniferous glaciation affected most of Gondwana. The ice sheet centered on the Antarctic part of Gondwana (e.g. Martin, 1981). Glacial evidence in western DML include bedrock striations on flat surfaces and the deposition of continental sediments upon these surfaces (Bauer et al., 1997). This thin sedimentary sequence consists of Permo-Carboniferous diamictites and cemented Permian clastic red-bed deposits intercalated with low-rank coal seams (Juckes, 1972; Bauer et al., 1997). Correlatives of these successions can be found elsewhere on all Gondwana fragments hosting as well Triassic red-beds and coals (e.g. Veevers and Powell, 1994).

(iii) *Karoo Magmatic Event.* Early Jurassic mafic rocks intruded the uppermost crust or continental flood basalts and were emplaced upon the surface. The igneous activity was short term but widespread and voluminous event that formed a large igneous province (Duncan et al., 1997). Origin and locus of the magma is recently debated and was either related to mantle plume upwelling or to upper mantle heat anomalies somewhere between East Africa and DML (Cox, 1992; e.g. Heinonen et al., 2010b). Karoo-related rocks can be found in western and central DML, and potentially in and near Lützow Holm Bay, whereas Sør Rondane lacks direct evidence of this magmatic episode (Tatsumi and Kizaki, 1969; Juckes, 1972; Belyatskii et al., 2006).

(iv) *Gondwana break-up and development of marginal seas.* Gondwana dispersal proceeded as well during the Jurassic. However, the interdependence between the Karoo Event and rifting to the major trigger of break-up is still questioned (Jokat et al., 2003). The DML margin is classified as a volcanic passive margin (Hinz and Krause, 1982; Leitchenkov et al., 1996; Leitchenkov et al., 2008). Kristoffersen et al. (2014) propose a narrow initial rift of 30 km width between western DML and South Africa. First true sea floor was formed at 155 Ma in the Riiser-Larsen Sea, followed at 147 Ma in the Weddell Sea and 140–135 Ma in the Lazarev Sea (Jokat et al., 2003; König and Jokat, 2006; Leinweber and Jokat, 2012). NNE–SSW trending depressions, strike slip ridges (for example, Astrid Ridge and Gunnerus Ridge) and transform



faults document oblique spreading between eastern and central DML and Mozambique (Jokat et al., 2003; Leitchenkov et al., 2008).

(v) *Eocene glaciation*. Substantial morphological modification of Antarctica was mostly initiated by climatic cooling, enhanced fluvial, and glacial incision (Sugden et al., 1995). A widespread ice-sheet in DML was already developed in the Late Eocene (Carter et al., 2017). Enhanced erosion is reflected by high deposition rates in the marginal basins (Solli et al., 2007; e.g. Huang et al., 2014).

## 12.4 Geomorphology of Eastern DML and Sør Rondane

The morphology of eastern DML is featured by a typical passive margin landscape. It comprises the marginal Riiser-Larsen-Sea with up to 7 km deep, potentially fault-bounded depocenters, a wide subglacial plain between the continental shelf and the high escarpment, on which Sør Rondane is located, whilst a lower inland plain is located south of Sør Rondane (Leitchenkov et al., 2008; Eagles et al., 2018). The depositional history in the Riiser-Larsen Sea is based on seismic evidence only and starts approximately at 158 Ma (Leitchenkov et al., 2008). Provenance of sediment fill in the depocentre in front of Sør Rondane is proposed to have had the input from the region northwards of Sør Rondane and from the Astrid Ridge volcanism (Eagles et al., 2018).

Sør Rondane hosts massifs of 1000–3200 m elevation that protrude up to 1600 m from the ice sheet. The terrain in Sør Rondane is highest in the southwest, slopes irregularly down to the north and redirects major ice streams from the polar plateau to the eastern and western terminations (e.g. van Autenboer and Declair, 1978; Rignot et al., 2011). To the east, Sør Rondane and the Belgica Mountains are dissected by a deep subglacial trough underneath West Ragnhild Glacier (Eagles et al., 2018). Glacial troughs in Sør Rondane are often overdeepened, and at least some of them seem to be fault-controlled (e.g. Gjelbreen; Pattyn et al., 1992; Mieth et al., 2014). A WSW-directed paleo-drainage system is proposed to have existed prior glaciation south of Sør Rondane (Eagles et al., 2018).

The mountain massifs are characterized by escarpment-bound summit plateau surfaces intersected by extensive ice-molded peaks. The flat or slightly undulating plateau surfaces occur throughout the area and are elevated between 1000 m in the north and 2600 m in the south (Figure 12.3). There is no lithological difference between plateau surfaces and the alpine-type peaks. The flat surfaces must have been formed prior to Cenozoic times, as the lowermost exposed surface (1284 m) does not provide any indication for Neogene to Quaternary ice-override (van Autenboer, 1964). In addition, some other surfaces were elevated significantly higher than maximum ice-sheet elevations since the Neogene, and evidences that they cannot have been formed during that time (Pattyn et al., 1989; Matsuoka et al., 2006; Sugauma et al., 2014). The same morphological pattern trends towards the west as well as to the east (for example, Belgica Mountains, Figure 12.3e). Hence, the morphology of DML can be constrained as one mega feature. Alpine landscape formation pre-dates the late Cenozoic and postdates paleosurface formation (Näslund, 2001). (Näslund, 2001) interpreted the flat surfaces in western and central DML as remnants of one or several regional planation surfaces. Flow



directions of the Permian ice sheet indicate regional low relief landforms in the Permian (Bauer et al., 1997). An exposition age of the paleosurface is given by the preserved thin remnants of the Carboniferous-Permian tillite in the western part. Striae on the basement paleosurface are in direct contact to the overlying diamictites (Poscher, 1992). This combination proves surface exposure, modification, and subsequent burial. Repeated near-surface exposure of the basement paleosurface and thin Permian strata is indicated by the intrusion of ca. 182 Ma aged sills, dykes and the effusion of lavas at least directly indicated in western DML and in parts of central DML (e.g. Duncan et al., 1997).

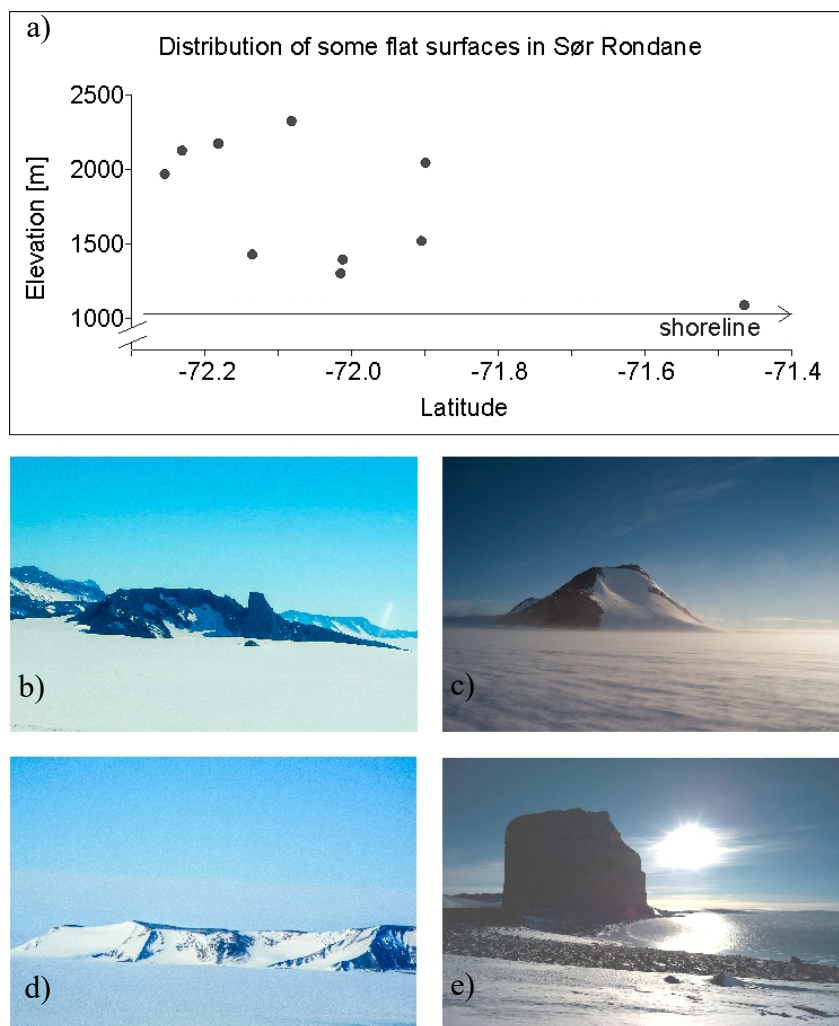


Figure 12.3: Elevation-latitude plot illustrates the recent dissection of some flat surfaces in Sør Rondane. It demonstrates that paleosurface elevation does not correlate with latitude or distance to the shoreline. Field photographs show examples of paleosurface remnants throughout Sør Rondane and Belgica Mountains (right below).

## 12.5 Brittle Fault-Slip Data

The brittle tectonic inventory of western Sør Rondane was studied during GEA II expedition (Geodynamic Evolution of East Antarctica, 2011–12) of the German Federal Institute for Geosciences and Natural Resources (BGR). Field data sets of brittle deformation were recorded from 8 localities and include measurements of fault planes and striations (Figure 12.4). The sense of movement of the hanging wall block is indicated by kinematic indicators like fiber



steps or Riedel shears on the slickensides. Lower hemisphere stereoplots and paleostress calculations were conducted with the software WinTENSOR (Delvaux and Sperner, 2003).

At least two composite paleostress tensor groups were obtained:

(i) NW-SE oriented contraction and NE-SW extension with corresponding E-W to WNW-ESE dextral, NNE-SSW sinistral, and NW-SE extensional faults.

(ii) N-S contraction and E-W extension with corresponding NE-SW sinistral, NW-SE dextral and NNW-SSE normal faults.

Paleostress tensor group I contains faults that can be related to the MSZ, which represents a nearly E-W oriented dextral shear zone with ductile and brittle increments of late Pan-African age (Ruppel et al., 2015). However, the data set may also contain additional, younger and thus post Pan-African faults. Paleostress tensor group II represents a separate, possibly younger event than the MSZ because of opposite kinematics and overprinting criteria of faults.

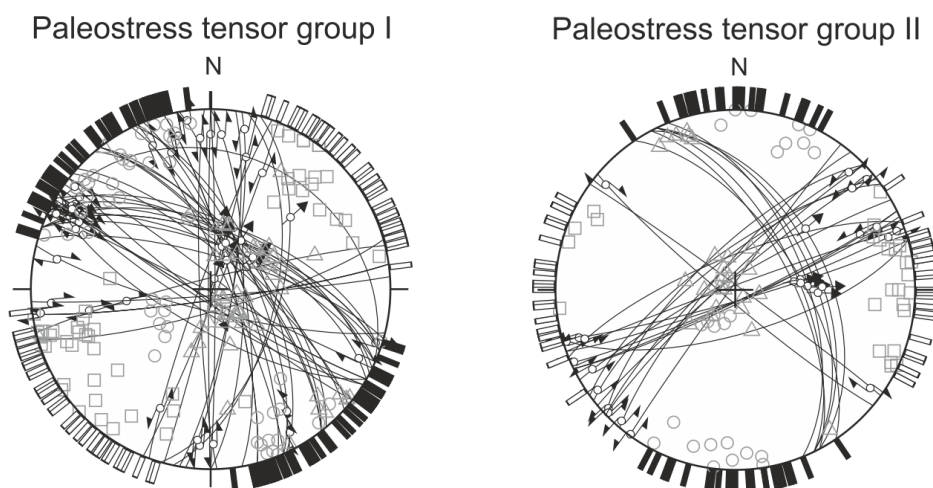


Figure 12.4: The two lower hemisphere stereographic projections are composite plots of brittle fault-slip data recorded in the study area. Based on overprinting criteria they are attributed to two composite paleostress tensor groups I and II. Faults are shown as great circles and striae and the motion of the hanging wall block as arrows. Circles, triangles, and rectangles indicate pressure-tension (P-B-T) axes calculated for each fault/striae pair. Black and white lines represent maximum and minimum horizontal stress, respectively.

## 12.6 Thermochronology

### 12.6.1 Sampling

Thirty in-situ rock samples for AFT and (U–Th–Sm)/He analysis were collected in western Sør Rondane during GEA I and II expeditions. Sampling intended to cover the entire relief between 1300–3200 m and all tectonic domains in order to investigate exhumation with respect to structural and geomorphological pattern (Figure 12.5). It includes a general horizontal N–S transect Perlebandet–Vikingshøgda–Widerøefjellet–Nils-Larssenfjellet, and traverses three litho-tectonic boundaries (Main Tectonic Boundary, Sør Rondane Suture, and MSZ). This transect also contains semi-vertical profiles of the two highest mountains, Widerøefjellet and Vikingshøgda. The two summits are separated by narrow standing and steep dipping strike-slip



shear planes of the MSZ that is utilized morphologically by the largely ice-free Dry Valley (Ruppel et al., 2015). Small paleosurface remnants are exposed between 1000 and 2800 m including the tops of Vikinghøgda and Nils-Larsenfjellet (Figure 12.5). We collected 22 specimen of this study from paleosurfaces, all other samples were obtained from alpine-type morphologies (Table F.1.1, ‘Electronic Appendix’). The dissection and the varying elevation of the paleosurface remnants, and the wide spatial sample distribution do not support vertical backstacking of the former paleosurface, and do not allow the calculation of paleogeothermal gradients from modelled paleotemperatures. Samples were prepared and analyzed at the University of Bremen according to standard techniques. Details and technical information are provided ‘Electronic Appendix F.1 and F.2’.

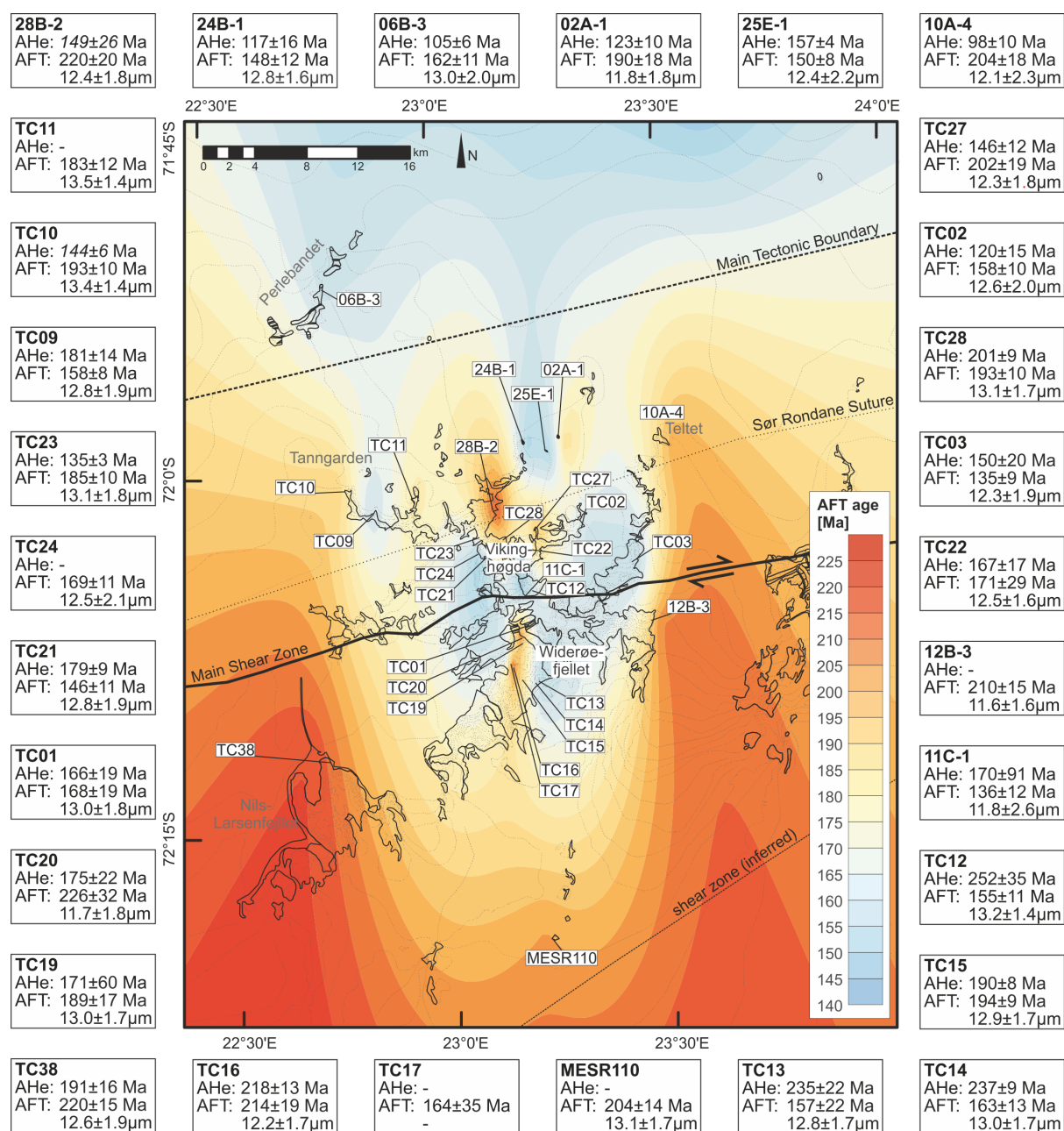


Figure 12.5: Map of sample locations and thermochronological results. Dotted lines represent topographic contours according to the Antarctic Digital Database. See Figure 12.2 for general overview of the area. Central AHe data in boxes were obtained with HelioPlot (Vermeesch, 2010).



## 12.6.2 Apatite Fission Track Results

Thirty AFT sample ages range from  $136 \pm 12$  to  $226 \pm 32$  Ma, and they are substantially younger than the times of rock formation, the latest metamorphic overprint, and initial (post-) orogenic exhumation indicated by 430–490 Ma K–Ar and Ar/Ar ages (Osanaï et al., 2013 and references therein; Table F.1.1).

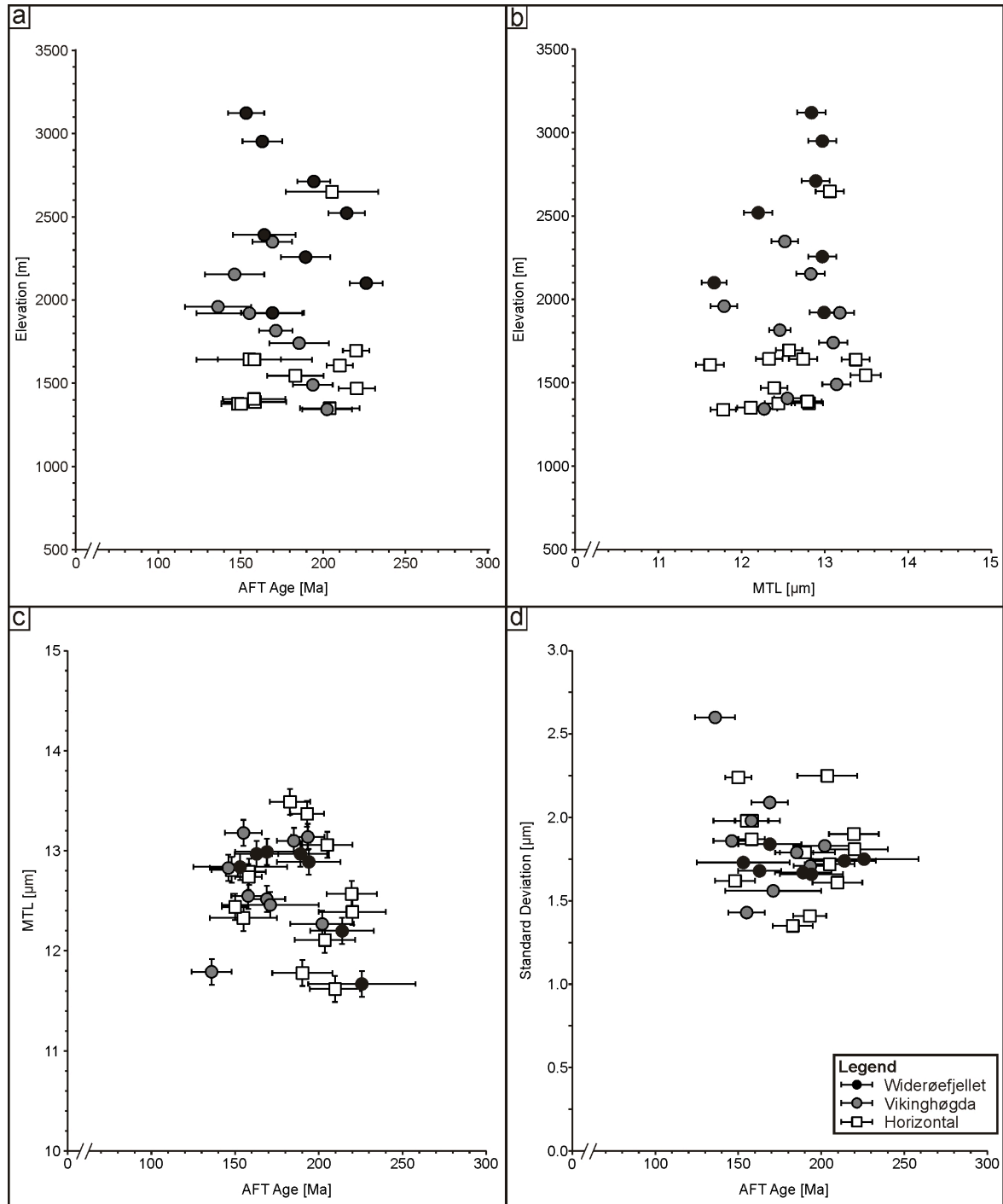


Figure 12.6: Plots of apatite fission track (AFT) data. a) Age vs. elevation. The AFT ages of the vertical profiles correlate inversely with elevation. Error bars indicate the standard deviation of fission track ages. b) Mean track lengths (MTL) vs. elevation, with  $1\sigma$  error bars. c) Mean track lengths vs. AFT ages. Vertical error bars indicate  $1\sigma$  error, horizontal error bars the standard deviation of pooled AFT ages. Note the long track length associated with ages of 180–210 Ma. d) Standard deviation of the MTL plotted against AFT age. The largest standard deviations occur in the youngest samples, whereas the lowest standard deviations are present in the samples with the largest MTL.



Ages of all samples except TC03 pass the  $\chi^2$  test with high probabilities referring to a single age population. Mean track lengths (MTL) vary between 11.6 and 13.5  $\mu\text{m}$  with broad track length spectra and standard deviations of 1.3–2.7  $\mu\text{m}$ . Values of the kinetic parameter  $D_{\text{par}}$  range between 1.5 and 2.2  $\mu\text{m}$ . Most shortened tracks are preserved in the oldest and youngest samples, while longer MTL of 13.1–13.5  $\mu\text{m}$  are associated with AFT ages between 183 and 193 Ma (Figure 12.6). The standard deviations of the MTL correlate inversely with MTL values (Figure 12.6). The AFT age and length data of this study do not show any systematic spatial cluster with respect to the different terranes of Sør Rondane. Also, ages and MTL of the scattered samples do not generally correlate with elevation (Figure 12.6). Only the AFT ages of the two vertical profiles from Widerøefjellet and Vikinghøgda show some inverse correlation with elevation. Apatite grains from Widerøefjellet are generally smaller in size compared to those from other locations and many grains could not be analyzed for curved dislocations, likely developed due to tectonic stress.

### 12.6.3 (U–Th–Sm)/He Results

79 single grain ages were calculated from 25 sample locations by applying the  $^4\text{He}$  ingrowth equation (Farley, 2002). Ages are listed in Table F.1.2 ‘Electronic Appendix’ and shown in Figure 12.7.  $F_T$ -corrected single grain ages vary strongly between  $44 \pm 6$  and  $348 \pm 41$  Ma. Most of the composite sample ages do not consist of replicating single grain ages but show either irregular age clustering or a randomly distributed age scatter. Central ages vary between  $98 \pm 10$  Ma and  $237 \pm 5$  Ma (Supplements). The youngest single grain age(s) of each sample are always younger than the corresponding AFT sample age, but many grain ages are significantly older. U–Th–He ternary plots identify only a few samples with replicating ages and uniform geochemistry (Supplements).

AHe single grain ages older than corresponding fission track ages are confined to proximity to the MSZ. 81 % aliquots from the Widerøefjellet have significantly higher AHe single grain ages than corresponding AFT ages. Analogously, 55 % Vikinghøgda AHe single grain ages predate the respective AFT ages, while only 22 % samples remote from the MSZ show such a reverse/inverse relationship. Apatite grains close to the MSZ are smaller and of poorer quality than the others, and some grains within the AFT mounts show indications of intracrystal deformation (curved dislocations) and irregular  $^{238}\text{U}$  and  $^{235}\text{U}$  zonation. The broad scatter of single grain ages reflects the typical scenario for cratonic regions (Flowers, 2009), and is also reported in adjacent regions (Emmel et al., 2007).

The AHe single grain ages generally correlate with elevation, except at Widerøefjellet and Vikinghøgda (Figure 12.7). Samples from higher locations tend to show a higher scatter of single grain ages. A broad scatter of individual ages is particularly obvious in samples from the Gabbro-Tonalite-Tronhjemite-Granodiorite subterrane. Aliquot and central ages of samples in the north are significantly younger than the corresponding AFT ages. This age difference decreases towards south where AHe ages are only somewhat younger than or equally old as AFT ages. Only samples from the top of the Widerøefjellet and Vikinghøgda vertical profiles show a distinctive crosscutting AHe/AFT age relationship. There, samples taken from elevations  $>2000\text{m}$  are characterized by AHe central and aliquot ages  $>200$  Ma.



Neither eU ratios (4–253 ppm) nor grain radius or mass do correlate with single grain AHe ages, which may be representative for radiation damage (Shuster et al., 2006; Flowers et al., 2009) (Figure 12.7). Only the Widerøefjellet vertical profile shows some diffuse correlation between  $F_T$ -corrected single grain ages and eU values ( $r^2=0.31$ ).

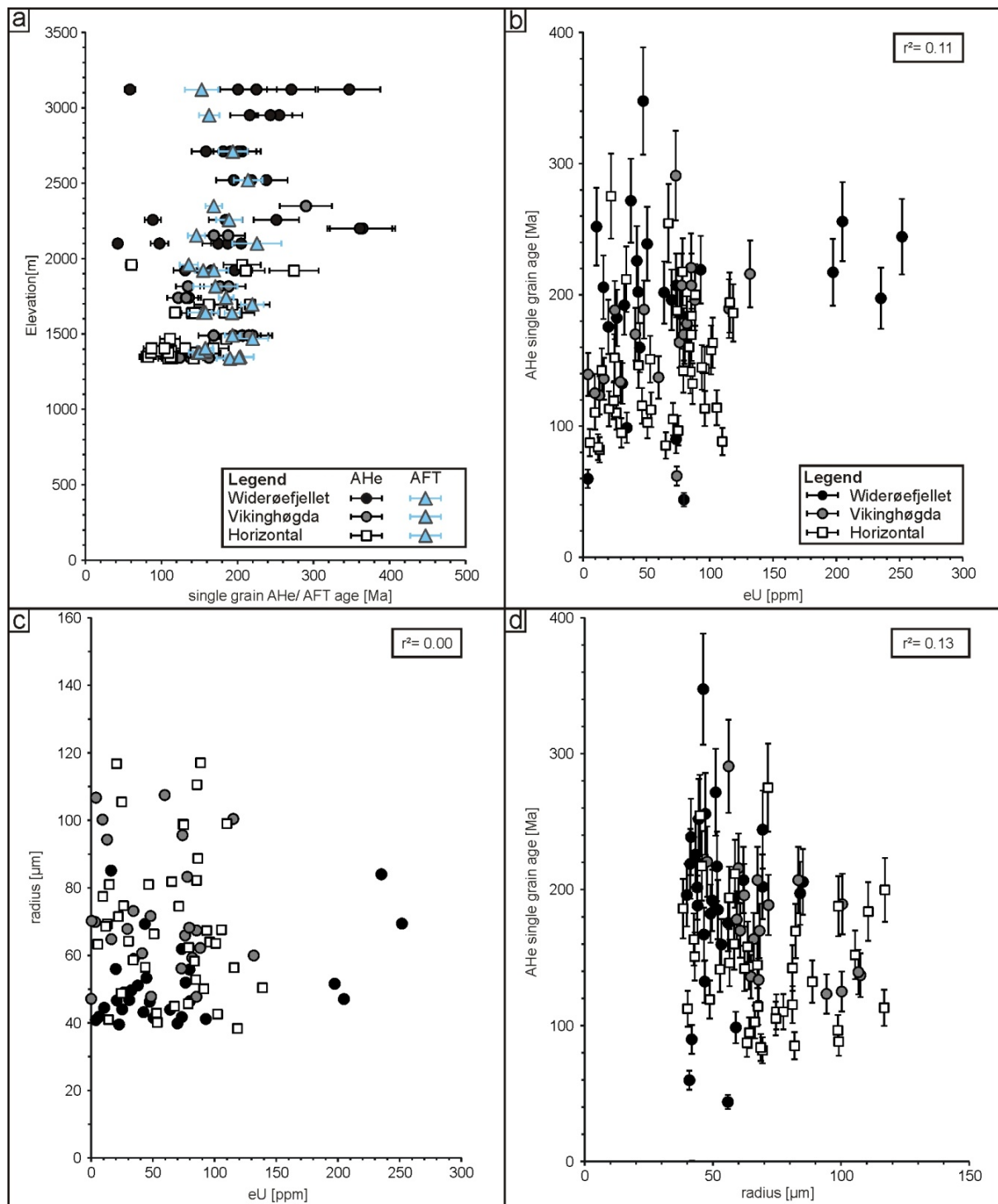


Figure 12.7: Apatite (U–Th–Sm)/He (AHe) results: a) AHe single grain ages and corresponding apatite fission track (AFT) ages were plotted against elevation. Error bars indicate the  $1\sigma$  error of the AHe data. b) eU values were plotted against AHe single grain ages, showing a rough correlation and broad distribution of eU values. Error bars indicate the  $1\sigma$  error of the AHe data. c) eU relation to the mean sphere radius of the distinctive apatite grains. No trends and no correlation are obvious. d) The  $F_T$ -corrected single grain ages correlate negatively with radius. Error bars indicate the  $1\sigma$  error of the AHe data.



## 12.6.4 Thermal History Modeling

Thermal history modeling with HeFTy (version 1.8.7; Ketcham, 2005) was applied to derive discrete time-temperature paths from thermochronological data and geological constraints. AFT samples with at least 20 dated apatite grains and more than 75 confined track length measurements and related AHe single grain ages without crossover relationships were selected for thermal history modeling. Twenty samples covering all tectonic domains met these requirements. The modeling procedure follows the approach suggested by Prenzel et al. (2013). It relies on the elementary assumption that a mountain range topped by a paleosurface results from consistent exhumation processes. Exhumation stages are marked by similar timing of cooling episodes for a common vertical sample suite, while maximum paleotemperatures of individual samples may vary depending on the geothermal gradient. AFT and AHe thermochronology covers a temperature range of 80 °C, referring to a vertical coverage of ca. 2.5 km within the crust. 2.5 km exceeds the recent vertical relief of 1.9 km in the analyzed area. Hence, interpretation of all samples must consider and allow Permian and Jurassic low-temperatures placement.

A crucial observation in western DML is the abundant occurrence of remnants of an early Permian erosion surface (Näslund, 2001). There is no direct evidence preserved in Sør Rondane, the wide distribution of formerly early Permian paleosurfaces formed or modified during Gondwana glaciation make it plausible to assume the flat surfaces in Sør Rondane as a Permian feature.

Following constraints were defined based on these considerations:

- (i) The last known time of higher paleotemperatures than 120 °C is provided by K–Ar and Ar/Ar ages of 430–490 Ma (Takigami et al., 1987). Whole rock ages obtained on biotite and hornblende rich gneiss mark paleotemperatures >300 °C.
- (ii) Upper Permian formation or re-exposition of low-relief erosional surfaces marks surface temperatures at ca. 300 Ma (cf. section 3).
- (iii) A probable Early Jurassic shallow crustal position and exposition of the paleosurface is narrowed down in section 3. Constraints were set between 15–60 °C, in the order of the recent paleosurface dissection.
- (iv) The recent mean annual surface temperature is -18 °C at Asuka Station (ca. 800 m) (calculated from Aoki, 1989; Yamanouchi et al., 1988; Matsuoka et al., 1990; Meshida et al., 1991; Iwasaki and Yamanouchi, 1992; Sukegawa and Yamanouchi, 1993). These temperatures were used to calculate the distinctive surface temperatures under consideration of the orographic gradient (supplements).
- (v) Further constraint boxes between 40–170 Ma and 200–300 Ma were set widely to allow all iterations between surface temperatures as well as complete resetting (i.e. temperatures higher as the apatite partial annealing zone). The lower temperature limit of boxes was adjusted to Mesozoic and Cenozoic surface temperatures.

The course of the inverse thermal history models is similar throughout, however with some paleotemperature variation (supplements). As constrained by K/Ar ages at ca. 450 Ma (Takigami et al., 1987) and Permian surface exposure, cooling proceeded from >350 °C to



temperatures between 60 and 0 °C. Since 300 Ma reheating to 80–110 °C is marked with subsequent cooling to below 60 °C around 180–230 Ma. The reheating between 250 and 200 Ma indicates an almost complete reset and hence, limits high-resolution thermal information to the time after 200 Ma. Thermal history models show some reheating between 160 and 135 Ma to temperatures of 50–110 °C, with subsequent cooling to present day surface temperatures, tentatively with an acceleration of cooling around 40 Ma. In general, the shapes of the paths and the maximum paleotemperatures do not correlate straightly with present elevation.

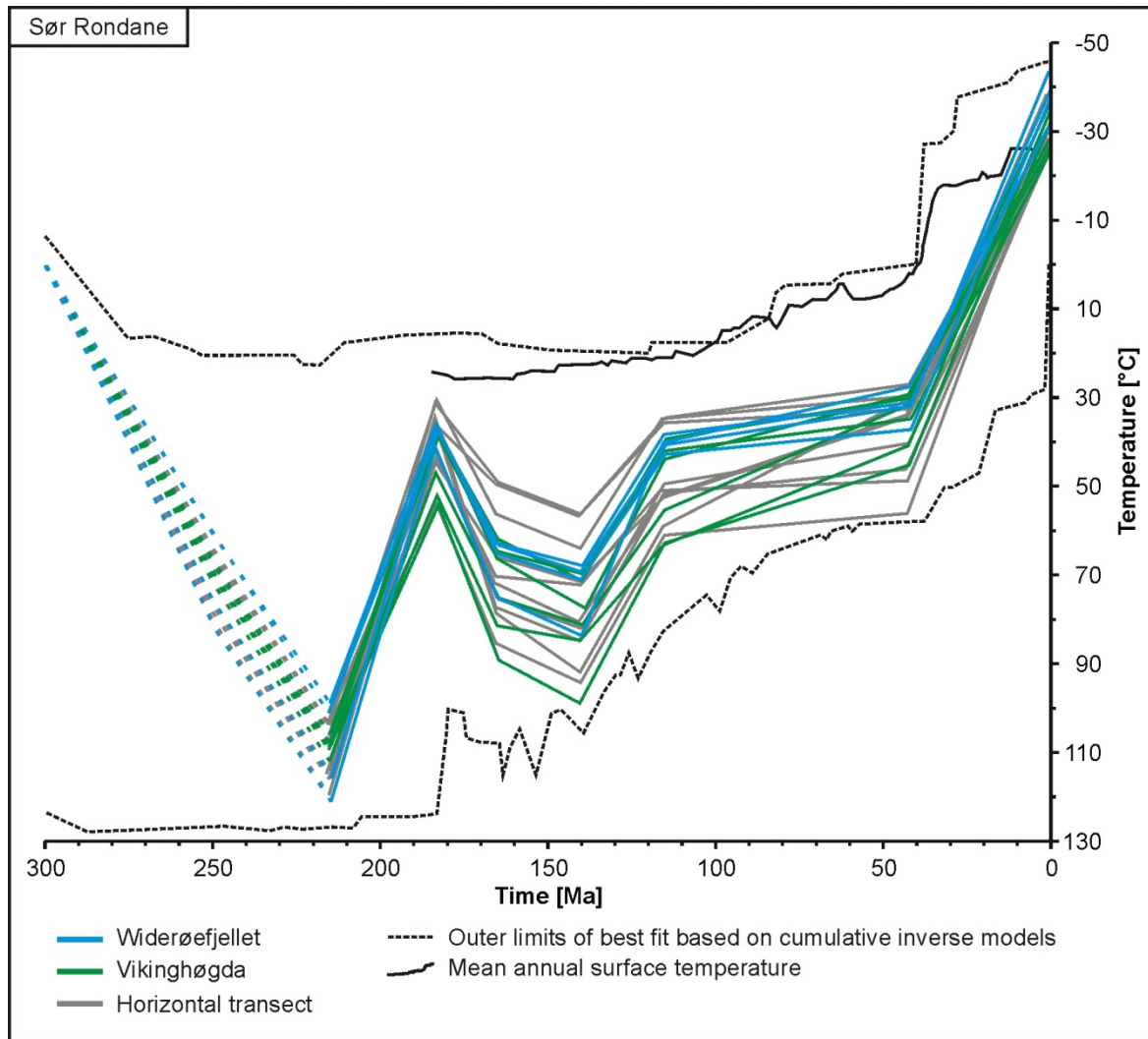


Figure 12.8: Compilation of thermal history models of Sør Rondane. All thermal history models (except TC14) are supported by a  $GOF > 0.5$ . The stippled lines illustrate times that are blurred by subsequent main cooling. For thermal history inversion see supplements. Temperature variation curve by Prenzler et al. (2014 and references therein).

Common thermal histories (Figure 12.8) of western Sør Rondane indicates temperatures of 95–110 °C at ca. 215 Ma with cooling to temperatures below 55 °C at ca. 180 Ma. Uniform reheating followed between ca. 180–140 Ma to maximum 100 °C. Cooling proceeded subsequently until ca. 115 Ma to temperatures below 60 °C. Between 115 Ma and 40 Ma cooling was more diverse with individual velocities (Figure 12.8). Since ca. 40 Ma the paleotemperatures of all thermal history models were below 40 °C. Hence, the thermal histories rely only on total cooling since then.



TC38 and TC24 were sampled closely beneath paleosurface remnants. The vertical relation between the samples and the surfaces appears to be undisturbed. Same courses and temperatures of thermal history models were interpreted here as representing the original paleosurface. All other samples are taken from alpine-type peaks and do not provide evidence to the original vertical distance to the paleosurface.

## 12.7 Exhumation of Western Sør Rondane

### 12.7.1 Permo-Triassic Sag Basin

The paleosurface remnants of Sør Rondane are not dated as overlying sediments or lava flows are lacking. As considered in section 4.4, an early Permian surface exposure of the basement appears as the most reasonable scenario also for Sør Rondane, and was integrated into thermal history modeling. The supposed, but very likely Early Permian paleosurface exposure in Sør Rondane implies that the examined part of basement was already subjected to aerial to very low temperatures at ca. 300 Ma. Uniformly higher paleotemperatures obtained by thermal history modeling at ca. 215 Ma (Figure 12.8) require homogenous reheating of basement and paleosurfaces between 300 and 215 Ma. The only mechanism to reheat consistently surface rocks over the great areal distance is substantial sedimentary burial, potentially superimposed by heatflow variation. The maximum paleotemperature corresponds to the maximum overburden comprising both the total of basement incision plus sedimentary thickness, whereas the paleosurfaces define the base of the former basin. Hence, sampled locations that lie close and undisturbed beneath the paleosurface provide implications for maximum sedimentary overburden. Approximate basin depths of Sør Rondane can be calculated as follows:

$$Z_x = (((T_{\max, x} - T_s) * \partial z / \partial T) - \Delta h_s).$$

Whereas  $Z_x$  = basin depth at point x,

$T_{\max, x}$  = maximum paleotemperature of sample x to time x;

$T_s$  = mean annual surface temperature. The estimated Triassic surface temperature is in the order of ca. 15 °C (e.g. Cantrill et al., 1995; Retallack and Krull, 1999).

$\partial z / \partial T$  = inverse geothermal gradient. Here, as geothermal gradients are unknown, we estimate a range of 25–40 °C\*km<sup>-1</sup>.

$\Delta h_s$  = vertical distance between sample x and paleosurface (no faulting between).

For  $\partial T / \partial z = 25$  °C/km

Southern Part: (105°C- 15°C)\*0.04 km\*°C<sup>-1</sup>-0.2 km=3.4 km

Central Part: (113°C-15°C)\* 0.04 km\*°C<sup>-1</sup>-0.4 km= 3.5 km

For  $\partial T / \partial z = 40$  °C/km

Southern Part: (105°C- 15 °C)\*0.025 km\*°C<sup>-1</sup>-0.2 km=2.0 km

Central Part: (113°C-15 °C)\* 0.025 km\*°C<sup>-1</sup>-0.4 km= 2.0 km



The higher paleotemperatures refer to the sum of sedimentary and basement overburden. The maximum paleotemperatures of the paleosurfaces refer to a maximum sedimentary overburden of 2.0–3.5 km, at least for the southern and central part. The similar burial depth of the paleosurface remnants and the small vertical differences of 0.6–0.8 km between top and bottom parts indicate a relatively smooth paleorelief of the basement and a continuous paleosurface in the Mesozoic and exclude faulting with more than a kilometer vertical offsets. It also implies the relative proximity to the recently eroded paleosurface in the whole study area. The recent vertical dissection of the paleosurface remnants throughout Sør Rondane (Figure 12.3, cf. section 12.4) would than indicate younger faulting, which could well correlate with some of the brittle faults measured in the study area (cf. section 12.5, Figure 12.4). However, this circumstance permits backstacking and calculation of the individual sediment thickness at locations where the paleosurface is completely eroded.

The relatively uniform burial depths throughout indicate the presence of a shallow basin. The areal extension of this basin is not known, but must have exceeded considerably the study area. Direct structural evidence is not available and individual cooling paths and the brittle fault-slip data do not provide implications for any structural control of the basin. The paleogeographic setting within Gondwana and the absence of any preferred fault orientations together with the assumed shallowness of the basin without implications to its adjacent terminations implies that western Sør Rondane was part of a continental sag basin.

Further evidence for continental subsidence is also indicated in the vicinity. Adjacent continental Permo–Triassic basins are known in western DML (Bauer et al., 1997), central DML (Emmel et al., 2009), South Africa (Catuneanu et al., 2005), Mozambique (Salman and Abdula, 1995) and further along East Africa (Kreuser, 1995) and Madagascar (Giese et al., 2012). The basins in western south Africa tend to be related to sags or to foreland basins (Tankard et al., 2009), whereas basins in the easternmost Africa/Madagascar are more related to rifting and graben development (Kreuser, 1995; Salman and Abdula, 1995) and are potentially driven by supraregional tectonic regimes within Gondwana (Catuneanu et al., 2005).

### 12.7.2 Early Jurassic Basin Inversion

The uniform Jurassic thermal history of the whole Sør Rondane area comprises stages of cooling and reheating. Thermal history models (Figure 12.8) show cooling with a long-term rate of ca. 2 °C/Ma commencing at ca. 215 Ma which terminated at temperatures between ca. 20 and 60 °C at ca. 180 Ma. Such slow and simultaneous cooling of the Sør Rondane basement can only be explained by erosional processes and slow stripping of sedimentary rocks due to basin inversion. At ca. 180 Ma, the Permian paleosurface was either re-exposed or covered by only a very thin or patchy sedimentary rock column, which implies more or less complete basin inversion and removal of its sedimentary infill.

The Mesozoic geological and tectonic setting of western Sør Rondane can be constrained by considering the geological record, the geothermal gradient, and the brittle tectonic inventory. The paleotemperature differences amongst the individual thermal history models remain consistent throughout the considered timeframe and support the persistence of a relatively stable paleogeothermal gradient. This is in agreement with the lacking on-site magmatism there. The absence of Mesozoic magmatism throughout Sør Rondane, the stable geothermal gradient,



low paleotemperatures, and missing correlation of local faults with continental margin orientation imply that Sør Rondane was not affected thermally or structurally by main rifting prior to Gondwana breakup. This places Sør Rondane to the hinterland of both initial rift and subsequent continental margins, and requires an alternative trigger for basin inversion.

Adjacent regions in DML experienced as well major cooling to low-temperatures in Late Triassic-Early Jurassic times that obviously terminated around the time of main igneous activity in the Early Jurassic (Jacobs and Lisker, 1999; Emmel et al., 2007; 2009). The time of basin inversion in Sør Rondane and hence likely in the adjacent regions within Gondwana predates the onset of main magmatic activity of the Karoo LIP by ca. 30 Ma. This fits to studies on the early surface effects of mantle flow with regional asthenospheric/crustal uplift prior to magmatism (e.g. Choudhuri and Nemčok, 2017 and references therein). However, the origin of the magma seems not to be related to a deep seated plume (Hastie et al., 2014). A differentiation of mantle processes is beyond topic here. However, we suggest the same or similar surface effects of melt accumulation beneath the uppermost crust regardless of its primary origin within the mantle. Such a rather slow process would be consistent with increasing melt production in the upper mantle that led to updoming in the overlying lithosphere. The surface uplift would also explain the geological record in western DML, where Jurassic magmatic rocks related to the Karoo LIP emplace thin remnants of basal Permian strata (Bauer et al., 1997). Erosion terminated around times of the zenith of Karoo magmatism at ca. 183 Ma (e.g. Duncan et al., 1997), even in non-igneous (Karoo) Sør Rondane. Remarkably, some locations in the Karoo Basins show similar thermochronological data (Green et al., 2017) or stratigraphic evidence to Late Triassic-Early Jurassic uplift (Turner, 1999) and the termination of the Karoo basin by Jurassic magmatism (Tankard et al., 2009).

In summary, slow exhumation, no correlation between local faults and margin orientation, lacking Jurassic volcanism in Sør Rondane plus the supra-regional event of basin inversion in the vicinity of the Karoo LIP can only be explained by mechanisms related to mantle flow leading to dynamic topography.

### 12.7.3 Jurassic-Early Cretaceous Continental Basin

The (near-)surface exposure at ca. 180 Ma potentially was a rather brief episode in western Sør Rondane, as thermal history models indicate a moderate reheating to maximum temperatures of ca. 60–100 °C between ca. 180 Ma and 140 Ma. Paleotemperature differences amongst the individual thermal history models remain consistent (Figure 12.8) and exclude substantial heat-flow variation. Also, the lack of obvious Jurassic or Cretaceous magmatism in Sør Rondane does not support thermal perturbation of the crust by any process related to magmatic cooling, and favor renewed sediment loading as the cause of long-lasting Cretaceous reheating. However, burial depths must necessarily remain speculative because the regional climate during this time is controversially debated and the geothermal gradient is not known. Late Cretaceous surface temperatures in the Weddell Sea-DML region are discussed in the literature between moderately cool including episodic ice sheet formation and warm with an annual maximum of 25°–30 °C (Miller et al., 2008; Jenkyns et al., 2012; Hay and Floegel, 2012). For this range of surface temperatures and a conventional geothermal gradient of 25°–30 °C, we



calculate burial between 0.9–1.5 km in the southernmost and 1.3–2.0 km central part of Sør Rondane.

The highest paleotemperatures were obtained in the western Vikinghøgda region and near Ketelersbreen, referring to paleo-depths of 2.3–3.1 km that comprise both some incised basement and sedimentary overburden. Burial to these depths requires the existence of some relief and suggests deposition within a depression during a time span of up to 40 Ma. Mechanisms of basin formation or implications for the basin type may be derived from the paleogeographic placement of Sør Rondane (cf. sections 6.1–6.2), including the margin type, and physical parameters of the lithosphere. Sør Rondane was placed in the hinterland of the rift. The topographic effects related to the development and evolution of passive margins are generally linked to flexural responses of the lithosphere, as expressed by the uplift of the rift flanks, and to the formation of bulges and depressions in the hinterland (Kusznir et al., 1991; Gilchrist and Summerfield, 1994; e.g. Basile and Allemand, 2002; Sacek et al., 2012a). The individual characteristics, style and duration of the topographic effects seem to depend on various thermal, rheological, tectonic and exogenic factors (Sacek et al., 2012a).

Moho depths and stretching factors of the crust beneath Sør Rondane are not yet studied in local resolution, however, an overview publication by An et al. (2015) infer recent Moho depths of up to 55 km in central and eastern DML.

Further physical parameters, such as the elastic thickness of the lithosphere are unknown, so that the characteristics and the extent of shallow continental depressions in some distance landwards off the rift axis/spreading center cannot further be constrained.

#### 12.7.4 Basin Inversion, Uplift and Major Geomorphological Modification

The thermal history models show subsequent homogenous cooling starting at ca. 140 Ma when temperatures between ca. 30–65 °C were recorded. Such cooling to almost surface temperatures (25–30 °C Jenkyns et al. (2012)) likely represents the erosion of the bulk sedimentary overburden in Sør Rondane throughout the Early Cretaceous with a mean erosion rate of 20–50 m\*Ma<sup>-1</sup>.

Potential trigger of basin inversion cannot be verified in detail but must have been related either by the decreasing flexure (progressive neutralization) because of rift/drift evolution or by far-field tectonic changes, or by both:

The onset of cooling is within resolution coincident with changes in the stratigraphic layers in the Riiser-Larsen Sea ca. 144 and 122 Ma (Leitchenkov et al., 2008). Cooling at ca. 140 Ma is also reported from central DML (Emmel et al., 2009). Simultaneously, the spreading direction in the Indian Ocean changed and also widespread igneous activity commenced in Riiser-Larsen Sea, Lazarev Sea and the adjacent marginal seas (for example, Astrid Ridge, Mozambique Ridge) (Hinze et al., 2004; König and Jokat, 2010; Leinweber and Jokat, 2012; Reeves, 2014). Coherence between far-away offshore tectonic changes and onshore exhumation along pre-existing faults near passive margins is reported by (Gallagher and Brown, 1997; Wildman et al., 2015). However, no direct implication of a tectonic event or fault reactivation in Sør Rondane has been identified.

The thermal history subsequent to the Early Cretaceous cooling stage is established only tentatively due to the limited resolution of the thermochronological data and the lack of external constraints, such as stratigraphic or datable geomorphological information. Thermal history



models collectively show a declination of cooling to 25–55 °C during Late Cretaceous to Eocene times (Figure 12.8). The general low cooling rate during this period seems to correlate with the long-term decrease of atmospheric temperature, however a more accelerated cooling is spotted for two places in the north, potentially indicate beginning basement incision (Figure 12.8).

The onset of final cooling at ca. 40 Ma from paleotemperatures of ca. 25–55 °C to surface temperatures of ca. 5 °C (Ivany et al., 2008) indicate 0.7–2.1 km of post-Eocene erosion comprising downwearing, incision and backstepping (Figure 12.8). A comparison of the plateau remnants with incised valleys in Sør Rondane implies post-Eocene uplift that triggered removal of up to 1.2 km basement or sedimentary overburden and at least the same amount of incision. Enhanced erosion of Sør Rondane due to uplift and increasing glaciation correlates with the deposition of up to 1.5 km thick sedimentary strata in the adjacent Riiser-Larsen Sea (Solli et al., 2007; Leitchenkov et al., 2008; Eagles et al., 2018). Morphological modification of the landscape and progressive relief formation is proposed to have begun by fluvial incision, followed by wet based glacial erosion, especially along pre-existing faults (Sugden et al., 1995). A positive feedback is suggested between rock incision and isostatic compensation that is manifested by increasing relief formation (Näslund, 2001; Sugden et al., 1995).

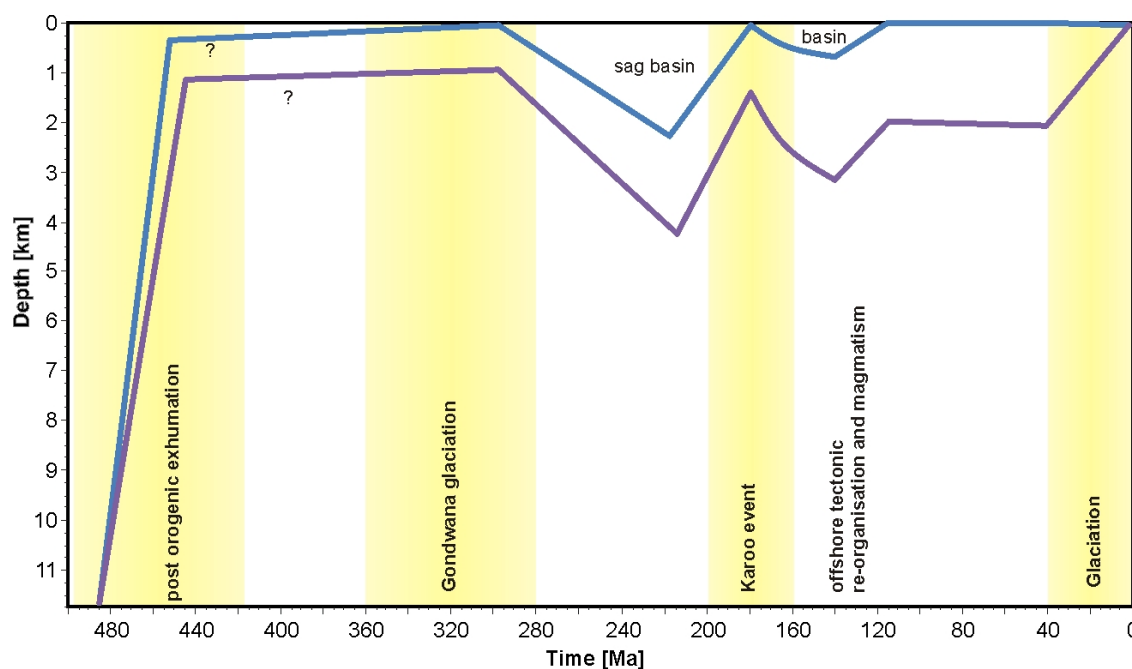


Figure 12.9: Combined sketch of geological and geomorphological evolution of western Sør Rondane, and major events in the vicinity. The blue line sketches the paleosurface level the violet line illustrates the maximum burial and incision.

Modeled thermal histories and paleotemperatures from the Widerrøefjellet summit (2950 m) and the northern foot of Vikinghøgda (1344 m) are very similar throughout, but are recorded at vertical elevations with 1600 m difference. This observation indicates post-Eocene faulting and dissection in the order of ca. 1.5 km. Similar offsets were also recognized from the amount of dissection of paleosurface remnants (c.f. section 12.4, and Figure 12.3), whereby the highest elevated paleosurface remnants occur in the south and on Vikinghøgda. Faulting and dissection might be represented by faults attributed to paleostress tensor group 2, and were likely caused during post-Eocene differential uplift. A similar scenario has been proposed by (Emmel et al., 2007) for central DML. In contrast, our thermal history models from Sør Rondane do not



support a post-Jurassic brittle tectonic event with local transpression as postulated for central DML (Owada et al., 2003; Läufer, in Press). Final exhumation and increasing relief formation is most probably superimposed by climate induced crustal response reinforcing uplift and further climatic changes. The preservation of the paleosurfaces is supported by the hyperarid conditions with very low Quaternary erosion rates (Matsuoka et al., 2006; Suganuma et al., 2014).

## 12.8 Conclusions

The integration of thermal history models of AFT and AHe data with surface exposure constraints provides insights into the passive margin evolution of eastern DML. The thermal histories indicate a complex evolution comprising various exhumation and burial stages since at least the Mesozoic (Figure 12.9). Long-term persistent shallow basins were interrupted by transient inversion phases:

- Sør Rondane was part of a 2.0–3.5 km deep Permian-Triassic sag basin of unknown extent, that was completely inverted in the Late Triassic, potentially as a consequence of dynamic topography.
- Sør Rondane became reburied by 0.9–1.5 km thick sediments until ca. 140 Ma and formed part of a continental depression in the hinterland of the developing passive margins.
- Far-field responses to tectonic and/or flexural changes trigger initial basin inversion at 140 Ma with slow erosion. Between ca. 115 and ca. 40 Ma, Sør Rondane was subject to low erosion.
- Major relief formed since the Cenozoic. It was characterized by paleosurface dissection of ca. 1.6 km, accelerated and differential erosion since ca. 40 Ma, and was potentially accompanied by uplift.

## 12.9 Acknowledgements

This work was supported by the German Research Foundation (DFG) in the framework of the priority program SPP 1158 ‘Antarctic Research with comparative investigations in Arctic ice areas’ by grants LI745/15 and LA 1080/9 to F. Lisker and A. Läufer. N. Krohne, J. Jacobs and M. Elburg are indebted to the BGR for the participation in the GEA II expedition. We thank the International Polar Foundation, Alain Hubert and the crew of Princess Elisabeth Station for support in the field and Alfred-Wegener-Institute for Polar and Marine Research in Bremerhaven for providing polar equipment. Many thanks go to the SkyHeli Helicopter Team, Trebbin, Germany. The brittle scientific results were obtained using Win-Tensor, a software developed by Dr. Damien Delvaux, Royal Museum for Central Africa, Tervuren, Belgium. Graeme Eagles is acknowledged for discussions and helpful comments. Rene Robert is thanked for providing field photographs of the Belgica Mountains (cf. Figure 12.3).



## Chapter 13

### 13. Synopsis

When Alfred Wegener published his continental drift theory (Wegener, 1912), scientists started to investigate the processes that have been involved in the formation of continents. To understand the nowadays configuration of plate tectonics, Antarctica represents an important crustal fragment due to its unique geographical position on the southern hemisphere, and because of its relative tectonic stability since the break-up of Gondwana in Jurassic times. Ever since, the Antarctic lithospheric plate was surrounded by mid-ocean ridges with the Antarctic Peninsula regarded as an exception. Thus, East Antarctica is considered a key location to study the pre-Mesozoic crustal evolution on least overprinted rocks. This thesis consists of several studies to advance a comprehensive understanding of the final amalgamation of Gondwana.

The concept of a stable East Antarctic shield was challenged by Fitzsimons (2000a) who reported on three distinct Grenville-aged basement provinces (Maud, Rayner, and Wilkes) separated by regions of intense Late Neoproterozoic/Early Cambrian tectonics related to the amalgamation of Gondwana. Since then, several plate tectonic models were developed to interpret geological observations and to study the final formation of Gondwana.

One scenario suggests the continuation of the East African Orogen (Stern, 1994) into Antarctica, which was proposed by several studies (Moyes et al., 1993; Grunow et al., 1996; Shackleton, 1996; Jacobs et al., 1998). However, all these studies suggest different locations for the E-W Gondwana suture between western and eastern Dronning Maud Land. Further scientific studies have been accomplished during the following years and have led to even more elaborate models (e.g. Meert, 2003; Fitzsimons, 2003; Boger et al., 2001; Boger and Miller, 2004). Boger (2011) provided an overview and discussed three main routes proposed for a second orogeny, the Kuunga Orogen (Figure 13.1) which is assumed to cross or intersect with the East African (-Antarctic) Orogen.

In these reconstructions, the region of Sør Rondane is situated in a key position to target the final collision processes of Gondwana more detailed and to address the question whether this region is potentially situated within two crossing orogens (Figure 13.1). Recent structural, geological and geochronological investigations were accomplished by Japanese Antarctic Expeditions across Sør Rondane (Satish-Kumar and Hokada, 2013). According to those studies, main granulite-facies metamorphism is documented at ca. 650-600 Ma (Shiraishi et al., 2008; Osanai et al., 2013) and related to a collision boundary, the Main Tectonic Boundary, being the result of the final closure of the Mozambique Ocean (Osanai et al., 2013). However, former studies suggest that the SW Terrane and NE Terrane of Sør Rondane were brought together during amphibolite-facies metamorphism at ca. 570 Ma (Shiraishi et al., 2008). Here, Satish-Kumar et al. (2013) admit that the conclusions regarding the collision scenario at ca. 650-600 Ma may be biased by existing concepts and consider the possibility of a completely different scenario being independent of the East African-Antarctic Orogen.



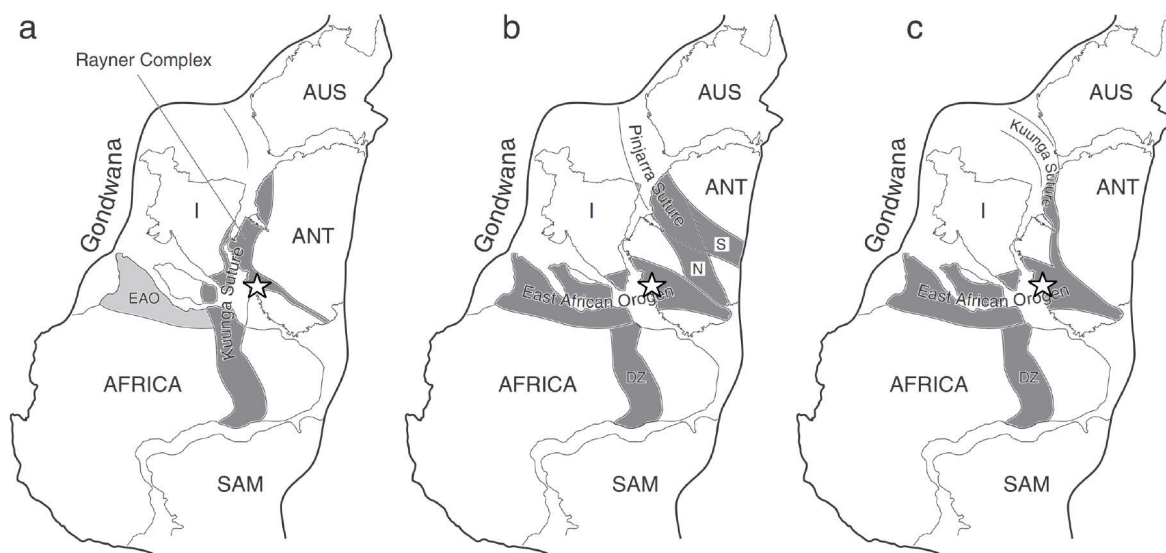


Figure 13.1: Overview of proposed routes of sutures originating from the amalgamation of Gondwana during the Late Neoproterozoic/Early Cambrian. The star marks Sør Rondane being situated at a key position within Gondwana (adapted from Boger, 2011). Proposed routes after (a) Meert (2003) (b) Fitzsimons (2003) (c) Boger et al. (2001) and Boger and Miller (2004).

Metamorphic U-Pb zircon ages between ca. 570-530 Ma (e.g. Picciotto et al., 1964; Pasteels and Michot, 1970; Shiraishi et al., 2008; Adachi et al., 2013; Grantham et al., 2013; Osanai et al., 2013) are documented across Sør Rondane and may suggest that this region is located within two apparently overlapping mobile belts (Satish-Kumar et al., 2013), which are represented by the East African-Antarctic Orogen (Jacobs et al., 1998) and the Kuunga Orogen (Meert, 2003; Boger, 2011).

Motivated by the persisting uncertainty about the final amalgamation of Gondwana, the region of Sør Rondane was targeted by the GEA project to provide detailed data on single aspects of its geodynamic history. Main advantage of the project was the combined acquisition of systematic aerogeophysical data and punctual field studies. The finding of an aeromagnetically distinct province in southeastern Dronning Maud Land, which is characterized by a subdued magnetic anomaly field with elongated parallel positive SE trending anomalies, was first interpreted as an orogenic belt of unknown age (Mieth and Jokat, 2014; Mieth et al., 2014). Nunataks between eastern (Sør Rondane) and central Dronning Maud Land are located within this magnetically distinct province and were targeted during the GEA II expedition. Field geology, geochronology and geochemistry facilitated ground-truthing of this mostly ice-covered area and provided evidence for a ca. 1000-900 Ma juvenile oceanic arc terrane (Jacobs et al., 2015). These juvenile Tonian rocks show close similarities to the GTTG complex of the SW Terrane in Sør Rondane and are jointly interpreted as a Tonian Oceanic Arc Super Terrane (TOAST) (Jacobs et al., 2015). These new findings are essential for the configuration of plate tectonics before the amalgamation of Gondwana and need to be included in future models. Nevertheless, this can only be done properly, if the dimensions of this new crustal fragment are being investigated. Ongoing systematically acquired aeromagnetic data over Sør Rondane (Mieth et al., 2014) and the largely ice-covered regions south and east of Sør Rondane provided first estimations of its minimum extent of approximately 5 % of East Antarctica (Ruppel et al., 2018).



## 13.1 Geophysical and Geo(chrono)logical Evidence Obtained from Sør Rondane

In areas with a comparably high density of exposures like Sør Rondane detailed high-resolution aeromagnetic data and their combination with geological information considerably improved our understanding of their tectonic and structural framework. Based on magnetic anomaly data former terrane boundaries and structures were redefined. Whereas the Main Tectonic Boundary is proven to be discontinued, the Sør Rondane Suture is not regarded as of major tectonic relevance anymore (Mieth et al., 2014). However, it is supposed to represent a part of the frontal fold zone of the collision of the NE- with the SW-Terrane (Osanai et al., 2013) and was imaged by magnetic anomaly data. Furthermore, magnetic anomaly data provide indication for a horizontal displacement along the dextral Main Shear Zone of roughly 40 km, whereas reliable geological edifice for the Main Shear Zone is only found west of the Gjellbreen Lineament (Figure 13.2). The new identification of the Sør Rondane corridor, which is based on magnetic anomaly data as well, suggests an extensional late Pan-African structure (Mieth et al., 2014).

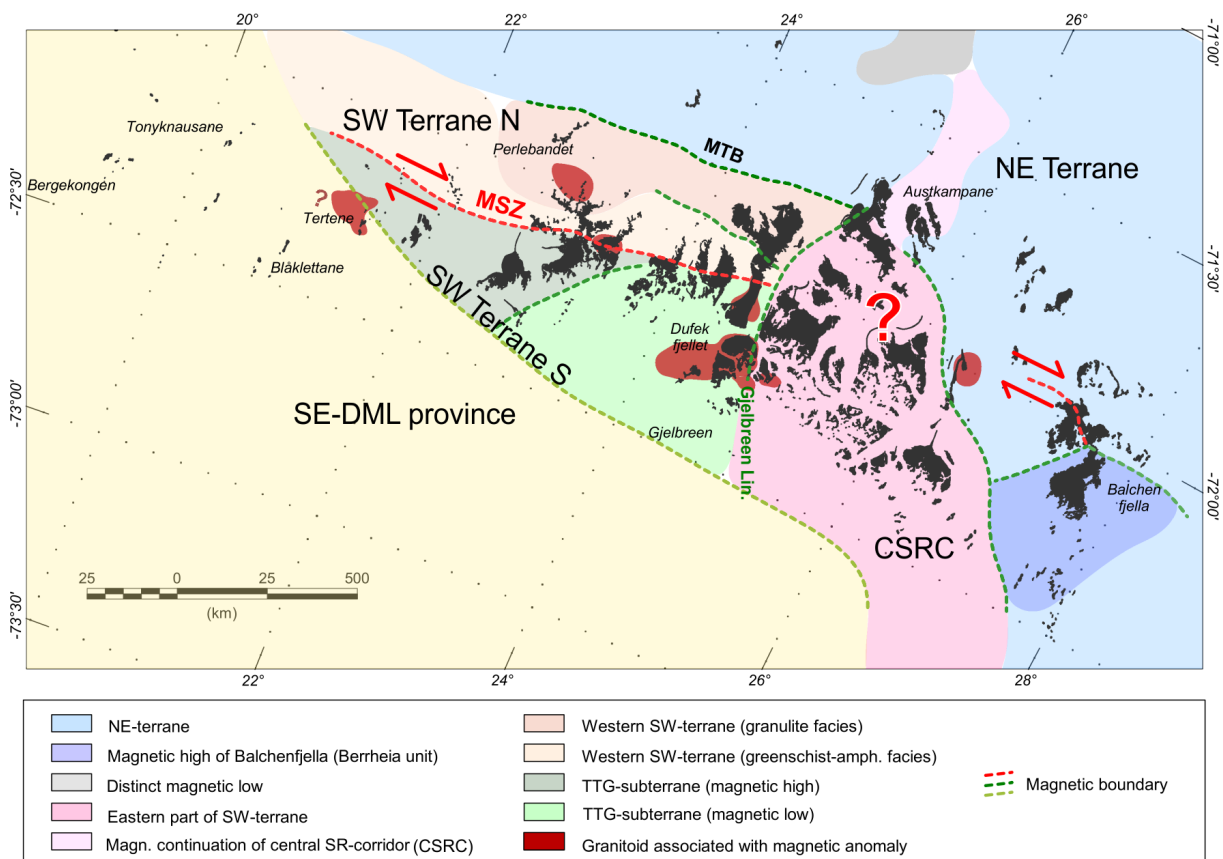


Figure 13.2: Interpretation of combined aeromagnetic and geological findings by Mieth et al. (2014). Note the highlighted trend of the dextral Main Shear Zone (MSZ) and a dextral shear zone at Balchenfjella, which are separated by the central SR-corridor (CSRC) of most likely extensional nature.

If the corridor postdates the Main Shear Zone, a younger extensional event might explain the abrupt end of this structure suggesting its prolongation eastwards of this magnetically defined corridor. Indeed, Ishikawa et al. (2013) report on a dextral shear zone, which is exposed in Balchenfjella and suggest a development under granulite- to amphibolite-facies conditions at ca. 600 Ma based on LA-ICP-MS U-Pb dating on zircons. These ages were obtained from the



rim of a garnet as well as from the matrix of a garnet-biotite-silimanite gneiss. However, the estimated age and metamorphic grade do not exactly correlate with the lower to medium grade metamorphic conditions and late Ediacaran to Cambrian age of the Main Shear Zone (Ruppel et al., 2015). Nevertheless, the U-Pb zircon ages from Balchenfjella represent a rough estimate for an upper age constraint of deformation. Here, additional Ar/Ar analyses might provide further indications of a possible prolongation of the Main Shear Zone.

Geochronological ages related to the timing of metamorphism, magmatic activity and cooling following the latest metamorphism in Sør Rondane are summarized and illustrated in Figure 13.3a-c. In general, peak metamorphism occurred around 650-600 Ma and is likely a result of the collision and overthrusting of the NE on the SW-Terrane (Osanai et al., 2013). The collision was followed by subsequent retrograde metamorphism, orogenic collapse, and exhumation, which was dated at ca. 570-530 Ma in both terranes (e.g. Shiraishi et al., 2008; Osanai et al., 2013 and references therein).

U-Pb zircon ages of igneous rocks provide evidence for at least four thermal pulses lasting 150 Myrs across the whole area at ca. 635 Ma, 565-545 Ma, 530 Ma and 510-500 Ma with the two oldest events associated with metamorphism. Nevertheless, the oldest and largest intrusion at Dufekfjellet of ca. 640-620 Ma (Li et al., 2006; Elburg et al., 2016), shows a volcanic arc and/or collisional signature (Li et al., 2003), with regard to an overthrusting scenario (Osanai et al., 2013), it is situated within the SW-Terrane S in the lower plate. In addition, the variations of inherited zircons between the NE and SW terranes (Osanai et al., 2013; Elburg et al., 2016) as well as the differences in Hf isotopic compositions between different sectors of the SW terranes together with the extended duration of magmatism suggest an accretionary collision history (Elburg et al., 2016).

New Ar/Ar mineral ages (Ruppel et al., in prep.) together with a few published Ar/Ar and K-Ar (Takigami et al., 1987; Takigami and Funaki, 1991) ages show a wide age range from 660-480 Ma. This Ar/Ar age distribution roughly correlates with the regional distribution of at least three generations of syn- to post-tectonic granitoids and is distinct for the five different tectonic domains recognised. The oldest Ar/Ar cooling ages of ca. 660 Ma are found in the SW Terrane S (Takigami and Funaki, 1991). This terrane consists of competent GTTGs and represents the mid-crustal part of a Tonian oceanic arc (Elburg et al., 2015), which is interpreted as a megaboudin since it lacks major deformation during the Late Neoproterozoic (Jacobs et al., 2015; Ruppel et al., in prep.). It further hosts the oldest and largest granitoid intrusion at Dufekfjellet dated to ca. 640-620 Ma (Li et al., 2006; Elburg et al., 2016).

The northern margin of the SW Terrane S coincides with the Main Shear Zone, which appears as a zone of strain concentration between the competent SW Terrane S and the rheological weaker SW Terrane N. Along this contact zone, U-Pb zircon ages of ca. 570-560 Ma are documented for syn-tectonic granitoids of the second generation whereas Ar/Ar amphibole and biotite ages of ca. 570-525 Ma suggest that deformation along the Main Shear Zone continued until ca. 525 Ma.

The youngest phase of magmatic activity is recorded in the four adjacent terranes surrounding the proposed megaboudin and correlates with the youngest Ar/Ar ages of ca. 510-480 Ma. Within these terranes an eastwards directed trend to younger Ar/Ar cooling ages away from the center of the East African-Antarctic Orogen may relate to a general outward growth and widening of the orogen over time. The application of Ar/Ar geochronology revealed a



differentially protracted Late Neoproterozoic/Early Paleozoic tectono-thermal cooling history over approximately 150 Myrs of the eastern part of the East African-Antarctic Orogen (Ruppel et al., in prep.). Together with the documented protracted magmatism and variations in the Hf isotopic composition (Elburg et al., 2016), Sør Rondane may have experienced rather a collage-style tectonism with repeated phases of accretion, magmatism and reactivation, prior to its integration into Gondwana (Elburg et al., 2016; Ruppel et al., in prep.).

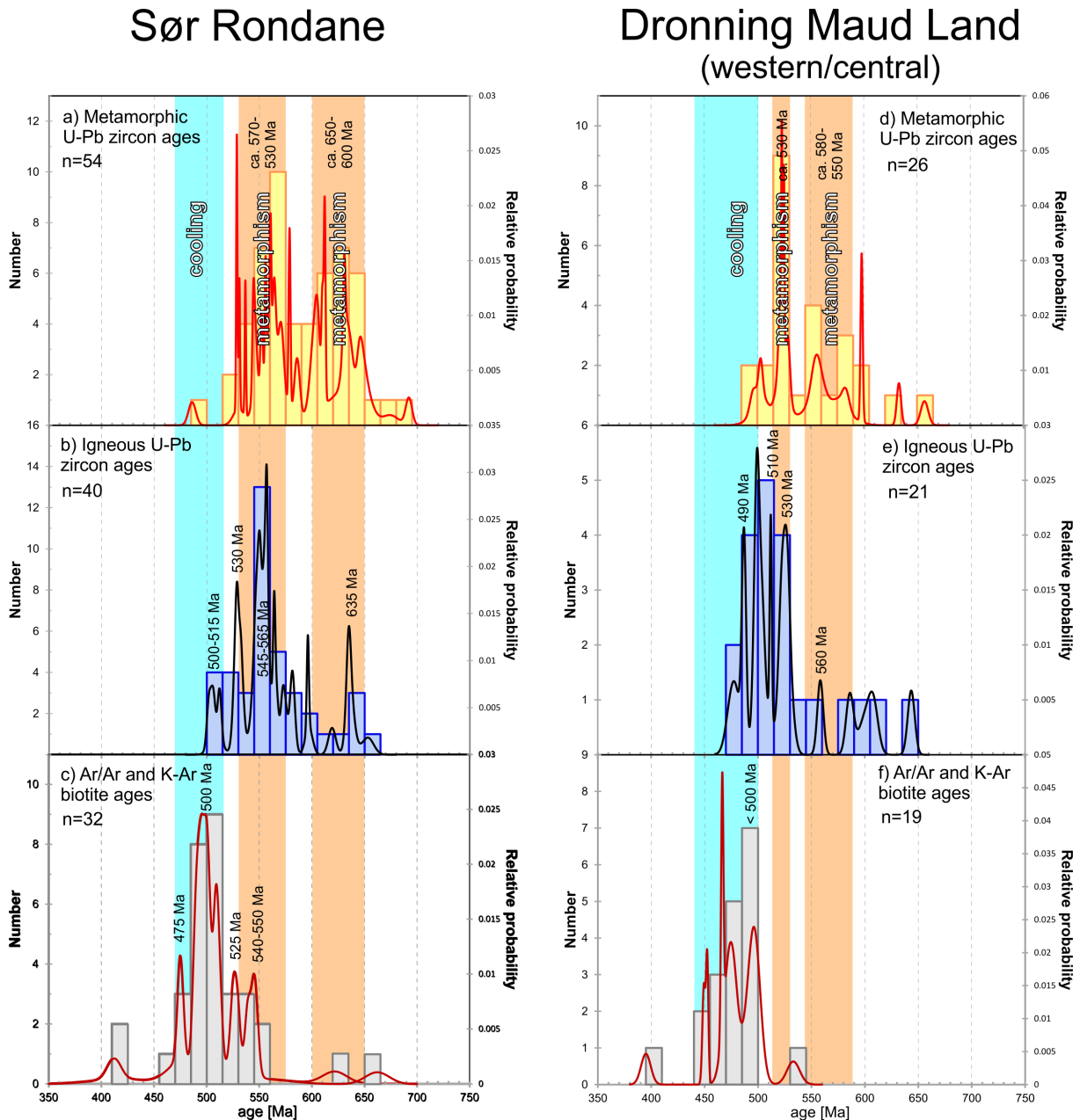


Figure 13.3: Geochronological data of Sør Rondane a)-c) and western/central Dronning Maud Land d)-e). Source for U-Pb zircon ages: (Harris et al., 1995; Mikhalsky et al., 1997a; Jacobs et al., 1998; Bauer et al., 2003b; Jacobs et al., 2003a, d; Jacobs et al., 2003c; Jacobs et al., 2003b; Paulsson and Austrheim, 2003; Shiraishi et al., 2003; Board et al., 2005; Ravikant et al., 2004; Bisnath et al., 2006; Li et al., 2006; Ravikant et al., 2007; Jacobs et al., 2008b; Shiraishi et al., 2008; Baba et al., 2010; Adachi et al., 2013; Grantham et al., 2013; Higashino et al., 2013; Hokada et al., 2013; Osanai et al., 2013; Owada et al., 2013; Nakano et al., 2013; Baba et al., 2015; Jacobs et al., 2015; Elburg et al., 2016; this study). Source for Ar/Ar and K-Ar biotite ages: (Takigami et al., 1987; Takigami and Funaki, 1991; Jacobs et al., 1995; Markl and Henjes-Kunst, 2004; this study).



To the west of Sør Rondane, two main metamorphic events can be differentiated. The first event is marked by the intrusion of anorthosites and charnokites at ca. 605 Ma and followed by deformation and metamorphism at ca. 580-550 Ma (e.g. Jacobs et al., 1998; Jacobs et al., 2003a; Board et al., 2005). This earlier event is regarded to be the result of crustal convergence whereas the second event between ca. 530 and 490 Ma was mostly of magmatic character and is marked by the intrusion of large volumes of post-tectonic granitoids during orogenic collapse (Ohta et al., 1990; Mikhalsky et al., 1997b; Jacobs et al., 1998; Jacobs et al., 2003a; Jacobs et al., 2003b; Roland, 2002; Paulsson and Austrheim, 2003, Figure 13.5d-e).

A number of ca. 500 Ma K-Ar and Ar/Ar amphibole and mica ages are reported from western Dronning Maud Land in the Heimefrontfjella (Jacobs et al., 1995; 2003c). In addition, a few K-Ar and Ar/Ar amphibole and biotite ages between ca. 490 and 450 Ma document cooling of ca. 540 Ma (U-Pb zircon age) post-kinematic charnokitic rocks in central Dronning Maud Land (Markl and Henjes-Kunst, 2004).

The comparison of the metamorphic, magmatic, and cooling history of Sør Rondane to adjacent regions to the west indicates a shift to a 20-40 Myrs older age (Figure 13.3c, f; only biotite ages are illustrated). These findings suggest a major crustal boundary between these regions and support the idea that this structural feature is represented by the Forster Magnetic Anomaly (Riedel et al., 2013). However, this may not be the only boundary as e.g. documented by Baba et al. (2015). These authors report on metamorphic ages of ca. 600 Ma and ca. 525 Ma obtained from Filchnerfjella and Hochlinfjellet, respectively, in central Dronning Maud Land. The age gap of ca. 80 Myrs between these two regions is suggested to be the result of different collisional events.

In general, different metamorphic ages within distinct regions of Dronning Maud Land, long lasting magmatism, and differential cooling as documented for Sør Rondane (Elburg et al., 2016; Ruppel et al., in prep.) support the hypothesis that different terranes were assembled most likely prior to the final collision with southern Africa (Kalahari craton).

In addition, the study of the so far poorly investigated region between Sør Rondane and central Dronning Maud Land as well as indications from moraine studies suggest that large parts of eastern Dronning Maud Land consist mostly of Late Mesoproterozoic/Early Neoproterozoic juvenile basement rocks with no indication of significant contribution from Palaeoproterozoic or Archaean continental crust (Elburg et al., 2015; Jacobs et al., 2015; Elburg et al., 2016). The exact number and the dimensions of single arcs/terranes of the TOAST remain yet unresolved whereas metamorphic overprint from about 850 to 580 Ma is suggested to result from ocean closure and the final amalgamation of Gondwana (Jacobs et al., 2017). However, a simplified concept of two discrete orogens - Kuunga and East African-Antarctic - is to be questioned and an accretionary model needs to be tested and investigated in more detail.

## 13.2 Crustal Provinces of East Antarctica

New findings of this study regarding the extent of the TOAST (Ruppel et al., 2018) within East Antarctica are integrated into previous interpretations of Golynsky et al. (2007). These authors identified major tectonic provinces of East Antarctica based on magnetic anomaly data of the ADMAP-1 compilation. A modified version is presented in Figure 13.4. This map indicates the location of major cratonic fragments with one of them being represented by the prominent Archaean Grunehogna craton/province in western Dronning Maud Land. This fragment was



prior to the break-up of Gondwana (~180 Ma) juxtaposed to the Kaapval craton in South Africa (Martin and Hartnady, 1986; Leinweber and Jokat, 2012). The Grunehogna province is fringed by the Namaqua-Natal-Maud Belt representing a Grenvillian (ca. 1.1 Ga) collision belt (Jacobs et al., 1998). The magnetic anomaly pattern changes abruptly along the transpressional Heimefront Shear Zone, which separates unaffected Mesoproterozoic rocks to the west from rocks with a Pan-African overprint to the east (Golynsky and Jacobs, 2001; Jacobs et al., 2003c). The western termination of the Maud Belt is distinguished by a change in the anomaly pattern of the neighbouring Coats Land Block and the Shackleton Range crustal block. In central Dronning Maud Land, the prominent 'Forster Magnetic Anomaly' delineates a major boundary and is interpreted as suture, which juxtaposes Mesoproterozoic rocks of the Maud Belt against the western boundary of the TOAST (Jacobs et al., 2015). The southern extent of the TOAST is less confined by the magnetic anomaly data presented in Ruppel et al. (2018). Lacking exposures prevent a reliable ground-truthing especially to the south. Further, major ice divides (Rignot et al., 2011) prohibit gaining geological ground control by the study of rock debris brought by continental glaciers.

Here, the interpretation of aeromagnetic data provides the sole possibility to define the extent of the TOAST. A change in the magnetic background values is observed in the south but the characteristic SE trend of the positive anomalies is still observed and challenges the interpretation whether this pattern still represents remnants of an oceanic arc complex. More recently, a new magnetic anomaly map of Antarctica (ADMAP-2) enables the first nearly complete mapping of the Valkyrie Cratonic Block situated inland of the TOAST (Golynsky et al., 2018) and most likely falls in line with the formerly presumed southern extent and border of the TOAST. East of the TOAST the Beaver-Rayner Mesoproterozoic province is delineated based on magnetic anomaly data (Golynsky et al., 2007), whereas the border between the TOAST and this province with Indian affinities is of transitional character (Ruppel et al., 2018). Overall, interpretation of magnetic anomaly data, if combined with surface geology where possible, provide a best estimate for the extent of the TOAST and the crustal architecture of East Antarctica, which can only be improved by considerable efforts, e.g. hard rock drilling.

### 13.3 From Rodinia to Gondwana

New findings of the geological nature and extent of the TOAST (Jacobs et al., 2015; Ruppel et al., 2018) raise the question of its place of origin and position during the final assembly of Gondwana. The normalized trace element pattern of GTTG gneisses west of Sør Rondane and tonalitic rocks of the SW-Terrane are typical for subduction-related magmas (Elburg et al., 2015; Jacobs et al., 2015). Further, the juvenile character without significant inheritance of older e.g. Archaean signatures and a lack of metamorphic overprint immediately following crustal formation suggest that this fragment was not an integral part of the supercontinent Rodinia and has evolved somewhere outboard (Jacobs et al., 2015). The nature of the southern boundary of the TOAST remains an open question. However, it can be speculated that the SE trending magnetic structures of the TOAST may indicate the general elongation of island arc terranes. These terranes were possibly accreted along the margin of the cryptic Valkyrie craton (Golynsky et al., 2018) that was situated in the south of the TOAST, before craton and TOAST together were sandwiched in between Kalahari and Indo-Antarctica (Figure 6.14, Figure 13.4). Alternatively, the island arc terranes could have accreted along a different place along blocks



of E- or W-Gondwana and were only translated into the present location. Due to lacking metamorphic overprint after crustal formation oceanic arc terranes may have amalgamated relatively late during early Paleozoic times before their final collision with Kalahari (Ruppel et al., in prep.).

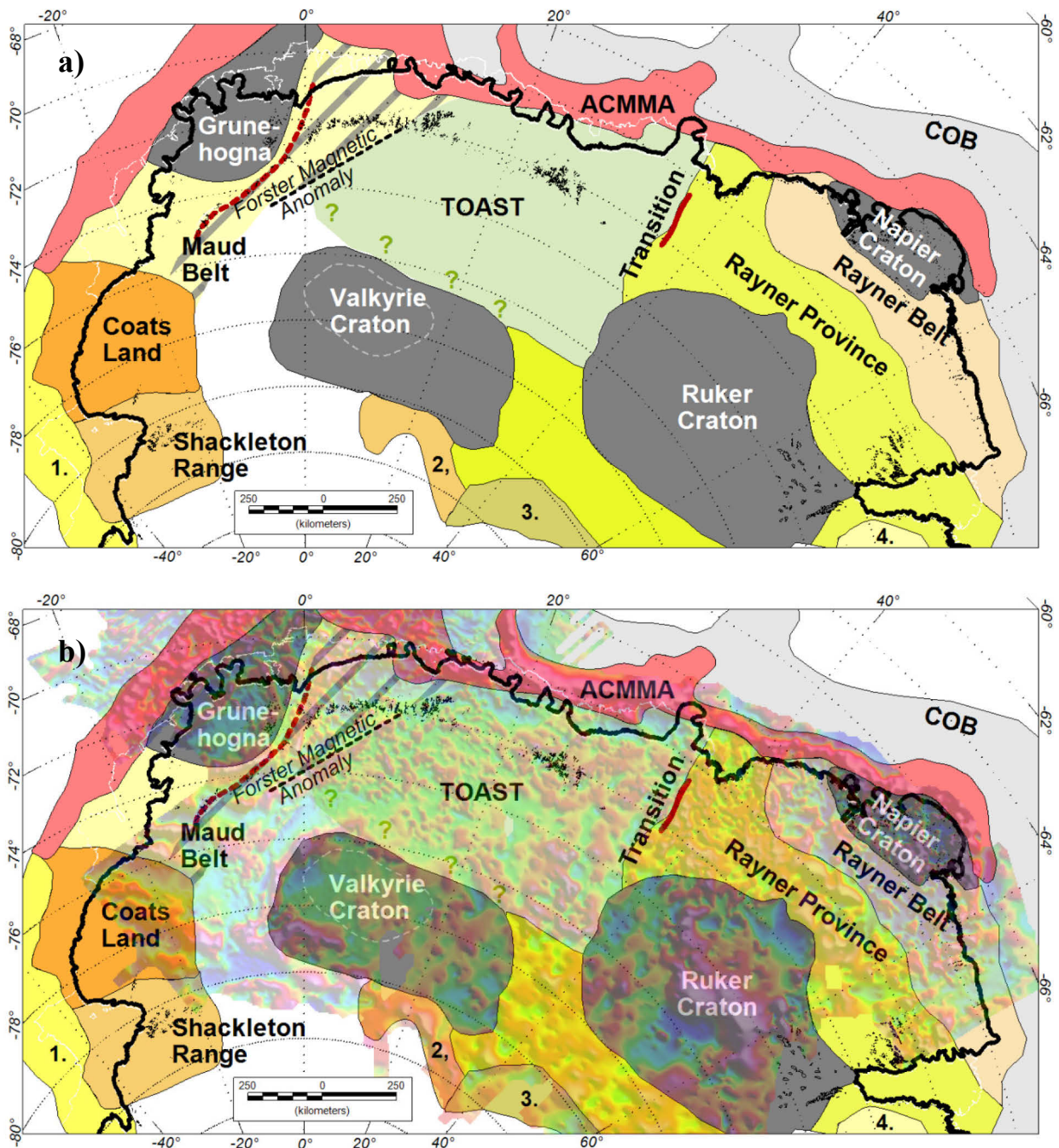


Figure 13.4: a) Revised map of major crustal provinces of East Antarctica modified after Golynsky et al. (2007). b) Superposition of Admap-2 (Golynsky et al., 2018) on crustal fragments presented in A). Abbrev: ACMMA: Antarctic Continental Magnetic Margin Anomaly; COB: Continent Ocean Boundary; TOAST: Tonian Oceanic Arc Super Terrane.



A recent study by Archibald et al. (2017) correlates the TOAST with a newly recognized Stenian to Tonian-aged arc magmatic suite (Dabolava Suite) in Madagascar. Similar to the TOAST, this arc is suggested to have formed in an oceanic arc tectonic setting outboard of Rodinia since it escaped sediment input from continental blocks that contain Archaean to Palaeoproterozoic rocks. Based on a comparison of isotopic compositions (Hf isotopic and Sr-Nd isotopic data) of contemporaneous Stenian to Tonian-aged magmatic arc rocks from different regions, Archibald et al. (2017) suggest the presence of an extensive oceanic or continental arc system that persisted outboard of Rodinia until the closure of the Mozambique Ocean (Figure 13.5). However, the position of the TOAST after its formation until its integration into Gondwana remains yet unknown.

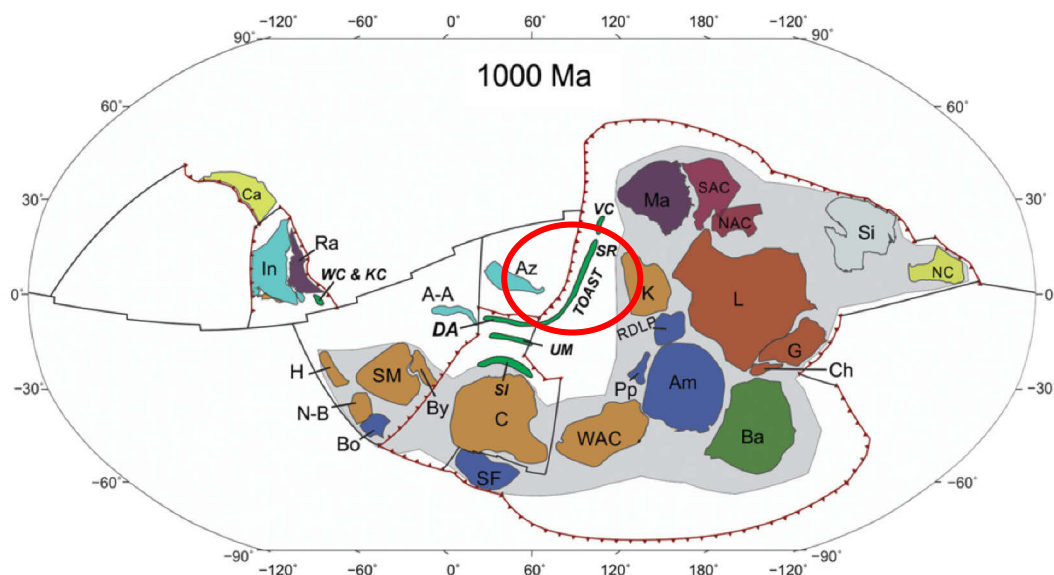


Figure 13.5: Tectonic geography of Rodinia (shaded in grey) at 1000 Ma (adapted from Archibald et al., 2017). Cratonic crust is coloured by present-day geography: North America, red (Ch, Chortis; G, Greenland; L, Laurentia); South America, dark blue; (Am, Amazonia; Bo, Borborema; Pp, Paranapanema; RDLP, Rio de la Plata; SF, São Francisco); Baltica, green; (Ba, Baltica); Siberia, grey; (Si, Siberia); India, Indian Ocean continents and the Middle East, light blue (A-A, Afif-Abas Terrane; Az, Azania; In, India); China, yellow (Ca, Cathaysia, South China; NC, North China); Africa, orange (By, Bayuda; C, Congo-Tanzania-Bangweulu Block; H, Hoggar; K, Kalahari; N-B, Nigeria-Benin; SM, Sahara Metacraton; WAC, West African Craton); Australia, crimson (NAC, North Australian Craton; SAC, South Australian Craton); Antarctica, purple (Ma, Mawson; Ra, Rayner); Meso- to Neoproterozoic Arcs, dark green; (DA, Dabolava Arc; SI, Southern Irumide; SR, Sør Rondane; TOAST, Tonian Oceanic Arc Super Terrane; UM, Unango-Marrupa; VC, Vijayan Complex; WC, Wann Complex; KC, Kadugannawa Complex).

Within a scenario proposed by Boger (2011), the amalgamation process of Gondwana started in Ediacarian times with the collision of the Kalahari craton, which comprised the combined Kaapvaal and Grunehogna cratons rimmed by the Natal-Maud Belt with the Coats Land Block (Figure 13.6). This event was followed by the collision of the combined Kalahari-Coats Land Block with (i) Precambrian Africa forming the Damara-Zambezi Orogen, with the (ii) newly defined TOAST, which was probably attached to the cryptic Valkyrie craton, and with (iii) the Indo-Antarctic craton. Evidence for the collision of Kalahari-Coats Land Block with the TOAST-Valkyrie craton is provided by the Forster Magnetic Anomaly in the west (Riedel et al., 2013; Mieth and Jokat, 2014; Jacobs et al., 2015; Ruppel et al., in prep.). This major anomaly projects directly into the outcropping Humboldt Mts. forming the western portion of



the Wohlthatmassive in central Dronning Maud Land. This area has only been studied at the reconnaissance level so far and is a key region to understand the amalgamation process of the TOAST. A change in the magnetic anomaly pattern to the east of the Yamato Mountains supports the hypothesis that relicts of the collision of the TOAST with Indo-Antarctica can be found in the Lützow-Holm Bay region (Boger, 2011; Nogi et al., 2013; Ruppel et al., 2018). The new findings of the dimensions of the TOAST and its speculated attachment to the Valkyrie craton with yet unknown affinities adds a new perspective to the amalgamation process. Nevertheless, the remote ice-covered regions inland of East Antarctica are insufficiently studied by e.g. airborne geophysical data and are desperately needed to investigate a more elaborated concept in particular with regard to the final amalgamation with parts of Australo-Antarctica as well as the dimensions and/or existence of the Crohn Craton.

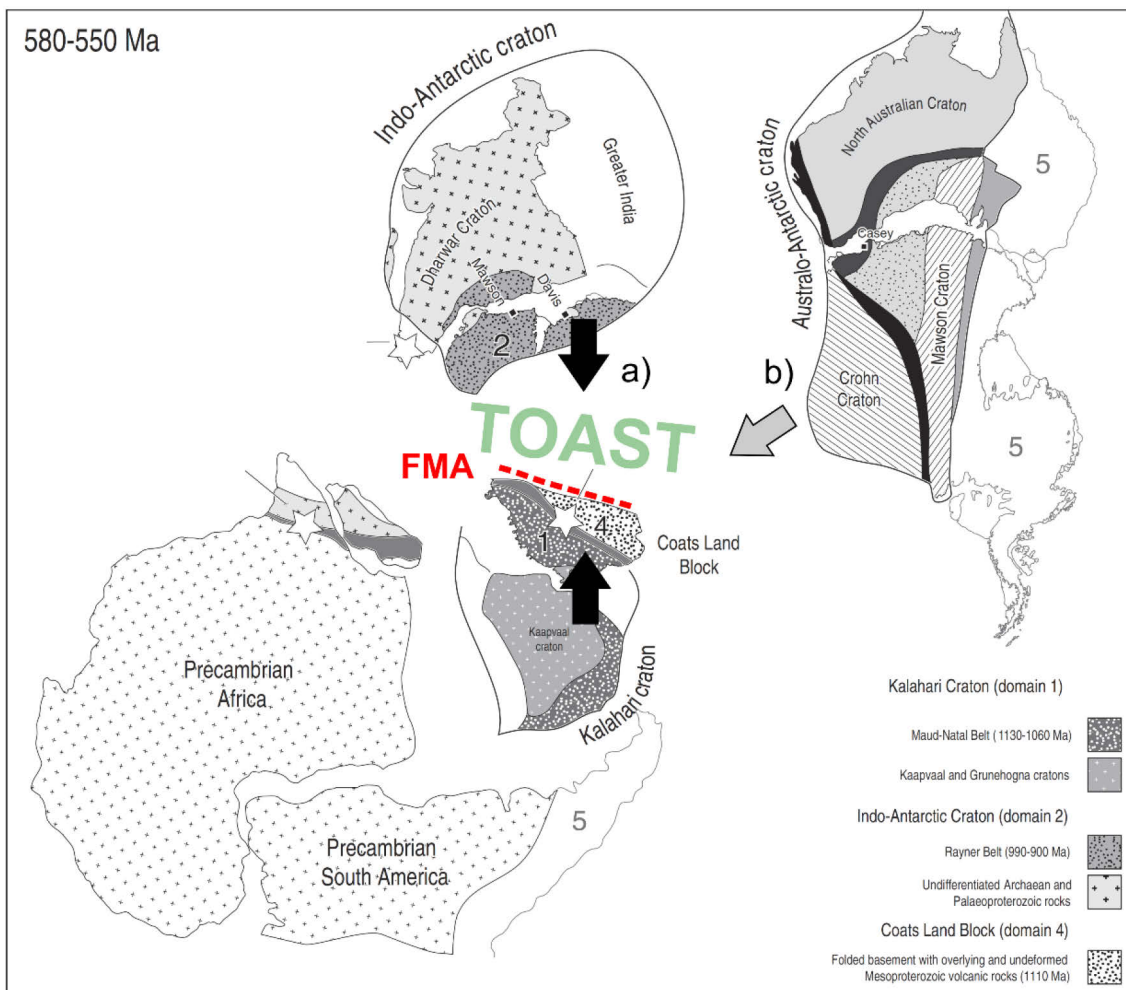


Figure 13.6: Assimilation of Gondwana (Boger, 2011). Antarctic palaeogeography in the Ediacarian. a) Collision of the combined Kalahari-Coats Land craton and Precambrian Africa with Indo-Antarctica in Ediacarian and early Cambrian (550-520 Ma) incorporating accreted juvenile oceanic arc terranes (TOAST) b) Final collision of Precambrian Africa, Precambrian South America, Coats Land, TOAST and Indo-Antarctica with Australo-Antarctica. 1: Maud-Natal Belt (African affinities); 2: Rayner Belt (Indian affinities); 3 (Australian affinities); 4: Coats Land Block (no known affinities); 5: Accreted pre- and post-Gondwana sediments, arc and para-autochthonous terranes.



## 13.4 Break-up of Gondwana

As stated above, the position and stability of Antarctica presents many advantages to study the amalgamation processes of Gondwana during Late Neoproterozoic/Early Paleozoic times. However, the lack of a Phanerozoic sedimentary record in Sør Rondane prevents a detailed reconstruction of geological processes after Gondwana was established. Here, first time low temperature geochronological data have provided new information about the Phanerozoic shallow crustal dynamics, the post-breakup uplift history and long-term landscape evolution of Sør Rondane. The new data show evidence for a dynamic geological evolution comprising various exhumation and burial stages. Cooling at 215-180 Ma is interpreted in terms of removal of 2.8 km overburden of a Permo-Triassic intracontinental basin in response of tectonic uplift. Furthermore, reburial of Sør Rondane in a local basin until 140 Ma is interpreted to be the response of ongoing extensional tectonism. Thermal models suggest a basin inversion at 140 Ma as a result of a far-field response to tectonic and/or flexural changes accompanied by slow erosion between ca. 115 and ca. 40 Ma. Major relief formed since ca. 40 Ma in the Cenozoic (Krohne, 2017; Krohne et al., in prep.).

Combined aerogeophysical data and seismic stratigraphy of offshore basins in the Riiser-Larsen Sea show that most of the erosion occurred during the ~40 Myrs following late Jurassic continental break-up (Leitchenkov et al., 2008; Eagles et al., 2018). Analyses of the seismic dataset illustrate that filling of basins located offshore still continued around ca. 160-140 Ma suggesting that the region of Sør Rondane has been characterized by high topography ever since. It is also assumed that reheating of Sør Rondane was rather triggered by the activity of the Astrid Ridge mantle plume accompanied by an increasing heat flow than by reburial (Eagles et al., 2018). However, it can be speculated that both studies refer to the same basin, which was most likely of a more regional scale with a sedimentary record between ca. 160-140 Ma that is today only preserved in the Riiser-Larsen Sea.





# Chapter 14

## 14. Conclusion

This study explored one of the most remote areas in East Antarctica, eastern Dronning Maud Land, feasible due to its high abundance of exposures. The chosen multi-methodological approach to accomplish the investigations by combining different fields of research, e.g. systematic airborne geophysical mapping of areas comparable in size to the Antarctic Peninsula, and age dating of minerals obtained from geological samples, has significantly improved our knowledge of the geodynamic evolution of the Sør Rondane region through Earth's history.

In addition, this study has sought to provide new data about an area which is of major importance for our understanding of the amalgamation and break-up histories of Rodinia and Gondwana, and hence the establishment of the modern configuration of plate tectonics.

Structural mapping, geochronology and isotope geochemistry were applied to study the evolution of the basement rocks, whereas shallow crustal dynamics were revealed by thermochronological methods. Newly acquired aeromagnetic data greatly supported structural and geological investigations, and thus provided profound information about the crustal architecture and fragments being involved in the supercontinent cycles. New ice-penetrating radar and gravity data delivered a first detailed image of the recent sub-ice topography enabling the exploration of hidden preglacial landscapes.

The following paragraphs refer back to the aims of this thesis (Chapter 1.2) and summarize the main conclusions of each method applied:

### **1) *Determination of the structural and metamorphic evolution of Sør Rondane with focus on Pan-African times***

#### **a) *Study of the Late Pan-African tectonic and structural evolution of Sør Rondane***

Structural investigations of the Main Shear Zone revealed information about its kinematics, its extent, timing, and role during the Pan-African orogenic cycle of which so far only little was known. This dextral high-strain ductile shear zone (under mostly upper low- to medium-grade metamorphic conditions) is interpreted as a large-scale late Pan-African strike-slip structure of late Ediacaran to Cambrian age, which is based on relative age constraints of magmatic rocks. This structure was formerly assumed to represent one candidate for the location of the suture or eastern boundary of the East African-Antarctic Orogen, which was not confirmed by this study. The Main Shear Zone is suggested to represent a lithotectonic boundary and is interpreted together with other shear zones in Dronning Maud Land to result from bipolar lateral escape tectonics of the EAAO.

#### **b) *Study of the cooling history of Sør Rondane by using geochronological methods***

Dating techniques have been systematically applied to improve our knowledge regarding the geodynamic evolution and the metamorphic history with focus on the Main Shear Zone as well as the cooling history of Sør Rondanes distinct terranes.



Combined Ar/Ar analyses and U-Pb dating on zircons revealed a Late Neoproterozoic/Early Paleozoic age for the Main Shear Zone. Syntectonic granites of ca. 560 Ma line up along the shear zone. Deformation along the Main Shear Zone continued until ca. 525 Ma, which is documented by Ar/Ar ages on amphibole and biotites ranging from ca. 570 to 525 Ma. The SW Terrane S records the oldest K-Ar cooling ages of ca. 660 Ma (Takigami and Funaki, 1991) in its interior and hosts the largest and oldest Late Neoproterozoic granitoid intrusions, the Dufek granitoid at ca. 640-620 Ma (Li et al., 2006; Elburg et al., 2016). It consists of competent GTTGs, exhibits a distinct NE-trending structural grain and is surrounded by tectonic domains, which are deformed significantly higher with different structural grains. These terranes are characterised further by younger intrusions and much younger cooling ages of ca. 510-480 Ma. These findings favor that the SW Terrane S might represent a mega-boudin within a broad, rheologically weaker crust overprinted by Late Neoproterozoic/Early Palaeozoic mobile belt(s). Overall, the record of a protracted over 150 Myrs long differential cooling history of the eastern part of the EAAO ranging from ca. 660 to 480 Ma may be explained by a collage style accretion related to the final stages of the assembly of Gondwana.

**c) *Study of different rock suites by using mainly U-Pb datings on zircons***

Exposures of a previously uncharted region west of Sør Rondane allowed the characterization and ground-truthing of a large and mostly ice-covered area that was inferred by preceding geophysical studies. Geochronological and geochemical analyses indicate that the basement of this region consists of juvenile Early Neoproterozoic rocks (ca. 1000-900 Ma) with close similarities to the SW Terrane S of Sør Rondane.

Meta-igneous rocks from the SW Terrane S were also studied in detail and yielded similar crystallization ages of ca. 1000 Ma. These rocks were also generated in an oceanic arc setting with an older subduction related magmatic phase (995-975 Ma) and a younger one which is geochemically more variable and supposedly reflects the end of subduction.

The geochemical characterization and the determination of the age of a younger phase of magmatism across Sør Rondane were combined with published igneous and metamorphic zircon ages and provided evidence for at least four magmatic pulses between 650 and 500 Ma suggesting that the area may be a collage of several different (sub-) terranes that amalgamated over an extended period of time.

**d) *Study of the Phanerozoic shallow crustal dynamics of Sør Rondane***

Integrated studies of thermal history models of AFT and AHe data and their combination with information of geological exposures yield new evidence for the passive margin evolution of Sør Rondane. The thermal histories indicate a complex evolution with various stages of exhumation and burial.

As part of a deep Permian-Triassic sag basin, Sør Rondane was inverted in the Late Triassic being the result of dynamic topography. Since then, Sør Rondane was reburied again until ca. 140 Ma ago, whereas far-field responses to tectonic and/or flexural changes triggered a second stage of inversion. Models suggest subsequent low erosion and formation of major relief starting during Cenozoic times.



## 2) *Characterization of the subglacial basement by combined aerogeophysical and geological studies*

Airborne geophysical investigations delivered new magnetic, gravity and ice-penetrating radar data that were collected with a line spacing of 10 km or less.

Aeromagnetic data across Sør Rondane indicate a correlation with the exposed geology and allow the projection of tectonic terranes and individual structures into ice-covered areas. Major new findings include (1) a new tectonic domain, the central Sør Rondane corridor, which separates the region into an eastern and western part, (2) a subdivision of the southern part of the SW Terrane that correlates with two distinct suites of intrusive meta-igneous rocks differing in age and geochemical composition, and (3) new evidence for the continuation of the SE DML province into southern Sør Rondane.

Aeromagnetic data of the largely ice-covered regions south and east of Sør Rondane revealed new information about the continuation of the SE DML province as well as an estimation of its extent. However, estimations represent a minimum extent of the so-called Tonian Oceanic Arc Super Terrane (TOAST) and most likely represent a remnant of the Mozambique Ocean.

Based on the currently available magnetic data it is not possible to exactly localize the eastern margin of the Pan-African East African-Antarctic Orogen, which is suggested to be situated further to the east of Sør Rondane.

Gravity and radar data provided a more recent image of nowadays East Antarctic Ice Shield and the subglacial bed topography of Sør Rondane. Analyses of the bed topography revealed a paleo-fluvial drainage system at the southern crest of the great escarpment with a SW directed drainage and a significant subglacial canyon representing the eastern termination of the escarpment and inland plateau.

### *Concluding remarks*

This study has offered a new perspective on an important, yet largely ice-covered area in East Antarctica. As a consequence of the sparse exposures, the geological field work was limited to only a small area compared to the large surface covered by aerogeophysical investigations. Therefore, a careful interpretation of the punctual geological data is necessary when inferring conclusions into the ice-covered region.

Overall, this study contributed to a more detailed picture of the interior of East Antarctica as not being just a single craton but comprising of several different fragments of evolved continental and juvenile nature, which are crosscut by various Late Neoproterozoic/Early Paleozoic mobile belts that assembled the Gondwana continent.





## Chapter 15

### 15. Continuing Work & Outlook

Antarctica is the least known continent on earth and the investigations carried out within this project revealed only a glimpse inside the geodynamic evolution of eastern Dronning Maud Land. The nature of research is to create new knowledge, and by addressing research questions, usually more questions will emerge. The Polar aircraft provides fundamental methods (radar, magnetics, and gravity) to map the ice-covered bedrock of Antarctica. However, especially potential field data provide several degrees of freedom in interpretation. Therefore, the combination with land-based studies is of particular benefit wherever possible. Nevertheless, the ice-free exposures are situated in a hostile and challenging environment, and sometimes these conditions make it impossible to access the necessary areas to realize comprehensive field studies.

The following chapter provides an overview of continuing studies and suggestions for future combined geophysical and geological research options.

#### 15.1 The Forster Magnetic Anomaly

Reading between the lines to better understand a major suture crossing central Dronning Maud Land (cited from Ruppel et al., 2017).

Combined aeromagnetic and geological investigations in the area of Dronning Maud Land have led to several hypotheses regarding the assembly of East Antarctica as an integral part of Gondwana (Figure 15.1). One hypothesis suggests that a prominent NE-SW trending magnetic lineament in central Dronning Maud Land, the Forster Magnetic Anomaly, represents a major suture between rocks with African affinities and Archean to Mesoproterozoic ages in the West

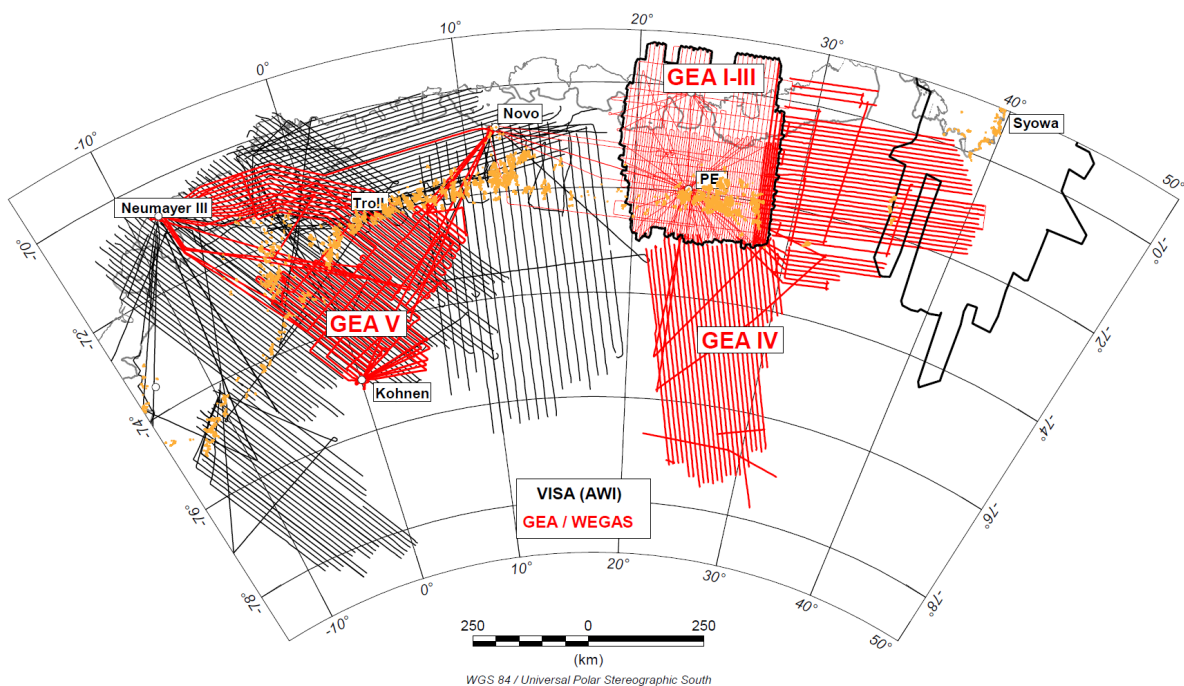


Figure 15.1: Flight line pattern of realized aerogeophysical campaigns in DML.



and juvenile Early Neoproterozoic rocks of the recently defined TOAST in the East. Consistent with this idea, satellite gravity data have recently revealed that a major change in lithospheric thickness coincides with the Forster Magnetic Anomaly. The Forster Magnetic Anomaly was first identified during aerogeophysical surveys carried out by the Alfred Wegener Institute, Helmholtz Centre for Polar and Marine Research (AWI) between 2001 and 2005, and lies well to the south of isolated mountainous outcrops that do not directly contribute to identify the

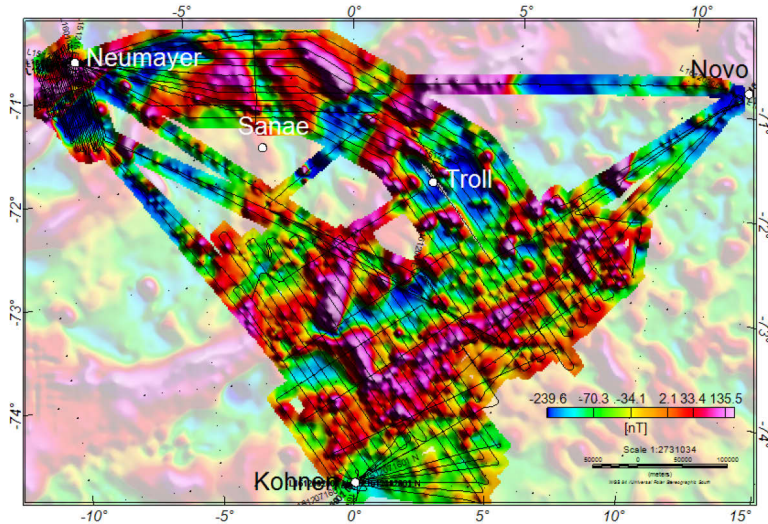


Figure 15.2: Preliminary results of the GEA V campaign (2015-2017) indicating the realized flight pattern and new magnetic anomaly data.

source of the anomaly. The AWI and the Federal Institute for Geosciences and Natural Resources collected aerogeophysical data in 2015-17 from Neumayer III and Kohner stations, with the objective to densify existing coverage of the Forster Magnetic Anomaly from a line spacing of 10 km up to a line spacing of 5 km (Figure 15.2). These new data provide a clearer image of the Forster Magnetic Anomaly itself, and need to be further analyzed and modelled to provide an interpretation of the transition from an African continental plate margin to Early Neoproterozoic accretionary rocks. Further, the combination with geological information will help to ground-truth the NE continuation of this anomaly. The Forster Magnetic Anomaly projects directly into the outcropping Humboldt Mts. forming the western portion of the Wohlthatmassive in central Dronning Maud Land. Here, geologists will try to accomplish detailed geological field work in the near future.

## 15.2 The Eastern and Southern Extent of the TOAST

GEA IV (Figure 15.3) was designed to investigate the southeastern continuation of the eastern Dronning Maud Land province. Ongoing field work and the newly acquired aeromagnetic data (see Chapter 5, Chapter 8) lead to the identification of a major tectonic province which is now considered as the TOAST. Its minimum extent is estimated based on the available aeromagnetic data but its southern and in particular eastern maximum continuation remains unknown. Additional integrated geological and geophysical studies will help to verify its dimensions. For verifying its eastern extent, a ground-truthing at the Belgica and Yamato Mts. within the GEA IV survey area is necessary. However, the exposures are situated in an extremely remote area regarding geological field work and can hardly be reached without a helicopter. The aerogeophysical investigation of the eastern extension can be realized by a flight line pattern from Syowa station (GEA X), whereas the area to the south of Syowa station needs higher



amount of logistical support by setting up a field camp that will include the preparation of a landing strip for polar 5/6 as well as an additional fuel depot (Figure 15.3).

The investigation of the southern extent of the TOAST and the presumed border to the Valkyrie craton (GEA Y) can be realized by logistical support from Neumayer III and Kohlen Station traversing fuel and camp material to a site further inland.

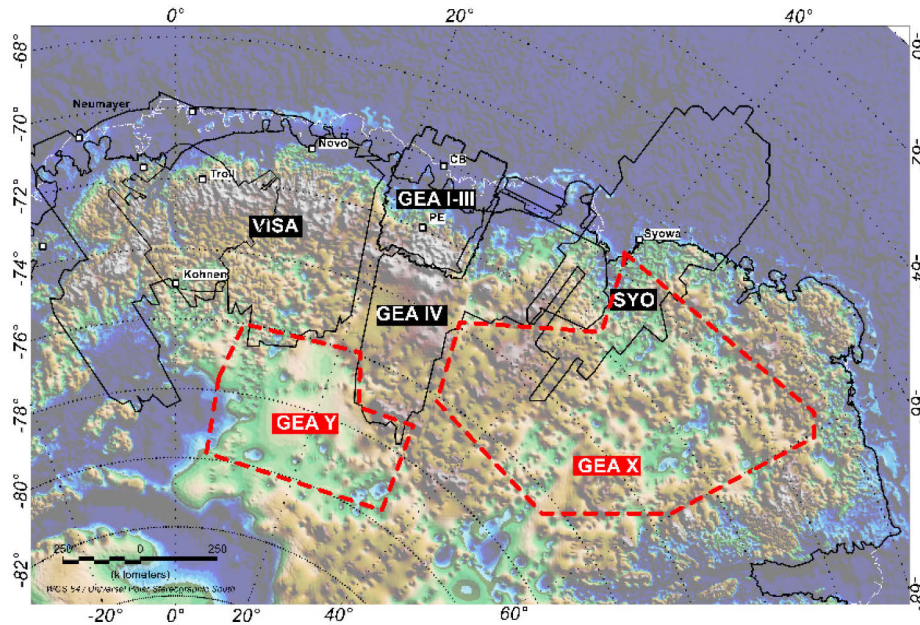


Figure 15.3: Eastern continuation of systematically acquired aerogeophysical data. Targets are east and south of Syowa station (SYO). Backdrop: Bedmap2 (Fretwell et al., 2013).

## 15.3 Unveiling the Cooling History of the SW Terrane S – Hints for a Distinct Geodynamic Evolution?

A new comprehensive dataset of Ar-Ar biotite cooling ages was presented for distinct terranes of Sør Rondane, but lacks data from the central and southern part of the SW Terrane S (Chapter 6). The SW Terrane S seems to represent a distinct crustal fragment of Tonian age with minor evidence for metamorphism and deformation. The northern margin of this terrane hosts the oldest Ar-Ar cooling ages whereas interpretations regarding the cooling history of the whole fragment rely on one age datum from previous studies. Therefore, investigations of equally distributed samples from the wider area of the SW Terrane S might provide a better understanding of its distinct cooling history and prove or disprove the hypothesis of the SW Terrane S hosting the oldest cooling ages representing a protected block within an accretionary tectonic setting. In addition, the integration of other dating methods like fission track dating on titanite and/or zircon are suitable for the same temperature window and need to be considered for future studies.





## 16. References

- Adachi, T., Osanai, Y., Hokada, T., Nakano, N., Baba, S., and Toyoshima, T., 2013, Timing of metamorphism in the central Sør Rondane Mountains, eastern Dronning Maud Land, East Antarctica: Constrains from SHRIMP zircon and EPMA monazite dating: *Precambrian Research*, v. 234, p. 136-160, <http://dx.doi.org/10.1016/j.precamres.2012.11.011>.
- An, M., Wiens, D. A., Zhao, Y., Feng, M., Nyblade, A. A., Kanao, M., Li, Y., Maggi, A., and Lévêque, J.-J., 2015, S-velocity model and inferred Moho topography beneath the Antarctic Plate from Rayleigh waves: *Journal of Geophysical Research: Solid Earth*, v. 120, no. 1, p. 359-383, <http://dx.doi.org/10.1002/2014JB011332>.
- Aoki, T., 1989, Meteorological data at Asuka Station, Antarctica in 1988: National Institute of Polar Research.
- Archibald, D. B., Collins, A. S., Foden, J. D., Payne, J. L., Macey, P. H., Holden, P., and Razakamanana, T., 2017, Stenian–Tonian arc magmatism in west–central Madagascar: the genesis of the Dabolava Suite: *Journal of the Geological Society*, v. 175, no. 1, p. 111-129, <http://dx.doi.org/10.1144/jgs2017-028>.
- Argus, D. F., Heflin, M. B., Owen, S. E., Gordon, R. G., Ma, C., Eanes, R. J., Willis, P., and Peltier, W. R., 2010, The angular velocities of the plates and the velocity of Earth's centre from space geodesy: *Geophysical Journal International*, v. 180, no. 3, p. 913-960, <http://dx.doi.org/10.1111/j.1365-246X.2009.04463.x>.
- Asami, M., Osanai, Y., Shiraishi, K., and Makimoto, H., 1992, Metamorphic evolution of the Sør Rondane Mountains, East Antarctica: *Recent Progress in Antarctic Earth Science*, p. 7-15.
- Asami, M., Suzuki, K., and Adachi, M., 1996, Monazite ages by the chemical Th–U–total Pb isochron method for pelitic gneisses from the eastern Sør Rondane Mountains, East Antarctica *Proceedings of the NIPR Symposium on Antarctic Geosciences*, v. 9, p. 49–64.
- Asami, M., Suzuki, K., and Adachi, M., 1997, Th, U and Pb data and CHIME dating of monazites from metamorphic rocks of the Rayner, Lützow-Holm, Yamato-Belgica and Sør Rondane Complexes, East Antarctica: *Proceedings of the NIPR Symposium on Antarctic Geosciences*, v. 10, p. 130-152.
- Asami, M., Suzuki, K., and Grew, E. S., 2005, Monazite and Zircon Dating by the Chemical Th-U–Total Pb Isochron Method (CHIME) from Alasheyev Bight to the Sør Rondane Mountains, East Antarctica: A Reconnaissance Study of the Mozambique Suture in Eastern Queen Maud Land: *Journal of Geology*, v. 113, p. 59-82.
- Baba, S., Hokada, T., Kaiden, H., Dunkley, D. J., Owada, M., and Shiraishi, K., 2010, SHRIMP Zircon U–Pb Dating of Sapphirine-Bearing Granulite and Biotite-Hornblende Gneiss in the Schirmacher Hills, East Antarctica: Implications for Neoproterozoic Ultrahigh-Temperature Metamorphism Predating the Assembly of Gondwana: *The Journal of Geology*, v. 118, no. 6, p. 621-639, <http://dx.doi.org/10.1086/656384>.
- Baba, S., Osanai, Y., Nakano, N., Owada, M., Hokada, T., Horie, K., Adachi, T., and Toyoshima, T., 2013, Counterclockwise P–T path and isobaric cooling of metapelites from Brattnipene, Sør Rondane Mountains, East Antarctica: Implications for a tectonothermal event at the proto-Gondwana margin: *Precambrian Research*, v. 234, p. 210-228, <http://dx.doi.org/http://dx.doi.org/10.1016/j.precamres.2012.10.002>.
- Baba, S., Horie, K., Hokada, T., Owada, M., Adachi, T., and Shiraishi, K., 2015, Multiple Collisions in the East African–Antarctica Orogen: Constraints from Timing of Metamorphism in the Filchnerfjella and Hochlinfjellet Terranes in Central Dronning Maud Land: *The Journal of Geology*, v. 123, no. 1, p. 55-77, <http://dx.doi.org/10.1086/679468>.
- Bahr, D. B., Hutton, E. W. H., Syvitski, J. P. M., and Pratson, L. F., 2001, Exponential approximations to compacted sediment porosity profiles: *Computers & Geosciences*, v. 27, no. 6, p. 691-700, [http://dx.doi.org/10.1016/S0098-3004\(00\)00140-0](http://dx.doi.org/10.1016/S0098-3004(00)00140-0).
- Barker, F., 1979, Chapter 1 - Trondhjemite: Definition, Environment and Hypotheses of Origin, *in* Barker, F., ed., *Developments in Petrology*, Volume 6, Elsevier, p. 1-12, <http://dx.doi.org/10.1016/B978-0-444-41765-7.50006-X>.
- Basile, C., and Allemand, P., 2002, Erosion and flexural uplift along transform faults: *Geophysical Journal International*, v. 151, no. 2, p. 646-653, <http://dx.doi.org/10.1046/j.1365-246X.2002.01805.x>.



- Bau, M., and Knittel, U., 1993, Significance of slab-derived partial melts and aqueous fluids for the genesis of tholeiitic and calc-alkaline island-arc basalts: Evidence from Mt. Arayat, Philippines: *Chemical Geology*, v. 105, no. 4, p. 233-251, [http://dx.doi.org/10.1016/0009-2541\(93\)90128-6](http://dx.doi.org/10.1016/0009-2541(93)90128-6).
- Bauer, W., Hagemann, H. W., Poscher, G., Sachsenhofer, R. F., and Spaeth, G., 1997, Permian Coals from western Dronning Maud Land - Composition, environment, and the influence of Jurassic magmatism on their maturity, *in* Ricci, C. A., ed., *The Antarctic Region: Geological Evolution and Processes*: Siena, Terra Antarctica Publication, p. 945-951.
- Bauer, W., Thomas, J., and Jacobs, J., 2003a, Proterozoic-Cambrian history of Dronning Maud Land in the context of Gondwana assembly in Proterozoic East Gondwana; supercontinent assembly and breakup: *Geological Society, London, Special Publications*, v. 206, p. 247-269.
- Bauer, W., Fielitz, W., Jacobs, J., Fanning, C., and Spaeth, G., 2003b, Mafic dykes from Heimefrontfjella and implications for the post-Grenvillian to pre-Pan-African geological evolution of western Dronning Maud Land, Antarctica: *Antarctic Science*, v. 15, no. 3, p. 379-391.
- Bauer, W., and Siemes, H., 2004, Kinematics and Geothermometry of Mylonitic Shear Zones in the Orvinfjella, Central Dronning Maud Land, East Antarctica., *in* Paech, H.-J. E., ed., *International GeoMaud Expedition of the BGR to Central Dronning Maud Land in 1995/96 - Vol. I: Geological Result Volume 96*: Stuttgart, Germany, Schweizerbart Science Publishers, p. 391-422.
- Beaumont, C., Kooi, H., and Willett, S., 2000, Coupled tectonic-surface process models with applications to rifted margins and collisional orogens: Chichester John Wiley, *Geomorphology and global tectonics*.
- Belyatskii, B. V., Sushchevskaya, N. M., Leichenkov, G. L., Mikhal'skii, E. M., and Laiba, A. A., 2006, Magmatism of the Karoo-Maud Superplume in the Schirmacher Oasis, East Antarctica: *Doklady Earth Sciences*, v. 406, no. 1, p. 128-131.
- Bingen, B., Jacobs, J., Viola, G., Henderson, I. H. C., Skår, Ø., Boyd, R., Thomas, R. J., Solli, A., Key, R. M., and Daudi, E. X. F., 2009, Geochronology of the Precambrian crust in the Mozambique belt in NE Mozambique, and implications for Gondwana assembly: *Precambrian Research*, v. 170, no. 3, p. 231-255, <http://dx.doi.org/10.1016/j.precamres.2009.01.005>.
- Bisnath, A., Frimmel, H. E., Armstrong, R. A., and Board, W. S., 2006, Tectono-thermal evolution of the Maud Belt: New SHRIMP U-Pb zircon data from Gjelsvikfjella, Dronning Maud Land, East Antarctica: *Precambrian Research*, v. 150, no. 1, p. 95-121, <https://doi.org/10.1016/j.precamres.2006.06.009>.
- Black, L. P., Kamo, S. L., Allen, C. M., Aleinikoff, J. N., Davis, D. W., Korsch, R. J., and Foudoulis, C., 2003, TEMORA 1: a new zircon standard for Phanerozoic U-Pb geochronology: *Chemical Geology*, v. 200, no. 1, p. 155-170, [http://doi.org/10.1016/S0009-2541\(03\)00165-7](http://doi.org/10.1016/S0009-2541(03)00165-7).
- Blakely, R. J., and Simpson, R. W., 1986, Approximating edges of source bodies from magnetic or gravity anomalies: *Geophysics*, v. 51, no. 7, p. 1494-1498, <http://dx.doi.org/10.1190/1.1442197>.
- Blakely, R. J., 1995, *Potential Theory in Gravity and Magnetic Applications*, Cambridge University Press.
- Board, W., Frimmel, H., and Armstrong, R., 2005, Pan-African tectonism in the western Maud Belt: P-T-t path for high-grade gneisses in the HU Sverdrupfjella, East Antarctica: *Journal of Petrology*, v. 46, no. 4, p. 671-699, <http://dx.doi.org/10.1093/petrology/egh093>
- Boger, S. D., Carson, C. J., Wilson, C. J. L., and Fanning, C. M., 2000, Neoproterozoic deformation in the Radok Lake region of the northern Prince Charles Mountains, east Antarctica; evidence for a single protracted orogenic event: *Precambrian Research*, v. 104, no. 1, p. 1-24, [http://doi.org/10.1016/S0301-9268\(00\)00079-6](http://doi.org/10.1016/S0301-9268(00)00079-6).
- Boger, S. D., Wilson, C. J. L., and Fanning, C. M., 2001, Early Paleozoic tectonism within the East Antarctic craton: The final suture between east and west Gondwana?: *Geology*, v. 29, p. 463-466.
- Boger, S. D., and Miller, J. M., 2004, Terminal suturing of Gondwana and the onset of the Ross-Delamerian Orogeny: the cause and effect of an Early Cambrian reconfiguration of plate motions: *Earth and Planetary Science Letters*, v. 219, p. 35-48.
- Boger, S. D., 2011, Antarctica - Before and after Gondwana: *Gondwana Research*, v. 19, no. 2, p. 335-371, <http://dx.doi.org/10.1016/j.gr.2010.09.003>.
- Boger, S. D., Hirdes, W., Ferreira, C. A. M., Schulte, B., Jenett, T., and Fanning, C. M., 2014, From passive margin to volcano-sedimentary forearc: The Tonian to Cryogenian evolution of the Anosyen Domain of southeastern Madagascar: *Precambrian Research*, v. 247, no. Supplement C, p. 159-186, <http://doi.org/10.1016/j.precamres.2014.04.004>.



- Boger, S. D., Hirdes, W., Ferreira, C. A. M., Jenett, T., Dallwig, R., and Fanning, C. M., 2015, The 580–520Ma Gondwana suture of Madagascar and its continuation into Antarctica and Africa: *Gondwana Research*, v. 28, no. 3, p. 1048-1060, <http://doi.org/10.1016/j.gr.2014.08.017>.
- Braun, J., and van der Beek, P., 2004, Evolution of passive margin escarpments: What can we learn from low-temperature thermochronology?: *Journal of Geophysical Research: Earth Surface*, v. 109, no. F4, <http://dx.doi.org/10.1029/2004JF000147>.
- Braun, J., 2018, A review of numerical modeling studies of passive margin escarpments leading to a new analytical expression for the rate of escarpment migration velocity: *Gondwana Research*, v. 53, p. 209-224, <http://dx.doi.org/10.1016/j.gr.2017.04.012>.
- Brown, R. W., Summerfield, M. A., and Gleadow, A. J. W., 2002, Denudational history along a transect across the Drakensberg Escarpment of southern Africa derived from apatite fission track thermochronology: *Journal of Geophysical Research: Solid Earth*, v. 107, no. B12, p. ETG 10-11-ETG 10-18, <http://dx.doi.org/10.1029/2001JB000745>.
- Callens, D., Matsuoka, K., Steinhage, D., Smith, B., Witrant, E., and Pattyn, F., 2014, Transition of flow regime along a marine-terminating outlet glacier in East Antarctica: *Cryosphere*, v. 8, no. 3, p. 867-875, <http://dx.doi.org/10.5194/tc-8-867-2014>.
- Callens, D., Thonnard, N., Lenaerts, J. T. M., Van Wessem, J. M., Van de Berg, W. J., Matsuoka, K., and Pattyn, F., 2015, Mass balance of the Sør Rondane glacial system, East Antarctica: *Annals of Glaciology*, v. 56, no. 70, p. 63-69, <http://dx.doi.org/10.3189/2015AoG70A010>.
- Campanile, D., Nambiar, C. G., Bishop, P., Widdowson, M., and Brown, R., 2008, Sedimentation record in the Konkan-Kerala Basin: Implications for the evolution of the Western Ghats and the Western Indian passive margin: *Basin Research*, v. 20, no. 1, p. 3-22, <http://dx.doi.org/10.1111/j.1365-2117.2007.00341.x>.
- Cantrill, D. J., Drinnan, A. N., and Webb, J. A., 1995, Late Triassic plant fossils from the Prince Charles Mountains, East Antarctica: *Antarctic Science*, v. 7, no. 1, p. 51-62.
- Carter, A., Riley, T. R., Hillenbrand, C.-D., and Rittner, M., 2017, Widespread Antarctic glaciation during the Late Eocene: *Earth and Planetary Science Letters*, v. 458, no. Supplement C, p. 49-57, <http://dx.doi.org/10.1016/j.epsl.2016.10.045>.
- Castelino, J. A., Eagles, G., and Jokat, W., 2016, Anomalous bathymetry and palaeobathymetric models of the Mozambique Basin and Riiser Larsen Sea: *Earth and Planetary Science Letters*, v. 455, p. 25-37, <http://dx.doi.org/10.1016/j.epsl.2016.09.018>.
- Catuneanu, O., Wopfner, H., Eriksson, P. G., Cairncross, B., Rubidge, B. S., Smith, R. M. H., and Hancox, P. J., 2005, The Karoo basins of south-central Africa: *Journal of African Earth Sciences*, v. 43, no. 1–3, p. 211-253, <http://dx.doi.org/10.1016/j.jafrearsci.2005.07.007>.
- Choudhuri, M., and Nemčok, M., 2017, Dynamic Crustal Uplift Due to Plume Activity, *in* Choudhuri, M., and Nemčok, M., eds., *Mantle Plumes and Their Effects*, Volume SpringerBriefs in Earth System Sciences: Cham, Springer.
- Claoué-Long, J. C., Compston, W., Roberts, J., and Fanning, C. M., 1995, Two Carboniferous ages: a comparison of SHRIMP zircon dating with conventional zircon ages and  $^{40}\text{Ar}/^{39}\text{Ar}$  analysis.
- Cockburn, H. A. P., Brown, R. W., Summerfield, M. A., and Seidl, M. A., 2000, Quantifying passive margin denudation and landscape development using a combined fission-track thermochronology and cosmogenic isotope analysis approach: *Earth and Planetary Science Letters*, v. 179, no. 3-4, p. 429-435, [http://dx.doi.org/10.1016/S0012-821X\(00\)00144-8](http://dx.doi.org/10.1016/S0012-821X(00)00144-8).
- Cordell, L., and Grauch, V. J. S., 1982, Mapping basement magnetization zones from aeromagnetic data in the San Juan Basin, New Mexico, SEG Technical Program Expanded Abstracts p. 246-247, <http://dx.doi.org/10.1190/1.1826915>.
- Corvino, A. F., Boger, S. D., Henjes-Kunst, F., Wilson, C. J., and Fitzsimons, I. C., 2008, Superimposed tectonic events at 2450Ma, 2100Ma, 900Ma and 500Ma in the North Mawson Escarpment, Antarctic Prince Charles Mountains: *Precambrian Research*, v. 167, no. 3, p. 281-302.
- Cox, K. G., Bell, J. D., and Pankhurst, J. R., 1979, *The Interpretation of Igneous Rocks*: Allen and Unwin, London, p. 464.
- Cox, K. G., 1992, Karoo igneous activity, and the early stages of the break-up of Gondwanaland: *Geological Society, London, Special Publications*, v. 68, no. 1, p. 137-148, <http://dx.doi.org/10.1144/gsl.sp.1992.068.01.09>.
- Dalrymple, G. B., and Lanphere, M. A., 1969, *Potassium-Argon Dating*: Freeman, San Francisco, 258 pp. p.



- Dalziel, I. W. D., and Elliot, D. H., 1982, West Antarctica: Problem child of Gondwanaland: *Tectonics*, v. 1, no. 1, p. 3-19, <http://dx.doi.org/10.1029/TC001i001p00003>.
- Dalziel, I. W. D., 1991, Pacific margins of Laurentia and East Antarctica, Australia as a conjugate rift pair: Evidence and implications for an Eocambrian supercontinent: *Geology*, v. 19, p. 598-601.
- Damaske, D., Marcinkowski, V., and Moller, H., 2005, Aeromagnetic survey in central Dronning Maud Land, East Antarctica, during the 1995/1996 GeoMaud expedition: layout, execution, and data processing: *Geologisches Jahrbuch Reihe B*, v. 97, p. 53.
- DeConto, R. M., and Pollard, D., 2003, Rapid Cenozoic glaciation of Antarctica induced by declining atmospheric CO<sub>2</sub>: *Nature*, v. 421, p. 245, <http://dx.doi.org/10.1038/nature01290>.
- Delvaux, D., and Sperner, B., 2003, New aspects of tectonic stress inversion with reference to the TENSOR program: Geological Society, London, Special Publications, v. 212, no. 1, p. 75-100, <http://dx.doi.org/10.1144/gsl.sp.2003.212.01.06>.
- Dougherty-Page, J. S., and Bartlett, J. M., 1999, New analytical procedures to increase the resolution of zircon geochronology by the evaporation technique: *Chemical Geology*, v. 153, no. 1, p. 227-240, [http://dx.doi.org/10.1016/S0009-2541\(98\)00158-2](http://dx.doi.org/10.1016/S0009-2541(98)00158-2).
- Duncan, R. A., Hooper, P. R., Rehacek, J., Marsh, J. S., and Duncan, A. R., 1997, The timing and duration of the Karoo igneous event: *Journal of Geophysical Research*, v. 102, no. B8, p. 18127-18138.
- Eagles, G., and König, M., 2008, A model of plate kinematics in Gondwana breakup: *Geophysical Journal International*, v. 173, no. 2, p. 703-717, <http://dx.doi.org/10.1111/j.1365-246X.2008.03753.x>.
- Eagles, G., Karlsson, N. B., Ruppel, A., Steinhage, D., Jokat, W., and Läufer, A., 2018, Erosion at extended continental margins: insights from new aerogeophysical data in eastern Dronning Maud Land: *Gondwana research*, v. 63, p. 105-116, <http://dx.doi.org/10.1016/j.gr.2018.05.011>.
- Eby, G. N., 1990, The A-type granitoids: A review of their occurrence and chemical characteristics and speculations on their petrogenesis: *Lithos*, v. 26, no. 1, p. 115-134, [http://dx.doi.org/10.1016/0024-4937\(90\)90043-Z](http://dx.doi.org/10.1016/0024-4937(90)90043-Z).
- Elburg, M., van Leeuwen, T., Foden, J., and Muhandjo, 2003, Spatial and temporal isotopic domains of contrasting igneous suites in Western and Northern Sulawesi, Indonesia: *Chemical Geology*, v. 199, no. 3, p. 243-276, [http://dx.doi.org/10.1016/S0009-2541\(03\)00084-6](http://dx.doi.org/10.1016/S0009-2541(03)00084-6).
- Elburg, M., Jacobs, J., Andersen, T., Clark, C., Läufer, A., Ruppel, A., Krohne, N., and Damaske, D., 2015, Early Neoproterozoic metagabbro-tonalite-trondhjemite of Sør Rondane (East Antarctica): Implications for supercontinent assembly: *Precambrian Research*, v. 259, no. 0, p. 189-206.
- Elburg, M., Andersen, T., Jacobs, J., Läufer, A., Ruppel, A., Krohne, N., and Damaske, D., 2016, One hundred and fifty million years of Pan-African magmatism in the Sør Rondane Mountains (East Antarctica): Implications for Gondwana assembly: *The Journal of Geology*, v. 124, no. 1, p. 1-26, <http://dx.doi.org/10.1086/684052>.
- Elburg, M. A., and Nicholls, I. A., 1995, Origin of microgranitoid enclaves in the S-type Wilson's Promontory Batholith, Victoria: Evidence for magma mingling: *Australian Journal of Earth Sciences*, v. 42, no. 4, p. 423-435, <http://dx.doi.org/10.1080/08120099508728212>.
- Elburg, M. A., Andersen, T., Bons, P. D., Simonsen, S. L., and Weisheit, A., 2013, New constraints on Phanerozoic magmatic and hydrothermal events in the Mt Painter Province, South Australia: *Gondwana Research*, v. 24, no. 2, p. 700-712, <http://dx.doi.org/10.1016/j.gr.2012.12.017>.
- Emmel, B., Jacobs, J., Crowhurst, P., and Daszinnies, M. C., 2007, Combined apatite fission-track and single grain apatite (U-Th)/He ages from basement rocks of central Dronning Maud Land (East Antarctica) -- Possible identification of thermally overprinted crustal segments: *Earth and Planetary Science Letters*, v. 264, no. 1-2, p. 72-88.
- Emmel, B., Jacobs, J., Crowhurst, P., Austegard, A., and Schwarz-Schampera, U., 2008, Apatite single-grain (U-Th)/He data from Heimefrontfjella, East Antarctica: Indications for differential exhumation related to glacial loading?: *Tectonics*, v. 27, <http://dx.doi.org/10.1029/2007TC002220>.
- Emmel, B., Jacobs, J., and Daszinnies, M. C., 2009, Combined titanite and apatite fission-track data from Gjelsvikfjella, East Antarctica - another piece of a concealed intracontinental Permo-Triassic Gondwana rift basin?: Geological Society, London, Special Publications, v. 324, no. 1, p. 317-330.
- Evensen, N. M., Hamilton, P. J., and O'Nions, R. K., 1978, Rare-earth abundances in chondritic meteorites: *Geochimica et Cosmochimica Acta*, v. 42, no. 8, p. 1199-1212, [http://dx.doi.org/10.1016/0016-7037\(78\)90114-X](http://dx.doi.org/10.1016/0016-7037(78)90114-X).



- Farley, K. A., 2002, (U-Th)/He dating: techniques, calibrations, and applications: *Reviews in Mineralogy and Geochemistry*, v. 47, no. 1, p. 819-844, <http://dx.doi.org/10.2138/rmg.2002.47.18>.
- Ferraccioli, F., Jones, P. C., Curtis, M. L., and Leat, P. T., 2005a, Subglacial imprints of early Gondwana break-up as identified from high resolution aerogeophysical data over western Dronning Maud Land, East Antarctica: *Terra Nova*, v. 17, no. 6, p. 573-579, <http://dx.doi.org/10.1111/j.1365-3121.2005.00651.x>.
- Ferraccioli, F., Jones, P. C., Curtis, M. L., Leat, P. T., and Riley, T. R., 2005b, Tectonic and magmatic patterns in the Jutulstraumen rift (?) region, East Antarctica, as imaged by high-resolution aeromagnetic data: *Earth, Planets and Space*, v. 57, no. 8, p. 767-780, <http://dx.doi.org/10.1186/BF03351856>.
- Ferraccioli, F., Finn, C. A., Jordan, T. A., Bell, R. E., Anderson, L. M., and Damaske, D., 2011, East Antarctic rifting triggers uplift of the Gamburtsev Mountains: *Nature*, v. 479, no. 7373, p. 388-392, <http://dx.doi.org/10.1038/nature10566>.
- Fitzsimons, I. C. W., 2000a, Grenville-age basement provinces in East Antarctica: Evidence for three separate collisional orogens: *Geology*, v. 28, no. 10, p. 879-882, [http://dx.doi.org/10.1130/0091-7613\(2000\)28<879:GBPIEA>2.0.CO;2](http://dx.doi.org/10.1130/0091-7613(2000)28<879:GBPIEA>2.0.CO;2).
- Fitzsimons, I. C. W., 2000b, A review of tectonic events in the East Antarctic Shield and their implications for Gondwana and earlier supercontinents: *Journal of African Earth Sciences*, v. 31, p. 3-23.
- Fitzsimons, I. C. W., 2003, Proterozoic basement provinces of southern and southwestern Australia, and their correlation with Antarctica: *Geological Society, London, Special Publications*, v. 206, p. 93-130.
- Fleming, A., Summerfield, M. A., Stone, J. O., Fifield, L. K., and Cresswell, R. G., 1999, Denudation rates for the southern Drakensberg escarpment, SE Africa, derived from in-situ-produced cosmogenic  $^{36}\text{Cl}$ : Initial results: *Journal of the Geological Society*, v. 156, no. 2, p. 209-212, <http://dx.doi.org/10.1144/gsjgs.156.2.0209>.
- Flowers, R. M., Ketcham, R. A., Shuster, D. L., and Farley, K. A., 2009, Apatite (U-Th)/He thermochronometry using a radiation damage accumulation and annealing model: *Geochimica et Cosmochimica Acta*, v. 73, no. 8, p. 2347-2365.
- Flowers, R. M., 2009, Exploiting radiation damage control on apatite (U-Th)/He dates in cratonic regions: *Earth and Planetary Science Letters*, v. 277, no. 1-2, p. 148-155.
- Förste, C., Schmidt, R., Stubenvoll, R., Flechtner, F., Meyer, U., König, R., Neumayer, H., Biancale, R., Lemoine, J.-M., Bruinsma, S., Loyer, S., Barthelmes, F., and Esselborn, S., 2008, The GeoForschungsZentrum Potsdam/Groupe de Recherche de Géodésie Spatiale satellite-only and combined gravity field models: EIGEN-GL04S1 and EIGEN-GL04C: *Journal of Geodesy*, v. 82, no. 6, p. 331-346, <http://dx.doi.org/10.1007/s00190-007-0183-8>.
- Frei, D., and Gerdes, A., 2009, Precise and accurate in situ U-Pb dating of zircon with high sample throughput by automated LA-SF-ICP-MS: *Chemical Geology*, v. 261, no. 3, p. 261-270, <http://dx.doi.org/10.1016/j.chemgeo.2008.07.025>.
- Fretwell, P., Pritchard, H. D., Vaughan, D. G., Bamber, J. L., Barrand, N. E., Bell, R., Bianchi, C., Bingham, R. G., Blankenship, D. D., Casassa, G., Catania, G., Callens, D., Conway, H., Cook, A. J., Corr, H. F. J., Damaske, D., Damm, V., Ferraccioli, F., Forsberg, R., Fujita, S., Gim, Y., Gogineni, P., Griggs, J. A., Hindmarsh, R. C. A., Holmlund, P., Holt, J. W., Jacobel, R. W., Jenkins, A., Jokat, W., Jordan, T., King, E. C., Kohler, J., Krabill, W., Riger-Kusk, M., Langley, K. A., Leitchenkov, G., Leuschen, C., Luyendyk, B. P., Matsuoka, K., Mouginit, J., Nitsche, F. O., Nogi, Y., Nost, O. A., Popov, S. V., Rignot, E., Rippin, D. M., Rivera, A., Roberts, J., Ross, N., Siegert, M. J., Smith, A. M., Steinhage, D., Studinger, M., Sun, B., Tinto, B. K., Welch, B. C., Wilson, D., Young, D. A., Xiangbin, C., and Zirizzotti, A., 2013, Bedmap2: improved ice bed, surface and thickness datasets for Antarctica: *The Cryosphere*, v. 7, no. 1, p. 375-393, <http://dx.doi.org/10.5194/tc-7-375-2013>.
- Fritz, H., Abdelsalam, M., Ali, K. A., Bingen, B., Collins, A. S., Fowler, A. R., Ghebreab, W., Hauzenberger, C. A., Johnson, P. R., Kusky, T. M., Macey, P., Muhongo, S., Stern, R. J., and Viola, G., 2013, Orogen styles in the East African Orogen: A review of the Neoproterozoic to Cambrian tectonic evolution: *Journal of African Earth Sciences*, v. 86, p. 65-106, <http://dx.doi.org/10.1016/j.jafrearsci.2013.06.004>.
- Frost, B. R., Barnes, C. G., Collins, W. J., Arculus, R. J., Ellis, D. J., and Frost, C. D., 2001, A Geochemical Classification for Granitic Rocks: *Journal of Petrology*, v. 42, no. 11, p. 2033-2048, <http://dx.doi.org/10.1093/petrology/42.11.2033>.



- Frost, C. D., and Frost, B. R., 2011, On Ferroan (A-type) Granitoids: their Compositional Variability and Modes of Origin: *Journal of Petrology*, v. 52, no. 1, p. 39-53, <http://dx.doi.org/10.1093/petrology/egq070>.
- Gallagher, K., and Brown, R., 1997, The onshore record of passive margin evolution: *Journal of the Geological Society, London*, v. 154, p. 451-457.
- Gazel, E., Hoernle, K., Carr, M. J., Herzberg, C., Saginor, I., den Bogaard, P. v., Hauff, F., Feigenson, M., and Swisher Iii, C., 2011, Plume–subduction interaction in southern Central America: Mantle upwelling and slab melting: *Lithos*, v. 121, no. 1–4, p. 117-134, <http://dx.doi.org/10.1016/j.lithos.2010.10.008>.
- Gerdes, A., and Zeh, A., 2006, Combined U–Pb and Hf isotope LA-(MC-)ICP-MS analyses of detrital zircons: Comparison with SHRIMP and new constraints for the provenance and age of an Armorican metasediment in Central Germany: *Earth and Planetary Science Letters*, v. 249, no. 1, p. 47-61, <http://dx.doi.org/10.1016/j.epsl.2006.06.039>.
- Giese, J., Seward, D., and Schreurs, G., 2012, Low-temperature evolution of the Morondava rift basin shoulder in western Madagascar: An apatite fission track study: *Tectonics*, v. 31, no. 2, p. n/a-n/a, <http://dx.doi.org/10.1029/2011tc002921>.
- Gilchrist, A. R., and Summerfield, M. A., 1990, Differential denudation and flexural isostasy in formation of rifted-margin upwarps: *Nature*, v. 346, no. 6286, p. 739-742, <http://dx.doi.org/10.1038/346739a0>.
- Gilchrist, A. R., and Summerfield, M. A., 1994, Tectonic models of passive margin evolution and their implications for theories of long-term landscape development: *Process models and theoretical geomorphology*, p. 55-84.
- Golynsky, A., and Jacobs, J., 2001, Grenville-age versus Pan-African magnetic anomaly imprints in western Dronning Maud Land, East Antarctica: *The Journal of Geology*, v. 109, p. 136-142.
- Golynsky, A., Blankenship, D., Chiapini, M., Damaske, D., Ferraccioli, S., Finn, C., Golynsky, D., Goncharov, A., Ishihara, T., Ivanov, S., Jokat, W., Kim, H. R., König, M., Masolov, V., Nogi, Y., Sand, M., and Studinger, M., 2007, New magnetic anomaly map of East Antarctica and surrounding regions, in Cooper, A., Raymond, C., and Team, I. E., eds., *Antarctica: A Keystone in a Changing World* Online Proceedings for the Tenth International Symposium on Antarctic Earth Sciences Volume 2007-1047, U.S. Geological Survey Open-File Report
- Golynsky, A. V., Masolov, V. N., Nogi, Y., Shibuya, K., Tarlow, C., and Wellman, P., 1996, Magnetic anomalies of Precambrian terranes of the East Antarctic Shield coastal region (20°E–50°E): *Proceedings of the National Institute of Polar Research Symposium on Antarctic Geosciences*, v. 9, p. 24–39.
- Golynsky, A. V., and Aleshkova, N. D., 2000, Regional magnetic anomalies of the Weddell Sea region and their geological significance: *Polarforschung*, v. 67, no. 3, p. 101-117.
- Golynsky, A. V., Ferraccioli, F., Hong, J. K., Golynsky, D. A., von Frese, R. R. B., Young, D. A., Blankenship, D. D., Holt, J. W., Ivanov, S. V., Kiselev, A. V., Masolov, V. N., Eagles, G., Gohl, K., Jokat, W., Damaske, D., Finn, C., Aitken, A., Bell, R. E., Armadillo, E., Jordan, T. A., Greenbaum, J. S., Bozzo, E., Caneva, G., Forsberg, R., Ghidella, M., Galindo-Zaldivar, J., Bohoyo, F., Martos, Y. M., Nogi, Y., Quartini, E., Kim, H. R., and Roberts, J. L., 2018, New Magnetic Anomaly Map of the Antarctic: *Geophysical Research Letters*, v. 45, no. 13, p. 6437-6449, <http://dx.doi.org/10.1029/2018GL078153>.
- Grantham, G. H., Macey, P., Ingram, B., Roberts, M., Armstrong, R., Hokada, T., Shiraishi, K., Jackson, C., Bisnath, A., and Manhica, V., 2008, Terrane correlation between Antarctica, Mozambique and Sri Lanka; comparisons of geochronology, lithology, structure and metamorphism and possible implications for the geology of southern Africa and Antarctica: *Geological Society, London, Special Publications*, v. 308, no. 1, p. 91-119.
- Grantham, G. H., Macey, P. H., Horie, K., Kawakami, T., Ishikawa, M., Satish-Kumar, M., Tsuchiya, N., Graser, P., and Azevedo, S., 2013, Comparison of the metamorphic history of the Monapo Complex, northern Mozambique and Balchenfjella and Austhameren areas, Sør Rondane, Antarctica: Implications for the Kuunga Orogeny and the amalgamation of N and S. Gondwana: *Precambrian Research*, v. 234, p. 85-135, <http://dx.doi.org/10.1016/j.precamres.2012.11.012>.
- Gray, D. R., Foster, D. A., Meert, J. G., Goscombe, B. D., Armstrong, R., Trouw, R. A. J., and Passchier, C. W., 2008, A Damara orogen perspective on the assembly of southwestern Gondwana: *Geological Society, London, Special Publications*, v. 294, no. 1, p. 257-278, <http://dx.doi.org/10.1144/sp294.14>.



- Green, P. F., Duddy, I. R., Japsen, P., Bonow, J. M., and Malan, J. A., 2017, Post-breakup burial and exhumation of the southern margin of Africa: *Basin Research*, v. 29, p. 96-127.
- Greene, A. R., DeBari, S. M., Kelemen, P. B., Blusztajn, J., and Clift, P. D., 2006, A Detailed Geochemical Study of Island Arc Crust: the Talkeetna Arc Section, South-Central Alaska: *Journal of Petrology*, v. 47, no. 6, p. 1051-1093, <http://dx.doi.org/10.1093/petrology/egl002>.
- Grew, E., Manton, W., Asami, M., and Makimoto, H., 1992, Reconnaissance geochronologic data on Proterozoic polymetamorphic rocks of the eastern Sør Rondane Mountains, East Antarctica: *Recent Progress in Antarctic Earth Science*, p. 45-54.
- Grew, E. S., Carson, C. J., Christy, A. G., Maas, R., Yaxley, G. M., Boger, S. D., and Fanning, C. M., 2012, New constraints from U-Pb, Lu-Hf and Sm-Nd isotopic data on the timing of sedimentation and felsic magmatism in the Larsemann Hills, Prydz Bay, East Antarctica: *Precambrian Research*, v. 206, p. 87-108.
- Griffin, W. L., Belousova, E. A., Shee, S. R., Pearson, N. J., and O'Reilly, S. Y., 2004, Archean crustal evolution in the northern Yilgarn Craton: U-Pb and Hf-isotope evidence from detrital zircons: *Precambrian Research*, v. 131, no. 3, p. 231-282, <http://dx.doi.org/10.1016/j.precamres.2003.12.011>.
- Grove, M., and Harrison, T. M., 1996,  $^{40}\text{Ar}^*$  diffusion in Fe-rich biotite, *Mineralogical Society of America*.
- Grunow, A., Hanson, R., and Wilson, T., 1996, Were aspects of Pan-African deformation linked to Iapetus opening?: *Geology*, v. 24, p. 1063-1066.
- Guillocheau, F., Rouby, D., Robin, C., Helm, C., Rolland, N., Le Carlier de Veslud, C., and Braun, J., 2012, Quantification and causes of the terrigenous sediment budget at the scale of a continental margin: A new method applied to the Namibia-South Africa margin: *Basin Research*, v. 24, no. 1, p. 3-30, <http://dx.doi.org/10.1111/j.1365-2117.2011.00511.x>.
- Gunnell, Y., and Fleitout, L., 1998, Shoulder uplift of the Western Ghats passive margin, India: a denudational model: *Earth Surface Processes and Landforms*, v. 23, no. 5, p. 391-404, [http://dx.doi.org/10.1002/\(SICI\)1096-9837\(199805\)23:5<391::AID-ESP853>3.0.CO;2-5](http://dx.doi.org/10.1002/(SICI)1096-9837(199805)23:5<391::AID-ESP853>3.0.CO;2-5).
- Hall, R., 2002, Cenozoic geological and plate tectonic evolution of SE Asia and the SW Pacific: computer-based reconstructions, model and animations: *Journal of Asian Earth Sciences*, v. 20, no. 4, p. 353-431, [http://dx.doi.org/10.1016/S1367-9120\(01\)00069-4](http://dx.doi.org/10.1016/S1367-9120(01)00069-4).
- Halpin, J. A., Daczko, N. R., Milan, L. A., and Clarke, G. L., 2012, Decoding near-concordant U-Pb zircon ages spanning several hundred million years: recrystallisation, metamictisation or diffusion?: *Contributions to Mineralogy and Petrology*, v. 163, no. 1, p. 67-85, <http://dx.doi.org/10.1007/s00410-011-0659-7>.
- Harris, P. D., Moyes, A. B., Fanning, C. M., and Armstrong, R. A., 1995, Zircon ion microprobe results from the Maudheim high-grade gneiss terrane, western Dronning Maud Land, Antarctica: *Centennial Geocongress*, p. 240-243.
- Harrison, M. T., 1982, Diffusion of  $^{40}\text{Ar}$  in hornblende: *Contributions to Mineralogy and Petrology*, v. 78, no. 3, p. 324-331, [10.1007/bf00398927](https://doi.org/10.1007/bf00398927).
- Hastie, W. W., Watkeys, M. K., and Aubourg, C., 2014, Magma flow in dyke swarms of the Karoo LIP: Implications for the mantle plume hypothesis: *Gondwana Research*, v. 25, no. 2, p. 736-755, <http://dx.doi.org/10.1016/j.gr.2013.08.010>.
- Hawkesworth, C. J., Dhuime, B., Pietranik, A. B., Cawood, P. A., Kemp, A. I. S., and Storey, C. D., 2010, The generation and evolution of the continental crust: *Journal of the Geological Society*, v. 167, no. 2, p. 229-248, <http://dx.doi.org/10.1144/0016-76492009-072>.
- Hay, W. W., and Floegel, S., 2012, New thoughts about the Cretaceous climate and oceans: *Earth-Science Reviews*, v. 115, no. 4, p. 262-272, <http://dx.doi.org/10.1016/j.earscirev.2012.09.008>.
- Heimsath, A. M., Chappell, J., Alimanovic, A., Finkel, R. C., and Fifield, K., 2006, Escarpment erosion and landscape evolution in southeastern Australia, *Special Paper of the Geological Society of America*, Volume 398, p. 173-190.
- Heinonen, A. P., Andersen, T., and Rämö, O. T., 2010a, Re-evaluation of Rapakivi Petrogenesis: Source Constraints from the Hf Isotope Composition of Zircon in the Rapakivi Granites and Associated Mafic Rocks of Southern Finland: *Journal of Petrology*, v. 51, no. 8, p. 1687-1709, <http://dx.doi.org/10.1093/petrology/egq035>.
- Heinonen, J. S., Carlson, R. W., and Luttinen, A. V., 2010b, Isotopic (Sr, Nd, Pb, and Os) composition of highly magnesian dikes of Vestfjella, western Dronning Maud Land, Antarctica: A key to the origins of the Jurassic Karoo large igneous province?: *Chemical Geology*, v. 277, no. 3-4, p. 227-244, <http://dx.doi.org/10.1016/j.chemgeo.2010.08.004>.



- Helferich, S., Läufer, A. L., Henjes-Kunst, F., and Kleinschmidt, G., 2004, Pan-African events in southern Kirwanveggen (western Dronning Maud Land, Antarctica) - evidence from structural geology and geochronology: *Zeitschrift der Deutschen Geologischen Gesellschaft*, v. 154, no. 4, p. 453-468.
- Higashino, F., Kawakami, T., Satish-Kumar, M., Ishikawa, M., Maki, K., Tsuchiya, N., Grantham, G. H., and Hirata, T., 2013, Chlorine-rich fluid or melt activity during granulite facies metamorphism in the Late Proterozoic to Cambrian continental collision zone—An example from the Sør Rondane Mountains, East Antarctica: *Precambrian Research*, v. 234, p. 229-246, <http://dx.doi.org/10.1016/j.precamres.2012.10.006>.
- Hinz, K., and Krause, W., 1982, The continental margin off Queen Maud Land/Antarctica: Seismic sequences, structural elements and geological development, *Geologisches Jahrbuch*, Volume 23, p. 17-41.
- Hinz, K., Neben, S., Gouseva, Y. B., and Kudryavtsev, G. A., 2004, A Compilation of Geophysical Data from the Lazarev Sea and the Riiser-Larsen Sea, Antarctica: *Marine Geophysical Researches*, v. 25, no. 3, p. 233-245, <http://dx.doi.org/10.1007/s11001-005-1319-y>.
- Hiroi, Y., Shiraishi, K., and Motoyoshi, Y., 1991, Late Proterozoic paired metamorphic complexes in East Antarctica, with special reference to the tectonic significance of ultramafic rocks: *Geological evolution of Antarctica*, p. 83-87.
- Hokada, T., Horie, K., Adachi, T., Osanai, Y., Nakano, N., Baba, S., and Toyoshima, T., 2013, Unraveling the metamorphic history at the crossing of Neoproterozoic orogens, Sør Rondane Mountains, East Antarctica: Constraints from U–Th–Pb geochronology, petrography, and REE geochemistry: *Precambrian Research*, v. 234, p. 183-209, <http://dx.doi.org/10.1016/j.precamres.2012.12.002>.
- Holbourn, A., Kuhnt, W., Schulz, M., and Erlenkeuser, H., 2005, Impacts of orbital forcing and atmospheric carbon dioxide on Miocene ice-sheet expansion: *Nature*, v. 438, p. 483, <http://dx.doi.org/10.1038/nature04123>.
- Huang, X., Gohl, K., and Jokat, W., 2014, Variability in Cenozoic sedimentation and paleo-water depths of the Weddell Sea basin related to pre-glacial and glacial conditions of Antarctica: *Global and Planetary Change*, v. 118, no. 0, p. 25-41, <http://dx.doi.org/10.1016/j.gloplacha.2014.03.010>.
- Huang, X., and Jokat, W., 2016, Sedimentation and potential venting on the rifted continental margin of Dronning Maud Land: *Marine Geophysical Research*, v. 37, no. 4, p. 313-324, <http://dx.doi.org/10.1007/s11001-016-9296-x>.
- Huhma, H., Mänttari, I., Peltonen, P., Kontinen, A., Halkoaho, T., Hanski, E., Hokkanen, T., Hölttä, P., Juopperi, H., and Konnunaho, J., 2012, The age of the Archaean greenstone belts in Finland: *Geological Survey of Finland, Special Paper*, v. 54, p. 74-175.
- Ikeda, Y., Shiraishi, K., and Yanai, K., 1997, Petrogenesis of the meta-trondhjemites from Cape Hinode, East Antarctica: *Proceedings of the NIPR Symposium on Antarctic Geosciences*, v. 10, p. 102-110.
- Ikeda, Y., and Shiraishi, K., 1998, Petrogenesis of the tonalitic rocks from the Sør Rondane Mountain, East Antarctica: *Polar Geoscience*, v. 11, p. 143-153.
- Ishikawa, M., Kawakami, T., Satish-Kumar, M., Grantham, G. H., Hokazono, Y., Saso, M., and Tsuchiya, N., 2013, Late Neoproterozoic extensional detachment in eastern Sør Rondane Mountains, East Antarctica: Implications for the collapse of the East African Antarctic Orogen: *Precambrian Research*, v. 234, p. 247-256.
- Ivany, L. C., Lohmann, K. C., Hasiuk, F., Blake, D. B., Glass, A., Aronson, R. B., and Moody, R. M., 2008, Eocene climate record of a high southern latitude continental shelf: Seymour Island, Antarctica.: *Geological Society of America Bulletin*, v. 120, no. 5-6, p. 659-678.
- Iwasaki, A., and Yamanouchi, T., 1992, Meteorological data at Asuka Station, Antarctica in 1990: *National Institute of Polar Research*.
- Jackson, S. E., Pearson, N. J., Griffin, W. L., and Belousova, E. A., 2004, The application of laser ablation-inductively coupled plasma-mass spectrometry to in situ U–Pb zircon geochronology: *Chemical Geology*, v. 211, no. 1, p. 47-69, <http://dx.doi.org/10.1016/j.chemgeo.2004.06.017>.
- Jacobs, J., Hejl, E., Wagner, G. A., and Weber, K., 1992, Apatite fission track evidence for contrasting thermal and uplift histories of metamorphic basement blocks in western Dronning Maud Land: *Recent Progress in Antarctic Earth Science*, Terrapub, Tokyo, p. 323-330.
- Jacobs, J., Ahrendt, H., Kreutzer, H., and Weber, K., 1995, K-Ar,  $^{40}\text{Ar}$ - $^{39}\text{Ar}$  and apatite fission-track evidence for Neoproterozoic and Mesozoic basement rejuvenation events in the Heimefrontfjella



- and Mannefallknausane (East Antarctica): *Precambrian Research*, v. 75, no. 3, p. 251-262, [http://dx.doi.org/10.1016/0301-9268\(95\)80009-7](http://dx.doi.org/10.1016/0301-9268(95)80009-7).
- Jacobs, J., Kaul, N., and Weber, K., 1996a, The history of denudation and re-sedimentation at the continental margin of western Dronning Maud Land, Antarctica, during break-up of Gondwana: *Geological Society, London, Special Publications*, v. 108, no. 1, p. 191-199.
- Jacobs, J., Bauer, W., Spaeth, G., Thomas, R. J., and Weber, K., 1996b, Lithology and structure of the Grenville-aged (~1.1 Ga) basement of Heimefrontfjella (East Antarctica): *Geologische Rundschau*, v. 85, no. 4, p. 800-821.
- Jacobs, J., Falter, M., Weber, K., and Jessberger, E. K., 1997,  $^{40}\text{Ar}$ - $^{39}\text{Ar}$  evidence for the structural evolution of the Heimefront Shear Zone (Western Dronning Maud Land), East Antarctica, In: Ricci, C.A. (Ed) *The Antarctic Region: Geological evolution and processes*. Terra Antarctica Publication, Siena, p. 37-44.
- Jacobs, J., Fanning, C. M., Henjes-Kunst, F., Olesch, M., and Paech, H. J., 1998, Continuation of the Mozambique Belt into East Antarctica: Grenville-age metamorphism and polyphase Pan-African high-grade events in central Dronning Maud Land: *The Journal of Geology*, v. 106, p. 385-406.
- Jacobs, J., and Lisker, F., 1999, Post Permian tectono-thermal evolution of western Dronning Maud Land, E-Antarctica: an apatite fission-track approach: *Antarctic Science*, v. 11, no. 4, p. 451-460.
- Jacobs, J., Bauer, W., and Fanning, C. M., 2003a, Late Neoproterozoic/Early Palaeozoic events in central Dronning Maud Land and significance for the southern extension of the East African Orogen into East Antarctica: *Precambrian Research*, v. 126, no. 1-2, p. 27-53, [http://dx.doi.org/10.1016/S0301-9268\(03\)00125-6](http://dx.doi.org/10.1016/S0301-9268(03)00125-6).
- Jacobs, J., Klemd, R., Fanning, C. M., Bauer, W., and Colombo, F., 2003b, Extensional collapse of the late Neoproterozoic-early Palaeozoic East African-Antarctic Orogen in central Dronning Maud Land, East Antarctica in Proterozoic East Gondwana; supercontinent assembly and breakup: *Geological Society Special Publications*, v. 206, p. 271-287.
- Jacobs, J., Fanning, C. M., and Bauer, W., 2003c, Timing of Grenville-age vs. Pan-African medium- to high grade metamorphism in western Dronning Maud Land (East Antarctica) and significance for correlations in Rodinia and Gondwana: *Precambrian Research*, v. 125, p. 1-20.
- Jacobs, J., Bauer, W., and Fanning, C. M., 2003d, New age constraints for Grenville-age metamorphism in western central Dronning Maud Land (East Antarctica), and implications for the palaeogeography of Kalahari in Rodinia: *International Journal of Earth Sciences*, v. 92, no. 3, p. 301-315, <http://dx.doi.org/10.1007/s00531-003-0335-x>.
- Jacobs, J., and Thomas, R. J., 2004, Himalayan-type indenter-escape tectonics model for the southern part of the late Neoproterozoic-early Paleozoic East African-Antarctic Orogen: *Geology*, v. 32, no. 8, p. 721-724.
- Jacobs, J., Pisarevsky, S., Thomas, R. J., and Becker, T., 2008a, The Kalahari Craton during the assembly and dispersal of Rodinia: *Precambrian Research*, v. 160, no. 1-2, p. 142-158, <http://dx.doi.org/10.1016/j.precamres.2007.04.022>.
- Jacobs, J., Bingen, B., Thomas, R. J., Bauer, W., Wingate, M. T. D., and Feitio, P., 2008b, Early Palaeozoic orogenic collapse and voluminous late-tectonic magmatism in Dronning Maud Land and Mozambique: insights into the partially delaminated orogenic root of the East African - Antarctic Orogen?: *Geological Society, London, Special Publications*, v. 308, p. 69-90.
- Jacobs, J., Bauer, W., Weber, K., Spaeth, G., and Thomas, R. J., 2009, Geology of the Sivorg Terrane, Heimefrontfjella, (East Antarctica), and new U-Pb zircon provenance analyses of metasedimentary rocks: *Polarforschung*, v. 79 no. 1, p. 11-19.
- Jacobs, J., Elburg, M., Läufer, A., Kleinhanns, I. C., Henjes-Kunst, F., Estrada, S., Ruppel, A. S., Damaske, D., Montero, P., and Bea, F., 2015, Two distinct Late Mesoproterozoic/Early Neoproterozoic basement provinces in central/eastern Dronning Maud Land, East Antarctica: the missing link, 15-21°E: *Precambrian Research*, v. 265, p. 249-272, <http://dx.doi.org/10.1016/j.precamres.2015.05.003>.
- Jacobs, J., Opås, B., Elburg, M. A., Läufer, A., Estrada, S., Ksienzyk, A. K., Damaske, D., and Hofmann, M., 2017, Cryptic sub-ice geology revealed by a U-Pb zircon study of glacial till in Dronning Maud Land, East Antarctica: *Precambrian Research*, v. 294, p. 1-14, <http://dx.doi.org/10.1016/j.precamres.2017.03.012>.
- Jacobsen, S. B., and Wasserburg, G. J., 1980, Sm-Nd isotopic evolution of chondrites: *Earth and Planetary Science Letters*, v. 50, no. 1, p. 139-155, [http://dx.doi.org/10.1016/0012-821X\(80\)90125-9](http://dx.doi.org/10.1016/0012-821X(80)90125-9).



- Janoušek, V., Farrow, C. M., and Erban, V., 2006, Interpretation of Whole-rock Geochemical Data in Igneous Geochemistry: Introducing Geochemical Data Toolkit (GCDkit): *Journal of Petrology*, v. 47, no. 6, p. 1255-1259, <http://dx.doi.org/10.1093/petrology/egl013>.
- Jenkyns, H., Schouten-Huibers, L., Schouten, S., and Damsté, J. S., 2012, Warm Middle Jurassic–Early Cretaceous high-latitude sea-surface temperatures from the Southern Ocean: *Climate of the Past*, v. 8, no. 1, p. 215.
- Jiang, G., Sohl, L. E., and Christie-Blick, N., 2003, Neoproterozoic stratigraphic comparison of the Lesser Himalaya (India) and Yangtze block (south China): Paleogeographic implications: *Geology*, v. 31, no. 10, p. 917–920.
- Johnson, P. R., and Woldehaimanot, B., 2003, Development of the Arabian-Nubian Shield: perspectives on accretion and deformation in the northern East African Orogen and the assembly of Gondwana: *Geological Society, London, Special Publications*, v. 206, no. 1, p. 289-325, <http://dx.doi.org/10.1144/gsl.sp.2003.206.01.15>.
- Johnson, P. R., Andresen, A., Collins, A. S., Fowler, A. R., Fritz, H., Ghebreab, W., Kusky, T., and Stern, R. J., 2011, Late Cryogenian–Ediacaran history of the Arabian–Nubian Shield: A review of depositional, plutonic, structural, and tectonic events in the closing stages of the northern East African Orogen: *Journal of African Earth Sciences*, v. 61, no. 3, p. 167-232, <http://dx.doi.org/10.1016/j.jafrearsci.2011.07.003>.
- Jokat, W., Boebel, T., König, M., and Meyer, U., 2003, Timing and geometry of early Gondwana breakup: *Journal of Geophysical Research: Solid Earth*, v. 108, no. B9, p. 2156-2202, <http://dx.doi.org/10.1029/2002jb001802>.
- Jöns, N., and Schenk, V., 2008, Relics of the Mozambique Ocean in the central East African Orogen: evidence from the Vohibory Block of southern Madagascar: *Journal of Metamorphic Geology*, v. 26, no. 1, p. 17-28, <http://dx.doi.org/10.1111/j.1525-1314.2007.00745.x>.
- Jukes, L. M., 1972, The Geology of North-Eastern Heimefrontfjella, Dronning Maud Land: *British Antarctic Survey Bulletin*, v. 65, p. 44.
- Kamei, A., Horie, K., Owada, M., Yuhara, M., Nakano, N., Osanai, Y., Adachi, T., Hara, Y., Terao, M., Teuchi, S., Shimura, T., Tsukada, K., Hokada, T., Iwata, C., Shiraishi, K., Ishizuka, H., and Takahashi, Y., 2013, Late Proterozoic juvenile arc metatonalite and adakitic intrusions in the Sør Rondane Mountains, eastern Dronning Maud Land, Antarctica: *Precambrian Research*, v. 234, p. 47-62.
- Kelly, N. M., Clarke, G. L., and Fanning, C. M., 2002, A two-stage evolution of the Neoproterozoic Rayner Structural Episode: new U–Pb sensitive high resolution ion microprobe constraints from the Oygarden Group, Kemp Land, East Antarctica: *Precambrian Research*, v. 116, no. 3, p. 307-330, [http://dx.doi.org/10.1016/S0301-9268\(02\)00028-1](http://dx.doi.org/10.1016/S0301-9268(02)00028-1).
- Kelly, N. M., and Harley, S. L., 2005, An integrated microtextural and chemical approach to zircon geochronology: refining the Archaean history of the Napier Complex, east Antarctica: *Contributions to Mineralogy and Petrology*, v. 149, no. 1, p. 57-84, <http://dx.doi.org/10.1007/s00410-004-0635-6>.
- Kent, R., 1991, Lithospheric uplift in eastern Gondwana: evidence for a long-lived mantle plume system?: *Geology*, v. 19, no. 1, p. 19-23.
- Ketcham, R. A., 2005, Forward and inverse modeling of low-temperature thermochronometry data: *Reviews in Mineralogy and Geochemistry*, v. 58, no. 1, p. 275-314, <http://dx.doi.org/10.2138/rmg.2005.58.11>.
- King, L. C., 1953, Canons of landscape evolution: *Bulletin of the Geological Society of America*, v. 64, no. 7, p. 721-752, [http://dx.doi.org/10.1130/0016-7606\(1953\)64\[721:COLE\]2.0.CO;2](http://dx.doi.org/10.1130/0016-7606(1953)64[721:COLE]2.0.CO;2).
- Kitano, I., Osanai, Y., Nakano, N., and Adachi, T., 2016, Detrital zircon provenances for metamorphic rocks from southern Sør Rondane Mountains, East Antarctica: A new report of Archean to Mesoproterozoic zircons: *Journal of Mineralogical and Petrological Sciences*, v. 111, no. 2, p. 118-128, <http://dx.doi.org/10.2465/jmps.151001>.
- Kleinhanns, I. C., Jacobs, J., Engvik, A., Bingen, B., Roland, N. W., Läufer, A., and Schoenberg, R., 2013, Pan-African granitoid magmatism in central Dronning Maud Land derived from a mantle source, not a lower crustal source: evidence from geochemical and Sr-Nd isotope signatures: *Berichte zur Polar- und Meeresforschung*, v. 659, p. 82–83.
- Kleinschmidt, G., Helferich, S., Henjes-Kunst, F., Jackson, C., and Frimmel, H. E., 2000, The pre-Permo-Carboniferous Rocks and Structures from Southern Kirwanveggen, Dronning Maud Land, Antarctica: *Polarforschung, Bremerhaven, Alfred Wegener Institute for Polar and Marine Research & German Society of Polar Research*, v. 66, no. 3, p. 7-18.



- Kleinschmidt, G., Buggisch, W., Läufer, A. L., Helferich, S., and Tessensohn, F., 2002, The ‘‘Ross orogenic’’ structures in the Shackleton Range and their meaning for Antarctica, *in* Gamble, J. A., Skinner, D. N. B., and Henrys, S., eds., *Antarctica at the close of a millennium Volume 35*, Royal Society of New Zealand, p. 75–83.
- Kojima, S., and Shiraishi, K., 1986, Note on the geology of the western part of the Sør Rondane Mountains, East Antarctica: *Memoirs of National Institute of Polar Research*, v. 43, p. 116–131.
- König, M., and Jokat, W., 2006, The Mesozoic breakup of the Weddell Sea: *Journal Geophysical Research*, v. 111, no. B12012, p. 1–28.
- König, M., and Jokat, W., 2010, Advanced insights into magmatism and volcanism of the Mozambique Ridge and Mozambique Basin in the view of new potential field data: *Geophysical Journal International*, v. 180, no. 1, p. 158–180, <http://dx.doi.org/10.1111/j.1365-246X.2009.04433.x>.
- Koppes, M. N., and Montgomery, D. R., 2009, The relative efficacy of fluvial and glacial erosion over modern to orogenic timescales: *Nature Geoscience*, v. 2, no. 9, p. 644–647, <http://dx.doi.org/10.1038/ngeo616>.
- Kounov, A., Niedermann, S., de Wit, M. J., Viola, G., Andreoli, M., and Erzinger, J., 2007, Present denudation rates at selected sections of the South African escarpment and the elevated continental interior based on cosmogenic  $^3\text{He}$  and  $^{21}\text{Ne}$ : *South African Journal of Geology*, v. 110, no. 2–3, p. 235–248, <http://dx.doi.org/10.2113/gssajg.110.2-3.235>.
- Kratzmann, D. J., Carey, S., Scasso, R. A., and Naranjo, J.-A., 2009, Role of cryptic amphibole crystallization in magma differentiation at Hudson volcano, Southern Volcanic Zone, Chile: *Contributions to Mineralogy and Petrology*, v. 159, no. 2, p. 237, <http://dx.doi.org/10.1007/s00410-009-0426-1>.
- Kretz, R., 1983, Symbols for rock-forming minerals: *American mineralogist*, v. 68, p. 277–279.
- Kreuser, T., 1995, Rift to drift evolution in Permian-Jurassic basins of East Africa: *Geological Society, London, Special Publications*, v. 80, no. 1, p. 297–315, <http://dx.doi.org/10.1144/gsl.sp.1995.080.01.14>.
- Kristoffersen, M., Andersen, T. O. M., and Andresen, A., 2013, U–Pb age and Lu–Hf signatures of detrital zircon from Palaeozoic sandstones in the Oslo Rift, Norway: *Geological Magazine*, v. 151, no. 5, p. 816–829, [10.1017/S0016756813000885](https://doi.org/10.1017/S0016756813000885).
- Kristoffersen, Y., Hofstede, C., Diez, A., Blenkner, R., Lambrecht, A., Mayer, C., and Eisen, O., 2014, Reassembling Gondwana: A new high quality constraint from vibroseis exploration of the sub-ice shelf geology of the East Antarctic continental margin: *Journal of Geophysical Research: Solid Earth*, v. 119, p. 9171–9182, <http://dx.doi.org/10.1002/2014JB011479>.
- Krohne, N., Lisker, F., Kleinschmidt, G., Klügel, A., Läufer, A., Spiegel, C., and Estrada, S., 2016, The Shackleton Range (East Antarctica): an alien block at the rim of Gondwana? : *Geological Magazine*, v. 155, no. 4, p. 841–864, <http://dx.doi.org/10.1017/s0016756816001011>.
- Krohne, N., 2017, From Active to Passive Margins: The Basin and Highland Evolution of the Weddell Sea Sector, East Antarctica, Doctoral dissertation.
- Krohne, N., Lisker, F., Läufer, A., Ruppel, A., Jacobs, J., Elburg, M., Damaske, D., and Spiegel, C., in prep., Exhumation and uplift of Sør Rondane (East Antarctica) – Inversion of an East Gondwana triple junction.
- Kröner, A., 2001, The Mozambique belt of East Africa and Madagascar: significance of zircon and Nd model ages for Rodinia and Gondwana supercontinent formation and dispersal: *South African Journal of Geology*, v. 104, no. 2, p. 151–166.
- Kröner, A., Rojas-Agramonte, Y., Kehelpannala, K. V. W., Zack, T., Hegner, E., Geng, H. Y., Wong, J., and Barth, M., 2013, Age, Nd–Hf isotopes, and geochemistry of the Vijayan Complex of eastern and southern Sri Lanka: A Grenville-age magmatic arc of unknown derivation: *Precambrian Research*, v. 234, no. Supplement C, p. 288–321, <http://dx.doi.org/10.1016/j.precamres.2012.11.001>.
- Kruhl, J. H., 1996, Prism- and basal-plane parallel subgrain boundaries in quartz: a microstructural geothermobarometer: *Journal of Metamorphic Geology*, v. 14, no. 5, p. 581–589, <http://dx.doi.org/10.1046/j.1525-1314.1996.00413.x>.
- Ksienzyk, A. K., and Jacobs, J., 2015, Western Australia-Kalahari (WAlahari) connection in Rodinia: Not supported by U/Pb detrital zircon data from the Maud Belt (East Antarctica) and the Northampton Complex (Western Australia): *Precambrian Research*, v. 259, p. 207–221, <http://dx.doi.org/10.1016/j.precamres.2014.11.020>.



- Kuiper, Y. D., 2002, The interpretation of inverse isochron diagrams in  $^{40}\text{Ar}/^{39}\text{Ar}$  geochronology: *Earth and Planetary Science Letters*, v. 203, no. 1, p. 499-506, [http://dx.doi.org/10.1016/S0012-821X\(02\)00833-6](http://dx.doi.org/10.1016/S0012-821X(02)00833-6).
- Kuritani, T., 2001, Replenishment of a mafic magma in a zoned felsic magma chamber beneath Rishiri Volcano, Japan: *Bulletin of Volcanology*, v. 62, no. 8, p. 533-548, <http://dx.doi.org/10.1007/s004450000117>.
- Kusznir, N. J., Marsden, G., and Egan, S. S., 1991, A flexural-cantilever simple-shear/pure-shear model of continental lithosphere extension: applications to the Jeanne d'Arc Basin, Grand Banks and Viking Graben, North Sea: Geological Society, London, Special Publications, v. 56, no. 1, p. 41-60, <http://dx.doi.org/10.1144/gsl.sp.1991.056.01.04>.
- Kuvaas, B., Kristoffersen, Y., Leitchenkov, G., Guseva, J., and Gandjukhin, V., 2004, Seismic expression of glaciomarine deposits in the eastern Riiser Larsen Sea, Antarctica: *Marine Geology*, v. 207, no. 1, p. 1-15, <http://dx.doi.org/10.1016/j.margeo.2004.04.004>.
- Lanphere, M. A., and Brent Dalrymple, G., 1976, Identification of excess  $^{40}\text{Ar}$  by the  $^{40}\text{Ar}/^{39}\text{Ar}$  age spectrum technique: *Earth and Planetary Science Letters*, v. 32, no. 2, p. 141-148, [http://dx.doi.org/10.1016/0012-821X\(76\)90052-2](http://dx.doi.org/10.1016/0012-821X(76)90052-2).
- Läufer, A. L., in Press, Geology and Geodynamic Evolution of Dronning Maud Land, East Antarctica., in Kleinschmidt, G., ed., *The Geology of the Antarctic Continent*: Stuttgart, Schweizerbart.
- Le Maitre, R. W., 2002, *Igneous rocks - A Classification and Glossary of Terms*: Cambridge, Cambridge University Press.
- Lee, J.-Y., Marti, K., Severinghaus, J. P., Kawamura, K., Yoo, H.-S., Lee, J. B., and Kim, J. S., 2006, A redetermination of the isotopic abundances of atmospheric Ar: *Geochimica et Cosmochimica Acta*, v. 70, no. 17, p. 4507-4512, <https://doi.org/10.1016/j.gca.2006.06.1563>.
- Leeuwen, T. v., Allen, C. M., Kadarusman, A., Elburg, M., Michael Palin, J., Muhandjo, and Suwijanto, 2007, Petrologic, isotopic, and radiometric age constraints on the origin and tectonic history of the Malino Metamorphic Complex, NW Sulawesi, Indonesia: *Journal of Asian Earth Sciences*, v. 29, no. 5, p. 751-777, <http://dx.doi.org/10.1016/j.jseaes.2006.05.002>.
- Leinweber, V. T., and Jokat, W., 2012, The Jurassic history of the Africa–Antarctica corridor — new constraints from magnetic data on the conjugate continental margins: *Tectonophysics*, v. 530-531, p. 87-101, <http://dx.doi.org/10.1016/j.tecto.2011.11.008>.
- Leitchenkov, G., Guseva, J., Gandyukhin, V., Griukurov, G., Kristoffersen, Y., Sand, M., Golynsky, A., and Aleshkova, N., 2008, Crustal structure and tectonic provinces of the Riiser-Larsen Sea area (East Antarctica): results of geophysical studies: *Marine Geophysical Researches*, v. 29, no. 2, p. 135-158, <http://dx.doi.org/10.1007/s11001-008-9051-z>.
- Leitchenkov, G. L., Miller, H., and Zatzepin, E. N., 1996, Structure and Mesozoic evolution of the eastern Weddell Sea, Antarctica; history of early Gondwana break-up, in Storey, B. C., King, E. C., and Livermore, R. A., eds., *Weddell Sea tectonics and Gondwana break-up*, Volume 108: London, Geological Society of London, p. 175-190.
- Leliak, P., 1961, Identification and Evaluation of Magnetic-Field Sources of Magnetic Airborne Detector Equipped Aircraft: *IRE Transactions on Aerospace and Navigational Electronics*, v. ANE-8, no. 3, p. 95-105, <http://dx.doi.org/10.1109/TANE3.1961.4201799>.
- Li, Z., Tainosho, Y., Shiraishi, K., Owada, M., and Kimura, J.-i., 2001, Geochemical characteristics of two types of early Paleozoic granitoids from the Sør Rondane Mountains, East Antarctica: *Polar geoscience*, v. 14, p. 119-138.
- Li, Z., Tainosho, Y., Kimura, J.-i., Shiraishi, K., and Owada, M., 2003, Pan-African Alkali Granitoids from the Sør Rondane Mountains, East Antarctica: *Gondwana Research*, v. 6, no. 4, p. 595-605.
- Li, Z., Du, Z., Yang, S., Chen, H., Song, B., and Liu, D., 2006, First report of zircon SHRIMP U-Pb dating from the Dufek granite in the Sør Rondane Mountains, East Antarctica, *Journal of Zhejiang University SCIENCE A*, v. 7, no. 2, p. 315-319.
- Lindeque, A., Martos, Y. M., Gohl, K., and Maldonado, A., 2013, Deep-sea pre-glacial to glacial sedimentation in the Weddell Sea and southern Scotia Sea from a cross-basin seismic transect: *Marine Geology*, v. 336, p. 61-83, <http://dx.doi.org/10.1016/j.margeo.2012.11.004>.
- Lisker, F., and Läufer, A. L., 2013, The Mesozoic Victoria Basin: Vanished link between Antarctica and Australia: *Geology*, v. 41, no. 10, p. 1043-1046, <http://dx.doi.org/10.1130/g33409.1>.
- Liu, X., Zhao, Y., and Hu, J., 2013, The c. 1000–900 Ma and c. 550–500 Ma tectonothermal events in the Prince Charles Mountains–Prydz Bay region, East Antarctica, and their relations to



- supercontinent evolution: Geological Society, London, Special Publications, v. 383, no. 1, p. 95-112, <http://dx.doi.org/10.1144/sp383.6>.
- Liu, X., Jahn, B.-m., Zhao, Y., Liu, J., and Ren, L., 2014, Geochemistry and geochronology of Mesoproterozoic basement rocks from the Eastern Amery Ice Shelf and southwestern Prydz Bay, East Antarctica: Implications for a long-lived magmatic accretion in a continental arc: *American Journal of Science*, v. 314, no. 2, p. 508-547.
- Ludwig, K., 2008, A user's manual for Isoplot 3.6/Ex: A Geochronological Toolkit for Microsoft Excel: Berkeley, CA, Berkeley Geochronology Center Special Publication, no. 4.
- Ludwig, K., 2011, A geochronological toolkit for Microsoft Excel: Berkeley Geochronology Centre Special Publications, v. 4.
- Ludwig, K., 2012, User's manual for Isoplot version 3.75-4.15: a geochronological toolkit for Microsoft. Excel Berkley Geochronological Center Special Publication Excel Berkley Geochronological Center Special Publication, v. No. 5, p. 1-75.
- Mandal, S. K., Lupker, M., Burg, J.-P., Valla, P. G., Haghpor, N., and Christl, M., 2015, Spatial variability of  $^{10}\text{Be}$ -derived erosion rates across the southern Peninsular Indian escarpment: A key to landscape evolution across passive margins: *Earth and Planetary Science Letters*, v. 425, p. 154-167, <http://dx.doi.org/10.1016/j.epsl.2015.05.050>.
- Mark, D. F., Stuart, F. M., and de Podesta, M., 2011, New high-precision measurements of the isotopic composition of atmospheric argon: *Geochimica et Cosmochimica Acta*, v. 75, no. 23, p. 7494-7501, <https://doi.org/10.1016/j.gca.2011.09.042>.
- Markl, G., and Henjes-Kunst, F., 2004, Magmatic Conditions of Formation and Autometasomatism of Post-Kinematic Charnockites in central Dronning Maud Land, East Antarctica: A Model of Magmatic Evolution: *Geologisches Jahrbuch Reihe B* v. 96, p. 139.
- Marschall, H. R., Hawkesworth, C. J., and Leat, P. T., 2013, Mesoproterozoic subduction under the eastern edge of the Kalahari-Grunehogna Craton preceding Rodinia assembly: The Ritscherflya detrital zircon record, Ahlmannryggen (Dronning Maud Land, Antarctica): *Precambrian Research*, v. 236, p. 31-45, <http://dx.doi.org/10.1016/j.precamres.2013.07.006>.
- Martin, A. K., and Hartnady, C. J. H., 1986, Plate tectonic development of the south west Indian Ocean: A revised reconstruction of East Antarctica and Africa: *Journal of Geophysical Research: Solid Earth*, v. 91, no. B5, p. 4767-4786, <http://dx.doi.org/10.1029/JB091iB05p04767>.
- Martin, H., 1981, The late Palaeozoic Gondwana glaciation: *Geologische Rundschau*, v. 70, no. 2, p. 480-496, <http://dx.doi.org/10.1007/bf01822128>.
- Matmon, A., Bierman, P., and Enzel, Y., 2002, Pattern and tempo of great escarpment erosion: *Geology*, v. 30, no. 12, p. 1135-1138, [http://dx.doi.org/10.1130/0091-7613\(2002\)030<1135:PATOGES>2.0.CO;2](http://dx.doi.org/10.1130/0091-7613(2002)030<1135:PATOGES>2.0.CO;2).
- Matsuoka, N., Moriwaki, K., Iwata, S., and Hirakawa, K., 1990, Ground temperature regimes and their relationship to periglacial processes in the Sør Rondane Mountains, East Antarctica: *Proceedings of the NIPR Symposium on Antarctic Geosciences*, v. 4, p. 55-66.
- Matsuoka, N., Thomachot, C., Oguchi, C. T., Hatta, T., Abe, M., and Matsuzaki, H., 2006, Quaternary bedrock erosion and landscape evolution in the Sør Rondane Mountains, East Antarctica: Reevaluating rates and processes: *Geomorphology*, v. 81, no. 3-4, p. 408-420, <http://dx.doi.org/10.1016/j.geomorph.2006.05.005>.
- Matthews, K. J., Maloney, K. T., Zahirovic, S., Williams, S. E., Seton, M., and Müller, R. D., 2016, Global plate boundary evolution and kinematics since the late Paleozoic: *Global and Planetary Change*, v. 146, p. 226-250, <http://dx.doi.org/10.1016/j.gloplacha.2016.10.002>.
- McCourt, S., Armstrong, R. A., Grantham, G. H., and Thomas, R. J., 2006, Geology and evolution of the Natal belt, South Africa: *Journal of African Earth Sciences*, v. 46, no. 1, p. 71-92, <http://dx.doi.org/10.1016/j.jafrearsci.2006.01.013>.
- McDougall, I., and Harrison, T. M., 1999, *Geochronology and Thermochronology by the  $^{40}\text{Ar}/^{39}\text{Ar}$  Method*, Oxford University Press on Demand.
- Meert, J. G., 2003, A synopsis of events related to the assembly of eastern Gondwana: *Tectonophysics*, v. 362, p. 1-40.
- Meert, J. G., 2012, What's in a name? The Columbia (Paleopangaea/Nuna) supercontinent: *Gondwana Research*, v. 21, no. 4, p. 987-993, <http://dx.doi.org/10.1016/j.gr.2011.12.002>.
- Meier, S., Jacobs, J., and Olesch, M., 2004, Tectono-thermal evolution of the continental margin of central Dronning Maud Land, East Antarctica: apatite fission-track thermochronology, *in* Paech, H.-J., ed., *International GeoMaud expedition of the BGR to central Dronning Maud Land in 1995/96 - Geological results, Volume B96*, Schweizerbart science publishers, p. 423-448.



- Mendonidis, P., Thomas, R. J., Grantham, G. H., and Armstrong, R. A., 2015, Geochronology of emplacement and charnockite formation of the Margate Granite Suite, Natal Metamorphic Province, South Africa: Implications for Natal-Maud belt correlations: *Precambrian Research*, v. 265, p. 189-202, <http://dx.doi.org/10.1016/j.precamres.2015.02.013>.
- Meschede, M., 1994, Methoden der Strukturgeologie: ein Leitfaden zur Aufnahme und Auswertung strukturgeologischer Daten im Gelände und im Labor, Enke, 169-169 p.
- Meshida, S., Azuma, N., Yukimatsu, A., and Yamanouchi, T., 1991, Meteorological data at Asuka Station, Antarctica in 1989: National Institute of Polar Research.
- Mieth, M., Steinhage, D., Ruppel, A., Damaske, D., and Jokat, W., 2013, Aerogeophysical survey over Sør Rondane Mountains and its implications for revealing the tectonic evolution of East Antarctica: EGU General Assembly 2013, Wien.
- Mieth, M., 2014, Aerogeophysical constraints for the geodynamic evolution of Dronning Maud Land, East Antarctica, Doctoral dissertation: University Bremen.
- Mieth, M., and Jokat, W., 2014, New aeromagnetic view of the geological fabric of southern Dronning Maud Land and Coats Land, East Antarctica: *Gondwana Research*, v. 25, no. 1, p. 358-367, <http://dx.doi.org/10.1016/j.gr.2013.04.003>.
- Mieth, M., Jacobs, J., Ruppel, A., Damaske, D., Läufer, A., and Jokat, W., 2014, New detailed aeromagnetic and geological data of eastern Dronning Maud Land: Implications for refining the tectonic and structural framework of Sør Rondane, East Antarctica: *Precambrian Research*, v. 245, p. 174-185, <http://dx.doi.org/10.1016/j.precamres.2014.02.009>.
- Mikhalsky, E., Beliatsky, B., Savva, E., Wetzel, H., Fedorov, L., Weiser, T., and Hahne, K., Reconnaissance geochronologic data on polymetamorphic and igneous rocks of the Humboldt Mountains, central Queen Maud Land, East Antarctica, *in Proceedings The Antarctic Region: Geological Evolution and Processes, Proc. VII International Symposium on Antarctic Earth Sciences, Siena-1995, Italy 1997a*, p. 45-53.
- Mikhalsky, E., and Jacobs, J., 2004, Orthogneisses in central Dronning Maud Land, East Antarctica: their origin and tectonic setting: *Geologisches Jahrbuch Reihe B*, v. 96, p. 49.
- Mikhalsky, E., Jacobs, J., and Fanning, C. M., 2011, New U-Pb zircon and Sm-Nd whole-rock data for metamorphic rocks of central Dronning Maud Land: implications for the structural evolution of Neoproterozoic to Cambrian events in Gondwana: 11th International Symposium on Antarctic Earth Sciences, p. 305.
- Mikhalsky, E. V., Beliatsky, B. V., Savva, E. V., Wetzel, H. U., Fedorov, L. V., Weiser, T., and Hahne, K., 1997b, Reconnaissance Geochronologic Data on Polymetamorphic and Igneous Rocks of the Humboldt Mountains, Central Queen Maud Land, East Antarctica, *in the Antarctic Region: Geological Evolution and Processes*, p. 45-54.
- Mikhalsky, E. V., and Sheraton, J. W., 2011, The Rayner tectonic Province of East Antarctica: Compositional features and geodynamic setting: *Geotectonics*, v. 45, no. 6, p. 496-512, <http://dx.doi.org/10.1134/s0016852111060057>.
- Milisenda, C. C., Liewa, T. C., Hofmanna, A. W., and Köhler, H., 1994, Nd isotopic mapping of the Sri Lanka basement: update, and additional constraints from Sr isotopes: *Precambrian Research*, v. 66, no. 1, p. 95-110, [http://dx.doi.org/10.1016/0301-9268\(94\)90046-9](http://dx.doi.org/10.1016/0301-9268(94)90046-9).
- Miller, H. G., and Singh, V., 1994, Potential field tilt - a new concept for location of potential field sources: *Journal of Applied Geophysics*, v. 32, no. 2, p. 213-217, [http://dx.doi.org/10.1016/0926-9851\(94\)90022-1](http://dx.doi.org/10.1016/0926-9851(94)90022-1).
- Miller, K. G., Wright, J. D., Katz, M. E., Browning, J. V., Cramer, B. S., Wade, B. S., and Mizintseva, S. F., 2008, A View of Antarctic Ice-Sheet Evolution from Sea-Level and Deep-Sea Isotope Changes During the Late Cretaceous-Cenozoic, *in Cooper, A. K., Barrett, P. J., Stagg, H., Storey, B., Stump, E., and Wise, W., eds., Antarctica: A Keystone in a Changing World. Proceedings of the 10th International Symposium on Antarctic Earth Sciences.* : Washington, DC, The National Academies Press, <http://dx.doi.org/10.3133/of2007-1047.kp06>
- Motoyoshi, Y., and Ishikawa, M., 1997, Metamorphic and structural evolution of granulites from Rundvågshetta, Lützow-Holm Bay, East Antarctica: *Sienna, The Antarctic Region: Geological Evolution and Processes*, 65-72 p.
- Moyes, A. B., Barton, J. M., and Groenewald, P. B., 1993, Late Proterozoic to Early Palaeozoic tectonism in Dronning Maud Land, Antarctica: supercontinental fragmentation and amalgamation: *Journal of the Geological Society*, v. 150, p. 833-842.



- Mueller, C. O., and Jokat, W., 2019, The initial Gondwana break-up: A synthesis based on new potential field data of the Africa-Antarctica Corridor: *Tectonophysics*, v. 750, p. 301-328, <http://dx.doi.org/10.1016/j.tecto.2018.11.008>.
- Muhongo, S., and Lenoir, J.-L., 1994, Pan-African granulite-facies metamorphism in the Mozambique Belt of Tanzania: U-Pb zircon geochronology: *Journal of the Geological Society*, v. 151, no. 2, p. 343-347, <http://dx.doi.org/10.1144/gsjgs.151.2.0343>.
- Nakano, N., Osanai, Y., Kamei, A., Satish-Kumar, M., Adachi, T., Hokada, T., Baba, S., and Toyoshima, T., 2013, Multiple thermal events recorded in metamorphosed carbonate and associated rocks from the southern Austkampane region in the Sør Rondane Mountains, East Antarctica: A protracted Neoproterozoic history at the Gondwana suture zone: *Precambrian Research*, v. 234, p. 161-182, <http://dx.doi.org/10.1016/j.precamres.2012.10.009>.
- Nardi, L. V. S., Formoso, M. L. L., Müller, I. F., Fontana, E., Jarvis, K., and Lamarão, C., 2013, Zircon/rock partition coefficients of REEs, Y, Th, U, Nb, and Ta in granitic rocks: Uses for provenance and mineral exploration purposes: *Chemical Geology*, v. 335, no. Supplement C, p. 1-7, <http://dx.doi.org/10.1016/j.chemgeo.2012.10.043>.
- Näslund, J. O., 2001, Landscape development in western and central Dronning Maud Land, East Antarctica: *Antarctic Science*, v. 13, no. 3, p. 302-311, <http://dx.doi.org/10.1017/S0954102001000438>.
- Nixdorf, U., Steinhage, D., Meyer, U., Hempel, L., Jenett, M., Wachs, P., and Miller, H., 1999, The newly developed airborne radio-echo sounding system of the AWI as a glaciological tool: *Annals of Glaciology*, v. 29, p. 231-238, <http://dx.doi.org/10.3189/172756499781821346>.
- Nogi, Y., Jokat, W., Kitada, K., and Steinhage, D., 2013, Geological structures inferred from airborne geophysical surveys around Lützow-Holm Bay, East Antarctica: *Precambrian Research*, v. 234, no. 0, p. 279-287, <http://dx.doi.org/10.1016/j.precamres.2013.02.008>.
- Ohta, Y., Tørudbakken, B. O., and Shiraishi, K., 1990, Geology of Gjelsvikfjella and western Mühlig-Hofmannfjella, Dronning Maud Land, east Antarctica: *Polar Research*, v. 8, no. 2, p. 99-126, <http://dx.doi.org/10.1111/j.1751-8369.1990.tb00380.x>.
- Ollier, C. D., 1984, Morphotectonics of continental margins with great escarpments, in Morisawa, M., and Hack, J. T., eds., *Tectonic Geomorphology, Volume Tectonic Geomorphology*: Boston Unwin Hyman, p. 3-25.
- Osanai, Y., Takahashi, Y., and Sakiyama, T., High-grade metamorphic rocks from the central part of the Sør Rondane Mountains, East Antarctica, in *Proceedings Proceedings of the NIPR Symposium on Antarctic Geosciences 1988, Volume 2*, p. 170.
- Osanai, Y., Shiraishi, K., Takahashi, Y., Ishizuka, H., Tainosho, Y., Tsuchiya, N., Sakiyama, T., and Kodama, S., 1992, Geochemical characteristics of metamorphic rocks from the central Sør Rondane Mountains, East Antarctica. In: Yoshida, Y., Kaminuma, K.; & Shiraishi, K. (Ed.) *Recent Progress in Antarctic Earth Science*, p. p. 17-27.
- Osanai, Y., Shiraishi, K., Takahashi, Y., Ishizuka, H., Moriwaki, K., Tainosho, Y., Tsuchiya, N., Sakiyama, T., Toyoshima, T. O. M., and Kojima, H., 1996a, Explanatory text of Geological Map of Brattnipene, Sør Rondane Mountains, Antarctica: *Antarctic Geological Map Series, National Institute of Polar Research, Tokyo*, v. Sheet 34, p. 1-29.
- Osanai, Y., Shiraishi, K., Takahashi, Y., Ishizuka, H., Moriwaki, K., Tainosho, Y., Tsuchiya, N., Sakiyama, T., Toyoshima, T., Owada, M., and Kojima, H., 1996b, Geological map of Brattnipene, Antarctica. *Antarctic Geological Map Series, Sheet 34, Scale 1:50,000*: National Institute of Polar Research, Tokyo.
- Osanai, Y., Shiraishi, K., Takahashi, Y., Ishizuka, H., Moriwaki, K., Tainosho, Y., Tsuchiya, N., Sakiyama, T., Toyoshima, T. O. M., and Kojima, H., 1996c, Geological map of the Sør Rondane Mountains, Antarctica. *Antarctica Geological Map Series, sheet 34, scale 1 : 25 0000*: National Institute of Polar Research, Tokyo.
- Osanai, Y., Nogi, Y., Baba, S., Nakano, N., Adachi, T., Hokada, T., Toyoshima, T., Owada, M., Satish-Kumar, M., Kamei, A., and Kitano, I., 2013, Geologic evolution of the Sør Rondane Mountains, East Antarctica: Collision tectonics proposed based on metamorphic processes and magnetic anomalies: *Precambrian Research*, v. 234, p. 8-29, <http://dx.doi.org/10.1016/j.precamres.2013.05.017>.
- Otsuji, N., Satish-Kumar, M., Kamei, A., Tsuchiya, N., Kawakami, T., Ishikawa, M., and Grantham, G. H., 2013, Late-Tonian to early-Cryogenian apparent depositional ages for metacarbonate rocks from the Sør Rondane Mountains, East Antarctica: *Precambrian Research*, v. 234, p. 257-278, <http://dx.doi.org/10.1016/j.precamres.2012.10.016>.



- Owada, M., Baba, S., Läufer, A., Elvevold, S., Shiraishi, K., and Jacobs, J., 2003, Geology of eastern Muehlig-Hofmannfjella and Filchnerfjella in Dronning Maud Land, East Antarctica: A preliminary report on a Japan-Norway-Germany joint geological investigation: *Polar Geoscience*, v. 16, p. 108-136.
- Owada, M., Baba, S., Osanai, Y., and Kagami, H., 2008, Geochemistry of post-kinematic mafic dykes from central to eastern Dronning Maud Land, East Antarctica: evidence for a Pan-African suture in Dronning Maud Land: Geological Society, London, Special Publications v. 308, p. 235-252.
- Owada, M., Shimura, T., Yuhara, M., Kamei, A., and Tsukada, K., 2010, Post-kinematic lamprophyre from the southwestern part of Sør Rondane Mountains, East Antarctica: Constraint on the Pan-African suture event: *Journal of Mineralogical and Petrological Sciences*, v. 105, no. 5, p. 262-267.
- Owada, M., Kamei, A., Horie, K., Shimura, T., Yuhara, M., Tsukada, K., Osanai, Y., and Baba, S., 2013, Magmatic history and evolution of continental lithosphere of the Sør Rondane Mountains, eastern Dronning Maud Land, East Antarctica: *Precambrian Research*, v. 234, no. 0, p. 63-84, <http://dx.doi.org/10.1016/j.precamres.2013.02.007>.
- Paech, H., Jacobs, J., and Bauer, W., 2004, Geological map 1: 500 000 of the central Dronning Maud Land; explanatory notes to the 1: 500 000 geological map of central Dronning Maud Land: *Geol. Jahrb. Reihe B*, v. 96, p. 97.
- Palme, H., and O'Neill, H. S. C., 2003, Cosmochemical estimates of mantle composition: *Treatise on geochemistry*, v. 2, p. 568.
- Partridge, T. C., and Maud, R. R., 1987, Geomorphic evolution of southern Africa since the Mesozoic: *South African Journal of Geology*, v. 90, no. 2, p. 179-208.
- Passchier, C. W., and Trouw, R. A. J., 2005, *Microtectonics*, 366 pp, Springer, Berlin.
- Pasteels, P., and Michot, J., 1968, Nouveaux résultats géochronologiques obtenus par la méthode U-Pb sur des zircons des monts Sør-Rondane (Antarctique): *Ann. Soc. Géol. Belg*, v. 91, p. 283-303.
- Pasteels, P., and Michot, J., 1970, Uranium-lead radioactive dating and lead isotope study on sphene and K-feldspar in the Sør-Rondane Mountains, Dronning Maud Land, Antarctica: *Eclogae Geologicae Helvetiae*, v. 63, no. 1, p. 239-254.
- Pattyn, F., Huybrechts, P., and Decler, H., 1989, Modeling glacier fluctuations in the Sør Rondane, Dronning Maud Land, Antarctica: *Zeitschrift für Gletscherkunde und Glazialgeologie*, v. 25, no. 1, p. 33-47.
- Pattyn, F., Decler, H., and Huybrechts, P., 1992, Glaciation of the central part of the Sør Rondane, Antarctica: glaciological evidence, in Yoshida, Y., Kaminuma, K., and Shiraishi, K., eds., *Recent Progress in Antarctic Earth Science*: Tokyo, Terra Scientific Publishing Company, p. 669-678.
- Pattyn, F., 2010, Antarctic subglacial conditions inferred from a hybrid ice sheet/ice stream model: *Earth and Planetary Science Letters*, v. 295, no. 3, p. 451-461, <http://dx.doi.org/10.1016/j.epsl.2010.04.025>.
- Paulsson, O., and Austrheim, H., 2003, A geochronological and geochemical study of rocks from Gjelsvikfjella, Dronning Maud Land, Antarctica—implications for Mesoproterozoic correlations and assembly of Gondwana: *Precambrian Research*, v. 125, no. 1, p. 113-138, [http://dx.doi.org/10.1016/S0301-9268\(03\)00109-8](http://dx.doi.org/10.1016/S0301-9268(03)00109-8).
- Pearce, J. A., Harris, N. B. W., and Tindle, A. G., 1984, Trace Element Discrimination Diagrams for the Tectonic Interpretation of Granitic Rocks: *Journal of Petrology*, v. 25, no. 4, p. 956-983, <http://dx.doi.org/10.1093/petrology/25.4.956>.
- Peate, D. W., Pearce, J. A., Hawkesworth, C. J., Colley, H., Edwards, C. M. H., and Hirose, K., 1997, Geochemical Variations in Vanuatu Arc Lavas: the Role of Subducted Material and a Variable Mantle Wedge Composition: *Journal of Petrology*, v. 38, no. 10, p. 1331-1358, <http://dx.doi.org/10.1093/ptroj/38.10.1331>.
- Pfänder, J. A., Sperner, B., Ratschbacher, L., Fischer, A., Meyer, M., Leistner, M., and Schaeben, H., 2014, High-resolution  $^{40}\text{Ar}/^{39}\text{Ar}$  dating using a mechanical sample transfer system combined with a high-temperature cell for step heating experiments and a multicollector ARGUS noble gas mass spectrometer: *Geochemistry, Geophysics, Geosystems*, v. 15, no. 6, p. 2713-2726, <http://dx.doi.org/10.1002/2014GC005289>.
- Picciotto, E., Deutsch, S., and Pasteels, P., 1964, Isotopic ages from the Sør Rondane Mountains, Dronning Maud Land.: In: Adie, R. J. (Ed.) *Antarctic Geology*, North-Holland, Amsterdam, p. 570-578.
- Poscher, G., 1992, Mikrotexturelle, sedimentpetrographische und geochemische Vergleichsuntersuchungen an jungpaläozoischen Diamiktiten der Ostantarktis, präkambrischen



- Diamiktiten Schottlands und glazialen Sedimenten der Ostalpen Jahrbuch der Kaiserlich-Königlichen Geologischen Reichsanstalt, v. 135, p. 493-511.
- Powell, C. M., and Pisarevsky, S., 2002, Late Neoproterozoic assembly of east Gondwana: *Geology*, v. 30, no. 1, p. 3-6.
- Prenzel, J., Lisker, F., Balestrieri, M. L., Läufer, A., and Spiegel, C., 2013, The Eisenhower Range, Transantarctic Mountains: Evaluation of qualitative interpretation concepts of thermochronological data: *Chemical Geology*, v. 352, p. 176-187, <http://dx.doi.org/10.1016/j.chemgeo.2013.06.005>.
- Prenzel, J., Lisker, F., Elsner, M., Schöner, R., Balestrieri, M. L., Läufer, A. L., Berner, U., and Spiegel, C., 2014, Burial and exhumation of the Eisenhower Range, Transantarctic Mountains, based on thermochronological, sedimentary rock maturity and petrographic constraints: *Tectonophysics*, v. 630, no. 0, p. 113-130, <http://dx.doi.org/10.1016/j.tecto.2014.05.020>.
- Raczek, I., Jochum, K. P., and Hofmann, A. W., 2003, Neodymium and Strontium Isotope Data for USGS Reference Materials BCR-1, BCR-2, BHVO-1, BHVO-2, AGV-1, AGV-2, GSP-1, GSP-2 and Eight MPI-DING Reference Glasses: *Geostandards Newsletter*, v. 27, no. 2, p. 173-179, <http://dx.doi.org/10.1111/j.1751-908X.2003.tb00644.x>.
- Rao, D. R., Rashid, S. A., and Panthulu, G. V. C., 2000, Origin of Mg-Metatholeiites of the Schirmacher Region, East Antarctica: Constraints from Trace Elements and Nd-Sr Isotopic Systematics: *Gondwana Research*, v. 3, no. 1, p. 91-104, [http://dx.doi.org/10.1016/S1342-937X\(05\)70060-5](http://dx.doi.org/10.1016/S1342-937X(05)70060-5).
- Ravikant, V., Bhaskar Rao, Y. J., and Gopalan, K., 2004, Schirmacher Oasis as an Extension of the Neoproterozoic East African Orogen into Antarctica: New Sm-Nd Isochron Age Constraints: *The Journal of Geology*, v. 112, no. 5, p. 607-616, <http://dx.doi.org/10.1086/422669>.
- Ravikant, V., 2006, Sm-Nd Isotopic Evidence for Late Mesoproterozoic Metamorphic Relics in the East African Orogen from the Schirmacher Oasis, East Antarctica: *The Journal of Geology*, v. 114, no. 5, p. 615-625, <http://dx.doi.org/10.1086/506163>.
- Ravikant, V., Laux, J. H., and Pimentel, M., 2007, Sm-Nd and U-Pb isotopic constraints for crustal evolution during Late Neoproterozoic from rocks of the Schirmacher Oasis, East Antarctica: geodynamic development coeval with the East African Orogeny, *in* Cooper, A. K., and Raymond, C. R., eds., *A Keystone in a Changing World-Online Proceedings of the 10th International Symposium on Antarctic Earth Sciences, Volume 1047, US Geological Survey Open File Report*.
- Reeves, C., 2005, *Aeromagnetic surveys: principles, practice and interpretation*, Geosoft.
- Reeves, C. V., 2014, The position of Madagascar within Gondwana and its movements during Gondwana dispersal: *Journal of African Earth Sciences*, v. 94, p. 45-57, <http://dx.doi.org/10.1016/j.jafrearsci.2013.07.011>.
- Renne, P. R., Mundil, R., Balco, G., Min, K., and Ludwig, K. R., 2010, Joint determination of 40K decay constants and 40Ar\*/40K for the Fish Canyon sanidine standard, and improved accuracy for 40Ar/39Ar geochronology: *Geochimica et Cosmochimica Acta*, v. 74, no. 18, p. 5349-5367, <https://doi.org/10.1016/j.gca.2010.06.017>.
- Retallack, G. J., and Krull, E. S., 1999, Landscape ecological shift at the Permian–Triassic boundary in Antarctica: *Australian Journal of Earth Sciences*, v. 46, p. 785-812.
- Reubi, O., and Blundy, J., 2009, A dearth of intermediate melts at subduction zone volcanoes and the petrogenesis of arc andesites: *Nature*, v. 461, p. 1269, <https://doi.org/10.1016/j.precamres.2013.05.01710.1038/nature08510>.
- Riedel, S., Jokat, W., and Steinhage, D., 2012, Mapping tectonic provinces with airborne gravity and radar data in Dronning Maud Land, East Antarctica: *Geophysical Journal International*, v. 189, no. 1, p. 414-427, <http://dx.doi.org/10.1111/j.1365-246X.2012.05363.x>
- Riedel, S., Jacobs, J., and Jokat, W., 2013, Interpretation of new regional aeromagnetic data over Dronning Maud Land (East Antarctica): *Tectonophysics*, v. 585, p. 161-171, <http://dx.doi.org/10.1016/j.tecto.2012.10.011>.
- Rignot, E., Mouginot, J., and Scheuchl, B., 2011, Ice Flow of the Antarctic Ice Sheet: *Science*, v. 333, no. 6048, p. 1427-1430, <http://dx.doi.org/10.1126/science.1208336>
- Roest, W. R., Verhoef, J., and Pilkington, M., 1992, Magnetic interpretation using the 3-D analytic signal: *Geophysics*, v. 57, no. 1, p. 116-125, <http://dx.doi.org/10.1190/1.1443174>.
- Rogenhagen, J., Jokat, W., Hinz, K., and Kristoffersen, Y., 2004, Improved Seismic Stratigraphy of the Mesozoic Weddell Sea: *Marine Geophysical Researches*, v. 25, no. 3, p. 265-282, <http://dx.doi.org/10.1007/s11001-005-1335-y>.



- Roland, N., 2002, Pan-African granitoids in central Dronning Maud Land, East Antarctica: Petrography, geochemistry, and plate tectonic setting, *Royal Society of New Zealand Bulletin, Antarctica at the close of a millennium*, v. 35.
- Roland, N. W., 2004, Pan-African granite-charnockite magmatism in central Dronning Maud Land, East Antarctica: petrography, geochemistry and plate tectonic implications: *Geologisches Jahrbuch Reihe B*, v. 96, p. 187.
- Rouby, D., Bonnet, S., Guillocheau, F., Gallagher, K., Robin, C., Biancotto, F., Dauteuil, O., and Braun, J., 2009, Sediment supply to the Orange sedimentary system over the last 150My: An evaluation from sedimentation/denudation balance: *Marine and Petroleum Geology*, v. 26, no. 6, p. 782-794, <http://dx.doi.org/10.1016/j.marpetgeo.2008.08.004>.
- Runcorn, S. K., 1962, Convection Currents in the Earth's Mantle: *Nature*, v. 195, p. 1248, <http://dx.doi.org/10.1038/1951248a0>.
- Ruppel, A., 2012, Structural evolution of the Main Shear Zone in Sør Rondane, East Antarctica: University of Bremen, Master Thesis p. 1-88.
- Ruppel, A., Eagles, G., Jacobs, J., Jokat, W., and Läufer, A., 2017, The Forster Magnetic Anomaly: reading between the lines to better understand a major suture crossing central Dronning Maud Land: *Geophysical Research Abstracts, EGU General Assembly*, v. 19, no. EGU2017-11750.
- Ruppel, A., Jacobs, J., Eagles, G., Läufer, A., and Jokat, W., 2018, New geophysical data from a key region in East Antarctica: Estimates for the spatial extent of the Tonian Oceanic Arc Super Terrane (TOAST): *Gondwana Research*, v. 59, p. 97-107, <http://dx.doi.org/10.1016/j.gr.2018.02.019>.
- Ruppel, A., Läufer, A., Jacobs, J., Krasniqi, K., Elburg, M., Krohne, N., and Lisker, F., in prep., New constraints on deformation and cooling history of Sør Rondane and their implications on the final assembly of Gondwana from Ar/Ar and U-Pb geochronology.
- Ruppel, A. S., Läufer, A., Jacobs, J., Elburg, M., Krohne, N., Damaske, D., and Lisker, F., 2015, The Main Shear Zone in Sør Rondane, East Antarctica: Implications for the late-Pan-African tectonic evolution of Dronning Maud Land: *Tectonics*, v. 34, no. 6, p. 1290-1305, <http://dx.doi.org/10.1002/2014TC003763>.
- Rust, D. J., and Summerfield, M. A., 1990, Isopach and borehole data as indicators of rifted margin evolution in southwestern Africa: *Marine and Petroleum Geology*, v. 7, no. 3, p. 277-287, [http://dx.doi.org/10.1016/0264-8172\(90\)90005-2](http://dx.doi.org/10.1016/0264-8172(90)90005-2).
- Rutte, D., Pfänder, J. A., Kolečka, M., Jonckheere, R., and Unterricker, S., 2015, Radial fast-neutron fluence gradients during rotating 40Ar/39Ar sample irradiation recorded with metallic fluence monitors and geological age standards: *Geochemistry, Geophysics, Geosystems*, v. 16, no. 1, p. 336-345, [10.1002/2014GC005611](https://doi.org/10.1002/2014GC005611).
- Sacek, V., Braun, J., and Van der Beek, P., 2012a, The influence of rifting on escarpment migration on high elevation passive continental margins: *Journal of Geophysical Research*, v. 117, no. B04407, p. 1-18, <http://dx.doi.org/10.1029/2011JB008547>.
- Sacek, V., Braun, J., and Beek, P., 2012b, The influence of rifting on escarpment migration on high elevation passive continental margins: *Journal of Geophysical Research: Solid Earth*, v. 117, no. B4.
- Salman, G., and Abdula, I., 1995, Development of the Mozambique and Ruvuma sedimentary basins, offshore Mozambique: *Sedimentary Geology*, v. 96, no. 1, p. 7-41, [http://dx.doi.org/10.1016/0037-0738\(95\)00125-R](http://dx.doi.org/10.1016/0037-0738(95)00125-R).
- Satish-Kumar, M., Hokada, T., Kawakami, T., and Dunkley, D. J., 2008, Geosciences research in East Antarctica (0°E-60°E): Present status and future perspectives: *Geological Society Special Publication*, v. 308, p. 1-20.
- Satish-Kumar, M., and Hokada, T., 2013, Crossing of Neoproterozoic orogens: *Precambrian Research*, v. 234.
- Satish-Kumar, M., Hokada, T., Owada, M., Osanai, Y., and Shiraishi, K., 2013, Neoproterozoic orogens amalgamating East Gondwana: Did they cross each other?: *Precambrian Research*, v. 234, p. 1-7.
- Scheinert, M., Ferraccioli, F., Schwabe, J., Bell, R., Studinger, M., Damaske, D., Jokat, W., Aleshkova, N., Jordan, T., Leitchenkov, G., Blankenship, D. D., Damiani, T. M., Young, D., Cochran, J. R., and Richter, T. D., 2016, New Antarctic gravity anomaly grid for enhanced geodetic and geophysical studies in Antarctica: *Geophysical Research Letters*, v. 43, no. 2, p. 600-610, <http://dx.doi.org/10.1002/2015GL067439>.



- Schlüter, J., Estrada, S., Lisker, F., Läufer, A., Kühn, R., Nitzsche, K. N., and Spiegel, C., 2011, First petrographical description of rock occurrences in the Steingarden area, Dronning Maud Land, East Antarctica: *Polarforschung*, v. 80, no. 3, p. 161-172.
- Schmädicke, E., and Will, T., 2006, First evidence of eclogite facies metamorphism in the Shackleton Range, Antarctica: Trace of a suture between East and West Gondwana?: *Geology*, v. 34, no. 3, p. 133-136.
- Sellwood, B. W., and Valdes, P. J., 2006, Mesozoic climates: General circulation models and the rock record: *Sedimentary Geology*, v. 190, no. 1, p. 269-287, <http://dx.doi.org/10.1016/j.sedgeo.2006.05.013>.
- Shackleton, R. M., 1996, The final collision zone between East and West Gondwana: where is it?: *Journal of African Earth Sciences*, v. 23, no. 3, p. 271-287.
- Shervais, J. W., 1982, Ti-V plots and the petrogenesis of modern and ophiolitic lavas: *Earth and Planetary Science Letters*, v. 59, no. 1, p. 101-118, [http://dx.doi.org/10.1016/0012-821X\(82\)90120-0](http://dx.doi.org/10.1016/0012-821X(82)90120-0).
- Shevenell, A. E., Kennett, J. P., and Lea, D. W., 2004, Middle Miocene Southern Ocean Cooling and Antarctic Cryosphere Expansion: *Science*, v. 305, no. 5691, p. 1766-1770, <http://dx.doi.org/10.1126/science.1100061>.
- Shiraishi, K., Asami, M., and Ohta, Y., 1982, Plutonic and metamorphic rocks of Massif-A in the Yanato Mountains, East Antarctica: *Memoirs of National Institute of Polar Research*. Special issue, v. 21, p. 21-31.
- Shiraishi, K., Asami, M., and Ishizuka, H., 1991, Geology and metamorphism of the Sør Rondane mountains, east Antarctica, *Geological Evolution of Antarctica*, 77-82 p, 77-82 p.
- Shiraishi, K., Osanai, Y., Tainosho, Y., Takahashi, Y., Tsuchiya, N., Kojima, S., Yanai, K., and Moriwaki, K., 1992a, Explanatory text of Geological Map of Widerøefjellet, Sør Rondane Mountains, Antarctica: *Antarctic Geological Map Series*, National Institute of Polar Research, Tokyo, v. Sheet 32, p. 1-20.
- Shiraishi, K., Hiroi, Y., Ellis, D., Fanning, C., Motoyoshi, Y., and Nakai, Y., 1992b, The first report of a Cambrian orogenic belt in East Antarctica - an ion microprobe study of the Lützow-Holm Complex: *Recent Progress in Antarctic Earth Science*. Terra Scientific Publishing Company, Tokyo, p. 29-35.
- Shiraishi, K., Osanai, Y., Tainosho, Y., Takahashi, Y., Tsuchiya, N., Kojima, S., Yanai, K., and Moriwaki, K., 1992c, Geological map of the Sør Rondane Mountains, Antarctica. *Antarctica Geological Map Series*, sheet 32, scale 1 : 25 0000: National Institute of Polar Research, Tokyo.
- Shiraishi, K., and Kagami, H., 1992, Sm-Nd and Rb-Sr ages of metamorphic rocks from the Sør Rondane Mountains, east Antarctica: *Recent Progress in Antarctic Earth Science*, p. 29-35.
- Shiraishi, K., Ellis, D. J., Hiroi, Y., Fanning, C. M., Motoyoshi, Y., and Nakai, Y., 1994, Cambrian Orogenic Belt in East Antarctica and Sri Lanka: Implications for Gondwana Assembly: *The Journal of Geology*, v. 102, p. 47-65.
- Shiraishi, K., Osanai, Y., Ishizuka, H., and Asami, M., 1997, Geological map of the Sør Rondane Mountains, Antarctica. *Antarctica Geological Map Series*, sheet 35, scale 1 : 25 0000: National Institute of Polar Research, Tokyo.
- Shiraishi, K., Hokada, T., Fanning, C., Misawa, K., and Motoyoshi, Y., 2003, Timing of thermal events in eastern Dronning Maud Land, East Antarctica: *Polar Geoscience*, v. 16, p. 76-99.
- Shiraishi, K., Dunkley, D. J., Hokada, T., Fanning, C. M., Kagami, H., and Hamamoto, T., 2008, Geochronological constraints on the Late Proterozoic to Cambrian crustal evolution of eastern Dronning Maud Land, East Antarctica: a synthesis of SHRIMP U-Pb age and Nd model age data: *Geological Society, London, Special Publications*, v. 308, no. 1, p. 21-67.
- Shuster, D. L., Flowers, R. M., and Farley, K. A., 2006, The influence of natural radiation damage on helium diffusion kinetics in apatite: *Earth and Planetary Science Letters*, v. 249, no. 3-4, p. 148-161.
- Siegert, M. J., Carter, S., Tabacco, I., Popov, S., and Blankenship, D. D., 2005, A revised inventory of Antarctic subglacial lakes: *Antarctic Science*, v. 17, no. 3, p. 453-460, <http://dx.doi.org/10.1017/S0954102005002889>.
- Sinton, J. M., Ford, L. L., Chappell, B., and McCulloch, M. T., 2003, Magma Genesis and Mantle Heterogeneity in the Manus Back-Arc Basin, Papua New Guinea: *Journal of Petrology*, v. 44, no. 1, p. 159-195, <http://dx.doi.org/10.1093/petrology/44.1.159>.
- Sirevaag, H., Jacobs, J., Ksienzyk, A. K., Dunkl, I., and Marschall, H. R., 2018a, Extent, thickness and erosion of the Jurassic continental flood basalts of Dronning Maud Land, East Antarctica: A low-T



- thermochronological approach: *Gondwana Research*, v. 61, p. 222-243, <http://dx.doi.org/10.1016/j.gr.2018.04.017>.
- Sirevaag, H., Ksienzyk, K. A., Jacobs, J., Dunkl, I., and Läufer, A., 2018b, Tectono-Thermal Evolution and Morphodynamics of the Central Dronning Maud Land Mountains, East Antarctica, Based on New Thermochronological Data: *Geosciences*, v. 8, no. 11, <http://dx.doi.org/10.3390/geosciences8110390>.
- Sláma, J., Košler, J., Condon, D. J., Crowley, J. L., Gerdes, A., Hanchar, J. M., Horstwood, M. S. A., Morris, G. A., Nasdala, L., Norberg, N., Schaltegger, U., Schoene, B., Tubrett, M. N., and Whitehouse, M. J., 2008, Plešovice zircon — A new natural reference material for U–Pb and Hf isotopic microanalysis: *Chemical Geology*, v. 249, no. 1, p. 1-35, <http://doi.org/10.1016/j.chemgeo.2007.11.005>.
- Solli, K., Kuvaas, B., Kristoffersen, Y., Leitchenkov, G., Guseva, J., and Gandjukhin, V., 2007, Seismic morphology and distribution of inferred glaciomarine deposits along the East Antarctic continental margin, 20°E–60°E: *Marine Geology*, v. 237, no. 3–4, p. 207-223, <http://dx.doi.org/10.1016/j.margeo.2006.12.002>.
- Sorbadere, F., Schiano, P., Métrich, N., and Bertagnini, A., 2013, Small-scale coexistence of island-arc- and enriched-MORB-type basalts in the central Vanuatu arc: *Contributions to Mineralogy and Petrology*, v. 166, no. 5, p. 1305-1321, <http://dx.doi.org/10.1007/s00410-013-0928-8>.
- Sperner, B., Ratschbacher, L., and Ott, R., 1993, Fault-striae analysis: a Turbo Pascal program package for graphical presentation and reduced stress tensor calculation: *Computers & Geosciences*, v. 19, no. 9, p. 1361-1388.
- Sperner, B., Jonckheere, R., and Pfänder, J. A., 2014, Testing the influence of high-voltage mineral liberation on grain size, shape and yield, and on fission track and  $^{40}\text{Ar}/^{39}\text{Ar}$  dating: *Chemical Geology*, v. 371, no. Supplement C, p. 83-95, <http://dx.doi.org/10.1016/j.chemgeo.2014.02.003>.
- Stacey, J. S., and Kramers, J. D., 1975, Approximation of terrestrial lead isotope evolution by a two-stage model: *Earth and Planetary Science Letters*, v. 26, no. 2, p. 207-221, [http://dx.doi.org/10.1016/0012-821X\(75\)90088-6](http://dx.doi.org/10.1016/0012-821X(75)90088-6).
- Steiger, R. H., and Jäger, E., 1977, Subcommittee on geochronology: Convention on the use of decay constants in geo- and cosmochronology: *Earth and Planetary Science Letters*, v. 36, no. 3, p. 359-362, [http://dx.doi.org/10.1016/0012-821X\(77\)90060-7](http://dx.doi.org/10.1016/0012-821X(77)90060-7).
- Stern, R. J., 1994, Arc-Assembly and Continental Collision in the Neoproterozoic African Orogen: Implications for the Consolidation of Gondwanaland: *Annual Review of Earth and Planetary Sciences*, v. 22, p. 319-351.
- Stern, R. J., 2002, Crustal evolution in the East African Orogen: a neodymium isotopic perspective: *Journal of African Earth Sciences*, v. 34, no. 3–4, p. 109-117, [http://dx.doi.org/10.1016/S0899-5362\(02\)00012-X](http://dx.doi.org/10.1016/S0899-5362(02)00012-X).
- Suda, Y., Kawano, Y., Yaxley, G., Korenaga, H., and Hiroi, Y., 2008, Magmatic evolution and tectonic setting of metabasites from Lützow-Holm Complex, East Antarctica: *Geological Society, London, Special Publications*, v. 308, no. 1, p. 211-233, <http://dx.doi.org/10.1144/sp308.11>.
- Suganuma, Y., Miura, H., Zondervan, A., and Okuno, J. i., 2014, East Antarctic deglaciation and the link to global cooling during the Quaternary: evidence from glacial geomorphology and  $^{10}\text{Be}$  surface exposure dating of the Sør Rondane Mountains, Dronning Maud Land: *Quaternary Science Reviews*, v. 97, p. 102-120, <http://dx.doi.org/10.1016/j.quascirev.2014.05.007>.
- Sugden, D. E., Denton, G. H., and Marchant, D. R., 1995, Landscape evolution of the dry valleys, Transantarctic Mountains; tectonic implications: *Journal of Geophysical Research*, v. 100, no. B6, p. 9949-9967.
- Sukegawa, Y., and Yamanouchi, T., 1993, Meteorological data at Asuka Station, Antarctica in 1991. JARE Data Rep.: National Institute of Polar Research.
- Tainosho, Y., Takahashi, Y., Arakawa, Y., Y. O., Tsuchiya, N., Sakiyama, T., and Owada, M., 1992, Petrochemical character and Rb-Sr isotopic investigation of the granitic rocks from the Sør Rondane Mountains, East Antarctica, *Recent Progress in Antarctic Earth Science*, 45-54.
- Takahashi, K., Tsunogae, T., Santosh, M., Takamura, Y., and Tsutsumi, Y., 2017, Paleoproterozoic (ca. 1.8Ga) arc magmatism in the Lützow-Holm Complex, East Antarctica: Implications for crustal growth and terrane assembly in erstwhile Gondwana fragments: *Journal of Asian Earth Sciences*, <http://dx.doi.org/10.1016/j.jseaes.2017.07.053>.
- Takahashi, Y., Arakawa, Y., Sakiyama, T., Osanai, Y., and Makimoto, H., 1990, Rb-Sr and K-Ar whole rock ages of the plutonic bodies from the Sør Rondane Mountains, East Antarctica: *Proceedings of the NIPR Symposium on Antarctic Geosciences*, v. 4, p. 1-8.



- Takigami, Y., Kaneoka, I., and Funaki, M., 1987, Age and paleomagnetic studies for intrusive and metamorphic rocks from the Sør Rondane Mountains, Antarctica: Proceedings of the NIPR Symposium on Antarctic Geosciences, v. 1, p. 169-177.
- Takigami, Y., and Funaki, M., 1991,  $^{40}\text{Ar}/^{39}\text{Ar}$  and K-Ar ages for igneous and metamorphic rocks from the Sør Rondane Mountains, East Antarctica: Proceedings of the National Institute of Polar Research Symposium on Antarctic Geosciences, v. 5, p. 122-135.
- Talarico, F., Kleinschmidt, G., and Henjes-Kunst, F., 1999, An ophiolitic complex in the northern Shackleton Range, Antarctica: *Terra Antarctica*, v. 6, no. 3/4, p. 293-315.
- Tankard, A., Welsink, H., Aukes, P., Newton, R., and Stettler, E., 2009, Tectonic evolution of the Cape and Karoo basins of South Africa: *Marine and Petroleum Geology*, v. 26, no. 8, p. 1379-1412, <http://dx.doi.org/10.1016/j.marpetgeo.2009.01.022>.
- Tatsumi, T., and Kizaki, K., 1969, Geology of the Lützow-Holm Bay Region and the "Yamato Mountains" (Queen Fabiola Mountains), Antarctic Map Folio Series, Volume Folio 12-Geology Sheets 9 and 10, Geology of the Lützow-Holm Bay Region and the "Yamato Mountains" American Society.
- Thébault, E., Finlay, C. C., Beggan, C. D., Alken, P., Aubert, J., Barrois, O., Bertrand, F., Bondar, T., Boness, A., Brocco, L., Canet, E., Chambodut, A., Chulliat, A., Coïsson, P., Civet, F., Du, A., Fournier, A., Fratter, I., Gillet, N., Hamilton, B., Hamoudi, M., Hulot, G., Jager, T., Korte, M., Kuang, W., Lalanne, X., Langlais, B., Léger, J.-M., Lesur, V., Lowes, F. J., Macmillan, S., Manda, M., Manoj, C., Maus, S., Olsen, N., Petrov, V., Ridley, V., Rother, M., Sabaka, T. J., Saturnino, D., Schachtschneider, R., Sirol, O., Tangborn, A., Thomson, A., Tøffner-Clausen, L., Vigneron, P., Wardinski, I., and Zvereva, T., 2015, International Geomagnetic Reference Field: the 12th generation: *Earth, Planets and Space*, v. 67, no. 1, p. 79, <http://dx.doi.org/10.1186/s40623-015-0228-9>.
- Thomson, S. N., Reiners, P. W., Hemming, S. R., and Gehrels, G. E., 2013, The contribution of glacial erosion to shaping the hidden landscape of East Antarctica: *Nature Geoscience*, v. 6, p. 203, <http://dx.doi.org/10.1038/ngeo1722>.
- Tinker, J., Kravtsov, A. V., Klypin, A., Abazajian, K., Warren, M., Yepes, G., Gottlöber, S., and Holz, D. E., 2008, Toward a Halo Mass Function for Precision Cosmology: The Limits of Universality: *The Astrophysical Journal*, v. 688, no. 2, p. 709-728, <http://dx.doi.org/10.1086/591439>.
- Toyoshima, T., Owada, M., and Shiraishi, K., 1995, Structural evolution of metamorphic and igneous rocks from the central part of the Sor Rondane Mountains, East Antarctica: Proceedings of NIPR Symposium on Antarctic Geosciences, v. 8, p. 75-97.
- Toyoshima, T., Osanai, Y., Baba, S., Hokada, T., Nakano, N., Adachi, T., Otsubo, M., Ishikawa, M., and Nogi, Y., 2013, Sinistral transpressional and extensional tectonics in Dronning Maud Land, East Antarctica, including the Sør Rondane Mountains: *Precambrian Research*, v. 234, p. 30-46.
- Trail, D., Bruce Watson, E., and Tailby, N. D., 2012, Ce and Eu anomalies in zircon as proxies for the oxidation state of magmas: *Geochimica et Cosmochimica Acta*, v. 97, no. Supplement C, p. 70-87, <http://dx.doi.org/10.1016/j.gca.2012.08.032>.
- Tsunogae, T., Yang, Q.-Y., and Santosh, M., 2015, Early Neoproterozoic arc magmatism in the Lützow-Holm Complex, East Antarctica: Petrology, geochemistry, zircon U–Pb geochronology and Lu–Hf isotopes and tectonic implications: *Precambrian Research*, v. 266, no. Supplement C, p. 467-489, <http://dx.doi.org/10.1016/j.precamres.2015.05.040>.
- Tsunogae, T., Yang, Q.-Y., and Santosh, M., 2016, Neoproterozoic–Early Paleoproterozoic and Early Neoproterozoic arc magmatism in the Lützow–Holm Complex, East Antarctica: Insights from petrology, geochemistry, zircon U–Pb geochronology and Lu–Hf isotopes: *Lithos*, v. 263, no. Supplement C, p. 239-256, <http://dx.doi.org/10.1016/j.lithos.2016.02.010>.
- Tuck-Martin, A., Adam, J., and Eagles, G., 2018, New plate kinematic model and tectono-stratigraphic history of the East African and West Madagascan margins: *Basin Research*, p. 1-23, <http://dx.doi.org/10.1111/bre.12294>.
- Turner, B. R., 1999, Tectonostratigraphical development of the Upper Karoo foreland basin: orogenic unloading versus thermally-induced Gondwana rifting: *Journal of African Earth Sciences*, v. 28, no. 1, p. 215-238.
- Van Autenboer, T., 1964, The Geomorphology and Glacial Geology of the Sør Rondane, Dronning Maud Land, Antarctica, *Medelingen van de Koninklijke Vlaamse Academie voor Wetenschappen, Letteren en Schone Kunsten van België*, Volume 24: Brussel, Koninklijke Vlaamse Academie voor Wetenschappen, Letteren en Schone Kunsten van België, p. 91.



- Van Autenboer, T., Michot, J., and Picciotto, E., 1964, Outline of the geology and petrology of the Sør-Rondane Mountains, Dronning Maud Land, in *Antarctic Geology*, In: Adie, R. J. (Ed) *Proceedings of the First International Symposium on Antarctic Geology*, Cape Town, 16-21 September 1963, p. 501-514, North-Holland Publishing Company, 501-514 p.
- Van Autenboer, T., 1969, *Geology of the Sør Rondane Mountains*. *Geologic Maps of Antarctica*, ed. by C. Craddock et al: American Geographical Society, v. (Antarctic Map Folio Ser., Folio 12), p. Sheet 8, Pl. VIII-Sheet 8, Pl. VIII.
- Van Autenboer, T., and Loy, V., 1972, Recent geological Investigations in the Sor Rondane mountains, Belgicafjella and Sverdrupfjella, Dronning Maud Land, Antarctica, *Proceedings SCAR-IUGS Symposium on Antarctic Geology*, Universitetsforlaget, Oslo, 563-571 p.
- Van Autenboer, T., and Declair, H., 1978, Glacier discharge in the Sør-Rondane, a contribution to the mass balance of Dronning Maud Land, Antarctica: *Zeitschrift für Gletscherkunde und Glazialgeologie*, v. 14, p. 1-16.
- Veevers, J. J., and Powell, C. M., 1994, Permian-Triassic Pangean basins and foldbelts along the Panthalassan margin of Gondwanaland: Boulder, CO, United States.
- Veevers, J. J., 2012, Reconstructions before rifting and drifting reveal the geological connections between Antarctica and its conjugates in Gondwanaland: *Earth-Science Reviews*, v. 111, no. 3-4, p. 249-318, [10.1016/j.earscirev.2011.11.009](http://dx.doi.org/10.1016/j.earscirev.2011.11.009).
- Verduzco, B., Fairhead, J. D., Green, C. M., and MacKenzie, C., 2004, New insights into magnetic derivatives for structural mapping: *The Leading Edge*, v. 23, no. 2, p. 116-119, <http://dx.doi.org/10.1190/1.1651454>.
- Vermeesch, P., 2010, HelioPlot, and the treatment of overdispersed (U-Th-Sm)/He data: *Chemical Geology*, v. 271, no. 3-4, p. 108-111.
- Watts, A. B., and Moore, J. D. P., 2017, Flexural Isostasy: Constraints From Gravity and Topography Power Spectra: *Journal of Geophysical Research: Solid Earth*, v. 122, no. 10, p. 8417-8430, <http://dx.doi.org/10.1002/2017JB014571>.
- Wegener, A., 1912, Die Entstehung der Kontinente: *Geologische Rundschau*, v. 3, no. 4, p. 276-292.
- Weis, D., Kieffer, B., Maerschalk, C., Barling, J., de Jong, J., Williams, G. A., Hanano, D., Pretorius, W., Mattielli, N., Scoates, J. S., Goolaerts, A., Friedman, R. M., and Mahoney, J. B., 2006, High-precision isotopic characterization of USGS reference materials by TIMS and MC-ICP-MS: *Geochemistry, Geophysics, Geosystems*, v. 7, no. 8, p. n/a-n/a, <http://dx.doi.org/10.1029/2006GC001283>.
- Whalen, J. B., Currie, K. L., and Chappell, B. W., 1987, A-type granites: geochemical characteristics, discrimination and petrogenesis: *Contributions to Mineralogy and Petrology*, v. 95, no. 4, p. 407-419, <http://dx.doi.org/10.1007/bf00402202>.
- Whitehouse, M. J., Kamber, B. S., and Moorbath, S., 1999, Age significance of U-Th-Pb zircon data from early Archaean rocks of west Greenland—a reassessment based on combined ion-microprobe and imaging studies: *Chemical Geology*, v. 160, no. 3, p. 201-224, [http://dx.doi.org/10.1016/S0009-2541\(99\)00066-2](http://dx.doi.org/10.1016/S0009-2541(99)00066-2).
- Whitehouse, M. J., and Kamber, B. S., 2005, Assigning dates to thin gneissic veins in high-grade metamorphic terranes: a cautionary tale from Akilia, southwest Greenland: *Journal of Petrology*, v. 46, no. 2, p. 291-318.
- Whittaker, J. M., Goncharov, A., Williams, S. E., Müller, R. D., and Leitchenkov, G., 2013, Global sediment thickness data set updated for the Australian-Antarctic Southern Ocean: *Geochemistry, Geophysics, Geosystems*, v. 14, no. 8, p. 3297-3305, <http://dx.doi.org/10.1002/ggge.20181>.
- Wiedenbeck, M., Allé, P., Corfu, F., Griffin, W. L., Meier, M., Oberli, F., Quadt, A. V., Roddick, J. C., and Spiegel, W., 1995, Three natural zircon standards for U-Th-Pb, Lu-Hf, trace element and REE analyses: *Geostandards Newsletter*, v. 19, no. 1, p. 1-23, <http://dx.doi.org/10.1111/j.1751-908X.1995.tb00147.x>.
- Wildman, M., Brown, R., Watkins, R., Carter, A., Gleadow, A., and Summerfield, M., 2015, Post break-up tectonic inversion across the southwestern cape of South Africa: New insights from apatite and zircon fission track thermochronometry: *Tectonophysics*, v. 654, p. 30-55, <http://dx.doi.org/10.1016/j.tecto.2015.04.012>.
- Wildman, M., Brown, R., Beucher, R., Persano, C., Stuart, F., Gallagher, K., Schwanethal, J., and Carter, A., 2016, The chronology and tectonic style of landscape evolution along the elevated Atlantic continental margin of South Africa resolved by joint apatite fission track and (U-Th-Sm)/He thermochronology: *Tectonics*, v. 35, no. 3, p. 511-545, <http://dx.doi.org/10.1002/2015TC004042>.



- Willbold, M., Hegner, E., Kleinschrodt, R., Stosch, H. G., Kehelpannala, K. V. W., and Dulski, P., 2004, Geochemical evidence for a Neoproterozoic magmatic continental margin in Sri Lanka—relevance for the Rodinia–Gondwana supercontinent cycle: *Precambrian Research*, v. 130, no. 1, p. 185-198, <http://dx.doi.org/10.1016/j.precamres.2003.11.003>.
- Williams, I. S., and Claesson, S., 1987, Isotopic evidence for the Precambrian provenance and Caledonian metamorphism of high grade paragneisses from the Seve Nappes, Scandinavian Caledonides: *Contributions to Mineralogy and Petrology*, v. 97, no. 2, p. 205-217, <http://dx.doi.org/10.1007/bf00371240>.
- Williams, I. S., 1998, U-Th-Pb geochronology by ion microprobe, *Reviews in Economic Geology, Applications of microanalytical techniques to understanding mineralizing processes*, 1-35 p.
- Williams, I. S., and Herget, J. M., 2000, U-Pb dating of Tasmanian dolerites: A cautionary tale of SHRIMP analysis of high-U zircon: *Lorne, Beyond 2000: new frontiers in isotope geoscience*, v. Abstracts and Proceedings, 185-188 p.
- Wilson, D. S., Jamieson, S. S. R., Barrett, P. J., Leitchenkov, G., Gohl, K., and Larter, R. D., 2012, Antarctic topography at the Eocene–Oligocene boundary: *Palaeogeography, Palaeoclimatology, Palaeoecology*, v. 335-336, p. 24-34, <http://dx.doi.org/10.1016/j.palaeo.2011.05.028>.
- Wilson, T. J., Grunow, A. M., and Hanson, R. E., 1997, Gondwana assembly: The view from Southern Africa and East Gondwana: *Journal of Geodynamics*, v. 23, no. 3, p. 263-286, [http://dx.doi.org/10.1016/S0264-3707\(96\)00048-8](http://dx.doi.org/10.1016/S0264-3707(96)00048-8).
- Woodhead, J. D., and Hergt, J. M., 2005, A Preliminary Appraisal of Seven Natural Zircon Reference Materials for In Situ Hf Isotope Determination: *Geostandards and Geoanalytical Research*, v. 29, no. 2, p. 183-195, doi:10.1111/j.1751-908X.2005.tb00891.x.
- Yamanouchi, T., Shibuya, K., and Sakai, R., 1988, Meteorological data at Asuka Camp, Antarctica in 1987. JARE Data Rep.: National Institute of Polar Research.
- Yildiz, H., Forsberg, R., Tscherning, C. C., Steinhage, D., Eagles, G., and Bouman, J., 2017, Upward continuation of Dome-C airborne gravity and comparison with GOCE gradients at orbit altitude in east Antarctica: *Studia Geophysica et Geodaetica*, v. 61, no. 1, p. 53-68, <http://dx.doi.org/10.1007/s11200-015-0634-2>.
- Yogodzinski, G. M., Lees, J. M., Churikova, T. G., Dorendorf, F., Wöerner, G., and Volynets, O. N., 2001, Geochemical evidence for the melting of subducting oceanic lithosphere at plate edges: *Nature*, v. 409, p. 500, <http://dx.doi.org/10.1038/35054039>.
- Yoshida, M., Funaki, M., and Piyadasa, W. V., 1992, Proterozoic to Mesozoic East Gondwana: The juxtaposition of India, Sri Lanka and Antarctica: *Tectonics*, v. 11, no. 2, p. 381-391.
- Zhao, J. X., Shiraishi, K., Ellis, D. J., and Sheraton, J. W., 1995, Geochemical and isotopic studies of syenites from the Yamato Mountains, East Antarctica: Implications for the origin of syenitic magmas: *Geochimica et Cosmochimica Acta*, v. 59, no. 7, p. 1363-1382, [http://dx.doi.org/10.1016/0016-7037\(95\)00050-A](http://dx.doi.org/10.1016/0016-7037(95)00050-A).



